FORMERLY ACTA GEODAETICA, GEOPHYSICA ET MONTANISTICA ACADEMIAE SCIENTIARUM HUNGARICAE

Acta Geodaetica, Geophysica et Montanistica Hungarica

VOLUME 19, NUMBERS 1–2, 1984

Akadémiai Kiadó, Budapest
AGGM 19 (1–2) 1–188 (1984) HU ISSN 0236-5758

ACTA GEODAETICA, GEOPHYSICA et MONTANISTICA HUNGARICA
A Quarterly Journal of the Hungarian Academy of Sciences

Acta Geodaetica, Geophysica et Montanistica (AGGM) publishes original reports on geodesy, geophysics and minings in English.

AGGM is published in yearly volumes of four numbers by

AKADÉMIAI KIADÓ
Publishing House of the Hungarian Academy of Sciences
H-1054 Budapest, Alkotmány u. 21.

Manuscripts and editorial correspondence should be addressed to

AGGM Editorial Office
H-9401 Sopron P.O. Box 5

Subscription information

Orders should be addressed to

KULTURA Foreign Trading Company
H-1389 Budapest P.O. Box 149

INSTRUCTIONS TO AUTHORS

Manuscripts should be sent to the editors (MTA Geodéziai és Geofizikai Kutató Intézete, AGGM Editorial Office, H-9401 Sopron, P.O.Box 5, HUNGARY). Only articles not submitted for publication elsewhere are accepted.

Manuscripts should be typewritten in duplicate, double-spaced, 25 lines with 50 letters each. The papers generally include the following components, which should be presented in the order listed.

1. Title, name of author(s), affiliation, dateline, abstract, keywords
2. Text, acknowledgements
3. References
4. Footnotes
5. Legends
6. Tables and illustrations

1. The *affiliation* should be as concise as possible and should include the complete mailing address of the authors. The *date of receipt* of the manuscript will be supplied by the editors. The abstract should not exceed 250 words and should clearly and simply summarize the most important methods and results. 5–10 significant expressions describing the content are used as *keywords*. Authors may recommend these keywords.

2. The *text* should be generally in English and as short and clear as possible. From Hungarian authors papers are also accepted in Hungarian.

The section heading should *not* be underlined or in capitals.

Please note that underlining denotes special types:

— single underlining: italics
— double underlining: bold-face roman

ACTA GEODAETICA, GEOPHYSICA et MONTANISTICA HUNGARICA

A Quarterly Journal of the Hungarian Academy of Sciences

VOLUME 19

Akadémiai Kiadó, Budapest
1984

AUTHOR INDEX

KEYWORD INDEX

CONTENTS

Book Reviews

CONTENTS

Proceedings of the 1st Symposium
of the KAPG Subproject 1.1
Budapest, September 8–14, 1982

GEOPHYSICAL AND GEODYNAMIC MODELS OF THE LITHOSPHERE OF THE CARPATHO-BALKAN REGION

Acta Geodaet., Geophys. et Montanist. Hung. Volume 19 (1—2), pp. 3—4 (1984)

GEOPHYSICAL AND GEODYNAMIC MODELS OF THE LITHOSPHERE OF THE CARPATHO-BALKAN REGION

(A NEW SUBPROJECT OF THE KAPG-COMMISSION OF THE ACADEMIES OF SCIENCES OF THE SOCIALIST COUNTRIES FOR PLANETARY GEOPHYSICS)

L STEGENA[1]

The Commission of the Academies of Sciences of the Socialist Countries for Planetary Geophysics (KAPG) decided to start with a new subproject entitled Geophysical and Geodynamic Models of the Lithosphere of the Carpatho-Balkan Region (KBR). After preparations, the subproject was discussed in Kiev, February 1981 and finalized at the KAPG Bureau-meeting in Varna, May 1981.

The subproject covers the area of the Carpatho–Balkan orogenic system and the areas jointed genetically (interarc basins like the Pannonian and Transylvanian basins, foredeeps, etc.). The scope of the subproject is: to improve our knowledge on the lithosphere, crust, tectonics and the geological evolution of the areas in question mainly by geophysical methods, for a better understanding of the evolution and structure of the geological mega-unit and to form this way a better basis for mineral explorations in the area. In the subproject the following strategies of operations are followed:

Magnetotellurics: to determine the deep geoelectric structures of the tectonic units using further MT soundings and taking into account the distortion (sedimentary-, edge- and coastal) effects of inhomogeneities on MT-soundings, comparisons of telluric data with the results of geothermics and of deep seismic soundings.

Wiese (Parkinson) vectors: further measurements, in function of period (GDS), quantitative interpretations along profiles.

Geomagnetism: construction of a magnetic normal field and a map of the regional vertical magnetic anomalies for the KBR; interpretations with up-to-date methods (frequency spectrum, filter theory).

Paleomagnetism: investigations of various parts of the KBR, for paleogeographic and tectonic reconstructions.

Magnetostratigraphy: comparison between paleomagnetic etalon-sections, construction of a regional magnetochronology for the Upper Neogene of the KBR.

Density models of the lithosphere: construction of a model for the region of the Carpathians, based on gravity, seismic and other data.

[1] Eötvös Loránd University, 1083 Budapest, Kun Béla tér 2.

Deep seismic soundings: further investigations down to the asthenosphere as far as possible, interpretation of $V(z)$ functions and its comparison with gravity, earthquake, electromagnetic and geothermic data.

Surface wave and other seismological studies, for a better knowledge of the KBR lithosphere.

Vertical and horizontal crustal movements: extension of the repeated levelings to the whole area of the KBR, starting the measurements of horizontal movements, study of the influences of rock compaction and other effects.

Rock stress measurements and its tectonic interpretation.

Geothermics: further heat flow density measurements, Moho-heat flow determinations; construction of geothermal models, implications of geothermics on tectonic evolution processes.

Special tectonic problems of the KBR: investigations of tectonic and stratigraphic problems and of ophiolites. Regional tectonic interpretation of satellite photos.

Volcanism: collecting data for age, volume, type and composition of the volcanic rocks of the KBR and the use of the data on regional maps.

Plate tectonics: investigations of the subduction — and collision — processes along the Carpathians and Balkan Mts. and of the development of the Infra-Carpathian basins.

Geotraverses: construction and interpretation of complex geotraverses along deep seismic profiles.

Data bank: collecting geophysical and geological data for the KBR.

About 30 scientific institutions of Bulgaria, Czechoslovakia, Hungary, Poland, Romania and the USSR are participating in the activity of the subproject.

The first scientific conference of the subproject was held in Budapest, September 8—14, 1982, with about 100 participants and 50 lectures. Varna and Lvov will probably host the succeeding conferences.

Those lectures of the Budapest conference are presented here, which refer to geophysical-geological problems of the KBR.

This volume contains some papers which were read at the KAPG conference on "Magnetotelluric deep soundings" (KAPG theme 1.1.4) in Sopron (Hungary), March 22—24, 1983 organized by A Ádám. The theme of these papers is the interpretation of the EM induction data measured also in the Carpatho–Balkan region. Simultaneously, this volume is a contribution to the ICL.

Acta Geodaet., Geophys. et Montanist. Hung. Volume 19 (1—2), pp. 5—13 (1984)

MARINE ELECTROMAGNETIC MEASUREMENTS ON THE BULGARIAN CONTINENTAL SHELF OF THE BLACK SEA

(PRELIMINARY REPORT)

L M ABRAMOVA,[1] S P GAIDASH,[1] A L KHARITONOV,[1] S M KOROTAEV,[1] S V SHABELIANSKY,[1] I L TROFIMOV[1]

The paper presents preliminary results of different marine electromagnetic measurements on the Bulgarian continental shelf: magnetotelluric sounding, magnetovariation profiling, magnetohydrodynamic profiling and magnetic survey. As final results the integral conductivity values of the sedimentary cover and the depths of magnetized bodies are given.

Keywords: Black Sea; continental shelf; magnetotellurics; magnetovariation profiling; sea electromagnetic measurements

Some complex geophysical measurements were carried out on the Bulgarian continental shelf by IZMIRAN and VC SOAN (USSR) with the participation of the Bulgarian Geological Committee between July and October 1981 with the aim to investigate the deep structure of the basement and of the sedimentary cover. A considerable part of the research program was done with electromagnetic methods, i.e. magnetotelluric sounding (MTS), magnetovariation profiling (MVP), magnetohydrodynamic profiling (MHDP) and magnetic survey.

Time variations were observed at stations lying roughly along a profile off Cape Kaliakra to SE (Fig. 1). The 5 components of the electromagnetic field were simultaneously measured at the station Balchik, too. 4 MTS stations, 8 MVP stations (6 with components and 2 with absolute value only) and 3 MHDP stations were measured. The variations of the magnetic field modulus were measured at the levels 0 and 300 m; thus, additional data were received for the method of gradient sounding.

The absolute geomagnetic field was observed over an area of about 160 × 160 km.

Fields induced by sea currents are present in the natural electromagnetic field of the sea; they have the same order of magnitude as the MT field, and, hence, disturb the MTS-method and, partly the MVP-method, but they give useful signals for the MHDP-method. That is why the measurements of sea currents were also included into the measurement complex.

Magnetic variations were measured by the following autonomic stations:

— three-component flux-gate station AMVS-3K with a scale value of about 1 nT, a time resolution of 1 min, and an automatical working period of 8 days;

[1] Institute of Terrestrial Magnetism, Ionosphere and Radio Wave Propagation (IZMIRAN) USSR Academy of Sciences Troitsk, Moscow Region, 142092

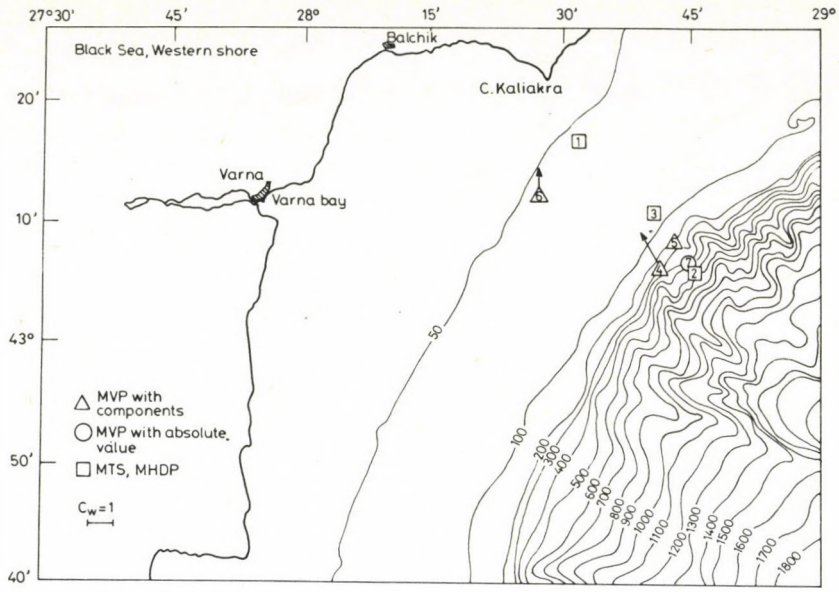

Fig. 1. Location of the variation points. Arrows are induction vectors determined from 1 h periods. Location of station 8 is shown in Fig. 8

— magnetostatic two-component station KDMVS-2, the parameters are similar to AMVS-3K;

— proton physical magnetic variometer-gradiometer AMPVG, with a sensitivity of 0.1 nT, time interval between two discrete measurements 1 min, a base of 300 m, and an automatism of 8 days.

Electric field variations were measured by an equipment consisting of two cable-lines of about 1000 m length at the sea-bottom and of Minigor recorders. As electrodes, graphite electrodes of the type Chernomor and Pb-$PbCl_2$-electrodes of the type IZMIRAN were used. The lines were laid out either parallelly and perpendicularly to the general sea current (at stations 1 and 2) or parallelly and perpendicularly to the magnetic meridian (at station 3) with an error of $\pm 1°$. The scale value of the equipment was about 0.1 $\mu V \cdot m^{-1}$, the time resolution 1 min.

Measurements on land were carried out by a 5-component station IZMIRAN-5.

Sea currents were measured by the instrument ATsIT which has a velocity sensitivity of 1 $cm \cdot s^{-1}$, and a direction sensitivity of $\pm 1°$. Beside currents, ATsIT also measured other hydrological elements of which the conductivity of water is important for the electromagnetic studies.

For the magnetic survey a towed absolute quantum magnetometer KM-8 was used; its data are: sensitivity up to 0.001 nT, absolute error ± 3 nT, time interval between two discrete measurements: 1s—0.01s.

The measurements were made by two vessels: the Evpatoria and the yacht A. Green. The following observation method was used: From board of Evpatoria, at small distances from each other (1.5—5 cable lengths) the flux-gate and the magnetostatic stations were brought into position together with a buoy from which A. Green laid out the electrode lines. Then A. Green moored herself to the buoy and recorded the variations of the electric field on her board. ATsIT was placed at a depth a little less than half of the depth of the electrodes of telluric measurements. Continuous synchronous observations of variations were made up to 10 days.

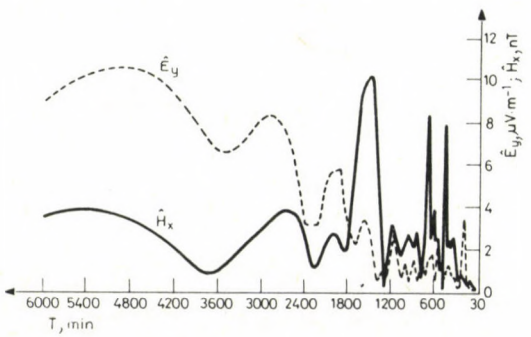

Fig. 2. Spectra of H_x and E_y at station 1

The magnetic survey was done on board of Evpatoria. In the centres of the survey regions, variations were recorded by the AMPVG nuclear magnetic instrument. The distances between the profiles varied between 1.5 − 15 km in dependence on the heterogeneity of the field.

The detection of the sea currents was an important preliminary step for the processing of the variations. Various currents of different types occur in the investigated area: synoptic and inertial ones, further those caused by wind, by mesoturbulence or even by seiches. The spectra of the fields of these currents are superposed to the spectrum of the MT field in the period range of 2 − 24 hours. The amplitudes of the sea current fields are especially great in the electric components where they usually exceed those of the telluric currents. As example the spectra of the orthogonal components H_x and E_y are shown in Fig. 2, as well as the spectrum of the corresponding component V_x in Fig. 3 (both at station 1). One can see that the sea current field is the highest at synoptic periods and it reaches about 4 nT in the magnetic and about 10 $\mu V \cdot m^{-1}$ in the electric field. According to our knowledge this was the first experiment of a synchronous measurement of the water current velocity and the magnetic field at the seafloor. The sea current field vanishes only at periods less than 2 hours. This circumstance highly disturbed the interpretation of the MT results, but on the other side it facilitated the realization of the MHDP method.

In the followings the preliminary results of the different methods are given.

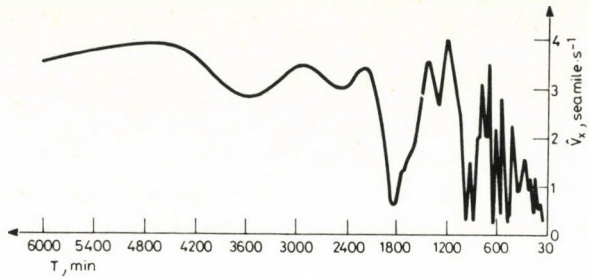

Fig. 3. Spectrum V_x (station 1)

Magnetotelluric sounding

The region is very complicated from the point of view of MTS not only because of the disturbance due to sea currents, but also because of the horizontal geoelectric heterogeneity caused by fracture tectonics and by the coastal effect. The data were processed by the method of amplitude and phase spectra and by that of the visual amplitudes and phases. Impedances were calculated as the solution of the equation system:

$$E_x(\omega) = Z_{xx}(\omega)\, H(\omega) + Z_{xy}(\omega)\, D(\omega)$$
$$E_y(\omega) = Z_{xy}(\omega)\, H(\omega) + Z_{yy}(\omega)\, D(\omega)$$

where E_x, E_y are the horizontal electric components, H, D the magnetic components, Z_{ij} impedance tensor components, ω is the frequency. The method of the visual amplitudes and phases gave better results.

In the period range between 10 minutes and several hours the electric field is linearly polarized in the direction perpendicular to the continental slope. Figure 4 shows impedance polar diagrams at the station Balchik. The diagrams of the main impedance have an orientation approximately perpendicular to the continental slope and an excentricity of 5 – 10. Figure 5 shows the MT-curve at the station Balchik (crosses are values from variations of the magnetic component polarized along the meridian, points are values from the impedance diagrams), Fig. 6 shows the MT curve of station 3. Both curves are H-polarized ones. The E-polarized curves can be determined only with great errors due to the high values of the secondary impedances lying along the minor axes of the diagrams. ϱ_T-values in the curve of Fig. 6 are by one order of magnitude less than those in the curve of Fig. 5. The interpretation of the curves gives for the integrated conductivity of the sediments $S = 60$ S at the station Balchik and about 1000 S at station 3, the latter being less reliable. Qualitatively the sea bed has a three-layer structure: conducting sediments–highly resistant basement–conducting mantle. The resistance of the basement below the seafloor is probably less than that of the continental basement.

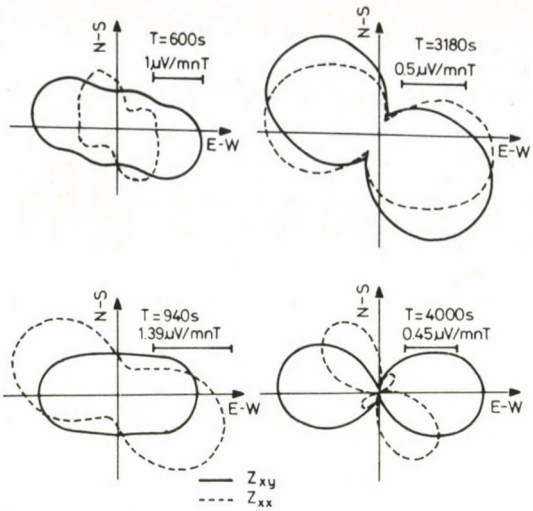

Fig. 4. Impedance polar diagrams at the station Balchik

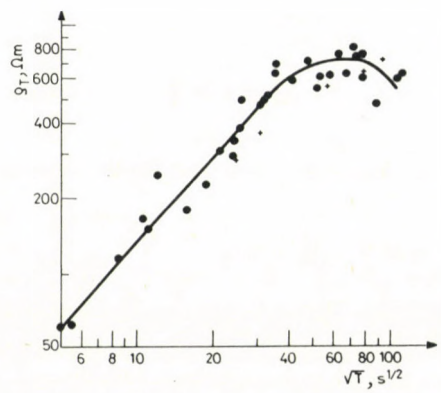

Fig. 5. MTS curve of the station Balchik

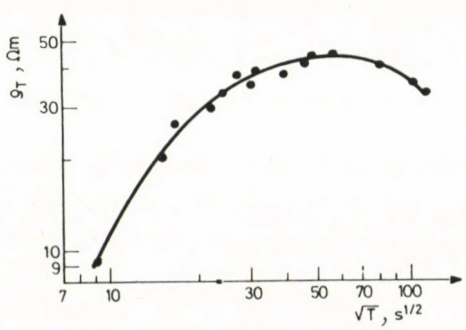

Fig. 6. MTS curve of station 3

Magnetovariation profiling

The polar diagrams of the magnetic transfer functions and the induction vectors (Schmucker's vectors) were calculated in the period range of 5 – 10 min by a method similar to that of the MTS. The example of the frequency dependence of the parameter η(station 4), related to the geomagnetic components H, D and Z by the equation:

$$Z(\omega) = \eta_{zx}(\omega)\, H(\omega) + \eta_{zy}(\omega)\, D(\omega),$$

is shown in Fig. 7.

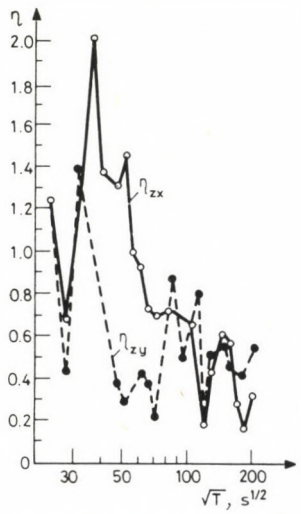

Fig. 7. Frequency dependent magnetic relations at station 4

The MVP-curves show at all points a maximum between 10 and 15 min and several maxima at longer periods. It was found that at the stations Balchik and 6 the induction vectors (i.e. real parts) determined by variations of the same period as of the main maxima are directed to the NE, but at station 4 to the SW. This indicates the existence of conducting inhomogeneity between these points. This inhomogeneity represents evidently the Kaliakra fracture. At a period of 1 hour all vectors are directed off the continental slope (Fig. 1). Consequently, the inhomogeneity corresponding to the Kaliakra fracture is a superficial anomaly, and the continental shelf is indicated by the deep geoelectric anomalies.

Magnetohydrodynamic profiling

This method is used to determine the integral conductivity of the sedimentary cover S by means of the electromagnetic field of sea currents. The method was realized in two variants reciprocally controlling each other: by the admittance of the current field on the seafloor:

$$S = H_{x,y}/E_{y,x} \tag{1}$$

and by the electric field and the average velocity $V_{x,y}$ along the vertical

$$S = S_0\left(\frac{V_{x,y}B_z}{E_{y,x}} - 1\right) \tag{2}$$

where S_0 is the integral conductivity of the water as a layer, B_z the vertical component of the geomagnetic field.

The first variant was used in the period range of maxima of the current field as determined from telluric disturbances as well as in the period range of the gradiometer method detecting the magnetic field of sea currents. The second variant was used in the period range where the variations of one of the electric components was similar to those of the perpendicular component of the velocity. The results received by variants (1) and (2) agree within a limit of 20%. The final results are: at station 1, $S = 320$ S; at station 3, $S = 600$ S; at 2, $S = 1900$ S.

Thus, there is an increase of S off land towards the deep basin. In the zone of the continental shelf the increase of S is more rapid. This is evidently in connection with the increase of the thickness of Eocene-Quaternary sediments. From preceding investigations it is known that the resistivities ϱ of the upper and lower sedimentary complexes are 2.0 and 40 Ohm · m, respectively. Supposing that the lower complex is the basement, one gets for the thicknesses of the upper complex from $h = S \cdot \varrho$ at the stations 1, 3 and 2, 640, 1200 and 3800 m, respectively. The basement is evidently Volanjin limestone.

One of the advantages of the MHDP-method with respect to MTS is its lower sensitivity against great changes of the resistivity in horizontal direction. This influence impeded the determination of S by MTS at stations 1 and 2 (at least, by conventional processing methods), and at station 3 the determination (1000 S) was less reliable than by MHDP (600 S). However, the discrepancy at station 3 can be explained by the fact that in contrary to the normal magnetotelluric field, the magnetic field of sea currents does not penetrate even through an infinitely thin insulating layer. Therefore, the difference in S may by caused by the difference in the leading horizons.

Magnetic survey

After correction for time variations, the total error of the survey has been $\leqq 10$ nT, thus it belongs to the category of high accuracy. The map of isodynams of the absolute value of the anomalous field ΔT is shown in Fig. 8. The problem of the interpretation was to determine the depths of the shallowest singular points of the magnetic anomalous bodies η. The interpretation was made by the method of the logarithms of the spatial spectrum of the anomalous field. The results are for profile 1: $h = 5$ km, for profile 2: $h = 7$ km. These values are quite reliable.

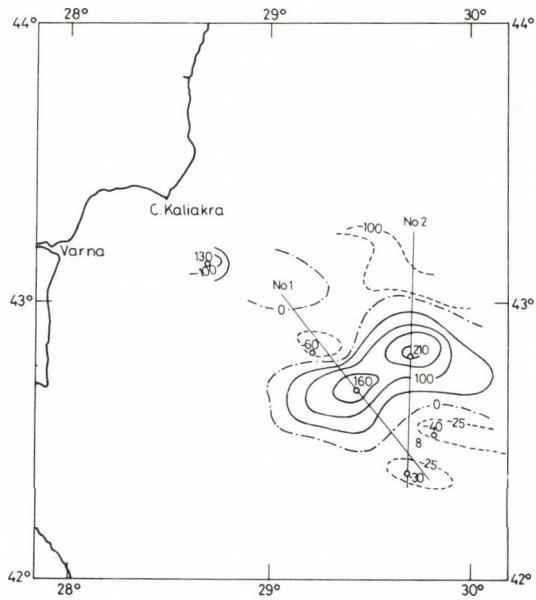

Fig. 8. The anomalous magnetic field ΔT and the profiles of interpretation. Isodynams bear numbers in nT

Conclusions

The two methods, MHDP and magnetic survey, allow at present to draw some final conclusions.

1. The thickness of the covering sediments increases along the sea profile from 640 to 3800 m. If the depth of the leading horizon will be defined by additional seismic data, it will be possible to use the received S-values to study the changes of the material composition of sediments along the profile.

2. The tops of the magnetic anomalous bodies in the continental shelf region lie in a depth of 5–7 km and correspond probably to the top of the basalt layer.

MVP gives qualitative information on the strikes of structures with a corresponding relative scale of depth.

MTS enabled so far only qualitative conclusions: the predominant strikes of the structures coincide down to depths of $\lesssim 100$ km with the direction of the continental shelf; the geoelectric structure is a three-layered one and the basement is more conducting under the seafloor than under the continent.

The interpretation of the data with the aim to construct a regional geoelectric and geomagnetic model will be continued.

Acta Geodaet., Geophys. et Montanist. Hung. Volume 19 (1—2), pp. 15—18 (1984)

GEOELECTRIC INHOMOGENEITIES IN THE EASTERN PART OF THE INTERNATIONAL GEOTRAVERSE V

(REGION OF THE KERCH AND TAMAN PENINSULAS)

L M ABRAMOVA[1], N G GOLUBEV[1], I V KARPMAN, N V KONDRASEVA[1], V S SHNEYER[1]

The paper presents results obtained by the magnetovariation profiling method in the Kerch–Taman depression. In summer 1975 and 1978, magnetovariation measurements were carried out at 10 sites. The total length of the profile is 250 km, and it crossed the Kerch strait. Wiese arrows and the distribution of the quantity H_z/H_x indicates a strong anomaly in the area. H_z has a zero value in the centre of the Kerch strait.

The anomaly was modelled by means of numerical 2–D modeling. Supposed geological structures were taken into account. Substantial differences between theoretical and experimental data can be attributed to 3–D-structures. Such a situation could arise from leakage currents from the deep water depression of the Black Sea—Azovian Sea sedimentary basins. Thus, the application of 3–D modeling is necessary.

Keywords: Black Sea; current channeling; Geotraverse V.; Kerch peninsula; magnetotellurics; magnetovariation profiling; Taman peninsula; Wiese arrow

In the year 1975, an extent magnetovariation anomaly was discovered by a team of the Maritime Magnetic Laboratory of IZMIRAN in the region of the Taman peninsula. An anomalous distribution of the magnetic components was observed not only by continental magnetovariation measurements, but also at sea buoy stations which indicated a continuation of the anomaly in the Black Sea. As since the profile did not cross the centre of the anomaly, a correct interpretation of the observed anomaly was not possible, therefore in 1978, some supplementary measurements were carried out in the same area: magnetovariation profiling across the general direction of the anomaly done along profiles of about 250 km total length.

The schematic map of the area (Fig. 1) shows the magnetovariation stations at the following sites: Strelka, Primorsky, Blagoveshchenskaya, Dzhemete, Cape Utrish, Yu. Ozereevka, Gelendzhik and Sokolovsky in the region of the Taman peninsula (at the Caucasian side) and Zavetnoe and Beregovoe in the region of the Kerch peninsula (at the Crimean side).

The magnetic field components D, H and Z were measured by the field magnetometer station IZMIRAN–4. The instruments were set up in rooms where the daily changes of temperature did not surpass 1–2 °C.

[1] Institute of Terrestrial Magnetism, Ionosphere and Radio Wave Propagation (IZMIRAN) USSR Academy of Sciences Troitsk, Moscow Region, 142092

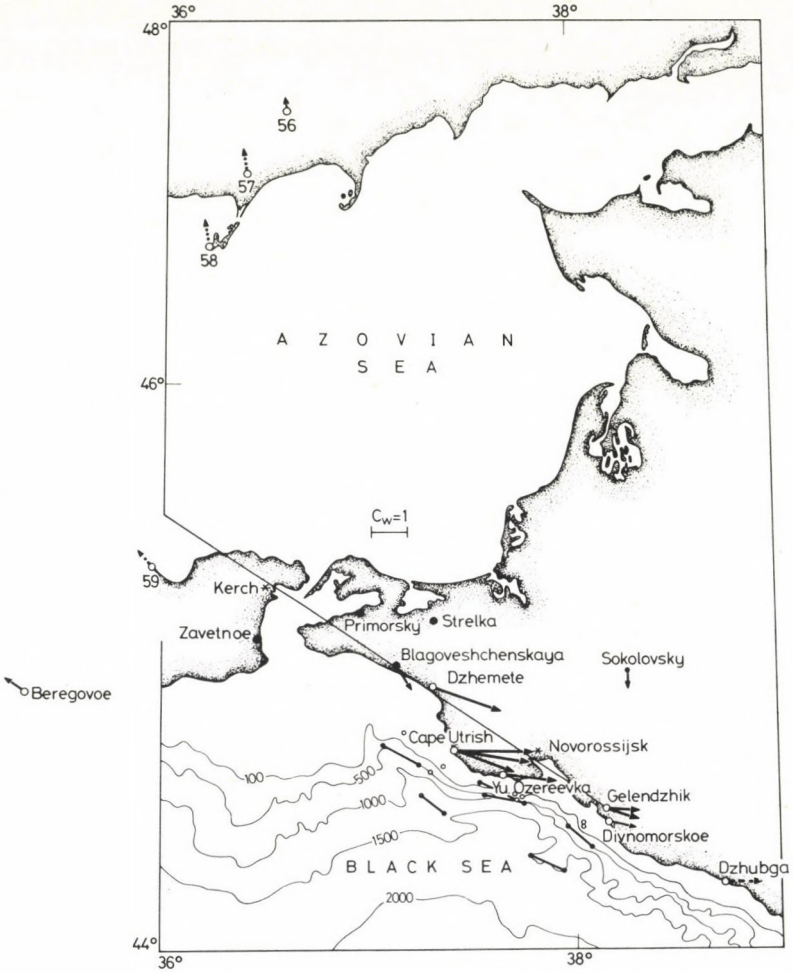

Fig. 1. Map with the observation points of the magnetic variations and the Wiese-arrows

The analogue magnetic records were made on photopaper with a recording speed of 20 mm/h, and the scale value of all components lay at about 1 nT/mm. Synchronous records were available from 7 stations of the 1978 profile and synchronous records from 4 stations in pairs of the 1975 profile.

These stations and the Wiese-vectors determined for them are shown in Fig. 1.

In the following, the geologic-tectonic situation of the area is summarized. The Western part of the Caucasus and the Kerch peninsula lying before it, are characterized by a very complicated geologic-tectonic structure. An explanation of the main features of the internal deep structure and the determination of the character of the different tectonic units and levels has a high practical importance.

The Taman and Kerch peninsulas lie in immediate contact with the Caucasus and the Crimean Mts and represent a deep depression filled with thick sediments of the Maikopian Mio-Pliocene series.

From a tectonic point of view the area of investigations belongs to the southern part of the Indolo-Kuban marginal foredeep and of the Western Caucasian periclinal foredeep, a major uniform tectonic depression being formed in the period of the general formation of the folded region of the Caucasus in the Oligocene-Neogene and lying at the moving edge of the epi-Paleozoic plate.

The Southern zone of the Indolo-Kuban marginal foredeep is the Kerch-Taman periclinal foredeep which includes parts of the continental shelf and continental margin.

The geological and geophysical investigations, and mainly the logging data enable to distinguish in the profile of this region four major geoelectric complexes (Fig. 2), they are characterized in the following by the indices of ϱ as ϱ_{1-4}.

For the construction of the geoelectric model of the region, a profile has been selected which represents best the experimental results (Fig. 1). The geoelectric layer sequence along this profile is given in Fig. 2. In the region of the strait of Kerch a

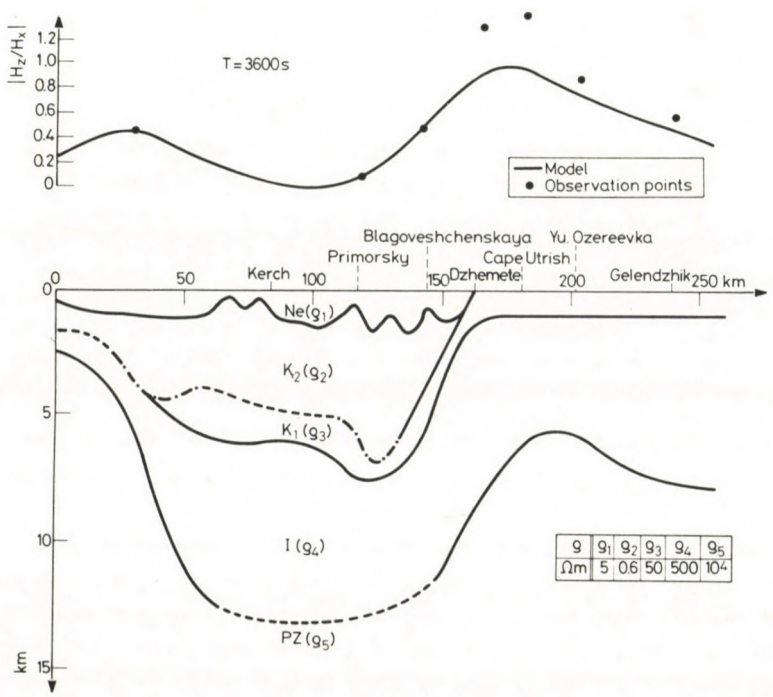

Fig. 2. Schematic geoelectric profile and the components of the magnetic field along the profiles

deepening can be observed practically in all layers till the Paleozoic of the Kerch–Taman foredeep.

The strong tilt at the flanks of the foredeep causes strong change of the specific resistivities which produces the anomalous inducing currents and geomagnetic variations.

The profiles presented were computed on the basis of the 2–D modeling using the finite difference method. For this purpose, the profile has been divided into a non-uniform network with 40×20 nodal points. The computations were carried out for the periods 3600, 2400 and 1200 s. In the first step there were significant differences between the experimental and theoretical curves, mainly in the short period range. By selecting appropriate hypothetic ϱ_k distributions along the profile, a better agreement could be reached between the experimental and theoretical values of the fields.

An increase of the theoretical values to the right of the axis of the conducting body could be achieved only by an increase of the conductivity contrast being in contradiction with present ideas about the structural geology of the region. Thus in the framework of the 2–D-modeling no acceptable model of the anomaly could be found.

In the future a 3–D-modeling will be attempted enabling to take into account the effect of the leakage of anomalous currents crossing the area from the deep-sea depression of the Black Sea towards the deep sedimentary basin of the Azovian Sea.

Acta Geodaet., Geophys. et Montanist. Hung. Volume 19 (1—2), pp. 19—34 (1984)

CRUSTAL CONDUCTIVITY ANOMALIES IN THE CARPATHIAN REGION

A ÁDÁM[1] and L POSPÍŠIL[2]

The main features of the two most characteristic crustal conductivity anomalies in the Carpathian region, i.e. the Carpathian and the Transdanubian anomaly are described taking into account other geophysical data which may help a better understanding of their development in time and space.

As a common feature the role of tectonics is emphasized in their development. The greatest difference appears in the depths what involves a large temperature difference, too.

The Transdanubian anomaly is tentatively interpreted as a pore fluid conduction while in case of the Carpathian anomaly partial melting of sediments is considered with water release during metamorphism or partial melting of crystalline rocks.

Keywords: Carpathians; crustal conductivity anomaly; magnetotellurics; partial melting; pore fluid conduction; Transdanubia

Introduction

From time to time the ideas on deep geophysical phenomena are reinterpreted using new data. A verification of these ideas with boreholes encounters generally great technical difficulties below a few km-s and would cause high expenses if it could be made at all. Therefore we try to reconsider the crustal conductivity anomalies in the Carpathian region with help of recent geologic and geophysical results.

The electric conductivity can be increased by the following physical and material factors:

— Electronic conduction of metallic minerals, graphite, etc.

— Ionic conduction of mineralized water solutions in rock pores and cracs (mainly in fractures). The conductivity of these solutions is highly influenced by the temperature (Berktold 1982).

— Partial melting of granite, or other crystalline rocks and that of sediments with water release during metamorphism (e.g. Rokityansky et al. 1976, Ádám 1978).

Almost each of these effects are connected with some kind of tectonics.

[1] Geodetical and Geophysical Research Institute of the Hungarian Academy of Sciences, H–9400 Sopron, Múzeum u. 6–8.

[2] Geofyzika, n.p. Geologická 18, 82552 Bratislava CSSR

In the Carpathians and Carpathian Basin two crustal conductivity anomalies merit attention:

— the Carpathian anomaly between the Inner and Outer Carpathians, mainly along the Pieniny Klippen Belt

— the Transdanubian anomaly in the Basin between the Rába- and Balaton-lines.

Carpathian anomaly

Geographic situation and previous interpretations

As early as in 1963, Wiese was the first to detect highly conductive formations in the Earth's crust of the Carpathians by geomagnetic deep sounding (GDS). Since this time a lot of profiles has been measured along the Carpathians by the GDS method which determined the position of a narrow conductive zone in the Earth's crust by the reversal of induction vectors (Fig. 1).

A conductivity anomaly was found in the West-Carpathians and in the Vienna basin. It continues in the Outer Flysch Carpathians with the exception of an area between the town Žilina and the High Tatra region where it penetrates relatively deeply into the Inner Carpathians. In the East-Carpathians, the anomaly passes again from the flysch zone to the Inner Carpathians near to the Marmaros zone. Further southeastward the anomaly hems the eastern margin of neovolcanic mountains, crosses the flysch belt and continues till the foredeep molasse zone of the South-Carpathians, where it disappears near the town Turnu Severin.

Estimations of the possible maximum depth of the upper edge of the anomalous conductive zone gave in the West-Carpathians 16–25 km (Praus et al. 1980), in the South-Carpathians 40 km (Rokityansky et al. 1976).

There are different suggestions about the nature and formation of the highly conducting body. These interpretations took into account often only theoretical physical assumptions, and rarely geologic—geophysical knowledge. For example:

— Rokityansky et al. (1976) interpreted the Carpathian conductivity anomaly in terms of regional metamorphism of the flysch complex below 10 km. This reasonable interpretation offers no explanation for the presence of flysch rocks at a depth of about 20 km and more in the foredeep molasse area of the South-Carpathians (Fig. 1).

— Jankowski et al. (1977) interprete the conductivity anomaly as "the extreme northwest position of the Slovakian block overthrusted to the southeastern slopes of the Bohemian Massif and covered by flysch sediments in the West-Carpathians". They suppose that the local enhancement of the temperature at a depth of 10–15 km is due to the low thermal conductivity of the crushed crystalline block. This interpretation can be accepted for the West- and East-

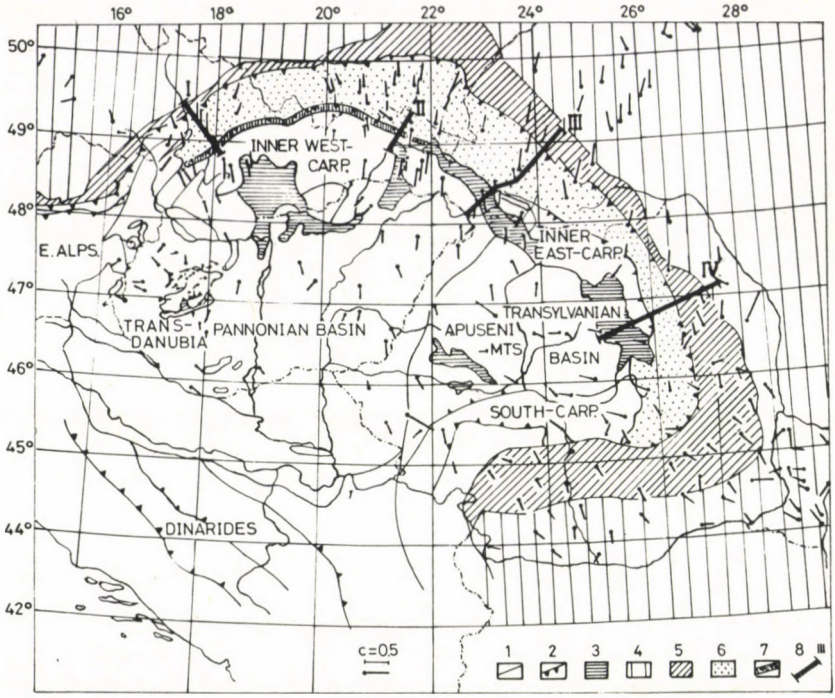

Fig. 1. Wiese induction vectors on a tectonic map of the Carpatho-Pannonian region for the $T \geqslant 20$ min period range. Keys: 1 — Boundary of main structural units; 2 — Main thrusts; 3 — Neogene calc-alkaline volcanic rocks on the surface; 4 — Stable European foreland; 5 — Foredeep molasse; 6 — Outer (Flysch) Carpathians; 7 — Pieniny Klippen belt; 8 — Geologic and geophysical profiles

Carpathian area, but in the South-Carpathians it should be somewhat modified.

— According to Ádám (1974) the process of dehydration can increase the conductivity of rocks at 600–700 °C if the overheated water cannot leave the rocks. The water-saturated silicate solutions can rise along deep fractures nearer to the surface in the zone of partial or complete anatexis. But Ádám himself call attention to several problems as the asymmetry of the geothermal gradient in both sides of the fracture zones, further rock transformation in the present final stage of the Carpathian orogeny and so on.

— Ney (1975) and Ádám et al. (1977) explain the electric anomaly as a manifestation of the southward lithospheric subduction. *Some objections against this interpretation as conclusion of one of the authors (P) are the following:*

a) predominantly terrigenous Cretaceous and Paleogene sediments are the fundamental feature of the flysch zone with Tertiary nappe structures. An own flysch

basin developed along the relative passive margin of the North-European platform which is a mighty, but light continental-type plate. Therefore it is very difficult to realize a litospherical subduction of the epi-Variscian platform. It is possible to consider only a shortening process in the upper part of the crust.

b) the distribution of neovolcanic products and their migration in time and space (Lexa and Konečny, 1974) with regard to the position of the conductivity anomaly does not confirm this explanation, either. In a comparison with typical convergent boundaries a substantial part of the andesite volcanoes lies very close or even directly over the klippen belt, which represents a surface exposure of the assumed subduction zone. It has been confirmed that andesite-rhyolite volcanism (Lower Badenian–Lower Pannonian, 17–10 mill years ago) and alcaline-basaltic volcanism (8.5–1.5 mill years ago) were transferred in time from south to north. This tendency is quite opposite as given by Ney (1975) and Ádám et al. (1977).

c) geophysical data (heat flow, seismic, gravity data and others), their mutual correlation from the point of view of building of whole lithosphere, can be more likely explained by a descending lithosphere of the "Pannonian Basin" under the epi-Variscian Platform than on the contrary [Pospíšil (in press), Pospíšil and Vass (in press)]. The reciprocal position of the anomaly sources is shown in a hypothetical model of the Carpathian lithosphere (Figs 2, 3).

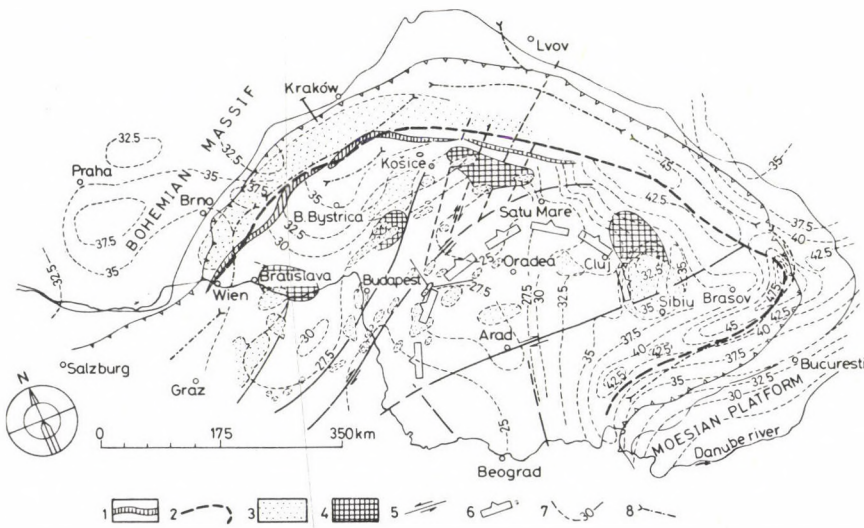

Fig. 2. The scheme of the main Carpathian geophysical anomalies (according Pospíšil and Vass 1982) Explanations: 1 — Pieniny Klippen belt zone; 2 — Electrical conductive zone; 3 — Magnetic anomalies from the pre-Tertiary basement; 4 — Intensive regional positive gravity anomalies; 5 — Supposed transcurrent faults; 6 — Border of mobile part of lithosphere (recent position); 7 — Contour of the Moho depth in km (mainly after Sollogub 1970, Beránek 1978, Zátopek 1979, Posgay et al. 1981); 8 — Axis of gravity low

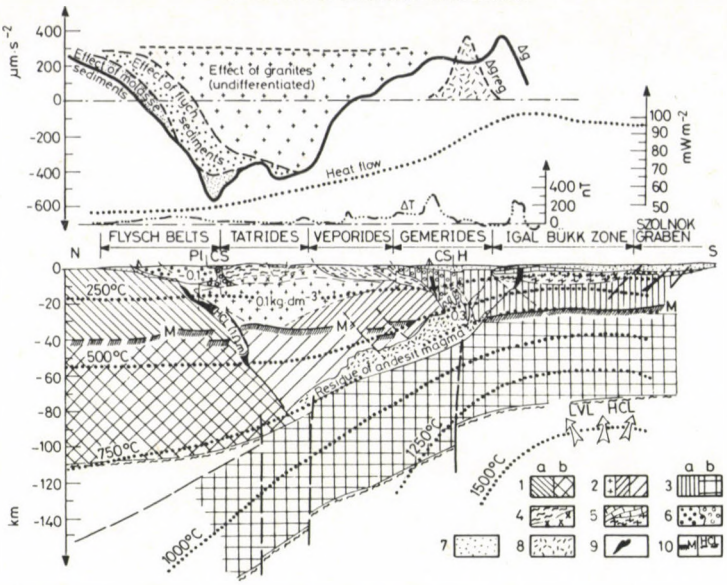

Fig. 3. The Geophysical Model of the West Carpathian lithosphere (according Pospíšil 1980) Explanations: 1 — Epi-Variscian platform (*a* — crust, *b* — mantle); 2 — "Island arc" (?) with granites; 3 — Lithosphere of the Pannonian basin (*a* — crust, *b* — mantle); 4 — Tatrides, Veporides and subtatric nappes; 5 — Igal–Bükk zone; 6 — Flysch zone and Pieniny Klippen belt; 7 — Molasse; 8 — Zone of mobilization of the calc-alkaline volcanism; 9 — Basic resp. ultrabasic rocks; 10 — Geophysical interface (*a* — Moho discontinuity, *b* — lithosphere-asthenosphere interface)

d) recent vertical movements, known from the Tertiary so far signalize an ancient tendency that can testify the collision at the contact of the Carpathians with the epi-Variscian platform.

— It is not probable that the narrow zone of highly mineralized water or sediments saturated by such water would extend for many hundred km in the subsurface layers, too. These sediments (flysch or molasse) saturated by mineralized water were detected by magnetotelluric soundings (MTS) at several places, at the side nearer to the platform (Pawliszyn and Pawliszyn 1978, Pícha and Chmelík 1980 and others).

The following interpretation of the Carpathian conductivity anomaly is based on geologic and geophysical (gravity, seismic, magnetic, remote sensing) data and on results of deep boreholes.

Geophysical informations and corresponding models

The main geophysical anomalies in the Carpathian area are shown in Fig. 2. A quantitative lithospheric model of the West-Carpathians is presented in Fig. 3.

This model was tested by solving the direct problems of gravity and geothermics.

The seismic data from profiles K–II, K–III (Beránek et al. 1979) show that the boundary zone of the Outer and the Inner West-Carpathians is strongly broken into blocs.

There is not a clear relationship between the zone of conductivity anomaly and the epicentres of earthquakes (cf. Jankowski et al. 1977). The depth of earthquake foci is seldom more than 10 km (Zátopek 1979), so the conductivity zone lies much deeper. The earthquakes may be provoked by movements at the sliding planes of the nappes or along the same fracture which contain the conductive formation.

A certain correlation can be seen between the conductivity anomaly and the Carpathian gravity low (CGL), lying mostly north or east of the conductivity anomaly.

The magnetic anomalies indicate the margin of the epi-Variscian platform and their intensity varies according to the thickness of the flysch complexes.

The local distribution of the surface heat flow (Čermák and Hurtig 1977) is not always a decisive indication of anomalous temperature conditions at crustal depths. Structural pecularities can cause local temperature enhancements (Jankowski et al. 1977). Therefore the regional heat flow value is more characteristic for a great tectonic unit.

The electric conductivity anomaly is also accompanied by an intensive recent crustal uplift (Joó et al. 1981).

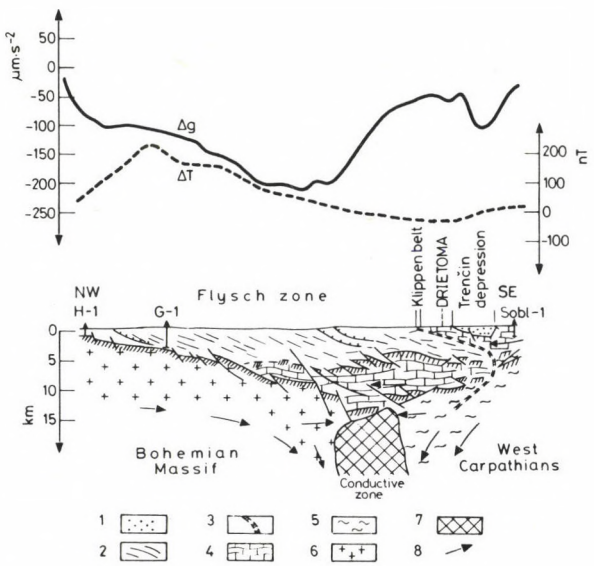

Fig. 4. The geologic profile I (Trenčin–Gottwaldov, according Kadlečik et al. 1979) Explanations: 1 — Molasse; 2 — Flysch; 3 — Pieniny Klippen belt zone, 4 — Para-autochthonous cover of the Platform eventually of the exotic block, central Carpathian nappes; 5 — West-Carpathian block; 6 — Bohemian Massif; 7 — High conductive zone; 8 — Direction of the movement of the unit

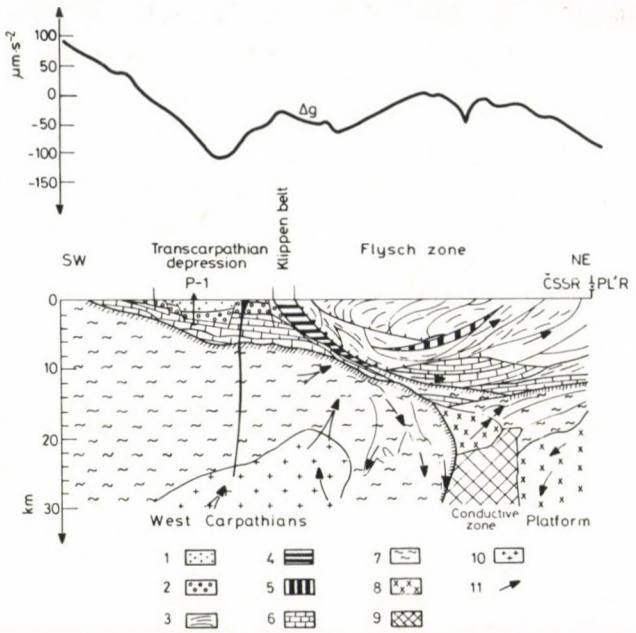

Fig. 5. The geologic profile II (Prešov–Svidník, according Pospíšil et al. 1982) Explanations: 1 — Molasse, 2 — Central Carpathian Paleogene; 3 — Flysch; 4 — Pieniny Klippen belt zone; 5 — Relict of the Dukla unit; 6 — Mesozoic (carbonatic) complex; 7 — Pre-Mesozoic basement; 8 — Epi-Variscian platform; 9 — High conductive zone; 10 — More viscous medium; 11 — Direction of the movement of the unit

The position of the conductive zone in the structure of the Carpathians is shown on several geologic profiles (Figs 4–7) constructed by different authors. The situation of the profiles is given in Fig. 1.

The electric conductivity anomaly separates clearly the platform from the Carpathians. The tectonic deformation of the contact zone between the upper part of the flysch belt and the Inner Carpathian is different at the profiles.

An important fact is that the conductive medium is covered by units with thick carbonate complexes.

From an analysis of all available data it is evident that the conductive zone is located in a strongly deformed tectonic zone which separates different great tectonic units. It may mark the outer boundary of collision zone of the Carpathians with the epi-Variscian platform. On the basis of the New Global Tectonics, the conductive zone may represent a suture, too, i.e. the extinction place of a flysch basin (back-arc-basin) with partly oceanic crust being formed between a relatively passive continent (the Eurasian plate) and an undefined island arc (the Krichevo–Iňačovce unit, the Bretila unit?). This interpretation was proposed by e.g. Dolenko–Danilovič (1976), Marschalko (1979), Pospíšil (in press). The suboceanic sedimentary flysch could be

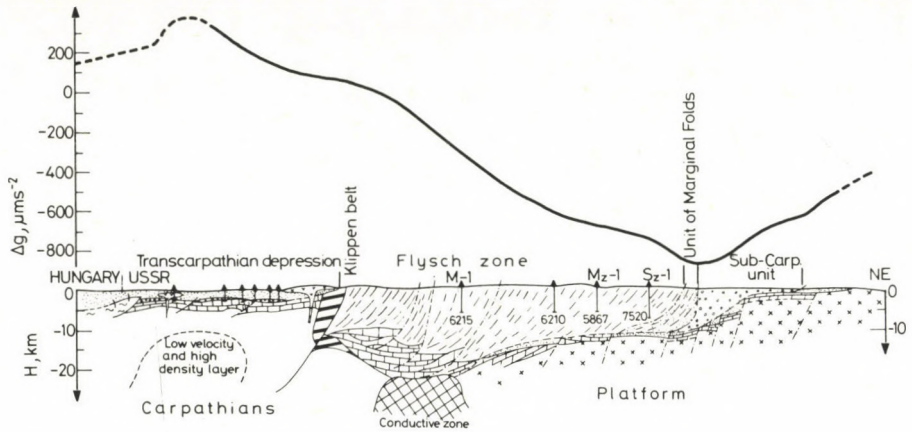

Fig. 6. The geologic profile III (Beregovo–Mezgorie–Szevczenko, according Glusko and Kruglov 1977, Utrobin and Glusko 1980, Czernicki and Starosielski 1982)

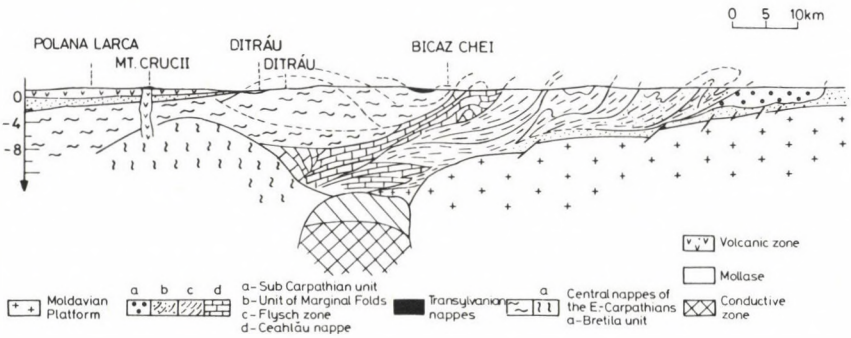

Fig. 7. The geologic profile IV (Polana Larca-Botesti, according to Sandulescu, in Mahel 1974)

totally destroyed by orogenic movements during the Neogene period. Outer parts of the flysch zone were transformed to nappes and overthrusted on the slope of the epi-Variscian platform. The inner and the southern parts of the flysch zone were strongly folded till being rolled and locally overthrusted to south, on the Inner Carpathians (Nemčok and Rudinec 1979, Pospíšil et al. 1982).

In a tectonically preformed zone where the sedimentary flysch was shortened (crustal subduction), it is possible to expect that the conductive anomaly is due to several factors simultaneously. Tectonics and probably the local effect of basic and ultrabasic complexes in the central part of the crust plays the most important role. The influence of local anomalous p–t conditions cannot be ignored.

Transdanubian anomaly

The Transdanubian anomaly with its horizontal conductivity of a few thousand S is one of the most characteristic crustal conductivity anomalies of the Earth. The apparent resistivity of the MTS curves is sometimes lower than 1 Ωm.

The anomalous area in the Transdanubian Mid-Mts (mainly in the Bakony Mts) and in its foreground is in an unknown way connected with Mezozoic basement carbonates (See Wein's geologic profile, 1972 in Fig. 8). The conducting formation crops out at the Rába-line in the north and at the northern shore of the Lake Balaton in the south where Permian sandstone lies on the surface instead of Mesozoic limestones. Its area, estimated on the basis of MT measurements is about 5000 km^2.

Southward from the Balaton–Velence granite belt an other very narrow (about 5–10 km wide) conducting zone appears in connection with the Balaton line, a main structural line [see the thick line south of Lake Balaton on the tectonic map, Fig. 9 and the conducting zone in Fig. 10 after Varga (1979)].

The average depth of the conductive zone is 7–10 km. The smallest depth values have been obtained along seismic active fault zones (or at the crossing of fracture lines), e.g. in Bakonybél the depth is between 2 and 3 km (Ádám 1976).

On the basis of the distortion theory it can be concluded that in the Bakony Mts and its immediate surroundings the conductivity increases in deep fractures (Ádám 1981).

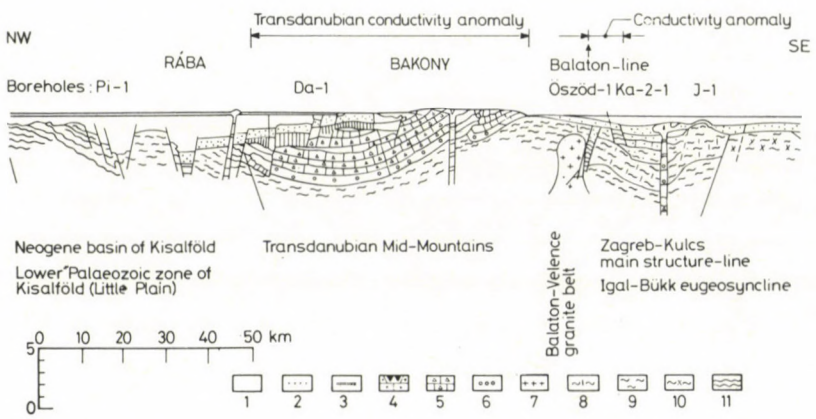

Fig. 8. Geologic profile across the Transdanubian conductivity anomaly after Wein (1972). 1 — Pliocene, Pleistocene, Holocene basin sediments, 2 — Miocene formation of the basin development, 3 — Upper Cretaceous epicontinental carbonates, 4 — Triassic-Jurassic-Lower Cretaceous formation of Mid-Mts development, 5 — Triassic-Jurassic-Lower Cretaceous formation of Igal–Bükk development, 6 — Permian continental formation, 7 — Lower Carboniferous migmatite-granite (Mórágy type), 8 — Lower Carboniferous epi-anhimetamorphic formation, 9 — Ordovician, Silurian, Devonian epimetamorphic formation, 10 — Precambrian polymetamorphic unseparable rocks, 11 — Precambrian crystalline rocks of the epi-meso-zones

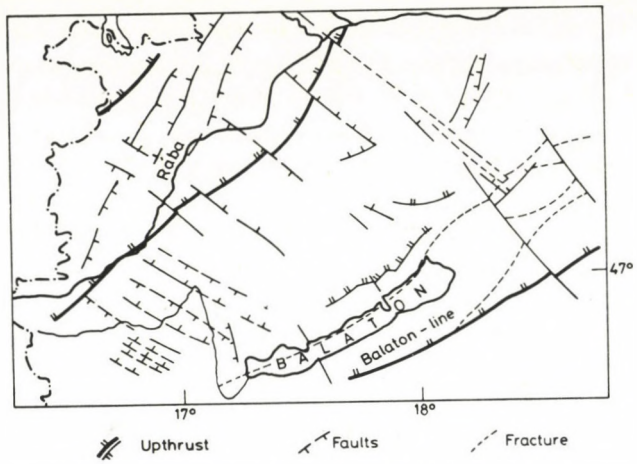

Fig. 9. Tectonic map of the NW part of Transdanubia

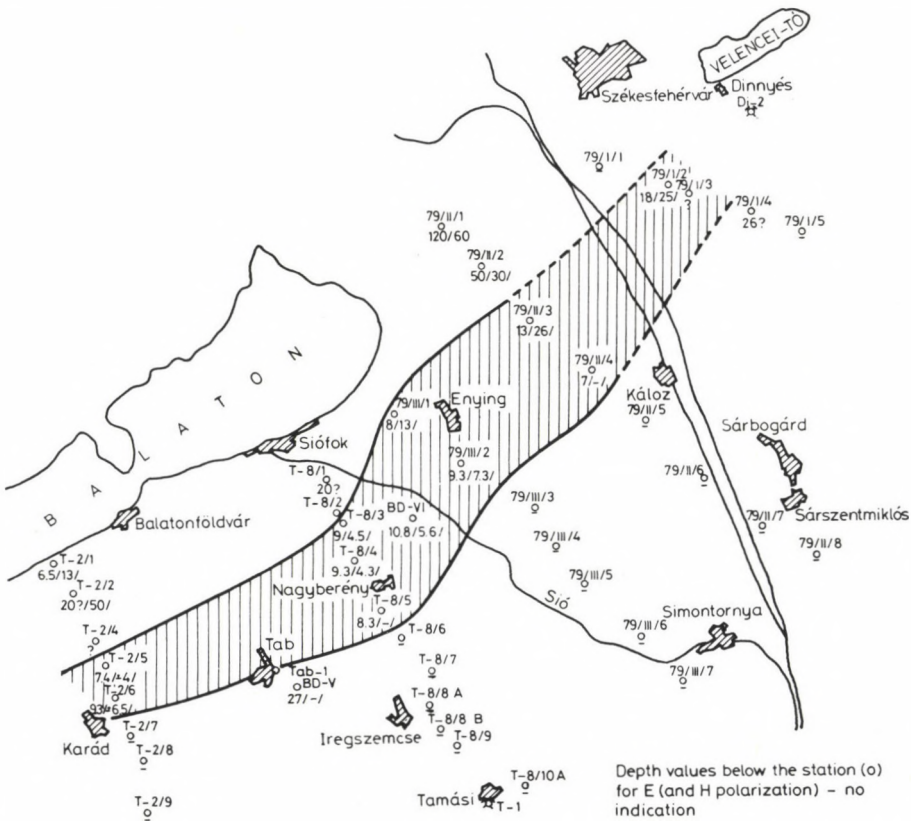

Fig. 10. Distribution and depth of conducting formations south from the Lake Balaton (along the Balaton tectonic line) after Varga (1979)

Below the Little Hungarian Plain the conductive zone shows a layer or an apparent layer structure on the MÁELGI MT profile measured with MTS point distances of 3–4 km. It should be remarked that in consequence of the character of the *E*-polarized MTS curves, the MT apparent resistivity structure of some neighbouring conducting bodies (e.g. fractures) is indiscernible from that of a conductive layer.

The conductivity increase has also been interpreted as the effect of fracture tectonics in Transdanubia by O Ádám (1977) who carried out a comprehensive study of all geophysical phenomenon in the Transdanubian Mid-Mts. His gravity profile and the corresponding deep structure (Fig. 11), demonstrate his ideas on the block structure of the basement bordered by deep fractures.

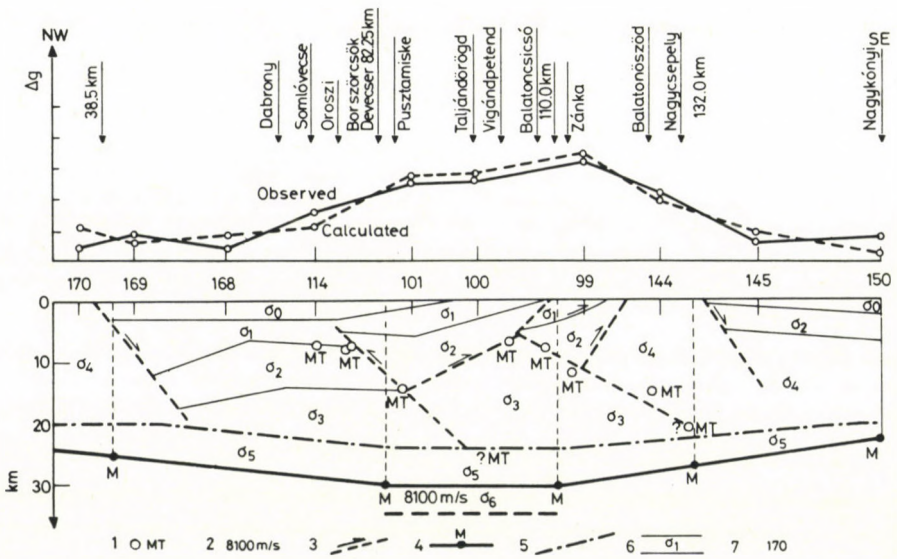

Fig. 11. Gravimetric and depth profile with the projectable crustal structure and depths of the high-velocity formation along the examined part of seismic profile NP–2 monitoring the Earth's crust after O Ádám (1977). 1 — Depth of the conducting formation by MTS measurements, 2 — Limiting velocity, 3 — Inferred fault line, 4 — The Moho discontinuity with pertinent depths points, 5 — Presumable position of the Conrad boundary, 6 — Data of rock density with geologic boundaries, 7 — First-order and second-order gravity stations

A field MT test measurement made in a shallow basin westward from the Bakony Mts around the village Ukk has also shown that the minimum ϱ values of the MT iso-ohm profile coincide with the locations of deep fractures. This fact hints also at a connection between conductivity increases and fractures, respectively.

After Berktold (1982) the highly mineralized water solutions (electrolytes) in the pores and cracks of the rocks reach its maximum conductivity at about 300–400 °C in consequence of a decrease of the viscosity of water (See Fig. 12 in case of KCl).

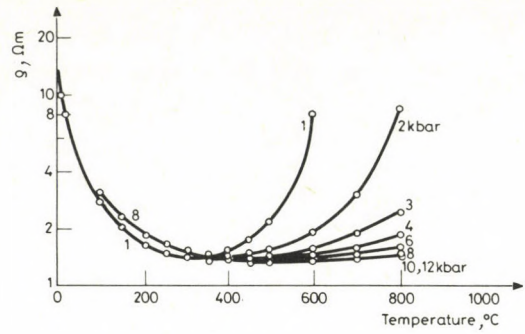

Fig. 12. Resistivity (ϱ) of a 0.01 molal KCl solution (0.745 263 g KCl/1 000 g solution) as a function of temperature and pressure after Berktold (1982)

Hermance (1973) calculated the rock resistivity as a function of depth for the pore path conduction component. The pore fluid is at lithostatic ($P_{\text{eff}}=0$) and hydrostatic pressure and the results for a range of NaCl concentration (0.01, 0.1 and 0.5 molal) are shown in Figs 13a and 13b after Hermance. A geothermal gradient of 60 °C/km and about 5 percent porosity are considered. The rock resistivity is equal to the fluid resistivity divided by the porosity squared according to Archie's Law in a simple form (Brace et al. 1965). In case of a geothermal gradient of 60 °C/km the minimum

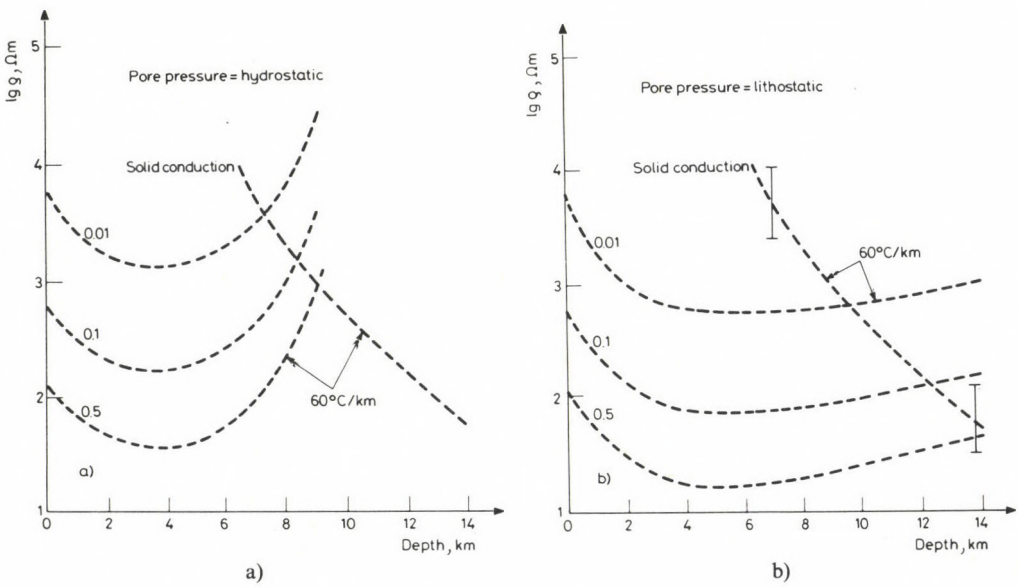

a) b)

Fig. 13. Pore fluid and solid rock resistivity as function of depth at hydrostatic *(a)* and lithostatic pressure *(b)* and for a range of NaCl concentrations (0.01, 0.1 and 0.5 molal) and a geothermal gradient of 60 °C/km after Hermance (1973)

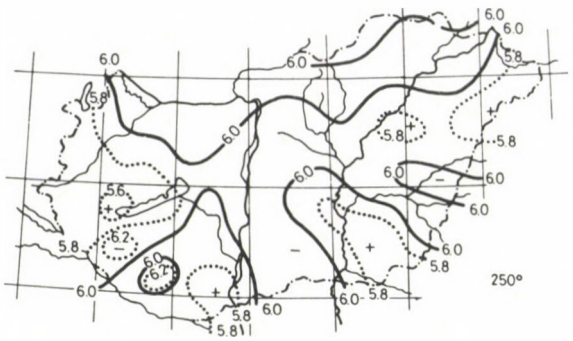

Fig. 14. Depth iso-lines corresponding to the temperature of 250 °C after Stegena (1976)

resistivity appears at a depth of about 5 km on Hermance's diagrams. Because the average geothermal gradient in the Pannonian Basin is somewhat lower than 60 °C/km [after Boldizsár 48–55 °C/km and after Stegena 32–56 °C/km; see in Horváth et al. (1979)] the conductivity anomaly originating in the pore fluid can be indicated here at about 7 km i.e. just in the average depth of the Transdanubian anomaly where the temperature reaches 300 °C (See Stegena's data in Fig. 14 about the depth of 250 °C). Only high porosity (10–20 percent) and high NaCl concentration (at least 1 molal) can assure the prerequisites for development of the low rock resistivity of the anomaly ($\leqq 1$ Ωm). At present we have no final information about these parameters. We suppose that these special conditions are connected with the above mentioned fracture zones created by an extensional stress field in the Transdanubian Mts. The shallowest depth of the conductivity anomaly in seismic active areas can be attributed to a higher crack porosity of rocks there.

We supposed earlier that the conductivity anomaly can be connected with graphite and graphitic schists in the basement rocks similarly to the graphite dykes of the Precambrian shield areas. Zhamaletdinov (1976) referred to these graphite dykes as gliding surfaces which might conduct the fracture tectonics. The role of the Mesozoic carbonates in the occurrence of the Transdanubian conductivity anomaly can be explained in this case, namely the thick carbonate layers protected the graphite from the erosion in this area.

There is no final conclusion about the origin of the Transdanubian conductivity anomaly. Both causes mentioned above can explain it sufficiently but the effect of tectonics is indisputable.

Conclusions

The two conductivity anomalies in the Carpathian region have both common and different features.

The greatest *difference* appears in their depths that involves a large temperature difference, too.

The maximum depth of the upper edge of the Carpathian anomaly varies between 16 and 25 km in the West-Carpathians and the depth of the Transdanubian anomaly is about 7 km. The corresponding temperatures are 600–700 °C and 300 °C, respectively. *If these differences really exist,* according to these different p–t conditions the conduction mechanism should also be different in the two conducting formations. The Transdanubian anomaly can be interpreted as pore (and crack)-fluid conduction which reaches its maximum value at a temperature of about 300 °C (or metallic, graphitic conduction?) while in case of the Carpathian anomaly partial melting of sediments with water release during metamorphism, partial melting of crystalline rocks (granite, basic, ultrabasic complexes) or deserpentinization should be taken into account.

These two quite different conduction mechanisms are clearly separated along the Deep Seismic Profile VI near to the Carpathians (See Fig. 6 in Pěčová et al. 1976) and cause splitting on the diagram of the empricial relation between the surface heat flow and the crustal well conducting layer (FCL) (Ádám 1978).

Among the *common* features of the anomalies at first the role of tectonics should be emphasized. Both anomalies are connected with some stress field, at the boundary of the Carpathians and the epi-Variscian platform (suture, shortening) and in the Hungarian Mid-Mts where basalt was erupted along open fractures during Pliocene and Pleistocene.

A common feature of both anomalies is that they occur below Mesozoic limestones which may play a genetic role in their development.

These recent ideas on the conductivity anomalies are mainly hypotheses which should be supported by further geologic, geophysical and geochemical researches.

References

Ádám A 1974: Electric crustal anomalies in the Carpathian Basin and their origin in the rock composition. *Acta Geol. Hung.*, 18, 13–22.

Ádám A 1976: Distribution of the electrical conductivity in seismic (deep) fractures in Transdanubia. *Acta Geod. Geoph. Mont. Hung.*, 11, 277–285.

Ádám A 1978: Geothermal effects in the formation of electrically conducting zones and temperature distribution in the Earth. *Phys. Earth Planet. Inter.*, 17, 21–28.

Ádám A 1981: Statistische Zusammenhänge zwischen elektrischer Leitfähigkeitsverteilung und Bruchtektonik in Transdanubien (Westungarn). *Acta Geod. Geoph. Mont. Hung.*, 16, 97–113.

Ádám A, Horváth F, Stegena L 1977: Geodynamics of the Pannonian Basin: geothermal and electromagnetic aspects. *Acta Geol. Hung.*, 21, 251–260.

Ádám O 1977: Deep structure of the Transdanubian Midmountains and its foregrounds on the basis of the geophysical results (in Hungarian). In: *M. Áll. Földtani Intézet évi jelentése az 1977 évről*, 269–287.

Beránek B 1978: Research of the Earth's crust on the CSSR area by seismic methods and transform gravity fields (in Czech.). MS-Geofyzika n.p., Brno

Beránek B, Lesko B, Mayerová M 1979: Interpretation of seismic measurements along the Trans-Carpathian profile K III. Final Report-Geodynamic Investigations in Czechoslovakia, VEDA Bratislava

Berktold A 1982: Electromagnetic studies in geothermal regions. Review paper read at the Sixth EM Induction Workshop, Victoria/B.C.

Brace W F, Orange A S, Madden T R 1965: The effect of pressure on the electrical resistivity of water-saturated crystalline rocks. *J. Geophys. Res.*, 70, 5669–5678.

Czernicki J, Starosielski M 1981: Geological and technical aspects of drilling deep boreholes in the Carpathians. *Nafta* (Kraków), 37, No 4, 111–115.

Čermák V, Hurtig F 1977: Preliminary Heat Flow Map of Europe, 1 : 5 000 000. Praha and Potsdam.

Dolenko G N, Danilovic L G 1976: New view on the geosynclinals and its application in the Ukrainian Carpathians (In Russian). *Zb. Geologica Carpathica* (Bratislava), 27, 1–9.

Glusko V V, Kruglov S S 1977: Reasons for oil and gas investigations in deep horizons of the Ukrainian Carpathians (In Russian). Naukova Dumka, Kiev

Hermance J F 1973: An electrical model for the sub-Icelandic crust. *Geophysics*, 38, 3–13.

Horváth F, Bodri L, Ottlik P 1979: Geothermics of Hungary and the tectonophysics of the Pannonian Basin "Red Spot". In: Terrestrial Heat Flow in Europe, Čermák V and Rybach L eds, Springer Verlag, Berlin–Heidelberg

Jankovski J, Petr V, Pěčová J, Praus O 1977: The Carpathian geoelectric anomaly and its relation to independent geophysical information. *Acta Geol. Hung.*, 21, 337–351.

Joó I, Csáti E, Jovanović P, Popescu M, Somov V I, Thurm H, Thury J, Totomanov I N, Vanko J, Wyrzykowski T 1981: Recent Vertical Crustal movements of the Carpatho-Balkan Region. *Tectonophysics*, 71, 41–52.

Kadlečik J, Roth Z, Stránik Z 1979: Deep structure of the Outer Carpathians in Moravia and Western Slovakia. In: *Proceedings of the conference: The main problems of the geological evolution and building of CSSR; Key areas and methods of solution* (In Czech.) Mahel M ed.

Lexa J, Konečny V 1974: The Carpathian Volcanic Arc: a Discussion. *Acta Geol. Hung.*, 18, 421.

Mahel' M 1973: Tectonics of the Carpathian-Balkan Regions. GÚDŠ Bratislava.

Marschalko R 1979: Considerations about Pienide flysch basins and their substratum in the Cretaceous and Paleogene (West-Carpathians). In: *Proceedings of the Conference: Czechoslovak Geology and Global Tectonics*, Smolenice, VEDA, Bratislava

Nemčok J, Rudinec R 1979: Geological cross-sections through the East-Slovakian flysch belt (In Czech.). In: *Tectonical profiles through the West Carpathians*, Mahel M ed. GÚDŠ, Bratislava

Ney R 1975: Tectogenesis of the Carpathians in the light of new tectonics of the Earth's Globe. *Mat. i Prace Inst. Geof.*, 82, 95–110.

Pawliszyn J, Pawliszyn J 1978: Use of magnetotelluric surveys for resolving complicated geological structures (In Polish). *Biuletyn Informacyjny Geofizika stosowana*, 2, 16–25.

Pěčová J, Petr V, Praus O 1976: Depth distribution of the electric conductivity in Czechoslovakia. In: *Geoelectric and Geothermal Studies, KAPG Geophys. Monograph.*, Ádám A ed., Akadémiai Kiadó, Budapest

Pícha B, Chmelík F 1980: Results of magnetotelluric sounding along the profile Osvetimany-Brezová p.B. profile (In Czeh.). In: *Proceedings of "The 7th Conference of geophysicists"*, Gottwaldov, Session S4-Geoelectrics-Radiometrics, SL–S6

Posgay K, Albu I, Petrovics I, Ráhner G 1981: Character of the Earth's crust and upper mantle on the basis of seismic reflection measurements in Hungary. *Earth Evolution Sciences*, 3–4, 272–279.

Pospíšil L, Nemčok S, Feranec S 1982: Analysis of the "Svidník-Stropkov nonlinear structure" identified by space photograph interpretation (in Czech.). *Minerália Slovaca, Bratislava*, 14, 539–548.

Pospíšil L: Geophysical Model of the West Carpathian Lithosphere: Discussion on the application of the subduction mechanism. *Geol. zbor. Geologica carpathica* (Bratislava) (in press)

Pospíšil L, Vass D 1983: Influence of the Structure of the Lithosphere upon the Formation and Development of Intramountane and Back Molasse Basins of the Carpathian Mts. (In Czech.). Geol. práce, Správy, GÚDŠ Bratislava (in press).

Praus O, Pěčová J, Petr V 1980: Present state of the research of the Carpathian geoelectrical anomaly (In Czech.). In: *Proceedings of "The 7th Conference of geophysicists"*, Gottwaldov, Session S6-complex geophysical interpretations and syntheses. Geofyzika n.p. Brno

Rokityansky I I, Amirov V K, Kulik S N, Logvinov I M, Shuman V N 1976: The electric conductivity anomaly in the Carpathians. In: *Geoelectric and Geothermal Studies, KAPG Geophys. Monograph*, Ádám A ed. Budapest, Akadémiai Kiadó

Sollogub V B 1970: Structure of the Earth Crust of the Ukraine (in Russian). *Geofyz. sb. AN USSR*, 38

Stegena L 1976: The variation of the temperature with depth in the Pannonian Basin. In: *Geoelectric and Geothermal Studies*, KAPG Geophysical Monograph. Ádám A ed. Budapest, Akadémiai Kiadó

Utrobin V N, Glusko V V 1980: Deep geological cross-sections of the Western Ukrainian parts; in connection with oil and gas perspectivity (In Russian). Naukova Dumka, Kiev

Varga G 1979: Geophysical investigation of geological basic profiles I. Report on the telluric and magnetotelluric measurements in 1979 (In Hungarian). MÁELGI Report. Manuscript

Wein Gy 1972: Summary of the geological structure development of Hungary before Neogene (In Hungarian). *Földrajzi Közlemények*, 20 (96), 302–328.

Wiese H 1963: Geomagnetische Tiefentellurik. Teil III: Die geomagnetischen Variationen in Mittel- und Südost-Europa als Indikator der Streichrichtung grossräumiger elektrischer Untergrundstrukturen. *Geofisica pura et applicata*, 56, 101–114.

Zátopek A 1979: On geodynamical aspects of geophysical synthesis in Central Europe. Final Report: Geodynamic investigations in Czechoslovakia. VEDA, SAV, Bratislava

Zhamaletdinov A A 1976: Electric conducting formation of the NW part of Kola peninsula and its effect on the deep sounding (In Russian). Thesis, Leningrad

Acta Geodaet., Geophys. et Montanist. Hung. Volume 19 (1—2), pp. 35—36 (1984)

MESOZOIC OPHIOLITES OF THE BÜKK MOUNTAINS (NORTH HUNGARY)*

(EXTENDED ABSTRACT)

Z BALLA[1], D HOVORKA[2], M KUZMIN[3], V VINOGRADOV[4]

Keywords: Bükk Mountains; ophiolite, Mesozoic; REE concentration

In the Bükk Mountains ophiolites are situated in the southwest, near the village Szarvaskő. They have sine-shape of about 8 × 3 km in size built up of nappe-fragments. An effusive horizon (basaltic pillow lavas) of about 400–500 m in thickness lies within a flysch-like sedimentary sequence. Beneath this horizon sills of basaltic to gabbroic composition are situated with clear intrusive contacts. The distance in stratigraphic sense from the effusive horizon to the deepest sill does not exceed 2 km.

Because of the metamorphism of prehnite-pumpellyite facies all rocks are altered (albite, chlorite, carbonate, serpentine, prehnite etc.), and mobile element (Li, Na, K, Rb, Cs, Sr, Ba, F, B) abundances and Sr-isotope ratios are increased, but according to all discriminant criteria using immobile elements (Fe, Ti, Zr, Nb, Rb, Y, REE, Cr, Ni) the Szarvaskő effusives are identical with oceanic tholeiites. Comparatively high Ti, Zr, Cr, Ni, REE concentrations may be related to the origin from a non-depleted mantle-source. High abundances of elements with high partition coefficients (Cr, Ni), the absence of a light-REE and Eu minimum seem to be caused by the very low degree of crystal fractionation before eruptions.

According to their stratigraphic position the Szarvaskő instrusives are equivalents of the sheeted-dyke complex of the standard ophiolite sequence. Indeed, their chondrite-normalized REE-curves coincide with those of the effusives. Crystallization and differentiation within intrusive bodies went under high P_{H_2O} probably because of water assimilation from surrounding clays. This resulted in the strong variation of crystallization degree within the bodies and in the appearance of magnetite and ilmenite in the first cumulate phases beside olivine, hypersthene and

* The full paper is published in Ofioliti (Florence), vol. 8 No. 1, 1983

[1] Hungarian Geophysical Institute, H–1145 Budapest, Columbus 17–23.

[2] Comenius University of Bratislava, Faculty of Natural Sciences, Gottwaldovo nám. 19, 886 02 Bratislava, Czechoslovakia

[3] Institute of Geochemistry, Siberian Department, USSR Academy of Sciences, 664033 Favorskogo 1–a, Irkutsk, USSR

[4] Institute of Geology, USSR Academy of Sciences 109017, Pyzhevsky 7, Moscow, USSR

basic plagioclase. Further accumulation led to the crystallization of bronzite, diallage and brown hornblende in large crystals and biotite as latest phase. Cumulation led to the forming of peridotites alternating in layered textures with rocks transitional to gabbro. Later differentiation at least partly caused by assimilation of country rocks resulted in appearance of acid rocks up to plagiogranites forming dykes within sills.

Main characteristics of the Szarvaskő sedimentary and magmatic rocks can be explained supposing their origin in a basin of marginal sea type. Their magmatism was related to the appearance of a new spreading zone and fixed earliest rifting events on an ancient oceanic crust.

Acta Geodaet., Geophys. et Montanist. Hung. Volume 19 (1—2), pp. 37—48 (1984)

INTERRELATION OF NEOGENE TECTONICS AND VOLCANISM IN THE PIENINY KLIPPEN BELT OF POLAND

K BIRKENMAJER[1]

There is a close interrelation between the Neogene fault pattern and the hypabyssal andesite intrusions in the area adjacent to the northern boundary fault zone of the Pieniny Klippen Belt of Poland (Carpathians). The Pieniny Andesite Line (PAL) directed WNW-ESE, obliquely traverses the northern boundary fault. Longitudinal strike-slip faults (f_1) of this system related to Savian (early Miocene) meridional compression and to subsequent transpression due to a clockwise rotation of the Inner Carpathian block in relation to the Outer Carpathians, predate the hypabyssal volcanism. Andesite magma started to penetrate tensionally-opened older fault (f_1) surfaces adjacent to the main transcurrent fault line during the Karpatian to Badenian stages, penecontemporaneously with horizontal meridional Styrian compression. There is an intricate relationship between andesite intrusions and transverse strike-slip faults (f_2) which formed partly simultaneously, partly post-date the intrusions. The youngest andesite intrusions (probably Badenian-Sarmatian boundary) used these strike-slip faults (f_2) if they were opened tensionally by right-lateral strike-slip translation along the PAL.

Keywords: Neogene tectonism; Neogene volcanism; Pieniny Klippen Belt

Introduction

The Pieniny Klippen Belt—the trace of an axial suture in the West-Carpathian arc (Fig. 1), is bordered on the north and the south by longitudinal faults and fault zones, respectively, best recognized in the Dunajec River area of the Belt (Fig. 2). It has been known since long that these vertical or subvertical faults represent fractures of major importance in the structure of the Carpathian fold belt. They are considered to be syntectonic with the early Neogene Savian Phase folding of the Pieniny Klippen Belt and the contacting flysch zones, i.e. the Outer Carpathian Magura Nappe (inner part) to the north, and the Inner Carpathian Podhale Paleogene syncline (outer part) to the south.

A major structural break between the Inner and Outer Carpathians along the Klippen Belt suture has also been indicated by deep seismic soundings (e.g., Sollogub et al. 1973, Uchman 1973, Ney 1975) which shows that the Moho discontinuity drops

[1] Institute of Geological Sciences, Polish Academy of Sciences, Tectonics Laboratory, ul. Senacka 3, 31–002 Kraków, Poland

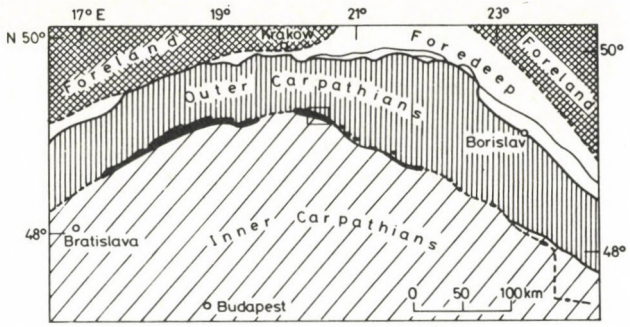

Fig. 1. Key map to show position of the discussed segment (rectangle) of the Pieniny Klippen Belt (in black)

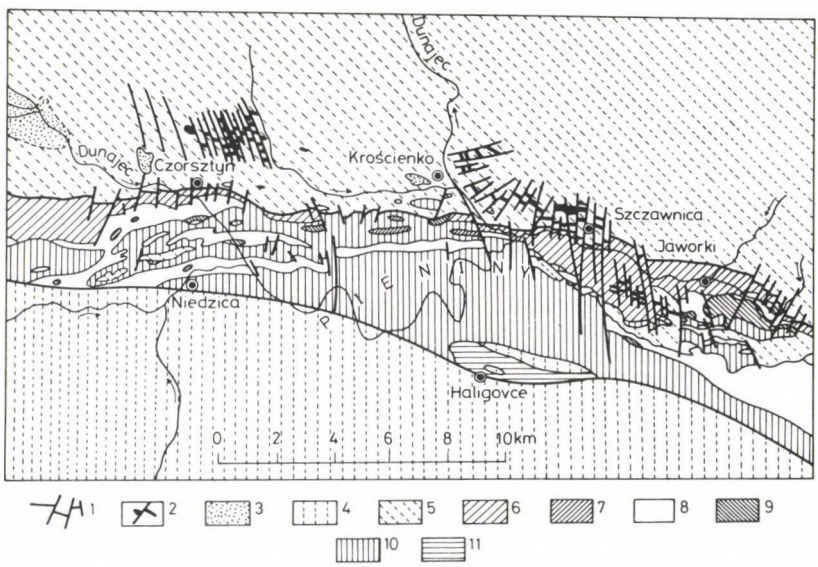

Fig. 2. Geologic map of the eastern sector of the Pieniny Klippen Belt of Poland. 1 — Miocene faults; 2 — Miocene andesite intrusions; 3 — Mio-Pliocene fresh-water deposits; 4 — Central Carpathian intra-arc Podhale Paleogene; 5 — Outer Carpathian Paleogene (Magura flysch trench deposits — Magura Nappe); 6 — Laramian Grajcarek Unit (Jurassic — Maastrichtian); 7 — Maastrichtian intra-arc molasse; 8 — Czorsztyn and Czertezik Units (Jurassic — Cretaceous); 9 — Niedzica Nappe (Jurassic — Cretaceous); 10 — Branisko and Pieniny Nappes (Jurassic — Cretaceous); 11 — Haligovce Unit (Triassic — Cretaceous); 8–11 — Klippen Successions

there, by about 15 km, down to about 50 km northward from the Belt. This has been interpreted in terms of a paleo-subduction zone active mainly during the late Cretaceous, early Paleogene and Neogene stages of folding, with after-effects as late as mid-late Miocene, Pliocene, and even Pleistocene (e.g., Birkenmajer 1976a, 1976b, 1978).

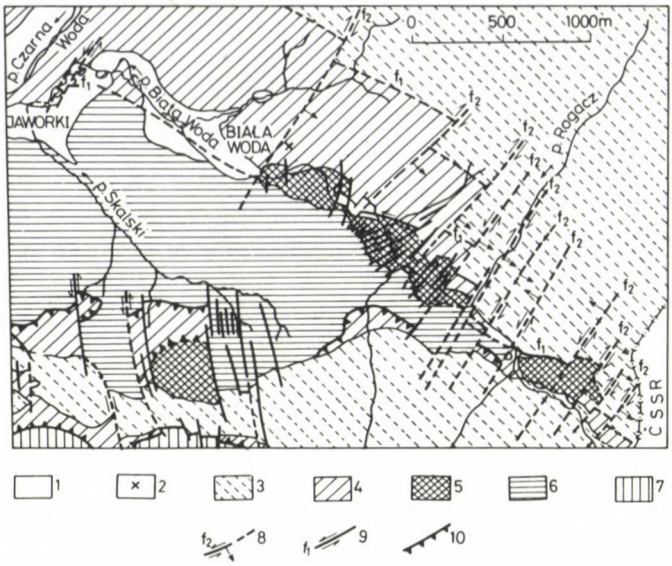

Fig. 3. Neogene fault systems in an area east of Szczawnica. 1 — Quaternary cover; 2 — basalt intrusion (Miocene); 3 — Magura Paleogene (Magura Nappe and Klippen Mantle); 4 — Laramian Grajcarek Unit; 5 — Czorsztyn Unit; 6 — Niedzica Nappe; 7 — Branisko Nappe; 8 — oblique-slip faults; 9 — strike-slip faults; 10 — pre-Eocene (Laramian and late Subhercynian) overthrusts

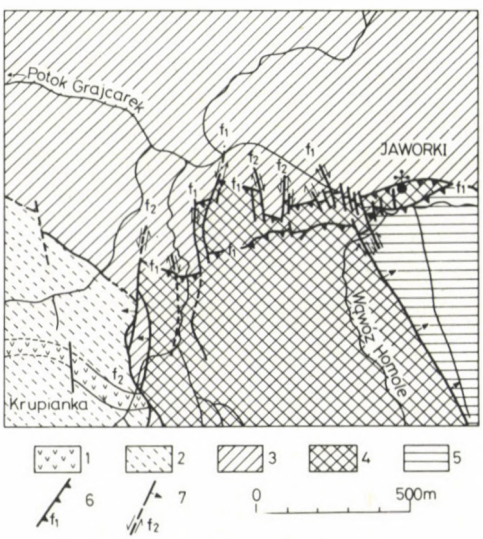

Fig. 4. Neogene fault systems and andesite intrusions in an area east of Szczawnica 1 — andesite dyke (Miocene); 2 — Magura Paleogene (Klippen Mantle); 3 — Laramian Grajcarek Unit; 4 — Czorsztyn Unit; 5 — Niedzica Nappe; 6 — Longitudinal thrust-faults (modified strike-slip faults); 7 — transversal strike-slip and oblique-slip faults

Fig. 5. Relation of Miocene andesite intrusions to faults between Szczawnica and Krościenko. 1 — Magura Paleogene (Nappe); 2 — Pieniny Klippen Belt horst, Laramian Grajcarek Unit inclusively; 3 — andesite dykes, subordinately sills, exposed to the surface; 4 — subsurface andesite intrusions (recognized on magnetometric survey); 5 — northern boundary strike-slip thrust-fault; 6 — transversal strike-slip faults

Horizontal striations on the surfaces of longitudinal faults in the northern boundary fault zone of the Pieniny Klippen Belt prove its strike-slip character (Birkenmajer 1981, 1983). There are some structural indications that the southern boundary fault is also of the strike-slip type (Figs 2, 7). The two border faults, however, differ from each other in their post-Savian history. The northern one was strongly modified, dissected and displaced by younger transverse strike-slip, oblique-slip and dip-slip faults related mainly to the Styrian Phase (mid-Miocene), possibly also by some still younger faulting, while the southern one remained almost untouched by the post-Savian deformations.

Another difference between the two border faults lies in the appearance o several Miocene hypabyssal andesite dykes and sills closely interrelated with transverse faulting along the northern boundary fault zone only.

1. Neogene fault system

There are two systems of Neogene faults in the Pieniny Klippen Belt of Poland (Figs 2, 7): 1. an older system of longitudinal faults corresponding to the Savian (early Miocene) compression and subsequent transpression, and 2. a younger system of transversal, often conjugate faults correlated mainly with the Styrian (mid-Miocene) compression (e.g., Birkenmajer 1970, 1974, 1981, 1983).

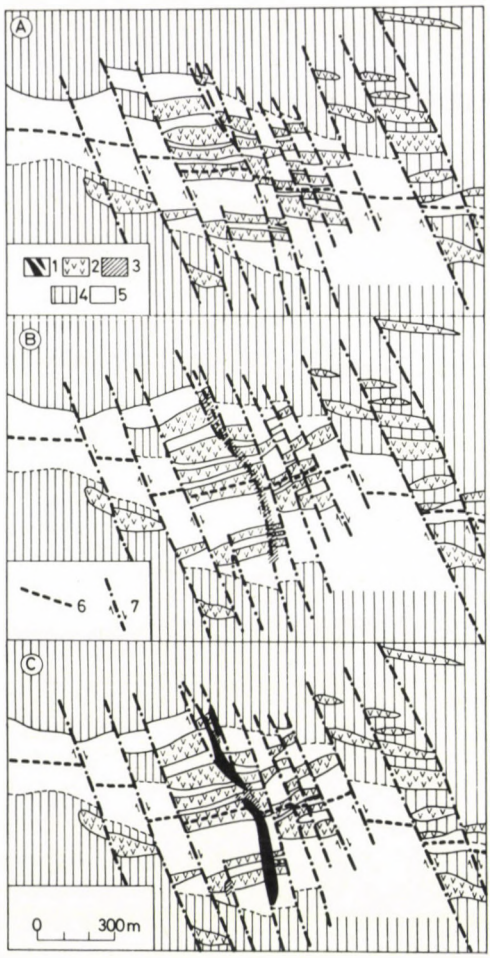

Fig. 6. Stages A–C (C — present stage) of formation of the Mt Wżar andesite dyke swarm, Czorsztyn area (after Birkenmajer and Nairn 1969). 1 — younger dykes; 2 — older dykes (dyke swarm); 3 — crush-breccia; 4 — Magura Paleogene, younger strata; 5 — Magura Paleogene, older strata (core of anticline); 6 — axis of the Mt Wżar anticline; 7 — strike-slip faults

There is also an evidence for post-Styrian, probably Moldavian (late-Miocene), and even Pliocene-Pleistocene faulting in the discussed area (Birkenmajer 1971, 1976b, Niedzielski 1971).

1.1 *Longitudinal faults* (f_1)

Two major border faults belong to this group which separate Mesozoic-Paleogene rocks of the Pieniny Klippen Belt horst from downthrown Paleogene flysches of the Outer and Inner Carpathians, respectively: 1.11 the southern boundary

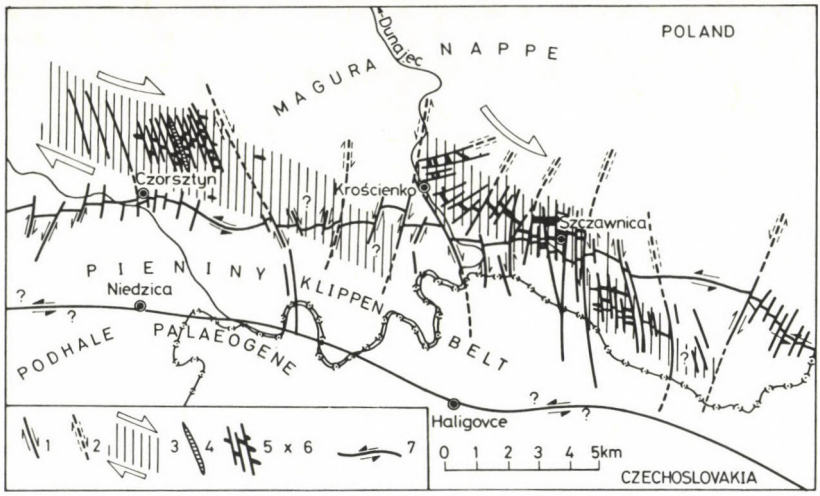

Fig. 7. Pieniny Andesite Line (PAL) and its relation to the Pieniny Klippen Belt. 1 — transversal strike-slip faults traceable at the surface; 2 — supposed transversal strike-slip faults in deep substratum of the Magura Nappe; 3 — PAL with sense of strike-slip translation marked; 4 — younger andesite dykes; 5 — older andesite dykes and sills; 6 — basalt intrusion; 7 — longitudinal strike-slip boundary faults

fault, and 1.12 the northern boundary fault. There is also a number of faults parallel with the above ones within the Klippen Belt horst itself, mainly in its northern part.

1.11 *The southern boundary fault* is extended along the whole length of the Pieniny Klippen Belt in the West-Carpathians. The fault surface is vertical or subvertical, the fault is normal (fault surface dipping south) or reverse (fault surface dipping north). The fault juxtaposes upturned, usually obliquely truncated Paleogene flysch strata on the downthrown southern side, and strongly folded, often obliquely truncated vertical folds, tectonic scales and horizontally bent sigmoids consisting of Mesozoic and Paleogene rocks on the northern, upthrown side. The character of the contact between these two units may suggest a strike-slip type of the fault. Its sense of translation (left-lateral ? — see Fig. 7) and magnitude of horizontal displacement are yet to be established.

1.12 *The northern boundary fault,* or zone, is much more complex than the southern one. In the Polish Klippen Belt area, it was well recognized at Szczawnica and to the east and west of this town, along the Grajcarek Stream (Gołab's Grajcarek Dislocation Zone, 1948), both by surface mapping and in boreholes (Figs 2–5) (Birkenmajer et al. 1979). The main fault surface is here subvertically dipping at 85 degrees to the south. The fault juxtaposes the downthrown Magura Nappe Paleogene intruded by Miocene andesites (mainly dykes) on the north, and the upthrown

Jurassic-Cretaceous rocks of the Grajcarek Unit and its Paleogene cover intruded by Miocene andesites (mainly sills) on the south (Figs 2, 5, 7).

The northern boundary fault was formed as a result of the early Miocene Savian meridional tangential compression (Birkenmajer 1970, 1974, 1983, Birkenmajer et al. 1979). The main fault surface is not enough exposed anywhere for a study of its character in details. Fortunately, there are a number of shorter, subordinate parallel faults of the same f_1 system well exposed to the south of the main transcurrent border fault (Figs 3, 4). These fault surfaces dip 65–85 degrees to the south, often becoming vertical, and show the presence of well developed horizontal fault striae and other tectoglyphs indicating left-lateral strike-slip translation (Birkenmajer 1983).

Despite of a close areal association of longitudinal f_1 faults and andesite dykes, the main northern boundary fault line remained impenetrable to magma intrusion during its whole history. On the contrary, the associated shorter parallel faults of the f_1 system both to the north and south of the main transcurrent fault line, often served as ways of penetration of the magma during the Miocene. This difference can be explained by assuming that a compressional (transpressional) regime was maintained at the main fault surface for a period exceeding the main Savian phase of folding, due to a clockwise rotation of the Inner Carpathian block relative to the Outer Carpathians. The subordinate, parallel f_1 faults tended to open as sites of stress release by strike-slip mechanism similar to that of tension gashes, thus allowing andesite magma to penetrate.

1.2 *Transversal faults (f_2)*

Faults transverse (oblique) to the f_1 system belong to the younger system (f_2). They are often radial with respect to the curvature of the Pieniny Klippen Belt. They occur usually as sets of parallel faults directed either SW-NE (resp. SSW-NNE) or SE-NW (resp. SSE-NNW), representing a conjugate system expressed alternately along the northern margin of the Belt and in the adjoining part of the Magura Nappe (Figs 2, 5–7).

The fault surfaces are straight or slightly curved, rarely bifurcating, vertical or steeply dipping. The striations and slickensides on fault surfaces are either horizontal (strike-slip faults) or oblique (oblique-slip faults), sometimes vertical (dip-slip faults), often superimposed on one another (Birkenmajer 1983). The scale of the strike-slip translation reaches from centimetres to several hundred metres.

These transverse faults were already known to Uhlig (1890) but the sense of motion on the fault surfaces has not been recognized until much later (e.g., Birkenmajer 1963, 1983, Jaroszewski 1968, Grochocka-Piotrowska and Kibitlewski 1974).

The transverse faults are considered to be syntectonic with the mid-Miocene (Badenian) Styrian compression and nappe-thrusting in the Outer West-Carpathians

(Birkenmajer 1970, 1974, 1983). The paleomagnetic dating of the andesite intrusions associated with these faults at Wżar (Birkenmajer and Nairn 1969) agrees with that age. Radiometric age of these andesite intrusions is yet to be established.

There seems to be a succession in transverse faulting, with the oldest strike-slip, followed by oblique-slip and dip-slip displacements of fault-blocks relative to one another, probably extending in time from mid-Miocene far into the late Miocene and even Plio-Pleistocene.

2. Andesite intrusions versus fault pattern

Neogene volcanism of the Dunajec River sector of the Pieniny Klippen Belt occupies a special position within the late to post-orogenic Neogene volcanic province of the Carpathians. It is represented entirely by small hypabyssal intrusions—dykes and sills, being predominantly of andesitic character and cutting through rocks of Jurassic to Paleogene ages (Birkenmajer 1957, 1958, 1962, 1970, Małoszewski 1962, 1963). They are areally restricted to the maximum bend and northward extension of the Klippen Belt arc. The Pieniny Andesite Line (PAL) has roughly a WNW-ESE direction and traverses obliquely the northern border fault zone (f_1) of the Belt (Figs 2, 7). It is of interest to note that the intrusions penetrate only through the Laramian Grajcarek Unit of the Belt and its Paleogene cover, and through the adjacent Paleogene flysch of the Magura Nappe, but not through any of the Klippen successions (Fig. 2). The Grajcarek Unit consists of Jurassic and Cretaceous rocks which were formed in the Outer Carpathian Magura trough north of the Pieniny Klippen Belt sedimentary realm, and were thrust backward (retro-arc) over late-Subhercynian Klippen nappes (Birkenmajer 1970, 1974).

The intrusive suite is represented mainly by andesites ranging from basic through normal (predominantly) to acid varieties (Małkowski 1958, Youssef 1978). Olivine-basalt occurrence is quite exceptional, dacite-rhyolite members of the suite have not been recognized. The andesites are considered to be products of hybridization of the primary mantle-derived basaltic magma on its way upward along tension fissures through the steeply bent downgoing slab of the Eurasian Plate and its tectonic overburden (Birkenmajer 1976a). When prolonged north-westwards, the PAL matches the Odra Fault line in Lower Silesia with its predominantly mantle-derived Tertiary basalts (Birkenmajer et al. 1973, 1977).

There are two systems of Neogene andesitic intrusions: 1. older, parallel with the PAL direction (subparallel or oblique with respect to the Pieniny Klippen Belt), and 2. younger, oblique to the PAL direction (Figs 2, 7).

2.1 *Older intrusions*

These intrusions, also called the first-phase andesites, occur in two areas: 2.11 east of Krościenko, and 2.12 in the vicinity of Czorsztyn (Figs 2, 7).

2.11 In the *area east of Krościenko* (between Krościenko and Jaworki) there occur mainly amphibole-andesites, subordinately amphibole-augite andesites, and even a small intrusion of olivine-basalt (at Biała Woda east of Jaworki — Fig. 3). The andesites post-date the Magura Paleogene flysch rocks, the early Miocene Savian fold structures of the Klippen Belt and the Magura Nappe. Preliminary paleomagnetic dating of andesites based on comparison with the Central Slovak volcanism suggests an early Miocene (probably Karpatian) age of the intrusions (Birkenmajer and Nairn 1969), a radiometric dating is yet to be performed.

A detailed study of thermal contacts of andesite sills with country rocks at Mount Jarmuta east of Szczawnica (Birkenmajer 1958) indicates that the magmatic intrusions were syntectonic with the short meridional (transversal) faults correlatable with the f_2 system: the country rocks are backed across these faults. Horizontal slickensides found on some of the transversal thermal joints in the andesite bodies indicate that the transversal strike-slip motion continued after cooling-off of the magma (during an early stage of the Styrian Phase?). A characteristic sinusoidal bend in the PAL direction which is also reflected in a radially arranged fault pattern, and in changes of the strikes of flysch rocks in an area between Krościenko and Szczawnica (Figs 2, 7) indicates a tectonic rotation of that area possibly during a late stage of the Styrian Phase.

2.12 The older-phase andesites of *Mount Wżar near Czorsztyn* (Figs 2, 6, 7) form a dyke swarm directed nearly E-W (Birkenmajer 1962). According to paleomagnetic dating (Birkenmajer and Nairn 1969) based on a comparison with the Central Slovak volcanic suite, they correspond to the early Badenian. The dykes may have intruded simultaneously with transversal faulting which apparently displaced them. There seems to be a succession of the intrusive events: from infrequent basic plagioclase-amphibole-andesite and magnetite-andesite dykes till more acidic normal amphibole-augite-andesite dykes which are most common (Youssef 1978).

2.2 *Younger intrusions*

The older andesite dykes at Mt Wżar are traversed by predominantly right-lateral strike-slip NW-SE-trending faults of the f_2 system (Fig. 6). An anticlockwise rotation of these dykes due to the accumulation of strike-slip movement along transverse faults is best expressed in a zone adjacent to the crush-breccia in the middle of the Wżar antlicline. It is supposed that this deformation corresponds to the Styrian

Phase of compression (mid-Badenian). The younger dykes, represented by mostly acid amphibole-augite-andesites follow the lines of transversal f_2 faults and associated crush-breccia, thus post-dating the Styrian deformation. Based on paleomagnetic dating, in comparison with the Central Slovak effusives, the younger andesite dykes at Wżar have been dated at the Badenian-Sarmatian boundary (Birkenmajer and Nairn, 1969); a radiometric dating of the dykes is yet to be performed. The dykes do not show visible traces of a tectonic deformation and thus may be regarded as post-tectonic with respect to the Styrian Phase, although Youssef (1978) considered a possibility of a transverse displacement caused by still younger WSW-ENE-directed faults.

The mechanism involved in the intrusion of the younger phase andesites at Wżar could be connected to the opening of the transversal fault planes (f_2) due to tension generated in the substratum of the Magura Nappe by a right-lateral strike-slip motion along PAL (Fig. 7).

3. Conclusions

1. There is a close interrelation between the Neogene fault pattern and the hypabyssal andesite intrusions in the area adjacent to the northern boundary fault zone of the Pieniny Klippen Belt in Poland.

2. The andesite intrusions post-date the Savian (early Miocene) meridional compression responsible for the intense folding of the Klippen Belt and the adjacent flysch zones. The northern boundary fault zone (f_1) having been formed then, continued to function as a left-lateral strike-slip transcurrent fault due to the subsequent clockwise rotation of the Inner Carpathian block relative to the Outer Carpathian zone. The fault itself was a site of transpression, while adjacent, parallel subordinate f_1 faults tended to open due to tension by stress release, to the north and south of the main translation surface.

3. The faults f_1 parallel to the main transcurrent fault thus became sites of the intrusion of older generation andesite magmas (dykes and sills) which seem to span the time from the Karpatian stage on the east (between Krościenko and Jaworki) to the early Badenian on the west (area of Czorsztyn).

4. Transverse faults f_2 were formed as result of a stress regime change from transpressive to compressive corresponding to the Styrian Phase (Badenian) of meridional tangential compression, simultaneously with the flysch thrust-nappe formation in the Western Outer Carpathians. The oldest transversal strike-slip faults were formed simultaneously with the intrusion of andesite magma, the faulting continued for some time after cooling-off of the intrusions causing a transverse strike-slip displacement in dykes and sills.

5. The youngest andesite intrusions attributed to the Badenian-Sarmatian boundary follow the lines of transversal faults (f_2) and are post-tectonic with respect to the Styrian compression.

6. The Pieniny Andesite Line (PAL) directed WNW-ESE, obliquely traverses the northern boundary fault zone (f_1) of the Pieniny Klippen Belt. This line seems to be an expression of a major rupture in the deep substratum of folded flysch masses (which are partly underthrust with respect to the Klippen Belt horst), probably within the down-buckled Eurasian Plate.

References

Birkenmajer K 1957: Andesite dykes of the Bryjarka Mt at Szczawnica, Pieniny Klippen Belt, Carpathians. *Przegl. Geol.*, 47, 62–65.

Birkenmajer K 1958: New contributions to the geology of magmatic rocks of the Szczawnica area within the Pieniny Klippen Belt. *Prace Muz. Ziemi*, 1, 89–103.

Birkenmajer K 1962: Remarks on geological form of the Mt Wżar andesites, Pieniny Mts, Carpathians. *Acta Geol. Pol.*, 12, 201–213.

Birkenmajer K 1963: Stratigraphy and paleogeography of the Czorsztyn Series, Pieniny Klippen Belt, Carpathians, in Poland. *Stud. Geol. Pol.*, 9, 1–380.

Birkenmajer K 1970: Pre-Eocene fold structures in the Pieniny Klippen Belt, Carpathians, of Poland. *Stud. Geol. Pol.*, 31, 1–77.

Birkenmajer K 1971: Origin of the Homole Gorge, Pieniny Klippen Belt, Carpathians. *Rocz, Ochr. Przyr.*, 36, 309–359.

Birkenmajer K 1974: Carpathian Mountains. In: *Mesozoic-Cenozoic orogenic belts — Data for Orogenic Studies* (A M Spencer ed.). *Geol. Soc. Lond. Spec. Publ.*, 4, 127–157.

Birkenmajer K 1976a: The Carpathian orogen and plate tectonics. *Publ. Inst. Geophys. Pol. Acad. Sci.*, A–2 101, 43–53.

Birkenmajer K 1976b: Pleistocene tectonic deformations at Szaflary, West Carpathians, Poland. *Ann. Soc., Géol. Pol.*, 46, 309–323.

Birkenmajer K 1978: Neogene to early Pleistocene subsidence close to the Pieniny Klippen Belt, Polish Carpathians. *Stud. Geomorph. Carp.-Balk.*, 12, 17–28.

Birkenmajer K 1981: Strike-slip faulting in the Pieniny Klippen Belt of Poland. Carp.-Balk. Geol. Ass., 12th Congr., Bucharest, Abstracts: 114–115.

Birkenmajer K 1983: Strike-slip faulting in the northern boundary zone of the Pieniny Klippen Belt, Carpathians. *Stud. Geol. Pol.*, 77, 89–112.

Birkenmajer K, Nairn A E M 1969: Paleomagnetic studies of Polish rocks. III. Neogene igneous rocks of the Pieniny Mountains, Carpathians. *Ann. Soc. Géol. Pol.*, 38, 475–489.

Birkenmajer K, Jeleńska M, Kądziałko-Hofmokl M, Kruczyk J, Nowakowski A 1973: Paleomagnetism and magnetic properties of Tertiary basaltic rocks from Gracze, Lower Silesia. *Acta Geol. Pol.*, 23, 245–271.

Birkenmajer K, Jeleńska M, Kądziałko-Hofmokl M, Kruczyk J 1977: Age of deep-seated fracture zones in Lower Silesia (Poland) based on K-Ar and paleomagnetic dating of Tertiary basalts. *Ann. Soc. Géol. Pol.*, 47, 545–552.

Birkenmajer K, Dudziak J, Jednorowska A 1979: Subsurface geological structure of the northern boundary fault zone of the Pieniny Klippen Belt at Szczawnica, Carpathians. *Stud. Geol. Pol.*, 61, 7–36.

Gołąb J 1948: Newly discovered mineral waters at Szczawnica (in Polish). *Biul. Państw. Inst. Geol.*, 42.

Grochocka-Piotrowska K, Kibitlewski S 1974: Remarks on tectonics of the Pieniny Klippen Belt near Czorsztyn. *Bull. Acad. Pol. Sci., Terre*, 21, 175–185.

Jaroszewski W 1968: Curved fault striae and the mechanism of faulting. *Acta Geol. Pol.*, 18, 233–238.

Małkowski S 1958: Volcanic processes in the geologic history of the Pieniny Mts area. *Prace Muz. Ziemi*, 1, 11–55.

Małoszewski, S 1962: Magnetic measurements of andesite occurrence in the vicinity of Szczawnica. *Prace Geol.*, 10, 1–140.

Małoszewski S 1963: Microtectonics of the Wżar Mountain and of its vicinities in the light of magnetometric research works. *Przegl. Geol.*, 7, 345–349.

Ney R 1975: Tectogenesis of the Carpathians in the light of new tectonics of the Earth's globe. *Publs Inst. Geophys. Pol. Acad. Sci.*, 82, 95–110.

Niedzielski H 1971: Tectonic origin of the eastern part of the valley of Nowy Targ. *Ann. Soc. Géol. Pol.*, 41, 397–408.

Sollogub V B, Prosen D et al. 1973: Crustal structure of central and south-eastern Europe by data of explosion seismology. *Tectonophysics*, 20, 1–33.

Uchman J 1973: Results of deep seismic sounding along International Profile V. *Publs Inst. Geophys. Pol. Acad. Sci.*, 60, 47–52.

Uhlig V 1890: Ergebnisse geologischer Aufnahmen in den westgalizischen Karpathen. II. Der pieninische Klippenzug. *Jb. geol. R.-A.*, 40, 559–824.

Youssef M M M 1978: Large-scale gelogical survey of the Mt Wżar andesites, Pieniny Mts, Poland. *Stud. Geol. Pol.*, 66, 1–30.

Acta Geodaet., Geophys. et Montanist. Hung. Volume 19 (1—2), pp. 49—51 (1984)

GEOPHYSICAL DATA BANK FOR THE CARPATHO-BALKAN AREA

(EXTENDED ABSTRACT)

I A BYCHVAROV[1], V N VADKOVSKY[2], V P GOLOVKOV[2], N A SERGEEVA[2], E P TIMOSHKINA[2], YU B TYUPKIN[2]

Keywords: Carpatho-Balkan geophysical data; geophysical data bank

Present geophysical surveys aim at a complex study of different areas. The analysis and generalization of the results of regional surveys is impossible without a previous collection of existing data on the geological and geophysical structure of the region. The results or any regional survey should coincide with the results on neighboring areas as well as with global data. The most adequate tool for such projects is the data bank (Shomie 1981).

The data bank is a complex of the following elements:

1. Data base — a sufficiently wide collection of data organized in a well-defined manner being accessible for a computer.
2. A control system of the data base which serves for the establishment and maintenance of the data base according to the actual situation and which enables any manipulation of the data.
3. A computer with adequate configuration.
4. Staff to carry out the activities of the bank (Ivanov 1977).

A data bank enables to concentrate great data quantities in a given place, any scientist has access to the data, the data sets can be utilized many times in a most versatile form, it facilitates data retrieval and handling, selection of necessary data and enables also for scientists to use their own special programmes. An important part of the data bank is the programme library with all important scientific programmes developed for the solution of geophysical problems.

A data bank takes the burden of a tedious and lengthy work from the scientists, e.g. to transcript data into or from a computer-readable format, to control such data and to construct programmes of data processing for these very data.

Since 1981, a project has been initiated in the framework of the cooperation of the Academies of Socialist Countries in the field of planetary geophysics (KAPG), i.e.

[1] Geophysical Institute of the Bulgarian Academy of Sciences, Akad. G. Bonchev str., block 13, 1113 Sofia, Bulgaria

[2] WDC B2, Soviet Geophysical Committee, Molodezhnaya 3, 117296 Moscow, USSR

Project 13 "Establishment of geophysical data banks". A topic of this project, topic 13.1, is "Establishment of a data bank for the geophysical data of the Carpatho-Balkan area". This bank should give possibility for a wide range of scientists to obtain data quickly, in great quantities and in comfortable format in geophysics and in related disciplines to carry out complex investigations in the Carpatho-Balkan area or for interdisciplinary research. The main functions of this bank are: selection, systematization and analysis of data, their incorporation into the data base to ensure continuous operation and access for all investigators.

In the data bank geophysical organizations and scientists of Bulgaria, Hungary, Romania, USSR and Czechoslovakia took part. The bank is realized in the United Mathematical and Mechanical Centre (ECMM) and in the Geophysical Institute of the Bulgarian Academy of Sciences, and also in World Data Centre B2 (WDC B2) of the Soviet Geophysical Committee of the Soviet Academy of Sciences. The technical tools of the bank are: a small series computer SM–4 (ECMM), a computer of the unified series 1022 (WDC B2) and 1040 (ECMM). The use of the data base control systems FORBIN, ADIOS, KATALOG (Vyrnev et al. 1983) enable the completion of the data base, the control of the existing data, their correction and re-organization, the actualization of the data base, an information-retrieval system to carry out different kinds of corrections and to realize any possible selection from an arbitrary data set according to some or other parameter or to a prescribed range of the values of a parameter, and also to construct a programme library of practical programmes being a supplementary and comfortable tool for the interpretation of geophysical data.

This establishment of the data base consists of the establishment of a file which contains a catalogue of data in the base and all relevant informations about any kind of data in it, and the data sets about different geophysical, geological and other similar parameters. Naturally, the data bank can meet the interest of scientists if it contains complete and reliable data sets in a wide range of disciplines and from different observation methods. The introduction of certain data into the data base is decided by the curators, who are scientists from different fields being invited to take part in the work of this KAPG-project.

The establishment of the data base is a continuous, lengthy task. A summary of data included into the data base (Table I) contains also data which are already in the data bank and can be used by scientists. The other data sets will be included during the years 1983–1985. It is also planned to add data to this data base from continuously operating observatories within the area of interest and also the results of geophysical investigations carried out in countries of the region, especially those being parts of KAPG-project 1.1: "Geophysical and geodynamical models of the Carpatho-Balkan area". It is further planned that geological, geochemical, tectonic etc. data will also be included into the data base.

In addition to data collection, supplementation of new information and data into the data base and to ensure comfortable access and utilization of different data

Table I. List of data sets about the geophysical discipline of the solid Earth, represented in the data base

Discipline, curator	Data set
1. Seismology V Kárnik, Geophysical Institute of the Czechoslovak Academy of Sciences	1. Digital seismogrammes from the world seismological network with records of earthquakes in the Carpatho-Balkan area 2. Seismological bulletins of the USSR and of the KAPG-countries 3. Catalogue of the earthquakes of the Carpatho-Balkan area and surrounding territories 4. Focal mechanisms of the earthquakes
2. Magnetic field I Bychvarov, Geophysical Institute of the Bulgarian Academy of Sci.	1. Mean yearly values of the geomagnetic field in the observatories of the Carpatho-Balkan area
3. Gravimetry A Venedikov, Geophysical Institute of the Bulgarian Academy of Sci.	1. Earth tides observation results from the Carpatho-Balkan area and from surrounding areas
4. Recent crustal movements P Vyskočil, WDC C of RCM, Czechoslovakia	1. Catalogue of stations where the vertical crustal movements have been determined in the Carpatho-Balkan area and in surrounding countries
5. Paleomagnetism V Vadkovsky, WDC B2, USSR	1. Catalogue of the average positions of paleomagnetic poles for the non-Alpine part of Europe 2. Catalogue of paleomagnetic data for the Carpatho-Balkan area
6. Heat flow V Čermák, Geophysical Institute of the Czechoslovak Academy of Sci.	1. Catalogue of the measured values of heat flow in Europe

sets for users it is also envisaged to enable graphic display (linear drawings, maps with isolines etc.) of the data about geophysical parameters.

At the end, the authors wish to express their gratitude to everybody who helped to establish the data bank about the Carpatho-Balkan area.

References

Ivanov A P 1977: Principles for a logical planning of data banks in Automatic system of data processing in planetary geophysics. Geophysical data banks. Publication of WDC B, Moscow.

Shomie Zh 1981: Data banks. Moscow, Energoizdat.

Vyrnev P 1983: Geophysical data bank of the Carpatho-Balkan area. Publication of WDC B, Moscow.

Acta Geodaet., Geophys. et Montanist. Hung. Volume 19 (1—2), pp. 53—56 (1984)

SOME COMMENTS ON THE HEAT FLOW DENSITY PATTERN IN EUROPE AND ITS INTERPRETATION

(EXTENDED ABSTRACT)

V ČERMÁK[1]

Keywords: crustal radioactivity; heat flow map, Europe; heat generation; Moho heat flow

Under the Project of the International Heat Flow Commission the Heat Flow Map of Europe was prepared and published in 1979 together with a comprehensive volume of papers discussing the results of the heat flow investigations in practically all the European countries (Čermák and Rybach eds 1979). The construction of the heat flow map of Europe was based on total 3076 existing observations which were complemented by all the available deep temperature measurements, heat flow density estimates and near surface temperature gradients. The contouring was adapted to a linear interpolation in the areas with sufficient data, in the areas with insufficient data coverage the course of the isolines was accommodated to the main tectonic features using the knowledge of the experimental relationship between the heat flow density and the age of the last tectono-thermal event.

Two papers interpreting the above map were prepared by the author recently (Čermák 1982a, 1982b). This extended abstract summarizes the main ideas of this interpretation together with the use of the surface heat flow density patterns for the calculation of the deep temperature distribution, Moho heat flow pattern and for the projection of the regional variation of the lithospheric thickness. Part of this work was presented during the KAPG 1.1 Workshop "Geophysical and Geodynamic Model of the Lithosphere of the Carpatho-Balkan Region" in Budapest, September 8–14, 1982.

a) The European continent is characterized by a large low heat flow zone covering the most of northern and eastern Europe, surrounded by normal to high heat flow density values spread in western, central, southern and southeastern Europe. The general "northeast" to "southwest" increase of the geothermal activity is the consequence of the geological evolution of Europe and the major heat flow provinces correlate relatively well with the principal tectonic units of Ur-Europe, Paleo-Europe, Meso-Europe and Neo-Europe. The first-order heat flow lows (< 40 mWm^{-2}) cover most of the East European platform including both the Baltic and the Ukrainian shields, i.e. the greater part of the European craton, the oldest ($> 1.5 \times 10^9$ yr) and the

[1] Geophysical Institute, Czechoslovak Academy of Sciences, 141 31 Praha-Spořilov, Bočni II/1401

most stable portion of the whole continent. Other heat flow lows include smaller units such as the Bohemian Massif, the Moesian Plate, etc., representing stable, consolidated segments, as well. Low heat flow is also typical for the Eastern Mediterranean Sea (probably the part of the African plate), with a thick stable mafic crust, and the Black Sea. Geothermal highs (>80 mWm^{-2}) are found in Iceland and its vicinity (part of the Mid-Atlantic Ridge), the Rhinegraben, the Alps, the Pannonian Basin, several locations in the Balkan, Turkey and the Caucasus (all geologically young structures, tectonically still active or recently active) and in the Western Mediterranean and the Aegean Sea (areas of the thin subcontinental crust).

b) The European heat flow density data display typical behaviour when related to the tectonic age. The characteristic curve is parallel to, but about 8–10 mWm^{-2} lower than the "all continents" curve. The Hercynian orogeny in Europe must have been characterized by an enormous, very deep thermal event, which may have strongly disturbed the thermal field; the corresponding "recollection" is still observable by the relatively high heat flow in most of the European Hercynian structures.

c) The number of combined heat flow (Q) — heat generation (A) measurements in Europe is still not sufficient and except for the Baltic ($Q=27.3+6.4\ A$) and the Ukrainian shield ($Q=25+8.0\ A$), it is not possible to determine the reliable values of the reduced heat flow for any other European heat flow province.

d) Crustal radioactivity, despite its local importance and contribution to the heat flow, does not play a decisive role from the regional point of view. Regionally, the terrestrial heat flow is dominated by the outflow of heat from the upper mantle. High heat flow is generally associated with the zones of a weakened (thin) crust, while low heat flow density is typical of regions with a thick crust. The explanation of this phenomenon is not quite clear yet, but it is believed to be connected with the role of the heat flow from the earth's depths in the long-term geological evolution, and with the nature of the Mohorovičić discontinuity as a complex transition phase under specific p,T conditions, the time factor definitely included.

The areas of thinner crust are usually younger in their origin than the relatively "colder" areas with a thick crust which belong to the oldest tectonic units. In the hyperthermal regions with a very high heat flow, high crustal temperatures associated with the increased heat flow from the depths may cause some "subcrustal erosion", i.e. the change of the crustal material into denser rocks having upper mantle properties. Crustal thickening in the younger mountains (such as the Alps) was caused by interthrusting in orogenes and the elevated heat flow may thus be a transient phenomenon. An important question that has to be solved, is the extent to which the position of the Mohorovičić discontinuity is time dependent. While in older areas the crust might have grown thicker due to cooling, the thick crustal bulge below the younger mountains may gradually diminish by the process of basification.

e) The map of the surface heat flow density in Europe was supplemented by the crustal thickness pattern and by data on crustal radioactivity and transformed then to

maps of deep temperature distribution and of mantle heat flow pattern. Using a model of radioactivity decreasing exponentially with depth $A(z)=A_0\exp(-z/D)$, with $A_0=2\,\mu Wm^{-3}$ and $D=10$ km, the generalized one-dimensional, steady-state, conductive temperature-depth curves for all the major tectonic units in Europe were computed. This model was further used to convert the surface heat flow pattern into a simplified regional representation of existing temperatures at the Moho depth and at a depth of 40 km. To be able to assess the upper mantle heat flow contribution the total crustal share due to the radioactive heat sources was estimated for $2^\circ \times 2^\circ$ surface grid elements from the characteristic vertical profiles of the v_p velocities known from explosion seismology. Heat generation was evaluated from the seismic velocities according to the experimental formula proposed by Rybach (1973) and the crustal heat contribution was then subtracted from the observed surface heat flow density.

The Moho discontinuity is neither an isothermal surface, nor is the heat flow from below it constant. Both the Moho temperature and/or the Moho heat flow may vary within broad limits which for the continent of Europe have been estimated as $280\,°C < T_M < 900\,°C$ and $15 < Q_M < 60$ mWm^{-2}, respectively. Relatively low temperatures (350–500 °C) at the Moho discontinuity, at depth of 45–50 km, are to be expected beneath the Precambrian shields and the East European platform, higher Moho temperatures of 500–600 °C were calculated for the Paleozoic folded units such as the Bohemian Massif or the Ural Mountains at depths of 35–45 km. Local temperature maxima of 600–700 °C seem to exist in the zones of a weakened crust or in the areas of deep faults, which are characterized by a higher heat flow density on the surface (up to 70–80 mWm^{-2}). Very high crustal temperatures (800–1000 °C) are probable in hyperthermal regions, such as the Pannonian Basin or in the Upper Rhinegraben, characterized by a relatively thin crust (25 km) and a very high heat flow on the surface (over 90 mWm^{-2}).

While even if the crustal rocks beneath the shields are considerably depleated in radioactivity, the heat flow from the upper mantle cannot exceed 15–20 mWm^{-2}. The normal Moho heat flow varies from 20–25 to 30–35 mWm^{-2} in the platform areas, in Paleozoic folded units and in the Cenozoic mountain belts. The hyperthermal areas of the Alpine intramontane depressions or of the young rift valleys must have a high Moho heat flow (minimum 40–50 mWm^{-2}), even if the crustal rocks are rich in radioactivity what is not likely. There must be substantial regional differences in the upper mantle heat flow contribution, up to the order of 30–40 mWm^{-2}. Such a regional variation in the energy outflow represents an important parameter in the tectonic evolution, as well as a critical limitation of the geophysical studies of the deep seated processes.

f) A geothermal model of the lithosphere was proposed (Čermák 1982b), in which the surface heat flow is in equilibrium with the heat flowing into the lithosphere at its base plus the heat generated within it. The deep lithospheric temperature distribution was calculated and the idea of Pollack and Chapman (1977) was used, i.e.

to use the calculated geotherms in combination with the mantle melting relations to estimate the top of a seismic low velocity channel. This channel characterizes the passage between the solid lithosphere and the viscous asthenosphere, the relatively sharp decrease of the seismic velocity may relate the fact that the existing temperatures at this depth reach or are close to the melting temperature of the surrounding mantle rocks. All the European territory was divided into regular $4° \times 4°$ latitude–longitude grid elements and the corresponding lithospheric thickness was determined in each element. By interpolating the individual data the regional pattern of the lithospheric thickness in Europe was projected. It was shown that in the Precambrian shield and the platform areas of northern and eastern Europe the lithosphere is more than 200 km thick, while thin lithosphere (less than 100 km) exists beneath the active tectonic units of the southern and southeastern European high heat flow zones.

References

Čermák V 1982a: Crustal temperature and mantle heat flow in Europe. *Tectonophysics*, 83, 123–142.

Čermák V 1982b: Regional pattern of the lithospheric thickness in Europe. In: *Geothermics and Geothermal Energy*, V Čermák and R Haenel eds 1–10. E Schweizerbart'sche Verlagsbuchhandlung, Stuttgart

Čermák V, Rybach L eds 1979: Terrestrial Heat Flow in Europe. Springer Verlag, Berlin–Heidelberg–New York

Pollack H N, Chapman D S 1977: On the regional variation of heat flow, geotherms, and lithosphere thickness. *Tectonophysics*, 38, 279–296.

Rybach L 1973: Wärmeproduktionsbestimmungen an Gesteinen der Schweizer Alpen. Beitr. Geol. Schweiz, Geotechn. Ser. 51, Kümmerly and Frey, Bern

Acta Geodaet., Geophys. et Montanist. Hung. Volume 19 (1—2), pp. 57—60 (1984)

MAGNETIC EFFECT OF THE CARPATHIAN CONDUCTIVITY ANOMALY AT DIFFERENT ALTITUDES

M V FISKINA[1]

New altitudinal experiments for the analysis of the Carpathian conductivity anomaly are discussed. The investigation possibilities of the geometrical parameters of this anomaly are illustrated in the framework of these experiments.

Keywords: altitudinal magnetic experiment; Carpathian conducting zone

The anomalous magnetic field in Central Europe essentially depends on the structure of the Carpathians. There is a well-known anomalous conductive body (ACB) under the central region of the Carpathians at a depth of 15–20 km; it can be estimated being 1000 km long and 20–25 km wide. The anomalous magnetic field due to induction in this ACB, gives important informations about this body. We consider the induction by the field of a plane wave in the cylinder, whereby the electric component E_0 is directed along the cylindrical axis y.

A theoretical or experimental study of this problem faces many difficulties. The following factors are important for the theoretical analysis:

a) Changes of the anomalous field due to the conductivity of the external medium.

b) Complicated form of the cylinder's cross section.

c) Influence of the Earth's surface.

d) Radial conductivity distribution inside the cylinder. The first two factors were analysed in a generalized form by Svetov (1973), the latter two recently by Wait and his coworkers (Mahmoud et al. 1981). The general induction formulae were applied to the problem of geomagnetic anomalies by Rokityansky (1975). The observation technique, however, does not permit at present to check a series of theoretical predictions. Therefore, the improvement of the observation techniques seems to be a very actual problem.

The altitudinal experiment, planned by IZMIRAN for the investigation of an anomalous conductive body, may be considered as a new experimental effort in this

[1] Institute of Terrestrial Magnetism, Ionosphere and Radio Wave Propagation (IZMIRAN). USSR Academy of Sciences, Troitsk, Moscow Region, 142092

field. The aim of this report is a preliminary discussion of the perspectives and difficulties of this experiment.

An ACB model having a form of a long circular cylinder predicts the anomalous magnetic field in the form

$$H_z = H_y = 0; \; H_\varphi = \frac{C}{2}; \; C = F(\omega; \sigma_e; \sigma_i; a)E_0. \tag{1}$$

The symmetrical structure of this field is produced by special assumptions about the geometry of the ACB. The symmetry of this idealized model may be due to the real factors (a–d) mentioned above; however, it is difficult to distinguish the effects of each of these factors in the measured field. Therefore, the application of methods based on the symmetry seems to be very useful. Let us consider some of these methods.

The determination of the depth of the ACB axis

The field components (1) in the plane (x, z), orthogonal to the y-axis, can be written as

$$H_z = \frac{Cx}{\Delta}; \; H_x = \frac{C(z+h)}{\Delta}; \; \Delta = x^2 + (z+h)^2. \tag{2}$$

The plane of symmetry (y, z) is determined by means of the zero value of the vertical component H_z. The depth h is calculated from the ratio of the H_x-values, measured in the plane $(x=0)$, *at the Earth's surface and at an altitude* z_0

$$h = z_0 \left[\frac{H(z_0)}{H(0)} - 1 \right]^{-1}. \tag{3}$$

This h-value can be checked by special measurements in three points. Namely, it is necessary to found three points, where the absolute value of the field $|\vec{H}|$ is equal. Two of these points lie on the surface $(z=0)$ at the points $(\pm d_0, 0)$, the third one determined by the altitudinal experiment lies in the plane of symmetry (z, y) at an altitude z_0. Let us draw a circle through these three points. The value h can be obtained then as:

$$h = \frac{d_0^2}{2z_0} - z_0. \tag{4}$$

The difference between the values h from Eq. (3) and from Eq. (4) will indicate the violation of the symmetrical model (1).

Violation of the symmetrical model

The changes of the field in the plane of symmetry (y, z) can be analysed by measuring the component H_x at altitudes z_0 and z_1. Theoretically it can be written for the component ratios, based on the distribution (1):

$$\frac{H_x(z_0)}{H_x(z_1)} = \frac{z_0+h}{z_1+h}. \tag{5}$$

Here the h-value was determined from Eq. (4). A comparison of the theoretical value of ratio (5) with the experimental one decides the applicability of model (1).

An additional control of model (1) can be connected with the ratio of the field components H_x/H_z at the Earth's surface. The deviation of the theoretical value of this ratio in the point $(d_0, 0)$ from the experimental one:

$$\left|\frac{H_z}{H_x}\right| = \frac{d_0}{h}; \tag{6}$$

indicates the influence of the Earth's boundary or the difference between the ACB cross section and the circular one.

Elliptical symmetry of ACB

A violation of the circular symmetrical model (1) can be interpreted by means of the ACB model with elliptical cross section. The depth h and the focal length $2a$ of such an elliptical cylinder can be determined by the generalization of some above mentioned altitudinal experiments. The violation of the circular symmetry, however, leads to an increase of the number of measurements.

The elliptical lines of equal magnitudes are characterized by some parameters $\varepsilon > 0$. The connection between the Cartesian co-ordinates (x, z) and the elliptical ones (ε, η) is given by the formulae

$$x = a \cdot \operatorname{ch} \varepsilon \cdot \cos \eta; \quad z = a \cdot \operatorname{sh} \varepsilon \cdot \sin \eta. \tag{7}$$

Let us find five points in the plane (x, z) having the same absolute value of field; one point $(0, z_0)$ lies on the symmetry axis; a pair of the points $(\pm d_0, 0)$ lie on the Earth's surface; the last two points $(\pm d_1, z_1)$ have intermediate positions; the co-ordinates of these points in the elliptical co-ordinate system can be written as $z = a \operatorname{sh} \varepsilon_0$; $z = a \operatorname{sh} \varepsilon_0$

$-z_0$; $z = a \operatorname{sh} \varepsilon_0 - (z_0 - z_1)$, respectively. The substitution of these values into Eq. (7) gives the following equation system governed by the unknown values a and ε_0

$$\left(\frac{d_0}{a \operatorname{ch} \varepsilon_0}\right)^2 + \left(\frac{z_0}{a \operatorname{sh} \varepsilon_0}\right)^2 - \frac{2z_0}{a \operatorname{sh} \varepsilon_0} = 0;$$

$$\left(\frac{d_1}{a \operatorname{ch} \varepsilon_0}\right)^2 + \left(\frac{z_0 - z_1}{a \operatorname{sh} \varepsilon_0}\right)^2 - \frac{2(z_0 - z_1)}{a \operatorname{sh} \varepsilon_0} = 0. \tag{8}$$

The depth h can be calculated by means of these values from

$$h = a \operatorname{sh} \varepsilon_0 - z_0. \tag{9}$$

The adequacy of this elliptical model with a real ACB can be checked by comparing the ratio of the components H_z/H_x, measured on the Earth's surface, with its theoretical value

$$\left|\frac{H_z}{H_x}\right| = \frac{1}{\operatorname{th} \varepsilon_0 \operatorname{tg} \eta_0}; \quad \operatorname{tg} \eta_0 = \sqrt{\frac{a^2}{d_0^2} \operatorname{ch}^2 \varepsilon_0 - 1}. \tag{10}$$

Thus it can be seen that altitudinal experiments give informations on the depth of ACB, and on the shape of its cross section; moreover, the accuracy of these determinations can be checked by means of several independent methods.

References

Mahmoud S F, Ali S M, Wait J R 1981: Electromagnetic scattering from a buried cylindrical inhomogeneity inside a lossy Earth. *Radio Sci.*, 16, 1285–1298.

Rokityansky I I 1975: Investigation of the conductivity anomalies by means of magnetovariation profiles (in Russian). Naukova Dumka, Kiev

Svetov B S 1973: Theory, methods and interpretation of the results of low frequency electromagnetic sounding (in Russian). Nedra, Moscow

Acta Geodaet., Geophys. et Montanist. Hung. Volume 19 (1—2), pp. 61—70 (1984)

PALEOMAGNETIC GEOCHRONOLOGICAL SCALE FOR THE NEOGENE OF THE CENTRAL PARATHETYS

A M GLEVASSKAYA[1], N P MIKHAILOVA[1], V N TSYKORA[1]

The construction of a magnetostratigraphic time scale for the Neogene of SE-Europe is a difficult problem. Some recent age determinations on paleomagnetic samples from the Soviet Carpathians enabled a more correct scaling. In this paper an attempt is made to create a uniform scale based on about 120 samples. The basis of this work was a separation of normal and reversed polarity epochs, the Transcarpathian (~8 m.y.), the Uzhgorod (12.5 m.y.), and some other earlier (20, 22, 24 m.y.) ones. All these epochs are compared with data from surrounding areas and on this basis their reality is tested. It is concluded that there are many open questions and at present only a first outline for this scale is possible.

Keywords: Central Parathetys; geochronological scale; Neogene time scale; paleomagnetism; Transcarpathian reversed epoch; Uzhgorod reversed epoch

It is a recent but still difficult problem to construct a magnetostratigraphic time scale for the Neogene of South-Eastern Europe and to correlate it with similar scales for the basins of the Black Sea and the Caspian Sea. The point is that the major part of the Neogene sequences were formed within basins of rough topography under conditions of tectonic mobility, heterogeneous facies and multiphase volcanic activity. For the Paratethys, however, the latter enabled to construct a paleomagnetic geochronological scale for the layers covering the magnetic anomaly zones, since these layers are characterized by their biostratigraphy and by their radiometrical age-determinations.

For the volcanic rocks of the Soviet Transcarpathians the paleomagnetic geochronological scale was compiled in the middle of the seventies (Bagdasaryan et al. 1970, Milanovsky et al. 1980) on the basis of detailed geological observations and paleomagnetic studies of practically all the volcanic sequences in the structural and facies zones Chop-Mukachevo and Solotvino, in the Transcarpathian Neogene trough, further by means of the K-Ar dating of the volcanic rocks (from over 60 determinations) whose polarity and magnetization directions were determined experimentally by combined magnetic and mineralogical methods. Fresh samples having been investigated paleomagnetically in the Institute of Geophysics, Kiev, with the purpose to separate the synchronous I_n component, were delivered to the

[1] S. I. Subbotin Institute of Geophysics, Academy of Sciences of the Ukranian SSR. 1252164 Kiev, prospect Palladina 32

Laboratory of Nuclear Geochronology, Institute of Geophysics, Academy of Sciences Armenian SSR where Bagdasaryan performed the K-Ar dating of the rocks. A few datings were made in the Laboratory of Absolute Age, Geological Institute, Academy of Sciences USSR, by Shanin and Arakelyants.

All this work enabled to determine the age interval for the Neogenic volcanism in the Soviet Transcarpathians (16–7[1] m.y.), to identify and describe radiometrically paleomagnetic zones and horizons as well as to trace the main features of the geomagnetic field changes during this period. In particular, from the Transcarpathian data the normal Transcarpathian and reversed Uzhgorod geomagnetic epochs have been defined as corresponding to the ninth and tenth geomagnetic epochs. On the basis of this scale a correlation between the volcanic structures in the Western and Eastern Transcarpathians and those in the Southern Transcarpathians, was established (Krynczyk et al. 1977), but at that time a lack of paleomagnetic and K-Ar datings did not allow to complete the work.

The present study is an attempt to construct a paleomagnetic chronological scale model from the paleomagnetic characteristics of the K-Ar dated volcanic layers representing the entire late-orogenic Carpathian volcanism as well as the platform volcanism manifesting itself within the consolidated structures of the Carpathian region. This work can be accomplished through revising and generalizing all the publications available till 1981 from Bulgaria, Hungary, GDR, Poland, Rumania, USSR and Czechoslovakia. In constructing the scale model we used more than 120 determinations of the Carpathian region each including the paleomagnetic and radiometric characteristics of the same geological object and 40 determinations from Africa, Japan and elsewhere meeting these requirements.

Unfortunately, in constructing the scale a lot of K-Ar datings were to be omitted due to lack of paleomagnetic characteristics. Some of them were made on cores from well-stratified and biologically characterized volcanic-sedimentary deposits. Meanwhile, in the Soviet Carpathians, the magnetization polarity has been determined on non-oriented cores to obtain sufficiently reliable results (Pevzner 1976).

We assume that the major component of the paleomagnetic chronological scale is a paleomagnetic event, i.e. a temporal equivalent of a zone of normal or reversed polarity within the paleomagnetic sequence. Chronological paleomagnetic levels were determined by constructing integral diagrams in which the age intervals were summed up with the determination accuracy (Fig. 1). Rocks showing normal and reversed paleomagnetic polarity were handled separately, i.e. two integral age profiles were plotted — one for the rocks with normal polarity and the other for the rocks with reversed polarity. Maxima on the integral curve of normal polarity and minima on those of reversed polarity made it possible to recognize N- and R-events. Closely

[1] The K-Ar data are recalculated with the decay constant $K = 0.585 \times 10^{-10} y^{-1}$ to provide a possibility of comparing with other planetary scales of geomagnetic inversions.

spaced extrema of opposite polarity provide a high accuracy in determining the ages of the inversions.

Let us analyse the paleomagnetic chronological scale model in Fig. 1. From the size of the areas framed by the integral curves it can be concluded that the Neogene epochs of normal and reversed polarity are almost tantamount, the latter even slightly dominant. Moreover, the amount of datings in relatively young volcanics—younger than 16 m.y. (the lower boundary of the Middle Miocene)—is surprisingly great. This may be explained by the absence of older volcanics in such a well-studied area as Soviet

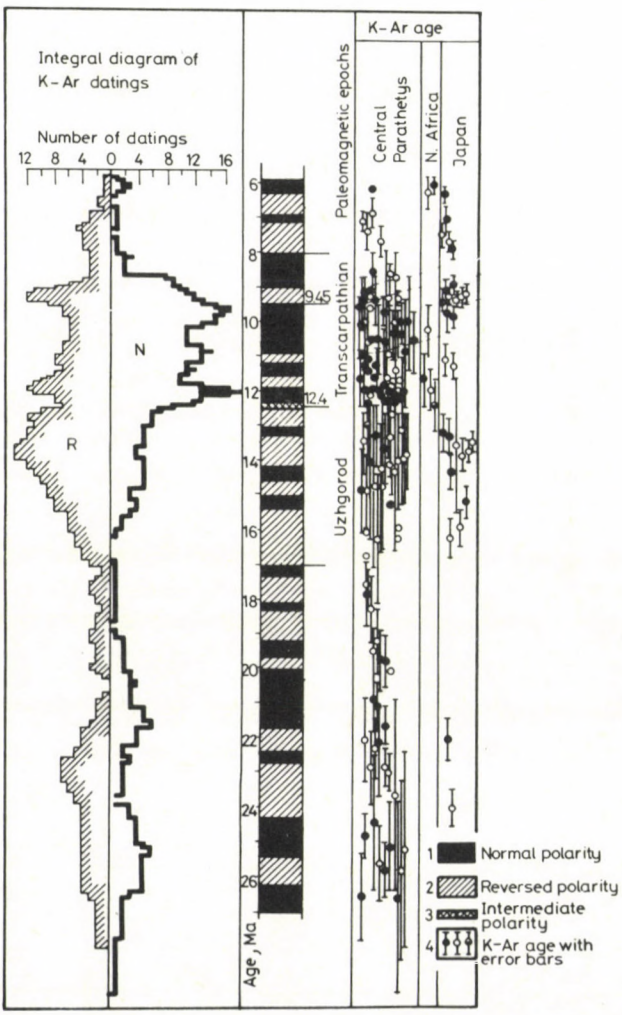

Fig. 1. Integrated diagrams of paleomagnetic data and K–Ar determinations for the Central Paratethys

Transcarpathia, but it is not beyond probability (on account of data from North Africa and Japan as well) that in the time period between 20 and 17 m.y. ago the volcanic activity was weak over vast areas of the Earth.

The existence of the Transcarpathian normal and Uzhgorod reversed epochs which were determined at first in the Soviet Union are supported by the followings: The inversion at 12.4 m.y. marking a transition from reversed to normal polarity seems to be very well confirmed on the scale. The time of 9.45 m.y. of the inversion from normal to reversed polarity is also determined quite reliably. We do not regard, however, this inversion to be the upper boundary of the Transcarpathian epoch, for among the volcanic rocks dated between 9 and 8.5 m.y. normally polarized rocks are dominating. This is probably the lower boundary of one of the reversed events in the Transcarpathian epoch.

The reversed polarity boundaries at the epochs 20 m.y., less than 22 m.y., 24 m.y. and some other ones are regarded as reliable. The ages of these and other inversions can be specified by increasing the accuracy of K-Ar dating, on the one hand, and by accumulating more paleomagnetic and isotopic datings, on the other.

The proposed procedure of constructing a paleomagnetic geochronological scale has of course some drawbacks. It would be better to generalize the scales derived from the most representative specific sections and evaluate their stratigraphy, age range, possible discontinuities, etc. This very way was followed at the first stage of paleomagnetic studies in the Soviet Transcarpathians (Glevasskaya and Mikhailova 1973, Milanovsky et al. 1980). Here, paleomagnetic sections were plotted on the basis of combined paleomagnetic studies and large scale geological mapping, but in the rest of the Carpathian region, this kind of work has not yet been completed. Moreover, the character of the volcanic section—consisting predominantly of continental type volcanic rocks and sedimentary components with reliable biostratigraphic characteristics being scarce—hamper the paleomagnetic and radiometric analyses of the correlated biostratigraphical levels what would be the most logical approach of the problem. In course of the paleomagnetic studies of volcanic rocks in the Transcarpathian trough the paleomagnetic and K-Ar data sometimes helped to introduce important corrections into the stratigraphic section of the volcanic layers (Glevasskaya and Mikhailova 1973). The difficulty is that we have to solve several problems at once, such as plotting paleomagnetic sections and correlating them separately (generally they have few data in common) by stratigraphic and paleomagnetic features. One thing is evident: a complete analysis of the paleomagnetic data together with K-Ar datings would be in itself very important.

Considering the mentioned difficulties we attempted to systematize the paleomagnetic data available on the Neogene of the Central Paratethys. Hereby we used the informations about the geochronology of the Neogene stratotypes in the Central Paratethys from Seneš (1979), Vass and Slavik (1978), Bagdasaryan et al. (1977) presented in Table I. The problem of comparing these data with the

Table I.

International geological time scala			Central paratethys			Standard biozones			K–Ar dating m.y.			Transcarpathian trough	
			Stages		Zones	Zone No.	NF	NP	Bagdasaryan et.al. (1977)	Vass (1979)	Seneš (1979)	Vyalov et.al. (1977)	
							Seneš (1979)					Biozones	Suites
Pliocene								19*		2.0			
	Upper		Rumanian			17		18*					Ilnitsky–Gutinsky
	Middle		Pannonian		G F	16		12* 11*	7.9–9.1	5.05	Pannonian–Rumanian radiometrically unspecified	E	
	Lower				E	15						Д	Koshelevsky
					C–D				10.7			Г В	
Miocene	Meotice				A–B according to Papp	14		11				Б A	Izovsky
	Sarmatian	Upper	Sarmatian	Upper	Nonion granosus	13	16	10	11.2	10.5 – 11.0		Porosononion subgranosum	Almashsky
		Middle		Middle	Elphidium haerinum	12	15		11.3 – 13.9	11.5 – 12.5		Quinguloculina reussi	Lukovsky
		Lower		Lower	Elphidium reginum	11	14	9	13.1 – 13.5			Cibicides aff. badenensis	Dorobratovsky
	Tortonian	Upper	Badenian		Rotalia	10 9	13	8 7	13.5 – 16.6	13.3	13.3–13.5	Streblus becc. cassibulina crista	Darolinsky Neresnitsky
					Bulimina bolivina								Tyachevsky Shandrovsky
					Arenaceous foraminifer	8	10	6				Arenaceous foraminifer	Solotvinsky
		Lower			Spirotectomzina carinata					15.0			Tereblinsky
					Langenidae	6–7	9	5	15.1 – 17.7	16.5		Urigerina asperula	Talaborsky
	Helvetian	Upper	Karpatian		Globigerina sicanus	5	8	4			16.5	Candorbulina universa	Novoselitsky
		Lower	Ottnangian		Globigerina trilobus	4	7						
	Burdigalian		Eggenburgian		Globigerina degescens		6	3	20.7	Radiometrically unspecified	19.0		Burlakovsky
							5	2	21.9		22.5		
	Aquitanian		Egerian		Globigerina primordus	3 2	4	1					Negrovsky
Chatt					Globigerina opima	1							

paleomagnetic chronological scale model becomes easier by the fact that both the K-Ar dating and and the track-dating (which often coincide) are considered to be the most reliable ones for the whole region. Moreover, a steadily increasing amount of data indicates coincidences of the paleomagnetic levels with stratigraphic boundaries, with tectonic reactivation, with increase or attenuation of the magmatism. In the following analysis of the paleomagnetic scale all these factors will be taken into account.

From the magnetization of the alkaline volcanoes in Lower Silesia (Krynczyk et al. 1977) and Saxony (Todt and Lippolt 1975) it has been concluded that the Miocene base is the epoch of the primarily normal polarity with some manifestations of reversed polarity, too. The epoch was followed by a long period of reversed geomagnetic field. The alkaline volcanoes belong mainly to the Egerian, but within that to different substages as an analysis of published data have proved. The boundary between normal and reversed polarity at the epoch 24 m.y. which is one of the most reliable in the model scale, is in surprisingly good agreement with the lower boundary of the Mediterranean Aquitanian (Seneš 1979) which passes within the Egerian and separates the Oligocene-Miocene "boundary stratotype" from the Upper Egerian. This may, therefore, suggest that the paleomagnetic boundary near 24 m.y. is the Lower Miocene, i.e. it marks the border between the Paleogene and the Neogene.

The next stage of the Early Miocene—the Eggenburgian—is estimated to about 3.5 m.y. (from 22.5 to 19.0 m.y. ago). This is a zone of mainly normal polarity, its lower age boundary corresponds probably to the boundary between the Egerian and the Eggenburgian.

It should be noted that components of this age are not present in the Miocene section of the Soviet Transcarpathians. In the Transcarpathian trough, the Neogene starts with the Burlakovsky sequence rich in Burdigalian mollusks, but the Helvetian formations overlying them, were almost totally destroyed by the Tortonian transgression. Reliable data on magnetization character and geochronology in this part of the Transcarpathian Neogene are very scarce. Some of them, however, can be found elsewhere. According to recent reports (Krynczyk et al. 1977), the Lower Eggenburgian is comparable with the Mediterranean Aquitanian; the Middle and Upper Eggenburgian as well as the younger Ottnangian and Karpatian with the Mediterranean Burdigalian. At the same time, the Central Paratethys Ottnangian corresponds to the Early Helvetian in West Ukraina and to the Kotsakhuri stage in West-Georgia. The Sakarauli-Kotsakhuri section (Ananishvili and Pevzner 1976) is characterized by R and N-polarities which are alternating. The Lower Helvetian in West-Ukraina and the Tarkhanian stage in the coastal area of the Black Sea are similar to the Karpatian. The Trakhanian stage has distinctly normal polarity (Milanovsky et al. 1980). The K-Ar dating of the South Slovakian rhyodacite tuffs intercalating with the Lower Karpatian pelagic sediments gives 20.7 and 19.4±1 m.y., respectively (Bagdasaryan et al. 1977). It follows from Seneš (1979), however, that the

geochronological Ottnangian interval is 19 to 17.7 m.y. old, while the top of the Karpatian rises up to 16.5 m.y. This version of the scale does not include a distinct and long enough magnetic period of normal polarity that could be compared with the Tarkhanian. The geochronology of this interval needs to be specified, as the number of paleomagnetic and K-Ar determinations is not sufficient.

Comparison between the Helvetian-Tortonian boundary (the Karpatian-Badenian in the new scale for the Central Paratethys) and the Mediterranean and Central Paratethys biozones gives for this boundary the age between 16.5 (Seneš 1979) and 16.27 (Vass and Slavik 1978) m.y. In the Transcarpathians, the Early Tortonian age is brought into connection with the earliest manifestations of the liparitic volcanism namely, to the Novoye Selo plagioliparite tuffs of 700 m thickness having the age of 15.7 ± 0.5 m.y. according to the K-Ar dating, (Bagdasaryan and Danilovich 1968) with reversed magnetization in the upper part of the section. Since all the Lower Badenian volcanic layers are placed within the age range between 17.7 and 15.1 m.y. (Seneš 1979), it is assumed that this magnetic period belongs to the upper part of the Lower Badenian (Lower Tortonian of West Ukraina).

In the section of the Transcarpathian Upper Tortonian, paleomagnetic horizons of opposite polarity alternate. The Talabor sequence is normal; both normal and reversed magnetizations are observed in the Treblinka sequence. A stable zone of normal magnetization is marked by the Nankov and Kovach tuffs widely developed in the Solotvin Depression. Thus the Later Tortonian, on the whole, can be considered as an epoch of predominantly normal polarity, which is in good agreement with the idea of similarity of the Late Tortonian and Late Badenian to the Konsky stage. The latter has mainly a normal polarization with an R-horizon in the middle of the section (Ananishvili and Pevzner 1976). The K-Ar datings of the Late Tortonian volcanic layers are concentrated within the range between 16.6 and 13.9 m.y. (Bagdasaryan et al. 1977), but the former number seems to be too big. The Transcarpathian plagioliparite tuffs from the second supersalt horizon (borehole in the village Bushtano), i.e. from the Teresvin sequence are dated as 15.7 m.y. (Bagdasaryan and Danilovich 1968).

The Upper Tortonian of the Central Paratethys marks the end of a long-lived connection with the basins of the Mediterranean Sea and Indian-Pacific Belt; the remaining basins are not connected, therefore, shallow pelagic and continental facies appear and the volcanism intensifies itself. With the present endemic fauna and the lack of organic remains the significance of paleomagnetic and geochronological data increases considerably.

The Sarmatian time lasted, probably, from 13.5 till 11–10.4 m.y. (Seneš 1979). If it is true, it is in the Sarmatian, that the most of the andesite-basaltic volcanoes of the East-Carpathian Belt were formed and the silicic volcanism of the Pannonian Massif came to an end. Meanwhile, most of the Transcarpathian geologists claim that the volcanic activity maximum, at least in the Soviet Transcarpathians, occurred in the

Pannonian and Levantinian age. Let us consider in detail the paleomagnetic and geochronological positions of these volcanic rocks.

In the Transcarpathian trough, the Sarmatian deposits are represented by the Lower Sarmatian Dorobratovsky sequence corresponding to the Nizhnevolynsky horizon (the zone with the species of *Cibicides badennensis* and *Elphidium reginum*), by the Lower Sarmatian Lukovsky sequence correlating with the Verkhnevolynsky horizon (the layers with *Cardium transcarpaticum, Quinqueloculina reussi*), as well as by the Middle Sarmatian Almashsky sequence. The Upper Sarmatian rocks together with the lower horizons of the Pliocenic section constitute the Pannonian deposits.

Ananishvili and Pevzner (1976) show that the lowermost part of the Lower Sarmatian has reversed magnetic polarity, whereas the overlying portion of the West-Georgian section includes a zone of reversed magnetization. On the Taman Peninsula, the Lower Sarmatian section of 115 m thickness is, mainly normally polarized, but in its middle part there are 17 m of abnormally polarized and 11 m of reversely polarized rocks. The Middle Sarmatian starts with rocks of normal polarization containing a 12 m thick reversed horizon in its middle, whereas the upper parts of the Middle and the lower parts of the Upper Sarmatian are weakly magnetized; then comes a normal stratum with an R-event in the middle.

The section of the Lower Sarmatian Dorobratovsky sequence revealed in the Beregovo region is considered as the most representative between the others in the Transcarpathians. Here, the layer sequence has a thickness of a few hundred meters and includes several subsequences and benches. The whole section of the Dorobratovsky sequence, perhaps with except of its lowermost part, has reverse magnetic polarization. All the components, composing the section of the middle and upper Dorobratovsky subsequences (sediments, silicic volcanic rocks, metasomatites) are uniformly magnetized and form a single paleomagnetic horizon. Similar magnetization is characteristic of the rhyolites whose domes and flows are, evidently, related to the boundary between the Dorobratovsky and Lukovsky time. The K-Ar dating of rhyolites gives 14 ± 0.2 m.y. for normal rocks (Mount Khaesh) (Milanovsky et al. 1980).

There are also some data on the Sarmatian volcanic layers in East Slovakia. In the Ruskovsky Basin, the marl deposits marked by *Elphidium reginum* typical of the Lower Sarmatian are underlain by normal andesite of an age of 13.6 ± 1 m.y. The andesite tuff intercalating with sediments of the Nyshlyansky layers and also containing *Elphidium reginum* is dated as 13.1 ± 1.1 m.y. Data of polarity are not available (Bagdasaryan et al. 1977). These volcanic rocks can evidently be related to the Lower Dorobratovsky time, but the low accuracy of K-Ar dating cannot ensure a comparison to the Transcarpathian sections. Similar ages are known for some perlites and rhyolites in the Beregovo region (Bagdasaryan and Danilovich 1968, Bagdasaryan et al. 1977), but the accuracy of the dating here is also low. The Middle Sarmatian

Almashsky sequence of the Transcarpathians is represented mainly by weakly magnetized and poorly studied rocks. Here, the Middle Sarmatian andesite near Shalanka is characterized by normal magnetization and a K-Ar age (recalculated for the new constant) of 13 ± 1 m.y.

All the younger rocks of the Transcarpathian trough belong geologically to the Pannonian and Levantinian. The K-Ar dating of the Soviet Transcarpathian volcanic rocks shows that they were formed not earlier than 7.6 ± 0.6 m.y. ago (Mikhailova et al. 1974); the younger complex volcanic structures of Rumania are dated in the volcanic massives of Kaliman (7.37 ± 0.66 m.y.) and Gurgiu (7.15 ± 0.60 m.y.) where the last eruption occurred 3.92 ± 0.20 m.y. ago.

Numerous polarity and age data on volcanic rocks in the Vyhorlat-Gutin Ridge show that there the zone of mainly reversed polarity was formed in the period between 13.3 and 12.4 m.y., which by no means corresponds to the Levantinian (the Upper Pliocene), but rather to the very beginning of the Pannonian, since the beginning of the Meotian (the Upper Pannonian, Kishelevsky sequence) is estimated as 12.4 m.y. ago. The boundary between the reversed Uzhgorod and the normal Transcarpathian geomagnetic epochs can be suggested to coincide with the interface marked in continental sections by hipparionic fauna. Gabunia and Rubinstein (1965), Milanovsky et al. (1980) consider it the boundary between Miocene and Pliocene. Nevertheless, considering paleomagnetic data on the Lower Pliocene derived from the Pontian-Caspian sections where the reversed zone includes both the Lower and Middle Meotian (with an N-event in the latter), the Upper Meotian is normal and the Pontian represents a new zone of stable reversed magnetization, and taking into account that the boundary between the Meotian and the Pontian is approximately at 10 m.y., one may suggest that the Uzhgorod epoch includes the major portion of the Meotian, whereas the Transcarpathian epoch includes, at least, its upper horizon. The upper boundary of the Transcarpathian epoch remains to be specified as does the correlation between the reversed volcanics in the Soviet and Rumanian Carpathians dated to 7 m.y. and the Pontian.

The foregoing makes it possible to reject the age determination of the volcanic rocks in the Vyhorlat-Gutin Ridge as Levantinian and do the same with regard to the most of the volcanic massives in Rumania. As known, the Levantinian deposits in Rumania are found above the Dakian stage which are the counterpart of the Pontian and Cimmerian in the Black Sea. Only the pyroxene postcalderic andesite of 3.92 ± 0.20 m.y. in the Maderash volcano can be considered as Levantinian, which, in combination with its reversed magnetization, can be related to the Gilbert geomagnetic epoch. Thus, in spite of a large amount of stratigraphic and geochronological data, our opinion is that the problem of constructing the paleomagnetic geochronological scale for the vast region of South-East Europe has been only outlined. It is quite evident that it cannot be solved without finding the connection between geochronological and biostratigraphical data and between them

and the detailed analysis of the geological environment in the areas of reference sections. It should be emphasized that it is absolutely necessary to study the paleomagnetic sections of the volcanic-sedimentary sequences in which the rocks must be dated by both methods.

References

Ananishvili G D, Pevzner M A 1976: Paleomagnetic section of the West Georgia Miocene. In: *All-Union Congress Abstracts, part 3, Main geomagnetic field and the problems of paleomagnetism* (in Russian). Moscow, 9.

Bagdasaryan G P, Danilovich L G 1968: New data on the absolute age of the Transcarpathian volcanic rocks (in Russian). *Izv. AN SSR, ser. Geol.*, No 9, 15–23.

Bagdasaryan G P, Glevasskaya A M, Mikhailova N P 1970: On the absolute dating of the paleomagnetic zones in the Vihorlat-Gutin ridge sections. In: *8-th Congress Materials, part 2 (The questions on paleomagnetism, geomagnetism and archaeomagnetism)* (in Russian). Kiev, Naukova dumka, 30–35.

Bagdasaryan G P, Slavik J, Gukasyan R K, Vass D 1977: Geocronology of the Parathetys Neogene (in Russian). *Izv. An AN SSSR, ser. Geol.*, No 2, 62–72.

Gabunia L K, Rubinstein MM 1965: Biostratigrafic parallelization of the Cenozoic sediments of Eurasia and North America in the light of absolute geochronology data (in Russian). *Izv. Geol. Soc. of Georgia AN GSSR*, 4, 7–27.

Glevasskaya A M, Mikhailova N P 1973: Transcarpathian Neogene volcanic rocks stratification in the light of paleomagnetic data (in Russian). In: *Volcanism and mineral deposits forming in the Alpine geosynclinal belt*. Novosibirsk. Ed. AN SSSR, 41–47.

Krynczyk J, Kadzialko-Hofmokl M, Elenska B, Birkenmajer K, Arakelyants M 1977: Tertiary polarity events in Lower Silesian basalts and their K-Ar age. *Acta Geophys. Polonica*, 25, 183–191.

Marton E P, Marton A M, Romanescu D, Glevasskaya A M, Mikhailova N P, Tretyak A N, Tsykora V N, Orlicky I, Pagach P, Pasteca W, Yanak F 1972: Paleomagnetism of volcanic formations of the Carpathian region (in Russian). *Geofiz. Sb. AN UkrSSR*, 45, 3–8.

Milanovsky E E, Kozhevnikov A V, Birman A S, Kopp M L, Raszvetaev L M, Trubikhin V M 1980: Upper cenozoic stratigraphy of Alpine belt of Eurasia on the paleomagnetic basis (in Russian). In: *Proceedings of the XI Congress of CBGA, Stratigraphy*. Kiev, Naukova dumka, 148–156.

Mikhailova N P, Glevasskaya A M, Tsykora V N 1974: Paleomagnetism of the volcanic rocks and neogene geomagnetic field reconstruction (in Russian). Kiev, Naukova dumka

Pevzner M A 1976: Paleomagnetism of the Taman peninsula Mio-Pliocene (in Russian). In: *All-Union Congress Abstracts, part 3 (Main geomagnetic field and the problems of paleomagnetism)*. Moscow, 73.

Seneš J 1979: Geochronologie des stratotypes des étages du Miocene inferieure et moyen de la Paratethys Centrale utilisable pour la correlation globale. *Geol. Zb. Geologica Carpathica*, 30, 99–108.

Todt W, Lippolt H 1975: K-Ar Altersbestimmungen an Vulkaniten bekannter paleomagnetischer Feldrichtungen. II. Sachsen, *Z. f. Geophys.*, 41, 641–650.

Tsykora V N 1976: Estimation of the magnetic polarity of the unoriented samples and magnetic orientation of cores. In: *Paleomagnetism, magnetism, geomagnetic field*. Kiev, Naukova dumka, 98–109.

Vass D, Slavik J 1978: The radiometric calibration of Paratethys Neogene. Geologicke prace. Spravy. Bratislava, *GUDS*, 63, 131–139.

Acta Geodaet., Geophys. et Montanist. Hung. Volume 19 (1—2), pp. 71—79 (1984)

COMPREHENSIVE ANALYSIS OF PHYSICAL FIELDS IN THE REGION OF THE CARPATHIANS AND DINARIDES

V V GORDIENKO[1]

Seismological, geothermal, geoelectrical, gravity and magnetic data are considered along five lines crossing various zones of the Carpathians and Dinarides and extending into other (platform and active) areas.

Anomalies of physical fields are shown to be related to lateral variations of the physical properties of crustal and upper mantle rocks. Mantle inhomogeneities can be accounted for by a deep process of polymorphic advection and partial alteration of the mantle material.

Keywords: Carpathians; crustal structure; Dinarides; geophysical model; tectonosphere

The anomalies of the fields studied in geophysics are caused by deviations in the physical parameters of the material in the Earth at a certain depth. These deviations again are the results of structural inhomogeneities in the Earth's crust, of lateral changes in the temperature and in the state of the mantle material.

In areas where the Earth's crust has been studied by seismic deep soundings (SDS), the effect of the first factor can be rather exactly taken into account. For this purpose density, magnetic and heat generation profiles should be constructed on the basis of the velocity profile of the crust and from them, the primary effects can be determined. In the present paper for the computation of these values the following formulas shall be used:

$$A_{os} = 1.35\ \mu\text{W m}^{-3}$$
$$A = 1.4 \exp 1.25\,(6 - V_p) \quad (V_p \text{ in kms}^{-1} \text{ units})$$
$$HF_m = 11 \pm 5\ \text{mWm}^{-2}$$
$$A = 1.4 \exp 5\,(2.7 - \sigma) \quad (\sigma \text{ in g cm}^{-3} \text{ units})$$
$$\sigma_{os} = 2.0 - 2.8 \quad \sigma_M = 3.3\ \text{g cm}^{-3}$$
$$\sigma = 2.7 + 0.25\,(V_p - 6)$$
$$I = V_p - 5.8 = 4\sigma - 10.6 \quad (I \text{ in } A\ \text{m}^{-1} \text{ units}), \text{ where}$$

A — heat generation, A_{os} — heat generation of sediments, V_p — compressional seismic velocity, HF_m — mantle heat flow from platform, σ — density, σ_{os} — density of sediments (from local data), I — magnetization.

[1] S. I. Subbotin Institute of Geophysics, Academy of Sci. of the UkSSR, 252164 Kiev–164, prosp. Palladina 32

This formulas establish connections between the velocity of the longitudinal seismic waves and other parameters of the crustal rocks. They were obtained for crustal temperatures in platform areas, in the warmer crust of the active areas a small correction is to be used. These formulas were confirmed by model experiments along DSS profiles on Precambrian platform areas, where no rapid changes of the mantle temperatures and therefore no changes connected with them can be expected. A comparison of the computed thermal and gravity fields along several thousand km long profiles on different platforms (East-European, North-American, Sibirian, Australian platforms) with the observed ones have shown that with few exceptions the formulas yield quite correct values for the regional anomalies. Thus they are reliable, and also the general lack of mantle anomalies due to lateral inhomogeneities of the mantle material holds. That means that in a first approximation it can be considered as of constant composition and the mantle anomalies in certain areas should be connected with thermal effects (and partly with polymorphous transformation of the rocks due to these thermal anomalies).

Naturally this confirmation could be understood only as within a certain error limit. This limit can be rather well expressed by the error limits of the computed fields: these are for the gravity field $20–25 \times 10^{-5}$ m s^{-2}, for the thermal field 5–7 mW/m^{-2} (Buryanov et al. 1980a, 1980b, Gordienko 1980, Gordienko et al. 1982). Evidently only anomalies of significantly greater amplitudes can be detected.

The expression for the magnetization of the rocks has not been confirmed by such a massive data material. Anyway it can be used for the explanation of many regional anomalies on platform areas, but the results of comparisons with observed fields also show that the connection is violated much more often than those of the density and of the heat generation. When modeling the magnetic field of greater areas it is unavoidable to collect local informations about the magnetization of the rocks.

A computation of the resistivities of rocks in the crust and in the mantle of platforms shows that within the whole tectonosphere (till the conducting bottom of the upper mantle, at 400 km) no zone of a sudden decrease of the resistivity due to thermal causes could be found where the summarized conductance would be more than a few hundreds S. Some isolated crustal conductive zones can be bound to various rock-types in the crust.

Thus in platform areas all regional anomalies of the fields are connected with crustal anomalies within the given accuracy limit. A completely other situation is present in active areas, mainly in recent geosynclines and in zones of fractural magmatic activization and the Carpatho-Dinarids area to be discussed belongs to these regions. When the computed effects due to crustal sources are compared with the observed ones on platforms adjacent to the Carpatho-Dinarids region, strong deviation is found in its central part. Evidently there are enormous mantle anomalies here which can be reliably separated and used in the interpretation. On the basis of the

interpretation of any of the fields, one particular aspect of the deep source is obtained. In addition they will have many unambiguities due to interpretational problems. A more complete and reliable result is obtained from a complex analysis of the physical fields. Its result will strongly depend on the primary hypothesis, i.e. on the first approximative model. Therefore it is logical to use as such models, geologically motivated ones which correspond to one hypothesis about the deep processes. We used as such a model the polymorphous-advective hypothesis.

This hypothesis considers the following sequence of events in the development of geosynclines (Gordienko et al. 1982). When the heating of the upper mantle reaches a certain level, its lower part loses its stability and lifts into the upper part in form of asthenolites, whereby relatively cold parts of the upper mantle take their place. Till the temperature of these masses reaches the temperature in their surroundings, some hundred million years pass away, therefore the asthenolites cannot return to their earlier place, thus the movements of the masses have a non-closed, advective character. The descent of cold masses into deeper parts of the upper mantle causes a decrease in the depth interval where asthenolites can be produced, thus the intensity of the process decreases exponentially with time, and 130 million years after the beginning of the process (about 60 million years after folding) it fully expires. The shift of these masses into different pressure and temperature conditions leads to polimorphous transformations with different signs in immense rock masses. This phenomenon together with the vertical branch of the streaming and with the forces of the isostatic adjustment (which appears with the crustal transformations) cause vertical movements in the corresponding region.

In wider geosyncline areas (as e.g. in the Carpatho-Dinarids region) the horizontal component of the movements is also significant, while in narrow ones (as e.g. the Caucasus) it is insignificant.

By summarizing the thermal effects of the asthenolites, a thermal model of the processes can be quite easily constructed in different stages (Fig. 1). With present values of the parameters of the crustal and mantle material a qualitative description can be given for the main events in the near-surface zone which corresponds to deep processes. The explanation starts with the sinking of the geosynclinal trough beginning about 110 million years ago, then the rebuilding of the crust follows—a thinning out below the centre of the geosyncline and a thickening at its peripheries—30 million years ago, the folding and the episodic magmatism began 25 million years ago and has continued till the near geologic past, the foredeep and the end of its sinking, the mountain-building in the folded zone and the formation of the transmountain deep are in the next stage of the development.

This hypothesis enables to explain (by a more limited advection than that below the geosyncline) other active geologic processes on the continents, too. This is especially true for the construction of a model for the magmatic activization in one of the forelands of the Carpatho-Dinarids area, i.e. in the Czech Massif.

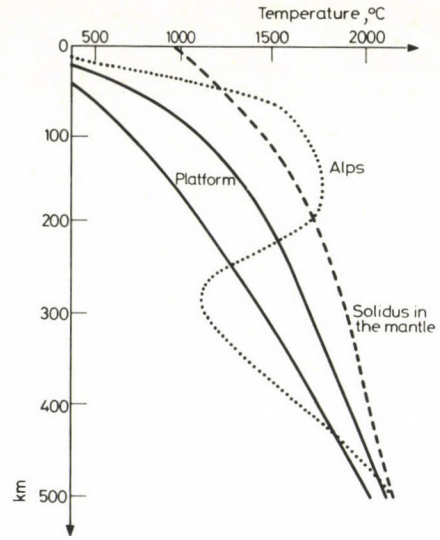

Fig. 1. Mantle temperatures in various regions

The thermal models in the core of the active regions, the ideas about the distribution of the anomalous temperatures till depths of about 500 km as deviations from the normal values also enable the construction of models for other physical parameters. They are generally connected with the temperature and also with the polimorphous transformations during the process. In the upper layers of the advection (mainly in the zones of the probable partial melting) the density, the velocity of the seismic waves, and the electric resistivity are strongly decreasing. The Curie-isotherm of the magnetic minerals is shifted upwards in relation to platform areas. In the lower layers the situation is just the opposite one. By taking into account the anomalies of the physical parameters, an estimation can be given for the primary effect and it can be compared to mantle anomalies. Such a study was made for many regions in Eurasia along DSS profiles. One part of them is shown in Fig. 2. Here profiles are also shown which cross the Carpatho-Dinarids system, starting from forelands of different types: from the Volyno-Podolian and Adriatic epi-Baikalian shields, from northeast through Poland (in latter case through a narrow zone of a Paleozoic platform), from the activated epi-Hercynian platform of the Czech Massif and from the Alpine zone of the Eastern Alps.

Figure 3 shows the profiles I and IV. Let us compare the observed and computed fields along them. The heat flow as result of the radioactive decay in the Earth's crust and of the normal heat flow from the non-activated platform-mantle, explains the value only in the area of the East-European platform. Further to the West, in the Carpathians and Alps, the heat flow reaches values of 40–50 mWm^{-2}. The

Fig. 2. Location of the profiles

introduction of a thermal model according to our hypothesis enables to reach a much better agreement. The same situation occurs in the gravity field: it can be fully explained by crustal effects on the platforms and it differs from this value by 200–250 m s^{-2} in Alpine areas. The difference in the comparatively narrow Alpine zone is less than in the wide Carpatho-Dinaride region. The effects of the anomalous mantle densities enable a much better approximation. The rest in Pannonia is not very big, but a stable difference of about $40 \cdot 10^{-5}$ m s^{-2} exists here. These differences can be well explained by the high temperatures and the corresponding lower velocities of the seismic waves in the crust and mantle of the Carpathians, Pannonia and Alps in comparison to platform areas. This decrease is especially strong (in the crust it cannot be seen due to the small scale of the picture) where according to thermal models, a melting is likely. Only the velocity in the zone of depths between 25 and 55 km in Pannonia is an exception. Here the observed value is significantly, by 0.8 km s^{-1} higher than the computed one.

The zones with higher electric conductivities in the crust and mantle can also be quite well explained by the situation of the zones of partial melting.

A strong change in the depth of the Curie-isotherm of the magnetite at the boundary of platforms and geosynclines—from 80 to 15 km—causes intensive anomalies which roughly coincide with the observed ones. In the active parts there are practically no regional anomalies: above the Curie-isotherm only weakly magnetized rocks can be found. This is also confirmed by independent data from an analysis of the edges of the local anomalies: they are in depths of 15 ± 4 km, and according to thermal models, in depths of 14 ± 1 km.

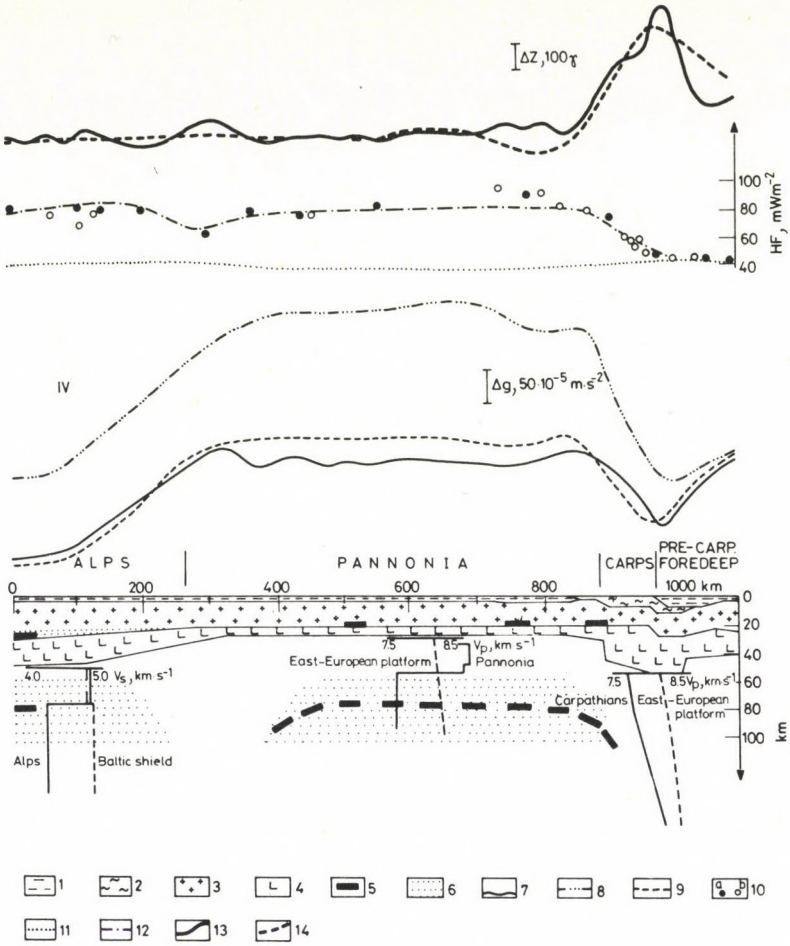

Fig. 3. Geophysical model for the tectonosphere along profiles I and IV. 1 — non-folded sediments, 2 — folded, 3 — "granitic" layer, 4 — "basaltic" layer, 5 — top of the conducting layer from MTS, 6 — partial melting intervals from the thermal model, 7–9 — gravity values: 7 — observed, 8 — crustal effect, 9 — effect with that due to anomalous densities in the mantle, 10–12 — heat flow: 10 — observed (a — single, b — groups of observations), 11 — background radiogenic, 12 — with thermal models for active regions, 13–14 — magnetic field: 13 — observed, 14 — computed

Similar results were obtained from the other profiles, too, see Figs 4 and 5. It deserves special attention that in the area of Profile III (Fig. 5) the field is completely anomalous as consequence of the fact that it reaches the area of the Czech Massif, where the effects of the Hercynian geosyncline and the Neogene activization are combined.

Thus the presented model for the interpretation (the hypothesis about deep processes) can explain not only the main geologic facts in this region, but also the

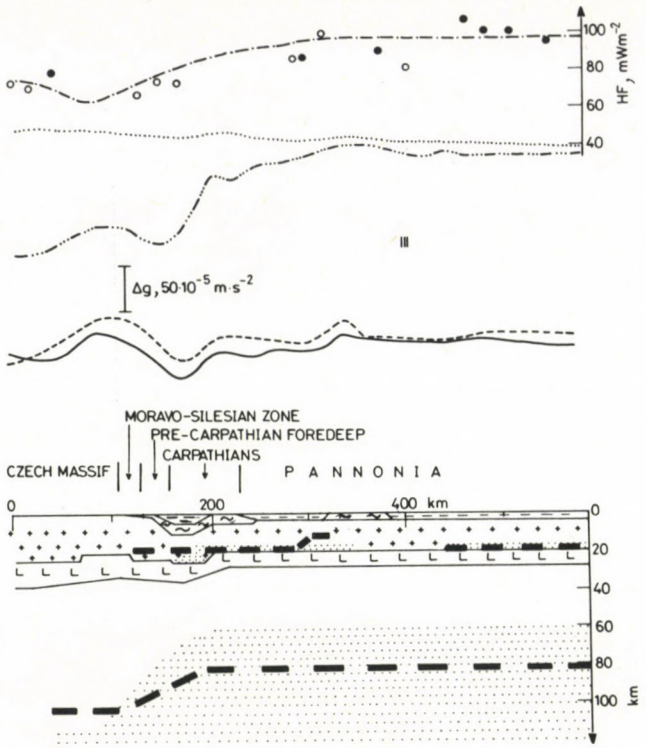

Fig. 4. Geophysical model for the tectonosphere along profile III. Legend as in Fig. 3

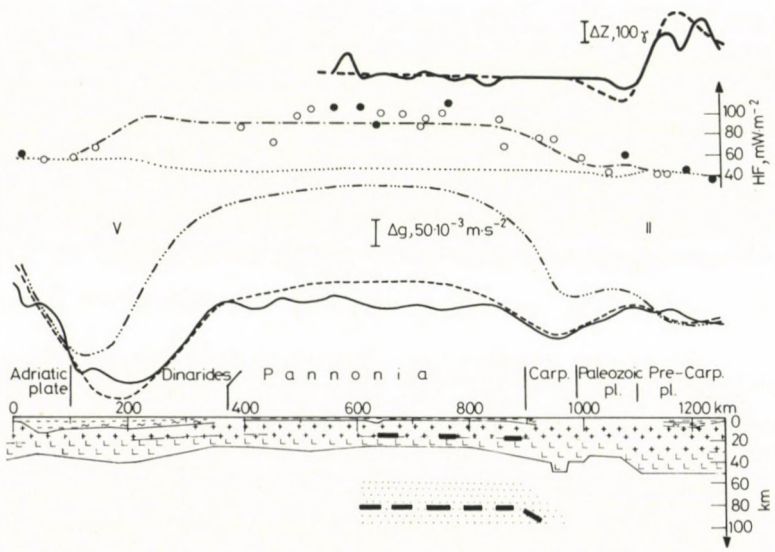

Fig. 5. Geophysical model for the tectonosphere along profiles II and V. Legend as in Fig. 3

anomalies of the physical fields along DSS profiles (Structure of the Earth's crust, 1978, 1981).

There remains only one difference of the computed and observed fields: the density of the mantle below Pannonia should be lower and the velocity of the seismic waves higher than the computed ones. For an explanation of this effect the fall of iron-containing minerals in the mantle rocks (Semenova 1982) is proposed. This process is according to the opinion of Abramovich and Klushin (1978) and others very characteristic for the topmost part of the mantle below magmatic zones and it is very common in the Pannonian Basin.

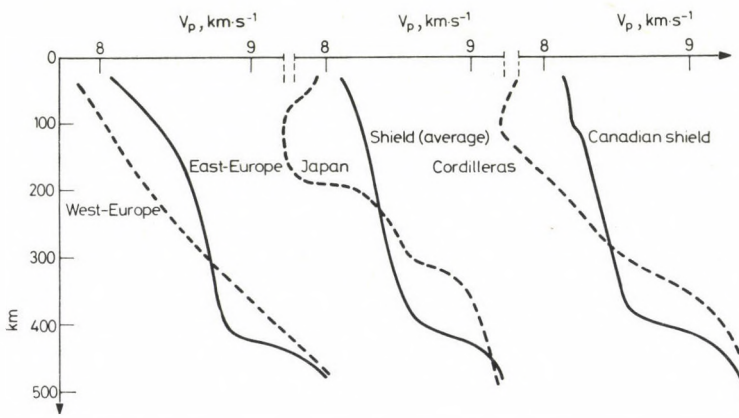

Fig. 6. Distribution of seismic velocities in the upper mantle in several regions

It is regrettable that there is no very deep velocity profile here. But exactly this would be the final proof of the correctness of the advection hypothesis: in the topmost part of the upper mantle the seismic velocity should be lower than the corresponding value below the platform areas, and in the lower parts it should be higher. Let us carry out such a comparison for the studied area (Fig. 6). It can be seen that a characteristic difference can be observed between the geosynclinal West-Europe and the platforms of East-Europe, between the Cordilleras and the Canadian shield, between Japan and the average profile of the shield areas.

References

Abramovich I I, Klushin I G 1978: Petrochemistry and deep structure of the Earth. Nedra, Leningrade

Buryanov V B, Gordienko V V, Kulik S N eds 1980a: Comprehensive geophysical model for the structure and evaluation of the lithosphere of the Carpathians and the Central European Hercyinides. In: *The tectonosphere below the Ukraine and other regions of the USSR*. Naukova Dumka, Kiev, 17–24.

Buryanov V B, Gordienko V V, Kulik S N eds 1980b: Comprehensive geophysical model for the lithosphere below the West-Carpathians, Czech Massif and Saxo-Thuringian zone (along the International DSS Profile). *Geophys. Zhurnal,* 2, No 3, 3–13.

Gordienko V V 1980: Radiogenic heat generation in the Earth's crust and heat flow from the mantle of ancient platforms. *Geophys. Zhurnal,* 2, No 3, 35–42.

Gordienko V V, Zavgorodnyaya O V, Yakoby N M 1982: Heat flow in continents. Naukova Dumka, Kiev

Semenova S G 1982: On petrophysical interpretation of the velocity distribution in the Earth's crust and in the upper mantle. *Geophys. Zhurnal,* 4, No 2, 73–77.

Structure of the Earth's crust and upper mantle in Central and Eastern Europe. 1978. Naukova Dumka, Kiev

Structure of the Earth's crust in Central and South-Eastern Europe. 1981. Naukova Dumka, Kiev

Acta Geodaet., Geophys. et Montanist. Hung. Volume 19 (1—2), pp. 81—91 (1984)

GEOELECTRIC ANOMALY IN THE CZECHOSLOVAK–POLISH SECTION OF THE CARPATHIANS ON THE BASIS OF GEOMAGNETIC AND MAGNETOTELLURIC SOUNDINGS

J JANKOWSKI[1], V PETR[2], J PĚČOVÁ[2], O PRAUS[2]

Geomagnetic variations recorded in *D*, *H* and *Z* components at almost 100 sites distributed over the Czechoslovak and Polish–Czechoslovak sectors of the Carpathians (West-Carpathians) were used to map the pronounced geoelectrical anomaly near the regional contact of the Central and Outer Carpathians. The anomaly axis is traced by the zero amplitude of the vertical component (*Z*) and by a reversal of its polarity in either sides of the zero amplitude zone.

Approximating the anomaly source by an infinite line current (a highly conductive lineament) we also estimated its maximum depth (Fig. 4). It was found to vary smoothly between 25 and 15 km in key regions of the Western-Carpathians.

The depth estimates were further refined by reinterpreting magnetotelluric sounding curves from sites located in the proximity of the anomaly centre. Sounding curves by Polish and Soviet authors were used together with our own sounding curves for solving a 1–D inverse problem. As result, we obtained a zone of decreased electrical resisitivity of about 2–5 ohm m at depths ranging from 7 to 12 km. This interpretation was further supported by 2–D forward and inverse numerical modelling.

The results obtained for the West-Carpathians together with investigations performed in other parts of the Carpathians proved the anomaly to be an important characteristic of this whole region. It is a regional structure in the contact zone of the Carpathian plate with adjacent geological units. Possible factors or their combinations were suggested to account for increased electrical conductivity of this zone.

Keywords: Carpathian conductivity anomaly; geoelectric model; geomagnetic deep sounding; magnetotellurics

Introduction

Since 1973 the recordings of geomagnetic variation components *D*, *H*, *Z* have been performed at almost 100 stations in the Czechoslovak and Polish–Czechoslovak section of the Carpathians. As a rule, 8–12 temporary geomagnetic observatories were established and operated as national or international Polish–Czechoslovak 1–D arrays. At certain localities magnetotelluric measurements were also organized to estimate the geoelectric cross section by a relatively independent method. Characteristics of the variations and their spatial variability are interpreted in terms of the internal electric conductivity distribution with implications on the composition and physical state of the matter inside the Earth. Also zones of strong geoelectric

[1] Institute of Geophysics Polish Acad. of Sciences. ul. Pasteura 3., 00–973 Warsaw, Poland
[2] Geophysical Institute of the Czechosl. Acad. Sci. 141 31 Prague 4 Spořilov, Bočni II/1401, Czechoslovakia

inhomogeneities are revealed. They are marked by zero amplitude in the variations of the vertical field component and by the reversal of their polarity in locations to either side of the "zero amplitude line". Their delineation provides a closer insight into the tectonic structure and development of the area covered by observations.

Location of the geoelectric anomaly

All geomagnetic variation events were used to estimate the induction vectors of the geomagnetic field according to Wiese's relation. In the next step the transfer functions were calculated from selected data samples to get a refined induction response of the field in the range of periods from about 600 s to 8000 s by a new method (Wieladek and Ernst 1977).

All well developed variation events were further used to separate the field into its internal and external parts (Pěčová 1982). By analysing the changing orientation of the internal field vectors and by assuming an infinite line current source, we were able to estimate the horizontal and vertical coordinates of the field source (location on the profile and its depth). The same parameters were also estimated by applying a physico-statistical approach (Petr 1980).

Having taken into account all these results, the centre of the anomaly could be localized with an accuracy of about ± 2 km in the key regions and, thus, the anomaly could be traced within the whole extent of the Czechoslovak and Polish–Czechoslovak Carpathians (Fig. 1). The detailed mapping of the anomaly substantially refined its course and position relative to important geological and tectonical features (the Klippen Belt, the Peripieninnian Lineament etc.). In particular, we found a characteristic bend of the anomaly trace into the inner Carpathian side of the Klippen Belt in the northwestern part of Slovakia. We suggested that this phenomenon was connected with tectonic movements and subsequent deformation in the wedge, where deep-rooted fault zones cross each other (Praus et al. 1981).

Further characteristics of the geoelectric anomaly can be deduced from the results of the calculated transfer functions and the related real and imaginary geomagnetic vectors (Schmucker vectors). The maximum real and, at the same time, the minimum imaginary geomagnetic vectors were obtained for periods between 1800 and 2000 s at almost all Carpathian profiles. It means that the character of the inducing process remains approximately the same in the whole regional extent and also the depth fluctuations of the anomaly source are not very large.

An important diagnostic feature of an anomalous field is the mutual orientation of the real and imaginary geomagnetic vectors. In our definition, real vectors are always perpendicular to a zone of increased electric conductivity (provided the inhomogeneous medium is strictly 2–D) and they are directed away from the zone. On the other hand, the imaginary vectors can change their orientation according to the

character of an anomaly. The model calculations show that an imaginary vector reverses its orientation with increasing periods if superficial effects are involved.

On analysing of the sets of vectors derived from the transfer functions for periods $T = 600$, 900, 1200, 1700, 2500, 3600 and 4800 s along four profiles traversing

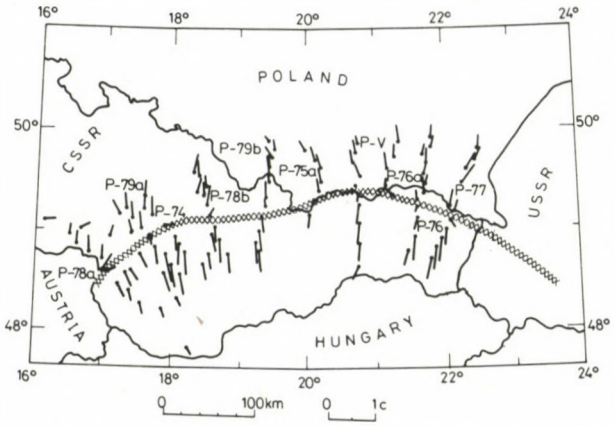

Fig. 1. Induction vectors in the Czechoslovak and Polish–Czechoslovak section of the Carpathians and the trace of the geoelectrical anomaly (cross-hatched line)

the transition zone between the Bohemian Massif and the Carpathians, we find that an approximately antiparallel orientation of the real and imaginary vectors is preserved from the long periods to about 1500 s at all stations in this area. It means that the anomaly has a two-dimensional character. At a period of about 1200 s, however, the imaginary vectors tend to reverse their orientation and lie parallel to the real ones at the Inner Carpathian side of each profile (compare Fig. 2 for periods $T = 2500$ s and Fig. 3 for periods $T = 1200$ s).

According to model calculations we think that a superficial induction is effective in the sediments of the marginal parts of the inner Carpathian basins and an increasing 3–D character of the structure in the Carpathian core mountains is the explanation of this feature.

Separating the variation field into external and internal parts and considering the spatial characteristics of the geomagnetic vectors at all Carpathian profiles we were able to estimate the depths of the anomaly source. Assuming an infinite line current approximation, we consider the estimated depths as maximum ones so that realistic geological structures corresponding to this schematized model may be expected at shallower depths.

The depths shown in Fig. 4 vary between 15 and 25 km with the maximum values in the Vienna basin and along the profile P–76 (the traverse through eastern Poland and Slovakia; see Fig. 1). This depth characteristic represents the averages of the sets

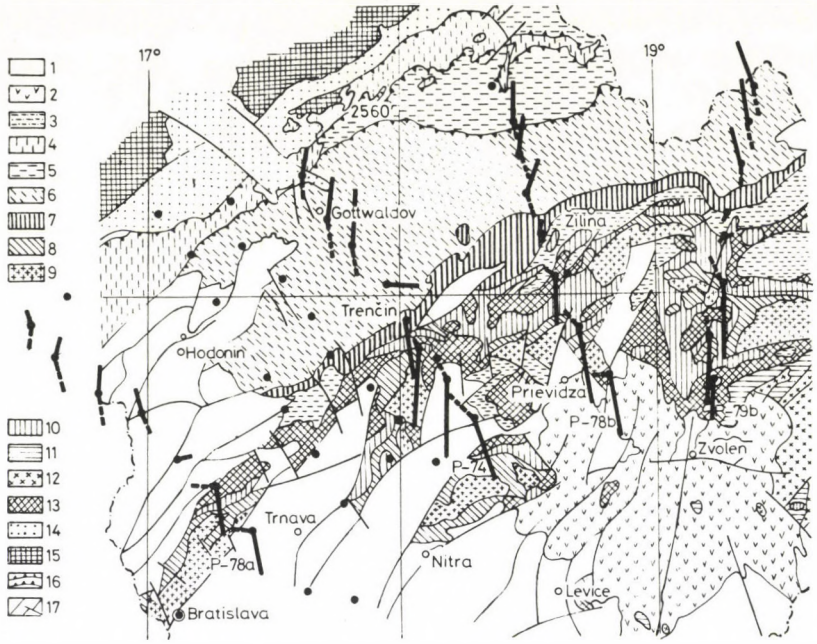

Fig. 2. Real (full) and imaginary (dashed) geomagnetic vectors in the transition zone between the Bohemian Massif and the Carpathians for the period $T = 2500$ s superimposed on the geological map of the region. Explanation of geological symbols: 1 — Neogene deposits of intramontane depressions; 2 — Neogene volcanic rocks; 3 — the Inner Carpathian Paleogene; 4 — the Frýdek (Subsilesian) and Ždanice units; 5 — the Silesian unit; 6 — the Magura unit; 7 — Mesozoic; 8 — the mantle series, late Paleozoic-Mesozoic; 9 — Crystalline; 10 — Paleozoic-Mesozoic (Fatric); 11 — late Paleozoic-Mesozoic (Veporic); 12 — Crystalline-early Paleozoic (Veporic); 13 — the Choč and Šturec nappe, late Paleozoic-Mesozoic (Hronic); 14 — Neogene Carpathian Foredeep; 15 — the Bohemian Massif; 16 — the nappe lines, the nappe overthrusts; 17 — faults and reverse faults

of individual estimates. Their detailed analysis, however, reveals remarkable peculiarities. For example, on all traverses the anomaly shows a pronounced asymmetry in the sense that its magnitude measured by moduli of geomagnetic vectors is substantially greater on the Inner Carpathian side of a specific profile than on the outer side. Variable thickness and longitudinal conductivity of the surface layer can account for some of these peculiarities. An obvious 3–D character of the structure in some regions and other factors also seem to be involved. They necessitate further investigations.

In applying the method of field separation into internal and external parts, we assumed an infinite line current approximation for the internal anomaly source. Consequently, we must consider the depths, thus obtained, as maximum estimates so that realistic geological features corresponding to this schematized model may be expected at shallower depths. This conclusion seems to be supported by the results of magnetotellurics and of numerical modelling presented further in this paper.

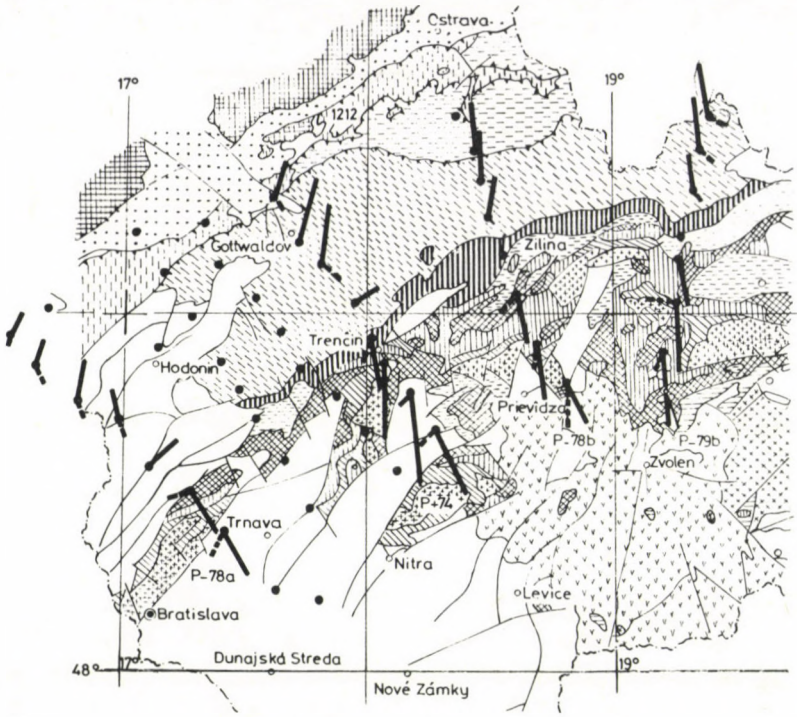

Fig. 3. The same as in Fig. 2 for the period $T = 1200$ s

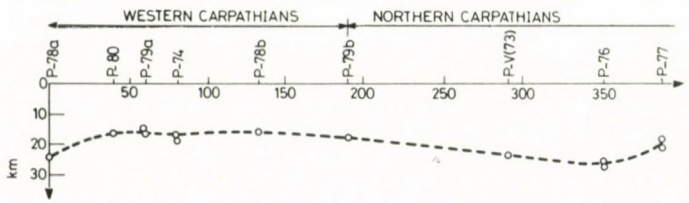

Fig. 4. Summary of source depth estimates for the geoelectrical anomaly along the Czechoslovak and Polish–Czechoslovak section of the Carpathians (from the Vienna basin to the USSR–CSSR frontier). Averaged estimates are shown for specific profiles traversing the anomaly (profile P–78a, etc)

Magnetotelluric results and geoelectric models

Further independent information on the internal geoelectric structure within the zone of anomalous induction was obtained from magnetotelluric soundings (MTS). They helped specifically in refining the depth estimates of a highly conductive zone, which was assumed to be responsible for the anomalous geomagnetic field of internal origin observed along the Carpathian traverses.

For this purpose we used the results of MT-soundings in different parts of the anomalous zone in Czechoslovak territory. The MTS curves published by Polish and Soviet authors were additionaly taken into account. The curves corresponded in all cases to the parallel mode and were interpreted by means of the 1–D inversion procedures developed by the Czechoslovak research group (Pěč et al. 1977, 1980; Pek and Červ 1979).

As the *first characteristic region* of the anomaly we define the transition zone between the Bohemian Massif and the West-Carpathians from the Austrian frontier to Považská Bystrica (about in the central part of the transition zone). The axis of the anomaly is shifted here to about 20 km from the Klippen Belt into the outer Carpathians, but it approaches gradually the Klippen Belt. The whole region represents a foredeep filled with sediments deposited on a non-conductive basement (Mesozoic crystalline rocks of the Bohemian Massif) dipping to depths estimated at 8–12 km in the deepest parts.

The MTS sites were located in the southernmost part of this region and they covered a section of the International DSS Profile No. VI. Inverting the MTS data on this profile, we proposed a tentative model of the internal geoelectric structure along it (Pěčová et al. 1980). Focusing our present discussion on the Carpathian foredeep only, we suggest a sequence of layers with decreased electric resistivity dipping from depths of about 15 km in the northwestern margin to about 25–30 km in the easternmost margin of the foredeep. Of special importance we consider, however, the highly conductive layer interpreted at the MTS site Hodonin (about 18 km northwestward from the centre of the anomaly, see Fig. 6, MTS curve Ho). Due to the inherent non-uniqueness of the inverse problem, this layer is characterized either by a resistivity of 7 ohm m at a depth of 4 km and 7 km thick, or by a resistivity of 4 ohm m at a the depth of 11 km and 3 km thick. We think that this layer together with a sequence of relatively well conductive layers in the deeper parts of the structure (Fig. 5) may represent the extension of the anomalous zone from its central part to the outer Flysch Carpathians. Both interpretations are acceptable as they seem to fit reasonably well the general tendency of the conductive layers emerging northwestwards from the Central Carpathians. According to the results at the MTS site Prievaly, located in the easternmost margin of the foredeep, there is no evidence of a similar conductive zone at the inner side of the Carpathians.

In this region a magnetotelluric survey was also performed at 20 MTS sites for the National Enterprise Geofyzika in the frame of a business contract by the Hungarian ELGI group. According to the MTS results (Varga et al. 1978) a layer with low resistivity of about 1 to 5 ohm m emerges from a depth of 12 and 15 km in the central part of the foredeep to about 4 km in the northwestern margin of the outer Flysch Carpathians.

A closer insight into the internal structure of this region was provided by the MTS results on profile P–74 shown in Fig. 6 (Ko, Ku, Dl). Only pulsation data were

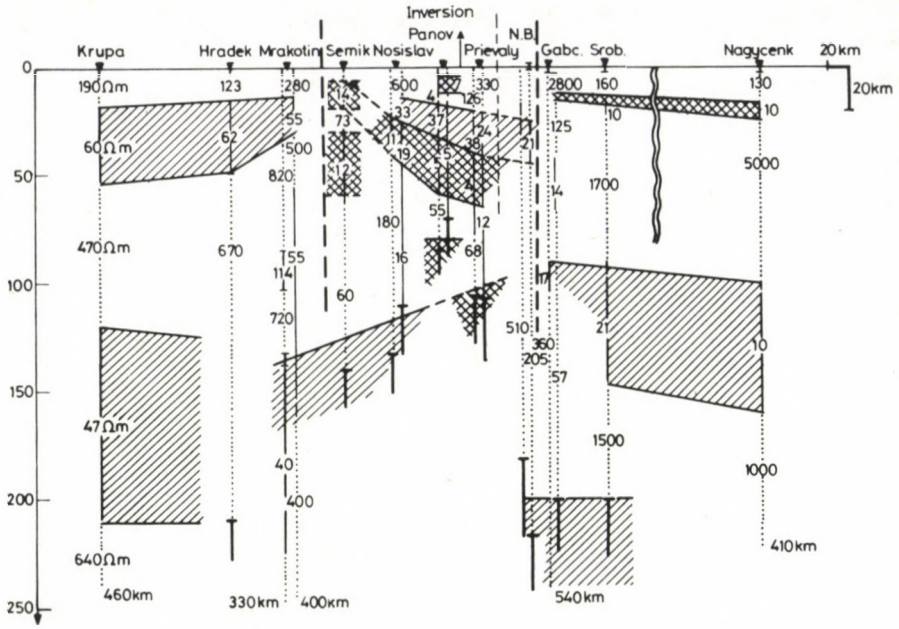

Fig. 5. Geoelectric cross section along the DSS profile No. VI on the basis of inversion results. Layers of decreased electrical resistivity are shown by cross-hatched regions

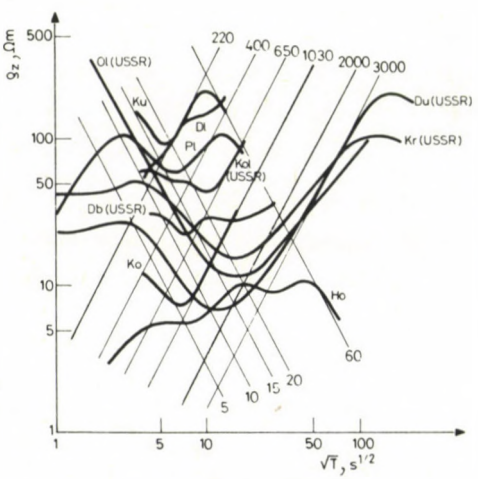

Fig. 6. Summary of MTS curves (parallel mode) in the vicinity of the geoelectric anomaly; families of H-depth lines (in km) and S-longitudinal conductivity lines (labelled in Siemens) are shown for orientation; notation of stations: Ho = Hodonin, Ku = Kudlov, Dl = Dolni Lhota, Ko = Kochavec, Pl = Plavnica (CSSR); Kol = Kolochava, Db = Dubrovitsa, Du = Dumen, Kr = Krasnoe, Ol = Olshany (USSR)

analysed, thus only the short period branches of the curves were determined. Layers with resistivities of about 2–3 ohm m were only found at the station Kochavec (Ko) at 4 km depth (a station located in the axis of the geoelectrical anomaly), and at the station Kudlov (Ku), (about 15 km from the axis), at a depth of 12 km. The sounding curve obtained at the station Dolni Lhota (Dl), between the two others did not fit into this general pattern (see the MTS curves in Fig. 6). Probably a complicated geology is responsible here for this result.

As *the second characteristic region* of the anomaly we define the area where the geoelectric anomaly penetrates into the inner Carpathian side of the Klippen Belt. It starts in the vicinity of Považská Bystrica, follows the northern margins of the Choč Mts. and of the High Tatra region and extends as far as the Pieniny Mts. Unfortunately, no MTS has been performed here as yet, mainly due to a high level of disturbing industrial currents. There is a great need, however, to find a suitable site for this purpose.

As initial zone of *the third characteristic region* of the anomaly we take DSS profile No. V, where the geoelectric anomaly returns to the outer side of the Klippen Belt and gradually resumes its position in the Outer Carpathians, about 30 km apart from it. This region may encompass the eastern Carpathians in Slovakia and Ukraina as far as the Rumanian frontier. It represents a transition zone from the Polish Paleozoic Platform, the East-European Platform and the Ukrainian Shield to the Carpathian unit.

The MTS sites within this sector cover the central zone of the anomaly. Specifically, on profile P–73 (coinciding with the international DSS profile No. V), a MTS curve was obtained at Plavnica (Pl) at about 8 km from the axis of the anomaly. South-eastwards from here, approximately on profile P–77 in Polish territory, two MTS curves at about 10 km from the inversion zone of the induction vectors were interpreted by Swiecicka-Pawlyszyn et al. (1978) (denoted by 1. and 2. in Fig. 7).

In Ukraina, several MTS curves along the anomaly were reported by Bilinsky et al. (1978); we used two of them with the axis of the anomaly in between for interpretation. Finally, three MTS curves from localities right above the axis of the anomaly were measured and published by Kulik et al. (1978).

The majority of these MTS curves were interpreted by applying 1–D inversion. If available, the authors' interpretation was used as a starting approximation. In few cases the process did not converge and the computations had to be repeated with a new starting approximation. The final results of inversion proved essentially the original estimates for the depths to about 60 km, while for greater depths the data did not allow a detailed discrimination of geoelectric structures.

The results of inversion are summarized as schematic models in Fig. 7. The most reliable depth estimates for the central part of the anomaly seem to be those based on the data by Kulik et al. (1978). Analysing the schematic models in Fig. 7, we can conclude that at most localities a zone of decreased electrical resistivity of about 2–5

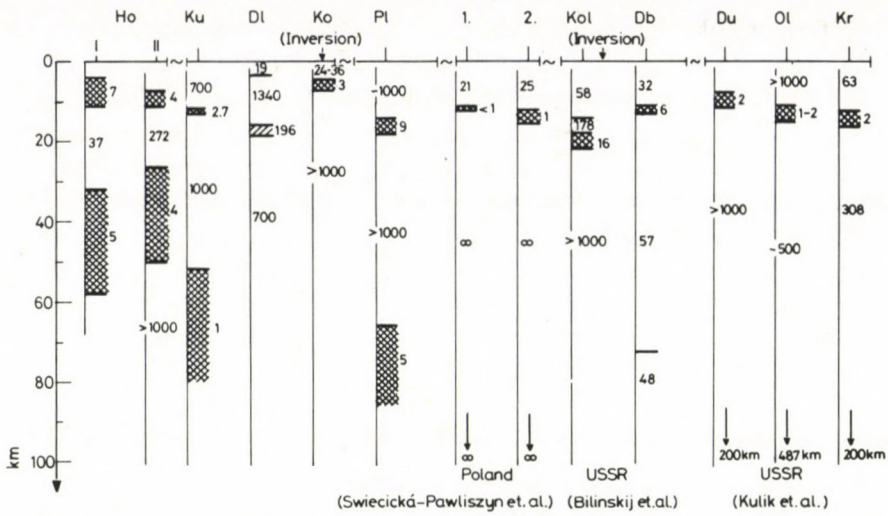

Fig. 7. Schematic geoelectric cross sections based on the results of solving the inverse magnetotelluric problem for MTS curves in the vicinity of the geoelectrical anomaly. Zones of decreased resisitivities are shown by cross-hatched regions. Notation of stations corresponds to Fig. 6

ohm m was obtained at depths ranging from 7 to 12 km. The thickness of the zone varies from 1 to 7 km. The variability of both the thicknesses and resistivities is mainly due to the electrical equivalence of the layers and, therefore, to the non-uniqueness of the inverse problem. It is important, however, that the cross sections at stations just above the anomaly are characterized by a high longitudinal conductivity of the zone ranging from 1000 to 3000 S. With increasing distances from the axis the longitudinal conductivity gradually decreases to about 200 S at localities lying at about 15–18 km apart.

Magnetotelluric, magnetovariational, and other geophysical and geological information was used to find a family of laterally non-homogeneous geoelectric structures of this region which fits the peculiarities of the field distribution. In proposing their geometry, we have taken subduction processes into account, which have been assumed to have occurred in certain sections of the Carpathians in the geological past. The modelling and corresponding field distributions were obtained in the first step by solving the forward 2–D problem numerically with adjusting the model parameters by trial and error to fit the experimental data. In the next step a 2–D inversion technique was applied to models with fixed geometry (Červ and Pek 1981).

From several models tested so far, we present here the one which fits reasonably well the real part of the geomagnetic vectors at three periods (Fig. 8). A common feature of all models tested was the existence of a well-conductive block with resistivities between 1 − 4 ohm m at depths from 8 to 12 km. This conclusion is in good accordance with the estimates of magnetotellurics.

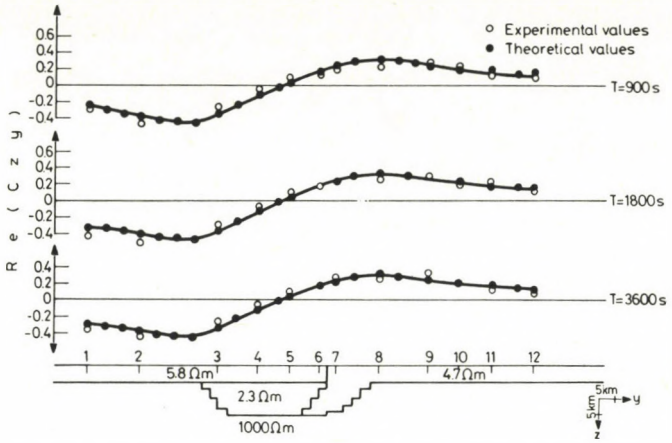

Fig. 8. Schematic model for a 2–D geoelectrically non-homogeneous structure (below) and the results of solving simultaneously at three periods the 2–D inverse problem for spatial distribution of real geomagnetic vectors (approximately in the vicinity of the profile P–73)

Conclusion

The results summarized here for the Czechoslovak and Polish–Czechoslovak sectors of the Carpathians together with interpretations performed in other Carpathian countries proved that the anomaly is an important characteristic of this geological unit as a whole. Therefore, it must have been produced by its specific tectonic development. The position of the anomaly near the contact with adjacent geological units, a deep-rooted relation to important tectonic features (the Klippen Belt, the Peripieninnian Lineament, etc.) and a correlation with anomalies of other geophysical fields (regional course of the gravity minimum, coincidence with the vertical jump at the Moho depth amounting to several kilometers and marking the contact of blocks with different thicknesses of the Earth's crust), suggest that the geoelectric anomaly indicates a regional structure in the contact zone of the Carpathian plate with adjacent blocks of the Bohemian Massif, the East-European Platform and the Ukrainian Shield. Increased electrical conductivity of this regional zone can be accounted for by the following factors or by their combinations:

a) the presence of thick sedimentary materials deposited in the Carpathian foreland subsiding due to subduction under the margin of the Carpathian lithospheric plate;

b) saturation of deposits by mineralized waters; high mineralization was proved in some boreholes in the transition zone between the Bohemian Massif and the West-Carpathians; for example in the Těšany borehole the highest salt water mineralization of 149 g/l and the corresponding resistivity of 0.09 ohm m was reported from the Devonian rocks at a depth of 3448 m;

c) increased temperatures and the effect of heating, mineralized waters, or even partial melting of rocks drawn into the crustal depths by subduction; increased temperatures have been reported recently from the borehole at Banska IG–1 in the region of the Pieninnian Klippen Belt (Jankowski et al. 1982);

d) heating and reduction effects in rocks containing various percentage of hydrocarbons according to a mechanism suggested by Bucha (1980).

References

Bilinsky A I, Kaufman M N, Shilova A M 1978: MTS curves in Transcarpathia. V. Vsesoyuz. shkola-seminar po elektromagn. zondirovaniyam. Kiev, Naukova dumka

Bucha V 1980: Geomagnetism of the External Flysch Czechoslovakian Carpathians and the possible causes of anomalous geophysical manifestations. *Studia geoph. et geod.*, 24, 227–251.

Červ V, Pek J 1981: Numerical solution of the two-dimensional inverse geomagnetic induction problem. *Studia geoph. et geod.*, 25, 69–80.

Jankowski J, Ney R, Praus O 1982: Are there thermal waters under the north-eastern part of the Carpathians? (in Polish). *Przeglad geologiczny*, 4, Rok XXX, 165–169.

Kulik S N, Logvinov I M, Rokityansky I I, Shul'man M G, Shuman V N 1978: Longitudinal MTS curves below the axis of the Carpathian anomaly. Kiev, Naukova dumka

Pěč K, Pěčová J, Praus O 1977: The inverse magnetotelluric problem for sounding curves in the Carpathian section of DSS profile No. VI. *Acta Geod. Acad. Sci. Hung.*, 21, 351–362.

Pěč K, Pěčová J, Praus O 1980: Inverse magnetotelluric problem for sounding curves from Czechoslovak localities. *Journ. Geomagn. Geoel. Suppl.* I, 32, 159–169.

Pěčová J 1982: Determination of the depth of a conducting anomaly by separating the geomagnetic variation field into its external and internal parts. *Travaux Géophysiques* (in press).

Pěčová J, Pěč K, Praus O 1980: Geoelectrical cross-section on the profile No. VI of the DSS (in Czech). Sbornik referátu 7. celostát. konfer. geofiziku. Sekce S–4-geoelektrika a radiometrie. Geofyzika n.p. Brno, Gottwaldov

Pek J, Červ V 1979: Solution of the one-dimensional inverse magnetotelluric problem. *Studia geoph. et geod.*, 23, 349–358.

Petr V 1980: A physico-statistical method for estimating the depth of a disturbing body from magnetovariational measurements (in Czech). Sbornik referátu 7. celost. konfer. geofiziku. Sekce S–4-geoelektrika a radiometrie. Geofyzika n.p. Brno, Gottwaldov

Praus O, Pěčová J, Petr V, Pěč K, Hvoždara M, Červ V, Pek J, Laštovičková M 1981: Electromagnetic induction and electrical conductivity in the Earth's body. In: *Geophysical Syntheses in Czechoslovakia*, Ed.-in-Chief A Zápotek. Veda, Bratislava, 297–315.

Swiecicka-Pawliszyn J, Pawliszyn J 1978: Zastosowanie badan magnetotellurycznych do rozpoznawania zolozonych struktur geologicznych. *Biul. Inform. Geofizyka Stosowana*, Warszawa, 16–25.

Varga G, Nemesi L, Draskovics P 1978: Magnetotelluric investigation in the Morava Basin. Veng. gos. geofiz. inst. L. Eötvös, Budapest. Archiv n.p. Geofyzika, Brno (unpublished)

Wieladek R, Ernst T 1977: Application of the method of least squares to determining impulse responses and transfer functions. Publ. Inst. Polish Acad. Sci., G–1, 1–12.

Acta Geodaet., Geophys. et Montanist. Hung. Volume 19 (1—2), pp. 93—106 (1984)

SOME NEW STRATIGRAPHICAL AND PALEOGEOGRAPHICAL DATA IN THE PALEOZOIC AND MESOZOIC OF THE PANNONIAN MEDIAN MASSIF AND ADJACENT AREAS

H KOZUR[1]

The hypothetical pre-Jurassic northern position of the Pannonian Median Massif beside the Tatricum cannot be supported by any stratigraphical, facial, paleobiogeographical or other data. On the other hand several data presented in this paper exlude a pre-Jurassic northern position of the Pannonian Median Massif.

Keywords: paleogeography; Pannonian Median Massif; Radiolaria; stratigraphy, Mesozoic; stratigraphy, Paleozoic

Introduction

A paleogeographical reconstruction or geodynamic model which contradicts well founded geological data should be abandoned, even if it is supported by *selected* geological (including paleontological and geophysical) data. The hypothesis about the pre-Jurassic northern position of the Pannonian Median Massif beside the Tatricum is such an example. This hypothesis was formulated by Patrulius et al. (1971). They came to the conclusion that the Finiş nappe of the Northern Apuseni Mts. (southern margin of the Pannonian Median Massif) and the Križna nappe of the West-Carpathians were deposited in the same Triassic trough because of the same Triassic facies successions in these nappes. But later Patrulius (1976) could show that these "similarities" were the consequence of former incorrect stratigraphical data from the Northern Apuseni Mts. According to newer stratigraphic data the Triassic sequence of the Finiş nappe is quite different from those of the Križna nappe or any other nappe in the West-Carpathians (Table I).

Some facial differences are possible within one trough, but not those of principal importance. The proximal units both in the Alps and in the West-Carpathians have Middle Carnian (Julian) dark clastical sediments (Lunz beds in the N and Raible beds in the S). This is connected with some tectonical movements and wet climate. Large amounts of clastical sediments were transported from the adjacent continental denudation areas both into the Tethyan realm and into the Germanic Basin (reed-sandstone). Grey shales or sandstones are lacking in the Middle Carnian only in the

[1] Magyar Állami Földtani Intézet, H–1143 Budapest, Népstadion út 14.

distal facies zones of the Alps and the West-Carpathians, far away from the continental margin. In the West-Carpathians the Lunz facies reaches far towards the south, it even occurs in the Choč nappe and in parts of the Stražov nappe.

On the contrary, in the Codru nappe system of the Northern Apuseni Mts. and even in the most proximal nappe (Vălani nappe) only limestones and dolomites are present in the Julian, but no clastical sediments can be found there. This big and decisive difference to all the proximal units in the Alps and the West-Carpathians can be easily explained. The sedimentation area even of the most proximal zone of the Codru nappe system was not situated at the northern border of the Tethys, but at the southern margin of an island area (Pannonian Median Massif) within the Tethyan realm.

The paleontological, paleobiogeographical, sedimentological and facies distribution data which seemingly support the pre-Jurassic northern position of the Pannonian Median Massif beside the Tatricum were carefully summarized by Kovács (1982). All these data, however, are either *selected* ones which do not support any paleogeographical reconstruction or they cannot be correct according to newer data. On the other hand there are some data which exclude a pre-Jurassic northern position of the Pannonian Median Massif beside the Tatricum.

Paleontological and paleobiogeographical arguments for the original position of the Pannonian Median Massif

1. The "northern" pelecypod and brachiopod faunas of the Peştiş Shale (Bihor Autochthon) with *Elegantinia elegans, Coenothyris vulgaris, Punctospirella fragilis,* etc. are not only typical for the Germanic Basin (*selected* data!), but in the same facies and age (Middle Triassic) also for the Southern Alps and other southern units. Otherwise *Aulacothyris geyeri* and *A.* cf. *incurvata,* also present in the Peştiş Shale are not present in the Germanic Basin and also unkown in the Austroalpine faunal province (Northern Alps, West-Carpathians north of the Meliata Unit), but present in the Dinarids. Hence, the Triassic brachiopods support rather a former southern position of the Pannonian Median Massif.

2. According to Kovács (1982 p. 631) "the presence of Upper Anisian reptiles of poor swimming ability in the Bihor Autochthon, which are also present in the Germanic Basin, points to the close connection of these two areas . . . and excludes the possibility that the Bihor Autochthon was to the south of the Meliata series at this time".

These reptiles (*Nothosaurus* and *Tanystropheus,* see Patrulius et al. 1979) from time equivalents of the *"Protrachyceras" reitzi* zone (lowermost Ladinian) in the Peştiş Shale were not only found there and in the Germanic Basin (*selected* data!). *Nothosaurus* is widespread in many non-pelagic Middle Triassic sediments of the

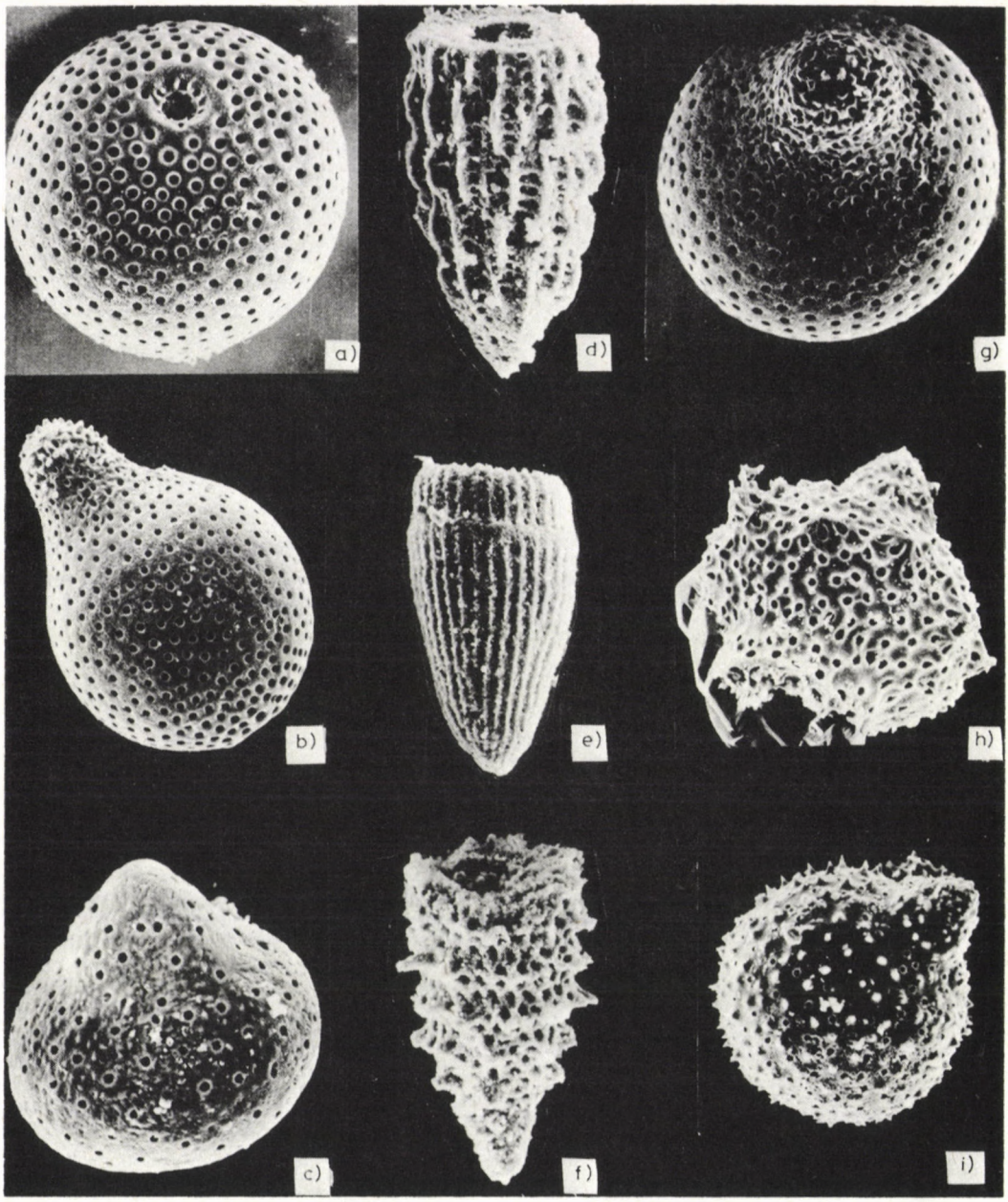

Fig. 1. Bajocian Radiolaria of the Bükk Mts. *a–c, g–i:* Csipkés-tető (southern Bükk Mts., $x = 557\,670$, $y = 607\,380$); *d–f:* Varga-tető (western Bükk Mts., $x = 556\,080$, $y = 694\,200$). *a, b, g) Praewilliriedellum cephalospinosum* n. sp., *a, g:* 360 x, *b:* 270 x; *c: Praezhamoidellum buekkense* n. sp., 630 ×; *d: Hsuum robustum* Pessagno et Whalen, 270 ×; *e: Archaeodictyomitra* n. sp., 270 ×; *f: Parvicingula* sp., 270 ×; *h: Syringocapsa buekkensis* n. sp. 400 ×; *i: Praewilliriedellum spinosum* n. sp. 400 ×

Tethys (e.g. Southern Alps). Bones of *Nothosaurus*, a typical *marine* reptile which surely could not cross larger land areas, were never found in continental Triassic sediments, but were found in the centre of the Germanic Basin, several 100 km far from any shoreline. It could not be a problem for such marine reptiles to come to the Bihor Autochthon from the SE (Moesian Platform) or along the southern margin of the Pannonian Median Massif even from the Southern Alps. These marine reptiles only indicate non-pelagic marine environments within a distance from not more than about 500 km off the shoreline of the continents or islands. Such conditions existed in the Pannonian Median Massif during the Middle Triassic in all possible paleogeographic positions. *Tanystropheus* occurs also in the Southern Alps and in Israel (!).

Moreover, during the Upper Anisian and Lower Ladinian no marine connection existed between the Germanic Basin and the West-Carpathians (see Kozur 1974, 1975). In this time the Germanic Basin was connected only in the SW with the Tethyan realm. During that time marine "northern" faunal elements including marine reptiles could migrate from the Germanic Basin to the Bihor Autochthon only across the Southern Alps.

3. The "northern" Jurassic brachiopod faunas of the Mecsek, Villány and Apuseni Mts. are not pelagic elements, but shallow water faunas. In the Transylvanian nappe system both the "northern" and the "southern" (pelagic) brachiopod faunas occur in dependence from the facies. The sedimentation area of the Transylvanian nappe system, however, was surely not situated both on the northern and southern margin of the Tethys.

4. The Upper Pelsonian and Lower Illyrian *Gondolella* (conodont) fauna of the Dinaric faunal province (Kozur 1980) is dominated by *G. bifurcata hanbulogi*. This can be observed both in pelagic sediments (with *Gladigondolella*) and in non-pelagic ones (without *Gladigondolella*). The same is true in the Mecsek and Villány Mts. Quite on the contrary, in the Austroalpine faunal province (Northern Alps, West-Carpathians from the Silica nappe to the north) and even in the Balaton Highland (lying at the southern margin of the Austroalpine faunal province with some transitions to the Dinaric one) *G. bifurcata bifurcata* is clearly dominating. Sometimes *G. bifurcata hanbulogi* is quite absent in the Austroalpine faunal province. In the Germanic Basin only *G. bifurcata bifurcata* is present in this time (under quite the same facial conditions as in the Mecsek and Villány Mts.).

If the Pannonian Median Massif had a northern position during the Triassic, then *G. bifurcata bifurcata* had to be at least as dominant as in the Austroalpine faunal province.

5. In the Vălani nappe, i.e. in the most proximal nappe of the Northern Apuseni Mts., an entirely southern microfauna (conodonts with *Pseudofurnishius*, holothurian sclerites with *Theelia tubercula*, ostracodes with *Falloticythere, Leviella sohni, L. bentori* etc.) occur in the Ladinian and Carnian (Kozur 1979). These southern faunal elements are known in the whole southern part of Tethys and in the epicontinental

seas south of it. They can be found in the Iberian-Northafrican faunal province (= Westmediterranean-Arabian = Sephardic faunal province), in the Southern Alps, Southern-Turkey, and Malaysia. But on the other hand these faunal elements are unknown in the West-Carpathians and Northern Alpine nappe systems (Austroalpine faunal province).

The typical southern Ladinian-Carnian microfaunas of the Vălani nappe are a clear argument against a northern position of the Pannonian Median Massif (beside the Tatricum) in the Triassic. If the Pannonian Median Massif had been in such a pre-Jurassic position, then an insular occurrence of Triassic southern faunal elements would exist within the Austroalpine faunal realm.

The paleontological data clearly exclude the northern position of the Pannonian Median Massif during the Triassic. A more southern, eastern or western pre-Jurassic position of the Pannonian Median Massif relative to the present adjacent areas cannot be excluded on the basis of faunal evidences, but they neither support nor reject it so far.

Sedimentological, geophysical and facies distribution data of the pre-Jurassic position of the Pannonian Median Massif

According to Kovács (1982 p. 628) "the absence of detrical Jurassic formations in the Bakony makes it quite impossible that these two areas (note: Mecsek and Bakony Mts.) were in their present position in the Lower and Middle Jurassic". The Pannonian Median Massif was at the beginning of the Liassic in its central part a low island, later successively subsided below sea level. The amount of sediment transport from such an island is low (compare the small clastical sediment transport from the Vindelizian island into the Germanic Muschelkalk sea during the Middle Triassic).

Even at the present distance between the denudation area south of the Mecsek Mts. and the sedimentation area in the Bakony it would be very improbable that clastical sediments from the Pannonian Median Massif, deposited in a rapidly sinking marginal trough at the northern margin of the Pannonian Median Massif (nearly 2000 m Liassic), would reach the Liassic sedimentation area of the Bakony, a slowly sinking carbonate platform. It is sure that the primary distance between the denudation area south of the Mecsek and the sedimentation area in the Bakony was considerably shortened during the Alpine orogeny.

Lateral relative movements between the Mecsek Mts and the Bakony Mts are probable, independently from the paleogeographic model. But, as pointed out above, even the absence of detrical rocks in the Bakony (some marls and shales are present here in the Toarcian and in the Middle Jurassic) would not be an argument against the present relative position of the Bakony and Mecsek Mts.

There is an assumption according to which the facies succeeded each other in the whole Pannonian Median Massif and its surroundings always from the north

(proximal facies, near to the margin of the sedimentation area) to the south (distal facies, more and more pelagic ones). At least the sediment transport should go always from the north to the south according to this assumption. It is correct for the northern Apuseni Mts. and the areas to the west of it, covered now by younger sediments. But here we are at the southern margin of the Pannonian Median Massif and in the transition area to the mobil belt south of it. Therefore, the distal facies had to be in the south.

Because the southern Bükkium is strongly southvergent in its southern parts (backfolding against the *northward* drifting Pannonian Median Massif), its southern part may be overthrusted by the northern part of the Pannonian Median Massif. If we regard the structure of the Northern Apuseni Mts. (eastern part of the Pannonian Median Massif), then large parts at least of the eastern Pannonian Median Massif can be regarded as basement nappes overthrusted from south to north. It is possible that the backfolding of the southern Bükkium was so strong that sediments of the Bükkium could overlie at some places the northern margin of the Pannonian Median Massif near to the Zagreb–Kulcs line. As consequence of this complicated tectonic situation and the thick cover of younger sediments, it is very probable that the transition of the northern margin of the Pannonian Median Massif to the mobile belt in the north will never be found.

On the other hand the central and northern parts of the Pannonian Median Massif outcrop or are only under a thin cover of younger sediments in the Mecsek Mts. and south of it. Here the Triassic-Liassic distal facies is in contrary to the above mentioned assumption in the *north* (Mecsek Mts. and northern foreland). In the thick sequence of the Mecsek Upper Triassic now brackish water ostracodes were found. At the same time the area *south* of the Mecsek Mts. belongs to the denudation area of the central Pannonian Median Massif. The same is true in the Liassic, where in the Mecsek Mts. nearly 2000 m detrical sediments (fresh water-paralic-marine) were deposited. The area *south* of the Mecsek Mts. belongs at that time still to the denudation area. Due to germanotype block faulting the degree of erosion was here quite different. In some places even the Precambrian basement was partly eroded, whereas in other places (e.g. in the Villány Mts.) the Middle Triassic is still present today.

Even in the Dogger of the Villány Mts. there are marine clastical sediments with land-derived plant remains. Therefore even in the Dogger there were still small denudation areas within the central Pannonian Median Massif and there is no possibility to work with any northern source area for these detrical rocks.

According to Kovács (1982) (referring to Nagy 1971) the sediment-transport in the Mecsek Upper Triassic and Liassic went from north to south, but this seems to be either a local event or a misinterpretation of the transport direction. The sediment transport of this area was surely not from the brackish (Upper Triassic) or from the fresh water, higher paralic and marine (Liassic) subsiding sedimentation trough in the Mecsek Mts. toward the denudation area south of it. Moreover, Lower Liassic

conglomerats have only been found in the southern part of the Mecsek sedimentation area.

If we study without preconceptions the facies changes in the marginal area of the Pannonian Median Massif then we can state the following: On its *southern* margin (Northern Apuseni Mts. and to the west of it) the distal facies lies in the *south* and on its *northern* margin the distal facies lies in the *north*. Quite the same trend can be observed from the Middle Triassic to Jurassic in the Bükkium. The Middle and Upper Triassic of the eastern Bükk Mts. in the south is by far more marginal than that of the Meliata Unit in the north (see Table II). The eastern Bükk development (including the central Bükk and much of the northern and southeastern Bükk development), however, is most probably a nappe. But even the Jurassic* sequences of the western and southwestern Bükk are more proximal compared with those of the Meliata Unit. No coarser clastical sediments, plant debris, coal stripes and even no limestones are known from the Jurassic of the Meliata Unit. It should be noticed again that in the same period, in which clastical sediments with plant debris, coals etc. were deposited on the northern margin of the Pannonian Median Massif in the Bükk Mts. clastical sediments, plant remains and coal stripes occur, too.

If we consider the Jurassic of the Bükk Mts. then the real rifting with magmatic activities derived from the mantle began in the Dogger. It is possible that some smaller magmatic activities began even in the Liassic. The clastical, slightly metamorphic Jurassic sequence with some cherts and a lot of mantle-derived volcanics is very similar to that of the Penninic rift trough. Such a Penninic type development can be found in the Jurassic-Lower Cretaceous always in transitional zones between the mobile geosynclinal realm and the more rigid parts, either at the margin of stable Europe (e.g. Penninicum) or at the margin of more rigid, earlier (most probably in the Precambrian) consolidated blocks within the Alpine orogene (e.g. Vardar Zone at the margin of the Serbo-Macedonian Massif).

* Jurassic sediments were unknown until now in the Bükkium, but all the clastical sequences in the Western and Southern Bükk Mts. belong to the Jurassic (Kozur, in press, see also Fig. 1) like the higher thick clastical sequence of the Meliata Unit (Kozur and Mock, in press). The limestones of the Liassic sequence in the Bükk Mts. (mostly olistolites in Middle Jurassic shale-chert sequences) show a continuous deepening from shallow water, partly oolithic limestones through moderately deep water micritic limestones with foraminifers and ostracodes (the same species as in the Middle Liassic of the Mecsek Mts.) to pelagic radiolarian-bearing limestones.

This deepening of the trough continued in the Middle Jurassic shale-chert sequence. All investigated cherts from this sequence yielded radiolarian faunas of Bajocian age. Most important are the radiolarian faunas of Varga-tető from beds nearly related to basic effusives. According to Pelikán, who sampled all these radiolarian-bearing cherts, the basic volcanics of this area had to be of the same age as the cherts or they are younger. The genus *Archaeodictyomitra* is already present in the Varga-tető radiolarian fauna (Fig. 1). This genus begins in the Stephanoceras humphresianum zone of the higher Middle Bajocian. *Hsuum robustum* is also very frequent (higher Middle Bajocian to deeper part of Upper Bajocian). Thus, at least parts of the pillow lavas in the western Bükk Mts. are from the higher Middle Bajocian or younger. The beginning of this volcanic activities in the Liassic (like in the Mecsek Mts. and other parts of the northern margin of the Pannonian Median Massif) is probable.

It is quite the same, whether we work with mantle diapirs or with convectional heat flow as the driving power of the tension in a geosyncline; at this boundary between more mobile and more rigid areas (discontinuities of crustal strength) the thinning or even removing of the continental crust will be the strongest. In the compressional phases the more rigid block is an abutment, thus even the youngest sediment filling (Jurassic-Lower Cretaceous) of these "Penninic type" rift troughs was metamorphosed and a vergency was caused which was always directed against the abutment.

For the "Penninic type" tectonic style of the Bükk Jurassic we also need the more rigid Pannonian Median Massif south of the Bükkium.

Marginal to the "Penninic type" rift trough of the Bükkium there were strong subsidence and magmatic activities during the Jurassic and Lower Cretaceous even in the northern part of the Pannonian Median Massif itself (Intrapannonian Mobile Belt). This subsidence and magmatic activities coincided with the main rifting and magmatic activities in the Bükkium.

Paleomagnetic data were often presented as evidence for a former northern position of the Mecsek Mts. (and the whole Pannonian Median Massif), because a polar path of stable Europe was assumed in the Mecsek Mts. If, however, the Mecsek Mts. were primarily beside the Tatricum, in the Mecsek Mts., an "African" polar path should be expected, too. The rift trough of the Pieniny Klippen Belt and its western and eastern continuations had separated the areas inside of these rifts from the stable Europe in the Jurassic and Lower Cretaceous. Although they were geographically parts of Europe, all the areas inside of these rifts (the Tatricum, too) rotated in this time together with the African plate. It is impossible to imagine that the Pannonian Median Massif was primarily a part of the stable Europe north of the Pieniny Klippen Belt, because in this case even the Codru nappe system had to be originated north of the Pieniny Klippen Belt.

New paleomagnetic data from the Mecsek Mts. (Márton 1980, 1981) show a polar path between those of the stable Europe and of Africa. The "anomalous" directions found for the Cretaceous volcanics were formerly explained by younger tectonic movements between the sampling points. But later (Márton 1980) the same "anomalous" Cretaceous directions were found together with "normal" Carboniferous directions in the same quarry of the Mórágy area immediately south of the eastern Mecsek Mts. The Cretaceous data are only anomalous, if we look for a polar path like that of the stable Europe. According to a personal communication by Márton, the pre-Tertiary polar path of the Mecsek Mts. would coincide with that of the Balaton Highland, if we regard the Cretaceous data as reliable and rotate it back to the present position. In this case the relative lateral position of the Mecsek and Balaton Highland should be unchanged until the Cretaceous and it had to be changed only in the (Upper Cretaceous and) Tertiary. But unfortunately, there are so far only very few paleomagnetic data to use it for any reconstruction.

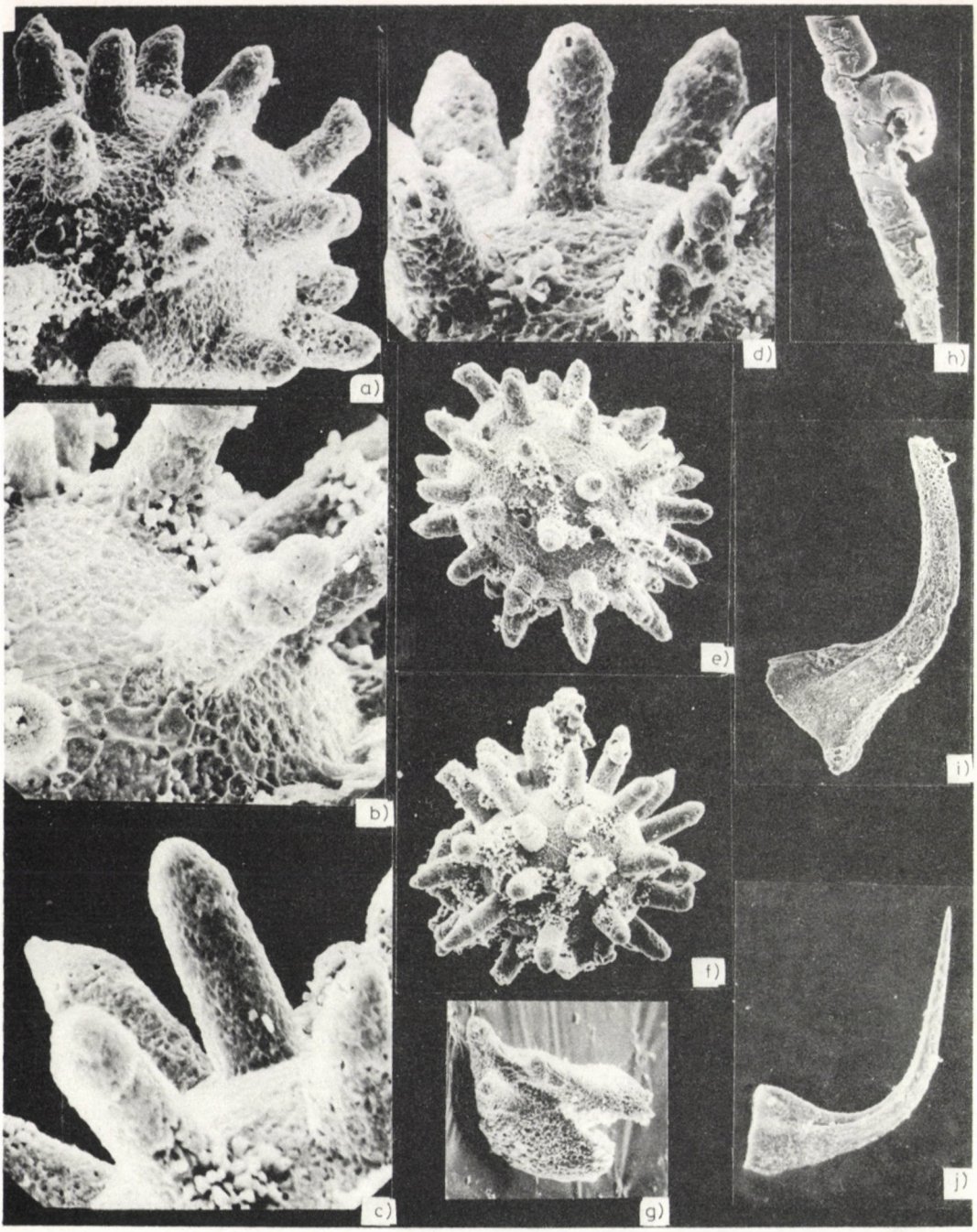

Fig. 2. a, b, c, d, e, f: Muellerisphaerida, Szalatnak–4 borehole, 635 m, amorphognathoides conodont zone (topmost Llandoverian to basal Wenlockian), excellent preservation of the organic matter. Even at very high magnifications no alterations caused by dynamometamorphosis are visible. *a:* 400×, *b, d:* 670×, *c:* 630×, *e:* 200×, *f:* 160× *g: Pseudooneotus tricornis* DRYGANT, 1974, 150×, conodont guide form for the amorphognathoides zone; sample, locality and age as for *a–f; h: Monograptus* ex gr. *exiguus* NICH, Alsóőrs (Máy János utca, corner of Április 4. utca), Balaton Highland. Even in this small magnification (67×) the dynamometamorphic alteration of the organic matter is well visible (cracks); *i, j: Dapsilodus praecipuus* BARRICK, 1977, *i:* 87×, *j:* 130×. Sample, locality and age as for *a–f*

There are only two time intervals in post-Hercynian age, where movements and rotations of the Pannonian Median Masif relative to its surroundings were possible: 1. the Jurassic-Lower Cretaceous time, in which the Pannonian Median Massif was surrounded by mobile belts in the west and north (Bükk–Igal trough), in the east-southeast (Mures trough) and in the south (dibranched Vardar zone); 2. the Paleogene during which the flysch trough of the Outer Carpathians was shortened at least in the rate 6 : 1. During the Miocene molasse sedimentation the movements of the Carpathians against the stable Europe also continued.

In the Tertiary the Inner West-Carpathians (south of the Pieniny Klippen Belt) as well as the Inner East-Carpathians should have been pushed against the stable Europe in the Carpathian arc. In this time relative lateral movements or rotations of the single units along younger faults or reactivated older ones should be expected. Perhaps the whole area south of the Pieniny Klippen Belt as well as the Eastern Alps were pushed at first to the north, later the inner West-Carpathians were pushed to the NE, whereas the area of the Hungarian Median Massif was pushed to the ENE or even to the east (in its eastern parts). Such relative movements would cause tensional features between the Eastern Alps and the West-Carpathians (e.g. Vienna Basin) and above all in the surroundings and within the Pannonian Median Massif so that a mantle diapir could rise in the area of the Pannonian Basin. The combination of this primary tension (secondarily intensified by the rising mantle diapir) and the mantle diapirism would explain the tensional features and the high heat flow in the Pannonian Basin. Compression in the Outer Carpathians and tension as well as high heat flow in the Pannonian Basin (Pannonian Median Massif and its surroundings) would be then related to the same driving forces.

Paleozoic data of the pre-Jurassic position of the Pannonian Median Massif

The Mesozoic paleogeographic reconstruction of the Carpathian area and the Pannonian Median Massif is almost exclusively based on Triassic and some Jurassic data, but also Paleozoic paleogeography, facies distribution and tectonic development are very important for any paleogeographic reconstruction in this area.

The Hercynian unmetamorphic sequence of the Bükk Paleozoic remains marine until the end of the Carboniferous (Balogh 1964). After a gap or very reduced continental sedimentation in the Lower Permian the marine sedimentation continued in the Middle Permian (lagoonal-marine) and Upper Permian. This sequence is similar to that of the Dinarids, but there marine Lower Permian can also be found.

This situation may be well explained by the existence of the Bükk–Igal trough northwest of the Pannonian Median Massif during the Upper Paleozoic. Of course, the

width of this trough was later, during the Alpine orogeny, considerably shortened (may be in a ratio of 3 : 1 to 6 : 1).

A quite different explanation was presented by Kovács (1982). He assumed a 300–500 km dextral slip along the Zagreb–Kulcs line during the Jurassic and Lower Cretaceous which would bring the Mecsek–Villány area from a pre-Jurassic position beside the Tatricum far in the NE of the sedimentation area of the Bükk Mts. into its present position far in the southwest of the Bükk Mts. But in such a hypothetical pre-Jurassic arrangement of the units, the primary dextral slip had to be by far larger than the amount of 300–500 km as estimated by Kovács (1982). According to this hypothesis the pre-Jurassic sedimentation area of the Bükk Mts. was a segment of the northwestern Dinarids, far in the southwest of its present position. On the other side, during the pre-Jurassic the southwestern margin of the basement of the Pannonian Median Massif should have been the direct continuation of the southern margin of the Tatricum in the north of the sedimentation areas of all West-Carpathian nappes (Kovács 1982, Fig. 3). After the considerable crustal shortening in the West-Carpathians during the Alpine orogeny (at least 3 : 1) the present distance between the southwestern margin of the basement of the Pannonian Median Massif and the southern margin of the Tatricum is still more than 500 km. So alone the Jurassic-Lower Cretaceous movement (before the crustal shortening!) of the Pannonian Median Massif relative to the Tatricum would require a dextral slip of minimum 1500 km. Such huge horizontal relative movements between the single units within the Carpathian realm having a pre-Alpine fixed outer frame (Bohemian Massif, East European Platform), not connected with the compressional shortening of the crust, seem to be highly improbable.

The displacement of the Bükk Mts. requires the lack of a large segment with marine Upper Paleozoic in the northwestern Dinarids, but no data support this. Moreover, the 400–500 km northeastward displacement of the Bükk Mts. from its Upper Paleozoic marine sedimentation area in the northwestern Dinarids had to cut away the marine Upper Paleozoic connections southwest of the present Bükk Mts. But quite on the contrary, according to the data of Kassai (1977) and Bérczi-Makk (1977) marine Upper Permian and/or marine Upper Carboniferous were found in boreholes south of Budapest (Bugyi), between Buda Mts. and Vértes Mts. (Alcsutdoboz), north and south of the Velence Mts. (Tabajd and Dinnyés), south of the middle Balaton (Karád, marine Upper Carboniferous) and south of the southwestern Balaton (Táska). Marine Lower Permian is present in the borehole Újfalu (SW Hungary). These data can be explained by the existence of a marine Upper Paleozoic trough between the northwestern Dinarids and the Bükk Mts. (Bükk–Igal trough), or by a northeastward meganappe-displacement of 400–500 km of the Bükk Mts. off from its former Paleozoic sedimentation area in the northwestern Dinarids.

Also the new data about the Lower Paleozoic of the Mecsek Mts. quite exclude any pre-Jurassic northern position of the Pannonian Median Massif beside the

Tatricum. In the Szalatnak–3 and Szalatnak–4 boreholes a thick Silurian sequence was found. It is dominated by dark siltstones, shales and tuffites. Lydites are very subordinate. Basic, intermediary and even rhyolithic volcanics also occur (Sz.–3 borehole). These synsedimentary volcanics, and above all Hercynian granodioritic to monzonitic subvolcanic, perhaps also plutonic rocks caused thermometamorphic alterations of different degree. Partly Knotenschiefer are present (as a part of the Silurian sequence in the Sz.–4 borehole), partly only thermic alterations of the organic matter can be observed, like in the Carboniferous to Lower Permian below the Gyűrűfű quartz porphyre (or mostly in a little higher degree).

In lydite intercalations well preserved Lower Silurian conodont faunas were found in the Sz.–3 borehole. In the Sz.–4 borehole rich conodont and acritarch associations of topmost Llandoverian to basal Wenlockian (amorphognathoides conodont zone) were found. No traces of dynamometamorphic alterations could be observed at these fossils even under higher magnifications (Fig. 2). On the contrary, the fossils of the weakly epimetamorphic Silurian sequences of the Balaton Highland and the Velence Mts. are clearly alterated by dynamometamorphic influences (Fig. 2). Silurian pebbles without any dynamometamorphic alterations are widely distributed in the continental higher Carboniferous and lowermost Permian of the Mecsek Mts.

This Silurian was sure part of the "Hüllenserie" wrapping series of the Precambrian metamorphics and granitoid rocks. In the Sz.–3 boreholes pebbles and inclusions of Cambrian to Ordovician limestones and pre-Silurian granitoid rocks could be found in synsedimentary volcanic agglomerates and tuffites. The Mecsek Mts. were therefore not Hercynian, but Precambrian consolidated (Jantsky 1979) with a last epimetamorphosis in the highest Precambrian or after the Precambrian and before the Silurian (in latter case most probably in the Upper Cambrian "Sardian Phase"). During the Hercynian orogeny only granodioritic to monzonitic magmas arose—like in other Precambrian consolidated areas—within or at the margin of the Hercynian orogen.

Quite on the contrary, the Tatricum underwent a high-degree Hercynian metamorphosis and in the whole West-Carpathians unmetamorphic Silurian is unknown. From the West-Carpathians to the south the Hercynian metamorphosis has been successively weaker: Higher epimetamorphic in the Gemerids, weakly epimetamorphic in the Velence Mts. and in the Balaton Highland, and no dynamometamorphic alterations in the Bükk* and Mecsek Mts. (anchimetamorphic alterations cannot

* Silurian rocks were until now unknown from the Bükkium. At the Strázsa-hegy near Nekézseny (southern margin of the Uppony Mts.) a large amount of weakly anchimetamorphic Silurian olistolites (or volcanotectonic blocks) were found in tuffites and tuffs and in inclusions within Middle Devonian schalstein and alterated diabases. The Silurian rocks consist of red and light to dark grey, fossiliferous, partly tuffitic limestones (including also nautiloid limestones). They contain rich Llandoverian to Přidolian conodont faunas (celloni to eosteinhornensis conodont zones, see Kozur, in press). These are the oldest faunas known until now from the Bükkium.

be excluded in both cases, because of some thermometamorphic alterations caused by younger magmatic rocks in the Mecsek Mts. and because of Alpine anchimetamorphic alterations in many parts of the Bükk Mts.).

For defending a pre-Jurassic northern position of the Mecsek Mts. beside the Tatricum, the Szalatnak Silurian will be surely regarded as a nappe by some geologists. But Alpine nappes may be excluded, because the Silurian sequence is overlain by the typical Lower Triassic Jakabhegy Sandstone Formation of the Mecsek Mts. Also a Hercynian nappe may be excluded from the geological situation. Otherwise such a hypothetical Hercynian nappe (there are no structural evidences for it!) could come only from the Dinarids or from the Bükk–Igal trough. This would also prove the pre-Jurassic southern position of the Mecsek Mts.

If the Mecsek was in pre-Jurassic time part of the Tatricum, a Hercynian nappe could be excluded. If the nappe would be pre-Sudetic, it had to be affected by the strong Hercynian metamorphosis of the Tatricum. If it would be post-Sudetic, then the nappe had to be pushed on a continental area (denudation area with some smaller continental basins in the higher Carboniferous), what is also impossible.

Acknowledgements

Prof. Dr. K Balogh, and Dipl. Geol. P Pelikán, MÁFI, Budapest, have my sincere thanks for guiding excursions, yielding important samples and giving very important explanations to the geology of the Bükk Mts. I thank also very much Mrs. Dr. A Barábas-Stuhl, Pécs, for her helps in studying the Szalatnak boreholes, Mrs. Dr. L Ravasz-Baranyai, MÁFI, Budapest, for petrological investigations of the Silurian rocks, Prof. Dr. B Jantsky, MÁFI, Budapest, and Dr. J Oravecz, Budapest, for guiding important excursions in the Precambrian of the Mecsek Mts. and in the Silurian of the Balaton Highland and Velence Mts., respectively.

References

Andrusov D 1965: Die Geologie der tschechoslovakischen Karpaten. II. 443 p., Bratislava.

Balogh K 1964: Die geologischen Bildungen des Bükk-Gebirges. *Jahrb. ungar. geol. Anst.*, 48, 245–719.

Bérczi-Makk A 1978: Upper Permian marine sediments in hydrocarbon exploring borehole Sári-2, southeast of Budapest (Hungary). *Földtani Közlöny*, 108, 313–327.

Jantsky B 1979: A mecseki gránitosodott kristályos alaphegység földtana. MÁFI Évkönyve, 60, 385.

Kassai M 1977: Data for a paleogeographic reconstruction of Transdanubia, Hungary, at the end of the Paleozoic time. *Acta Mon. Petrogr.*, 23, 41–48.

Kovács S 1982: Problems of the "Pannonian Median Massif" and the plate tectonic concept. Contributions based on the distribution of Late Paleozoic-Early Mesozoic isopic zones. *Geol. Rdsch.*, 71, 617–640.

Kozur H 1974: Probleme der Triasgliederung und Parallelisierung der germanischen und tethyalen Trias. Teil I: Abgrenzung und Gliederung der Trias. *Freiberger Forsch.-H.*, C 298, 139–197.

Kozur H 1975: Probleme der Triasgliederung und Parallelisierung der germanischen und tethyalen Trias. Teil II: Anschluss der germanischen Trias an die internationale Triasgliederung. *Freiberger Forsch.-H.*, C 304, 51–77.

Kozur H 1979: Einige Probleme der geologischen Entwicklung im südlichen Teil der Inneren Westkarpaten. *Geol. Paläont. Mitt. Innsbruck*, 9, 155–170.

Kozur H 1980: Revision der Conodontenzonierung der Mittel- und Obertrias des tethyalen Faunenreichs. *Geol. Paläont. Mitt. Innsbruck*, 10, 79–172.

Márton E 1980: Multicomponent natural remanent magnetization of migmatites, Mórágy area, southwest Hungary. *Earth Plan. Sci. Letters,* 47, 102–112.

Márton E 1981: Tectonic implication of paleomagnetic data for the Carpatho-Pannonian region. *Earth Evol. Sci.,* 3–4, 257–264.

Nagy E 1971: Der unterliassische Schichtenkomplex von Grestener Fazies im Mecsek-Gebirge (Ungarn). *Ann. Inst. Geol. Hung.,* 54, 155–159.

Patrulius D 1976: Les formations mesozoiques des Monts Apuseni septentrionaux: Correlation chronostratigraphique et faciale. *Rev. Roum. Geol., Geod., Geophys., Geogr.,* 20, 49–57.

Patrulius D, Bleahu M et al. 1971: Guidebook to excursions of the second Triassic Colloquium Carpatho-Balkan Association: The Triassic Formations of the Apuseni Mountains and of the East Carpathian Bend. *Guidebook to excursions,* 8, 86.

Patrulius D, Bleahu M et al. 1979: The Triassic Formations of the Bihor Autochton and Codru nappe-system (Apuseni Mountains). Guidebook to field trips. IIId. Triassic Colloquium of the Carpatho-Balkan Geological Association, 1979. Bucharest

Acta Geodaet., Geophys. et Montanist. Hung. Volume 19 (1—2), pp. 107—114 (1984)

GEOELECTRIC MODEL OF THE ALPINE REGIONS IN EUROPE

S N KULIK and I M LOGVINOV[1]

An analysis of the magnetotelluric soundings and frequency responses of anomalous fields in the Alpine folded area shows that in the geoelectric structure there is generally a mantle layer of high electric conductivity (asthenosphere) however, of a variable integrated conductance. Thus, below the Northern Pyrenees, H is 70 km, S about 3500 S; below the Alps, H is about 90 km, and S more than 6000 S; below the Pannonian Basin H is 80 km; below the Caucasus, H is about 90 km.

The Earth's crust of the Alpine regions is characterized by zones of high electric conductivity which produce anomalies in the geomagnetic variations. The depth till the top of the conductors is 10 to 15 km below the Carpathians and the Northern Pyrenees, and 7–13 km below some parts of the Pannonian Basin. The anomalous bodies lying below the Alps and the Caucasus have complex shapes.

Keywords: Alpine region; Alps; asthenosphere; Carpathians; Caucasus; conductivity anomaly; geoelectric model; magnetotellurics; Pannonian Basin, Pyrenees

Geologic processes taking place in the activated areas of the Earth must be reflected in the physical parameters of the rocks of the crust and upper mantle. The changes of these parameters in the course of the geologic evolution can be used as sources of information about deep processes. According to this idea, Gordienko et al. (1981) constructed a geoelectric model of the Hercynian folded areas in Europe. In the present paper an analysis of the geoelectric data will be presented about the areas of the Alpine folding. The investigated areas include the Northern Pyrenees, the Alps, the Carpathians, the Pannonian Basin and the Caucasus.

Babour et al. (1977) discovered and studied a zone of anomalous geomagnetic variations in the Northern Pyrenees. The results of this investigation is a map of the induction arrows, graphs of the anomalous fields along profiles and frequency characteristics of the anomalous field. The centre of the anomalous currents lies according to an analysis of the distribution of the anomalous currents not deeper than 20–25 km. A more exact analysis of the distribution of the anomalous currents yielded according to Vasseur and Weidelt (1977) a depth of 17 km. In their opinion the cause of the anomalous geomagnetic variations is a concentration of currents induced by ionospheric-magnetospheric sources in the surrounding Atlantic ocean and the Mediterranean Sea, in a conducting body below the studied area.

[1] Institute of Geophysics of the Academy of Sciences of the Ukranian SSR. 1252164 Kiev, Prospekt Palladina 32, USSR

When interpreting this material, an explanation of the excitation mechanism of the anomalous field in local inhomogeneities can be adopted as a redistribution of currents between the anomalous body and the embedding material and as a concentration of the anomalous currents in the medium with increased electric conductivity. As input data for the following computations frequency depending values of the modulus and of the argument of the anomalous field were used which is characterized by the maximum modulus of the anomalous field and the crossing of the value zero by the argument around $\sqrt{T} = 30\ s^{1/2}$ (in the first case, Fig. 1a), and in the second case a monotonous decrease of the modulus of the field with increasing period and also a crossing the value zero by the argument near to $\sqrt{T} = 20\ s^{1/2}$ (Fig. 2a). The total longitudinal conductance of the 2–D-body, G, is in this case $1.0–1.6 \times 10^8\ S \cdot m$. Accordingly the body causing the anomaly and having a cylindrical form with a radius of not more than 7 km must have a specific conductivity of about $1\ S \cdot m^{-1}$.

As the average conductivity of sediments is according to published data about 30 ohmm, the maximum thickness of the sediments about 5000 m, and the maximum width of the sedimentary basins 10^5 m, the value $G_{sed} = 10^7\ S \cdot m^{-1}$ has been obtained. This value is by one order of magnitude less than the above computed estimation of G

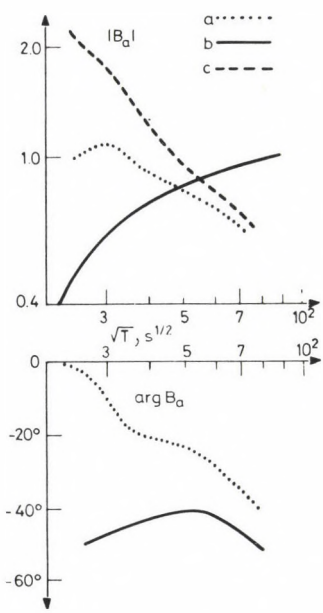

Fig. 1. a) Frequency dependence of the modulus and argument of the horizontal component of the anomalous field computed from the Fourier-transform of the impulse response,
b) the function $V(T)$ for models with circular and ellipsoidal cylinders, $G = 10^8\ S \cdot m$ and $\sigma_i/\sigma_e = 10^3$,
c) impedance of the surrounding medium (Z_0)

for the anomalous body. Therefore only an unsignificant part of the anomalous current flows in the sedimentary rocks, and the major part is concentrated in greater depths.

In Figs 1b and 2b, the impedances of the embedding medium are presented as computed on the basis of the connection existing between the anomalous field, the parameters of the anomalous body and the impedance of the embedding medium.

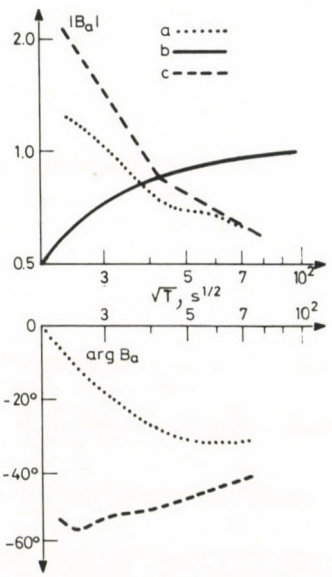

Fig. 2. a) Frequency dependence of the modulus and argument of the horizontal component of the anomalous field computed from spectral estimates of observed time series, *b)* and *c)* similarly to *b)* and *c)* in Fig. 1

From the impedances the value ϱ_k could be computed which characterizes the embedding medium. In Fig. 3 the values ϱ_k computed so are compared with the theoretical curves for different dimensions of the conductor in depths of 50–100 km. The best fit of the experimental curve with the theoretical one is obtained for the following set of parameters: thickness of the sedimentary rocks, (h_1) 3 km, their electric conductivity (ϱ_1) 30 ohmm; $h_2 = 67$ km, $\varrho_2 = 2000$ ohmm; thickness of the conducting body (h_3) 36 km, $\varrho_3 = 10$ ohmm; total longitudinal conductance 3600 S, $h_4 = 294$ km, $\varrho_4 = 1000$ ohmm. The lowest part of the profile is represented by a layer in which the resistivity continuously decreases from 10 to 0.1 ohmm.

As a result of the analysis of the magnetovariation profile, the geoelectric profile in this area can be characterized by the presence of a crustal conducting body, with a maximum depth of about 17 km, $G = 1.0–1.6 \times 10^8$ S · m and a deep conductor of 3600

S total longitudinal conductance in a depth of 70 km and therefore it can be identified with the asthenosphere.

In the area of the pre-Alpine molassic depression, in the Hohe Tauern, in the Zillertal Alps and elsewhere in Austria measurements were made using the methods of magnetovariation profiling (MVP) and magnetotelluric sounding (MTS) (Kemmerle

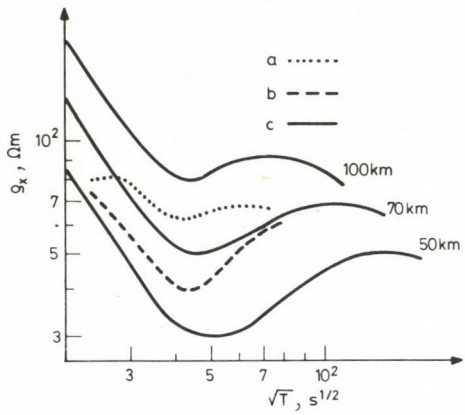

Fig. 3. Observed and theoretical MTS curves:
a) ϱ_k corresponding to the frequency dependence in Fig. 1a,
b) ϱ_k corresponding to the frequency dependence in Fig. 2a numbers on the curves give the depth values to the top of the conducting layers,
c) theoretical MTS curves, the index of the curve is the depth of the conducting layer

1974, Berktold et al. 1976, Duma 1980, Ádám et al. 1981). The MVP data along the meridian 12.5° confirm the existence of two distinct areas with anomalous geomagnetic variations, the first of them coincides with the pre-Alpine molassic depression and was caused by induction effects in the sedimentary rocks. The second zone is in the Hohe Tauern-area, where the maximum intensity of the variation field was obtained at periods of 500 s confirming the existence of an anomalous body in greater depths.

In course of the interpretation of the data from the Hohe Tauern area, at first the induction effect was estimated by the method of Kulik and Logvinov (1980b). As a next step of interpretation a best fitting horizontally layered model was chosen for the experimental MTS curves. The geoelectric profile confirms the existence of two deep conductors. The top of the upper conductor is in a depth of 30 km and appears very sharply in the Hohe Tauern area. This layer is pinching out toward the north which causes anomalies in the variations of the geomagnetic *H*-component. The second conductor appears in a depth of about 90–100 km.

Some features of the MTS curves obtained by Austrian and Hungarian geophysicists in Austria allow only to suppose the presence of a conductor in depths of about 20–40 km.

The highest intensity of the anomalous field confirms on the basis of the Wiese-vectors the complicated structure of the conductor below the Alps. The MVP measurements in the Caucasus revealed a similar distribution, where the presence of a conductor was supposed on the basis of the MVP data in depths of less than 20 km below the Big Caucasus (Vanyan et al. 1981).

From a geoelectric point of view, the Pannonian Basin can hardly be approximated by a 2–D-model (Fig. 4). Consequently its continuous sediments are isometric in plane and they are in contact with the resistive rocks of the surrounding mountain systems. This situation causes apparently a great scatter of the measured values (Ádám 1980). The main distorting factor can be the induction effect, the galvanic effect and the flow-around effect; in such a complicated geoelectric situation the smoothing out of the mentioned effects can be very easily reached by an average MTS curve characterizing the whole area.

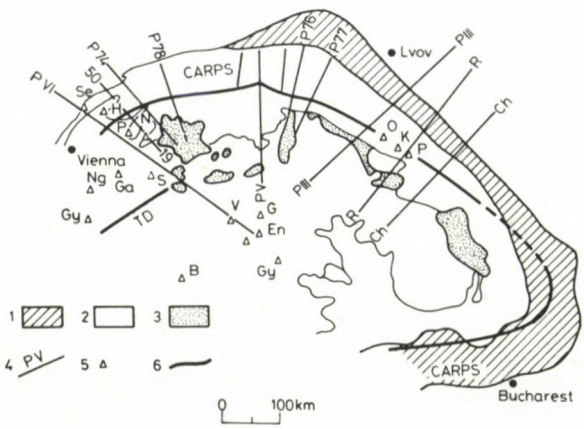

Fig. 4. Observation profiles and points (MVP and MTS) in the Carpathian region. 1: Carpathian Foredeep, 2: Carpathians, 3: Areas of Neogene volcanism, 4: MVP profiles, 5: MTS, 6: projection of the axis of the conductivity anomaly (CARPS is the area of the Carpathian anomaly, TD the Transdanubian anomaly)

The averaging of the experimental curves has been carried out separately for the Vienna and the Pannonian sedimentary basins and it was found that the average curves ϱ_k coincide (Fig. 5) allowed for a difference in the total longitudinal conductivities. Such a coincidence enables to conclude that the whole area between the Alps from west and the East-Carpathians from east has a uniform deep geoelectric structure.

The anomaly of the geomagnetic variations in the folded Carpathian area were also detected by electromagnetic methods (Bondarenko et. al. 1972, Ádám et al. 1972, Rokityansky et al. 1975, Pečova et al. 1979) in the last 20 years. These investigations have shown that the anomaly of the geomagnetic variations can be explained only by

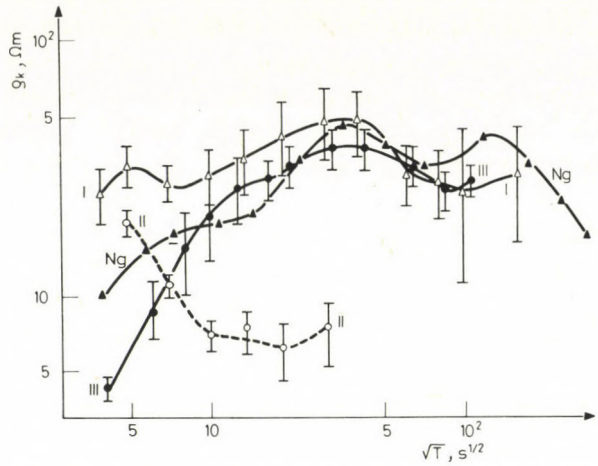

Fig. 5. ϱ_k curves, I for the Vienna basin, II for Transdanubia, III for the Pannonian basin. Vertical error bars are shown for ϱ_k

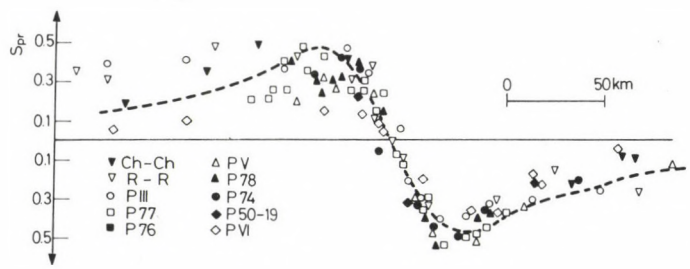

Fig. 6. Induction Wiese-vectors (S_{pr}) projected on the line normal to the axis of the Carpathian conductivity anomaly. The location of the line is shown in Fig. 4

an anomalous body of high conductivity. Detailed studies using the MVP method along many profiles across the Carpathians enabled a determination of the surface projection of the axis of this anomaly along the whole chain of the Carpathians (Fig. 4).

The main result of the MVP method is a summarized graph of the projections of Wiese's induction vectors (S_{pr}) for the period range 10–80 min (Fig. 6) in a direction normal to the axis of the anomaly. On the basis of these vector projections, the depth of the upper edge of the anomalous body can be estimated as 25–35 km (Kulik and Logvinov 1980a). In the region of the Soviet Carpathians the MTS data have confirmed the top of the anomalous body in a minimum depth of 10–14 km (Kulik et al. 1978).

Along some profiles in different regions of the Carpathians, a dependence of the anomalous fields on the periods were found and according to these data, the total longitudinal conductance of the anomalous body can be estimated to $2–5 \cdot 10^8$ S · m.

The decrease of the S_{pr}-value in the West-Carpathians indicates a pinching out of the anomalous body in the transitional zone between the West-Carpathians and the Alps.

A comparison of the experimental data with the computed curves for the crustal conductor shows an asymmetry of the observed anomalous fields in the inner and outer zones of the Carpathians. This fact can be explained by the presence of the asthenosphere below the whole Pannonian Basin and its pinching out in the direction of the East-European platform.

Electromagnetic data from the area of the Alpine folding show everywhere the presence of conductors in the Earth's crust and mantle and enable some conclusions about the structure of the Alpine geosynclines and interarc basins.

The horizontal dimension of the conductors in the Earth's crust of the folded areas surpass in most cases several times the transversal dimensions (Carpathians, Northern Pyrenees). Below the Alps and the Caucasus the conductor has a more complicated form. The tops of the conductors lie in different depths, 10-15 km below the Carpathians and the Northern Pyrenees, and 30 km below the Alps. Below a part of the Pannonian Basin (in Transdanubia) there is a conducting layer in depths between 17 and 18 km.

The conductors in the upper mantle lie about 70 km deep below the Northern Pyrenees and the Carpathians, about 90 km deep below the Alps, about 80 km deep below the Pannonian Basin and about 90 km deep below the central chain the Big Caucasus (Guganava 1981). The highest conductivity of this layer was found below the Pannonian Basin (more than 6000 S), the lowest below the Alps and probably below the Caucasus.

References

Ádám A 1980: The change of electrical structure between an orogenic and an ancient tectonic area (Carpathians and Russian Platform). *J. Geomag. Geoelectr.*, 32, 1–46.

Ádám A, Verő J, Wallner Á 1972: Regional properties of geomagnetic induction arrows in Europe. *Acta Geod. Geoph. Mont. Hung.*, 12, 251-287.

Ádám A, Märcz F, Verő J, Wallner Á, Duma G, Gutdeutsch R 1981: Magnetotelluric sounding in the transitional zone between the Eastern Alps and Pannonian Basin *J. Geophys.*, 50, 37-44.

Babour K, Menvielle M, Rossignol J C, Vasseur G 1977: Some features of a geomagnetic anomaly in Northern Pyrenees. *Acta Geod. Geoph. Mont. Hung.*, 12, 81-85.

Berktold A, Beblo M, Kemmerle K 1976: On the distribution of the electrical conductivity below the eastern Alps. *Geol. Rundschau*, 65, 715–732.

Bondarenko A P, Bilinsky A I, Sedova F I 1972: Geoelectromagnetic variations in the Soviet Carpathians. Naukova Dumka

Duma G 1980: Magnetotellurik vom Grazer Becken in die Ostalpen. In: Prot. über Koll.: *Elektromagnetische Tiefenforschung* (Berlin-Lichtenrade)

Gordienko V V, Kulik S N, Logvinov I M 1981: Asthenosphere of Epi-Hercynian Platforms *Geofiz. Zhurn.*, 3, No. 2, 202–216.

Guganava G E 1981: Connections between some geophysical fields and the deep structure of the Caucasus. Tbilisi, Mecniereba

Kemmerle K 1974: Magnetotellurik am Alpen-Nordland. In: Prot. über Koll.: *Erdmagnetischen Tiefensondierung* (Grafrath)

Kulik S N, Logvinov I M 1980a: Geoelectric model of the Carpathian regional lithosphere (according to data of MVP and MTS along the 6th international profile of DSS). *Geofiz. Zhurn.*, 2, No. 4, 79–85.

Kulik S N, Logvinov I M 1980b: Estimation of the induction effect of MTS. DAN USSR, ser. B, No. 12, 6–8.

Kulik S N, Logvinov I M, Rokityansky I I, Schulman MG, Schuman VN 1978: Longitudinal MTS curves below the axis of the Carpathian anomaly. In: *V. Vsesoyuznaya Shkola-Seminar po Electromagnitom Zondirovaniyam (Mukachevo), Abstr. of papers,* Kiev

Pečova J, Petr V, Praus O 1979: Internal electrical conductivity distribution on Czechoslovak territory. Geodynamic investigation in Czechoslovakia. Bratislava, Veda

Rokityansky I I, Kulik S N, Logvinov I M, Schuman V N 1975: The electric conductivity anomaly in the Carpathians. *Acta Geod. Geoph. Mont. Hung.*, 10, 277–286.

Vanyan L L, Gugunava G E, Dadunashvili N S Logvinov I M, Rokityansky I I, Schumann V N 1981: Some results of magnetovariation observations in the Caucasus. *Geofiz. Zhurn.*, 3, No. 6, 93–96.

Vasseur G, Weidelt P 1977: Bimodal electromagnetic induction in nonuniform thin sheets with an application to the northern Pyrenean induction anomaly. *Geophy. J. R. astr. Soc.*, 51, 669–690.

Acta Geodaet., Geophys. et Montanist. Hung. Volume 19 (1—2), pp. 115—124 (1984)

GEODYNAMIC STUDIES OF THE LITHOSPHERE IN THE WEST-CARPATHIANS

V G KUZNETSOVA[1] and M I MELNICHUK[1]

At present spatial-temporal characteristics of the geomagnetic variations of different periods are investigated which are connected with geotectonic-geodynamic processes in the Earth's crust of the Carpatho-Balkan region. For this study data of 20 observatories have been used which lie in different geostructural regions of Europe. The amplitudes and the phases of the variations at the observatories lying within the Carpatho-Balkan region differ from the corresponding values of observatories on the West-European platform. The results confirm the existence of immense inhomogeneities in the lithosphere; they differ corresponding to differences in the structure of the Earth's crust, heat flow, seismicity etc., i.e. a connection was found between anomalous effects in the geomagnetic long period variations and lithospheric structure.

The results presented here were obtained at stations of the Carpathian geodynamic polygon. Anomalous effects connected with present geodynamic processes were separated in the temporal variations of the geomagnetic field.

Keywords: Carpatho-Balkan region; conductivity anomaly; fracture tectonics; geomagnetic secular variation

For the interpretation of the connection between the spatial anomalous values of the geomagnetic field and the character of the strains in the Earth's crust, a tectonophysical crustal model for the Transcarpathian foredeep has been constructed. Movements of the big blocks of the foredeep were studied, resulting in compressional strain-nodes found in the Earth's crust in connection with earthquakes (e.g. the Uglya region).

A complex of several geophysical methods is often used for the study of the recent structure and dynamics of the tectonosphere. The information content of these methods is increasing from year to year. Such investigations are systematically used in the Carpathian polygon which was established at the Southwestern slope of the East-Carpathians and which covers the following tectonic elements: Folded Carpathians, Transcarpathian foredeep and zone of the Transcarpathian deep fracture (Carpathian Geodynamic Polygon 1978).

The main task of these complex investigations is to study the interrelations of the physical fields with seismicity as well as with deep structure and dynamics of the Earth's crust. The most important task is to collect data on temporal variations of physical parameters.

[1]Institute for Applied Problems of Mechanics and Mathematics of the Ukrainian SSR, 290047 Lvov-47, ul. Nauchnaya 3b

The temporal variations of the geomagnetic field can be considered as a geophysical phenomenon whose study enables to collect informations about the physical parameters of the terrestrial material, beginning with processes in the Earth's core and mantle up to the crust. Just for this purpose, the study of the spatial-temporal variations of the geomagnetic field with different periods has an utmost importance in detecting geotectonic and geodynamic processes. This can be illustrated by the results of a study of different period variations of the Carpatho-Balkan region.

The study was carried out using material from geomagnetic observatories in Central and Eastern Europe and several years long observations of the secular change at stations of the Carpathian geodynamic polygon. A combination of these informations enabled to study variations with different periods and spatial dimensions (local and regional changes) in the geomagnetic field and to connect them to structural and geodynamic regions.

For a study of the regional characteristics of the secular variation in the Carpatho-Balkan area for the interval 1960–1980, data of 20 observatories were used which lie in different structural zones. The smooth part of the field, the trend, reflecting the global characteristics of the secular change was approximated by a second order polynomial in all the three components of the geomagnetic field (Kuznetsova and Chigin 1981). From the remaining field, being the difference between the observed field and the trend, a part of nearly 10-years periodicity can be split off whose source could not be unambiguously identified. It is supposed that these variations are caused by the superposition of two sources, one in the ionospheric ring current having a cyclic variation due to changes of its parameters within the solar cycle, the other within the Earth (Rivin 1979). A comparison of the amplitudes and phases of this variation shows that at the observatories Hurbanovo, Grocka, Tihany, Surlari, Panagyurishte which lie within the Carpatho-Balkan mountain system, distortions of the 10-years period can be observed (Fig. 1).

The mentioned observatories lie in a big inhomogeneous zone of the lithosphere which differs in its crustal structure, thermal field, seismicity, and recent crustal movements from the consolidated ancient East-European platforms in the East and from the tectonically more stable areas of Hercynian foldings in Northwest and West.

The results correspond sufficiently well to those of Mundt (1980) who analyzed the average five-years values of the secular variation on the whole area of Europe for 1950-1975 on the basis of the yearly averages of 44 geomagnetic observatories. In Central Europe he observed a northwest-southeast striking zone which can be identified on the basis of the sign of the anomalies in the secular variation being different from that in neighborous territories. Just within this zone we observed the 10-years periodic variations.

Thus a connection was found between anomalous effects in long period variations (4–10 years) with the structure of the lithosphere. Shorter period variations were analyzed using monthly averages of the four observatories Surlari, Odessa,

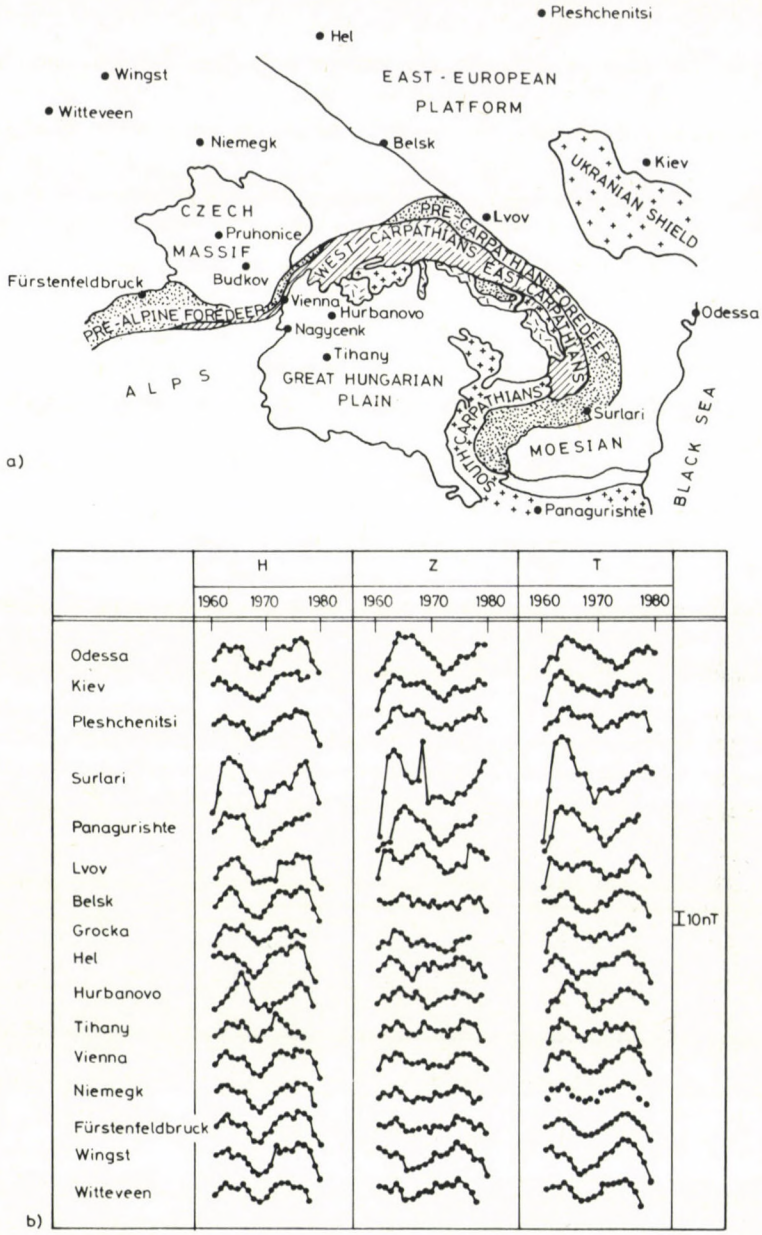

Fig. 1. Result of the analysis of the 10-years variation of the geomagnetic field in the Carpatho-Balkan region
a) distribution of the observatories
b) curves of the variations of the rest field for the interval 1960–1980

Panagyurishte and Kiev (Maksimchuk 1981). The observatories were selected so that a comparison of these variations should be possible for the seismoactive region of the Carpathians (observatories Surlari and Panagyurishte) with observatories lying in tectonically quiet areas. In the residual, field variations with periods of about two years could be separated which appear most significantly at the observatory Surlari lying at a distance of 150 km from the Vrancea epicentral zone of deep focus earthquakes. In a number of cases the anomalous effects in the geomagnetic field coincide temporally with the moments of strong earthquakes.

Thus in the regional characteristics of the secular variations of the Carpatho-Balkan region, some local effects could be found which were observed during long observation series at stations of the Carpathian geodynamic polygon.

The task of the studies at the polygon was to separate anomalous effects in the temporal variations of the geomagnetic field connected with present tectonic movements. The measurements at a number of points were processed using the method of synchronous observations referred to a basic station, and the parameter studied is the difference ΔT betwen the station studied and the basic station. The temporal variations of this quantity ΔT (the values $\Delta\Delta T$) show an anomalous temporal variation of the geomagnetic field.

For a study of the general characteristics of the spatial distribution of the anomalous areas in the years 1976–1981, the dispersion (σ^2) of the quantity ΔT was used at each station in the interval studied (Fig. 2). At stations where the value ΔT has no change between the different years of the studied interval the value of σ^2 shows the scatter of the data due to different random sources (measurement errors, disturbances). In such cases σ^2 is less than 2 nT. At stations where during the interval some anomalous changes of the field are present, the dispersion increases significantly.

The results of the studies at the polygon gave following results:

1. On the basis of many repeated measurements, a linearly extended zone could be identified in the Carpathians which spatially coincides with the Transcarpathian seismoactive deep fracture, where σ^2 can be as high as 10 nT. In this zone, anomalous changes of the geomagnetic variations could be detected in a wide range of periods from short period bay-type disturbances (1.5–2 hours) to daily variations, Sq. These deviations of the geomagnetic variations are connected with the Carpathian zone of geoelectric inhomogeneities which lies at the contact of the Inner and Outer Carpathians and it has a Transcarpathian strike. These data show the possibility of the mapping of active deep fractures in which the anomalies of the electric conductivity appear (Kuznetsova and Maksimchuk 1979).

2. Systematic tectonomagnetic studies at the polygon enabled to detect local areas of anomalous variations of the field (σ^2 up to 4 nT) which lie in areas of volcanic rock complexes of high magnetic parameters (up to 1 CGS) (Kuznetsova 1981). There is a connection between these anomalous variations and seismic events. The supposed seismic origin of the anomalous variations opens the possibility to study the changes of

the strain-deformation state of the crust on the basis of continuous geomagnetic measurements. Such observations were already initiated in some anomalous areas. From this follows the possibility of the application of tectonomagnetic studies for prognostic purposes.

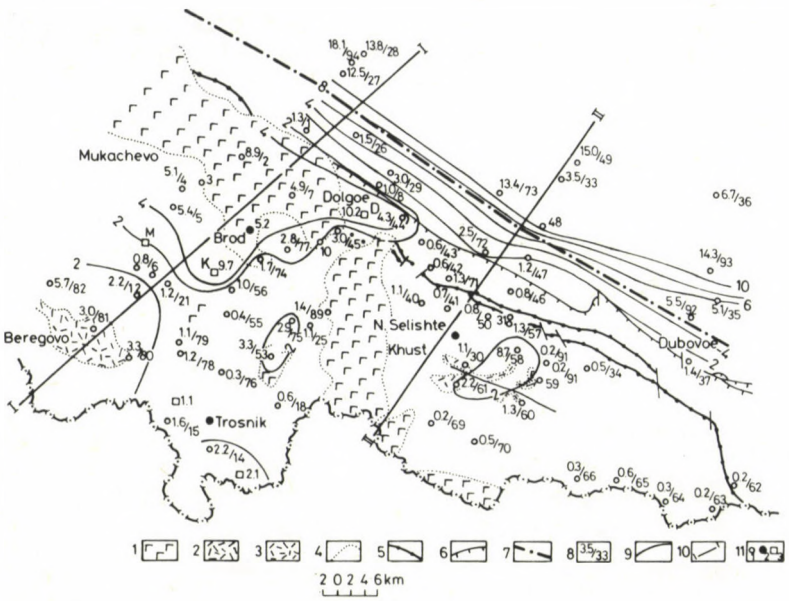

Fig. 2. Map of the spatial distribution of the dispersion of ΔT in the Carpathian geodynamic polygon. 1 — volcanogenic formations of the Gutin suite, 2 — axis of volcanogenic rocks and their tuffs in the Beregovo Hills, 3 — layers of Nankovian tuffs, 4 — boundary of the volcanogenic formations, 5 — downwards and upwards faults, 6 — regional upthrusts, 7 — axis of the Carpathian electroconductivity anomaly, 8 — nominator: dispersion of the value ΔT for the period 1976–1981 (σ^2) at the stations in nT, denominator: number of the station, 9 — isolines of σ^2 in nT, 10 — position of the profiles I and II, 11 — sites of the geomagnetic observations 1: normal set, 2: stationary stations, 3: secular universal basic station

3. On the maps of the anomalous variations of the field some areas can be selected where the temporal variations have identical character and sign. Each of these zones is elongated along the Carpathian chain and confirms the longitudinal extension of the zones of the main structural elements being characteristic for the tectonics of the Carpathians. It is interesting that the position of the zero isoline coincides with tectonic fractures which border blocks of different crustal structures and within which the slow variations ΔT have nearly identical character. These data also confirm the connection of the temporal variations of the geomagnetic field with the crustal structure.

In addition to geomagnetic studies, the investigation of geodynamic processes at the Carpathian polygon included an analysis of the seismic activity, studies of recent crustal movements and tectonophysical modeling.

For an explanation of the connection between the areas of the anomalous changes of the geomagnetic field and the crustal strains, tectonophysical models were constructed for the Transcarpathian foredeep. This modeling was made by the Tectonics Laboratory of the Institute of Earth Physics of the Academy of Sciences of the URSS led by Osokin.

Let us consider the movements of the megablocks of the Transcarpathian foredeep and the crustal strains. Repeated measurements on the position of triangulation points carried out in 75 years have shown that the crustal blocks of the foredeep are moving in different directions (Melnichuk 1978, Sobakar et al. 1975). Thus in the Perechin-Dolgoe area there is a connection between four blocks: the Uzhgorod, Zaluzh and Perechin, Svalyava fractures cross there. At the section Dolgoe-Solotvino the blocks Solotvino and Folded Carpathians connect each other, which move toward northeast as a single block. As an effect of such movements of the crustal blocks in the Transcarpathian region, the Transcarpathian fracture at the section Perechin-Dolgoe is an extensional zone, and at the section Dolgoe-Solotvino, a compressional one (Fig. 3, Melnichuk 1975, 1978). A somewhat different situation has been observed in the zone of the Prepannonian fracture. Thus in the zone Chop-Beregovo there is a compressional zone, and to the south, in the Solotvino depression on the Beregovo-Vyshkovo section there is an extensional zone. As result of these movements of the blocks, both the Transcarpathian and the Prepannonian fractures are submitted to the effect of extensional forces on certain sections, on others to compressional forces. Repeated levelings show that within the limits of the Transcarpathian region there are no differences in the vertical movements (Sobakar et al. 1975). This fact confirms in a certain extent our hypothesis about the character of the deformations of this zone. Figure 3 shows that the Uzhgorod block is moving toward west-southwest, and the Svalyava block toward northeast with a tendency to rotate toward north. These movements yield in the region of Dolgoe a strain node in compressional sense and at the same time in the region Svalyava, there is a region of extensional forces, i.e. the characteristic Transcarpathian fractures with sliding deformations which are connected evidently with the earthquakes.

The observed compressional and extensional zones are the results of oscillatory motions of the megablocks of the crust in the foredeeps. Only such periodic oscillations of the basement can explain the observed vertical and horizontal crustal movements and their spatial-temporal character.

The strain in the crust of the foredeeps can be identified first of all by means of the epicentral maps (Fig. 3) connected with the blocks (Carpathian Geodynamic Polygon 1978, Melnichuk 1982). The connection of the seismicity with the tectonics can be characterized by the force field, its effect on the structural elements of the foredeep which are connected with the accumulation and discharge of the strains.

Evidently the observed rifts of the Jurassic limestone (Pieniny belt zone of the Transcarpathian fracture) are the results of the breaking up of the monolith due to the

periodically changing force field and the discharge of the critical strain which surpass the strength of the limestone.

A typical example of the connection of the strain in the crust with the earthquakes is the region around Uglya and Kolodno (Pronishin and Pustovitenko 1981). Here earthquakes with intensities of 6–7° occurred on August 23 and September 22, 1979 with hypocentral depths of 4 km in both cases. It should be remarked that these earthquakes occurred in the zone of the Transcarpathian fracture where earlier earthquakes could also be observed: Chumalevo (1935), 5–6°, Dragovo (1937) 6–7°, Dulovo, Tereblya and a series of others within a radius of 25 km occurring in the years 1781, 1830, 1870, 1886, 1894 and 1926 with intensities of 6–7° and depths of the hypocentres of 10 km. An analysis of the earthquakes near to Uglya ($M = 3.5$) by Pronishin and Pustovitenko (1981) led to a conclusion about the similarity of the type of the impulses in the focus of both earthquakes and the identity of the focus regions of the two earthquakes of August 23 and September 22, 1979.

The isoseists of these earthquakes show that the energy of the seismic waves propagating toward northeast met the complicated Transcarpathian fracture zone

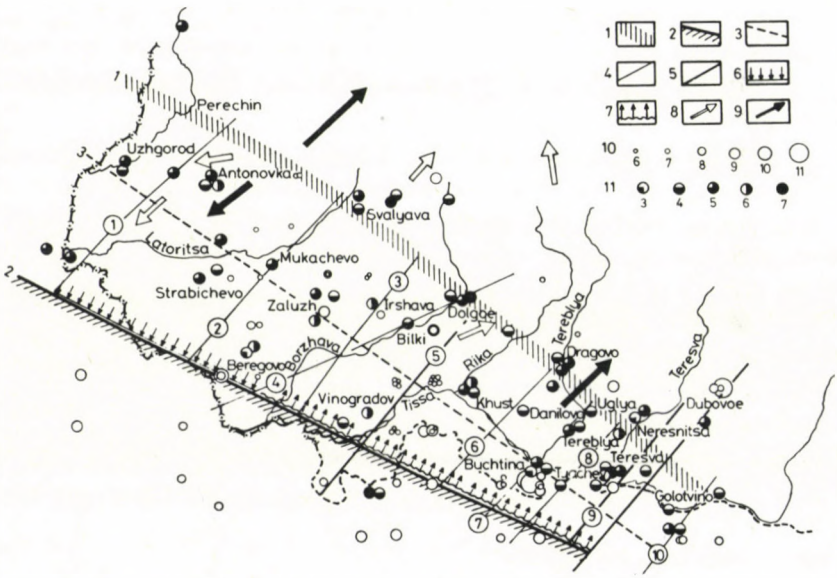

Fig. 3. Fracture tectonics of the Transcarpathian foredeep 1 — Zakarpatsky deep fracture, 2 — Pannonian boundary fracture, 3 — Central (Uzhgorod-Tyachev) zone of the impulsive ruptures from shallow sources, 4 — perpendicular fractures (with numbers in circles) 1: Chop, 2: Latoritsa (Mukachevo), 3: Shalanki-Irshava, 4: Borzhava, 5: Vinogradovo, 6: Velyatin-Dragovo, 7: Tereblya, 8: Novoselitsa, 9: Dubovoe-Grushevo, 10: Kobiletskaya-Polyana, 5 — Shopurkino-Nadvornaya-Monastirska fracture of the Pannonian-Volynian cross-depression in the East-Carpathians, 6 — compressional zones, 7 — extensional zones, 8 — vectors of the linear displacement of stations in the triangulation network, 9 — direction of the horizontal movement of megablocks of the Earth's crust, 10 — magnitude of the earthquakes, 11 — epicentres of earthquakes (intensities)

which absorps a part of this energy, and the other part propagates further toward the Folded Carpathians where it completely disappears. The seismic waves which propagate toward southwest meet the central zone of the fracture where a part of the energy is also absorbed decreasing so the destroying effect to southwest from this fracture zone.

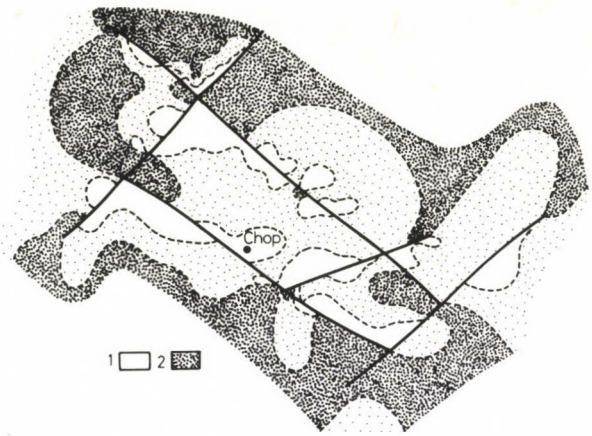

Fig. 4. Strains in the crust of the Transcarpathian foredeep. 1 — normal background strains, 2 — local strain fields.

It should be mentioned that according to Pronishin and Pustovitenko's (1981) data the rupture striked in focus of both earthquakes near Uglya and Kolodno from southwest to northeast with a strike direction of the breaking around 45°. The movement of the Solotvino megablock is directed in the same direction.

A quantitative estimation of the strain field and its connection with the tectonics was obtained from modeling of the strains in the crustal foredeep with special equipment.

The first model of the foredeep was bordered by immense longitudinal and perpendicular fractures and included one perpendicular fracture at Borzhavo. In case of an uniaxial strain, the field in the foredeep can be characterized by a normal state except increased strains at the junctions of the fractures (Fig. 4).

The second foredeep model contained the same fractures but the supposed deformation zones and the movements of the big crustal blocks were also included. For an imitation of the compressed zone and the extensional zone, respectively, supplementary frictions were introduced in the crossing zones of the Transcarpathian and Prepannonian fractures. In the case of uniaxial compression a completely different crustal stress field was observed in the foredeep (Fig. 4). In addition to the normal strain field, local fields appeared coinciding with the fractures, mainly in the Transcarpathian region. In connection with these field appreciable earthquakes have

also appeared. The most interesting one is the wide zone of increased strains in the region at Uglya.

The physical modeling of the strains in the crust of the foredeep shows that without taking into account the partial discharge of the strains near Uglya, the whole zone is in a strained state and the possibility of repeated earthquakes in the near future cannot be excluded.

The seismic potential of the Transcarpathian zone is determined mainly by the complicated structures which are responsible for the strain field of the foredeep. The different foci of the earthquakes are connected with existing structures and their strains. A typical example for this supposition is the Uglya earthquake which appeared and was connected with an existing structure, the Solotvino block and the fractures bordering this block, being responsible for the earthquakes. It is evident that the greater crustal volumes are included into the strains, the stronger the expected earthquakes will be. In the present case this is the volume of the crustal material of the Solotvino block (bordered by the Belyatin-Dragovo, Novoselitsa and Zakarpatsky fractures and the central fracture zone of ruptures) which means according to our computations more than 1000 km^3 rocks and which was included in the Uglya earthquake. The accumulation of the strains in this volume of the crust lasted more than 40 years (Pronishin and Pustovitenko 1981).

Estimating the seismic hazard in the Transcarpathian zone it should be remarked that it is determined by the seismic potential mainly of the active fractures and existing structural elements in the Earth's crust.

The strains of the crust of the foredeep have a complicated character. The different structural elements of the foredeep have different strains, therefore the Transcarpathian foredeep can be considered as a zone of present tectonic activity, where different values of the crustal strains can be observed and they determine the scale and type of the force fields there.

A study of the complex processes determining the geodynamic conditions is the task of our future investigations. It is of great importance to compare the results of the geodynamic investigations along the whole Carpathian arc and to interpret their characteristics together.

References

Carpathian Geodynamic Polygon. Sov. Radio, 1978.

Kuznetsova V G 1981: Local temporal variations of the geomagnetic field in the seismoactive Transcarpathian foredeep. *Geofiz. Zhurnal*, 2, No. 6, 105–110.

Kuznetsova V G, Chigin A I 1981: Character of the secular variation of the geomagnetic field in the Carpatho-Balkan region. In: *II. All-union conference: The geomagnetic main field, rock magnetism and paleomagnetism*, Part I, Tbilisi.

Kuznetsova V G, Maksimchuck V K 1979: Possibility to detect anomalies of the electric conductivity by repeated high-precision observations of the geomagnetic field. *Geofiz. ob.*, No. 89, 31—35.

Maksimchuk V E 1981: Connection of the variation of the horizontal component of the geomagnetic field in the observatory Surlari with seismicity of the Southern Carpathians. In: *II. All-union conference: The geomagnetic main field, rock magnetism and paleomagnetism,* Part I, Tbilisi

Melnichuk M I 1975: Some characteristics of the appearance of deep processes in the tectonics of the Transcarpathian foredeep. *Geofiz. ob.,* 66, 11–18.

Melnichuk M I 1978: Possible zones of deformations of the Earth's crust in the Transcarpathian foredeep. In: *Geologic structure of the mineral resources of Ukraina.* Kiev, Naukova Dumka

Melnichuk M I 1982: Genetic connection of the seismic processes with tectonics in the Carpathian region. *Geofiz. Zhurnal,* 4, No. 2, 34–41.

Mundt W 1980: The character of the geomagnetic secular variation in Europe. *Gerlands Beitr., Geophysik,* 89, 451–466.

Pronishin R S, Pustovitenko B G 1981: Character of the processes in the epicentral zones of the Transcarpathian carthquakes in 1979. *Geofiz. Zhurnal,* 3, No. 6, 71–84.

Rivin Yu R 1979: Spherical harmonic analysis of the 10-years variations of the geomagnetic field. *Geomagnetizm i aeronomiya,* 19, 120–125.

Sobakar G T, Somov B I, Kuznetsova V G 1975: Present dynamics and structure of the Earth's crust in the Carpathians and neighborous areas. Naukova Dumka

Acta Geodaet., Geophys. et Montanist. Hung. Volume 19 (1—2), pp. 125—134 (1984)

GEOTHERMAL SITUATIONS OF THE CARPATHO-BALKAN AREA

E A LUBIMOVA[1]

Geothermics plays an important role in the discussion on the origin of the Carpathians and the basin within it. After a survey of present ideas in this field, a new analysis of existing data is presented. The fractures of the area are described and those four belonging to the Alpine geotectonic cycle selected, the sedimentation effects as well summarized.

Heat flow has a maximum in the Pannonian Basin, and it decreases toward the Carpathian arc and further. Using other geophysical data, the depths of the partial melting is estimated to 16–20 km and 60–110 km, respectively. These values are compared to data on the electrical conductivity from induction studies. Conclusions are drawn about the possible geologic history of the area.

Special attention is devoted to the low heat flow in Transylvania, probably due to a sinking plate.

Keywords: Carpathians; conductivity anomaly; deep fractures, geothermics; Earth's crust; Flysch zone; heat flow

Introduction

The study of the geothermal situation in the Carpatho-Balkan area is one of the main possibilities to explain the machanism of this folded system. As it is known there is a long lasting discussion if the Carpathian arc is a result of the collision of two continental plates or the result of a deep mantle diapir. At present, however, it is not yet decided what a thermal profile should originate from such a structure.

According to a whole series of different data, the Carpatho-Balkan region lies in a zone, where earlier the oceanic region of the Thetys should have existed which later closed itself. Some remnants of the disappeared lithospheric plates being covered by the ocean can be traced on the basis of the intermediate and deep seismic activity in certain areas along the extended Alpine-Himalayan zone of attenuation, particularly also below the Carpathian arc. In Romania, the seismic activity in a depth of 200 km outlines the surface of a nearly vertical plate which is immersed into the Carpathian arc (Roman 1970). The fact of the immersion is endorsed by negative anomalies of the gravity field, by high thermal fluxes, by the attenuation of seismic waves and by the presence of andesites. The approximate position of the Romanian seismic zone and the distribution of the strains are presented in Fig. 1 (curve 1) in comparison with the

[1] Institute of Physics of the Earth. 123810 Moscow, Bolshaya Gruzinskaya 10.

configuration of the Hindukush (2) and Kurilian zones (3). As it can be seen, the Romanian zone of the seismic foci is nearly vertical. The whole zone can be characterized by compressive strains in depths between 100 and 200 km. This fact has a primary importance in the construction of tectonic models and models of the thermal evolution. Thermal and tectonic parameters are clearly connected, even if the interpretation of this fact is not always the same.

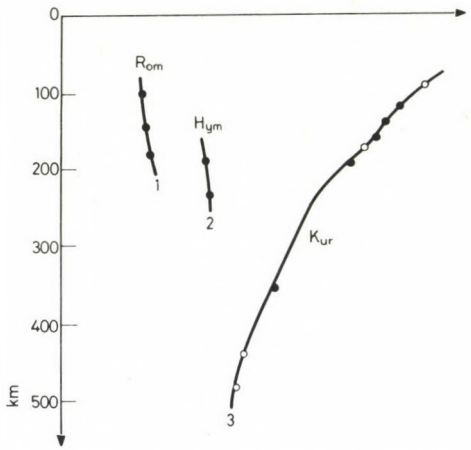

Fig. 1. Approximate position of seismic zones and the distribution of strains along the dipping planes. Open circles: mechanism with the axis of the compression, full circles: with the axis of stretching for the dipping zone (after Isaks and Molnar 1971)

International Deep Seismic Profiles III and VI cross the present region in the area of Hungary, Czechoslovakia and the GDR (Chekunov 1972, Sollogub and Chekunov 1978). Some experiments were made to construct complex geophysical models along Profile VI for the lithosphere of the West-Carpathians, the Czech Massif and the Saxo-Thuringian zone taking into account their magmatic history, gravity and thermal data and magnetotelluric soundings. The basis of this model was the activization of the mantle (Subbotin et al. 1976, Buryanov et al. 1980) causing a rise of the liquidus. This rise of the liquidus must have ensured some magmatism which appeared only in the area crossed by fractures of Carpathian and West-Sudetian strikes, and the crust was heated here till partial melting in an area being more extended than the West-Carpathians.

Some complex models were presented about the position of the tectonic plates and about a proposed mechanism of the collision of continental plates, i.e. the mechanism "continent-continent collision" (Bodri and Bodri 1977, Horváth et al. 1977, Horváth and Royden 1981, Stegena 1976), created by an overthrust of the Carpathian region to the European Massif. In both suggestions geothermal and MT

data and many conclusions about the anomalous heating of the Pannonian Basin and the Pre-Carpathian region played an important role.

In the following, geothermal data will be once again analyzed and compared with tectonic and other conclusions and the most urgent tasks in the study of the thermal model of the Carpatho-Balkan area will be raised.

Tectonic fractures

We are mostly interested in the development of the geothermal conditions, therefore the first problem to be discussed is tectonics, not only deep tectonics, but also the tectonics of the Earth's crust, its block structure and the character of the tectonic fractures. There are quite recent results of the refraction seismics and deep seismic soundings of the West-Ukrainian geophysical exploration expedition and of the Spetsgeofizika trust, and the distribution of the fractures in the Carpathian region has been corrected taking into account borehole data, too (Zayats 1980). Some projecting sections were found in the granitic layer which represents the surface of the consolidated crust (in the Early Proterozoic) which later descended to depths of 7–20 km in the area Nadvornaya–Ivano-Frankovsk–Kolomiya and were subsequently filled by sediments. During 900–1000 million years the immense sedimentary complex became a metamorphized layer of the Earth's crust. A scheme of the fractures is given in Fig. 2. The parallel course of nine fractures should be observed here which intersect the tenth one, that of Tyachevsk.

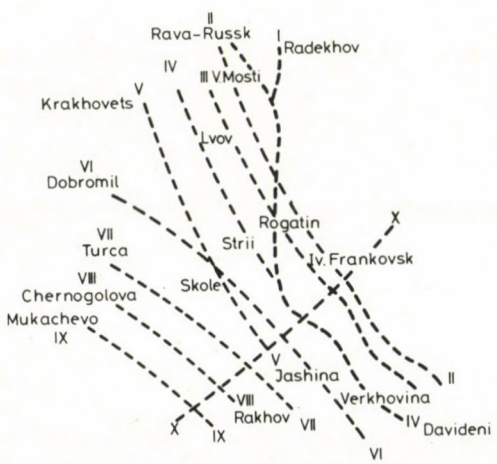

Fig. 2. Main deep fractures of the Carpathian region. I Radekhov-Rogatin region, II Nesterovo-Chernovits, III Veliko Mosti-Storozhenetsk, IV Rava-Russk-Davideni, V Krakovets-Ko-Verkhovina, VI Predkarpatsky, VII Uzhok, VIII Chernogolova, IX Zakarpatsky, X Tyachev-Nadvornya-Monastirshen

The Ivano-Frankovsk foredeep lies on the pre-Riphean crystalline basement. The sedimentation form of the Lvov and Podolian foredeeps have been cofirmed. The Ivano-Frankovsk foredeep is filled with sediments of the Upper Proterozoic having a total thickness of up to 10 km.

These facts are important when studying the distribution of the heat flow values, as the process of sedimentation causes a deformation or more exactly a decrease of the original heat flow and the fractures ensure the fluid component.

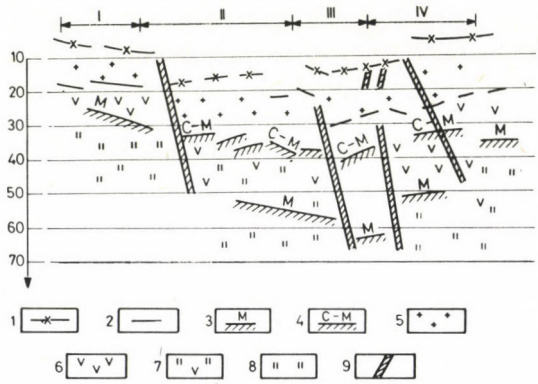

Fig. 3. Structure of the Earth's crust and deep crustal mantle fractures along the geotraverse "Zakarpatsky foredeep–Flysch Carpathians–Predkarpatsky foredeep". Notations: 1. surface of the crystalline basement, 2. boundaries in the granite layer, 3. bottom of the crustal-mantle complex, 4. top of the crustal-mantle complex, 5. "granitic" layer, 6. "basaltic" layer, 7. crustal-mantle complex, 8. mantle, 9. deep fractures

At the surface of the Baykalian basement the Baykalide orogen (Mozhaisko-Dobrudzhian chains) appears together with the pre-mountain foredeeps. These structures are bordered from northwest by the Krakovets-Verkhovina (Fig. 2, V) and Rava-Russk–Davideni (Fig. 2, IV) deep fractures. The axis of the pre-mountain foredeep of the Baykalides bordered by these fractures, are directed toward Gorodok-Verkhovina. The axis of the Krakovets-Verkhovina foredeep lies around Skole-Yasinya. The root of the fracture is fixed at the surface by the pre-Riphean crystalline basement which reaches the depth of 20 km and the depth of the Mohorovičić surface.

The Alpine movements were the most active ones among all geotectonic movements. The Alpine tectonic activity is connected with deep subcrustal processes below the Great Hungarian Plain.

The Uzhok and Predkarpatsky fractures (Fig. 2, VII, VI) lie about 4–5 km far from each other and reach depths of about 12 km. They are overlain by a sedimentary cover overthrusted from southwest. The direction of the Predkarpatsky deep fracture follows the regional Carpathian gravity minimum which diverges from the

Predkarpatsky fracture only toward southeast and continues toward Verkhovina. Toward northwest, the Baykalide structure covers the formations of the inner zone of the Predkarpatsky foredeep. Towards southwest it disappears under the overthrust of the Folded Carpathians. Thus on the surface of the pre-Riphean crystalline basement of the Carpathians, four deep fractures can be distinguished belonging to the Alpine geotectonic cycle: Predkarpatsky (VI), Uzhok (VII), Chernogolova (VIII), Zakarpatsky (IX). They determine the block structure of the surface of the consolidated crust, the Predkarpatsky and Inner Carpathian grabens and the Carpathian horst.

Figure 3 gives and example for the general structure of the crust which is broken up by fractures through the Zakarpatsky foredeep, the Flysch Carpathians and the Predkarpatsky foredeep. When interpreting the boundaries of the parts in the profile of the Carpatho-Balkan region (CBR), attention should be paid to the fluctuations which violates the phase equilibrium due to changes in the thermal conditions and due to changes in the pressure (Rakhimova and Altman 1980). The effect of the changes in the load were studied at the shift of the phase boundary basalt (gabbro)-eclogite. This can be the alternation of sedimentation and erosion. Due to changes of the pressure, polymorphous transitions appear much earlier than any changes of the thermal conductivity due to sedimentation. Nevertheless, the thermal background determines the development of tectonic movements which cause rises and descents of the Moho-boundary. Let us see the geothermal data.

Geothermal data

Significant contributions to the study of the geothermic conditions of the Carpatho-Balkan region (CBR) were made by Soviet, Romanian, Czechoslovak, Hungarian, Polish and Bulgarian scientists (Shushpanov 1966, Gordienko 1975, Kutas 1978, Majorovicz 1977, Čermák 1976, Stegena 1976, Veliciu and Visarion 1982, Demetrescu 1977). Already the first measurements of the heat flow in the Transcarpathian region by IFZ in Zaluzh and Mukachevo have shown a high value of about 110 mWm^{-2} (Shushpanov 1966). Since that many measurements have shown that the heat flow values are around 100–110 mWm^{-2} in the central area of the Pannonian Basin (Stegena 1976), it decreases to 65–70 mWm^{-2} in the Carpathians, and slightly decreases towards northwest to 50–60 mWm^{-2}. The profile of the heat flow along the International Geotraverse VI through the West-Carpathians to the Saxo-Thuringian zone is shown in Fig. 4. The previously listed levels are complicated by the presence of local structures. Their small extension and coincidence with geologic structures confirm the connection with near-surface structures, with fractures and other zones of disturbances. The distribution of the heat flow has been used for constructing the geotherms of the Carpathians e.g. across the Pannonian depression—Voronezh Massif (Kutas 1978).

If the earliest Cretaceous is accepted as the earliest sedimentation period in the history of the development of the Carpathians, and considering the depth of 38 km as the equilibrium depth of the phase boundary, then the phase temperature of the equilibrium will be 570 °C according to the Clapeyron-equation. Nearly the same

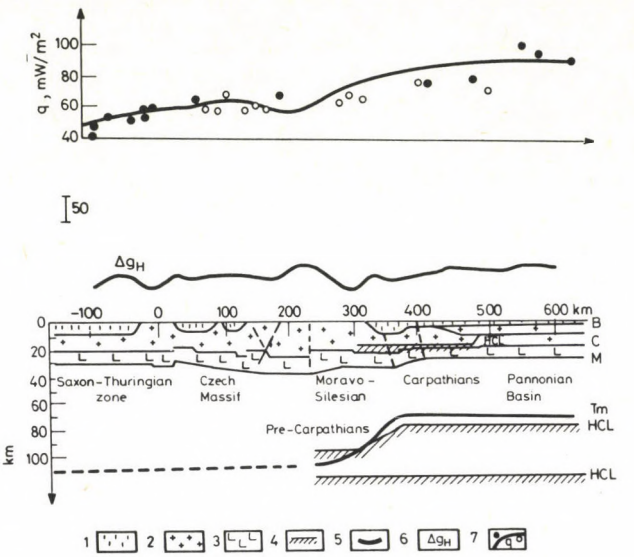

Fig. 4. Profile of the observed heat flow q_H, distribution of gravity anomalies in a scale of 50 mg and the lithospheric profile along the International Deep Seismic Profile VI across the West-Carpathians, the Czech Massif, and the Saxo-Thuringian zone. Notations: 1. sedimentary rocks of the cover and folded basement, 2. rocks of the granitic layer, 3. "basaltic" layer, 4. possible boundaries of the high electric conductivity layers (HCL), 5. supposed temperatures of the partial melting, 6. observed variations of the gravitational force (after Buryanov et al. 1980)

isotherm, i.e. that of 580 °C crosses in the lithosphere model of the West-Carpathians the zone of the connection between the Precarpathian foredeep and the West-Carpathians in a depth of 40 km (Kutas 1978). In the Transcarpathian foredeep and in the Transcarpathian deep fracture zone the temperature is significantly higher, i.e. above 700 °C.

Taking into account the velocity of the sedimentation and its duration in different sedimentation periods, the huge temporal changes of the phase surface can be estimated.

The heat production can be estimated on the basis of empiric formulas and 1.4–1.5 μWm^{-3} result for the sedimentary layer and the upper layer of the consolidated crust (granite layer), 0.5 μWm^{-3} for the basalt layer and 0.3 μWm^{-3} for

the layers below. For the density range $\varrho = 2.65$–2.95 gcm^{-3} the heat generation A can be described by the exponential equation:

$$A = 1.3 \exp 5\ (2.7 - \varrho)$$

or its connection with the seismic velocity

$$A = 2.7 + 0.25\ (V_p - 6).$$

Based on the values of q or A, the zone of partial melting is in depths of 16–20 km below the Carpathians and the Pannonian Massif. Its top can be identified with the geotherm 650 °C, its bottom is at the Conrad boundary (Buryanov et al. 1980). The second zone of partial melting is in the mantle at depths of 60–110 km (Fig. 4).

A comparison of geothermal models with geodynamic and complex geophysical data

The high heat flow in the Pannonian depression was correlated with the somewhat elevated position of the electrically highly conducting layer (HCL) (Ádám 1965, Stegena 1976, Berdichevsky et al. 1973). A similar correlation was observed for the South-Caspian depression which is else a remnant of the here supposed big ocean Thetys. The thickness of the sedimentary layer in Southern Caspia is even greater than in Pannonia due to the continuous sedimentation in the present inner sea and this process absorps a part of the heat.

According to recent data on the longitudinal conductance of the sedimentary cover of the Carpathian region (Kravchenko and Sapuzhak 1980) the maximum value of the total conductance is 1000–1500 S, and it was detected in the area of Irshava and Zaluzh where the heat flow anomaly approximates its maximum. In the surrounding area, there are some local highs in a general level around 500 S in the conductance up to 750 S near the town "40 p" and a minimum in the region of Uzhgorod.

The main part of the conducting sediments in the Transcarpathian foredeep are Tortonian and Lower Sarmatian, i.e. Neogene rocks. For the computation of the total conductance of all sedimentary layers the conductance of deeper sediments was as determined from borehole logging and seismological data. The longitudinal conductance is first of all correlated with the thickness of the sedimentary layers.

The conductor of the Carpathian anomaly (computed as the magnetic field of a spheroid in the field of direct currents) is supposed to extend over 700 km in both directions from the centre of the East-Carpathians and it happens to meet the conductor below the Alps. The Carpathian anomaly of the electric conductivity has its axis below the Pienniny Klippen Belt. For a model of a circular cylinder, the maximum depth of the conductor is 35 km, for an elliptic cylinder 18 km (Jankowski et al. 1977, Buryanov et al. 1980).

The data of MTS enable to distinguish three conducting zones in the Pannonian Basin and in the Carpathians (Fig. 4): the lowest is the conductive basement of the upper mantle (it was detected in all regions of the Carpathian region, but not all MT curves enable their identification), the intermediate layer which can be identified with the top of the asthenosphere, in the Pannonian Basin and in the Carpathians at depths of 80–120 km, in the Czech Massif in 100–120 km, then an upper crustal conducting layer appearing most clearly in the Alpine profiles at depths of 10–20 km which is clearly connected with the effusive rocks of the Alpine part and also with the appearance of the deep melting in the extended zone of deep fractures which can be found at the connection of the West- and East-Carpathians with the West-European platform. This fracture is accompanied by Neogene magmatism.

According to temperature computations, the top of the 100 km thick asthenosphere occurs at a depth of around 110 km below the central zones of the Hercynides and it deepens to depths of around 130–150 km in its surroundings. The contribution of melt material in the pyrolithic or lherzolitic material of the mantle, corresponding to the asthenosphere, is at a level of about 15–25%. In the period of the Alpine activization (in the Carpathians the main phases occurred 25 and 12 million years b.p.) the fractures in the area of the Czech Massif were rejuvenized and very strong disjunctive dislocations appeared at its contact with the folded zones, the Hercynides, and weaker ones in the least strong part of the massif, in the Tepel-Barranden zone (Buřyanov et al. 1980). Based on the geothermal model two periods of melting can be supposed in the subcrustal part of the mantle: 25 million years b.p. in the depth interval of 35–55 km, and 12 million years b.p. in the depth range 55–75 km with 50% substitution of the material there. Corresponding to this the deeper lithospheric layer had to deepen its position by 20 km and the asthenosphere by 10 km as follows from the density model. The volcanism at the end of the Pliocene can also be explained. In this period the melting interval was in a depth of 70–75 km. This hypothetic mechanism of the activization is the "mobilization" of the mantle according to one model (Buryanov et al. 1980).

The other mechanism is connected with the tectonic plates and the hypotheses of the supposed continent-continent collision, the folded zones of the Carpathians and the increase of the heat flow as it should be in case of island arc-systems.

On the other side according to Stegena's (1976) opinion the hot mantle diapir is the most likely cause of the increased heat flow in the Pannonian Basin. It seems that the two mechanisms complement each other.

Thermal conditions in the Romanian Carpathians

A great and important contribution to the study of the heat flow, of the deep isothermal structure and of the geothermal conditions of the Balkan, and specially in Romania were made by Romanian scientists (Veliciu 1977, Demetrescu 1977). They compared mainly the thermal field of the Transcarpathian depression, the Pannonian Basin, the East-Carpathians, using data on the distribution of deep temperatures, heat conductivity and heat flow. The Transylvanian Basin and the crystalline zone of the East-Carpathians, the Moesian platform are characterized by low heat flow values (30–60 mWm^{-2} and 30–80 mWm^{-2} respectively). The Pannonian Basin and the zone of the Neogene volcanism represent areas of high heat flow (72–132 mWm^{-2}).

Veliciu and Visarion (1982) proposed a geothermal model for the lithosphere below the Romanian Carpathians by modelling the tectonic plates. In case of the East-Carpathians, the heat production by radiogene sources and the processes which accompany the decrease of the lithosphere in the very long period of the subduction can explain many features of the observed high heat flow. For the explanation of the low heat flow in Transylvania which is an intermountain basin of Neogene age, three models of the heat generation were proposed in order to explain the conditions in the basin which differ from those in other ensialic interarc basins.

The study of the thermal structure in the crust and upper mantle along several DSP shows that the horizontal variations of the thermal parameters depend on the structure and composition of the crust inside of which conductive processes determine the heat flow. In a regional scale the contribution from mantle processes is significant and means a contribution of the convective transport. The mantle heat flow for Transylvania is 20–30 mWm^{-2}, and the temperature at the basis of the crust is 600 °C, being much lower than the corresponding value in the Pannonian Basin, where $T_m = 800$–900 °C. Consequently geothermics confirms the existence of a more rigid and colder lithosphere in the Transylvanian region.

References

Ádám A 1965: Einige Hypothese über den Aufbau des oberen Erdmantels in Ungarn. *Gerlands Beiträge zur Geophysik*, 74, (1), 20–40

Ádám A, Horváth F, Stegena L 1977: Geodynamics of the Pannonian basin: Geothermal and electromagnetic aspects. *Acta Geod. Acad. Sci. Hung.*, 21, 251–260.

Bodri L, Bodri B 1977: Induced convection. — A possible source mechanism of heat anomaly of the Pannonian basin. *Acta Geologica Hung.*, 21, 277–285.

Boldizsár T 1956: Terrestrial heat flow in Hungary. *Geofis. Pura Appl.*, 34, 66-70.

Buryanov V B, Gordienko V V, Kulik S N, Logvinov I M 1980: Complex geophysical model of the lithosphere in the West-Carpathians, in the Czecz Massif and in the Saxon-Thuringian zone (Along International Deep Seismic Profile VI). *Geof. Zhurn.*, 3, 3–13.

Čermák V 1976: Heat flow investigation in Czechoslovakia. In: *Geoelectric and Geothermal Studies*. A Ádám ed. Akadémiai Kiadó, Budapest, 414–424.

Chekunov A V 1972: Structure of the Earth's crust and tectonics of the horn of the European part of the USSR. Naukova Dumka, Kiev

Demetrescu C 1979: On the geothermal regime of some tectonics units in Rumania. In: *Geothermics and Geothermal Energy*. L Rybach and L Stegena eds, Basel and Stuttgart, 124–134.

Gordienko V V 1975: Thermal anomalies of geosynclines. Naukova Dumka, Kiev

Gordienko V V 1980: Radiogene heat production in the Earth's crust and heat flow from the mantle of ancient platforms. *Geof. Zhurn.*, 2, No 3, 35–42.

Haenel B 1973: Heat flow measurements in Austria and heat flow maps of Central Europe. *Zeit. Geoph.*, 3, 425–440.

Horváth F, Royden L 1981: Mechanism for the Formation of the Intra-Carpathian Basins: A Review. *Earth Evolution Sciences*, 1, 307–316.

Horváth F, Vörös A, Onuoha K M 1977: Plate-tectonics of the Western Carpatho-Pannonian region: a working hypothesis. *Acta Geologica Hung.*, 21, 207–221.

Horváth F, Bodri L, Ottlik P 1979: Geothermics of Hungary and the Tectonophysics of the Pannonian Basin "Red Spot". In: *Terrestrial Heat Flow in Europe*. V Čermák and L Rybach eds, Springer Verlag, Berlin-Heidelberg, 206–217.

Isacks B, Molnar P 1971: Distribution of stresses in the descending lithosphere from a global survey of focal-mechanism solutions of mantle earthquakes. *Rev. Geophys. Space Phys.*, 9, 103–104.

Jankowski I, Szymanski A, Pec K, Cerv V, Petr V, Pecová J, Praus O 1977: Induction anomaly in the Carpathians. *Studia Geoph.*, 21, 1, 35–57.

Kravchenko A P, Sapuzhak 1980: Conductivity of the sedimentary cover in the Carpathian region. *Geof. Zhurn.* 2, No 3., 73.

Kutas P I 1978: Heat flow field and thermal model of the Earth's crust. Naukova Dumka

Majorowicz J 1977: Contribution of the mantle to the heat flow in Northern Central Europe. *Acta Geologica Hung.*, 21, 269–275.

Praus O, Pecová J, Petr V, Dvorak Z, Tobyasová M 1970: Magnetotelluric inhomogeneity of the transition zone between Bohemian massif and the West-Carpathians. *Geophys. Sb.*, 18, 403–432.

Rakhimova I Sh, Altman A D 1980: The effect of the phase transition of the material on the boundaries in the Earth's crust of the Ukrainian Carpathians. *Geof. Zhurn.*, 2, No 3, 78–84.

Roman C 1970: Seismicity in Romania — evidence for the sinking lithosphere. *Nature*, 228, 1176–1178.

Shushpanov A P 1966: On the thermal regime of the Carpathian area of the USSR. In: *Problems of the terrestrial heat flow*. E A Lubimova ed., Nauka, 133–143.

Sollogub V B, Chekunov A V 1978: Deep structure of the Soviet Carpathians. Kiev, Naukova Dumka.

Stegena L 1976: Geothermics, magnetotelluric and tectophysics of the Pannonian Basin. In: *Geoelectric and Geothermal Studies*. A Ádám ed. Akadémiai Kiadó, Budapest, 572–585.

Subbotin S I, Sollugob V B, Chekunov A V 1976: Structure and evolution of the Earth's crust in the Ukraine and in the neighborous regions of Thetys according to new data and ideas. *Geof. sb., vip.*, 70, 17.

Veliciu S 1977: Some results on the mantle heat flow investigation in Romania. *Acta Geol. Sci. Hung.*, 21, 256–258.

Veliciu S, Visarion M 1982: On the low heat flow in the Transylvanian Basin. In: *Geothermics and Geothermal energy*. V Čermák and R Haenel eds, Schweizerbart'sche Verlagsbuchandlung, Stuttgart, 91–100.

Zayats Kh B 1980: The general surface of the Earth's crust in the Carpathian region and the deepening of the Ukrainian shield before it. *Geof. Zhurn.*, 2, No 3, 29–34.

Acta Geodaet., Geophys. et Montanist. Hung. Volume 19 (1—2), pp. 135 (1984)

SOME REPRESENTATIVE SEISMIC SECTIONS IN THE PANNONIAN BASIN OF HUNGARY

(EXTENDED ABSTRACT)

Z NAGY,[1] GY POGÁCSÁS,[1] J RUMPLER,[1] B SZANYI[1]

Keywords: Pannonian Basin; seismic sections; stratigraphy

Seismic time sections acquisited in the Pannonian basin of Hungary for hydrocarbon surveys and viewed as representative sections for the stratification of extensional basins were presented at the conference. Advances in seismic profiling, data processing and data display make it possible to carry out geological interpretation about the evolution of sedimentary basins and sub-basins including their relation to early and Neogene tectonics. The interpretation of seismic data contains many pitfalls. Ambiguities involved in our interpretation were openly debated among the participants. To solve some of the geological interpretation problems of the seismic sections other geophysical methods are called upon. An example was cited for electromagnetic deep soundings by the EM FRS method that supplemented the seismic data in the foothills of Bükk mountains.

The paper put the emphasis on the interpretation of regional and stratigraphic features. Special interest was paid to fault types incl. growth faults, listric faults, etc.

[1]Geophysical Exploration Company. 1068 Budapest, Gorkij fasor 42., Hungary

Acta Geodaet., Geophys. et Montanist. Hung. Volume 19 (1—2), pp. 137—138 (1984)

SEISMIC STRATIGRAPHY IN HUNGARY

(EXTENDED ABSTRACT)

Gy POGÁCSÁS[1]

Keywords: Neogene depression; Pannonian Basin; seismic stratigraphy

In the Hungarian part of the Pannonian Basin a depression system separated into several units in the depth was developed during the Neogene-Quaternary.

In the variously subsiding parts of the Pannonian Basin the Neogene sedimentation was subdivided into several cycles. Due to the sporadic arrangement of boreholes and to discontinuous core sampling, extension and relationships of the sedimentary facies especially at the deep zones cannot be revealed by traditional direct (paleontological, petrological) investigations. The up-to-date multifold coverage seismic measurements provide a lot of new data and a relatively uniform spatial distribution of the informations. The most characteristic depositional sequences of the East Hungarian Neogene depressions and their stratigraphic classification were interpreted and correlated on the basis of amplitudes, frequencies, continuity and configurations of the reflection horizons. The structure of the sediments deposited in different environment varies and this is indicated on the seismic profiles. The seismic stratigraphic classification of the different depressions was reviewed by Késmárky et al. (1982) and by Pogácsás and Völgyi (1982) and by Pogácsás et al. (1982).

Based on the subsequently overlying seismic facies the following main phase of paleogeography and evolution can be verified. In the area of deep depressions basin filling sedimentation took place in the Badenian and Sarmatian which continued also in the Lower Pannonian (seismic facies *A* and *B*). No erosion unconformity or hiatus can be recognized in the Pannonian sediments of the deep depression (Fig. 1).

The Lower Pannonian is characterized by a gradual transgression (facies *C*). The transgression formations are overlain by regression sequences (facies *D* and *E*). The picture of facies *D* characterized by prograding reflections reminds one of a delta front and that of facies *E* of a delta-background-like sedimentation environment. Facies *F* is represented by lacustrine-fluviatile sediments.

Analysing the coincidence and the overlapping of stratigraphic classifications based on different geophysical methods, Gy Pogácsás and L Völgyi compiled the correlation table of these coincidences (Fig. 2).

[1]Geophysical Exploration Company. Budapest, Népköztársaság útja 59., H-1062, Hungary

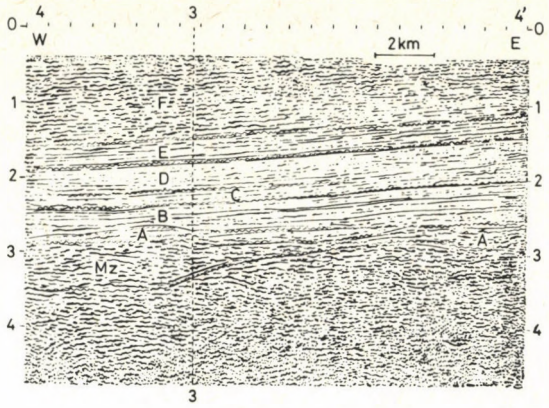

Fig. 1. Seismic stratigraphy in the Pannonian Basin

Seismic facies		Lithogenetic units	Lithostratigraphic units	
			Formation	Member
F		Pa_2	HEVES IV	Nagyalföld 2
				Zagyva 1
E	E_2 / E_1		CSONGRÁD III	Törtel 2
D	D_2 / D_1	Pa_1^2		Algyő 1
C	C_2		JÁSZKUNSÁG II	Szolnok 2
	C_1	Pa_1^{1b}		1 Nagykörű
B	B	Pa_1^{1a}	MAROS I	4 Tótkomlós / Vésárhely 3 / 2 Békés / Dorozsma 1
	B			
A	A'	-	Miocene	
Cr	Mz	-	Basement	

Fig. 2. Correlation between stratigraphies

References

Késmárky I, Pogácsás Gy, Szanyi B 1982: Seismic stratigraphic interpretation in neogene-quartenary depressions of eastern Hungary. (In Hungarian) *Magyar Geofizika,* 23, 20–30.

Pogácsás Gy, Völgyi L 1982: Seismic representation of Pannonian lithostratigraphic and lithogenetic units in eastern Hungary (in Hungarian). *Magyar Geofizika,* 23, 82–93.

Pogácsás Gy, Lukács Z, Tóth S 1982: Comparative analysis of deep geology in the Zala and Drava Basins on the basis of seismic time sections (in Hungarian). *Magyar Geofizika,* 23, 178–193.

Acta Geodaet., Geophys. et Montanist. Hung. Volume 19 (1—2), pp. 139—144 (1984)

MODELING OF THE ELECTROMAGNETIC FIELD IN THE CARPATHIAN REGION

I I ROKITYANSKY[1] and M N YUDIN[2]

3-D model computations were carried out in several variants for the explanation of the Carpathian and Transdanubian anomalies. The parameters (depth, conductivity) of the conductor introduced into the model are discussed and the resulting anomalous fields compared to experimental results. The effect of highly conducting sediments within the basin is also studied. Anomalies outside of the Carpathians are possible, too. It is proposed to continue these model calculations.

Keywords: Carpathians; conductivity anomaly; electromagnetic distorsion; Pannonian Basin; three dimensional numerical modeling

The Carpathian region is covered by a dense network of electromagnetic observations which shows a complex geoelectrical structure of the region (Ádám 1976, Rokityansky 1982). The most characteristic feature of the region is the presence at depths of 10–15 km of an electrical conducting zone in the crust which is elongated along the Folded Carpathians (Fig. 1). The second crustal anomaly is the Transdanubian one which lies to the North of Lake Balaton. The existence and the location of the anomalies have been determined with high reliability.

A deeper conducting zone is the asthenosphere. The presence of a high heat flow anomaly in the Hungarian basin leads to a conclusion on the anomalous heating of the deep material and to supposition of the existence of a well-developed asthenosphere. A very important point is the confirmation of this supposition by geoelectrical measurements. A considerable amount of deep magnetotelluric soundings (DMTS) carried out by the group lead by Ádám (1970, 1976) shows a complicated form of the MTS-curves, with significant variations from station to station within the Hungarian basin. Some curves allow a conclusion about the existence of the asthenosphere of high conductivity, but it has not been proved by all the curves, consequently there is some doubt about this result. One of the considerations which fed this doubt about the asthenospheric parameters in the Carpathian region, is the shunt-effect of the electric field through the crustal conductive anomaly inside of the Carpathian arc. The present paper contains the first results on the mathematical modeling for the investigation of

[1]Institute of Geophysics, Academy of Sciences of the UkSSR, 252164 Kiev-164, Prosp. Palladina 32.
[2]Moscow Geological Exploration Institute (MGRI)

the effect of the Carpathian crustal anomaly on the results of DMTS in connection with the problem of existence of the asthenosphere and evaluation its parameters.

The computations were carried out using the finite difference method with the algorithm proposed by Yudin (1980) with a grid consisting of $14 \times 14 \times 14$ elements with the results obtained in 15×15 grid points at the surface. The programme automatically selects the network for the computations depending on the given model

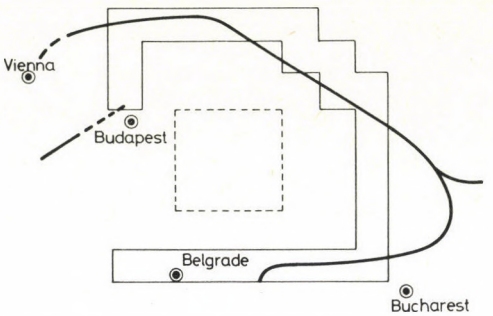

Fig. 1. The Carpathian (thick line from Vienna to near to Belgrade) and the Transdanubian (near to Budapest) crustal anomalies of the electric conductivity (Rokityansky 1982) and the contours of the models used in the computations

to obtain the best possible results in an optimization. The first model of the Carpathians was too complicated and no reliable results were obtained. Then in a next step the model was simplified to the form presented in Figs 1–3. As can be seen from Fig. 1, it roughly corresponds to the location of the Carpathian and Transdanubian anomalies with the supposition that they became united in the northwestern part of the figure. The model has been "composed" on an equally spaced grid of 8×8 elements with the dimensions 60×60 km for each element and this model is presented in Figs 1–3. The programme has transformed this model into an even simpler one so that the inhomogeneities were concentrated in the central 6×6 elements of the grid with dimensions 80×80 km for each in order to enable the field to attain its normal value at the boundaries of the model. The results of the computations for the modulus and for the argument of all six components of the electromagnetic field were obtained in digital form for 15×15 grid points from which 7×7 were above the inhomogeneities. For an easier survey of the results they are presented in form of isolines. If analyzing these digital results it should not be forgotten that they were obtained in a loose network with big elements. Therefore the details in the isoline map (Figs 2, 3) should not be considered as reliable ones.

The computations were carried out up to now only for one polarization — for a current flying in N–S direction (along the axis X). The phases were not yet analyzed.

The first model was without asthenosphere and high conducting sedimentary layers and consisted of a conducting, homogeneous sedimentary layer with a longitudinal conductivity of 50 Ω^{-1}, a thick (499 km) layer with a low conductivity (1000 Ohmm), within which the conducting body is in depths between 15 and 23 km in the form of a non-closed square with an open oblique angle section corresponding to the Carpathian crustal conductivity anomaly. The parameters of this body correspond to estimates (Rokityansky 1975, 1982, Ádám 1976) obtained from field measurements for the Carpathian anomaly. Below 500 km the conducting mantle follows roughly corresponding to the data obtained from a global GDS. Figure 2 shows the results of

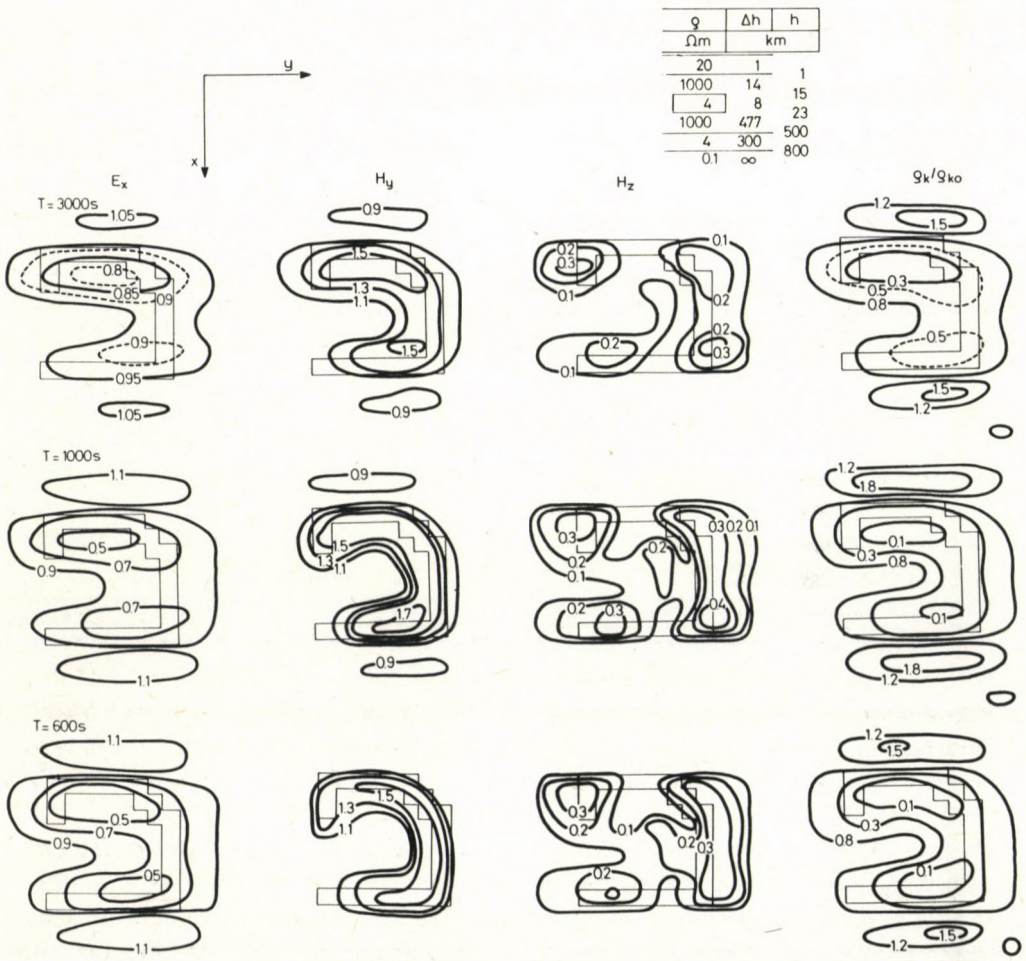

Fig. 2. Results of the computations on the model of the Carpathians for the cross section shown in the upper right corner. The inhomogeneities occur in depths of 15–23 km. ϱ_{ko} is the apparent resistivity far from the inhomogeneity. The primary field is a plane wave of vertical incidence with an electric field polarized along the *X*-axis

the computations for three periods. The values of E_x and H_y at the boundary of the grid approximate the value 1. The isolines of H_y agree (if one takes into account the very rude approximation used in this model) with the values measured in field.

The isolines H_z can be understood after taking into account the phase data which are indicative to such important informations as the change of sign in H_z when crossing the anomaly. However, as this change of the sign has a local character, its appearance in our rough grid is not clear and it should be specially investigated. Thus in the followings data about H_z will not be considered any more.

The frequency dependence of the maximum anomalous fields E_x and H_y correspond approximately to estimates on the basis of 2-D models (Rokityansky 1982). With increasing periods the anomalous area of the field E_x is widening in the direction Y which corresponds the situation in case of E-polarization in 2-D models. The appearance of additional anomalies E_x and H_y with opposite sign at frontal areas of the inhomogeneity (to the north and to the south of it) can be explained by a concentration of the current in the embedding rocks which flow through the conductivity anomaly (concentration effect). This effect can be observed in case of 2-D models for the E-polarization, it is local and reaches its maximum value at longer periods (up to D.C.). In the maps of the ϱ_a-isolines the maximum values in these supplementary anomalies reach 2.2, inside of the isoline 1.8 at a period of $T = 1000$ s and they are quickly decreasing both with increasing and decreasing periods. By taking into account the rough, approximative character of the model, this effect can attain a much greater amplitude in certain local regions and this fact should be kept in mind when interpreting MT anomalies mainly in the area to the north of the Carpathian anomaly. As the effect is strongly dependent on frequency it can cause additional curvatures or extrema on the MTS curves.

The main anomaly which appears as a decrease of E_x and ϱ_k includes the greatest part of the area inside of the arc of the crustal conductivity anomaly with exception of the western, latitudinally central part of the region. This anomaly-free zone must be the greater the shorter the periods of the variations are. Nevertheless, the computations did not reveal such a situation what can be explained by the too rough grid of the elements in the model. In the remaining area inside of the arc of the crustal conductivity anomaly, E_x and ϱ_k are considerably lower due to the effect of the anomaly, and this is especially true in the places near to the anomaly (northern and southeastern part of the area inside of the arc).

In the second model (Fig. 3) the crustal conductivity anomaly does not differ from that in the first model, but the normal cross section differs considerably: the resistivity of the poor conductor in depths between 1 and 500 km decreased from 1000 to 4000 Ohmm, and in the depths between 100 and 150 km a conducting asthenosphere has been introduced ($\varrho = 10$ Ohmm, $S = 5000\ \Omega^{-1}$). In addition, in the centre of this model a quadratic surface inhomogeneous zone has been introduced in an area of the dimension 180×180 km roughly corresponding sediments in the centre of the

Pannonian Basin. A comparison between Fig. 2 and Fig. 3 shows that the anomalous field of the second model is considerably less than that of the first one in spite of the same anomalous body in both models.

The maximum of the anomalous field H_y reaches 10 % (isoline 1.1 in Fig. 3) being less than the observed value in the area of the real Carpathian anomaly. This difference shows that the normal profile (first of all, the asthenosphere) has been chosen as too conductive in the second model.

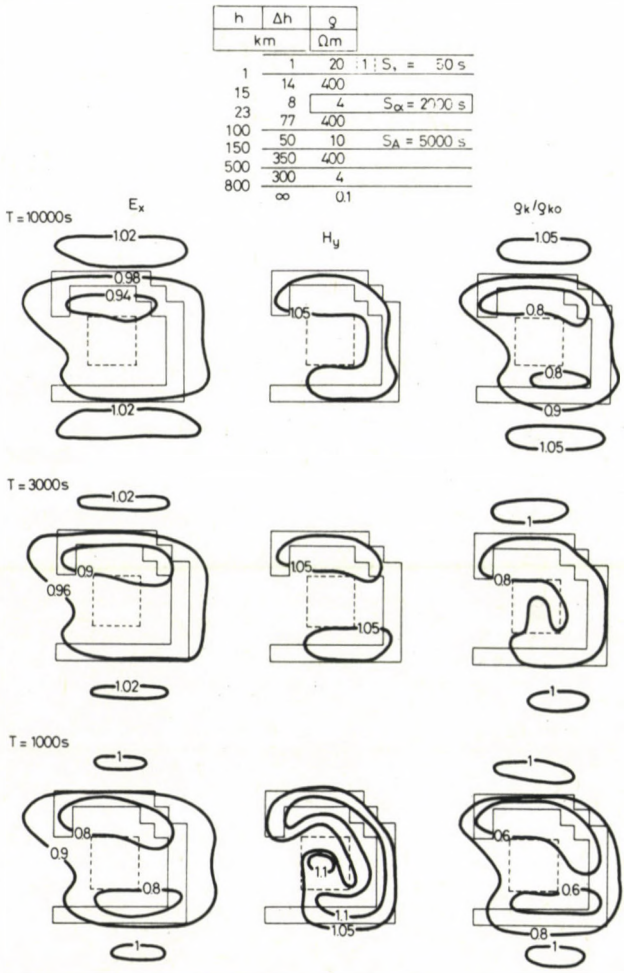

Fig. 3. Results of the computations on the model of the Carpathians with an asthenosphere of conductivity 5000 Ω^{-1} and an inhomogeneous sedimentary cover of 1000 Ω^{-1} (within the dotted line). See also the legend of Fig. 2

The inhomogeneity of the sedimentary cover (in the square of 180×180 km) with a summarized longitudinal conductivity of $S = 1000\ \Omega^{-1}$ in comparison with the surrounding value of $S_0 = 50\ \Omega^{-1}$ does not result in any considerable anomaly in the field E_x but this result seems rather strange.

Conclusion

1. In case of the given configuration and conductivity of the crustal anomaly, the conductivity of the surrounding material (10^{-3} ohm^{-1} m^{-1}) was high enough to give a strong anomalous field in H_y due to a concentration of currents in the anomaly (Model I). A further increase of the conductivity to 2.5×10^{-3} ohm^{-1} m^{-1} did not cause an increase of the anomalous field (Model II) but on the contrary, it decreased it due to a decrease of the impedance of the normal cross section.

2. Outside of the arc of the electric conductivity anomaly, E_x- and H_y-anomalies of signs opposed to the main one can be observed. They are caused by the concentration of the currents and may cause the strong distortions of the MTS curves.

3. The main anomalous field E_x (and ϱ_k) can be observed above the anomaly of the electric conductivity spreading in directions transverse to the primary field E_o and inside of the arc.

For an explanation of the character of the field variations in the central area of the arc of the Carpathian conductivity anomaly further computations are necessary with a finer grid.

References

Ádám A 1970: Problems of electric upper mantle research in the Hungarian basin. Bull. Geod. Geophys. Res. Lab., Sopron

Ádám A ed. 1976: Geoelectric and Geothermal Studies. KAPG Geophys. Monograph. Budapest, Akadémiai Kiadó

Rokityansky I I 1975: Investigation of the electrical conductivity anomalies with magnetovariational profiling. Kiev, Naukova Dumka

Rokityansky I I 1982: Geoelectromagnetic Investigation of the Earth's Crust and Mantle. Berlin-Heidelberg-New York, Springer

Yudin M N 1980: Computation of the 3D magnetotelluric problem with the method of variational difference. In: *Problems of the sea electromagnetic investigations*, Moscow, IZMIRAN, 96-102.

Acta Geodaet., Geophys. et Montanist. Hung. Volume 19 (1—2), pp. 145—146 (1984)

APPLICABILITY OF DIFFERENT ORGANIC MATURATION PARAMETERS

(EXTENDED ABSTRACT)

Cs Sajgó[1], J Lefler[1], Z A Horváth[1]

Keywords: organic maturation; temperature, time history; vitrinite reflectance

During the last two decades numerous empirical methods were introduced to characterize the transformation or maturation of dispersed organic matter in sediments as a function of subsidence.

The goal of experts was the same in every case to set up an auxiliary scale for hydrocarbon generation processes. Methods include optical ones (vitrinite reflectance, palynomorph colouration, fluorescence of liptinites), gross analyses of kerogen (pyrolysis, elemental, ESR), abundance and quality of bitumens and gaseous hydrocarbons and molecular parameters (ratios of products in different isomerization, aromatization and cracking reactions of hydrocarbons).

All the mentioned methods have been successfully applied in petroleum exploration. Nevertheless, most of them are not applicable in general owing either to the absence of the component required or to the absence of the universal scale. The greatest part of the petroleum geochemists believes the applicability of the above mentioned parameters to depend on the reliability of their calibrations as a function of temperature and time (e.g. time-temperature index). This opinion is especially widespread in case of vitrinite reflectance.

On the basis of our experience and theoretical considerations, most of the parameters (except those based only on the cracking process) may not be used as direct and universal parameters of oil generation. Namely, on the basis of their scales these may not predict the genuine values of onset, peak and deadline of petroleum genesis.

The main problem of these parameters is that they are governed by different reactions from the free radical cracking which is the main reaction of oil generation, and so they have different frequency factors and activation energy values, too, consequently the temperature dependence of their reaction rates is not similar to that of oil generation. In different reactions the reaction volume changes variously, therefore not only the temperature dependence, but the pressure dependence must be also different in the quasi-closed system of petroleum genesis.

[1] Laboratory for Geochemical Research, Hungarian Academy of Sciences. H-1112 Budapest, Budaörsi út 45.

To check the thermal history of basin formation, three organic reactions were chosen (the conversion of 20R − 5α(H), 14α(H), 17α(H) − steranes, and 22R − − 17α(H), 21β(H) − hopanes to 20S and 22S isomers, resp. and aromatization of 5α(H) and 5β(H) − 20 $R-C_{29}$ C-ring monoaromatic steroid hydrocarbons to 20 $R\,C_{28}$ − triaromatic steroid hydrocarbons). The reactants are ubiquitous in sedimentary rocks at the stage of diagenesis. They derived from buried natural products and belong to the so-called biological marker compounds.

The activation energy (E) and frequency factor (A) values were determined in samples of the Hód-*I* borehole (Pannonian Basin, near to Szeged). The absolute ages of samples can be determined relatively reliably on the basis of biostratigraphy due to the existence of a superthick Neogene sequence. The temperature data used were based on corrected logging data by the help of some static measurements. We accepted the present geothermal gradient to be maximal and assumed that the progress of three reactions could be described by unimolecular first-order reaction laws. Thus, the temperature-time integration could be carried out numerically. We obtained A and E of $1.46 \cdot 10^{12}\ ma^{-1}$ and 92.3 kJ mol^{-1} for sterane isomerization, $4.8 \cdot 10^{12}\ ma^{-1}$ and 91 kJ mol^{-1} for hopane isomerization and $9.68 \cdot 10^{16}\ ma^{-1}$ and 126 kJ mol^{-1} for aromatization. These reactions have different temperature/time ranges and, of course, we can only use them within their ranges.

The task of future is to test the general validity of reaction parameters. If they are proven applicable to other sedimentary sequences, the temperature/time histories of basins will be reconstructable from some analytical measurements. If the reaction constants are not universal, they need to be determined in every instance, but in this case we can solve the problem by the synthesis and successive approaches of geochemical data and geophysical model.

This study shows that some biological marker compounds in sedimentary sequences can record the temperature/time history of a basin within certain temperature/time ranges.

Acta Geodaet., Geophys. et Montanist. Hung. Volume 19 (1—2), pp. 147—152 (1984)

CRUST AND UPPER MANTLE INVESTIGATION BY MAGNETOTELLURIC SOUNDINGS IN ROMANIA

D STĂNICĂ[1] and M STĂNICĂ[1]

This paper presents a synthesis of magnetotelluric investigations in the last 4 years and provides an experimental contribution to the study of the distribution of the electrical conductivity in the Earth's crust and upper mantle. The soundings reveal materials of the crystalline basement whose top occurs at depths ranging from 3 to 18 km and the partial melting of the asthenospheric material in the depth ranges from 80 to 250 km.

Keywords: asthenosphere; Carpathians; geoelectric structure; Moesian Platform area

Magnetotelluric measurements were made at 25 field stations in the main structural units of Romania. Data were taken in the frequency range from 10^{-4} to 1 Hz which corresponds to depths from about 2 to 250 km.

From a geological point of view the sites were selected in order to get information in connection with elongated sedimentary depressions, crystalline massifs, flysch zones and platforms (Fig. 1).

Field measurements were made using two components of the electric field (E_x, E_y) with the y direction along the magnetic meridian, and three components of the magnetic field (H_x, H_y, H_z) in time intervals of 3 to 6 hours at each site by the Soviet MTL-71 equipment.

Data analysis

The graphic records were sampled at varied intervals (Δt) by a Hewlett-Packard digitizer. After the elimination of the linear effect due to the electrode polarization and to temperature differences between the electrodes, all data sets were analyzed on an IBM-370 computer using spectral analysis, including power density spectra, cross spectra, coherency and polarization from which the following quantities were computed: ϱ_{xy}, ϱ_{yx}, $\varrho_{||}$, $\varrho_{\perp}$ and ϱ_{ef} (Ádám 1976a, Cantwell and Madden 1960, Kaufman and Keller 1981, Rokityansky 1982, Word et al. 1971).

[1] Institute of Geology and Geophysics. Caransebes 1., Bucharest, Romania

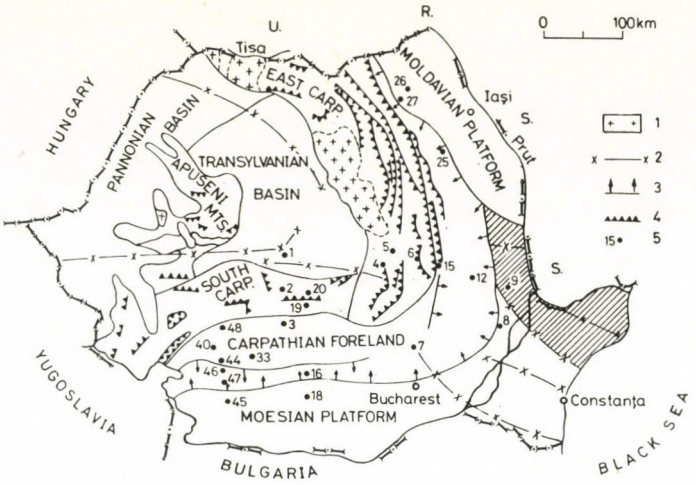

Fig. 1. MTS locations on a tectonic sketch map (1 — Neogene volcanics, 2 — deep fractures, 3 — area of flexures, 4 — thrusts, 5 — MTS location)

Results

For an interpretation of the magnetotelluric curves, resistivities of the sedimentary layers were calculated using logs from nearby wells, then an attempt was made to fit the observed curves to theoretical models. The resistivities plotted for $\varrho_{\parallel}$ and $\varrho_{\perp}$ indicate that the geoelectric section to depths of about 250 km is divided into three principal layers: a uniform layer of low resistivity near the surface, overlying a layer of higher resistivity which in turn overlies a semiinfinite medium of high conductivity.

The Carpathian foreland has an asymmetric cross section being, in general, bordered by outcrops of ancient low conducting mountain building rocks on one side and passing into a gentle sloping platform on the other side (Stănică and Stănică 1981). The sediments have an integrated conductivity of about 1000–2700 mho in the exterior of the South-Carpathians (Figs 2 and 3) and 700–1200 mho in the Carpathian Arc zone (Figs 4 and 5).

The level of longitudinal curves (Fig. 2) is lower over the central part of the foredeep than over its northern and southern parts. This feature is an indication of the superchanneling of the telluric currents. The apparent resistivity values on the transverse curves are higher in the outside part of the foredeep than inside of it.

At short periods, the transverse and longitudinal curves are either coincident or parallel (Fig. 6), but starting from about 400–600 s they are widely separated. The results of the modeling show that, at long periods, the distortions are similar to those of the direct current and cause a vertical displacement of the curves.

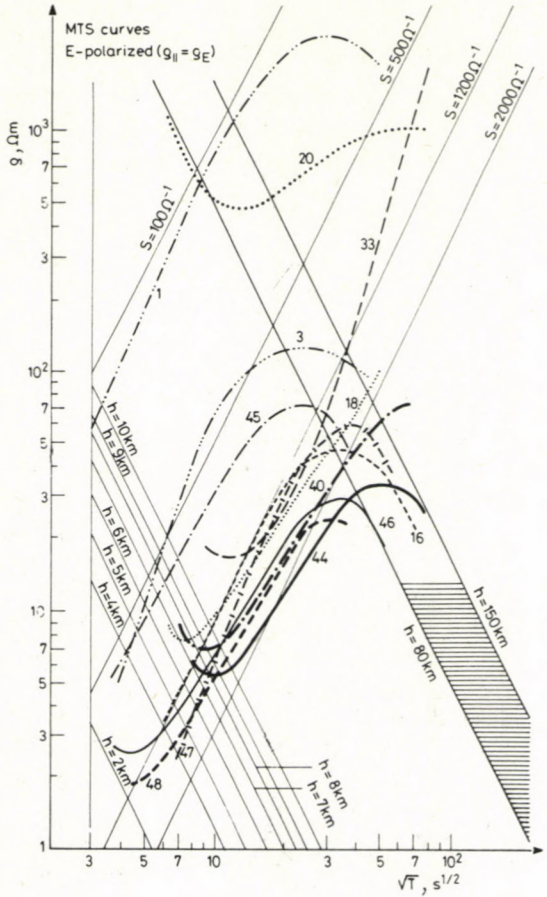

Fig. 2. Magnetotelluric curves for E polarization ($\varrho_{\parallel} = \varrho_E$)

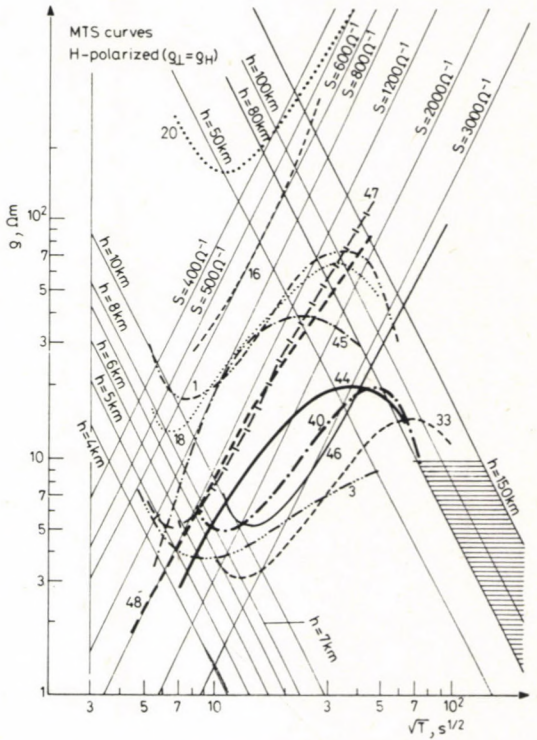

Fig. 3. Magnetotelluric curves for H polarization ($\varrho_{\perp} = \varrho_H$)

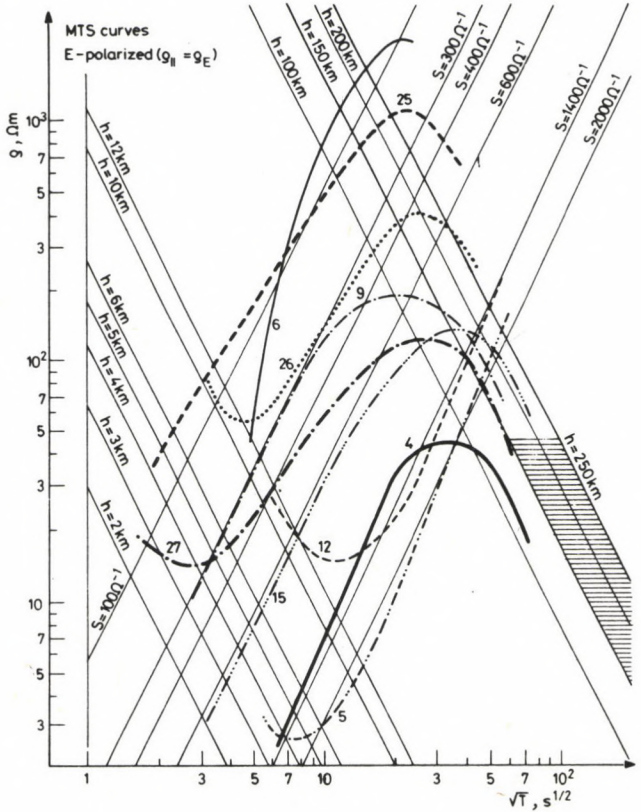

Fig. 4. Magnetotelluric curves for E polarization ($\varrho_{\parallel} = \varrho_E$)

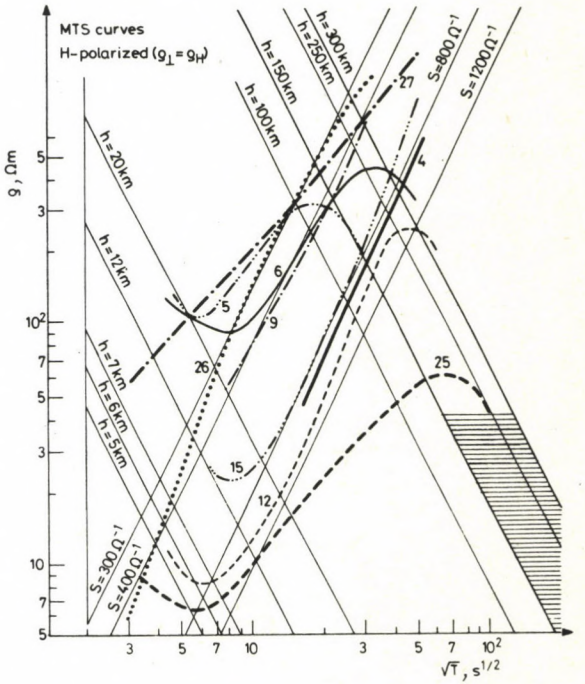

Fig. 5. Magnetotelluric curves for H polarization ($\varrho_{\perp} = \varrho_H$)

In platform areas the rocks composing the basement are mostly bad conductors but they are often cut through by a net of highly conducting formations which produce strong distortions in telluric currents. Another source of the distortions is the inhomogeneity of the upper sedimentary layer characterized by the "*S*-effect" and the "induction effect", too (Sounding 45, Figs 2 and 3).

The level of Sounding 20 (Figs 2 and 3) is higher than 2.10^2 ohm m and reflect the normal geoelectric cross section of the crystalline massif of the South-Carpathians.

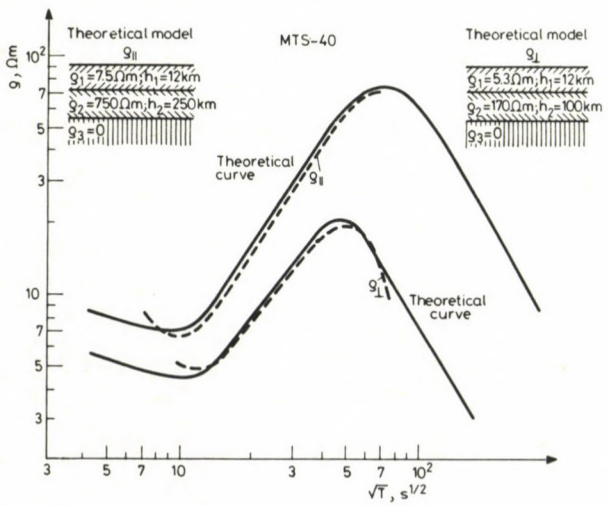

Fig. 6. Theoretical and experimental model for MTS-40

Conclusions

A comparison of the magnetotelluric data with the expected geological structure shows a good agreement for most major features of the conductivity distribution. So the characteristic features of the Carpathian foreland are: a longitudinal conductivity of 700–2700 mho, a super-channeling effect of the telluric currents at long periods and the presence of conducting layers at depths of about 80–150 km in the South- and 180–250 km in the East-Carpathians.

For the crystalline massifs of the South-Carpathians, the most important feature is the presence of a conducting layer at about 50–80 km (MTS-20). In platform areas the longitudinal conductivity is between 400–1200 mho with a conducting layer at about 80–150 km (Moesian Platform) and 180–250 km (Moldavian Platform) (Ádám 1976a, 1976b).

References

Ádám A ed. 1976a: Geoelectric and Geothermal Studies (East Central Europe and Soviet Asia). KAPG Geophysical Monograph. Akadémiai Kiadó, Budapest

Ádám A 1976b: Quantitative connections between regional heat flow and the depth of conductive layers in the Earth's crust and upper mantle. *Acta Geod. Geoph. Mont. Hung.*, 11, 503—509.

Cantwell T, Madden T R 1960: Preliminary report on crustal magnetotelluric measurements. *J. Geophys. Res.*, 65, 4202—4205.

Kaufman A A, Keller G V 1981: The magnetotelluric sounding method. Elsevier Scientific Publishing Comp. Amsterdam–Oxford–New York

Rokityansky I I 1982: Geoelectromagnetic investigation of the Earth's crust and mantle. Springer Verlag, Berlin–Heidelberg–New York

Stănică M, Stănică D 1981: The use of the natural electromagnetic field of the Earth for the construction of a structural model of the East Carpathian arc (in Romanian). *St. cerc. geol., geofiz., geogr., Geofizica*, 19, 41–51.

Word D R, Smith H W, Bostick F X Jr 1971: Crustal investigations by the magnetotelluric tensor impedance method. Geoph. Monograph. series, 14, 145–167.

Acta Geodaet., Geophys. et Montanist. Hung. Volume 19 (1—2), pp. 153—160 (1984)

REVIEW OF THE PANNONIAN BASIN

L STEGENA[1] and F HORVÁTH[1]

The Pannonian Basin is characterized by Neogene-Quaternary sediments, with a thickness of 2.5 km in average. The Miocene sediments are, usually slightly and locally heavily affected by extensional tectonics. During the Miocene, intensive calc-alkaline and in the Plio-Pleistocene, less intensive alkali-basaltic volcanism occurred in the basin.

The basin exhibits a thin crust (25-30 km); the velocity of *P* waves drops from 8.2 km/s to 7.7-7.8 km/s in a relatively shallow depth, between 50-60 km. The basin area is characterized by pronounced geothermal highs (80-130 mW/m^2). Also the Moho boundary has an elevated temperature (700-1000 °C). Paleo heat flow determinations showed that the basin was heated up in the last 15–5 my. Magnetotellurics showed the highly conducting layer in the mantle in an elevated position (45-65 km), in accordance with seismic and geothermal results. Moreover, gravity measurements suggest a relatively light upper mantle beneath the Pannonian Basin, in agreement with its high temperature.

The elevated, hot, light upper mantle of the Pannonian Basin represents a pronounced mantle diapir, which is suggested to be the primary cause of the development of the Pannonian Basin.

Keywords: Carpathians; evolution, basin; geological structure, Pannonian Basin; geophysical model, Pannonian Basin

Geological overview

The intra-Carpathian basins are now completly surrounded by a mountain ring which is made up of the Eastern Alps, West-, East- and South-Carpathians and the Dinarids. Figure 1 summarizes the division and main tectonic features of the deformed mountain arc and shows the different units of the backarc region.

The basin surrounded by the folded arc is not uniform. The Neogene-Quaternary subsidence affected large areas, however, some ranges remained emergent and/or uplifted. They divide the backarc area into several sub-basins. The central part is the Pannonian Basin which is further surrounded by peripheral basins as the Vienna basin, the Transcarpathian depression and the Transylvanian basin. The Pannonian Basin is separated by the Little Carpathians from the Vienna basin on the northwest, and by the Apuseni Mts. from the Transylvanian basin on the east (Fig. 1). The Pannonian Basin can be further subdivided. The basinal area to the NW from the

[1]Eötvös Loránd University, Kun B. 2, H-1083 Budapest, Hungary

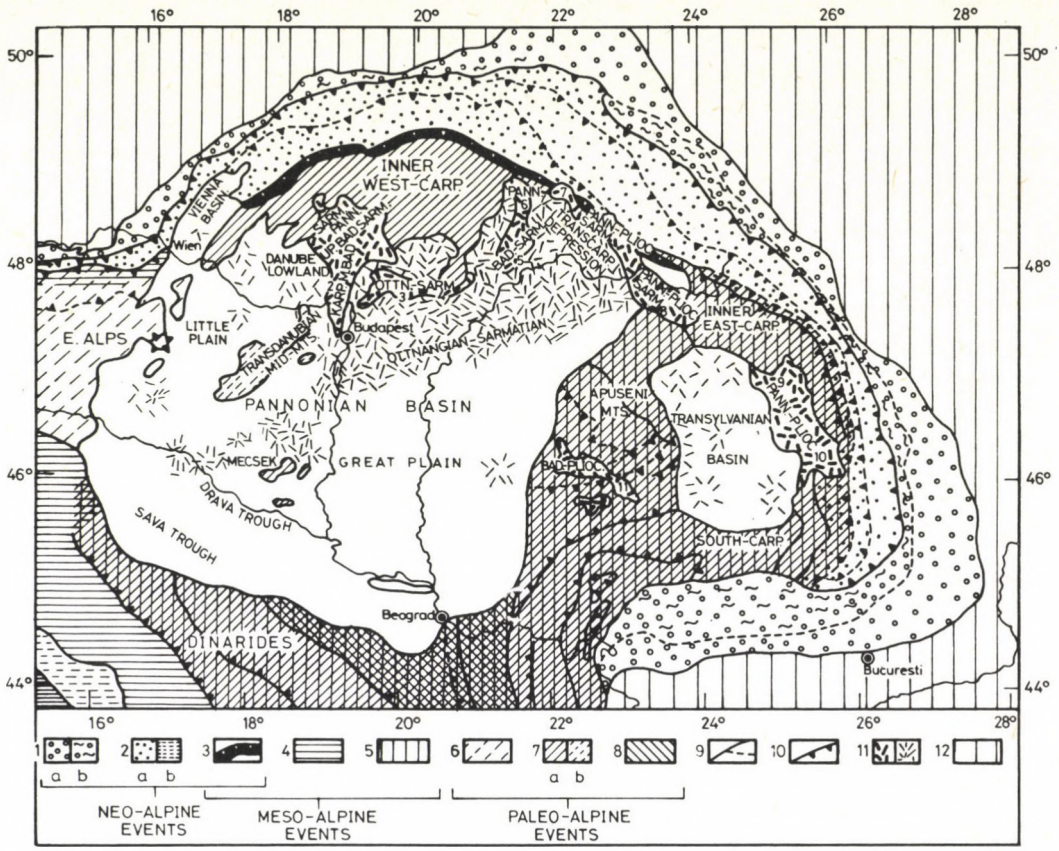

Fig. 1. Tectonic sketch of the Pannonian back-arc basin and the associated folded area (mainly after Mahel 1974 and Lexa and Konecny 1974).Keys: 1 — Foredeep molasse; undeformed (a), folded during the Pliocene-Quaternary (b). 2 — Outer (Flysch) Carpathians strongly deformed during the Late Oligocene-Early Miocene (a). Other tectonic units deformed during this interval (b). 3 — Pienniny Klippen belt, strongly deformed during the Late Oligocene-Early Miocene and the Latest Cretaceous-Paleocene intervals. 4 — Area of Late Eocene-Early Oligocene deformation. 5 — Area of Latest Cretaceous-Paleocene deformation. 6 — Area of Late Cretaceous deformation. 7 — Area of mid-Cretaceous intensive (a) and slight (b) deformation. 8 — Area intensive (a) and slight (b) Late Jurassic-Early Cretaceous deformation. 9 — First order (a) and second order (b) tectonic boundary. 10 — Main thrusts. 11 — Neogene calc-alkaline volcanic rocks on the surface (a) and below younger sedimentary cover (b) and their age. 12 — Foreland. The numbers indicate the main units of the volcanic area. 1. Central Slovakia, 2. Börzsöny Mts., 3. Mátra Mts., 4. Bükk Mts., 5. Tokaj Mts., 6. Presov Mts., 7. Vihorlat Mts., 8. Gutin Mts., 9. Calimani Mts., 10. Harghita Mts., 11. Apuseni Mts., 12. Stable European foreland

Transdanubian Mid-Mts. is called Little Hungarian Plain and the Slovakian part Danube Lowland. The southeastern part is the Great Hungarian Plain, northeast from it lies the Transcarpathian depression. Towards the Dinarids two elongated depressions can be considered as part of Pannonian Basin: the Drava trough and Sava trough.

Structure and geology of the emergent ranges, deep drillings and geophysical data show that the peripheral basins, and the Danube Lowland and Little Hungarian Plain are depressions superimposed on the deformed pre-Neogene arc. Circumstantial evidences (facies and faunal affinites, structural trend) suggest that the Transdanubian Mid-Mts. also belong to the Austroalpine nappes.

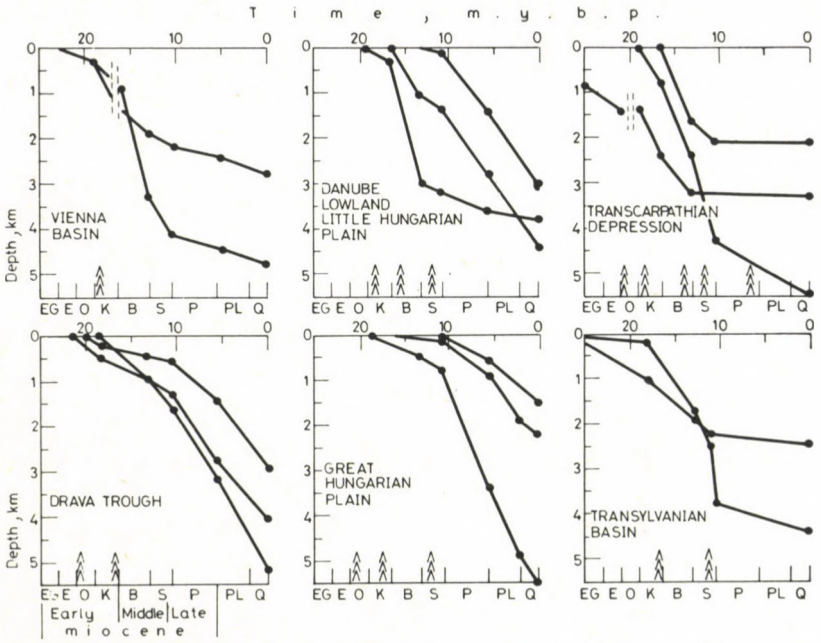

Fig. 2. Sedimentation versus time diagrams for different units of the intra-Carpathian depression (after Horváth and Berckhemer 1982). Stacked triangles indicate the time of calc-alkaline volcanism

The tectonic structure of the pre-Neogene bedrock of the Great Hungarian Plain is under discussion, although extensive thrustings have been demonstrated even by drilling. It is, however, generally accepted that the pre-Neogene basement is deformed and composed of belts which can be well correlated with the different units of the Apuseni Mts. and Inner East-Carpathians.

The pre-Neogene bedrock of the Great Hungarian Plain, as well as the basement of the other intra-Carpathian basins were part of the Late Cretaceous-Paleogene orogenic belt, as demonstrated by a flysch-trough in the Central Great Hungarian Plain and by the Paleogene basin in northern Hungary. Thereafter they became area of extension and subsidence during the Neogene-Quaternary.

The Neogene-Quaternary sediments of the intra-Carpathian basins are mostly sands, sandstones, clays, shales and limestones, with a mean thickness of about 2.5 km. The younger sedimentary fill of the Pannonian Basin is tectonically not or slightly

affected, but intensive normal faulting occurred during the middle Miocene. Figure 2 shows some characteristic sedimentation histories of the intra-Carpathian basins.

During the Miocene, intensive calc-alkaline and in the Plio-Pleistocene, less intensive basaltic volcanism occurred in the Pannonian Basin.

Geophysics

Data relevant for the basin evolution consist of crustal profiling, geothermal and electromagnetic measurements, gravity and magnetic anomaly maps, seismological and paleomagnetic data.

Several long seismic profiles were measured in the Carpatho-Pannonian region (Fig. 3). One representative profile is shown in Fig. 4. The Outer Carpathians and the Dinarides are characterized by thick crust (40-65 km). A very interesting feature is the doubling of the lower crust below the Outer Carpathians, which is probably the result of the early Miocene continental collision. The Pannonian Basin, the peripheral basins

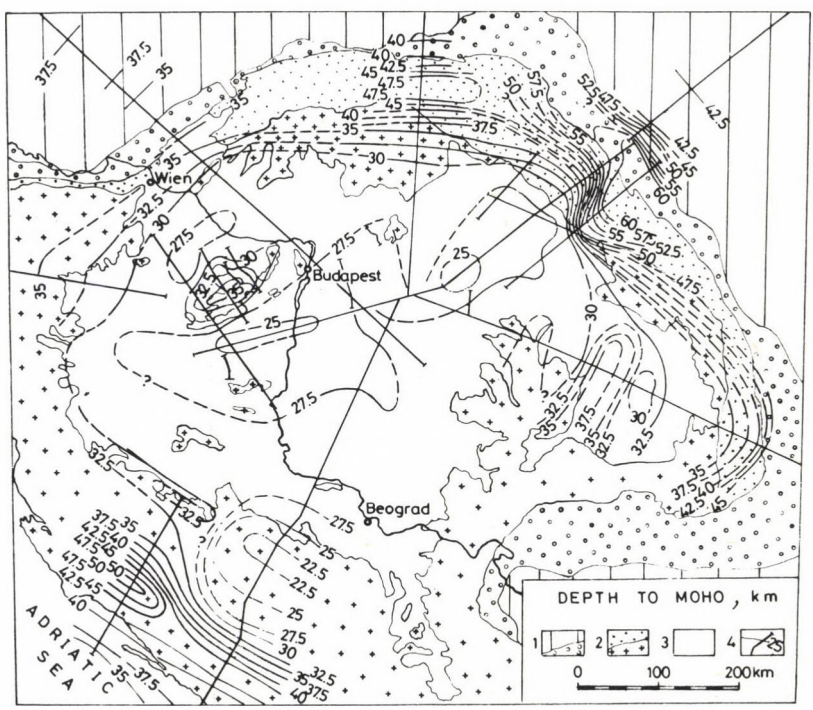

Fig. 3. Depth to Moho (in km) in the Carpatho-Pannonian region (after Horváth and Royden 1981). 1 — Stable Europe and the foredeep, 2 — Outer and Inner Carpathians, 3 — Carpathian basins, 4 — Seismic profiles and Moho depths (in km)

and also partly the Inner Carpathians exhibit thin crust (25-30 km). Velocity determinations have shown that the upper mantle right below the Moho is normal (V_p=8.0-8.2 km/s) all along the sections. However, in the Pannonian Basin the velocity of *P* waves drops from 8.2 km/s to 7.7-7.8 km/s in a relatively shallow depth, between 50 and 60 km (Posgay 1975, Fig. 4).

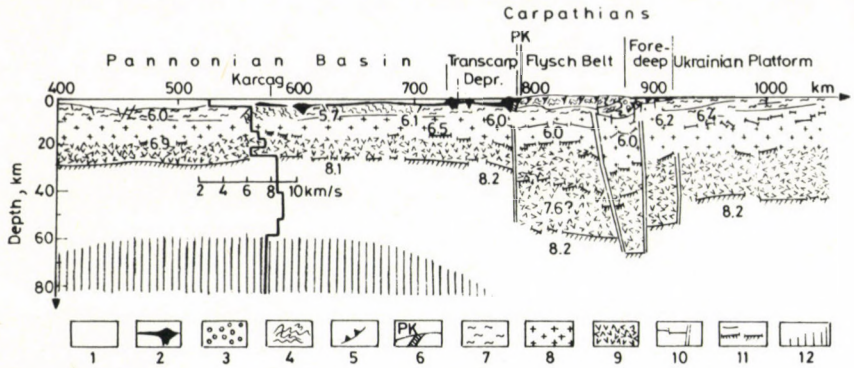

Fig. 4. Crustal structure of the Pannonian basin, Carpathians and Ukrainian platform along the IP-III seismic line (modified after Sollogub et al. 1973). The velocity vs. depth function was determined by Posgay (1975) in the vicinity of Karcag. Keys: 1 — Neogene-Quaternary sediments. 2 — Mio-Pliocene calc-alkaline volcanoes and volcanoclastics. 3 — Molasse of the Carpathian foredeep. 4 — Upper Cretaceous/Paleogene flysch. 5 — Major thrust plane. 6 — Pienniny Klippen Belt. 7 — Paleozoic and earlier basement, locally including Mesozoic rocks. 8 — Upper crust. 9 — Lower crust. 10 — Local and major faults, resp. 11 — Seismic reflector, Conrad and Moho discontinuity resp., and seismic velocity in km/s. 12 — Subcrustal lithosphere and asthenosphere resp.

The area of the Pannonian Basin is characterized by pronounced geothermal highs. Several thousand temperature measurements carried out in boreholes demonstrated that the temperature at 1 km depth is in the 40-90 °C interval (Horváth et al. 1981). Heat flow density determinations have given values from 80 to 130 mW/m². Figure 5 shows that the Pannonian Basin, particularly the Great Plain is a significant heat flow high. Recently, a reconsideration of the Hungarian heat flow determinations concluded that in the Pannonian Basin the thermal field is just slightly and locally disturbed by convective disturbances and the Pannonian thermal high reflects real anomalous temperature condition of the lithosphere. Calculation shows that the Moho heat flow and temperature are in the range 60-70 mW/m² and 700-1000 °C, respectively, for the Great Hungarian Plain. Two dimensional temperature model calculations along seismic sections gave concordant results.

The Transdanubian Mid-Mts. are made up by thick (up to 4 km) Mesozoic carbonates, and are characterized by a low thermal gradient (10 to 20 °C/km) and heat flow (50 mW/m²). In these regions, however, convective heat transport is significant:

Meteoric water infiltrates into the complex in the central parts of the mountains and then enters to the surface in hot springs at the margins of the mountains. Provided that this hydrothermal cycle is a stationary process the convective heat transport can be estimated and corrected. Calculations suggest that the undisturbed (conductive) heat flow must be as high as 100 to 120 mW/m², i.e. similar to the value characteristic for the

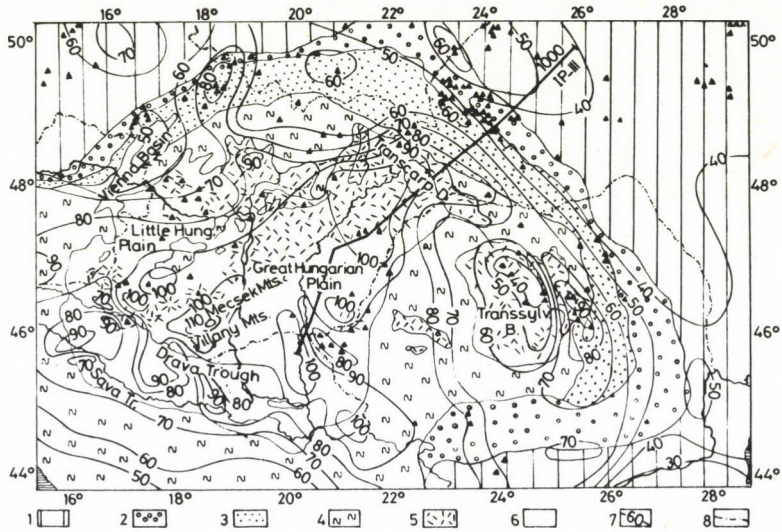

Fig. 5. Heat flow map of the Carpatho-Pannonian region (modified after Čermák and Hurtig, 1979). Keys: 1 — Stable European foreland. 2 — Molasse foredeep. 3 — Flysch Carpathians. 4 — Folded mountain arc of the Alps, Inner Carpathians, Apuseni Mts. and Dinarides. 5 — Outcrops of Neogene calc-alkaline volcanic complex. 6 — Intra-Carpathian depression. 7 — Heat flow isoline, in mW/m². 8 — Political boundary of Hungary

Great Hungarian Plain. In contrast, the peripheral Vienna basin and Transylvanian basin is cold, their average heat flow is about 50 mW/m². The Danube Lowland and Little Hungarian Plain is characterized by slightly higher heat flow values (72 mW/m² in average).

Paleo-heat flow density determinations, based on vitrinite reflectance data, sedimentary history and recent geothermics of some Pannonian boreholes show that the basin was heated up in the last 15–5 my, having previously a normal ($\sim$ 50 mW/m²) heat flow density value.

Numerous magnetotelluric deep soundings have been carried out in the Pannonian Basin and its surroundings. They show that the top of the first highly conducting layer of the mantle lies in an elevated position (45-65 km). Ádám et al. (1977) have demonstrated that it is the result of thermal processes. They interpreted the seismic velocity and electric conductivity characteristics of the Pannonian upper mantle in terms of a thin lithosphere (50-60 km) and updomed asthenosphere.

Gravity anomaly maps of the region (Bureau Gravimetrique International, 1962-65) show that the Carpathian arc is characterized by negative Bouguer anomalies (up to −120 mgal), the axis of which does not follow exactly the trend of the main tectonic zones. The Pannonian Basin exhibits slight positive and negative values (−20 to +25 mgal) with an average of about +10 mgal. Gravity modeling along crustal profiles has shown that the negative anomaly associated with the Carpathian arc is caused by the thickening of the crust and by the light molasse wedge of the foredeep. Moreover, it suggests that the Pannonian upper mantle is relatively light, in agreement with its high temperature. These highly consistent data for the elevated position of the asthenosphere below the Pannonian Basin are also supported by the positive travel-time residuals (+0.7 to +2.6 s) characteristic for the region.

The magnetic anomaly map of the region (Posgay 1967) shows lineated anomaly features trending ENE-WSW. They may be associated with dikes intruded into the crust during the phase of extension, but more probably they are caused by mafic rocks, emplaced during the juxtaposition of the supposed two Mesozoic units of the Carpathian-Pannonian area.

Paleomagnetic measurements on Mesozoic rocks have given paleodirections which agree with the contrasting character of the two Carpatho-Pannonian units (Márton and Márton 1978, Márton 1981). From the point of view of basin development, however, age determination of young sedimentary rocks by measuring the direction of primary magnetization is the most important. Cooke et al. (1979) have quite recently carried out such magnetostratigraphic measurements on sediments derived from two, fully cored boreholes in southeastern Hungary. Both holes being about 1200 m deep are situated on the fast subsiding part of the Great Hungarian Plain. Several hundred cores were measured in each hole and stable inclination versus

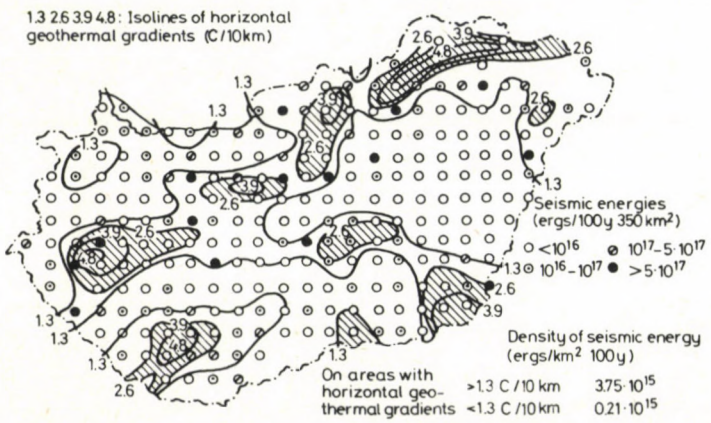

Fig. 6. Horizontal geothermal gradients (for the depth of 1 km) and earthquake energies between 1859–1958, computed for a 350 km² grid (after Stegena 1979)

depth plots were constructed. The plots are highly consistent and can easily be matched the generally accepted paleomagnetic time scale (La Brecque et al. 1977). One of the most important results is that the depth-age plot in both hole is strongly linear for the 0-6 my interval, indicating a remarkably uniform average sedimentation vs. subsidence rate (160 m/my and 175 m/my) for the Quaternary-top Miocene time.

The earthquakes of the intra-Carpathian basins are of weak, sporadic, crustal quake character. It was suggested by a comparison with the heat flow map (Fig. 6), that these quakes (and also the similar earthquakes of Central Europe) can be generated mostly by temperature differences in the crust and not by large-scale tectonic forces (Stegena 1979).

References

Ádám A, Horváth F, Stegena L 1977: Geodynamics of the Pannonian basin: geothermal and electromagnetic aspects. *Acta Geol. Acad. Sci. Hung.*, 21, 251–260.

Cermák V, Hurtig E 1979: Heat flow map of Europe. In: *Terrestrial heat flow in Europe*. V Čermák and L Rybach eds, Springer Verlag, 1–318.

Cooke H B B, Hall J M, Rónai A 1979: Paleomagnetic sedimentary and climatic records from boreholes at Dévaványa and Vésztő, Hungary. Paper presented at the field conference of 128 IGCP project, 1979, Budapest

Horváth F, Berckhemer H 1982: Mediterranean backarc basins. *Geodynamics Series*, 7, 141–173.

Horváth F, Royden L 1981: Mechanism for the formation of the intra-Carpathian basins: a review. *Earth Evol. Sci.*, 1, 307–316.

Horváth F, Dövényi P, Liebe P 1981: Geothermics of the Pannonian basin. *Earth Evol. Sci.*, 1, 285–291.

La Brecque J L 1977: Revised magnetic polarity time scale for Late Creaceous and Cenozoic time. *Geology*, 5, 330–335.

Lexa J, Konecny V 1974: The Carpathian volcanic arc: a discussion. *Acta Geol. Acad. Sci. Hung.*, 18, 279–293.

Mahel M ed. 1974: Tectonics of the Carpathian-Balkan Regions. Geol. Ustav D. Stur, Bratislava, 1–380.

Márton E 1981: Tectonic implication of paleomagnetic data for the Carpatho-Pannonian region. *Earth Evol. Sci.*, 1, 257–264.

Márton E, Márton P 1978: Tectonic implications of a new paleomagnetic result from the Jurassic of the Transdanubian Central Mountains. *Tectonophysics*, 45, T1–T6.

Posgay K 1967: A comprehensive survey of geomagnetic masses in Hungary. *Geophys. Trans. Budapest*, 16, 1–118.

Posgay K 1975: Mit Reflexionsmessungen bestimmte Horizonte und Geschwindigkeitsverteilung in der Erdkruste und in Erdmantle. *Geophys. Trans. Budapest*, 23, 13–17.

Sollogub V B, Prosen D and co-workers 1973: Crustal structure of Central and Southeastern Europe by data of explosion seismology. In: *The structure of the Earth's crust based on seismic data*. S Müller ed. *Tectonophysics*, 20, 1–33.

Stegena L 1979: Geothermics and seismicity in the Pannonian basin. In: *Terrestrial and Space Techniques in Earthquake Prediction Research*, A Vogel ed. Vieweg, Braunschweig, 467–471.

Acta Geodaet., Geophys. et Montanist. Hung. Volume 19 (1—2), pp. 161—171 (1984)

CRITICAL COMPARISON OF SOME METHODS FOR THE GEOTHERMAL RECONSTRUCTION ON THE BASIS OF VITRINITE REFLECTANCE

I VETŐ[1], P DÖVÉNYI[2], I KONCZ[3]

The knowledge of the burial history and of the present geothermal conditions offers — at least in principle — a possibility to assess the maturity of organic matter in sedimentary basins. In the last decade, about ten such calculation methods have been suggested in the literature and some of them obtained a broad acceptance. Four published methods (Lopatin 2, Bostick, Hood et al., Waples-Lopatin) were compared. This work was done on 52 profiles taken from the literature. Their burial history, rock temperature and reflectance data are known.

Since a pure statistical approach of the calculation errors would have little sense, we tried to investigate the problem by the study of the following relations:

— errors vs. geological age,
— errors vs. type of burial history,
— errors vs. measured reflectance.

By this way we are able to discuss the limits of application of the studied methods.

Keywords: organic maturity; Pannonian Basin; thermal history; vitrinite reflectance

Introduction

The relation between organic maturity, temperature and time was drawn up in several papers (Karweil 1956, Lopatin 1971, Bostick 1973, Hood et al. 1975, Lopatin 1976, Cornelius 1975, Karpov et al. 1975, Shibaoka and Bennett 1977, Tissot and Espitalié 1975, Waples 1980, Buntebarth 1982) and methods have been proposed to calculate the maturity on the basis of the supposed thermal history, or to reconstruct the thermal history on the basis of the maturity and burial history. The basic assumption of the calculations is that the temperature and the time needed to achieve a given maturity are more or less complementary. The differences of the methods are how the authors take into consideration this complementarity.

The usefulness of the methods were documented on actual geological examples and the errors were proved to be remarkably small. All of them made the geologists interested and some methods have been applied widely in different basins.

[1]Hungarian Geological Institute, H-1143 Budapest, Népstadion út 14, Hungary
[2]Geophysical Department, Eötvös University, H-1083 Budapest, Kun B. tér 2, Hungary
[3]Hungarian Hydrocarbons Institute, H-8801 Nagykanizsa, Vár u. 8, Hungary

The question arises what reasons this or that method was chosen for? In the papers no answer can be found so we are afraid the choice was often made either by sympathy or by the knowledge of only one method. Very little effort was made with the aim to compare the advantages and the limits of the different methods (Kettel 1981, Vető 1981). The goal of our paper is to fill this lack.

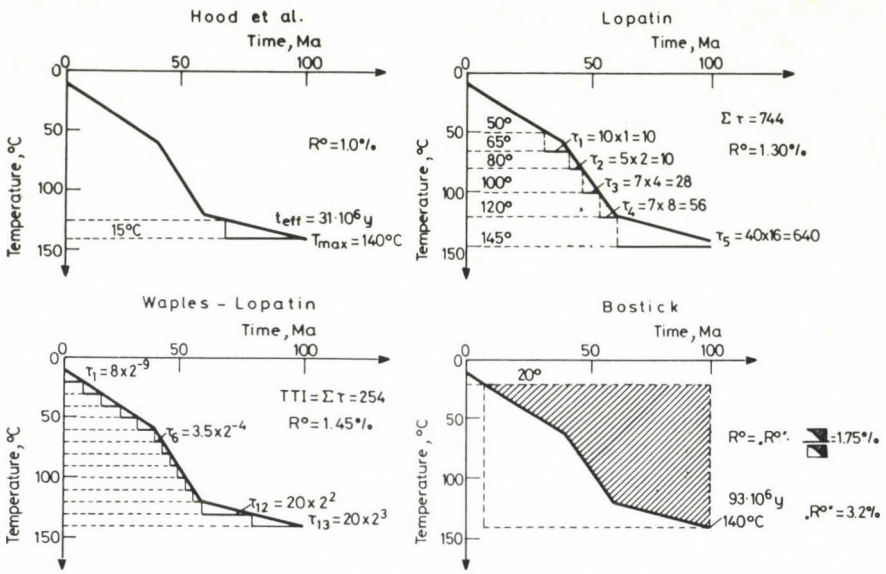

Fig. 1. Principles of the considered methods on the example of a simple thermal history

The four methods involved in our study are the most widely accepted ones in the literature. All of them make calculations with the present geothermal gradient and surface temperature data throughout the whole burial history and give the maturity in terms of vitrinite reflectance. Figure 1 shows the principles of the methods on the example of a simple thermal history.

Lopatin (1976) assumes that the reaction rate increases with temperature but the increase is (more and more) slower and slower. He divides the thermal history above 50 ° C into intervals and multiplies the time (in million years) an organic particle spent in these intervals by 1, 2, 4 and so on. Then he summarizes these so-called individual heat impulses. The vitrinite reflectance is assumed to be the function of this summarized value ($\Sigma\tau$). Lopatin introduced a limitation for the time-temperature complementarity; he supposed that a minimum temperature is needed to achieve a given maturity.

Bostick (1973) derives an "$R°$" value from the maximum temperature and the time the organic particle spent at temperatures higher than 20 ° C. The actual vitrinite

reflectance is calculated by multiplication of "$R°$" with the ratio of hatchured area to the area of the time-temperature rectangle in Fig. 1.

Hood et al. (1975) assumes the maturity can be calculated from the maximum temperature (T_{max})and the "effective heating time" (t_{eff}). This latter is the time the organic matter spent in the [T_{max}, $T_{max} - 15\,°C$] interval.

Waples (1980) accepts Lopatin's (1971) original assumption about the maturation rate increase with temperature but modifies the empirical relationship between maturity and time-temperature index.

Results

To compare these methods we have collected data from the literature. They should be well documented, namely we have to know their temperature profile, their burial history and some vitrinite reflectance data. Our collection consists of 52 profiles coming mainly from the sedimentary basins of Australia, North America and Western Europe (Fig. 2). Geological ages vary between Devonian and Pliocene. For all points where measured reflectance data were available we have derived the thermal histories and calculated the reflectances following the four methods.

Fig. 2. Location map of boreholes from which data were collected

Before we attempt to compare the advantages and the limits of these methods we line up the possible sources of the calculation errors. They may be grouped in two families:

i) errors in the data, ii) errors in the method.

The first family consists of i) reflectance measurement error,

ii) errors in burial history (bad interpretation of stratigraphic hiatus, uncertainty in age determination, neglection of the compaction),

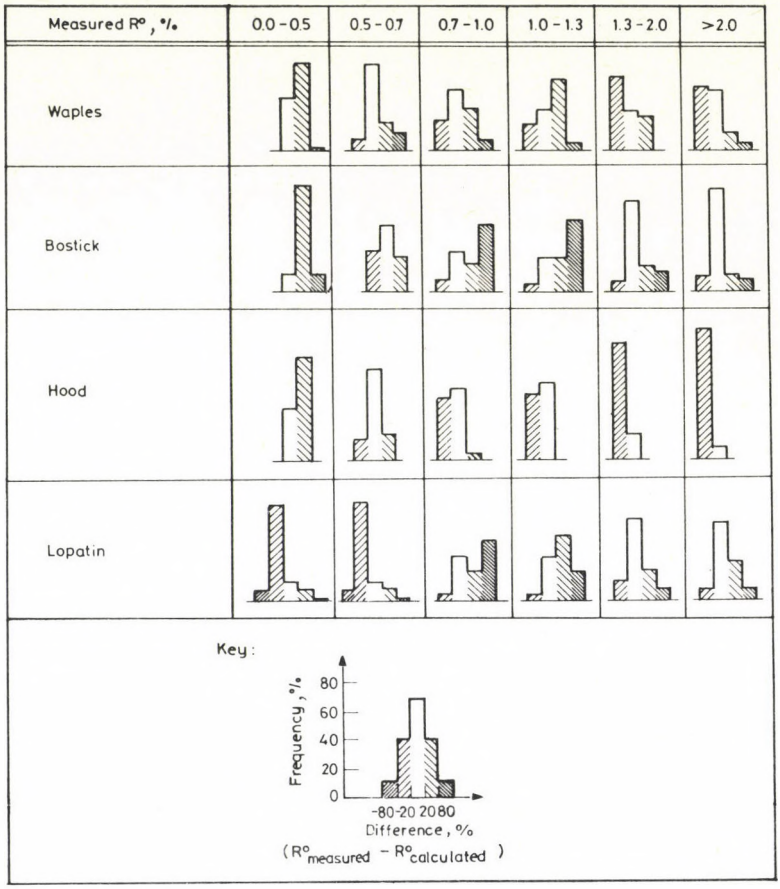

Fig. 3. Histograms of differences between the calculated and measured vitrinite reflectances as a function of the measured ones

iii) errors in temperature measurements,

iv) differences between the present geothermal gradient and the former ones,

v) differences between the present surface temperature and the former ones.

The two last are suspected to be of particular importance.

The second family consists of the errors in the kinetic model of the maturation: assumption of a common response of vitrinite for a given thermal history, although differences between vitrinite reflectances of same thermal history are well documented (Bostick and Foster 1974, Künstner 1974, Blanquart and Mériaux 1974) in several basins.

Taking into account the great diversity of error sources a pure statistical approach of the calculation errors would have little sense. So it seems to be more

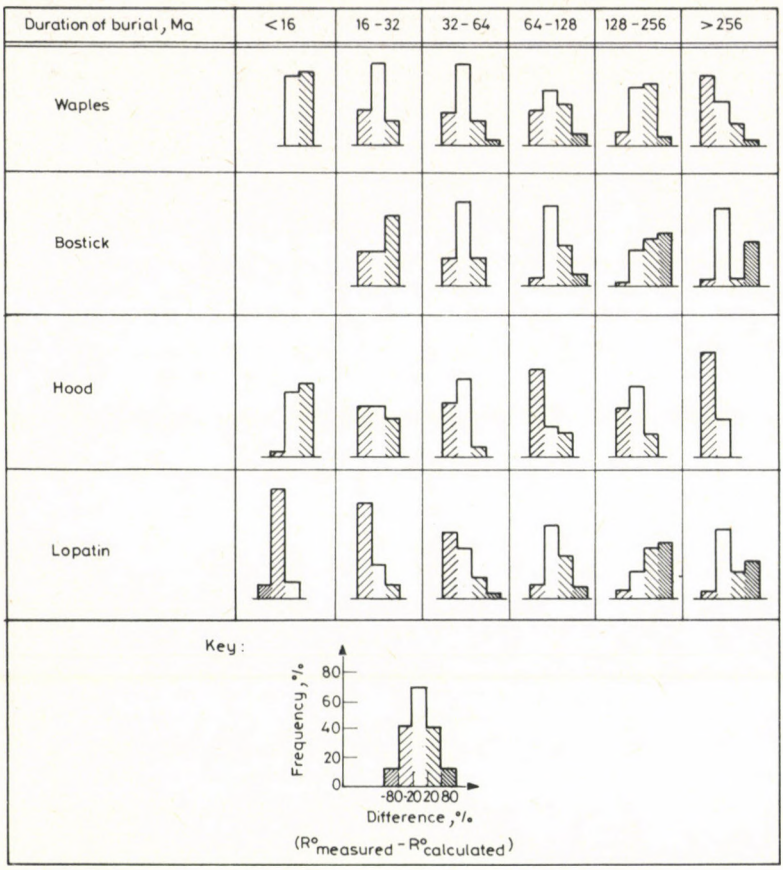

Fig. 4. Histograms of differences between the calculated and measured vitrinite reflectances as a function of the geological age

appropriate to study them in function of maturity and of two parameters playing a role in the maturation, namely the geological age and the burial type. The points were grouped according to the measured R° values and for every group a histogram was drawn (Fig. 3). The blank columns in the middle of them represent good calculations (-20% to $+20\%$ relative error). The over- and underestimations are shown by hatchured columns to the right and left, respectively.

The Waples (W) and Hood et al. (H) histograms show a remarkable similarity: in the immature group ($R^\circ < 0.5\%$) both methods give overestimation, in the beginning of the oil window (R° between 0.5 and 0.7%) they work well although the H definitively better, in the rest of the oil window (up to 1.3%) none of them is successful enough. For $R^\circ > 1.3\%$ both methods result in an underestimate. The Bostick (B) and Lopatin (L) methods also show a similarity, in the oil window they both give

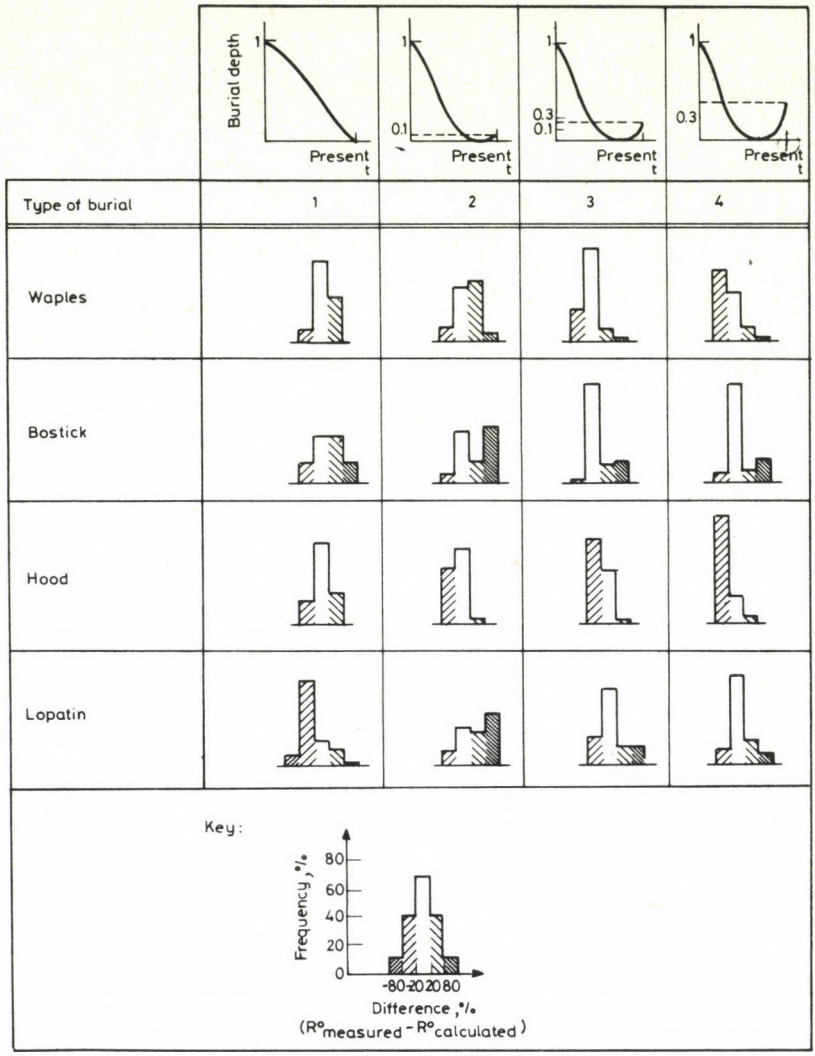

Fig. 5. Histograms of differences between the calculated and measured vitrinite reflectances as a function of burial types

overestimation, but L at the beginning of the oil window an underestimate. In the overmature groups they work well but B definitively better.

Accordingly only the beginning of the oil window and the overmature zone are well described, the first by the W and H methods, the second by the B and L ones.

Error histograms were drawn according to the geological ages, too (Fig. 4). The W and H methods show a remarkable similarity, here too. They work well in the early Neogene-Paleogene groups and result in overestimation and underestimation

respectively in the late Neogene and late Paleozoic groups. In the Mesozoic groups the number of under- and overestimations are nearly the same, and the amount of good calculations is only 30–40%. The B and L methods also show some similarity. In the Cenozoic-Mesozoic groups a shift of the maximum can be seen from the underestimation toward the overestimation with increasing ages. The late Paleozoic histograms show two well defined maxima: in the column of the good calculation and of the strong posiuve error.

The histograms of Fig. 5 were drawn from errors grouped according to the burial types which are as follows:

i) continuous burial,
ii) burial followed by stagnation,
iii) burial followed by a moderate uplift,
iv) burial followed by a strong uplift, in some cases with a second burial.

The W histograms show the dominance of the good calculations in the first and third groups meanwhile the overestimations and underestimations dominate respectively the second and fourth groups. The four H-histograms show a regular change: in the case of continuous burial the method works well then the underestimations become more and more overwhelming. The B and L histograms show strong similarities. Both methods work well in the case of uplift. In the stagnant one the histograms have two maxima in the columns of the good values and of the overestimations. The L method gives mainly underestimations for continuous burial history.

Discussion

The picture above is not very comforting but it was not to be expected else since the maturation history of the vitrinite can not be characterized by only one reaction. For instance the immature stage is dominated by the loss of oxygen and the oil window by that of the hydrogen. So it is not surprising to see a method working properly only in a limited part of the maturation history. Of course the errors can be caused by other factors, too. The most important of them, at least we believe so, is the temporal change of the geothermal gradient. In the following we try to elucidate the error sources in the different maturity stages.

We think the geothermal gradient in a young, continuously sinking basin has a better chance to remain constant than in an old, uplifted one. We have drawn histograms (Figs 6, 7 and 8) for these two basin types separately for the same maturity stages with the aim to be able to elucidate the error sources.

In the immature stage the W and H methods both give overestimation in both basin types so the principal source of the errors can be suspected in the kinetic models. In the oil window for continuously sinking basins the H method works well while the

W method shows a mild overestimating tendency. So we conclude the kinetic model of the H method is correct in this case. Finally in the overmature stage both methods underestimate in both basin types so the principal source of the errors can be suspected in the kinetic models. The L method gives underestimation in the immature stage in

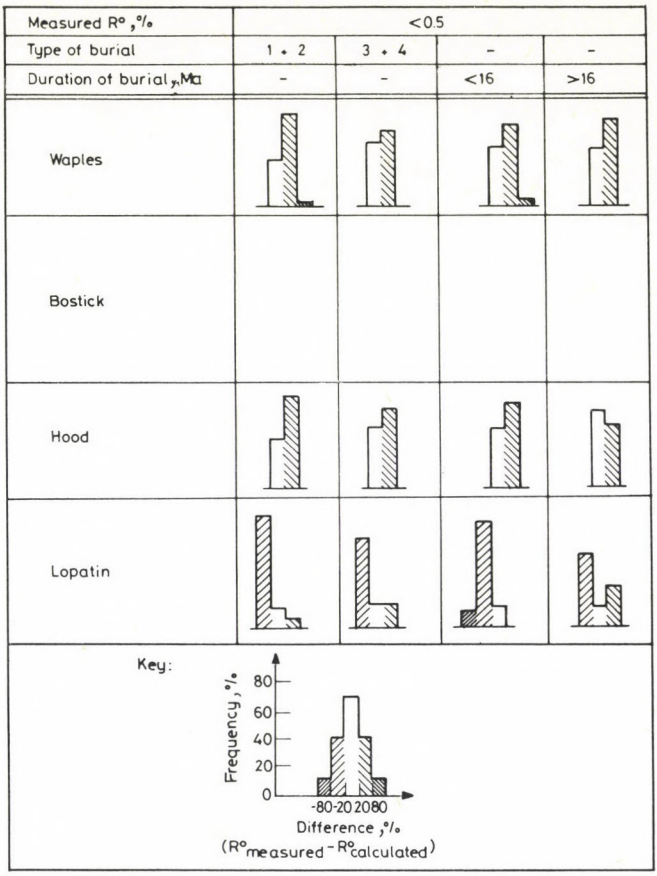

Fig. 6. Histograms of differences between the calculated and measured low vitrinite reflectance data as a function of burial type and the duration of burial, resp.

both basin types so the principal source of the errors is in the method. In the oil window both the L and B methods give overestimation in both basin types so the principal error is due to the methods. The differences between the two histograms for the same maturity stage reflect the decrease in time of the geothermal gradient in the uplifted basins. In the overmature stage the histograms for the two basin types show marked differences, in the continuously sinking basins both methods are dominated by

overestimation, while in the uplifted basins they work excellently. We believe in the latter case the decrease of the geothermal gradient counterbalances the overestimations due to the methods. To show even better this counterbalancing we have plotted histograms for the samples with R ° values over 2% (Fig. 9) and marked the part of the

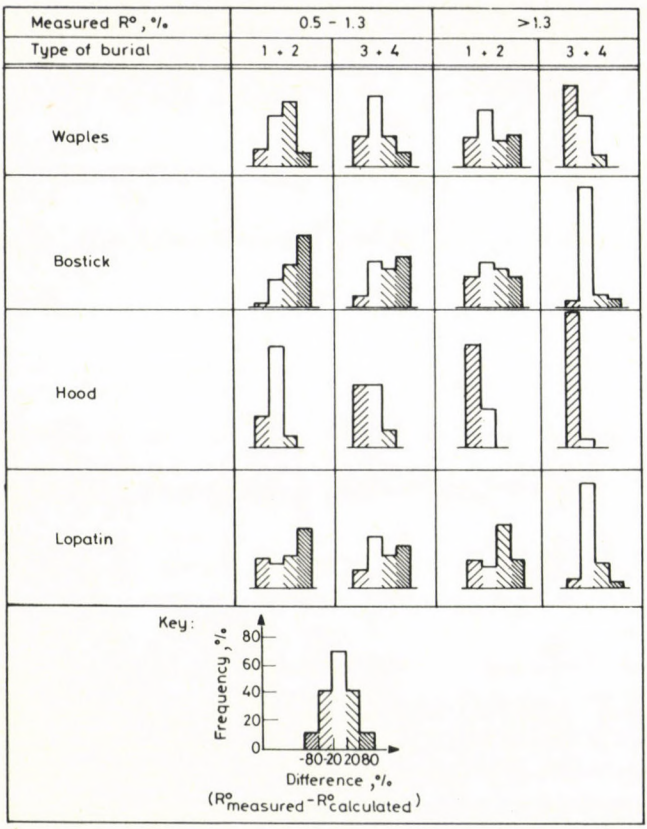

Fig. 7. Histograms of differences between the calculated and measured vitrinite reflectance data as a function of measured R^o and the type of burial

Münsterland 1 well. This well is located in the FRG, near the Ruhr basin where the maturation of the coal measures of the same age as in the Münsterland 1 were stopped before the Permian (Teichmüller and Teichmüller 1979). The Münsterland 1 coal measures suffered two rapid burials in the Upper Carboniferous and in the Upper Cretaceous times. The L and B calculations obtained very good values with more than 100 million years as acting time although the maturation took place very likely before the Permian so in less then 20 million years.

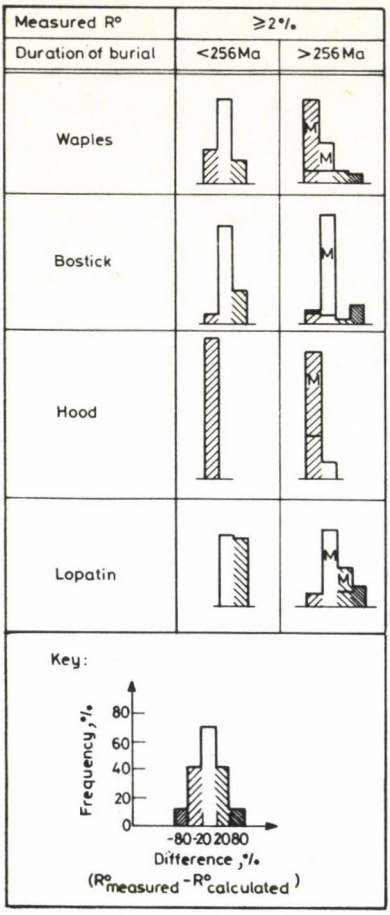

Fig. 8. Histograms of differences between the calculated and measured vitrinite reflectances in uplifted basins

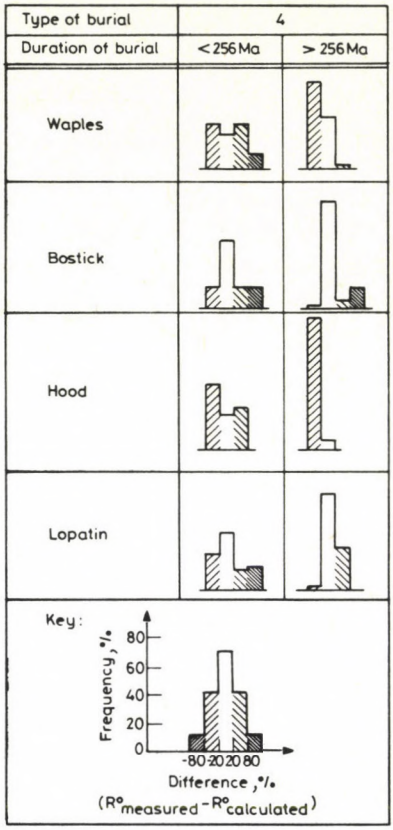

Fig. 9. Histograms of differences between the calculated and measured high vitrinite reflectance data

Conclusions

1. No one of the methods can be used in the immature and overmature stages.

2. The Hood et al. method is suggested to be used in the mature stage but we should note the use of this method for geothermal reconstruction is very limited in the case of a rapid subsidence and high geothermal gradients—e.g. the Pannonian Basin—since it takes into account only the last 15 °C which is a relatively minor part of the thermal history.

References

Blanquart P, Mériaux E 1974: Étude comparative du pouvoir réflécteur de veines, passées, lits, veinules, filets et grains de matière organique dispersée dans quelques sédiments du bassin houiller du Nord et du Pas-de-Calais. In: *Coll. Intern. Petr. Mat. Org. Sed.* Alpern B ed., 17–39.

Bostick N H 1973: Time as a factor in thermal metamorphism of phytoclasts (coaly particles). C. R. 7e Congr. Int. Str. Géol. Carbonifère

Bostick N H, Foster J N 1974: Comparison of vitrinite reflectance in coal seames and in kerogen of sandstones, shales, and limestones in the same part of sedimentary section. In: *Coll. Intern. Pétr. Mat. Org. Séd.* Alpern B ed. 13–25.

Buntebarth G 1982: Geothermal history estimated from the coalification of organic matter. *Tectonophysics,* 83, 1–2, 101–108.

Cornelius C D 1975: Geothermal aspects of hydrocarbon exploration in the North Sea area. *Norges geologiske undersokelse,* N ° 316, 29–68.

Hood A, Gutjahr C C M, Heacock R L 1975: Organic metamorphism and the generation of the petroleum. *AAPG Bulletin,* 59, 6, 986–996.

Karpov, P A, Stepanova A. F, Soloveva N V, Agulov A P, Gozhaja A L, Golikov V A, Tsaitsky VP P 1975: Quantitative estimation of the role of temperature and geological time in the coalification of dispersed coaly particles and possibility of its application in the oil geology (in Russian). *Izv. AN URSS ser. Geol.,* 103–113.

Karweil J 1956: Die Metamorphose der Kohlen von Standpunkt der physikalischen Chemie. *Z. dt. geol. Ges.,* 107, 132–139.

Kettel D 1981: Maturitätsberechnungen für das nordwestdeutsche Oberkarbon—ein Test verschiedener Methoden. *Erdöl-Erdgas Z.* 97, 395–404.

Künstner E 1974: Vergleichende Inkohlungsuntersuchungen unter Berücksichtigung mikrophotometrischer Reflexionsmessungen an Kohlen, Brandschiefern und kohlehaltigen Nebengesteinen. *Freiberger Forschungshefte, Reihe C,* No 287.

Lopatin N V 1971: Effect of temperature and geological time in the coalification (in Russian). *Izv. AN URSS Ser. Geol.,* 3, 95–106.

Lopatin N V 1976: Estimation of the effect of temperature and geological time in the catagenetic processes of coalification and oil genesis (in Russian). Study of the organic matter in ancient and recent sediments. Vassojevich N B ed. 361–366.

Shibaoka M, Bennett A J R 1977: Patterns of diagenesis in some Australian basins. *APEA Journal,* 17, 58–63.

Teichmüller M, Teichmüller R 1979: Diagenesis of coal (coalification). In: *Diagenesis in sediments and sedimentary rocks.* Larsen G, Chillingar G V eds, 207–246.

Tissot B, Espitalié J 1975: L'évolution thérmique de la matière organique des sédiments: application d'une simulation mathématique. *Revue IFP* 30, 743–777.

Vető I 1981: An examination of the timing of catagenesis of organic matter using three published methods. In: *Adv. Org. Geoch. 1979.* Douglas A G and Maxwell J R eds, 163–169.

Waples D W 1980: Time and temperature in petroleum formation: application of Lopatin's method to petroleum exploration. *AAPG Bull.,* 64, 916–926.

Acta Geodaet., Geophys. et Montanist. Hung. Volume 19 (1—2), pp. 173—184 (1984)

DEEP-STRUCTURE OF THE REGION BETWEEN THE MOTRU VALLEY AND ARGEŞ VALLEY (ROMANIA) AS SHOWN BY THE RESULTS OF GEOPHYSICAL SURVEYS

M VISARION[1], D STĂNICĂ[1], M STĂNICĂ[1]

Magnetotelluric researches carried out along four profiles situated at the exterior of the South-Carpathians, in the region between the Motru Valley and the Argeş Valley, give new information on the spatial distribution of the main discontinuities of the Earth's crust, especially of the boundary between the sedimentary formations and the crystalline basement. According to these data, the zone of maximum depth of the crystalline basement (cca 12 km) is in the area of the localities Peşteana-S Mateeşti.

The results obtained, supplemented by informations provided by other methods of investigation (gravimetric, magnetic, seismic, seismologic and borehole logging), enabled to sketch a structural model which contributes to the increase of the knowledge on the deep structure in this area.

Keywords: Argeş Valley; Carpathians; geomagnetic field; gravity; magnetotellurics; Moesian Platform; Motru Valley; tectonics

Introduction

The present area was covered by numerous geophysical surveys which contributed significantly to some regional geological structure problems (Airinei 1982, Cornea et al. 1978, Gavăt et al. 1965, Socolescu et al. 1964) as well as to the fitting of the area into the concept of global tectonics (Airinei 1982). It belongs mostly to the western part of the Moesian Platform, characterized by strong erosion reliefs, intrusive bodies in the basement and eruptive rocks in the Permo-Triassic cover. Towards N and NW, the investigated area extends also into the Danubian Autochthon, the lowermost unit of the South-Carpathian structural sequence.

The present paper is a part of the research programme of the deep structure on Romanian territory, within which special account is paid to magnetotelluric researches due to their information about the discontinuity of the lithosphere — and with moderate expenses, and data supplied by other geophysical methods as seismics, gravimetry and seismology were considered, too. In this context, this paper represents a continuation of previous researches (Stănică and Stănică 1979, 1981) carried out along profiles crossing Carpathian units and their foreland with a view to synthetize in a unitary concept all evidence yielded by an integrated interpretation of the available data. They resulted in a tectonic sketch which offers new elements on the structure of the basement as well as on some peculiarities of the Earth's crust in this region.

[1]Institute of Geology and Geophysics, Caransebes 1, Bucharest, Romania

Primary data and the methodology of processing and interpretation

The paper is based on the results of the magnetotelluric soundings in 32 points, along 4 profiles, generally trending N-S which cross the major structural units of the area. The measurements were carried out with the equipment MTL-71 which enables the simultaneous recording of the Earth's natural electromagnetic components (E_x, E_y, H_x, H_y, H_z) in the frequency range 10^{-4} — 1 Hz, within a time interval of 3-6 hours.

Primary data were processed by spectral analysis, using Fast Fourier Transform applied to a time function $f(t)$ (Hermance 1973, Soare et al. 1978).

For the interpretation of the magnetotelluric sounding curves invariant quantities of the impedance tensor were determined which allowed to conclude to the type of the geological structures (1-, 2- and 3-D) and to compute the corresponding parameters ϱ_{xy}, ϱ_{yx}, $\varrho_{||}$, $\varrho_{\perp}$, and ϱ_{ef} (Berdichevsky 1968, Kaufman and Keller 1981, Rokityansky 1975).

As the magnetotelluric profiles cross geological units with clearly different structures, the determination of the complex connection between the electric and magnetic components required the elimination of the dispersion effects from the amplitude spectrum and the utilization of statistic methods of approximation based on the methods of least squares fitting and of the polynomial regression of the orders I-VI (Soare et al. 1978).

The interpretation of the magnetotelluric sounding curves was based on the estimation of the effective impedance; however, in certain sectors transversal and longitudinal resistivity curves were also successfully used.

The selection of the transversal or longitudinal resistivities in the interpretation of the magnetotelluric sounding curves is influenced by the weight of the galvanic and induction distortions and of the superchanneling or strait effect.

With a view to ensure a correct interpretation of the data one took into account when choosing the curves ϱ elements connected to the dip angle of the upward branch as well as the shape and elongation of the impedance tensor polar diagrams (Berdichevsky and Zhdanov 1981, Word et al. 1971).

The magnetotelluric soundings were quantitatively interpreted, both on the basis of master curves and analytically (Vanyan and Butkovskaya 1980). This enabled to obtain the effective conductance (S_{ef}) and depth values (H). Finally a structural map was constructed for the level of the basement of the sedimentary cover.

The gravimetric and magnetic data were taken over from the national maps Δg_B and Δz, with a scale of 1 : 200,000 (Airinei et al. 1971, Vencov et al. 1957). Considering certain seismic data related to the depth of the Moho discontinuity in Oltenia (Cornea et al. 1978, Rădulescu, 1979) gravity anomalies were processed using Socolescu et al's. (1964) calculation method to obtain an idea on the depth changes of this surface within the area. On one of the MTS profiles the gravitation effect due to the sedimentary cover

was evaluated on the basis of a hypothetic geological structure (considered to be 2-D), in order to make a direct comparison between gravimetric and magnetotelluric results.

The integrated study of the gravimetric and seismic data completed with seismologic informations, enabled to trace the principal basement fractures. The magnetic anomalies Δz were used for the separation of basements with different petrographic constitutions as well as for the location of the intrusive and effusive rock bodies.

Results of the magnetotelluric survey

The map of the effective conductance (Fig. 1) shows a zone with a high density of isolines in the area north of the Tg. Jiu-Rîmnicu Vîlcea alignment; it hints at the existence of major fractures in the basement, with deeper southern flanks.

Southwards there is a large zone of high conductivity, its axis lies in the direction of the localities Tg. Cărbuneşti and Slătioarele indicating a considerable thickening of the sedimentary cover. To the south the anomaly is bordered by a gradient belt, more obvious in the Drăgăşani area which corresponds to a major step of the platform basement to the north.

An important minimum anomaly, with a SW-NE axis through the localities Bratovoeşti, Slatina, Potcoava, indicates the uplift of the platform basement in the Balş-Optaşi area.

The depth of the resistive horizon, corresponding to the crystalline basement, was calculated on the basis of master curves in direct connection with the S_{ef} values. The isobath map (Fig. 2) gives a general image on the relief of the crystalline basement. According to the data obtained the zone of the maximum depth of the basement (10–11 km) trends along the Tg. Cărbuneşti-S Rîmnicu Vîlcea alignment. Southwards, an uplift of the basement can be observed up to the Balş-Potcoava area where it is found at approximately 3 km and 4 km, respectively. The southeastern part is characterized by a rapid sinking of the basement, in connection with the Alexandria Depression.

In order to achieve a more thorough image on the possibilities of the magnetotelluric method, three deep sections are presented which are correlated with the variation curves of the values S_{xy}, S_{yx} and S_{ef} as well as of the telluric parameters E_m and J.

Profile I-I' (Fig. 3), approximately trending N-S, crosses the localities Baia de Fier, Zătreni, Iancu Jianu and Studina. The variation of the effective conductance S_{ef} localizes the zone of maximum thickening of the sedimentary cover between Mateeşti and Zătreni. The northern part of the profile is characterized by a strong anisotropy of the electric parameters, the values S_{xy}, S_{yx} and S_{ef}, as a result of the complex structure of the cover with intra-Senonian tectogenesis and of the Precarpathian unit. Southwards the transition to the platform cover, with gentle sloping layers, is marked by a grouping of the values. After the elimination of the distortion effects from the

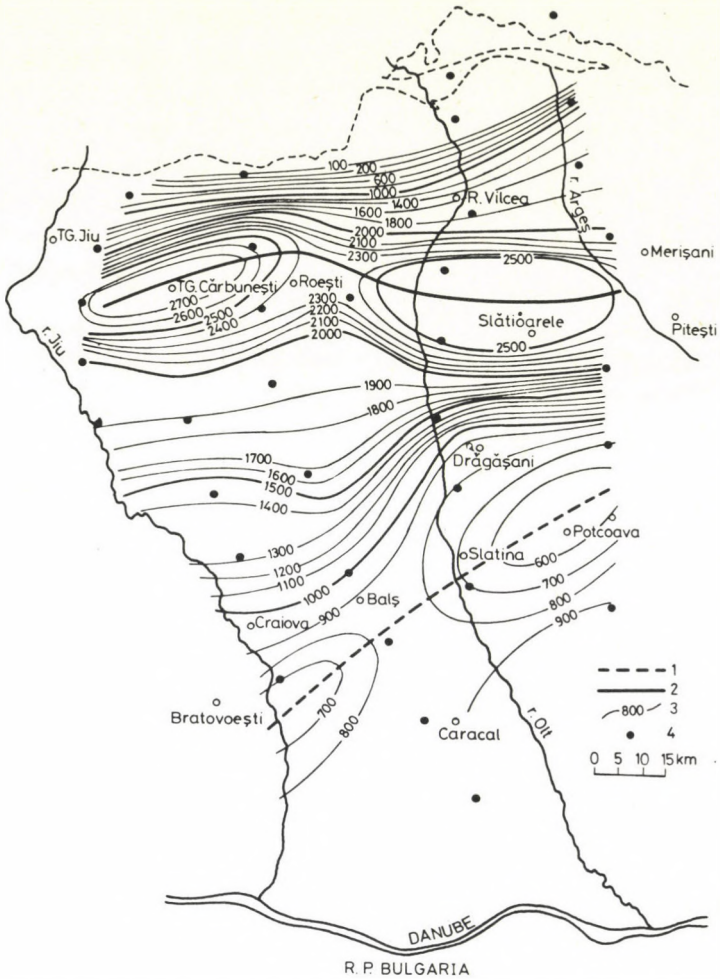

Fig. 1. Map of the effective conductance distribution S_{ef} (1 — axis of the minimum zone S_{ef}; 2 — axis of the maximum zone S_{ef} 3 — S_{ef} isolines; 4 — location of magnetotelluric soundings)

MTS curves, one could obtain the spatial changes of the basement which, at least in the southern part of the profile, could be correlated with the results of seismometric surveys and deep drilling.

On the same profile, on the basis of the dependence between the apparent conductance and the penetration depth, two boundaries have been separated at depths ranging from 18–24 km to 30–38 km, probably corresponding to the Conrad and Moho discontinuities.

The use of 1-D inversions (Word et al. 1971, Kaufmann and Keller 1981) might cause the appearance of further errors in case of complex geological structures. In

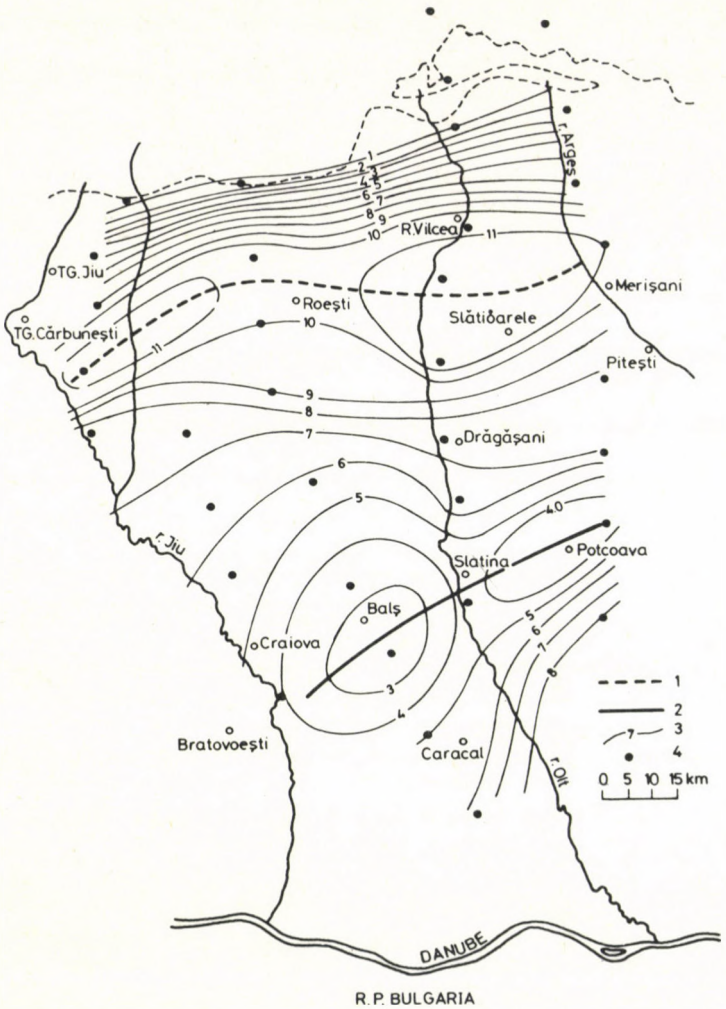

Fig. 2. Isobath map at the level of the crystalline basement (1 — axis of the zone of maximum depth of the basement; 2 — axis of the zone of maximum uplift of the basement; 3 — isobaths drawn at levels of 1 km; 4 — MTS locations)

order to make a more correct interpretation of the magnetotelluric data one used both the set of master curves and the longitudinal resistivities given by well logs.

On the profiles II-II' and III-III' (Fig. 4), situated through the localities Muşeteşti-Ceplea and Stoina-Malu Mare, respectively, the curves S_{xy}, S_{yx} and S_{ef} show configurations similar to the above-mentioned one, corresponding to the intensively folded formations in the northern part and to gentle-sloping platform formations in the southern part.

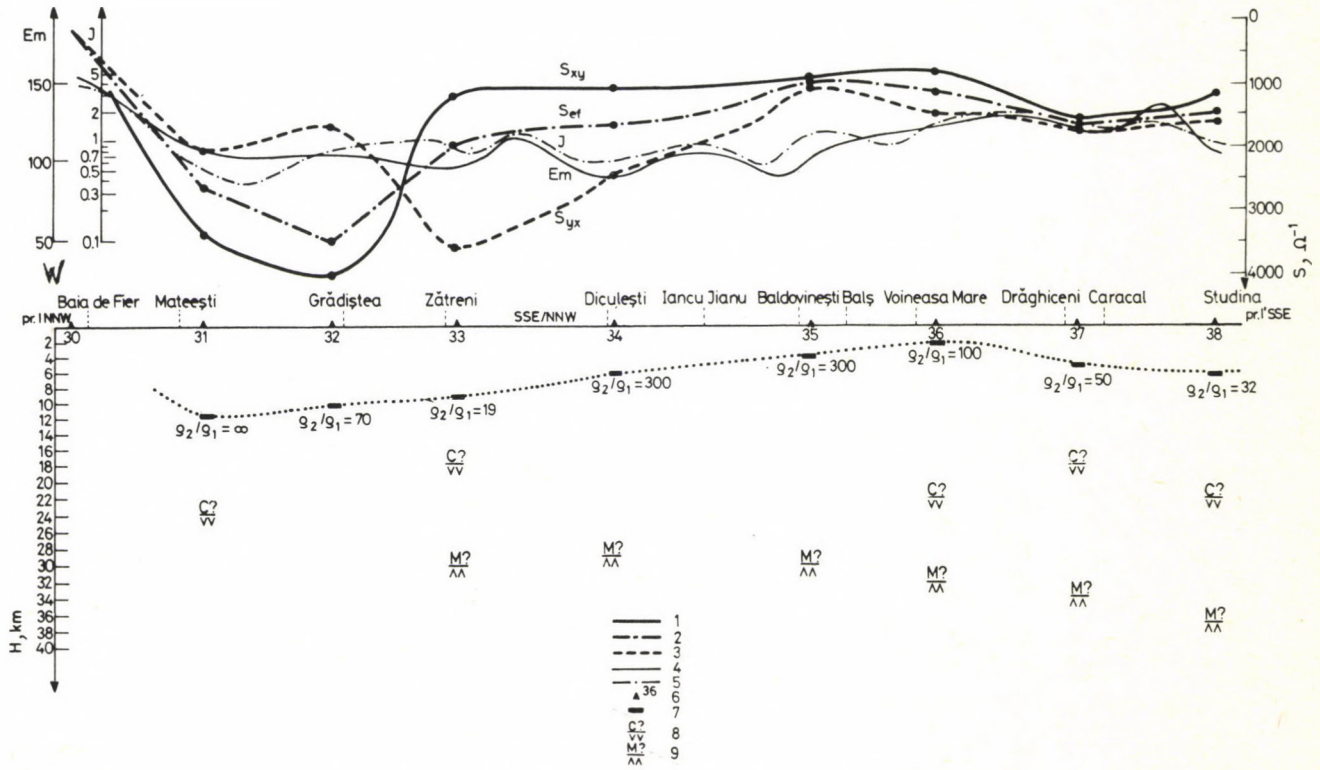

Fig. 3. Deep section on the basis of magnetotelluric data along the profile I–I' (1, 2, 3 — curves of the conductances S_{xy}, S_{ef}, S_{yx}; 4 — average of the telluric field E_m; 5 — invariant J; 6 — MTS locations; 7 — surface of the crystalline basement; 8, 9 — assumed position of the Conrad and Moho discontinuities)

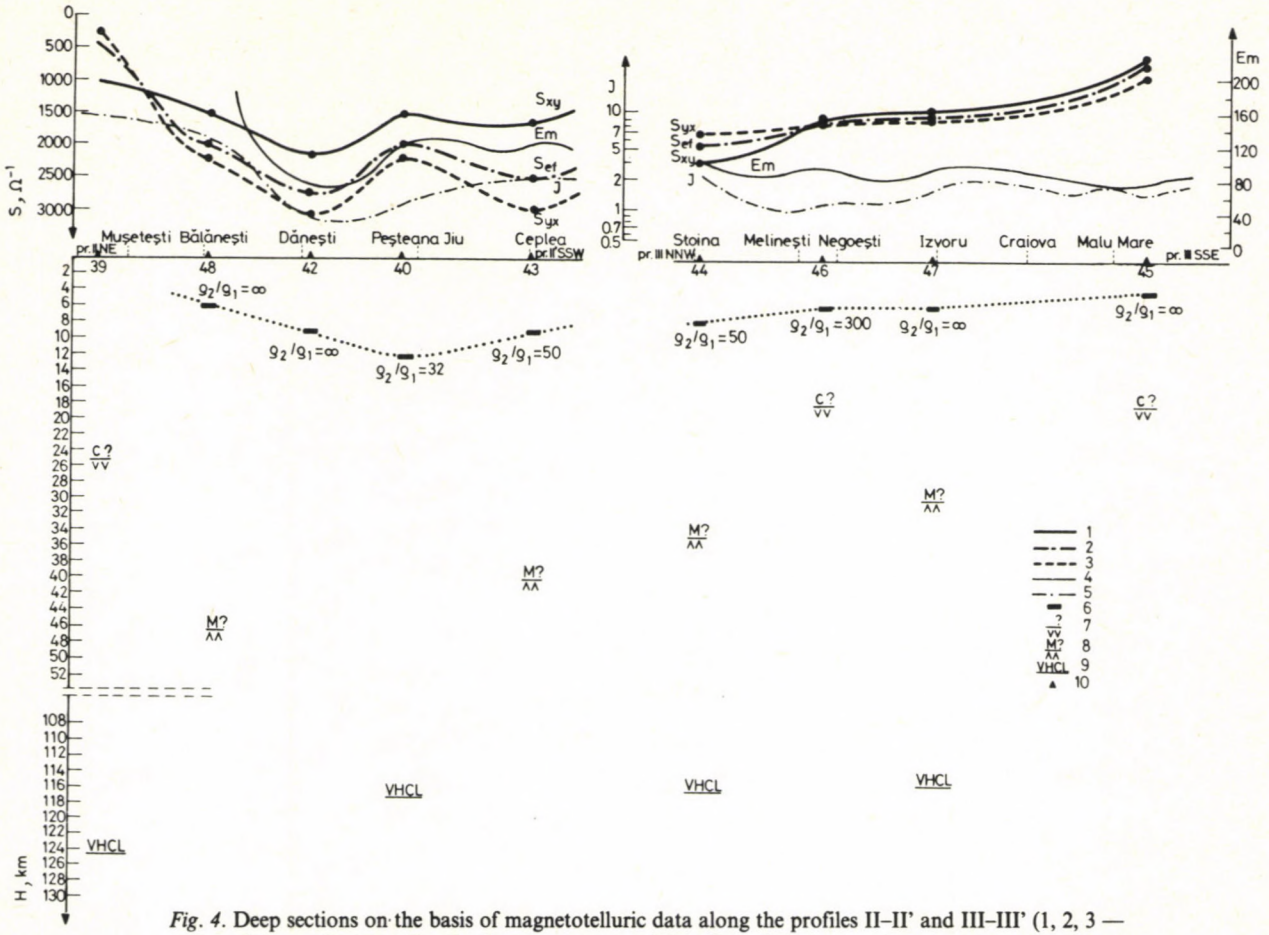

Fig. 4. Deep sections on the basis of magnetotelluric data along the profiles II–II' and III–III' (1, 2, 3 — curves of the conductance S_{xy}, S_{ef}, S_{yx}; 4 — average of the telluric field E_m; 5 — invariant J; 6 — surface of the crystalline basement; 7, 8 — assumed position of the Conrad and Moho discontinuities; 9 — upper limit of the high conductivity layer; 10 — MTS locations)

A detailed analysis of the MTS curves, along the Stoina-Malu Mare profile, using the same methods of 1-D inversion of the impedance-frequency function in a conductance-depth estimation, led to the identification of four boundaries within the lithosphere. The first boundary — at depths of 6 km at Bălăneşti, 12 km at Peşteana-Jiu, and 4 km at Malu Mare — corresponds to the basement. The second boundary was found at depths between 25 km (in the north) and 18 km (in the south). The third boundary was confirmed on the curves ϱ_{eff} of 4 MTS, at a depth of 30 km at Izvoru and of 48 km at Bălăneşti. The latter value is doubtful and is not likely to be the depth of the Moho discontinuity.

Most of the soundings along profile III-III' point to the presence of a fourth boundary, for the range of periods from 600 to 3000 s, at depths of 110–120 km, being the top of the high conductivity layer at the basis of the lithosphere.

General considerations on the deep geological structure

The complementation of magnetotelluric data with the informations given by gravimetric, seismic, magnetic and seismologic surveys, as well as by boreholes allowed to present a structural sketch of the area (Fig. 5).

The basement of the region is constituted by the Danubian Autochthon or by the basement of the Moesian Platform. The boundary between the two units was outlined mainly on the basis of the magnetic anomaly Δz; it has a different course, especially in West-Oltenia than the one previously indicated (Gavăt et al. 1965). Taking into account the gradient belt which corresponds to the minimum gravimetric anomaly northwards, this boundary is assumed to have a tectonic origin being the S Călimăneşti-Tg. Jiu fracture. It represents the contact between folded Hercynian elements (metamorphosed Paleozoic) and their foreland (platform Paleozoic). In this interpretation it has been admitted the hypothesis* that, south of this fracture, there occurs a thickening of the Upper Paleozoic formations, as confirmed by deep sounding which indicates a strong development of the Permo-Triassic in the northern part of the Bibeşti fracture. West of Tg. Jiu, the mentioned fracture intersects the Timoc fault, active till the Neogene.

The area of the Moesian Platform west of the River Olt is dominated by basement fractures with a general E-W trend. A major element of the platform is the Filiaşi-Drăgăşani uplift, an equivalent of the Oltenian threshold (Dumitrescu et al. 1962). Northwards several fractures can be observed, among them two major ones which result in a significant sinking of the platform basement. In the zone of maximum depths, the basement would be at 14–15 km, according to gravimetric data, and at

*Visarion et al. (1981). Report, I.G.G. Archives, Bucharest

11–12 km, according to magnetotellurics. The difference may be due to the Hercynian marginal depression the effect of which has not been taken into account in the model.

South of the Filiaşi-Drăgăşani threshold, the platform basement is divided into blocks with different spatial positions bordered by fractures, from which the Balş-Optaşi uplift block is separated. The location of the Permo-Triassic effusions (of basic origin) on the uplift blocks and in their vicinity indicates that the fractures bordering

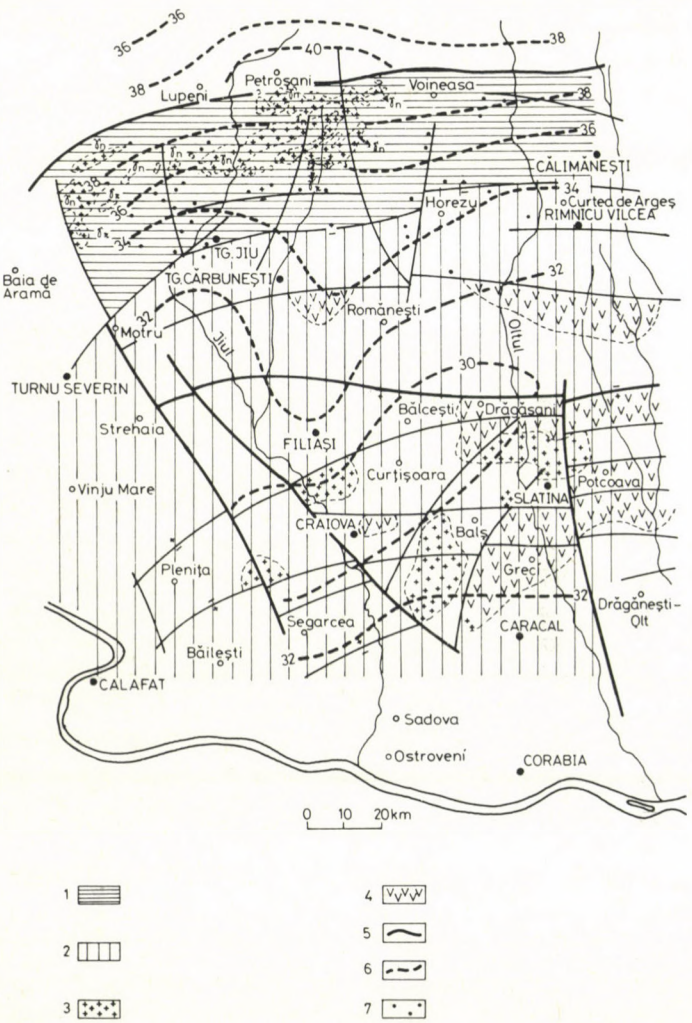

Fig. 5. Structural sketch of major geological units between the Argeş and the Motru Valleys (1 — Danubian Autochthon; 2 — Moesian type basement; 3 — bodies of intrusive rocks; 4 — Permo-Triassic effusions; 5 — crustal and basement regional fractures; 6 — surface of the Moho discontinuity; 7 — epicentres of normal earthquakes)

them constituted the principal ways of access for the magmas. The magnetic and borehole data show that the Permo-Triassic magmatic activity is characteristic for the platform west of the intra-Moesian fault.

Two important fractures — the Jiu and Motru fractures — affect the platform basement and it is probably that, especially the latter one, should be of crustal origin.

West of the Motru River a modification of the basement is indicated by magnetic anomalies, which probably includes granitic bodies of considerable sizes. In any case this area belongs to the platform, too, as the boreholes crossed Paleozoic formations specific to this unit.

The Danubian Unit is developed north of the S Călimănești-Tg. Jiu fault and west of the Timoc fault. We shall not give further details on it as surface geological data are sufficient for its characterization. However, a present uplift of the mountainous zone by 3–4 mm/year should be mentioned; it might explain the more advanced erosion of the Getic Nappe and the wide outcropping of the Danubian Autochthon in this region. Another new element is constituted by the extension of the Cerna fault to the east, at least up to the Voineasa area, as indicated by some geophysical and remote-sensing data.

Information on the lithospheric structure

The comparison of magnetotelluric and gravimetric data with seismic ones (Cornea et al. 1978, Rădulescu 1979) enables to trace the configuration of the Moho discontinuity, with acceptable errors.

According to available data, two different zones exist separated by a conventional line situated at the parallel of the locality Tg. Jiu.

The southern zone is characterized by a less pronounced relief of the Moho discontinuity, at depths ranging from 30 to 35 km. In the Balş area there is a wide swell, limited by the isoline of 30 km. Southwards a tendency of sinking has been found, which is extended till Bulgarian territory, with depths typical of the epi-Hercynian platforms.

Generally, the crust constitution is relatively homogeneous in this region, according to seismic and magnetic data on the position of the Conrad discontinuity. A special case seems to be the Balş area, where the residual gravimetric anomaly shows the existence of an intrusive massif at the basis of the granitic layer (Socolescu et al. 1958).

North of the parallel of the locality Tg. Jiu, the crust is rapidly thickening so that under the Petroşani Depression, on the eastern prolongation of the Cerna graben, the Moho discontinuity is situated at 40–42 km.

Magnetotellurics also yields information on the thickness of the lithosphere, showing the upper part of the high conductivity layer at depths of 100–120 km. Considering the results from the bend zone (Stănică and Stănică 1981), where this layer

is located at 180—250 km, there results a thinning of the lithosphere from east to west. As compared to the region from the interior of the Carpathians, where the basis of the lithosphere is at about 80 km, in the present area it is thicker, with values close to those corresponding to the regional average (Ádám 1980).

Conclusion

The comparison of magnetotelluric data with informations provided by other geophysical methods and by deep soundings enabled to conclude about the Danubian Unit and its foreland in the area studied. The results specify the thickness of the sedimentary cover, refer to crustal and regional fracture systems as well as to the position of the Moho discontinuity. Data on the upper limit of the high conductivity layer, corresponding to the top of the asthenosphere, are also given.

The central-western part of the Moesian Platform displays some peculiarities, among which mention should be made of the intense magmatic activity, materialized by the presence of acid and basic intrusions in the basement (probably Paleozoic), as well as of ample Permo-Triassic effusions, as indicated by a remarkable modification of the geothermic situation west of the intra-Moesian fault.

The continuation of these researches is necessary for the inclusion of the Romanian territory into the global tectonics concept, some of the models proposed being insufficiently supported by available data.

References

Ádám A 1980: The change of electrical structure between an orogenic and an ancient tectonic area (Carpathians and Russian Platform). *J. Geomagn. Geoel.*, 32, 1–46.

Airinei St 1982: Geodynamics relations of the Moesian microplate with the Carpatho-Balkanic arc in Romanian territory. *St. cerc. geol. geofiz., geogr., Geofizica*, 20, 3–10.

Airinei St, Stoenescu Sc, Velcescu G 1971: Magnetic map of Muntenia and Oltenia. (in Romanian) *St. cerc. geol. geogr. geofiz., Ser. geofiz.*, 9, Nr 1, 27–38.

Berdichevsky M N 1968: Electric prospecting with the method of magnetotelluric profiling (in Russian). Izdat. Nedra, Moscow

Berdichevsky M N, Zhdanov M S 1981: Interpretation of the variable electromagnetic field of the Earth (in Russian). Izdat. Nedra, Moscow

Cornea I, Varodin V Chişcan V, Costescu M, Rădulescu F, Răileanu V 1978: Deep crustal reflections in Romania. *Rev. Roum. Géol., Géophys. et Géogr., Série de Géophysique*, 22, 3–13.

Dumitrescu I, Săndulescu M, Lăzărescu V, Mirăută O, Pauliuc S, Georgescu C 1962: Mémoire pour la carte tectonique de la Roumanie. *Ann. Com. Geol.*, 32.

Gavăt I, Airinei St, Botezatu R, Socolescu M, Stoenescu Sc, Vencov I 1965: Contributions de la gravimétrie et de la magnétometrie à l'étude de la structure profonde du territoire de la R. P. Roumanie. *Rev. Roum. Géol., Géophys. et Géogr., Série de Géologie*, 9, 81–107.

Hermance J F 1973: Processing of magnetotelluric data. *Physics of the Earth and Planetary Interiors*, 7, 349–364.

Kaufman A A, Keller G V 1981: The magnetotelluric soundings method. *Methods in geochemistry and geophysics*, 15, Elsevier Sci. Publ. Comp. Amsterdam–Oxford–New York.

Radulescu F 1979: Seismic study of the crustal structure in Romania (Dr thesis) (in Romanian). Univ. Bucharest.

Rokityansky I I 1975: Study of the anomalies of the electrical conductivity with the magnetotelluric profiling method (in Russian). Nauk. Dumka, Kiev.

Rokityansky I I 1981: Induction sounding of the Earth (in Russian) Nauk. Dumka, Kiev.

Rokityansky I I 1982: Geoelectromagnetic investigation of the Earth's crust and mantle. Springer Verlag, Berlin.

Soare A, Stănică D, Cucu G, Plavită R 1978: Some techniques of magnetotelluric data processing. *Rev. Roum. Géol., Géophys. et Géogr., Série de Géophysique*, 22, 107–112.

Socolescu M, Bişir D, Georgescu M, Popovici D, Visarion M 1958: Determination of residual anomalies from gravimetric measurements. (in Romanian) *St. cerc. geofiz.*, 9, Nr 1, 115–126.

Socolescu M, Popovici D, Visarion M, Roşca V 1964: Structure of the earth's crust in Romania as based on the gravimetric data. *Rev. Roum. Géol. Géophys., Géogr., Série de Géophysique*, 8, 3–11.

Stănică M, Stănică D 1979: Telluric and magnetotelluric research in the Getic depression (in Romanian). *St. techn. econ., Ser. D. Prosp. geofiz.*, 12, 139–146.

Stănică M, Stănică D 1981: The use of the natural electromagnetic field of the Earth for the construction of a structural model of the East-Carpathian arc (in Romanian). *St. cerc. geol., geofiz., geogr., Sec. Geofizica*, 19, 41–51.

Vanyan L L, Butkovskaya A I 1980: Magnetotelluric sounding of layered media (in Russian). Nedra, Moscow.

Vencov I, Stoenescu Sc, Esca Al 1957: Recherches gravimétriques en Olténie et en Valachie. *Rev. Géol. et Géogr.*, 1, 11–25.

Word D R, Smith H W, Bostick F X Jr 1971: Crustal investigations by the magnetotelluric tensor impedance method. *Geophys. Monograph Series*, 14, 145–167.

Acta Geodaet., Geophys. et Montanist. Hung. Volume 19 (1—2), pp. 185—188 (1984)

SYNCHRONOUS MAGNETOTELLURIC MEASUREMENTS ALONG A PROFILE IN THE SOVIET CARPATHIAN REGION

M S ZHDANOV[1], M N BERDICHEVSKY[2], V S SHNEYER[1], E B FAINBERG[1], V N BOBROV[1], A I BILINSKY[3], S N KULIK[4], I M LOGVINOV[4]

The paper presents some results of magnetotelluric measurements in the Soviet Carpathians in summer 1981. 8 electromagnetic stations and three magnetometers were operated along 500 km of the international Geotraverse II (KAPG). The recordings lasted 2–2.5 months.

The data obtained show the effect of the 2-D conductive body below the central part of the Carpathians. The measurements were strongly disturbed by industrial noises at some places. Nevertheless, MT data could be analyzed. All data will be used in the solution of the direct and inverse problems.

It would be important to carry out synchronous measurements at a MT array in the Carpathian zone of the USSR, Hungary, Czechoslovakia, Poland, Romania and Bulgaria. It is desirable to use uniform instruments and processing methods.

Keywords: Carpathians; Geotraverse II.; magnetotellurics; synchronous measurements

The study of the distribution of the electric conductivity below the Soviet Carpathians by the magnetotelluric method was started by Ukranian geophysicists in the mid-sixties. In the past years magnetovariational (MV) and magnetotelluric (MT) measurements were carried out in different intervals at several tens of stations.

As a result of these measurements, maps of the total longitudinal conductance were prepared for this region which enabled to detect and localize several geoelectric inhomogeneities, and among them as most important one the Carpathian MT-anomaly which is one of the greatest of such anomalies known presently.

At the stations the depth of the top of the conductor has been estimated corresponding to the asthenosphere which enables the determination of the temperature distribution in greater depths.

Nevertheless, all these computations had the imperfection that the results at different stations were obtained not in the same time and mostly within relatively short time intervals.

[1] Institute of Terrestrial Magnetism, Ionosphere and Radio Wave Propagation (IZMIRAN) USSR Academy of Sciences Troitsk, Moscow Region, 142092

[2] Moscow State University Computer Center and Geological Department, 117311 Moscow, Leningory

[3] IPP MM AN USSR, 290047 Lvov, ul. Nauchnaya 3b.

[4] Institute of Geophysics of the Academy of Sciences of the Ukranian SSR, 1252164 Kiev, prospekt Palladina 32

The present methods for the solution of the inverse problem and for the interpretation of the experimental observations are based on the splitting of the fields into parts of internal and external origins, to normal and anomalous parts or on analytic continuations, etc., and necessitate synchronous measurements along profiles or over certain areas.

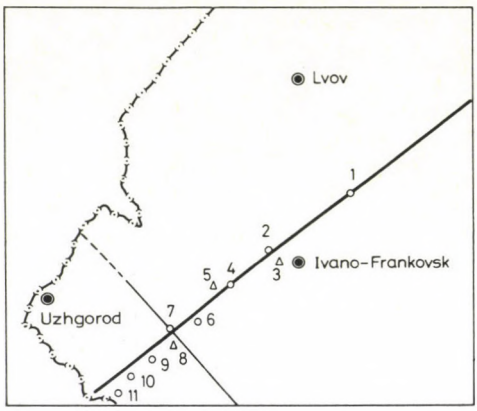

Fig. 1. The map of the measuring sites
1 Snegurocka, 2 Mizun, 3 Dolina, 4 Vyshkov, 5 Torun, 6 Mezhgorye, 7 Lisichevo, 8 Kushnitsa, 9 Irshava, 10 Kvasovo, 11 Varyevo; ○ Five-component MT station (MEVS-5); Δ Three-component Bobrov-system

Corresponding to the plans of the KAPG, in summer 1981 several institutions of the Soviet Academy of Sciences carried out synchronous MT measurements during longer time intervals along a geologic-geophysical profile (corresponding to Geotraverse II of the KAPG) with a total length of about 500 km, starting in the southwestern part of the Russian platform (Podolian high), crossing the central part of the Carpathians and ending in the Pannonian Basin.

8 five-component MT stations (MEVS-5) and 3 three-component MV stations of the Bobrov-system were established along the profile (Fig. 1). The latter stations were set up for a densification of the profile mainly near to the greatest gradients of the field in the vicinity of the Carpathian anomaly.

These instruments apply magnetostatic quartz variometers and galvanometers, and the recordings are run in analogue form on photopaper. The scale values of the magnetic records were between 0.2 to 0.5 nT/mm and of the electric records, 0.1–0.2 mV/km · mm; recording speed was 60 mm/h, precision of time signals ± 1 min. In order to decrease thermal drifts, the instruments were put into pits dug out for this purpose or into abandoned cellars being freed from all magnetic materials. The temperature changes during the measurement interval were always less than 5 ° C. The orientation of the instruments corresponded to the main magnetic directions, thus the

recorded components were D, H, Z, and E_x (N–S magnetic), E_y (E–W magnetic), respectively. The lengths of the electric lines were 150–300 m, and plumb electrodes were used. Longer electrode distances can hardly be used in mountaineous regions.

The instrument at each station was operated by 2–3 persons, they supervised the correct functioning of the instruments, ensured the time service, determined the scale values and took care for development and identification of the magnetograms. The erection of the stations and the repair of the instruments were made by members of the instrument team. The instruments recorded at each station 2–2.5 months in average.

During the measurement period MT recordings with a rich content in different frequency signals were obtained, the spectrum reached from daily variation till substorms and pulsations.

Figure 2 shows some example of the synchronous records of bay disturbances at 6 stations. It can be easily seen how much the components change when one proceeds from the platform area through the Carpathian anomaly to the Pannonian Basin.

The amplitude of the H_z component increases from the platform in the flanks of the anomaly, then crosses a minimum in its centre. This distribution concludes to a 2-D-conductor below the axis of the Carpathians. The axis of the anomaly is supposed in the area of the station Lisichevo. The ratio of the vertical component to the horizontal

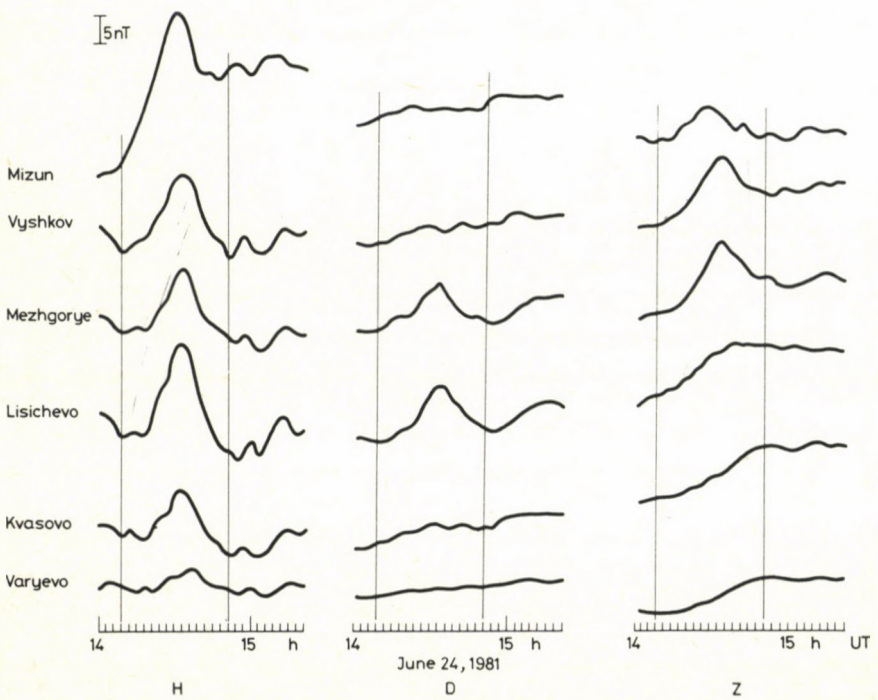

Fig. 2. Synchronous records of bay disturbances at 6 stations

one shows that the direction azimuth of the axis of the anomaly is about 145 °. At the station Varyevo a phase reversal of the H_z-component was observed. The second maximum of the H_z-component lies apparently in Hungary. For an interpretation of the Carpathian anomaly it would be very important to continue this profile till the ratio reaches its normal level.

The electric field was at several stations very much disturbed by artificial noises. The amplitudes of these industrial noises reached at some places several tens of mV/km with periods of some to some tens of seconds. The noise level could be decreased in a part of the stations by means of capacitive filters. The noises are also filtered mathematically by computers.

At present, the results obtained are being processed by computers using a special programme package for the statistical evaluation of long period variations. The processed data will be used in a geological-geophysical interpretation using MTS and MVP direct and inverse solution methods.

In the year 1982 the MT measurements in the Soviet Carpathians were continued by measurements along a profile of about 50–100 km to the W from the first one and running parallelly with it.

There are plans to continue these MT profiles along the international geotraverses in the area of Hungary, Czechoslovakia, Bulgaria and Poland. For the most complete homogenization of the measurements it would be the best to use uniform instruments e.g. those of the type MEVS-5, and to carry out processing and interpretation with the same methods, too. Deep geoelectromagnetic studies in the Carpatho-Balkan area necessitate a close cooperation of the corresponding groups from all participating countries.

PRINTED IN HUNGARY

Akadémiai Kiadó és Nyomda, Budapest

Acta Biochimica et Biophysica

ACADEMIAE SCIENTIARUM HUNGARICAE

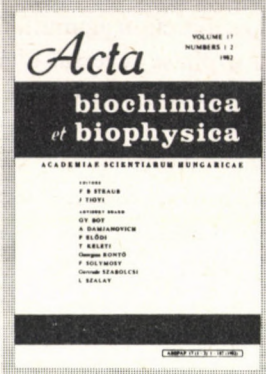

EDITORS
F. B. STRAUB and J. TIGYI

Acta Biochimica et Biophysica publishes original papers on biochemistry and biophysics in English. Papers on proteins (structure and synthesis), enzymes, nucleic acids, regulatory and transport processes, bioenergetics, excitation, muscular contraction, functional structure and ultrastructure will be accepted.

Published in one volume (4 issues) annually
Subscription rate per volume $ 40.00

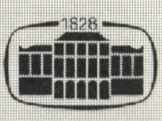

AKADÉMIAI KIADÓ
Publishing House of the Hungarian Academy of Sciences
Budapest

Distributed by KULTURA
Hungarian Foreign Trading Co.
PO Box 149, H-1389 Budapest

CONTENTS

VOLUME 17, NUMBERS 3–4

— treble underlining: bold-face italics
— red underlining: Greek letters
— green underlining: script letters.

Rules for mathematical-physical notations:

— trigonometric, logarithmic, analytic symbols, symbols for units and functions are in roman type (not underlined)
— letter symbols in mathematical and physical formulas, scalars, and subscripts of algebraic and physical quantities are in italics (underlined)
— vectors, matrices, operators in probability theory are in bold-face roman type (double underlining)
— tensors, operators and some special functions are in script letters (green underlining). These cannot be bold.
— Greek letters (red underlining) cannot be bold or extra bold type (thus they cannot be used for vectors or tensors)
— void upper lines e.g. for vectors
— avoid possible confusion between o (letter) and 0 (zero), l (letter) and 1 (one), ν (Greek nu) and v, u (letters) etc.
— explain ambiguous or uncommon symbols by making marginal notes in pencil
— be careful about superscripts and subscripts
— formulae must be numbered consecutively with the number in parentheses to the right of the formula. References in text to the equations may then usually be made by the number in parenthesis. When the word equation is used with a number, it is to be abbreviated, Eq. or Eqs in the plural
— the International System of Units (SI) should be used.

Authors are liable for the cost of alteration in the *proofs*. It is, therefore, the responsibility of the author to check the text for errors of facts before submitting the paper for publication.

3. *References* are accepted only in the Harvard system. Citations in the text should be as:

...(Bomford 1971)...or Bomford (1971)

...(Brosche and Sündermann 1976)...

...(Gibbs et al. 1976b)...

The list of references should contain names and initials of all authors (the abbreviation et al. is not accepted here); for *journal articles* year of publication, the title of the paper, title of the journal abbreviated, volume number, first and last page.

For *books* or *chapters in books*, the title is followed by the publisher and place of publication.

All items must appear both in the text and references.

Examples:

Bomford G 1971: Geodesy. Clarendon Press, Oxford

Brosche P, Sündermann J 1976: Effects of oceanic tides on the rotation of the earth. Manuscript. Univ. of Bonn

Buntebarth G 1976: Temperature calculations on the Hungarian seismic profile-section NP-2. In: *Geoelectric and Geothermal Studies (East-Central Europe, Soviet Asia), KAPG Geophysical Monograph.* Akadémiai Kiadó, Budapest, 561–566.

Gibbs N E, Poole W G, Stockmeyer P K 1976a: An algorithm for reducing the bandwidth and profile of a sparse matrix. *SIAM J. Number. Anal.*, 13, 236–250.

Gibbs N E, Poole W G, Stockmeyer P K 1976b: A comparison of several bandwidth and profile reduction algorithms. *ACM Trans. on Math. Software*, 2, 322–330.

Szarka L 1980: Potenciáltérképezés analóg modellezéssel (Analogue modeling of potential mapping). *Magyar Geofizika*, 21, 193–200.

4. *Footnotes* should be typed on separate sheets.

5. *Legends* should be short and clear. The place of the tables and figures should be indicated in the text, on the margin.

6. *Tables* should be numbered serially with Roman numerals. Vertical lines are not used.

All the illustrations should contain the figure number and author's name in pencil on the reverse.

Figures will be redrawn. Therefore the most important point is clearness of the figures, even pencil-drawings are accepted (with a duplicate).

Photographs and *half-tone* illustrations should be sharp and well contrasted.

If a specific reduction or enlargement is required, please indicate this in blue pencil on the figure.

The editors will send information to the first author about the *arrival* and acceptance of the papers. A galley proof is also sent to the first author for *correction*. Hundred *offprints* are supplied free of charge.

Periodicals of the Hungarian Academy of Sciences are obtainable at the following addresses:

AUSTRALIA
C.B.D. LIBRARY AND SUBSCRIPTION SERVICE
Box 4886, G.P.O., *Sydney N.S.W. 2001*
COSMOS BOOKSHOP, 145 Ackland Street
St. Kilda (Melbourne), Victoria 3182

AUSTRIA
GLOBUS, Höchstädtplatz 3, *1206 Wien XX*

BELGIUM
OFFICE INTERNATIONAL DE LIBRAIRIE
30 Avenue Marnix, *1050 Bruxelles*
LIBRAIRIE DU MONDE ENTIER
162 rue du Midi, *1000 Bruxelles*

BULGARIA
HEMUS, Bulvar Ruszki 6, *Sofia*

CANADA
PANNONIA BOOKS, P.O. Box 1017
Postal Station "**B**", *Toronto, Ontario M5T 2T8*

CHINA
CNPICOR, Periodical Department, P.O. Box 50
Peking

CZECHOSLOVAKIA
MAD'ARSKÁ KULTURA, Národní třida 22
115 66 Praha
PNS DOVOZ TISKU, Vinohradská 46, *Praha 2*
PNS DOVOZ TLAČE, *Bratislava 2*

DENMARK
EJNAR MUNKSGAARD, Norregade 6
1165 Copenhagen K

FEDERAL REPUBLIC OF GERMANY
KUNST UND WISSEN ERICH BIEBER
Postfach 46, *7000 Stuttgart 1*

FINLAND
AKATEEMINEN KIRJAKAUPPA, P.O. Box 128 *SF- 00101 Helsinki 10*

FRANCE
DAWSON-FRANCE S. A., B. P. 40, *91121 Palaiseau*
EUROPÉRIODIQUES S. A., 31 Avenue de Versailles, *78170 La Celle St. Cloud*
OFFICE INTERNATIONAL DE DOCUMENTATION ET LIBRAIRIE, 48 rue Gay-Lussac
75240 Paris Cedex 05

GERMAN DEMOCRATIC REPUBLIC
HAUS DER UNGARISCHEN KULTUR
Karl Liebknecht-Straße 9, *DDR-102 Berlin*
DEUTSCHE POST ZEITUNGSVERTRIEBSAMT Straße der Pariser Kommüne 3–4, *DDR-104 Berlin*

GREAT BRITAIN
BLACKWELL'S PERIODICALS DIVISION
Hythe Bridge Street, *Oxford OX1 2ET*
BUMPUS, HALDANE AND MAXWELL LTD.
Cowper Works, *Olney, Bucks MK46 4BN*
COLLET'S HOLDINGS LTD., Denington Estate *Wellingborough, Northants NN8 2QT*
WM. DAWSON AND SONS LTD., Cannon House *Folkstone, Kent CT19 5EE*
H. K. LEWIS AND CO., 136 Gower Street
London WC1E 6BS

GREECE
KOSTARAKIS BROTHERS INTERNATIONAL BOOKSELLERS, 2 Hippokratous Street, *Athens-143*

HOLLAND
MEULENHOFF-BRUNA B. V., Beulingstraat 2,
Amsterdam
MARTINUS NIJHOFF B.V.
Lange Voorhout 9–11, *Den Haag*
SWETS SUBSCRIPTION SERVICE
347b Heereweg, *Lisse*

INDIA
ALLIED PUBLISHING PRIVATE LTD., 13/14
Asaf Ali Road, *New Delhi 110001*
150 B-6 Mount Road, *Madras 600002*
INTERNATIONAL BOOK HOUSE PVT. LTD.
Madame Cama Road, *Bombay 400039*
THE STATE TRADING CORPORATION OF INDIA LTD., Books Import Division, Chandralok 36 Janpath, *New Delhi 110001*

ITALY
INTERSCIENTIA, Via Mazzé 28, *10149 Torino*
LIBRERIA COMMISSIONARIA SANSONI, Via Lamarmora 45, *50121 Firenze*
SANTO VANASIA, Via M. Macchi 58
20124 Milano
D. E. A., Via Lima 28, *00198 Roma*

JAPAN
KINOKUNIYA BOOK-STORE CO. LTD.
17-7 Shinjuku 3 chome, Shinjuku-ku, *Tokyo 160-91*
MARUZEN COMPANY LTD., Book Department, P.O. Box 5050 Tokyo International, *Tokyo 100-31*
NAUKA LTD. IMPORT DEPARTMENT
2-30-19 Minami Ikebukuro, Toshima-ku, *Tokyo 171*

KOREA
CHULPANMUL, *Phenjan*

NORWAY
TANUM-TIDSKRIFT-SENTRALEN A.S., Karl Johansgatan 41–43, *1000 Oslo*

POLAND
WĘGIERSKI INSTYTUT KULTURY, Marszalkowska 80, *00-517 Warszawa*
CKP-I W, ul. Towarowa 28, *00-958 Warszawa*

ROUMANIA
D. E. P., *Bucuresti*
ILEXIM, Calea Grivitei 64–66, *Bucuresti*

SOVIET UNION
SOJUZPECHAT — IMPORT, *Moscow*
and the post offices in each town
MEZHDUNARODNAYA KNIGA, *Moscow G-200*

SPAIN
DIAZ DE SANTOS, Lagasca 95, *Madrid 6*

SWEDEN
GUMPERTS UNIVERSITETSBOKHANDEL AB
Box 346, *401 25 Göteborg 1*

SWITZERLAND
KARGER LIBRI AG, Petersgraben 31, *4011 Basel*

USA
EBSCO SUBSCRIPTION SERVICES
P.O. Box 1943, *Birmingham, Alabama 35201*
F. W. FAXON COMPANY, INC.
15 Southwest Park, *Westwood Mass. 02090*
READ-MORE PUBLICATIONS, INC.
140 Cedar Street, *New York, N. Y. 10006*

YUGOSLAVIA
JUGOSLOVENSKA KNJIGA, Terazije 27, *Beograd*
FORUM, Vojvode Mišića 1, *21000 Novi Sad*

Index: 26.031

Acta Geodaetica, Geophysica et Montanistica Hungarica

VOLUME 19, NUMBERS 3–4, 1984

Akadémiai Kiadó, Budapest
AGGM 19 (3–4) 189-479 (1984) HU ISSN 0236-5758

ACTA GEODAETICA, GEOPHYSICA et MONTANISTICA HUNGARICA
A Quarterly Journal of the Hungarian Academy of Sciences

Acta Geodaetica, Geophysica et Montanistica (AGGM) publishes original reports on geodesy, geophysics and minings in English.

AGGM is published in yearly volumes of four numbers by

AKADÉMIAI KIADÓ
Publishing House of the Hungarian Academy of Sciences
H-1054 Budapest, Alkotmány u. 21.

Manuscripts and editorial correspondence should be addressed to

AGGM Editorial Office
H-9401 Sopron P.O. Box 5

Subscription information

Orders should be addressed to

KULTURA Foreign Trading Company
H-1389 Budapest P.O. Box 149

INSTRUCTIONS TO AUTHORS

Manuscripts should be sent to the editors (MTA Geodéziai és Geofizikai Kutató Intézete, AGGM Editorial Office, H-9401 Sopron, P.O.Box 5, HUNGARY). Only articles not submitted for publication elsewhere are accepted.

Manuscripts should be typewritten in duplicate, double-spaced, 25 lines with 50 letters each. The papers generally include the following components, which should be presented in the order listed.

1. Title, name of author(s), affiliation, dateline, abstract, keywords
2. Text, acknowledgements
3. References
4. Footnotes
5. Legends
6. Tables and illustrations

1. The *affiliation* should be as concise as possible and should include the complete mailing address of the authors. The *date of receipt* of the manuscript will be supplied by the editors. The abstract should not exceed 250 words and should clearly and simply summarize the most important methods and results. 5–10 significant expressions describing the content are used as *keywords*. Authors may recommend these keywords.

2. The *text* should be generally in English and as short and clear as possible. From Hungarian authors papers are also accepted in Hungarian.

The section heading should *not* be underlined or in capitals.

Please note that underlining denotes special types:

— single underlining: italics
— double underlining: bold-face roman

CONTENTS

Book reviews

Acta Geodaet., Geophys. et Montanist. Hung. Volume 19 (3–4), pp. 189–196 (1984)

KINEMATICAL ANALYSIS OF VERTICAL MOVEMENTS ABOVE WORKING PITS

G BARTHA[1] and L BÁNYAI[1]

[Manuscript received February 7, 1983]

On a local network established above working pits levelings were carried out to observe the vertical displacement of the area. Isocontour maps (displacements, velocities, accelerations) were developed for the kinematical characterisation of the area. On the basis of these maps the motion tendencies were determined. For prediction purpose a least squares collocation was applied and it was tested by measured data.

Keywords: kinematical analysis; least squares collocation; leveling network; movements above mines; vertical crustal movements

1. Introduction

In the frame of the cooperation work between the Mecsek Coal-Mine Company and the Geodetic and Geophysical Research Institute of the Hungarian Academy of Sciences levelings were made on a local network established in an area above working pits in order to detect the vertical movements of the surface. Between 1979 and 1982 the levelings on nearly hundred bench marks were repeated four times. Significant displacements could be observed at about forty of them during this time interval; they ranged between 1 cm and 190 cm.

In this paper attention is only paid to the kinematic description of the displacements, without their dynamical interpretation, i.e. rock mechanical considerations are not investigated here. Our purpose is to give a detailed kinematic picture about the vertical displacement, further to show a general method to process such kinds of leveling data.

Using a simple model the velocities and accelerations of vertical displacements were computed for each point at different time intervals. From the observed vertical displacement data and from the computed velocities and accelerations, three kinds of isoline maps (displacements, velocities, accelerations) were developed for three time

[1] Geodetic and Geophysical Research Institute of the Hungarian Academy of Sciences, H-9401 Sopron, P.O.B. 5, Hungary

periods by means of a finite element interpolation method. On the basis of these maps the movement trends were investigated, and quantitative considerations were made for predictional purposes by using a least square collocation method.

2. Approach of the problem

The problem of vertical movements of a topographic surface can be approached from two aspects. The first — it is called a dynamical approach — is a deductive method, it consists of constructing a theoretical model based on rock-mechanical or tectonical considerations, and its validity should be proved by the measurements. The theoretical models usually contain strict premises for the sake of simplicity of the mathematical treatment, therefore their application is in many cases limited or senseless, respectively.

The second possibility — it can be called the kinematical approach — is an inductive way when the displacements are carefully traced by measurements and using the measured data a model is constructed for the motion.

For the problem mentioned in the introductory note, we used the inductive method for the following reasons:

— due to lack of informations about the geological structure;

— the mining activities have been carried out in a complex, difficult structure in consequence of the sloped, separated coal layers.

To perform the inductive approach, two methods could be used. The first would be to approximate the shape of dip by a mathematically well treatable "smoothed" 2-D function (functional model) and to determine its parameters by a least squares adjustment process for a certain epoch from the measured displacements. Having repeated this process for several epochs, when measurements were carried out, the time dependence of the parameters of the function can be determined.

This problem has been well known for long in mining survey and many authors delt with the shape determination of such a kind of sinking field. However, they concentrated on the determination of the final shape and the time history of the phenomenon was formulated by an empirical factor; moreover, they investigated only simpler cases of mining activity (Martos 1969, Somosvári 1967, Turza 1980). It is sufficient to look at Fig. 3a, where the displacement isolines are shown, to realize that there does not exist any chance for the approximation of the dip form by a "smoothed" surface function.

Due to the mentioned facts the second method, i.e. the kinematic approach for each point was chosen. In spite of creating a functional model for the dip shape, the motion of each measured point was investigated in order to determine their kinematic parameters (displacement velocities and accelerations) at overlapping time intervals. Values in unmeasured points were approximated by the finite element method and they

were used to plot the isolines. These monitoring maps are useful for drawing conclusions about the motion tendencies. The "separate" treatment of each point was also followed to predict the displacements by using a collocation process.

Attention should be paid to some special conditions which had to be taken into consideration. In contrary to "classical" vertical movement investigations the present area is very small (1.5×1.5 km^2), where displacements were produced by artificial activity. Therefore in our case:

— the displacements reach a significant level after a very short time and their magnitudes are extraordinary in comparison with the usual vertical crustal movements;

— since the significant movements are concentrated on a small area, outside of it fixed points can be defined;

— as displacements have been produced by mining activity, they have the same direction, i.e. the moving area is sinking.

In summary the kinematic approach seems to be useful from two aspects. Partly it gives a general method to process vertical displacements, partly it yields informations about the development of the dip above a mining area.

3. Kinematic description of the vertical movement of a single point

Levelings had been carried out at five epochs, therefore four displacement data were available for each observed point. To determine the kinematic parameters of the vertical motion in a point P, a second order time polynomial was fitted to its data set. This simple approximation is very common in the practice (Holdahl 1975, Mälzer et al. 1979) and the fitting of this polynomial seems to be good enough. For some points the fitting is shown in Fig. 1. The fitted polynomials are denoted by dashed lines. The time polynomial for a displacement Δh was:

$$\Delta h = v_0 \Delta t + \frac{a}{2} \Delta t^2 \tag{1}$$

$$\Delta t = t - t_0$$

where:

v_0 = velocity at t_0

a = acceleration (assumed to be constant).

From Eq. (1) we get:

$$v(t) = v_0 + a\Delta t. \tag{2}$$

In this approximation the assumption of a uniformly accelerated motion is a serious restriction which does not match the reality. To overcome this problem, the total

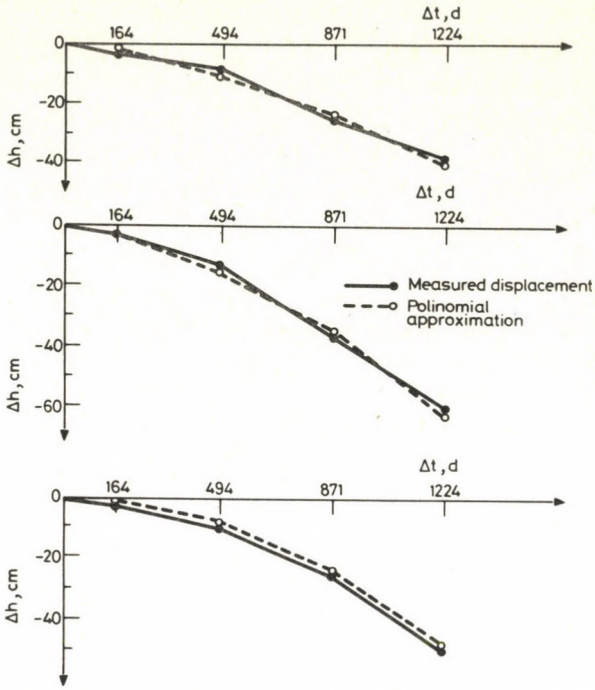

Fig. 1. Polinomial approximation of displacements

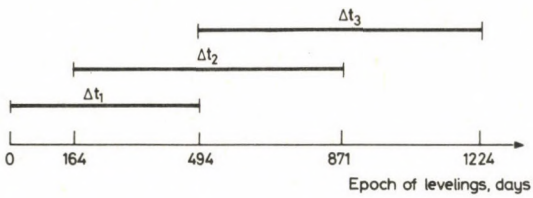

Fig. 2. The segmentation for polinomial approximation

motion was segmented, and the time polynomial was adjusted to each segment separately.

One segment should contain at least two displacements to obtain the parameters v_0 and a. In order to get as many segments as possible, the total time period was divided into overlapping intervals, as it can be seen in Fig. 2.

An inconsistency resulted from this process, since double values of the kinematic parameters belonged to the common parts of overlapping intervals. In spite of this contradiction the motion process could be followed well on the isoline maps which were constructed for the time periods $\Delta t_1, \Delta t_2, \ldots$ etc. of Eq. (1) (Fig. 3a, b, c) by taking the means.

4. Motion tendencies

A displacement data series consisted of four measured data on an observed point which were segmented into overlapping parts (Fig. 2) and the time polynomial Eq. (1) was separately adjusted to each part. These adjustments were carried out for all observed points. Therefore, for each point three parameter sets (each of them consists of the values Δh, v_0, a) were produced belonging to the three overlapping time intervals ($\Delta t_1 = 0-494$, $\Delta t_2 = 164-871$, $\Delta t_3 = 494-1224$ days; see on Fig. 2), whereby the values v_0 belonged to the beginning time points t_0 of the intervals (0, 164, 494 days; see on Fig. 2). The first measurement epoch was taken as the zero point of the time axis.

Figure 3 shows the maps plotted from these parameter sets. The isolines were deduced by a finite element interpolation method (Kalmár 1983). In Fig. 3a, the measured relative displacements are plotted in cm, in Figs 3b and 3c the computed values v_0 in cm/10^3 days and values a in cm/(10^3 days)^2.

The displacements and velocities are negative (sinking field) but the signs of the accelerations can change depending on the tendency of the motion. Positive acceleration means a deceleration in the sinking while negative acceleration means an acceleration in the sinking. In Fig. 3c negative acceleration isolines are denoted by dashed lines, zero isolines by dotted lines.

It follows from Fig. 3: The isolines of the velocities and displacements are roughly concentric around an imaginary centre. The isolines of accelerations are around different centres (Fig. 3c). The NW part of the sinking field showed a deceleration, while the SE part an acceleration during the time interval Δt_1. The sinking process can be well traced on the next maps, as during time interval Δt_2 the accelerating area decreased and moved toward South. During Δt_3, the centre of acceleration became the centre of the deceleration and a new acceleration centre appeared in the SW part. This indicates that significant displacements can be expected in this direction.

5. Prediction of the motion in a single point

To solve the prediction problem, the least squares collocation method was applied (Moritz 1973). We used a programme package developed by Závoti (1979). The basic equations of this method are (Moritz 1973):

$$\mathbf{x} = \mathbf{AX} + \mathbf{s}' + \mathbf{n}$$

$$\mathbf{X} = (\mathbf{A}^T\bar{\mathbf{C}}^{-1}\mathbf{A})^{-1}\mathbf{A}^T\bar{\mathbf{C}}^{-1}\mathbf{x}$$

$$\mathbf{s} = \mathbf{C}_{sx}\bar{\mathbf{C}}^{-1}(\mathbf{x} - \mathbf{AX})$$

$$\bar{\mathbf{C}} = \mathbf{C} + \mathbf{D}$$

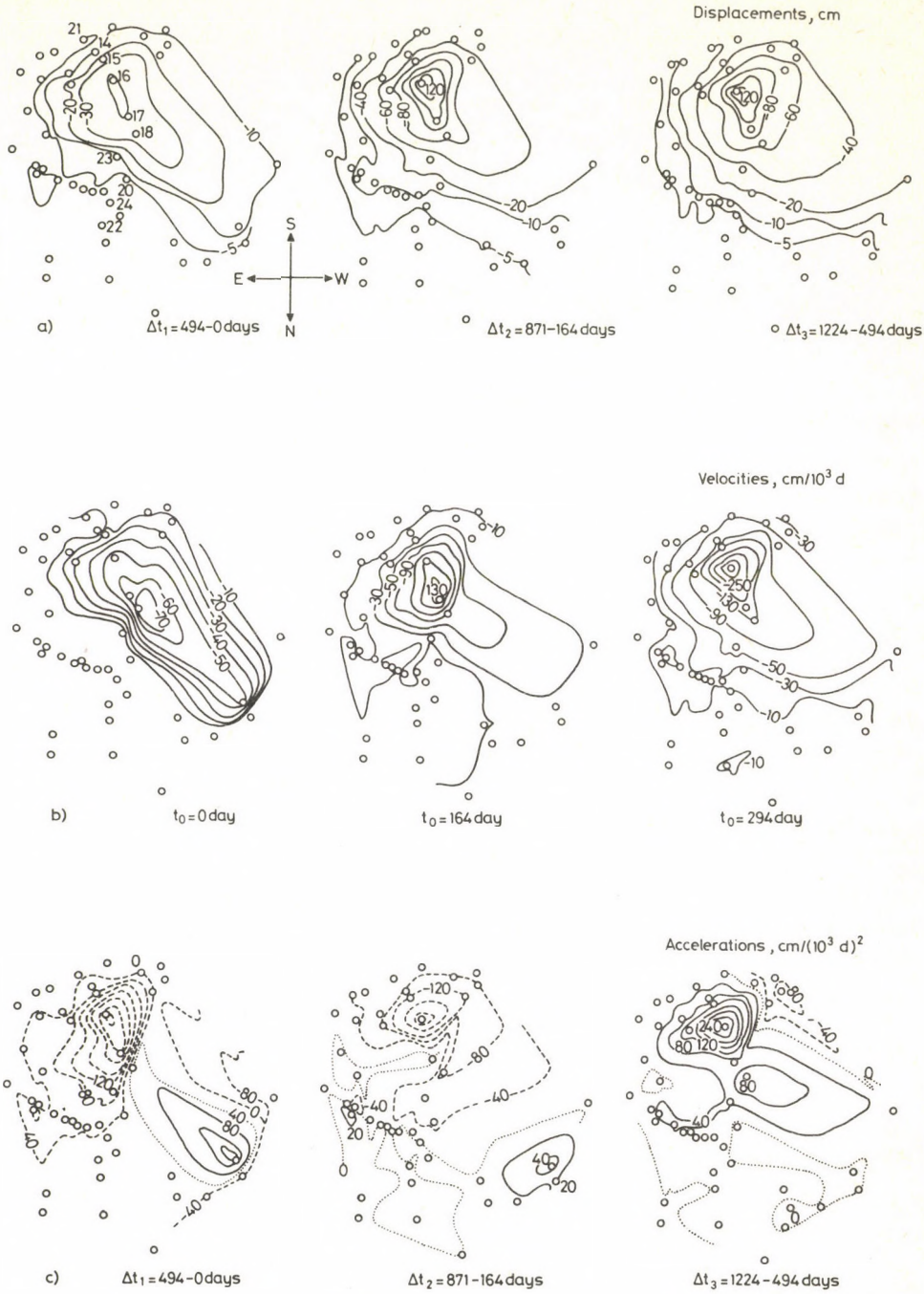

Fig. 3. Contour maps for vertical displacements, velocities and acceleration

Table I

Predicted value Δh (cm) at $\Delta t = 0-1224$	Observed value Δh (cm) at $\Delta t = 0-1224$
43.76	44,20
71.82	69.50
204.19	191.20
109.76	102.90

where:

$\mathbf{x}$ = vector of measurements,
$\mathbf{s}$ = signal vector ($\mathbf{s}'$ signal at observation points),
$\mathbf{A}$ = coefficient matrix of the functional model,
$\mathbf{X}$ = vector of unknowns,
$\mathbf{n}$ = noise vector,
$\mathbf{C}$ = signal covariance matrix,
$\mathbf{D}$ = noise covariance matrix,
$\mathbf{C}_{sx}$ = cross covariance matrix,

The elements of the vector of measurements were the displacements observed in a single point at the intervals $\Delta t_1 = 0-164$, $\Delta t_2 = 0-494$, $\Delta t_3 = 0-871$, $\Delta t_4 = 0-1224$. For getting the best prediction we used some functional models and covariance functions. The best prediction was yielded by the linear functional model:

$$\Delta h = v_0 \Delta t \tag{3}$$

and the covariance function:

$$C = c_0 e^{-b\Delta t^2} \tag{4}$$

where $c_0 = 0.3$ and $b = 0.001$ were estimated empirically.

In this model the "second order part" was included into the stochastic part of the model. The predictions were tested by a very simple process. The parameters v_0, c_0 and b were determined from three displacements in a single point at Δt_1, Δt_2 and Δt_3; and the fourth displacement at Δt_4 was predicted. The predicted values and observed ones for some measured points are compared in Table I.

6. Conclusions and future perspectives

As it was shown the pure kinematic investigation of a moving area gives some possibility to determine the trend of the motion and to predict future displacements. A good prediction was provided by the collocation method.

According to our opinion it would be very useful to extend the above outlined kinematic analysis to the investigation of the total area, i.e. to transform the one-

dimensional problem to a two-dimensional one. As mentioned for this purpose a 2-D function of the topographic surface is to be determined as a function of time. It is very likely that by splitting the topographic surface into a harmonical series a very useful tool would result in this respect. In the future work we are going to step forward into this direction.

References

Holdahl S R 1975: Models and Strategies for Computing Vertical Crustal Movements in the United States. International Symposium on Recent Crustal Movements, Grenoble, France

Kalmár J 1983: Digital Terrain Model for Geodetic Purpose. (in press)

Mälzer H, Schmitt G, Zippelt K 1979: Recent vertical movements and their determination in the Rhenish Massif. *Tectonophysics*, 52, 167–176.

Martos F 1969: Bányakártan (Damages of mining activity). Tankönyvkiadó, Budapest

Moritz H 1973: Least-Squares Collocation. *DGK Reiche A: Theoretische Geodäsie*, Nr. 75.

Somosvári Zs 1967: Néhány külszíni kőzetsüllyedést közelítő függvény vizsgálata (The Investigation of some Approximate Functions of Surface Sinking). *Bányászati és Kohászati Lapok*, 12, 803–806.

Turza I 1980: A süllyedés dimenzió nélküli típusgörbéjének közelítő meghatározása a Mecseki Szénbányáknál (Approximate Determination of the Dimensionless Standard Curve of the Sinking at Mecsek Coal-Mines). *Bányászati és Kohászati Lapok*, 13, 335–338.

Závoti J 1979: Ideas on the Practical Application of Collocation. *Acta Geod. Geoph. Mont. Hung.*, 14, 111–124.

Acta Geodaet., Geophys. et Montanist. Hung. Volume 19 (3–4), pp. 197–205 (1984)

OBSERVATIONS OF THE DEFORMATION OF THE EARTH'S CRUST IN THE "MÁTYÁSHEGY"-CAVE NEAR BUDAPEST

L A LATININA[1], GY SZABÓ[2], P VARGA[2]

[Manuscript received July 27, 1983]

A quartz extensometer with a length of 21 m has been in operation in the "Mátyáshegy"-cave since the spring of 1980. On the basis of observations in 1980–81 it was found that the distance between the two ends of the extensometer increased by 46 μm during 17 months.

The study of the periodic lunisolar component of the observation material proved the correct recording of earth tides.

Extensometers can also be used as long period seismographs.

Keywords: crustal deformation; extensometer; Mátyáshegy-cave; quartz rod

Extensometers measure the relative displacement of two rock-points in a distance of some 10 m-s from each other. The ratio between displacement and the distance between the two points gives the average horizontal deformation in the azimuth of the extensometer. The sensitivity of extensometers is generally given as the ratio between the smallest change of distance yet measurable and the length of the instrument; this value is in general 10^{-7}–10^{-10}.

A very wide spectrum of movements taking place in the solid Earth can be observed by means of extensometers, from long period earthquake waves (10^{-3}–1 μm/sec), through earth tides (10^{-1}–1 μm/day) till recent crustal movements (1–10^{2} μm/year). Since almost only such instruments can be used for the continuous observation of the latter long period variations, extensometers are very important instruments of the geodynamic research.

The Hungarian 1st order gravimeter basic point and in connection with it, a geodynamic station for the continuous study of Earth tides and long period geodynamic phenomena was installed by the Loránd Eötvös Geophysical Institute in the "Mátyáshegy"-cave in Budapest in 1979–80. The measurement of the absolute g as well as relative gravimetric measurements were carried out in the cave since that time. Besides the extensometer (Fig. 1), observations are run with three recording gravimeters and a pair of horizontal pendulums (Fig. 2). The cave lies in the area of

[1] Institute Physics of the Earth B. Gruzinskaya 10, Moscow D-242
[2] Geophysical Institute 'Loránd Eötvös' Budapest, Columbus u. 17–23, H-1145

Budapest, the geographic coordinates are: $\varphi = 47° 33'$ N, $\lambda = 19° 01'$ E, altitude = 202 m. The cave produced by thermal water activity lies in the upper Eocene nummulitic limestone which is dissected by fissures and breaks and interlaced by a natural cave-system (Jaskó 1948). Some parts of the cave-net were artificially widened and built out during World War II.

The quartz extensometer was built in cooperation by the O Yu Smidt Institute of Earth Physics of the Soviet Academy of Sciences and the Loránd Eötvös Geophysical Institute according to the working plan of KAPG (Cooperation of Academies of Socialist Countries on the Field of Planetary Geophysics). The instrument has been installed in the "Mátyáshegy"-cave at a distance of 30–35 m both from the entrance and

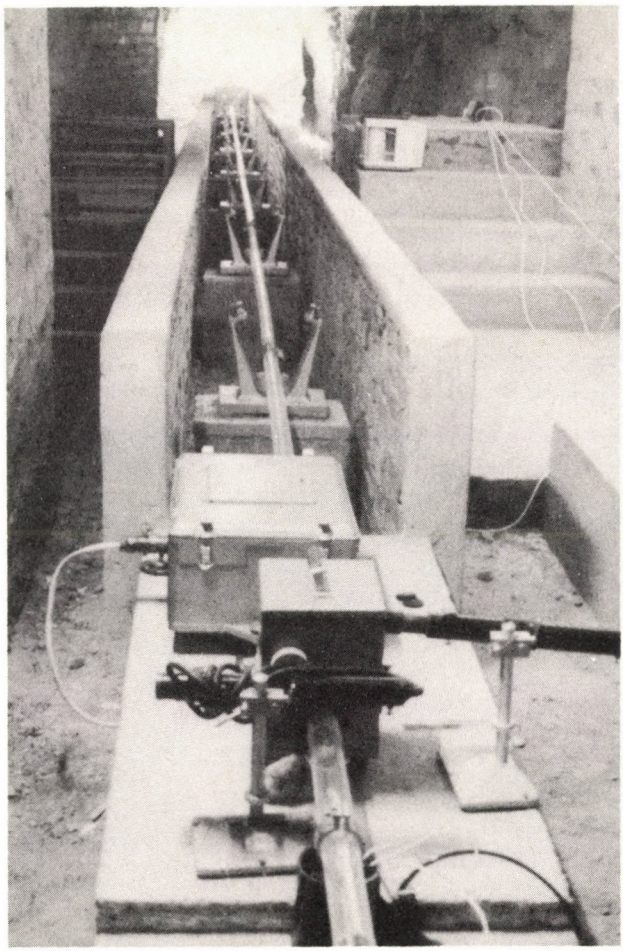

Fig. 1. Quartz extensometer in the "Mátyáshegy" cave in Budapest

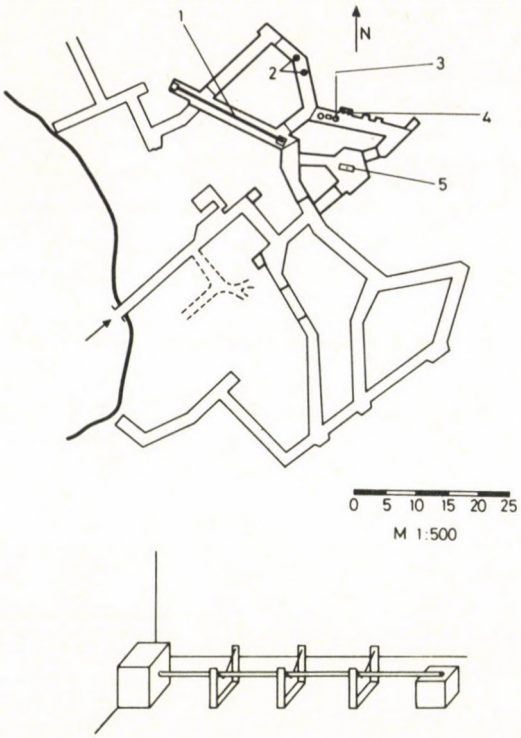

Fig. 2. Plan of the observation station in the "Mátyáshegy" cave in Budapest and sketch of the extensometer. 1 — extensometer, 2 — Heiland gravimeters, 3 — Askania gravimeter, 4 — Horizontal pendulums, 5 — Gravimetric 1st order basis point

the surface. The azimuth of the quartz rod is W24° N. In order to decrease the cave effect (Harrison 1976) the posts were arranged in a way that the quartz-tube lies almost in the axis of the cave. For the extensometer silica glass tubes of 45 mm diameter and 2–3 mm thickness were used, which have a linear thermal extension coefficient of $0.45 \cdot 10^{-6}$. The lengths of the individual tube pieces are 2.5–3 m, they were fastened together by invar profile pieces and epoxy-resin. The total length of the instrument is 21.1 m. The fixed end of the extensometer is connected through a magnetostrictive calibration unit (coil with permendure-core of about 40 ohm) to the rock. The linear deformations of the calibration unit caused by the effect of currents of different intensities were determined by a laser interferometer, the displacement of the system was measured by a roller-interference instrument placed to the free end of the system (Fig. 3).

The displacement at the free end of the measuring system is indicated by a capacitive sensor. Its resolving power enables observations with a relative sensitivity of at least $5 \cdot 10^{-10}$. The high sensitivity and the exactness of the re-adjustment getting

necessary from time to time meant serious difficulties in the development of the mechanics of the capacitive sensor. According to experiences the behaviour of the extensometer will deflect from normal when somebody enters the cave or due to an adjustment by hand. A mechanical adjustment of adequate precision by remote control with servo-motor was successfully made by F Holló, coworker in the Loránd Eötvös Geophysical Institute (Fig. 4).

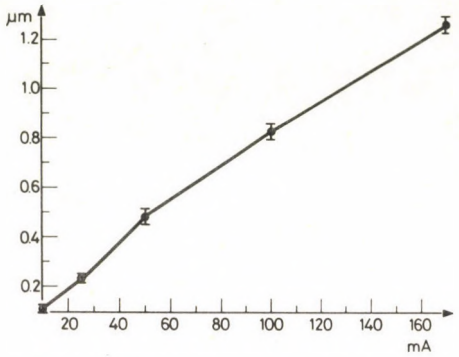

Fig. 3. Calibration curve of the extensometer

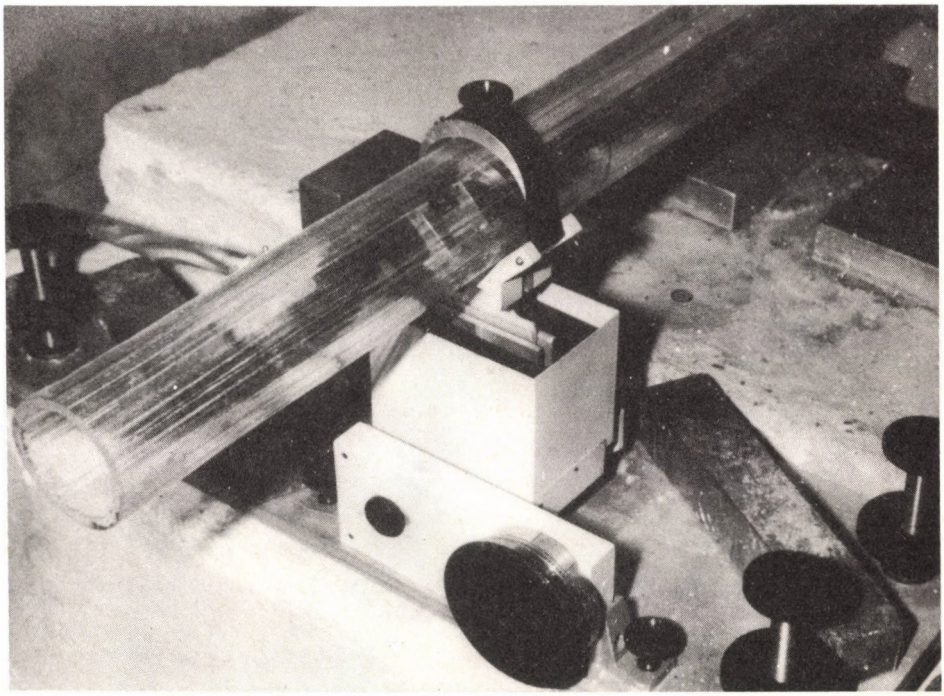

Fig. 4. The free end of the extensometer with the capacitive sensor

The signal received from the capacitive sensor is recorded in analogue form by a compensograph, in digital form by a digital voltmeter and a calculator HP-97S.

In course of processing and interpretation the main difficulty arose with the determination of the sensitivity with adequate accuracy. The study of the calibrating unit showed that the scale value of the record can be determined with a 1.5% inner accuracy at 0.1% stability of the calibrating current. Taking into account the error of interferometric and rolling calibration, too (Latinina 1975) one can speak only of a 5% calibration accuracy. The histogramme of 175 sensitivity determinations are shown in

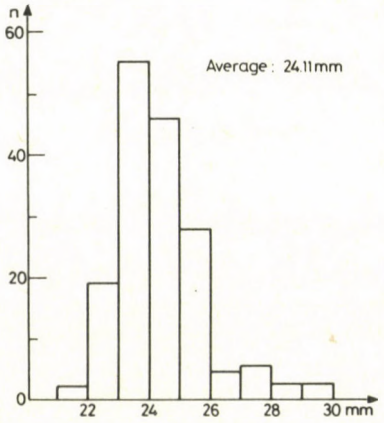

Fig. 5. Histogram of the determinations of scale values

Fig. 5 where a near to normal distribution can be observed. Thus it can be supposed that the scatter of the calibration values is of random character and has no systematic components, therefore their average can be well used for the processing of the observed data. Calibration was made once in a day, hence it could be observed, whether a change in the operation of the extensometer had occurred. The calibration unit enabled also the linearity control of the total system.

External effects — e.g. meteorological and hydrological ones — were studied on the basis of long period variations, this point will be discussed in detail later.

From the meteorological effects a connection between barometric variations and the observed time-series could not have been proved on the basis of the material observed so far. An effect of the change of outdoor air temperature, however, could have been determined. It was found that about 1 μm displacement corresponds to 1 °C in the yearly temperature variation. Some hydrological factors in the environment of the station are the river Danube flowing about 2 km far and the karstic water in the mountain. The observed material does not show any connection with the water-level changes of the Danube, but a connection with the variation of the level of karstic water

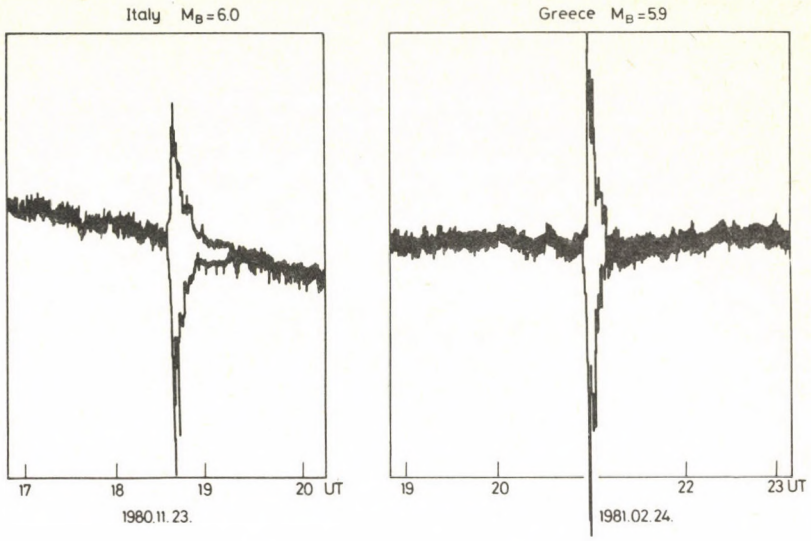

Fig. 6. Earthquakes on extensometer records

was found in several cases — since a systematic observation of the latter was initiated. Longer and intensive investigations are necessary to clear this connection, because it is a complicate one.

As already mentioned, extensometers have the favorable property that they enable to investigate geophysical phenomena of entirely different character and origin in a very large frequency range (rock-stresses, earthquakes, earth tides, crustal movements). Extensometers can be used as seismographs, too (Bisztricsány 1974). Two of the numerous earthquakes visible on the records are shown in Fig. 6.

The interpretation of earth tides observations with extensometer offers an interesting possibility inspite of the fact that calibration is less reliable than that of other earth tides recording instruments (e.g. recording gravimeters). The expectable difference from theoretical values is in case of gravimeters 20%, in case of horizontal pendulums 30–35%. In case of extensometers, however, even 20–100% differences from theoretical values were found in dependence of the geological situation of the station. In seismically active areas and in the zones of great movements along great tectonic fracture lines even greater differences occurred, e.g. at the station Sari-Pul in Central Asia the amplitudes of tidal waves surpassed the theoretical values by 200–300% (Latinina et al. 1978). A detailed analysis of these observations is presented in Table I.

When interpreting the results presented, it must be taken into consideration that they are based on a relative short observation series of only 106 days, but even here the five main tidal waves were unambiguously revealed. The Love number ratio h/l (Melchior 1978) determined from the amplitudes shows a good agreement with the h/l

Table I

Results of the harmonic analysis of observed data (The interpretation is based on the amplitudes of the waves O_1 and M_2)

Wave	Amplitude ($\times 10^{-9}$ relative)	Phase	$h/1$ (from measurements)	$h/1$ (from a theoretical Earth model)
Diurnal				
O_1	5.36 ± 0.36	$-1°.3 \pm 3°.8$	0.153	0.146
K_1	5.53 ± 0.33	$2°.6 \pm 3°.4$	0.130	0.183
Semi-diurnal				
N_2	0.55 ± 0.19	$8°.0 \pm 20°.3$	0.130	0.146
M_2	2.67 ± 0.17	$-10°.3 \pm 3°.7$	0.125	0.146
S_2	1.26 ± 0.16	$-16°.5 \pm 7°.1$	0.111	0.146

ratio received on the basis of the Gutenberg–Bullen earth model, but the data series is by far not long enough and the results — with expect of the wave K_1 — are also distorted by the ocean tide. The deviation of the h/l ratio of the wave K_1 indicates that the extensometer is not free of the effect of temperature (the period of K_1 is almost exactly 24 h) despite the fact that the extensometer in the cave is at a proper distance from the measurements of 0.1 °C accuracy no variations with daily periods were detected.

It should be further studied how great the area is where the results of the extensometer are valid. It is generally accepted that observations with extensometers are able to characterize the movements of a certain geological unit (Rikitake 1976). Extensometers are sensitive to the effects of the immediate environment, first of all to cavity and topographic effects — even if their sensitivity is less than that of horizontal pendulums. The amplitudes of tidal waves observed by extensometers show in certain geological environments changes in time (Latinina and Rizaeva 1976).

The small variations detectable with extensometers mean a third type of deformation besides those caused by seismology and earth tides. In our investigations the waves with periods shorter than one day were filtered out by an appropriate filter. The filtered data series is shown in Fig. 7 together with the meteorological and hydrological variations. The aperiodic component indicates a deformation being linear in time. With linear approximation and at reliability factor of 90%, the end points of the instrument got by 46 μm farther away from each other during 17 months, i.e. the horizontal component of the crustal movement is 0.03 mm/year.

A comparison by correlation between the yearly wave of temperature and the long period variation of the extensometer (dotted line in Fig. 7) gave with a reliability of 0.75 a thermal variation of 2 μm for a temperature change of 15 °C at the surface.

Concerning the possible instrumental causes of the aperiodic variations, a definitive statement could only be made if two extensometers were operated parallel at the observation station. At stations, however, where observations are run with two

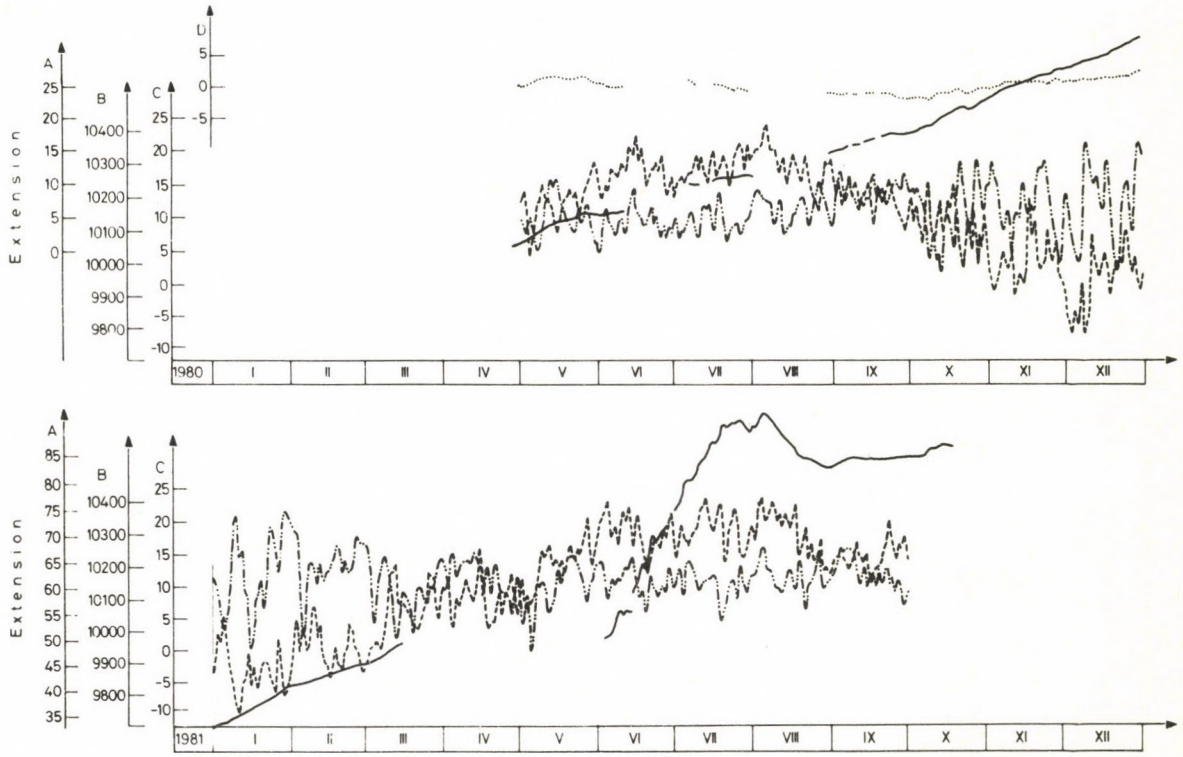

Fig. 7. Deformation variation in 1980–81. A ——— Displacement of the end point of the extensometer (μm); B– . .–. . air pressure (mbar); C – – – – – – – temperature (°C); D ..... extensometer residual (μm)

parallel instruments, aperiodic variations were found always similar to those observed in our station. Taking this similarity into consideration it is probable that the monotonous variation shown in Fig. 6 is of geological origin.

At several points of the Earth a similarly large, $1.5 \cdot 10^{-6}$/year extending movement has been observed. As example one can mention that $1.6 \cdot 10^{-6}$/year was found at the station Osakayma in Japan on the basis of a 20 years long observation series (Ozawa 1971) and the Soviet stations in Central-Asia are characterized by roughly similar data. The relative velocity was determined as $(0.2–0.25) \cdot 10^{-6}$/year from a 2 years long observation series in Protvino on the Russian platform (Latinina 1975). In our case, however, the data series is not long enough for an unambiguous characterization of the connection between the velocity of relative variations and the activity of tectonic movements.

References

Bisztricsány E 1974: Engineering seismology (in Hungarian).

Harrison J C 1976: Cavity and topographic effects in tilt and stain measurement. *J. Geophys. Res.*, 81, No. 2.

Jaskó S 1948: The Mátyáshegy cave (in Hungarian). MÁFI report on scientific sessions, No. 3.

Khalisev L E 1978: Secular and tidal deformations recorded in the fault zone of the northeastern Tien Shan. Proc. of the International Workshop on Monitoring Crustal Dynamics in Earthquakes Zones. Friedr. Vieweg & Sohn, Braunschweig/Wiesbaden.

Latinina L A 1975: On horizontal deformations at faults recorded by extensometers. *Tectonophysics*, 29.

Latinina L A, Rizaeva S D 1976: On tidal strain variations before earthquakes. *Tectonophysics*, 31.

Melchior P 1978: The tides of the planet Earth. Pergamon Press. Oxford, New York, Toronto, Sydney, Paris, Frankfurt.

Ozawa I 1971: Observations of the secular and annual changes of the crustal stains at Osakayama. Contrib. Geophys. Inst. Kyoto Univ., No. 11.

Rikitake T 1976: Earthquake prediction. Elsevier Scientific Publishing Company, Amsterdam–Oxford–New York.

Acta Geodaet., Geophys. et Montanist. Hung. Volume 19 (3–4), pp. 207–214 (1984)

TRANSFER FUNCTIONS OF DIGITAL TERRAIN MODEL INTERPOLATION METHODS

J Závoti[1]

[Manuscript received November 11, 1983]

The aim of this paper is to compare the interpolation methods of different orders. For this purpose transfer functions were determined theoretically for a number of different interpolation algorithms. Thus, the transfer functions of the stepwise-, linear-, second- order spline- and third order spline-interpolations were deduced.

Keywords: digital terrain model; interpolation; spline method; transfer function

Introduction

Some interpolation methods usable in case of one single variable are investigated in the paper. Interpolation methods can be well characterized by their transfer functions; the transfer functions give information about the effectivity of the different methods.

Since Fourier analysis is the means to investigate the accuracy of the digital terrain model, its concepts are used here for the discussion of the interpolation methods of the digital terrain model.

Mathematical basis of the interpolation

Stepwise interpolation

This interpolation method is applied especially in the solution of many numerical problems due to its simplicity.

The basic function, i.e. weight function of the stepwise interpolation is:

$$\varphi_0(t-i)=\begin{cases}1 & |t-i|<\frac{1}{2}\\ 0 & \text{else}.\end{cases} \tag{1}$$

Function $\varphi_0(t)$ is defined as a spline function of zero order.

[1] Geodetic and Geophysical Research Institute of the Hungarian Academy of Sciences, H-9401 Sopron, P.O.B. 5, Hungary

The following interpolation function:

$$f_0''(t) = \sum_{i=-\infty}^{\infty} f_i \varphi_0(t-i) \tag{2}$$

is ordered to the values $\{f_i\}_{i=-\infty}^{\infty}$ by this interpolation method.

The Fourier transform of the spline of 0th order can be determined from Eq. (2.1) in (Brigham 1974):

$$\Phi_0^i(f) = \int_{i+\frac{1}{2}}^{i+\frac{1}{2}} 1 e^{-j2\pi ft}\,dt = \frac{\sin \pi f}{\pi f} e^{-j2\pi fi}. \tag{3}$$

Using a feature of the Fourier transform (Brigham 1974, Eq. 3.1) one gets the transfer function of the spline-interpolation of 0th order as defined in Eq. (48) by Tempfli (1982):

$$F\left[\sum_{i=-\infty}^{\infty} f_i \varphi_0(t-i)\right] = \frac{\sin \pi f}{\pi f} \sum_{i=-\infty}^{\infty} f_i e^{-j2\pi fi} =$$

$$= \frac{\sin \pi f}{\pi f} F(f). \tag{4}$$

The transfer function $F_0(f) = \frac{\sin \pi f}{\pi f}$ of the spline-function of 0th order is presented in Fig. 1.

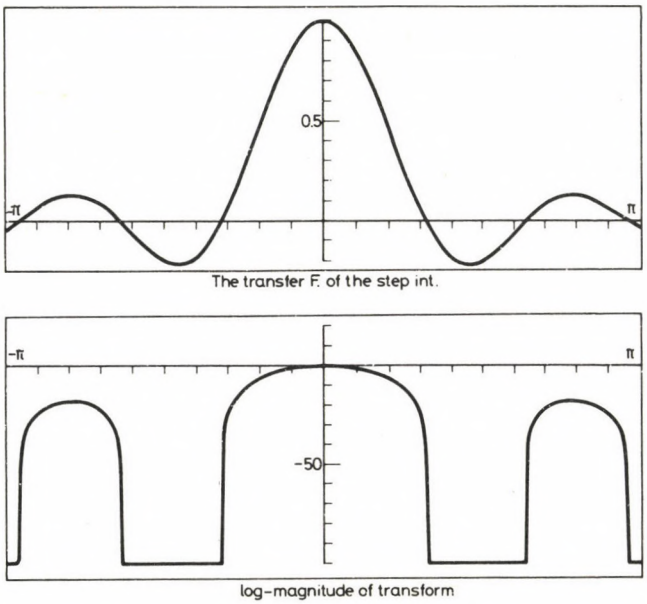

Fig. 1

Linear interpolation

Linear interpolation has a more advantageous characteristics than the stepwise interpolation.

The basis function or weight function of the linear interpolation is:

$$\varphi_1(t-i)=\begin{cases}1-|t-i| & |t-i|<1\\ 0 & \text{else}\end{cases}. \tag{5}$$

The function $\varphi_1(t)$ is defined as a spline-function of first order.

One gets the corresponding interpolation function by combining the basic functions:

$$f_1''(t)=\sum_{i=-\infty}^{\infty} f_i\varphi_1(t-i)\,. \tag{6}$$

Let us consider the convolution of the 0th order spline-functions defined in Brigham's Eq. (4.1) (1974)

$$\varphi_0(t-i)*\varphi_0(t-i)=\int_{-1}^{1}\varphi_0(t-i-\tau)\varphi_0(t-i)\,\mathrm{d}\tau=\varphi_1(t-i)\,. \tag{7}$$

On the basis of a property (Eq. 4.11 at Brigham 1974) of the Fourier transform, the transfer function of the linear interpolation can also be determined:

$$F\left[\sum_{i=-\infty}^{\infty} f_i\varphi_1(t-i)\right]=\left(\frac{\sin\pi f}{\pi f}\right)^2\sum_{i=-\infty}^{\infty} f_i e^{-j2\pi f i}=$$

$$=\left(\frac{\sin\pi f}{\pi f}\right)^2 F(f)\,. \tag{8}$$

The transfer function $F_1(f)=\left(\frac{\sin\pi f}{\pi f}\right)^2$ of the first order spline-interpolation is illustrated in Fig. 2.

Second-order spline-interpolation

The basis function of the spline-interpolation of second order will be defined recursively; it was shown that the basis function φ_1 of the first order spline-interpolation is the convolution of the basic function φ_0 of the zero order spline-interpolation with the function φ_0.

Be on the basis of the definition:

$$\varphi_2(t-i)=\varphi_1(t-i)*\varphi_0(t-i)\,. \tag{9}$$

Now one gets for the basic function of the second order spline-interpolation the following explicit expression:

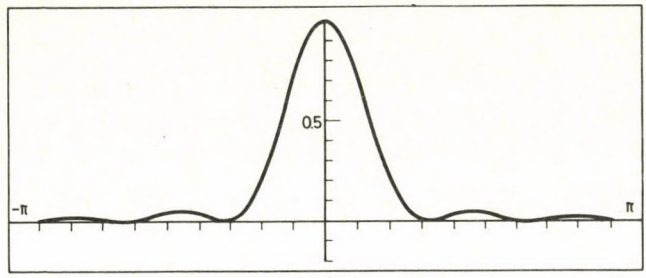

The transfer F. of the linear int.

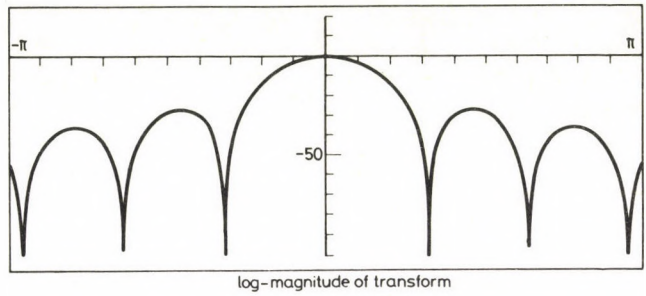

log-magnitude of transform

Fig. 2

$$\varphi_2(t-i)=\begin{cases}\dfrac{3}{4}-(t-i)^2 & |t-i|\le\dfrac{1}{2}\\[2ex] \dfrac{1}{2}\left(\dfrac{3}{2}-|t-i|\right)^2 & \dfrac{1}{2}\le|t-i|\le\dfrac{3}{2}\\[2ex] 0 & \text{else}\end{cases}. \tag{10}$$

The function φ_2 defined in this way does not satisfy the concept of the so-called sampling function ($\varphi_2(0)=1$, $\varphi_2(i)=0$ $i\neq 0$).

Thus, let us consider the following infinite series (Sünkel 1981):

$$\varphi_2'(t-i)=\sqrt{2}\sum_{k=-\infty}^{\infty}(-1)^k(\sqrt{2}-1)^{2|k|}\varphi_2(t-i-k). \tag{11}$$

The conditions for a sampling function are already satisfied for this function.

Hence, even in case of second order spline-interpolation, the interpolation function can be produced by the linear combination of the basic functions:

$$f_2''(t)=\sqrt{2}\sum_{i=-\infty}^{\infty}f_i\sum_{k=-\infty}^{\infty}(-1)^k(\sqrt{2}-1)^{2|k|}\varphi_2(t-i-k). \tag{12}$$

On the basis of the property (Eq. 4.11 at Brigham) of the Fourier transform the transfer function of the second order spline-interpolation can be derived as follows:

$$F\left[\sum_{i=-\infty}^{\infty} f_i\sqrt{2}\sum_{k=-\infty}^{\infty}(-1)^k(\sqrt{2}-1)^{2|k|}\varphi_2(t-i-k)\right]=$$

$$=F\left[\sqrt{2}\sum_{k=-\infty}^{\infty}(-1)^k(\sqrt{2}-1)^{2|k|}\varphi_2(t-i-k)\right]\sum_{i=-\infty}^{\infty}f_i e^{-j2\pi f i}=$$

$$=F\left[\sqrt{2}\sum_{k=-\infty}^{\infty}(-1)^k(\sqrt{2}-1)^{2|k|}\right]F[\varphi_2(t-i)]F(f)\,. \tag{13}$$

Since we got φ_2 as the convolution of φ_1 and φ_0, the connection $F'_2(f) = F_1(f)\cdot F_0(f)=\left(\frac{\sin \pi f}{\pi f}\right)^3$ is obvious.

Using the symmetry property of the Fourier series of the infinite series, the deduction can be continued:

$$=\sqrt{2}(1+2\sum_{k=1}^{\infty}(\sqrt{2}-1)^{2k}\cos 2\pi f k)\cdot F'_2(f)\cdot F(f)\,. \tag{14}$$

The infinite series can be written according to Demidovich (1974, Eq. 2967), in a closed form, too:

$$=\sqrt{2}\frac{1-(\sqrt{2}-1)^2}{1-2(\sqrt{2}-1)\cos 2\pi f+(\sqrt{2}-1)^4}\cdot F'_2(f)\cdot F(f)\,. \tag{15}$$

By means of identical transformations the following form is obtained:

$$=\frac{4}{3+\cos 2\pi f}\cdot F'_2(f)\cdot F(f)\,. \tag{16}$$

The transfer function $F_2(f)=\frac{4}{3+\cos 2\pi f}\cdot\left(\frac{\sin \pi f}{\pi f}\right)^3$ of the second order spline-interpolation is presented in Fig. 3.

Third order spline-interpolation

The basic function (1) will be convolved with basic function (9) and in sense of the recursion supposal we get the basic function φ_3 of the third order spline-interpolation:

$$\varphi_3(t-i)=\varphi_2(t-i)*\varphi_0(t-i)\,. \tag{17}$$

After expanding, function $\varphi_3(t-i)$ has the form:

$$\varphi_3(t-i)=\frac{1}{6}\begin{cases}3|t-i|^3-6(t-i)^2+4 & |t-i|\le 1\\ (2-|t-i|)^3 & 1\le|t-i|\le 2\\ 0 & \text{else}\,.\end{cases} \tag{18}$$

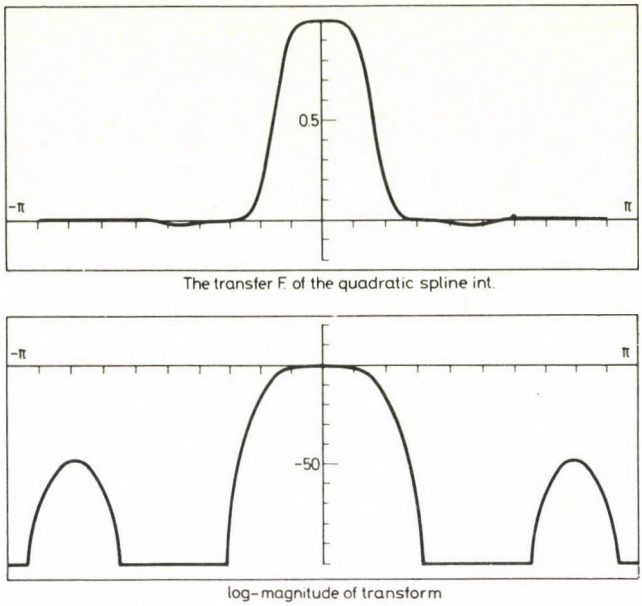

Fig. 3

Similarly to the second-order spline-interpolation third order sampling spline-functions will be introduced by means of the functions $\varphi_3(t-i)$. Be on the basis of Sünkel (1981):

$$\varphi'_3(t-i)=\sqrt{3}\sum_{k=-\infty}^{\infty}(-2+\sqrt{3})^{|k|}\cdot\varphi_3(t-i-k)\,. \tag{19}$$

Now one gets the third order spline-interpolation polynom by the linear combinations of the basic functions:

$$f''_3(t)=\sqrt{3}\sum_{i=-\infty}^{\infty}f_i\sum_{k=-\infty}^{\infty}(-2+\sqrt{3})^{|k|}\cdot\varphi_3(t-i-k)\,. \tag{20}$$

For the Fourier transform we get by a similar deduction as in the foregoing section:

$$F\left[\sqrt{3}\sum_{k=-\infty}^{\infty}(-2+\sqrt{3})^{|k|}\right]F[\varphi_3(t-i)]\cdot F(f)\,. \tag{21}$$

On the basis of the convolution theorem defined by Eq. (4.1) in Brigham (1974) the connection $F'_3(f)=F'_2(f)\cdot F_0(f)=\left(\dfrac{\sin\pi f}{\pi f}\right)^4$ is valid.

Again the expanded infinite Fourier series can be summed on the basis of Demidovich (1974, Eq. 2967) and one gets the following result:

$$\sqrt{3}\frac{1-(-2+\sqrt{3})^2}{1-2(-2+\sqrt{3})\cos 2\pi f+(-2+\sqrt{3})^2}\cdot F'_3(f)\cdot F(f)\,. \tag{22}$$

By means of identical transformations one gets the following expression:

$$=\frac{3}{2+\cos 2\pi f}\cdot F'_3(f)\cdot F(f)\,. \tag{23}$$

The transfer function $F_3(f)=\dfrac{3}{2+\cos 2\pi f}\cdot\left(\dfrac{\sin \pi f}{\pi f}\right)^4$ of the third order spline-interpolation is presented in Fig. 4.

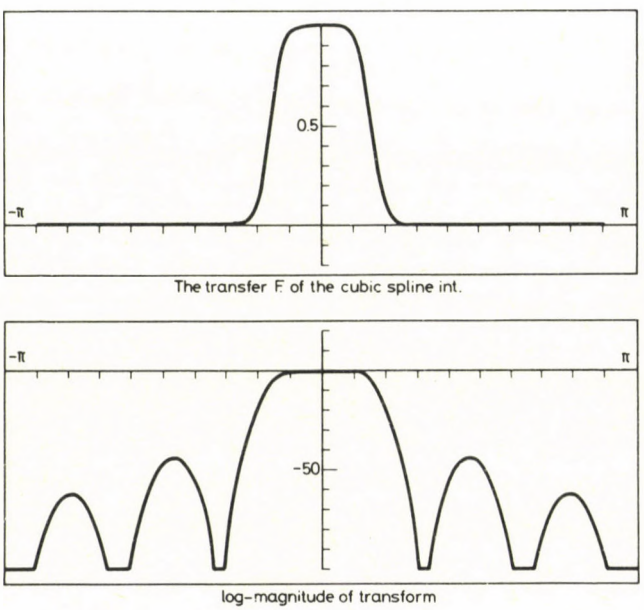

Fig. 4

This paper aims to show the advantageous features of the third order spline-interpolation by the deduction of the transfer functions of the interpolations of different orders. Advantages of the application of the third order spline-interpolàtion are also visible from the diagrams of the transfer functions.

References

Birgham E O 1974: The fast Fourier transform. Prentice-Hall, Inc. Englewood Cliffs, New Jersey

Demidovich B P 1974: Mathematical analysis. Tankönyvkiadó, Budapest

Sünkel H 1981: Cardinal interpolation. Reports of the Department of Geodetic Science, Report No. 312 Colombus, Ohio

Tempfli K 1982: Genauigkeitsschätzung digitaler Höhenmodelle mittels Spektralanalyse. *Geowissenschaftliche Mitteilungen*, Heft 22, Wien

Acta Geodaet., Geophys. et Montanist. Hung. Volume 19 (3–4), pp. 215–223 (1984)

DETECTION OF LOCAL HORIZONTAL MOVEMENTS OF THE EARTH'S SURFACE BY ERROR ELLIPSES

M VERŐ-HETÉNYI[1]

[Manuscript received December 12, 1983]

Two mathematical models of the adjustment of geodetic measurements for the detection of horizontal movements are described. All epochs are computed independently, but the form matrix is the same, which results in a reduction of the computational work. The significance of the displacements is determined by error ellipses of the points for each epoch, thus making an immediate comparison of any epoch possible. An experimental area in Hungary is used as test area for the method proposed.

Keywords: error ellipse; local horizontal movement; test area

If geodetic measurements are carried out in an industrial area with the aim to detect local movements, then measurements in horizontal and vertical sense are to be made repeatedly at geodetic points established in the area to be surveyed. Such measurements include generally direction and distance measurements in a network, further a network of height measurements (levelings).

In the present paper only mathematical models for the detection of horizontal movements shall be discussed.

Such network have to fulfil the following requirements:

1. Measurements should be at least twice repeated;
2. The plan for measurements should be the same in all epochs;
3. Due to the possibility of widespread movements, the lowest possible number of stable points should be supposed.

The last requirement means for the construction of the model that experiments are to be made to determine the possible lowest number of fixed parameters using which the system of normal equations does not become singular (that means also that a conventional adjustment is used here, and not a free one).

In the following two mathematical models will be described in which measurement results are adjusted independently in each epoch, and they are also independently interpreted.

[1] Geodetic and Geophysical Research Institute of the Hungarian Academy of Sciences, H-9401 Sopron, P.O.B. 5, Hungary

a) In the first case the correction equations (for sake of simplicity, referring to only two measurement epochs, with index *I* for the initial, and with index *II* for the repeating epoch):

$$\mathbf{v}^{\mathrm{I}} = \mathbf{A}\begin{pmatrix}\delta\mathbf{x}^{\mathrm{I}}\\ \delta\mathbf{y}^{\mathrm{I}}\end{pmatrix} + \mathbf{l}^{\mathrm{I}}. \tag{1}$$

The computation of the unknowns:

$$\begin{pmatrix}\delta\mathbf{x}^{\mathrm{I}}\\ \delta\mathbf{y}^{\mathrm{I}}\end{pmatrix} = (\mathbf{A}^{\mathrm{T}}\mathbf{P}\mathbf{A})^{-1}\mathbf{A}^{\mathrm{T}}\mathbf{P}\mathbf{l}^{\mathrm{I}}, \tag{2}$$

where the matrix of the reciprocal weights is the following:

$$(\mathbf{A}^{\mathrm{T}}\mathbf{P}\mathbf{A})^{-1} = \mathbf{N}^{-1} = \mathbf{Q}^{\mathrm{I}}_{x,y}. \tag{3}$$

The initial approximate coordinates are corrected by the coordinate changes computed for the first interval. In that sense one has:

$$\begin{aligned} x_i^{\mathrm{I}} &= x_i^0 + \delta x_i^{\mathrm{I}} \\ y_i^{\mathrm{I}} &= y_i^0 + \delta y_i^{\mathrm{I}}. \end{aligned} \tag{4}$$

When adjusting the repeat measurements, the coordinates of the points after the adjustment of the first measurement series can be used as approximate coordinates.

Thus the correction equations are in the repeat epoch:

$$\mathbf{v}^{\mathrm{II}} = \mathbf{A}'\begin{pmatrix}\delta\mathbf{x}^{\mathrm{II}}\\ \delta\mathbf{y}^{\mathrm{II}}\end{pmatrix} + \mathbf{l}^{\mathrm{II}}, \tag{1a}$$

and the unknowns:

$$\begin{pmatrix}\delta\mathbf{x}^{\mathrm{II}}\\ \delta\mathbf{y}^{\mathrm{II}}\end{pmatrix} = (\mathbf{A}'^{\mathrm{T}}\mathbf{P}\mathbf{A}')^{-1}\mathbf{A}'^{\mathrm{T}}\mathbf{P}\mathbf{l}^{\mathrm{II}} \tag{2a}$$

($A' \neq A$, as though the coordinates of the basic points are the same, the approximate coordinates differ from each other).

The matrix of the reciprocal weights:

$$(\mathbf{A}'^{\mathrm{T}}\mathbf{P}\mathbf{A}')^{-1} = \mathbf{N}'^{-1} = \mathbf{Q}^{\mathrm{II}}_{x,y}. \tag{3a}$$

In this epoch the coordinates are the following:

$$\begin{aligned} x_i^{\mathrm{II}} &= x_i^{\mathrm{I}} + \delta x_i^{\mathrm{II}} \\ y_i^{\mathrm{II}} &= y_i^{\mathrm{I}} + \delta y_i^{\mathrm{II}}. \end{aligned} \tag{4a}$$

b) In the second case the approximate coordinates of the initial epoch are used throughout the whole measurement series as approximate coordinates, as measurement results are referred to the first measurement's epoch. This second model will be

treated in more details, as this is the basis for the common adjustment of many measurement epochs.

In the second case the matrix of the correction equations is the following in the initial epoch:

$$\mathbf{v}^{\mathrm{I}} = \mathbf{A}\begin{pmatrix}\delta\mathbf{x}^{\mathrm{I}}\\ \delta\mathbf{y}^{\mathrm{I}}\end{pmatrix} + \mathbf{l}^{\mathrm{I}}. \tag{5}$$

This is the same as Eq. (1) for the first case, but it is also identical with the matrix of the following Eqs (2) and (3), too.

Naturally the computed coordinates

$$\begin{aligned} x_i^{\mathrm{I}} &= x_i^0 + \delta x_i^{\mathrm{I}} \\ y_i^{\mathrm{I}} &= y_i^0 + \delta y_i^{\mathrm{I}} \end{aligned} \tag{6}$$

are also identical with Eq. (4) for the first epoch. The matrix of the correction equations in the repeat epoch is the following:

$$\mathbf{v}^{\mathrm{II}} = \mathbf{A}\begin{pmatrix}\delta\mathbf{x}^{\mathrm{II}}\\ \delta\mathbf{y}^{\mathrm{II}}\end{pmatrix} + \mathbf{l}^{\mathrm{II}}. \tag{7}$$

As it can be seen, the form matrix **A** is identical with the form matrix of the initial epoch, the free term $\mathbf{l}^{\mathrm{II}}$ naturally differs from the same term in the first epoch.

The unknowns can be computed from the following equations:

$$\begin{pmatrix}\delta\mathbf{x}^{\mathrm{II}}\\ \delta\mathbf{y}^{\mathrm{II}}\end{pmatrix} = (\mathbf{A}^{\mathrm{T}}\mathbf{P}\mathbf{A})^{-1}\mathbf{A}^{\mathrm{T}}\mathbf{P}\mathbf{l}^{\mathrm{II}}. \tag{8}$$

The matrix of the reciprocal weights is:

$$(\mathbf{A}^{\mathrm{T}}\mathbf{P}\mathbf{A})^{-1} = \mathbf{N}^{-1} = \mathbf{Q}^{\mathrm{II}}_{x,y}. \tag{9}$$

That means that the matrix of reciprocal weights is in this case identical with the weight reciprocal matrix in the first epoch,

$$\mathbf{Q}^{\mathrm{I}}_{x,y} = \mathbf{Q}^{\mathrm{II}}_{x,y}.$$

The Geodetic and Geophysical Research Institute of the Hungarian Academy of Sciences has a test area where measurements are repeatedly carried out for the detection of horizontal movements.

The following experiments were made with this test area (Fig. 1). The net included 35 geodetic points. When the measurements were made, care was taken that all points could be determined at least from an other point as polar points. The connection of points determinable from at least two points was made by precise trilateration (distance) polygons. If in a traverse three or more sides met in a point, then this point was considered as a nodal point. Using such measurements the preliminary

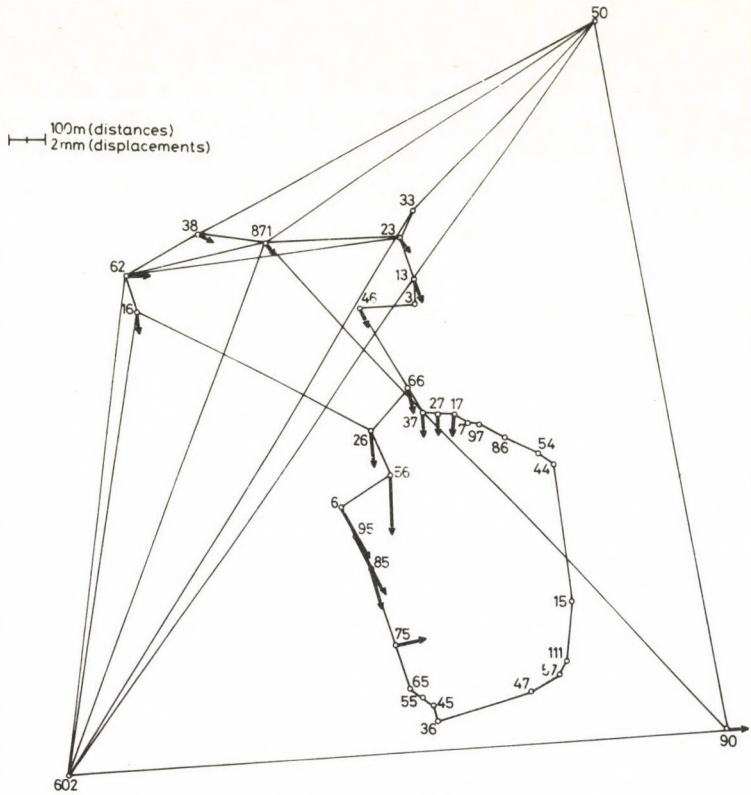

Fig. 1. The test network and the computed displacements

coordinates of all points, could be determined including both points without horizontal movements and new points (where movements were supposed). The correction equations for the direction and distance measurements from both new and given points, further the linearization of these equations are supposed to be known. The linear equations of the direction measurements are after the expanding into a series:

$$L_{ij}+v_{ij}=-\delta z_i+a_{ij}\delta x_i-b_{ij}\delta y_i-a_{ij}\delta x_j+b_{ij}\delta y_j\,, \tag{10}$$

where L_{ij} means the contradictions of free terms:

$$L_{ij}=l_{ij}-\alpha_{ij}^c+z_i^c\,, \tag{11}$$

the coefficients of the coordinate changes are the following:

$$a_{ij}=\frac{\partial\alpha_{ij}}{\partial x_i}\,; \qquad b_{ij}=\frac{\partial\alpha_{ij}}{\partial y_i}\,.$$

As according to requirement 3 the lowest possible number of movement-free points should be used, the majority of the first part of the correction equations are equations of direction measurements between two new points Eq. (10), where the unknowns are the coordinates i and j.

The correction equations for the point 50, lying further away from the area of movements and having given coordinates are the following (in this case point i has known, point j unknown coordinates): (see also Fig. 1):

$$L_{ij}+v_{ij}=-\delta z_i-a_{ij}\delta x_j+b_{ij}\delta y_j\,. \tag{10a}$$

By this point 50 which is supposed to be stable, the position of the net is also fixed. As the direction of points 50 and 602 has also been fixed, the orientation of the net became also unambiguous.

In connection with the direction supposed to be errorfree, a condition is to be introduced. As it is known, z_a is the average of the orientation angles measured in point i, with weights corresponding to a weighted average with the distances as weights.

E.g. in case of three measured directions:

$$z_{\text{average}}=\frac{z_1 s_1+z_2 s_2+z_3 s_3}{s_1+s_2+s_3}\,, \tag{12}$$

with the averages determined so, the free terms can be determined:

$$l_1=z_a-z_1$$

$$l_2=z_a-z_2$$

$$l_3=z_a-z_3\,.$$

When interpreting the direction measurements made from point 50 of given coordinates, the value z_{average} has not been computed, instead of that the value $z_{(50-602)}$ was used as reference of the measured directions, and the free terms have been computed:

$$z_{(50-602)}=\alpha^c_{(50-602)}-\alpha^m_{(50-602)}$$

$$l_1=z_{(50-602)}-z_1$$

$$l_2=z_{(50-602)}-z_2$$

$$l_3=z_{(50-602)}-z_3\,. \tag{13}$$

The second part of the adjustment consisted of correction equations based on distance measurements.

The linearized correction equations are the following:

$$L_{ij}+v_{ij}=-s_{ij}\chi-c_{ij}\delta x_i-d_{ij}\delta y_i+c_{ij}\delta x_j+d_{ij}\delta y_j\,. \tag{14}$$

Here also prevail correction equations between two unknown points.

If one of the end points is the known point 50, then one gets:

$$L_{ij}+v_{ij}=-s_{ij}\chi+c_{ij}\delta x_j+d_{ij}\delta y_j\,. \tag{14a}$$

(In Eqs (14) and (14*a*) χ is an instrumental correction depending on the distance.) In the two measurement epochs correction equations based on Eqs (10), (10*a*), (14) and (14*a*) include 103 unknowns; there are 113 such equations. Having solved this system of equations, the interpretation could be commenced. The low number of superfluous measurements is due to the very rough topography and the covered area. Figure 1 shows that the line 66-37-27-17-7-97-86-54-44-15-111-57-47-36-45-55-65-75-85-95-6-56-26 could be measured only with the lowest possible number of measurements between any of the points.

After the adjustment, one had the following unknowns:

$$\delta x^{\mathrm{I}}\,,\ \delta y^{\mathrm{I}}\,,\ \delta z^{\mathrm{I}}\,,$$

and

$$\delta x^{\mathrm{II}}\,,\ \delta y^{\mathrm{II}}\,,\ \delta z^{\mathrm{II}}\,.$$

The approximate coordinates which were the same in both adjustments have been changed by these values.

The question to be answered is now, if differences between the coordinates in the two epochs are significant or not, i.e. they are due to horizontal movements of the points or due to random errors?

Error ellipses have been determined for both ends of the "displacement vector", and these ellipses were used for subsequent conclusions. (Figure 1 does not contain the ellipses, some of them are presented on separate figures, as illustrative examples.)

Figure 2 shows the error ellipses for point 95 in two measurement epochs. The vector connecting the two centres, i.e. the displacement vector is very great in respect of the error ellipses. The rigorous method would be the determination of relative error ellipses. The simplified method presented here can be used for quick comparison. The mean square error is approximated by the following equation:

$$\sigma=\frac{\Delta}{\sigma_\Delta}\,, \tag{15}$$

where:

Δ = the length of the displacement vector (the distance between the centres of the two ellipses)

$\sigma_\Delta=\sqrt{\sigma_{\mathrm{I}}^2+\sigma_{\mathrm{II}}^2}$ where σ_{I} is the distance between the centre of the error ellipse and the periphery of the ellipse in direction of the displacement vector in the first measurement epoch; and σ_{II} is the distance between the centre of the error ellipse and the periphery of the ellipse in direction of the displacement vector in the second measurement epoch.

The probability of a quotient happening to be greater than that in Eq. (15) can be found in a table of the normal distribution (Detrekői 1974) (i.e. supposing random

errors). This value gives the significance level of a displacement. This level is in the present case-for point 95 99.98 percent, thus the displacement is highly significant.

In case of point 55 (Fig. 3) no significant displacement can be observed, as the level of significance is below 80 percent. This can be already surmised from Fig. 3, as the two error ellipses intersect each other quite strongly. A similar situation was found for point 44 (Fig. 4).

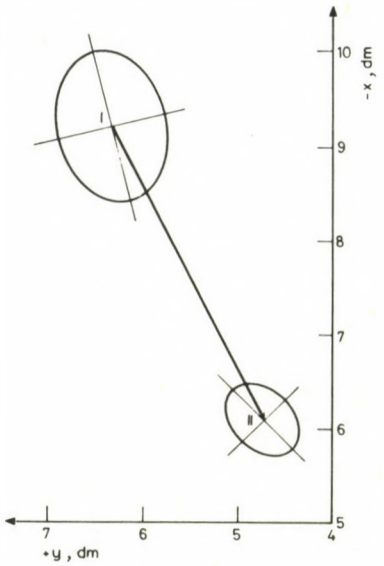

Fig. 2. Error ellipses and displacement in point 95

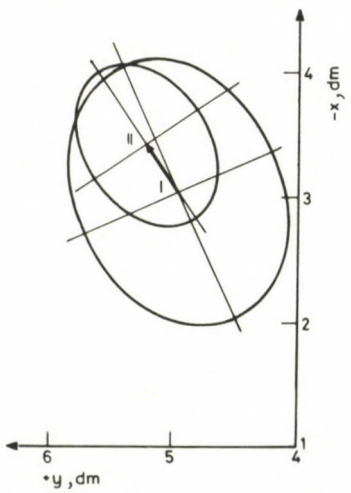

Fig. 3. Error ellipses and displacement in point 55

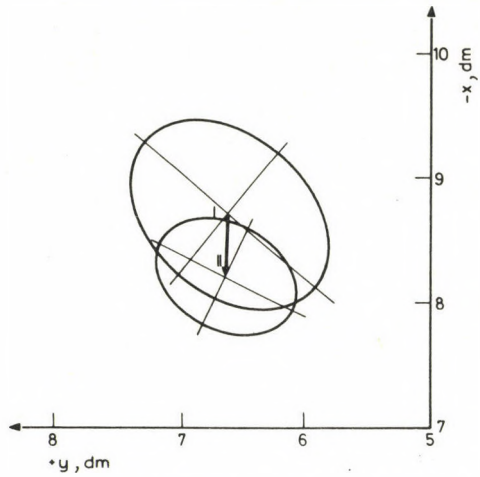

Fig. 4. Error ellipses and displacement in point 44

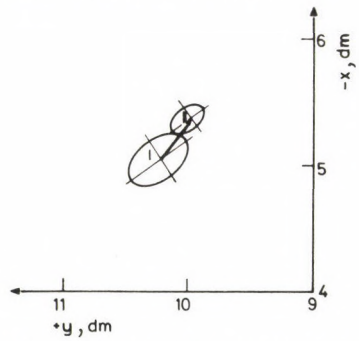

Fig. 5. Error ellipses and displacement in point 33

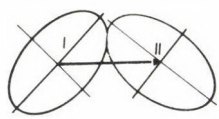

Fig. 6. Sketch of the error ellipses and the displacement in a point, where the approximation used in this paper is not valid

The error ellipses of point 33 (Fig. 5) just touch each other. The level of significance for a movement is here 80 percent, thus the displacement is not proven.

The rigorous method would consist in a determination of the relative error ellipse of the displacement vector from the error ellipses of the two end points (V Hetényi 1972, 1983), and the significance of the displacement vector could be deduced then from this ellipse. The proposed simple method yields with the exception of some extreme cases, as shown e. g. in Fig. 6, quite reliable results.

Such an analysis has been made for all points, and the significance of the displacement determined for all points. The vectors represented in Fig. 1 show that highest significance levels occur in points 85, 95, 6, 56, 26, where it is well above 96 percent.

An advantage of the method is that the interpretation can be continued for any following epoch, and error ellipses in the third, fourth.. epoch can be compared to the first or to second one. The displacement vector and error ellipses yield directly the probability level for a movement between any two epochs, not only for consecutive ones. This can be rigorously carried out as the plan for determination of the points, and therefore the form matrix **A** were the same in each epoch. This means less computational work, further error ellipses increase in dimensions when getting farther away from the point with given (fixed) coordinates (V Heténvi 1973). As these points are the same in all measurement epochs, thus the error ellipses of the points increase and decrease in the same manner, thus a comparison is reliable. The most serious setback of the present method could be that the displacements increase with time so strongly, that the linearization is no more allowed; in such cases the application of the first suggested method (Eqs 1—4a) solves the problem, but in such cases the computational work is greater.

Acknowledgement

I should like to thank here my colleague J Kalmár, who carried out the computations in connection with the adjustment on the HP—1000 E computer of the Institute.

References

Detrekői Á 1974: Kiegyenlítő számítások (Adjustment computations). Tankönyvkiadó, Budapest

V Heténvi M 1972: A hálózati relatív hibaellipszisek számítása (Computation of the relative error ellipses in a network). *Geodézia és Kartográfia*, 24, 344—348.

V Heténvi M 1973: Önálló háromszoghálózatok kiegyenlítéséről (On the adjustment of independent networks). *Geodézia és Kartográfia*, 25, 248—253.

V Heténvi M 1983: Detection of horizontal movements by relative error ellipses. In: *Scient. Bull. of the Stanislaw Staszic Univ. of Mining and Metallurgy No.* 949 *Geodesy b.* 79. *Cracow 1983*, 145—148.

Acta Geodaet., Geophys. et Montanist. Hung. Volume 19 (3–4), pp. 225–233 (1984)

A NEW APPARATUS FOR TESTING BUBBLE VIALS, ELECTRONIC LEVELS AND AUTOMATIC LEVELS

J SOMOGYI[1], K KRAUSZ[1], GY MENTES[1]

[Manuscript received December 28, 1983]

In spite of the appearance of new measurement methods in geodetic survey, the importance of the bubble level did not decrease. The increase of the accuracy is one of the most important tasks of geodetic research. In this connection, the reliability of the testing of high-precision bubble levels must be also increased. This purpose is served by an apparatus for testing bubble vials which fulfils up-to-date demands. The smallest measurable rotation angle is 0.1 second of arc, the smallest measurable displacement 0.01 mm. Measurement results can be interfaced directly to computers. In addition to test of instrument levels, it can be also used for the calibration of tiltmeters and for the control of automatic leveling instruments.

Keywords: automatic levels; bubble vials; electronic levels; testing of leveling instruments; tiltmeter

The technical development of the last decades gave impetus also to the development of surveying instruments. The continuous spread of electro-optical distance-meters, laser techniques and computerization have increased the accuracy of geodetic measurements and computations. The geodetic application of artificial satellites resulted in significant improvements from the point of view of both instrumental and measurement techniques. In spite of all these changes the role and importance of classical geodetic measuring devices, such as bubble vials and various levels did not decrease.

In order to ensure the necessary accuracy, high-precision bubble vials, leveling instruments and electronic levels should be tested from time to time. For testing bubble vials investigations have been started at the Geodetic and Geophysical Research Institute of the Hungarian Academy of Sciences in 1953. Together with some measurement and computational methods, several types of bubble triers have also been produced Tárczy-Hornoch (1961a, 1961b), Tárczy-Hornoch et al. (1972).

An important task of geodetic researches is to increase the accuracy. Several significant results have been achieved in this field leading to an increase of the role of geodesy in geosciences (e.g. determination of geometric and physical parameters

[1] Geodetic and Geophysical Research Institute of the Hungarian Academy of Sciences, H-9401 Sopron, P.O.B. 5, Hungary

needed for geodynamical investigations). That means that the accuracy of astrogeodetic measurements and high precision leveling must be also increased. A part of this task is a more correct qualification of different levels and leveling instruments. For this purpose a new level trier (tiltmeter) has been constructed in our Institute taking into account earlier experiences.

The main aspects of the construction of this new apparatus were the following Somogyi and Mentes (1978):

1) more accurate measurement of the tilt angle,
2) more accurate measurement of the bubble movement,
3) electronic sensing and digital display of the measured values,
4) on-line connection to the computer
5) decrease of the effect of outer disturbances during measurements and comfortable handling.

The level trier enables the step-by-step control of tilt-in or free bubbles of any accuracy, of electronic levels, of automatic levels or any other kind of tilt meters, its main aim is, however, the control of high-precision levels needed in astrogeodetic measurements. In order to ensure a high precision, the tilt of the level trier is measured by a capacitive transducer, the displacements of the bubble by the movement of an optical system of changeable base using a measuring screw. Both values can be digitally

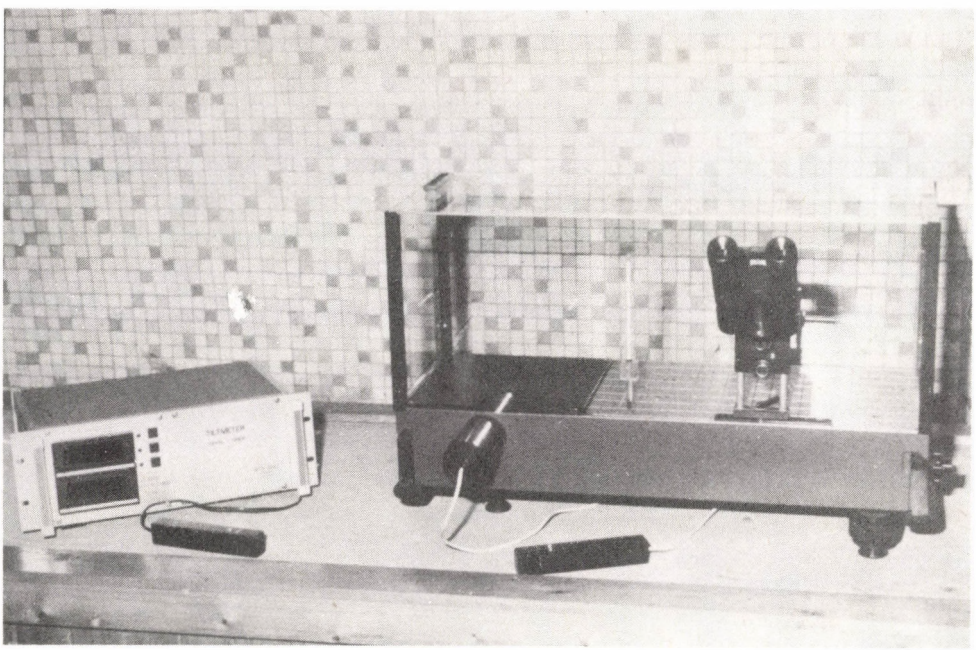

Fig. 1

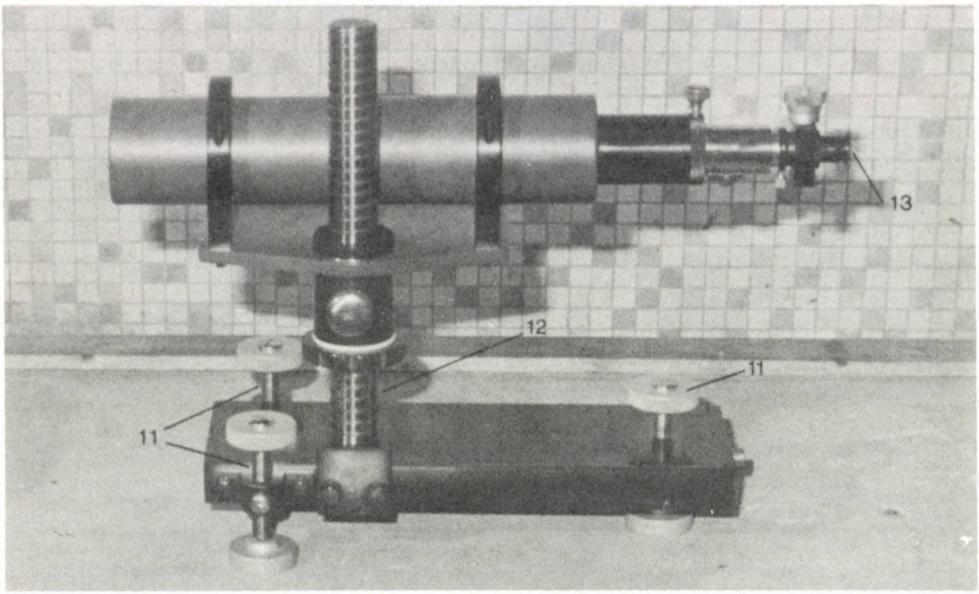

Fig. 2

displayed. The smallest rotation angle measurable by the transducer is 0.1 second of arc, the smallest measurable displacement of the bubble is 0.01 mm.

In order to eliminate the effect of the heat radiated from the observer, the upper part of the level trier is covered by a plastic box. This means that outer temperature changes can disturb less the level during the measurements. The comfort of the measurement is ensured by a suitable observing facility.

The main units of the whole apparatus are:

1. the level trier (tiltmeter) (Fig. 1)
2. the electronic unit (Fig. 1)
3. the measuring collimator (Fig. 2).

The tiltmeter consists of two parts (Fig. 3):

a) fixed unit

b) moving unit.

The basis of the fixed part is the basic frame (1) of the instrument. It is supported by a fixed foot (2) and by two foot screws (3). The following units are connected to the basic frame: the horizontal rotation axis, the fixed part of the capacitive transducer and the carriage of the optical system with the incremental angular encoder, are settled inside, outside one can see the measuring screw (4) which follows the movements of the level and the lifting unit (5) which can be connected to a remote control unit (Fig. 1).

The moving unit of the instrument consists of the tiltable rigid plate (6) for the setting of the level to be controlled (different level holders can be mounted on it) (see 7 in

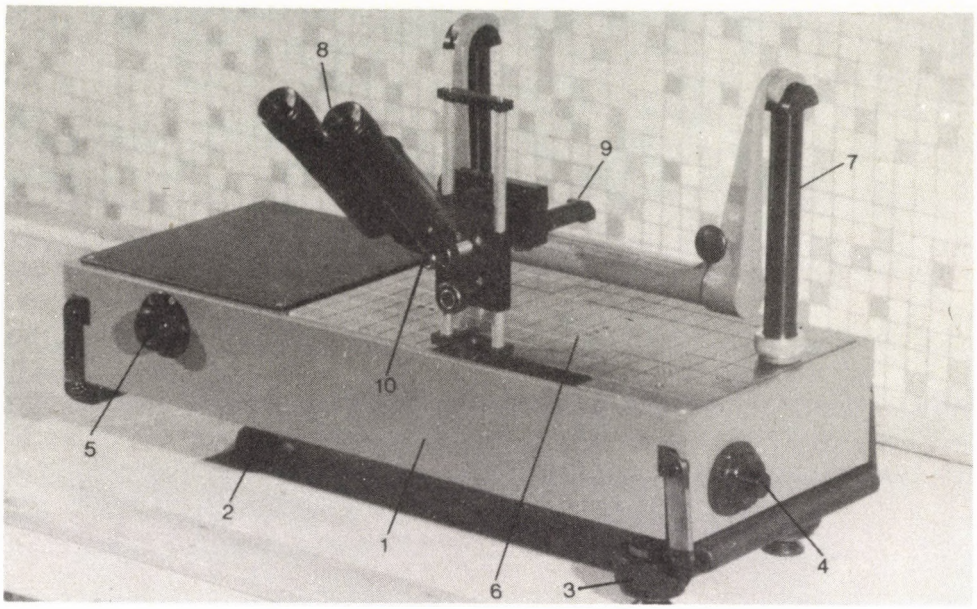

Fig. 3

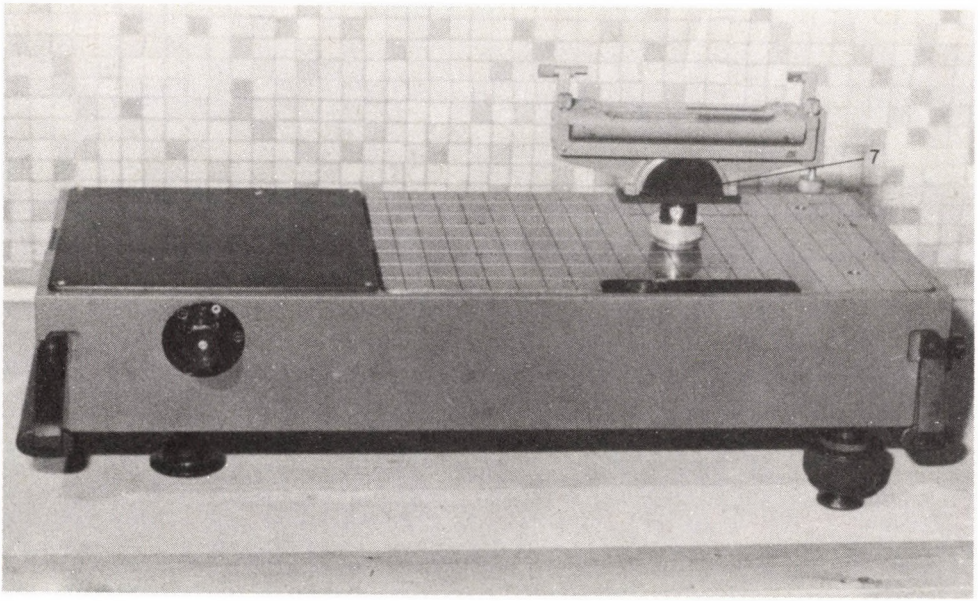

Fig. 4

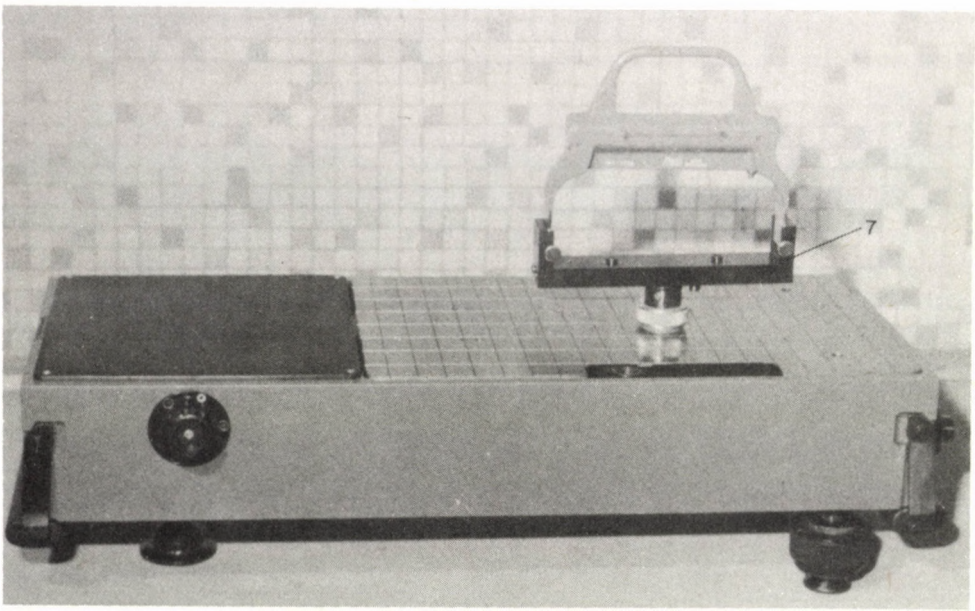

Fig. 5

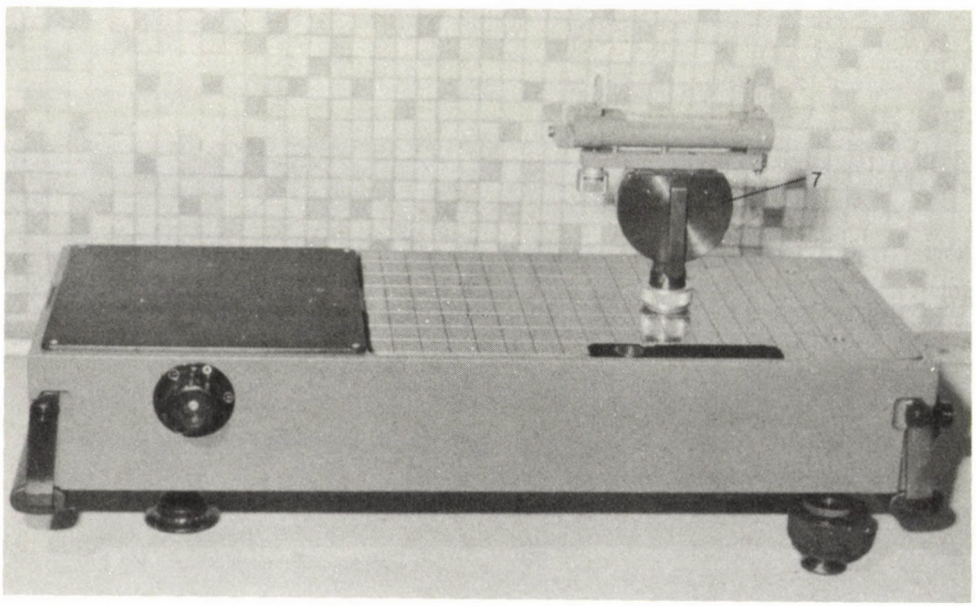

Fig. 6

Figs 3, 4, 5, 6), and of the movable optical system (8). The pins (9) of the optical system can be brought to a distance corresponding to the actual bubble length by the base-length setting screw (10).

Operation of the electronic unit of the level trier:

The electronic construction of the tiltmeter is presented in Fig. 7. The changes of the tilt are transformed by a capacitive transducer into electronic signals.

The device consists of a differential condenser where the area of the opposite surfaces changes due to an angular rotation. Using this method the transducer has linear characteristics in a wide range. The capacitive transducer in the bridge-circuit is supplied by an oscillator of high amplitude stability in order to reach a high precision of the measurements. The output signal of the bridge is amplified to the necessary level by a carrier frequency amplifier. The amplification can be digitally programmed in three steps using the pushbutton GAIN, thus three different angular ranges or sensitivity steps can be obtained. The output signal of the amplifier is transformed into digital signals by an A/D converter and it reaches the bus of the built-in microprocessor through a parallel interface.

In the most sensitive range, tilts between $+20$ and -20 seconds of arc can be measured. The error of a measurement is ± 0.3 seconds of arc. This range is used for the control of high precision levels. The other two ranges have scale values set according to the demands of the user. By increasing the measurement range, the resolution power and the accuracy of the angular measurement decrease, too. In case of the control of

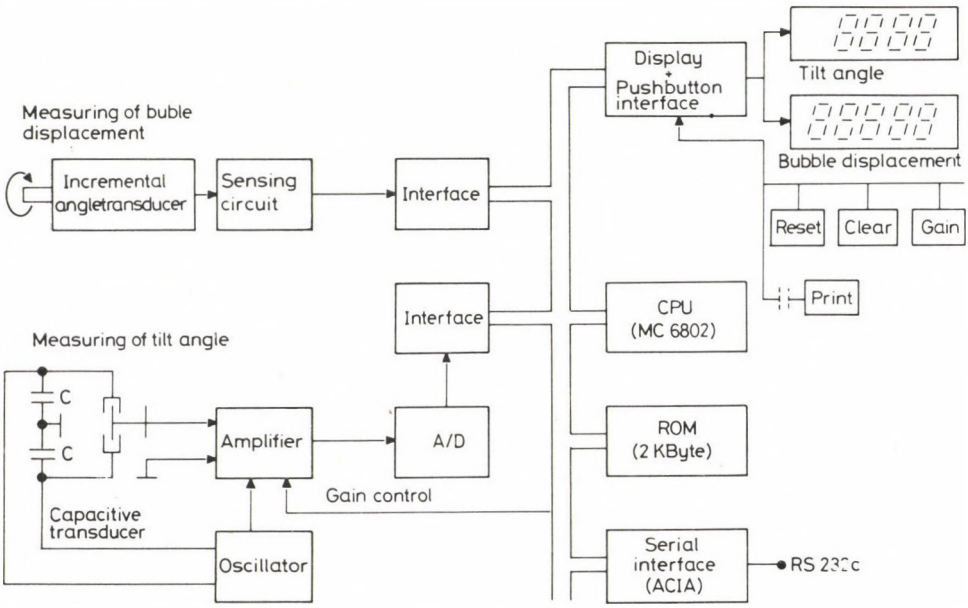

Fig. 7

conventional levels, the rotation of the moving screw of the microscope which follows the movements of the bubble is felt by an incremental angular encoder. The two out-of-phase signals of the angular encoder are processed by the microprocessor using the corresponding software.

The resolution in the display of the bubble movements is 0.01 mm, the measurement range is 120 mm.

The display of the tilt and of the bubble movement is carried out continuously. If the pushbutton PRINT is pressed, then the built-in microprocessor yields output data about corresponding tilts and bubble positions by the serial RS232 C interface. Thus they can be directly fed into a computer or to a printer, and the characteristic curve of the level can be automatically drawn.

The transfer rate of the serial interface lies between 75 bits/s and 9600 bits/s.

The use of the tiltmeter is supported by the remote control of the lifting unit. In certain cases its use is unavoidable (collimator measurements). Lifting and lowering can be made with two different speeds, thus arbitrarily small angles can be set.

The measuring collimator is used for testing automatic leveling instruments. The collimator can be set up in a stable position using the big foot screws (1) (see Fig. 2). The adjustment of the collimator tube in elevation can be carried out by the setting screw (2) on the vertical supporting column. The eye-piece micrometer of the collimator (3) is interchangeable. The presently used eye-piece micrometer is a product of the firm Jenoptik and has divisions of 0.01 mm and the measuring range is 8 mm. The complete error of pointing and reading is obtained if the vertical or horizontal wire of the tested instrument is several times made to be flanked by the double wire of the eye-piece micrometer of the collimator and the standard error of this measurement series is computed. Its *a priori* value is about 0.3 seconds of arc. In order to increase the reading accuracy, the measuring screw should be read through a hole diaphragm to avoid parallax.

As it has been told, the level trier can be used for different tasks but its main aim is the control of high precision levels. This measurement is made as follows. The level to be controlled is set on the basis frame and one of the extremal pars-divisions is brought into coincidence with the end of the bubble. In the observing system one sees the bubble ends in coincidence and they touch the initial division. The fixed rotation value chosen for the incremental measurement is set on the raising unit, its value appears on the display. One lets the bubble ends once more to coincidence with the aid of the measuring screw and the bubble displacement due to the tilt change can now be measured. Its value appears also on the display. The chosen angular value can be set again on the raising unit and the operations are repeated till the bubble reaches the far end of the divisions.

In order to test the stability and measuring accuracy of the instrument, a lot of different investigations were carried out. The results of these investigations comply with the specified requirements.

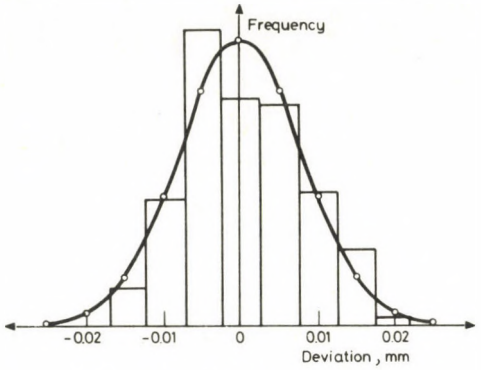

Fig. 8

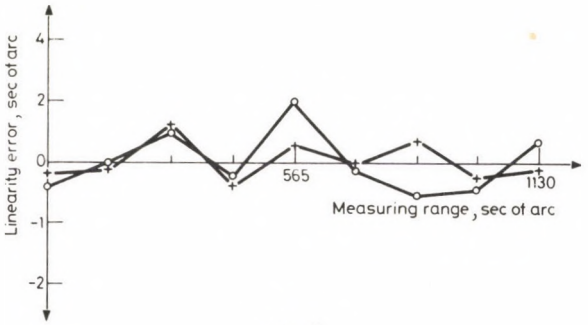

Fig. 9

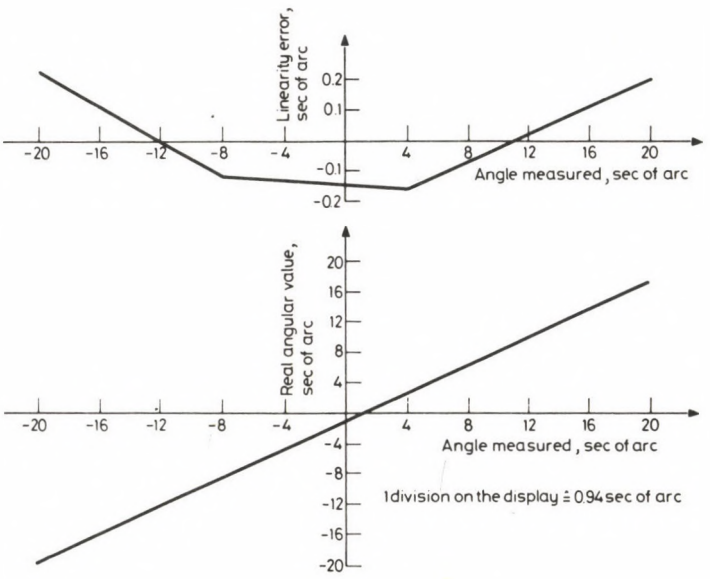

Fig. 10

The accuracy of the observations has been determined by the bubble of a Horrebow-level belonging to a Wild T4 instrument. In order to exclude environmental effects, short measurement series consisting of 10 measurements each were carried out with nine repetitions. The observation accuracy of the bubble lies between ± 0.005 and 0.013 mm; on the basis of 90 measurements, the expected error is ± 0.008 mm (Fig. 8).

The linearity of the collimator has been controlled by a Wild T3 theodolite. The images of the centres of the wire crosses have been brought into coincidence, then the measuring eye-piece of the collimator has been set at 1.00 mm. The angular values belonging to different positions of the measuring eye-piece have been read on the theodolite (Fig. 9).

The bottom part of Fig. 10 shows the characteristics of the level trier in the range between $+20$ and -20 seconds of arc. The tangent of the first order regression line gives the calibration constant of the level trier, being in the present case 0.94 seconds of arc for one unit displayed. Top of Fig. 10 shows the deviations of the actual characteristics from the regression line with a greater scale, i.e. the linearity errors belonging to points of the measuring range.

References

Somogyi J, Mentes Gy 1978: A new apparatus for testing bubble vials. *Bulletin Géodésique*, 52, 223—227.

Tárczy-Hornoch A 1961*a*: Ein neuer automatischer Libellenprüfer für Sekundenlibellen. *Geofisica Pura e Applicata*, 48, 27—34.

Tárczy-Hornoch A 1961*b*: Über einen halbautomatischen Libellenprüfer für Libellen mittlerer Genauigkeit. *ÖZfV*, 49, 65—73.

Tárczy-Hornoch A, Alpár Gy, Bummer A 1972: Bubble level testing with a fully automatic level trier. *MOM Review* 4, 3—7.

Acta Geodaet., Geophys. et Montanist. Hung. Volume 19 (3–4), pp. 235–248 (1984)

SOME REMARKS TO THE NOTION OF UNCERTAINTY

L CSERNYÁK[1] and F STEINER[2]

[Manuscript received May 21, 1982]

Numerical characterization possibilities of the uncertainty of a physical quantity are dealt with in the present paper mainly from a practical point of view. It is desirable that the values characterizing the uncertainty should be finite for any class of distributions. Among the often used values, however, not only the scatter, but also the entropy can be infinite for whole classes of distributions.

The measures of the uncertainty for a single measurement are to be treated separately from those for the estimates calculated from samples with a high number of elements (see the Table). In latter case the uncertainty changes of course with the method used for estimation: (for symmetrical distributions) it is $1/[2f(0)]$, if medians are used; it is $\varepsilon/\sqrt{n(\varepsilon)}$, if the most frequent value of certain data is calculated, and is the scatter (σ) of $f(x)$, if averages are computed (according to the least squares method). Therefore, the relation of uncertainty well known in the theory of the Fourier transforms (and having generally known physical consequences, too) is bound to a given method of estimation—which even is not applicable in general—and further it does not describe the connection of primary distribution-pairs (of parent distributions).

Keywords: entropy; most frequent value; scatter; uncertainty

1. If measurements made on a certain quantity yield always the same result x_0, then this quantity if fully determined from one cause or more; in such cases it is superfluous to use probability theory or mathematical-statistical methods. It is naturally possible to speak even in such cases from a distribution having a density function in form of a Dirac- δ, i.e. a so-called causal distribution, as it is made e.g. by Korn and Korn (1961).

If certain data are found to have a "causal distribution", it is not necessary to suppose in them "infinitely exact" measurements of an absolutely stable quantity. Let us use e.g. a digital voltmeter, where the last digit means 100 V-s. The voltage in a power network oscillating around 220 V (supposing that black-out intervals are excluded, i.e. no measurements are made in such intervals) will always be read as exactly 200 V, and the data will have a causal distribution.

In this somewhat paradox example the very low accuracy of the measurements produced the causal distribution of the measured data. Thus, this can be interpreted as

[1] School of Finances and Public Accountances Budapest, Buzogány u. 10/12 H-1149, Hungary
[2] University for Heavy Industry, Miskolc-Egyetemváros H-3515, Hungary

an admonition that even those quantities can be qualified as exactly determined ones where a certain range of statistical oscillation, i.e. the uncertainty can be neglected from the very first, that means that between distributions of causal or non-causal character does not necessarily exist a difference in their quality.

If the statistical oscillations cannot be neglected, the uncertainty should be anyhow characterized. As it will be shown, the case of a single measurement must be discussed separated from its opposite: the case, where starting from a high number of data, the estimate of location is looked for by an arbitrary algorithm.

The case where the number of data, n is not high enough to adopt the formulas valid for the case $n \to \infty$ is a good approximation: i.e. the so-called "transitional range" is very important, or even the most important from a practical point of view, but its treatment is difficult, since it can be treated analytically only in case of some simple estimation methods or certain distributions (see Csernyák and Steiner 1983a, where examples are shown for the curious character of the averages in this transitional range).

2. Let be $F(x)$ the functional form for the probability p that the result of a measurement will be less than x. This function $F(x)$ (commonly known as distribution function) defines exactly the uncertainty of the case of a single measurement, as it gives for the characterization of the uncertainty for all p-s $0<p<1$ the interval (x_p, x_{1-p}) which has the width:

$$q(p) \equiv F^{(-1)}(1-p) - F^{(-1)}(p)$$
$$F^{(-1)}(y) = \inf \{x : F(x) = y\,;\; 0 \leqq y \leqq 1\}\,. \tag{1}$$

(These intervals are known as the confidence intervals.) As the level of the uncertainty should be given by as few data as possible, instead of the set of all $q(p)$-s, the range for one or those for a few p-s are considered as sufficient; most often the range $q(p)$ corresponding to $p=0.25$, the so-called interquartile range, or the range corresponding to small values of p (e.g. 0.05, 0.025, 0.005 or even 0.0005, 0.00005 or less) will be given outside of which the occurrence probability of a single measured value is $2p$ (in which cases one speaks for the above examples of confidence intervals at a 90, 95, 99,99.9, 99.99 percent probability level; in these cases the percentages mean the probability that the value lies inside the interval).

3. In the following only symmetrical distributions shall be considered. The question is to define the uncertainty for an estimate of the symmetry point, if the estimation is made on the basis of a high number of measurements. However, this question has (in contrast to the case studied in section 2), a sense only if the algorithm of the estimation is fixed in advance.

3.1 If the algorithm of the estimation is simply the computation of the algebraic mean, and the distribution has a finite scatter σ and the symmetry point m, then in case of a high number n of measured values—according to the law of the central limit distribution, e.g. Korn and Korn (1961, p. 556)—the distribution of the means has a

Gaussian distribution with the same symmetry point m, but with a $\sqrt{n}$-times lower scatter. As the distribution function of the Gaussian distribution, denoted generally by $\Phi(x)$, is well known, therefore in cases with finite scatter, the uncertainty of the means of n data from a parent distribution with a distribution function $f(x)$ can be characterized in the same way (for $n \to \infty$), as the characterization of single data was made in Section 2: the complete characterization is given by $\Phi(x)$, as a single datum; as uncertainty the value of $q(p)$, corresponding to a certain p, can be used in the practice. In such a sense, the quantity $2\sigma/\sqrt{n}$ yields the confidence interval for the 68 percent level. Multiplied this by 0.6745, the interquartile range will be obtained, and in any case, a numerical value belongs unambiguously to each p value (or to each confidence level), which gives the range $q(p)$ when multiplied by $\sigma/\sqrt{n}$ (multiplying by the numerical value 5.2, the confidence limit for 99 percent, by 3.3, that for the 90 percent confidence limit will be obtained).

If n is not "sufficiently high", the numerical value of the uncertainty cannot be obtained, as in such a case the density function of the averages, obtained by n-times convolution:

$$f_n(x) = n \cdot [f(n \cdot x)]^{n*} \tag{2}$$

can significantly differ from the Gaussian bell-shaped curve. One problem is just this: in the practice it is not known whether for a given distribution and for a given value of n, the density function (2) means a good approximation of the Gaussian curve, i.e. is the value of n "sufficiently high" for the determination of the uncertainty by the simple method based on $\sigma/\sqrt{n}$, according to the previous considerations? If $f_n(x)$ would be computed from Eq. (2) in order to decide this question, then its integral from $-\infty$ to x would yield the distribution function of the means of n elements,—and a simplification due to the law of the so-called central limit distribution would not be any more necessary. Anyway, if the convolutions according to Eq. (2) are carried out for the values of $n = 2, 3, 4, \ldots$ (or more advantageously for $n = 2, 4, 8, 16 \ldots$) till a sufficiently high value of n, then it will be known for which values of n case be computed the uncertainty from $\sigma/\sqrt{n}$ for a given $f(x)$, further the uncertainty in the transitional range can be also given (as done by Csernyák and Steiner (1983b) for the interquartile range).

For the characterization of the uncertainty the quantity $\sigma/\sqrt{n}$ can be used therefore only outside of the transitional range in an asymptotic sense; where it certainly cannot be used, is the uncertainty of a single measurement, i.e. the case of $n = 1$. A very high error, sometimes of several orders of magnitude is made if the values $q(p)$ characterizing the uncertainty of a single measurement would be computed from σ on the basis of the distribution function $\Phi(x)$ (e.g. using the previously given factors), and if the scatter is infinite, then the impossible situation arises that the result of a very precise measurement would be burdened with infinitely high uncertainty. (An extreme example: if a distance of 1 km would be measured within the precision of ± 1 micron in such a manner that only every one measurement out of a million differs from the

symmetry point by more than 1 micron, then it would be absolutely erroneous to emphasize the infiniteness of the uncertainty as it appears in case of a data set of Cauchy-distribution.) *For the characterization of the uncertainty of a single measurement the scatter is therefore perfectly inadequate*, it yields information only about the asymptotic uncertainty of the means.

3.2 If medians are determined, the density function of the medians for $2n+1$ data will be:

$$f_M(n, x) = \binom{2n}{n} (2n+1) (F(x))^n (1-F(x))^n f(x)$$

(f and F are respectively the density and distribution functions of the parent distribution), since out of the $2n+1$ data, one must lie at x, and n each to the right and to the left of it.

Be the symmetry point in the origin (this will be supposed in the followings, too). When in case of $n \to \infty$ the distribution of the medians converges to the normal distribution, the limit value of $f_M(n; 0)$ must be the value of the density function of the corresponding normal distribution at $x=0$, i.e.

$$\lim_{n \to \infty} f_M(n; 0) = \frac{1}{\sqrt{2\pi}\,\sigma},$$

where σ is the scatter of the limit distribution. By applying Stirling's formula:

$$n! \approx \left(\frac{n}{e}\right)^n \sqrt{2\pi n} \qquad (n \gg 1),$$

and $F(0) = 1/2$, one gets:

$$f_M(n; 0) = \frac{(2n)!}{(n!)^2} \frac{(2n+1)}{2^{2n}} f(0) \approx \frac{\left(\frac{2n^{2n}}{e}\right.}{\left(\frac{n}{e}\right)^{2n}} \frac{\sqrt{2\pi}\,\sqrt{2n}}{(\sqrt{2\pi}\,\sqrt{n})^2} \frac{2n+1}{2^{2n}} f(0) =$$

$$= \frac{1}{\sqrt{2\pi}} \sqrt{2n} \frac{2n+1}{n} f(0) \approx \frac{2}{\sqrt{2\pi}} \sqrt{2n+1}\, f(0).$$

Supposing that $f(0)$ is finite and differs from 0, the above equations yield:

$$\sigma \approx \frac{1}{2f(0)\sqrt{2n+1}}. \tag{3}$$

This result, Eq. (3) can be obtained in an other way, too, which shall not be given in details.

Landy et al. (1982) have shown that for the medians the law of great numbers is not always valid. It is really clear from Eq. (3) that in case of $f(0)=0$ the asymptotic uncertainty of the medians is infinite.

3.3 If the most frequent value is determined from a sample with a high number of elements, the scatter of the limit distribution of the same Gaussian type will be:

$$\frac{1}{\sqrt{n}} \cdot \frac{\varepsilon}{\sqrt{n(\varepsilon)}} \tag{4}$$

in that case the asymptotic uncertainty will be characterized by $\varepsilon/\sqrt{n(\varepsilon)}$. Csernyák and Steiner (1983) gave its detailed theoretical and tabular presentation, thus it is superfluous to give more details in addition to Eq. (4) about the uncertainty of the most frequent values.

4. Concerning the uncertainty of the value of a single measurement it is a necessary property of the measure that the value for $\frac{1}{c} \cdot f\left(\frac{x}{c}\right)$ should be c-times the value for $f(x)$ as it is visibly valid for the asymptotic measure of the estimates.

4.1 At first we consider the function $q(p)$ introduced in Section 2. The notion of the confidence interval is supposedly as old as the engineering demand for a numerical characterization of uncertainty; Box et al. (1978) consider so much as a primary quantity the sequence of these ranges that they introduce the density function based on these values.

Though the function $q(p)$ yields a complete possibility for the characterization of the uncertainty of a single measurement, we look for single numerical values in order to aid comparisons and generally for simplicity. If the uncertainty is measured by the following integral:

$$U[w(p)] = \int_0^{0.5} w(p) \cdot q(p)\, \mathrm{d}p \tag{5}$$

then for this value the demand is fulfilled that c-times stretching of the density function results in an c-times increase of the uncertainty U, too. By taking different choices of the function $w(p)$, different definitions of U will be obtained.

4.11 Be $w(p)$ the unit Dirac-δ at $p=0.25$, then one has obviously

$$U[w(p)=\delta(0.25)] = \int_0^{0.5} \delta(0.25) \cdot q(p)\, \mathrm{d}p = q(0.25)\,, \tag{6}$$

i.e. the numerical value will be the interquartile range.

4.12 If $w(p) \equiv 1$, then

$$U[w(p) \equiv 1] = \int_0^{0.5} q(p)\, \mathrm{d}p\,. \tag{7}$$

— Definition (5) can be clearly used for all distributions having an expectance, as for them Eq. (5) yields always finite values (it is, however, for the Cauchy-distribution already infinite).

— The finiteness of $U[w(p)\equiv 1]$ for distributions having an expectance can be proven as follows:

It follows from Eq. (5) (using the prerequisite symmetry) that

$$U=\int_0^{0.5} q(p)\,\mathrm{d}p=\int_{-\infty}^{0} F(x)\,\mathrm{d}x+\int_0^{\infty}[1-F(x)]\,\mathrm{d}x=2\int_{-\infty}^{0} F(x)\,\mathrm{d}x=$$

$$=2\int_{-\infty}^{0}\int_{-\infty}^{x} f(t)\,\mathrm{d}t\,\mathrm{d}x=-2\int_{-\infty}^{0}\int_0^t f(t)\,\mathrm{d}x\,\mathrm{d}t=-2\int_{-\infty}^{0} tf(t)\,\mathrm{d}t=$$

$$=2\int_{-\infty}^{0}|t|f(t)\,\mathrm{d}t=\int_{-\infty}^{\infty}|t|f(t)\,\mathrm{d}t\,.$$

4.13 The uncertainties of greater groups of distributions can be characterized by functions $w(p)$ for which $w(0)=0$. For the simplest of such functions, $w(p)=p$, one has:

$$U[w(p)=p]=\int_0^{0.5} p\cdot q(p)\,\mathrm{d}p\,. \tag{8}$$

Definition (8) enables already the characterization of the uncertainty of probability functions having a Cauchy-distribution, too.

4.14 Each definition of $w(p)$ means a decision about the weights with which the series of $q(p)$-s is taken into account. If therefore a certain range of p is especially important from a certain point of view, then it should be emphasized, while attention should be paid that the less important values of $q(p)$ have not to play an important roie in the value of U. Thus special points of view necessitate special $w(p)$-s (and they have according to the actual situation different forms), on the other hand, however, it should be generally considered that in the case $p\to 0$ the often valid $q(p)\to\infty$ should not lead to an automatic preponderance of this range. It is therefore advantageous that not only $w(0)=0$ should be fulfilled (as in case of Eq. 8) but also $w'(0)=0$. This is fulfilled e.g. if $w(p)=\sin^2(\pi p)$ when the interquartile range obtains the half of the maximum weight:

$$U[w(p)=\sin^2(\pi p)]=\int_0^{0.5}\sin^2(\pi p)\cdot q(p)\,\mathrm{d}p\,. \tag{9}$$

4.15 In some cases it can be necessary to suppress even more radically the very great $q(p)$-s belonging to small p-s. According to this let it be:

$$w(p)=100\cdot e^{-\frac{1}{p}}, \tag{10a}$$

in which case one has:

$$U[w(p)=100\cdot e^{-\frac{1}{p}}]=\int_0^{0.5} 100\cdot e^{-\frac{1}{p}}\cdot q(p)\,\mathrm{d}p\,. \tag{10b}$$

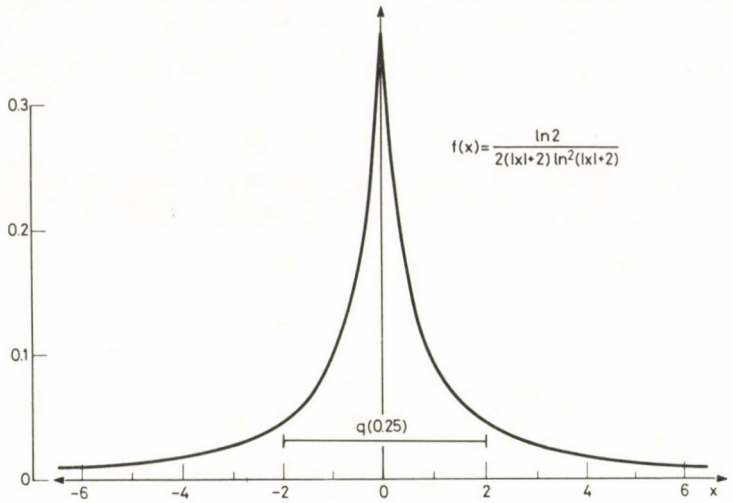

Fig. 1. Density function according to Eq. (11). The area belonging to the narrow stripe above the denoted abscissae, further to its upper edge (at $x = \pm 17.6$) joining flanks is 0.303

With this definition of uncertainty, a finite value is obtained for the distribution function defined by the following density function:

$$f(x) = \frac{\ln 2}{2(|x|+2)\ln^2(|x|+2)} \tag{11}$$

(Fig. 1). This density function has extremely elongated flanks as it is shown by the extremely slow convergence to 1 of the distribution function

$$F(x) = 1 - \frac{\ln 2}{2\ln(x+2)} \qquad (x \geqq 0) \tag{12}$$

(Fig. 2). Correspondingly, $q(p)$-s are at small values of p extremely great, as it can be computed from the expression

$$q(p) = 2\left[e^{\frac{\ln 2}{2p}} - 2\right] \tag{13}$$

valid for this case. This $q(p)$ with the weight function Eq. (10a) (its form can be seen in Fig. 3a) yields not only a finite integral for U, but the integrand itself is alway finite, too (Fig. 3b).

4.16 The weight function (10a) is in vain greater than 0 for all p with the exception of $p = 0$, what is realized is in fact a neglection, truncation of even the $q(p)$-s which according to Eq. (13) increase very quickly for the case $p \to 0$ outside of a certain range

(as shown by Fig. 3). If in practice a truncation is already made, the use of the following weight function should be considered (for a previously given truncation level of p_{min}):

$$w(p)=\begin{cases} p-p_{min}, & \text{if} \quad p>p_{min} \\ 0, & \text{if} \quad p\leqq p_{min} \end{cases}. \tag{14}$$

Infinite U-s will only in this way not appear; it can be easily seen that for any positive

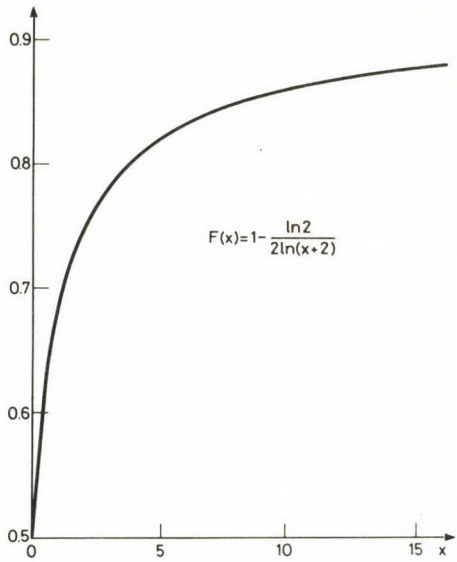

Fig. 2. The distribution function belonging to the density function of Fig. 1

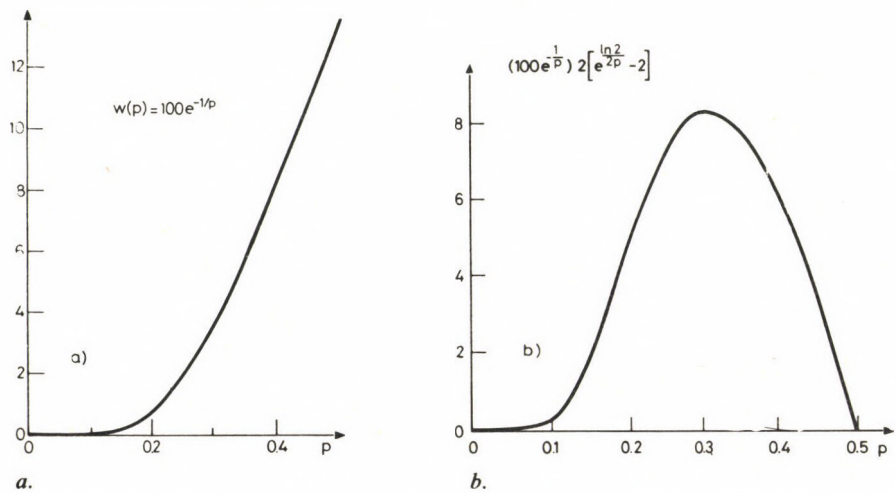

Fig. 3a. The weight function of Eq. (10a)
Fig. 3b. Integrand of U for the weight function of Fig. 3a and for the distribution of Eq. (11)

p-s, with any convergence to 0 for a fixed $w(p)$ a distribution can always be found for which the integral (5) has an infinite value.

In Section 4 the possibilities in connection with U have been surveyed (without aiming to completeness). The proposed $w(p)$-s are more intended as experiments than as suggestions. It should be mentioned further that by an appropriate choice of the weight function $w(p)$ a close connection can be established between U and the average deviation of the medians from samples with n elements of the original distribution. Namely using the density function of the medians, mentioned already in Section 3.2:

$$f_M(n; x) = \binom{2n}{n} (2n+1)\,(F(x))^n (1-F(x))^n f(x)$$

their average deviation is given by the following integral:

$$d_M = \int_{-\infty}^{\infty} |x| f_M(n; x)\,\mathrm{d}x = \binom{2n}{n} (2n+1) \int_{-\infty}^{\infty} |x|\, F^n(x)\,(1-F(x))^n f(x)\,\mathrm{d}x\,.$$

By introducing the substitution $F(x)=p$:

$$d_M = \binom{2n}{n} (2n+1) \int_0^1 |F^{-1}(p)|\,[p(1-p)]^n\,\mathrm{d}p =$$

$$= \binom{2n}{n} (2n+1)\,2 \int_0^{0.5} q(p)\,[p(1-p)]^n\,\mathrm{d}p\,.$$

And the weight function is:

$$w(p) = \binom{2n}{n} (2n+1) 2 [p(1-p)]^n \qquad 0 \leqq p \leqq 0.5\,.$$

4.2 When computing the most frequent value, as it has been shown by Csernyák (1973), a Cauchy-density distribution is looked for which is (according to a criterion based on the Schwarz-inequality) most similar to the given density distribution. This criterion is insensitive to any actually elongated flanks, therefore if a measure of the uncertainty is looked for which is free of the effect of such flanks and is based mainly on high values of $f(x)$, then the interquartile semi-range of a Cauchy-distribution fitted to the given distribution should be chosen. This value is denoted by ε in papers dealing with theoretical and practical problems of the most frequent value. This measure of uncertainty is finite for all distributions.

4.3 The notion of the entropy which is quite natural in the information theory for the discrete case, is generally transposed to the continuous case with hinting at the problems connected with it (e.g. Reza 1966, p. 318). A disadvantageous property of the formula for the continuous case is that it yields infinite values for certain distributions, e.g. for the distribution of Eq. (11). The entropy is expressed sometimes by 2-based, sometimes by Neper-logarithms. In the latter case the entropy, denoted by $H(f)$ for the

distribution with the density function $f(x)$ according to its definition is the following:

$$H(f)=\int f(x)\ln\frac{1}{f(x)}\,dx\,. \tag{15}$$

The integration is to be carried out for all values of x, where $f(x)\neq 0$.

It is evident that when passing from $f(x)$ to its c-times stretched function: $\frac{1}{c}\cdot f\left(\frac{x}{c}\right)$, then $H(f)$ increases by $\ln c\cdot H(f)$, as a measure of the uncertainty fits the best the requirements of information theory, but in its original form it does not fulfil the demand of the engineering applications mentioned at the beginning of Section 4: namely that if the distribution is stretched c-times, the measure of uncertainty should increase to its c-times. A practically useful measure is obtained if instead of $H(f)$, the value

$$e^{H(f)} \tag{16}$$

is used, as if $H(f)$ increases by $\ln c$, then this value increases really to its c-times. As the

Table I.

$f(x)$	$F(x)$	$q(p)$ $0\leqq p\leqq 0.5$
$\frac{1}{2}e^{-\lvert x\rvert}\quad -\infty<x<\infty$	$\begin{cases}\frac{1}{2}e^{x} & x\leqq 0\\ 1-\frac{1}{2}e^{-x} & x>0\end{cases}$	$2\ln\frac{1}{2p}$
$\frac{1}{\sqrt{2\pi}}e^{-\frac{x^2}{2}}=\varphi(x)$	$\Phi(x)$	$\Phi^{-1}(1-p)-\Phi^{-1}(p)$
$\frac{1}{\pi}\frac{1}{1+x^2}\quad -\infty<x<\infty$	$\frac{1}{\pi}\left(\arctan x+\frac{\pi}{2}\right)$	$2\tan[\pi(0.5-p)]$
$\frac{\ln 2}{2(\lvert x\rvert+2)\ln^2(\lvert x\rvert+2)}\quad -\infty<x<\infty$	$\begin{cases}\frac{\ln 2}{2\ln(\lvert x\rvert+2)} & x\leqq 0\\ 1-\frac{\ln 2}{2\ln(x+2)} & x>0\end{cases}$	$2\left(2^{\frac{1}{2p}}-2\right)$
$\begin{cases}0.5 & \lvert x\rvert<1\\ 0 & \lvert x\rvert\geqq 1\end{cases}$	$\begin{cases}0 & (x\leqq -1)\\ 0.5(1+x) & -1<x\leqq 1\\ 1 & x>1\end{cases}$	$2(1-2p)$

exponential function is everywhere monotonous, this transformation yields an uncertainty measure of higher numerical value, if the entropy is higher: if comparing two distributions, relations cannot change sign in consequence of this transformation. Further the advantage should also be mentioned that after the transformation only positive measures of uncertainty can be obtained, while the entropy can have negative values, too, which as a measure of uncertainty is quite unusual to the practical mind (Rényi 1962, p. 446). (The immediate correspondence is quoted from Korn and Korn, 1961: "$H(x)$ (entropy of x) is a measurement of the expected uncertainty involved in a measurement of x" (p. 549)).

Here are some measures of uncertainty according to Eq. (16): for a Gaussian distribution $\sqrt{2\pi e}.\sigma$ (Reza 1966, p. 335), for a Cauchy-distribution $4\pi\varepsilon$ (Hajagos 1982), ε is here the interquartile semi-range; for a Laplace-distribution $2\beta e$ (Korn and Korn 1961, p. 566), and finally for a uniform distribution in the range (a, b): $(b-a)$ (Reza 1966).

5. Now some illustrations will be given for the previous sections. Table I gives the density functions $f(x)$, the distribution functions $F(x)$, the functions $q(p)$, further the measures of uncertainty for a single measurement according to the subsections of Section 4, and for the different methods of estimation the measures of indefiniteness

Uncertainty measures for a single measurement							Uncertainty measures of estimations made by different methods on the basis of a high number of measurements		
$q(0.25)$	$U=\int_0^{0.5} w(p)q(p)\,dp$				Entropy $e^{H(f)}$	ε	Median $\frac{1}{2\cdot f(0)}$	E-fitting σ	M-fitting $\varepsilon/\sqrt{n(\varepsilon)}$
	$w(p)\equiv 1$	$w(p)=p$	$w(p)=\sin^2(\pi p)$	$w(p)=100\cdot e^{-\frac{1}{p}}$					
1.386	1	$\frac{1}{8}=0.125$	0.205	0.901	$2e=5.437$	0.807	1	$\sqrt{2}=1.4142$	1.076
1.349	$\sqrt{\frac{2}{\pi}}=0.7979$	0.117	0.202	0.481	4.133	0.925	1.253	1	1.165
2	∞	0.221	0.319	1.311	$4\pi=12.57$	1	1.571	∞	1.414
4	∞	∞	∞	2.046	∞	0.748	1.386	∞	1.312
1	1.5	0.0833	0.149	0.740	2	0.719	1	0.577	0.871

described in Section 3 for the Laplace, Gaussian, and Cauchy distributions, for the distribution defined by Eq. (11), having an infinite entropy and for the uniform distribution. (In the case of Section 3, the limit distributions have a known form, from this single datum the uncertainty defined by any formula can be computed — as it has been already mentioned —, e.g. $q(0.25)$ as the $2 \cdot 0.6745 = 1.349$-times of the scatter belonging to the actual estimate.)

The possible uncertainty of the asymptotic measures is to be understood literally that if n increases over all limits the numerator of the expression

$$\frac{\text{measure}}{\sqrt{n}}$$

cannot be finite. For the cases in the Table that means that the averaging, as an estimation method, cannot be used for the Cauchy-distribution and for the distribution according to Eq. (11).

The infinite value of the measures of uncertainty for a single measurement arises already doubts in the definition of uncertainty itself; namely for an arbitrarily small probability p a factor can be found for the decrease of the scale factor in case of all distribution types for which the measured values lie outside of an arbitrarily small interval only with this very small probability p -and in such a case it has no sense to speak of infinite uncertainty. This can be naturally said so that the infinitely high values indicate that the actual distribution is outside of the group of distributions for which the definition of uncertainty can be applied.

If the measures of uncertainty characterizing the parent distribution, but relative to the same σ, namely $q(0.25)$ and ε (further from the experimental ones those corresponding to $w(p)=p$ and $w(p)=\sin^2(\pi p)$) are compared for the Laplace- and Gaussian distributions (this can be made easiest by dividing the measures for the Laplace distribution by $\sqrt{2}$), then all uncertainties are less for the Laplace-distribution than for the Gaussian one. Concerning the measure of uncertainty dedueed from the entropy, $e^{H(f)}$, a similar result is obtained. The latter is a special case of a theorem known from the information theory: from distributions having the same scatter, the normal distribution has the highest entropy (Reza 1966, p. 335). This theorem seems for the first glance paradox, but looses this character, if one reminds the fact that the entropy (and together with it, also $e^{H(f)}$) is a measure of the uncertainty of a single measurement, i.e. it characterizes the parent distribution, while the scatter means something rather different: the distribution resulting from $f(x)$ by n-times convolution of the type of Eq. (2) (which approximates for great n values the Gaussian distribution), which after an n-times stretching, however, (having restituted $n=1$) results in a density function absolutely dissimilar to the parent distribution. The latter case is the more conspicuous the greater the deviation of the flanks of the parent distribution from those of the Gaussian one is, as Eq. (2) amplifies the characteristics of the flanks (which was

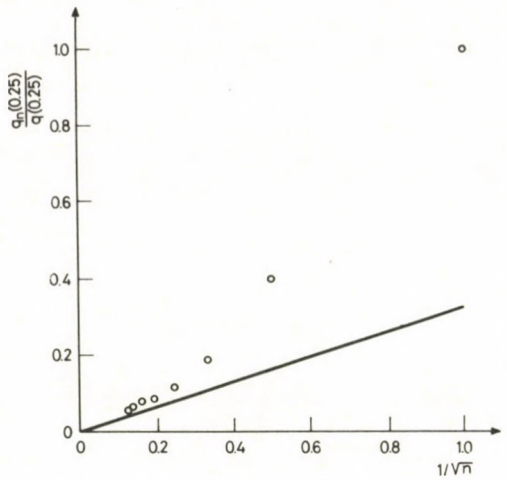

Fig. 4. Interquartile ranges of some estimates of locations obtained by the method of the most frequent value for different elements n in a sample, in comparison to the interquartile range of Eq. (11) in function of $1/\sqrt{n}$

for certain measures of uncertainty absolutely not taken into account, e.g. for certain kinds of U).

The scatter of the parent distribution is the exclusive characteristics of the estimation looking for the symmetry point as for the expected value E, i.e. the exclusive characteristics of the arithmetic means (E-fitting). As in the uncertainty relation of the Fourier-transforms (which has physical consequences, too) the uncertainty characterizing the parent distribution does not appear, further as the scatter is *only one* (and generally not always applicable) measure of the uncertainty, this complex of problems has several points which need a clarification (see also Steiner 1982) to which authors intend to return in the future.

At last the use of the median and of the most frequent value will be proved to be very advantageous from a mathematical-statistical point of view for the distribution defined by Eq. (11) and having an infinite entropy. These advantages were already shown by the asymptotic uncertainty measures of the Table ($1/[2f(0)] = 1.386$ and $\varepsilon/\sqrt{n(\varepsilon)} = 1.312$).

A data system characterized by the density function (11) was produced using a random number generator for different n-s. 200 samples have been chosen for each n and for each of these samples the median was chosen and the most frequent value computed. Thus for each n and for each method of estimation we obtained the interquartile range ($q_n(0.25)$) on the basis of 200 data which was then compared to the interquartile range of the parent distribution, being $q(0.25)$ equal to 4. As it can be seen from Figs 4 and 5, the values tend (as $1/\sqrt{n}$) in reality asymptotically in function of n toward a straight line through the origin with a tangent of $2 \cdot 0.6745 \cdot 1.386/4 = 0.4675$

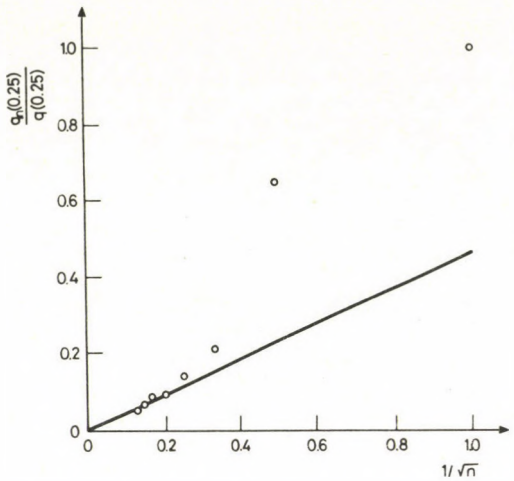

Fig. 5. Interquartile ranges of some estimates of locations using medians for different numbers of elements n in a sample, in comparison to the interquartile range of the parent distribution of Eq. (11) in function of $1/\sqrt{n}$

and $2 \cdot 0.6745 \cdot 1.312/4 = 0.3280$. Consequently, the infinite entropy in this example shows only the limited application range of this value as uncertainty measure, on the other hand, it is clear that even a distribution as Eq. (11) can be treated from a mathematical point of view without any problem, if adequate methods are used.

References

Box G E P, Hunter W G, Hunter J S 1978: Statistics for Experimenters. John Wiley and Sons, New York

Csernyák L 1973: On the most frequent value and cohesion of probability distributions. *Acta Geod. Geoph. Mont. Hung.*, 8, 397–401.

Csernyák L, Steiner F 1983a: Limit distribution of the most frequent values from symmetrical distributions. *Acta Geod. Geoph. Mont. Hung.* 18, 135—140.

Csernyák L, Steiner F 1983b: Decision between two estimates of location: the most frequent value and the arithmetic mean. *Acta Geod. Geoph. Mont. Hung.* 18, 141—156.

Hajagos B 1982: Der häufigste Wert, als eine Abschätzung von minimalem Informationsverlust, und zugleich als die beste "maximum likehood"—Abschätzung. Publications of the Technical University for Heavy Industry, Series A Mining, 37 (1)

Korn G A, Korn T M 1961: Mathematical Handbook for Scientists and Engineers. McGraw-Hill, New York

Landy I, Lantos M, Steiner F 1982: Untersuchungen von U-Verteilungen. Publications of the Technical University for Heavy Industry, Series A Mining, 37 (1)

Rényi A 1962: Wahrscheinlichkeitsrechnung. Deutscher Verlag der Wissenschaften, Berlin

Reza F M 1966: Introduction to information theory. Műszaki Könyvkiadó, Budapest

Steiner F 1982: Über die Unzulänglichkeiten des Streuungsbegriffes. Publications of the Technical University for Heavy Industry, Series A Mining, 37 (1)

Acta Geodaet., Geophys. et Montanist. Hung. Volume 19 (3–4), pp. 249–255 (1984)

PERIODICITY OF THE RELEASE OF SEISMIC ENERGY AND THE ANOMALISTIC GREAT CYCLE OF THE MOON

O NEKOVETICS[1]

[Manuscript received December 30, 1982]

The paper hypothesizes a connection between the seismic energy release of the Northern hemisphere and the long-period lunar intervals, mainly the anomalistic long period of 8.85 years. It seems that in such a frame of reference the maxima of the energy release follow a regular pattern.

Keywords: anomalistic lunar period; earthquake energy release; seismic energy

In previous papers (Nekovetics 1973, 1974) it was suggested that global and local periodicities of 3 years exist in the seismic and volcanic processes of the Earth. Periods corresponding to multiples of 3 years could also be detected in the seismic series. As the anomalistic and draconistic long periods of the Moon's orbit (8.85 and 18.6 years) are quite near to the multiples of 3 years, a comparison of these periodicities seemed reasonable.

The present investigation includes high energy seismic events ($M > 7.75 \cdot 10^{24}$ erg) according to the list published by Duda (1965) for the time interval January 1, 1897 till December 31, 1964, supplemented by later events till the end of 1978.

The anomalistic (perigee) point of the Moon's orbit makes a complete revolution respective to the direction of stars in $AS = 3232.596\,104$ days (roughly 8.85 years). This period is distributed into six sections of roughly equal length (for details see Fig. 1). The sections are denoted by the letters A–F, the boundaries between the sections can be determined easily and are contained in Table I.

The Northern and Southern hemispheres of the Earth are rather different from a seismic point of view. About 3/4 of the seismic energy was released in the investigated period in the Northern hemisphere, and only about 1/4 in the Southern hemisphere. In

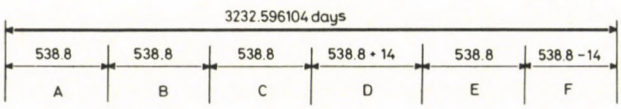

Fig. 1. Boundaries of the sectors within the anomalistic year

[1] Dimitrov tér 7/105, H-8300 Tapolca, Hungary

Table I

Limits of the sectors *A–F* for the years 1897–1964

Anomalistic long period	First day of the sectors					
	A	*B*	*C*	*D*	*E*	*F*
1.						Oct. 8. 1897
2.	March 17. 1899	Sept. 6. 1900	Febr. 26. 1902	Aug. 19. 1903	Febr. 22. 1905	Aug. 15. 1906
3.	Jan. 20. 1908	July 13. 1909	Jan. 2. 1911	June 25. 1912	Dec. 29. 1913	June 21. 1915
4.	Nov. 27. 1916	May 20. 1918	Nov. 10. 1919	May 1. 1921	Nov. 5. 1922	Apr. 27. 1924
5.	Oct. 4. 1925	March 26. 1927	Sept. 15. 1928	March 8. 1930	Sept. 12. 1931	March 3. 1933
6.	Aug. 10. 1934	Jan. 30. 1936	July 23. 1937	Jan. 13. 1939	July 18. 1940	Jan. 8. 1942
7.	June 17. 1943	Dec. 7. 1944	May 29. 1946	Nov. 19. 1947	May 25. 1949	Nov. 15. 1950
8.	Apr. 22. 1952	Oct. 13. 1953	Apr. 5. 1955	Sept. 25. 1956	March 31. 1958	Sept. 21. 1959
9.	Febr. 26. 1961	Aug. 19. 1962	Febr. 9. 1964	Aug. 3. 1965	Febr. 7. 1967	July 30. 1968
10.	Jan. 5. 1970	June 28. 1971	Dec. 22. 1972	June 10. 1974	Dec. 15. 1975	June 9. 1977
11.	Nov. 16. 1978					

addition, the seismically active zone of the Northern hemisphere is a nearly continuous band from the Azores (30W) through Eurasia, the Aleuts, Northern and Central America till the Eastern part of the Antilles (65W). That means that about 9/10 of the longitudes is covered by this active zone. On the Southern hemisphere there are two active zones unconnected with each other: they lie between Sumatra (100E) and Samoa (170W) and between Ecuador (80W) and Tierra de Fuego (65W), respectively. Thus in

Table II

Conversion of earthquake magnitudes into released energy

Magnitude	Energy
7.75	$0.2 \cdot 10^{24}$ erg
7.8	$0.3 \cdot 10^{24}$ erg
7.9	$0.4 \cdot 10^{24}$ erg
8.0	$0.6 \cdot 10^{24}$ erg
8.1	$0.9 \cdot 10^{24}$ erg
8.2	$1.3 \cdot 10^{24}$ erg
8.25	$1.6 \cdot 10^{24}$ erg
8.3	$1.9 \cdot 10^{24}$ erg
8.4	$2.8 \cdot 10^{24}$ erg
8.5	$4.0 \cdot 10^{24}$ erg
8.6	$5.8 \cdot 10^{24}$ erg
8.7	$8.3 \cdot 10^{24}$ erg
8.9	$17.4 \cdot 10^{24}$ erg

the Southern hemisphere only about 30 percent of the longitudes contain seismically active zones, and even these in two disrupted parts.

Due to this situation, it seems to be reasonable to study the seismic energy release of the Northern hemisphere. Table II contains the energies of the earthquakes of different magnitudes. The time distribution of the energy release from the Northern hemisphere according to the sections in Table I can be seen in Table III and Fig. 2. This curve can be characterized by quick and great excursions. These excursions are, however, not randomly distributed, they follow each other in a regular pattern. Figure 3 shows that there are two series of maxima, each of them having a time interval of 6 units between subsequent maxima (i.e. the interval is exactly 8.85 years). The maxima of the two series follow each other after 2 and 4 units, respectively.

The existence of these two series confirms that the release of the seismic energy in the Northern hemisphere is a periodic phenomenon. The periodicity of the energy release is equal with the period of the perigee point of the Moon's orbit in relation to stars. It is supposed that due to this coincidence the Moon influences the energy release of terrestrial earthquakes. The shaded areas in Fig. 4 show the time intervals when the seismic risk is high. If the perigee point of the Moon's orbit reaches these shaded zones,

Table III

Sum of the released energies in the sectors of the anomalistic long periods

Anomalistic long period	Sector (No. in Fig. 2, 3)	Energy (in 10^{24} ergs)	Anomalistic long period	Sector (No. in Fig. 2, 3)	Energy (in 10^{24} ergs)
1	E (1)	36.1		D (24)	0.8
	F (2)	9.0		E (25)	20.6
2	A (3)	11.6		F (26)	3.2
	B (4)	7.8	6	A (27)	0.9
	C (5)	16.5		B (28)	0.0
	D (6)	11.7		C (29)	8.3
	E (7)	40.8		D (30)	0.6
	F (8)	7.9		E (31)	11.5
3	A (9)	4.6		F (32)	3.2
	B (10)	2.5	7	A (33)	2.3
	C (11)	18.7		B (34)	1.9
	D (12)	2.1		C (35)	4.7
	E (13)	9.6		D (36)	1.9
	F (14)	2.3		E (37)	9.6
4	A (15)	1.2		F (38)	6.6
	B (16)	4.2	8	A (39)	2.8
	C (17)	7.7		B (40)	0.6
	D (18)	0.9		C (41)	0.3
	E (19)	6.6		D (42)	4.6
	F (20)	0.0		E (43)	10.3
5	A (21)	2.3		F (44)	0.0
	B (22)	2.3	9	A (45)	0.0
	C (23)	5.8		B (46)	1.6
				C (47)	4.0

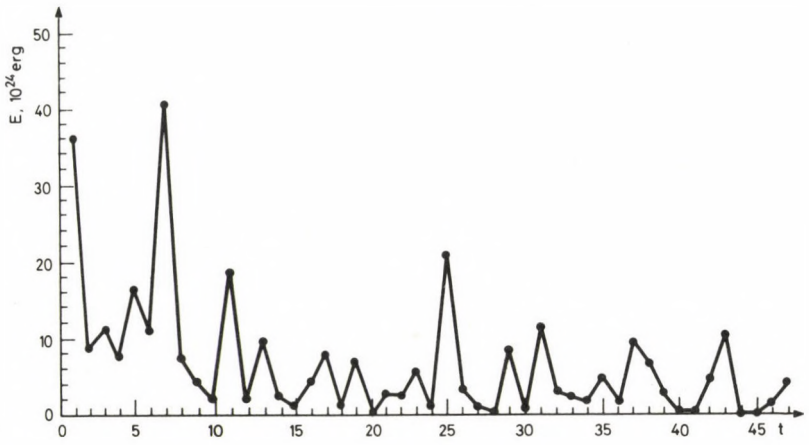

Fig. 2. Seismic energy release within the years 1897–1964 time unit roughly 8.85/6 years

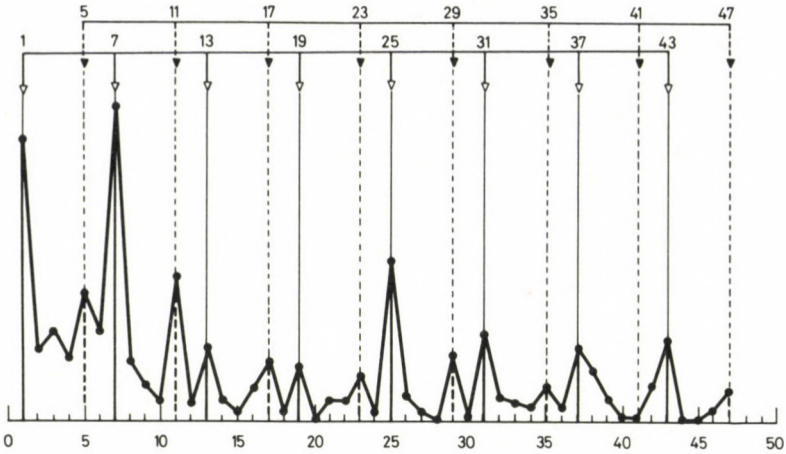

Fig. 3. As Fig. 2, but with the two periodic series of maxima

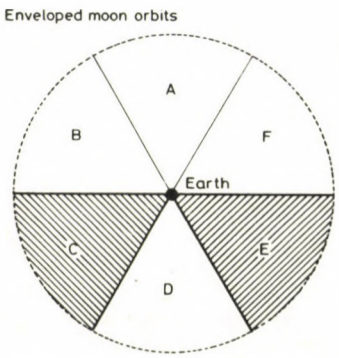

Fig. 4. Sectors of the anomalistic month favourable for great earthquakes

the probability of great earthquakes is increasing. The sectors oriented to the stars are connected to the terrestrial environment so that their position relative to the Earth's rotation axis remains unchanged, as the rotation axis of the Earth (irregarding some minor changes) points always to the same place of the space.

Secondary characteristics of the energy release curve

The maxima of the two series have in the energy release curves values which at first decrease continuously, then they increase abruptly. The order of the maxima in the first series is the following:

$$\begin{array}{ll} & 1 \\ 7>13>19 & 1<7 \\ & 19<25 \\ 25>31>37 & 37<43. \\ 43 & \end{array}$$

The same for the other series:

$$\begin{array}{ll} & 5 \\ 11>17>23 & 5<11 \\ & 23<29 \\ 29>35>41 & 41<47. \\ 47 & \end{array}$$

The "maximum" at the abscissa 41 does not exist in the strict sense of the word, but the sequence necessitates just at this place a quite small value which happened to be less than the neighborous values. Anyway this value is the only exception from the above rule.

The secondary characteristics of the curve can be thus summarized as in a period of $3 \cdot 8.85$ years three maxima occur which have continuously decreasing values. The series from the 16 maxima of the curve form a regular sequence which would occur randomly less than once in 1000 cases according to a rough estimation.

It should be mentioned that even between the maxima at time intervals of twice the basic interval, clear minima appear which confirm the existence of the periodicity.

The time series of the seismic energy release of the Northern hemisphere has been used in an autocorrelation analysis (Fig. 5). In this case the interval for individual

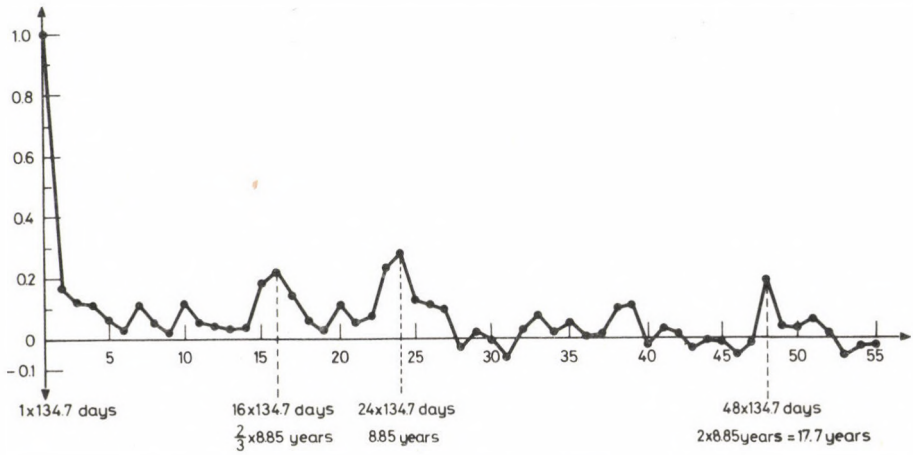

Fig. 5. Autocorrelation function of the time series in Fig. 2

values has been chosen to be 8.85/24 years, roughly 135 days. The main maximum appeared at 8.85 years, the second and third at $2/3 \cdot 8.85$ and $2 \cdot 8.85$ years. The peak at $2/3 \cdot 8.85$ years corresponds to the 4 units ($2/3 \cdot 6$ units) difference between the maxima of the two series in Fig. 3 the peak at $2 \cdot 8.85$ years corresponds most probably twice the main periodicity of the series. Thus the autocorrelation function of the series has confirmed the existence of the two periodic components in the original series.

Else the two series could be traced also in the continuation of Duda's earthquake energy release series covering more 13 years, too. It can be considered as a supplementary proof of the supposed regularities.

Conclusions

The statement offered in earlier papers of the author (Nekovetics 1973, 1974) that near celestial bodies (Sun, Moon) play a greater role in the seismic energy release process than supposed hitherto could be confirmed by a systematic study of the energy release in great earthquakes of the Northern hemisphere. The maxima of the energy release curve are clearly connected with the position of the anomalistic point of the Moon's orbit in respect to a frame of reference fixed to the stars.

Acknowledgements

The author acknowledges the help by M Varga and J Verő in the computations and in collecting recent earthquake data.

References

Duda J 1965: Secular seismic energy release in the circumpacific belt. *Tectonophysics*, 2, 5.

Nekovetics O 1973: Periodicity of seismic phenomena (in Hungarian). *MTA X. Osztályának Közleményei*, 6, No. 1, 40.

Nekovetics O 1974: Connection between the position of nearby celestial bodies and high-energy shallow focus earthquakes (in Hungarian). *MTA X. Osztályának Közleményei* 7, No. 1, 2.

Acta Geodaet., Geophys. et Montanist. Hung. Volume 19 (3–4), pp. 257–266 (1984)

INVESTIGATION OF THE INDUCTIVE EXCITATION OF DEEP CONDUCTING ZONES USING PHYSICAL MODELING*

M N BERDICHEVSKY[1], A I BILINSKY[1], V M KOBZOVA[1], I P MOROZ[1]

[Manuscript received March 25, 1983]

A physical modeling equipment was built up to model the Earth's structure having a conductor-isolator-conductor profile using a homogeneous plane wave field. Conductivity inhomogeneities were placed not only in the conducting upper layer (electrolyte) but also in the high resistivity layer modeled by an air space.

The physical modeling has shown that the inductive excitation mechanism of deep conducting zones can give a noticeable contribution to MT anomalies. The conductive current redistribution due to fractures essentially increases the resolution power of deep MT soundings.

Keywords: conducting zone; deep conducting zone; geoelectric modeling; inductive excitation

Introduction

For several years the magnetotelluric method was more and more frequently used to investigate the Earth's structure. A large amount of measured data obtained by deep magnetotelluric soundings has been accumulated in the Soviet Union and also in other countries. However, for a correct interpretation one has to know the magnetotelluric effects of deep conductivity inhomogeneities.

Tectonical and geophysical data give informations on geoelectric inhomogeneities in the crust and in the upper mantle: subduction zones, geosutures, asthenolites and asthenospheric layers give a conductivity drop from hundreds to several thousands siemenses. Therefore the most important problems are as follows: morphology of the anomalous magnetotelluric field caused by typical deep structures, their genesis and determination of the resolution power of the MT method. Physical modeling has more chance in solving such problems than mathematical modeling, as some basic difficulties appear when calculating EM fields of arbitrary 3-D inhomogeneities in multilayered media using computer methods (Dmitriev 1981).

The magnetotelluric physical modeling equipment built up in the Institute of Applied Problems in Mechanics and Mathematics of the Ukrainian Academy of

* Paper presented at the KAPG-Symposium on Electromagnetic Induction, Sopron, March 1983

[1] Institute of Applied Problems in Mechanics and Mathematics of the Ukrainian Academy of Sciences, Lvov

Sciences enables to model the Earth's deep structure having a conductor-isolator-conductor profile using a homogeneous plane wave field (Moroz et al. 1975). Conductivity inhomogeneities are placed not only in the conducting upper layer which is modeled by a NaCl-solution, but also in the high resistivity layer (air). The high conductivity mantle is modeled by the basement of the equipment made of metal. There are some conducting embeddings in the second layer as crustal or asthenospheric models. The anomalous EM field of such inhomogeneities can be divided into galvanic and inductive parts. The galvanic effect connected with the redistribution of currents in the medium decreases the resolution power of MT soundings, because the conducting zone is screened by high resistivity lithospheric rocks. In the inductive mechanism there is no screening effect and as a consequence informations can be obtained from the galvanically screened conducting zones in the crust and in the upper mantle.

The inductive excitation mechanism of asthenospheric zones was studied by physical modeling experiments.

Description of models

Discs, ellipsoid, cylinder, prisms made of duralumin ($\rho \sim 3 \cdot 10^{-8}$ ohm) served as models of high resistivity zones. Dimensions of the models and parameters of the modeling profile can be seen in Figs 1, 2, 3 and 4. Coefficients of similarity ($K_i = 6 \cdot 10^5$, $K_\rho = 100$, $K_T = 3.6 \cdot 10^9$) were chosen so that the modeling frequency range 0.1–10.0 MHz should correspond to geoelectromagnetic variations between 10 and 0.1 hours. E_0 is directed along the axis. Dimensions of the conducting models correspond to the characteristic dimensions and to the depth of the active zone. The electrical conductivity of the partly liquid material is much higher than that of the solid phase.

It is significant that in these models there is practically no galvanic connection between the layer ρ_1 and the embeddings. The factor $\rho^{\perp} = \dfrac{a}{\sqrt{S_1 T_2}}$ (where $S_1 = h_1/\rho_1$ and $T_2 = (h - h_1)/\rho_2^*$) was determined to characterize the screening (Moroz et al. 1975). h_1 means the thickness, ρ_1 the specific resistivity of the surface layer (electrolyte). h means the depth, a the linear dimension of the conducting embedding. In the calculation of the transversal resistivity of the second layer (air) ρ_2^*, the displacement current was taken into account: $\rho_2^* = \dfrac{1}{\sqrt{1/\rho_2^2 + (2\pi f \rho_0)^2}}$. In case of $a = 0.40$ m and $f = 10.0$ MHz as a maximum, the factor $\rho^{\perp}$ is not more than 1.3. This means an almost perfectly screened conducting embedding. As there is no galvanic connection between the layer ρ_1 and the embeddings, the observed effects must be of inductive origin. The parameter $|ka|$ (where k is the wave number, a is the dimension of the embeddings) is for all the investigated models at least 1000. This means an intensive inductive domain which exists already if $|ka| \geq 10$.

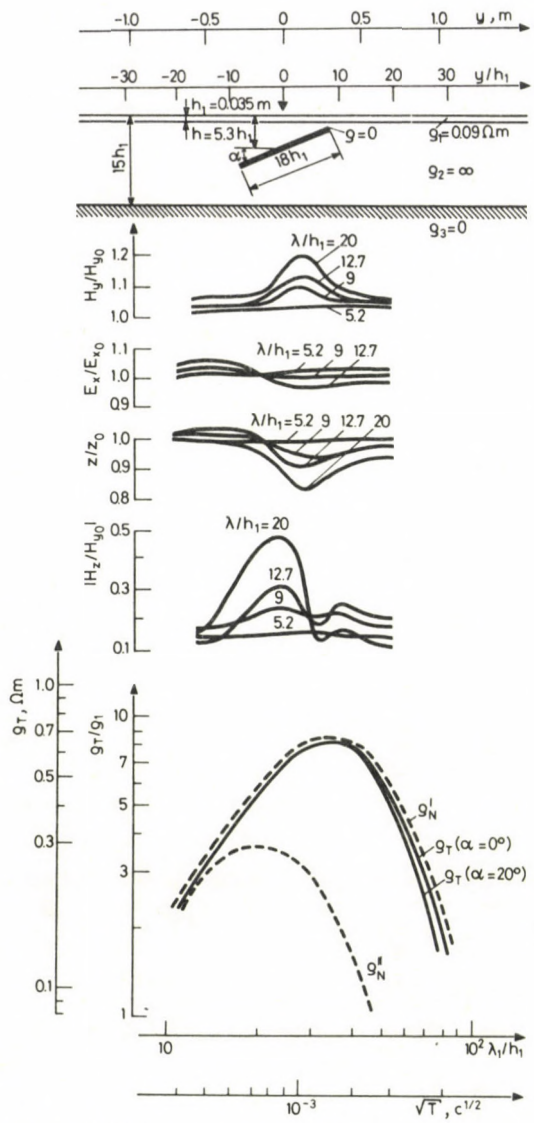

Fig. 1. Electromagnetic field components and MT sounding curves over a conducting disc ρ_N^{I} and ρ_N^{II} — normal (1–D) MT sounding curves for $d=0$ and $d=\infty$

Eddy currents inducted in conductive embeddings produce an anomalous field on the surface. The spatial distribution of the relative amplitudes H_y/H_0, E_x/E_0, H_z/H_0 of the components are shown for a disc in Fig. 1, for an ellipsoid in Fig. 2, for a cylindrical horst in Fig. 3, for a conducting layer and a vertical embedding in Fig. 4. With the exception of the thin horizontal disc, the anomalous fields for all the conducting embeddings are similar.

Thin horizontal copper discs (of 1.5 mm thickness) having diametres from 0.16 m to 1.28 m did not change the induced field. The physical explanation is as follows: in case of a thin, horizontally layered conducting zone the primary magnetic field is parallel to its surface and in a disc of limited extension the eddy currents can be neglected (as if the disc would be absent). In case of an inclined disc a primary magnetic

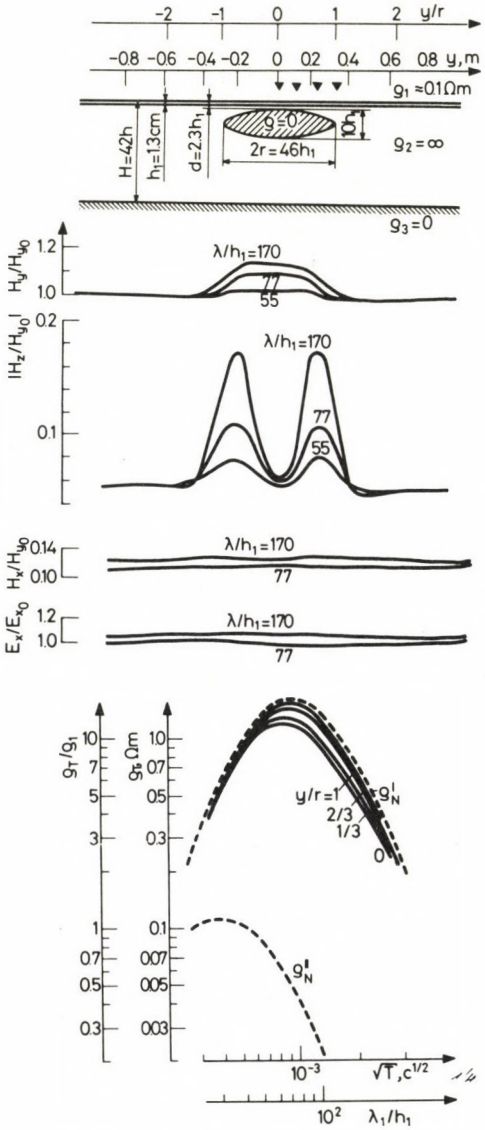

Fig. 2. Electromagnetic field components and MT sounding curves over a conducting ellipsoid. ρ_N^I and ρ_N^{II} — normal (1–D) MT sounding curves for $r=0$ and $r=\infty$

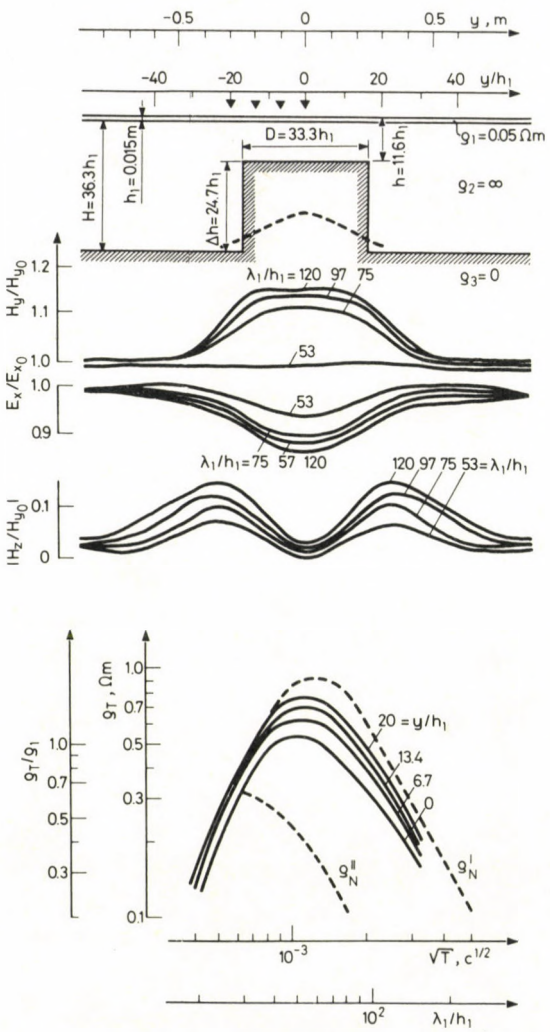

Fig. 3. Electromagnetic field components and MT sounding curves over a cylinder-like rise of the high conductivity basement.
ρ_N^I and ρ_N^{II} normal (1–D) MT sounding curves for $D=0$ and $D=\infty$

field component appears perpendicular to its surface, which component generates significant eddy currents. This is the reason of the anomalous electromagnetic field on the surface of the profile. E.g. if the inclination is 20°, the magnetic field over the embedding can be increased by more than 50%. According to experiments the anomaly of the disc-like conducting zone models increases when increasing the diameter of the embedding and the inclination. The anomaly almost linearly attenuates when

immersing the disc. There is no surficial effect if the depth of its centre is greater than $10h_1$.

For a thick ($10h_1$) conducting embedding an ellipsoid of rotation served with axes 0.65 m and 0.13 m ($a/b = 5$) which corresponds to a conducting asthenospheric zone about 80 km thick, 360 km long and 20 km deep. The electric conductance of the upper layer was $S = 750$ S, and the depth of the conducting mantle 320 km.

To study the anomalous field of conducting embedding being united with the conducting layers of the mantle, a conducting circular cylinder horst over the

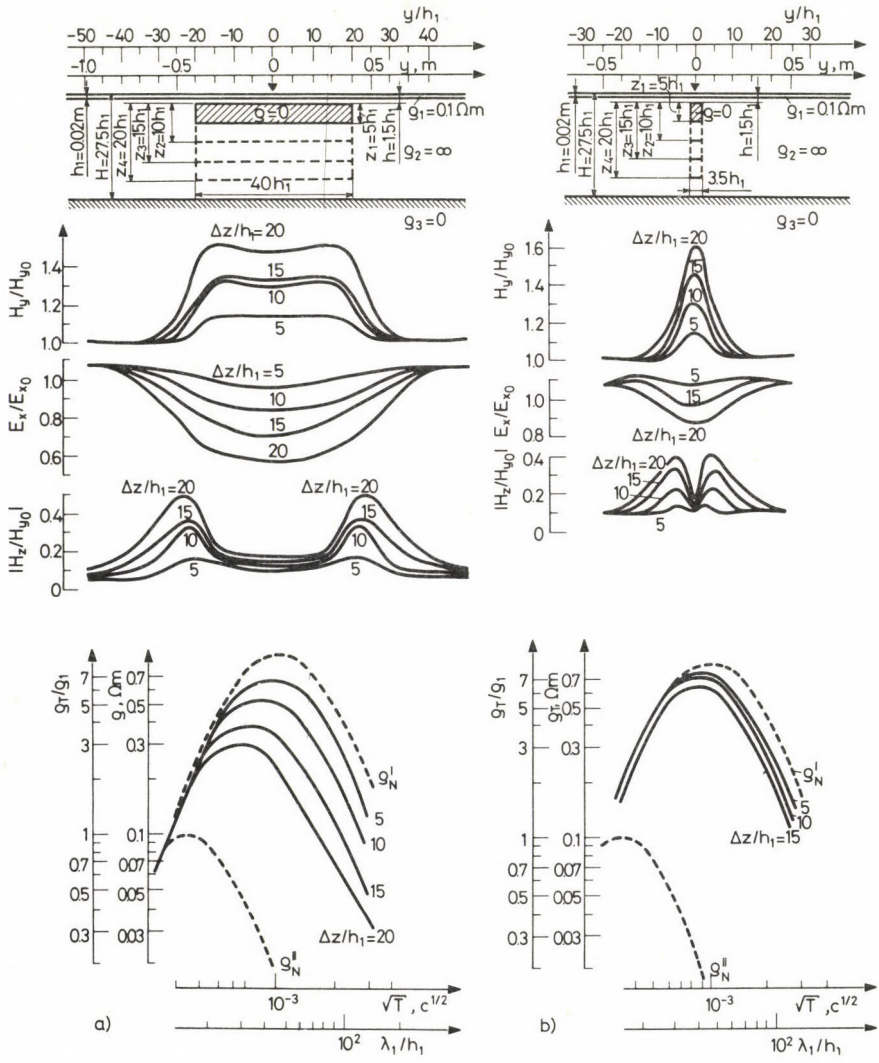

Fig. 4. Electromagnetic field components and MT sounding curves over a conducting sheet (*a*) and dyke (*b*). ρ_N^I and ρ_N^{II}-normal (1–D) sounding curves for $y = 0$ and $y = \infty$

conductive basement of the equipment was used. The diameter of the horst was 0.5 m, its height 0.37 m. In field conditions these values correspond to a strike of 300 km, a height of 220 km and the depth of the high conductivity mantle 330 km.

The effect of geometric dimensions was studied using metal prisms. The upper boundary of models was in a depth $h=0.05$ m, their dimensions changed as follows: $\Delta x=0.5$–4.0 m, $\Delta y=0.5$–0.8 m, $\Delta z=0.1$–0.4 m (in field conditions these mean $h=30$ km, $x=300$–2400 km, $y=300$–480 km, $z=60$–240 km).

Characteristics of MT anomalies

The basic characteristics of the anomalous EM field generated in an inductive way being the same for all investigated model types were as follows:

— each anomalous field component can be higher by 50% than the primary field;

— the maximum anomaly appears at the lowest frequencies and the anomaly is attenuated very strongly in function of the frequency (there is no anomaly if $\lambda_1/h_1<40$);

— the anomaly depends on Δx and Δz and only slightly on Δy. It means that the electromagnetic induction in the conducting embeddings is related to the cross-section perpendicular to the inducing magnetic field.

MTS curves ρ_T in case of $\lambda_1/h_1>40$ (when MT anomalies appear) deviate downwards from the curve ρ_N^{I} obtained over a three-layered profile in absence of embeddings. The deviation of the curve ρ_T from ρ_N^{I} depends on the dimensions of the embeddings. A zone with vertical and horizontal dimensions two and five times larger than its depth, can be taken as a limiting value, as the deviation between the curves ρ_T and ρ_N^{I} is not more than 5%. In case of embeddings of large dimensions this deviation can reach several ten percents, but the curves ρ_T did not have duplicate asymptotes and they did not approximate the normal curve ρ_N^{II} corresponding to the upper boundary of the embedding. A formal interpretation of MT sounding curves does not indicate the presence of an isolated conducting embedding and shows a fictitious rise in the conducting basement layer of the mantle. This behaviour of the magnetotelluric field can be explained by the three-dimensionality of the embeddings. For this reason it has to be concluded that in case of isolated zones using inductive generation the formal interpretation of MT curves in the class of 1-D Tikhonov–Cagniard models leads to rough mistakes.

One has to observe still that in real geological situations the induction effect can seem to be far weaker than in models giving just the maximum effect. However in the nature in spite of the accepted view, the inductive excitation can add a significant contribution to the anomalous EM field, as it can be seen from the parameter $|ka|$. E.g. for asthenospheric zones of specific resistivity $\rho=100$ ohmm, of 150 km effective radius, for periods $T=1$ min the induction is significant as $|ka|=18$, but if $T\geq 5$ min, that means $|ka|\leq 8$, the induction effect becomes weaker.

Role of the deep fractures

The resolution power of MT soundings over screened deep conducting zones can be enhanced by means of conductive current redistribution between sedimental overburdens and conducting zones in the crust or in the mantle which redistribution can be realized by deep fractures. In this connection a simple 3-D model has been studied to give a qualitative description on the role of deep fractures. MT soundings were made over a copper disc (of diameter $d=1.1$ m, thickness 0.2 m, $\rho \sim 3 \cdot 10^{-8}$ ohmm) placed at the bottom of the electrolyte layer ($h_1=2.2$ cm, $\rho_1 \sim 0.1$ ohmm), then an isolator film made of polyethylene was stuck on the same disc and at last in the film two holes of diameter 1 mm and at 1 m from each other were made along the diameter of the disc which was parallel to the inducing field. In this model the layer ρ_1 modeled the sedimentary overburden; the disc modeled the deep conducting zone; the polyethylene film modeled high resistivity rocks in the crust and in the upper mantle; and the holes in the film modeled conducting channels related to fractures. All of these three cases of MTS curves are shown in Fig. 5.

The completely opened disc behaves as a high conductivity basement of a two layered model giving an accordance between the curve ρ_T^d and the normal curve ρ_N^{II} calculated for $d=\infty$. For the isolated disc, the curve ρ_T^i is close to the normal curve ρ_N^I

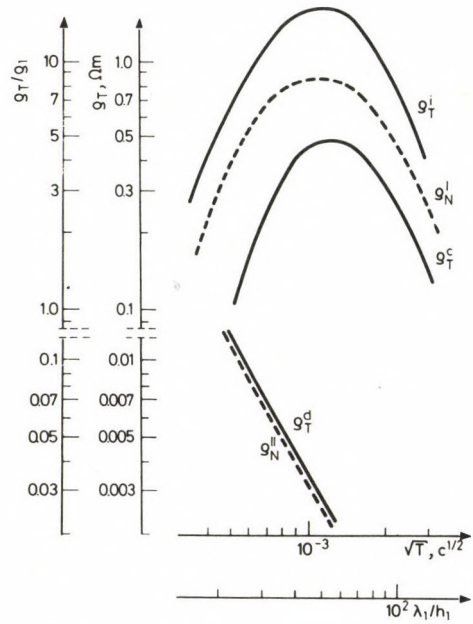

Fig. 5. MT sounding curves over the conducting disc having contact with the superficial layer.
ρ_N^I and ρ_N^{II}-normal (1-D) MT sounding curves for $d=0$ and $d=\infty$
ρ_T^i — MT sounding curve over the isolated disc
ρ_T^c — MT sounding curve over the isolated disc having contact with ρ_1

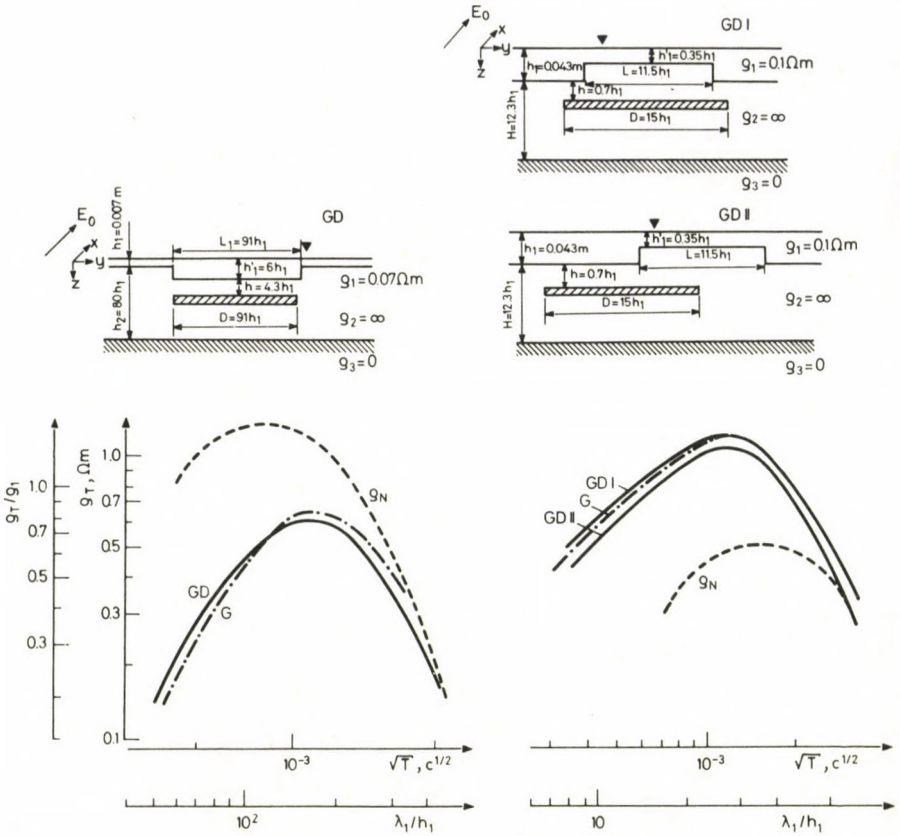

Fig. 6. MT sounding curves of the conducting layer in field of an inhomogeneous superficial layer. ρ_N — normal (1–D) MT sounding curve if $h'_1 = h_1$ G — MT sounding curve if $D = 0$ GD, GDI, GDII — MT sounding curves over the corresponding models

without the disc ($d = 0$). The imperfectly isolated disc shows another picture. In this case the curve ρ_T^c is below the curve ρ_N^I. The values ρ_T are about 8 times less than ρ_N^I, that means a threefold decreasing in the electric field. In this manner the holes in the insulating film, the area of which is 10^6 times less than that of the disc, can activate the galvanic mechanism. Through these holes a significant part of the current flowing in the layer ρ_1 branches into the conducting disc appearing clearly on MT curves.

The studied case gives a clear evidence that — due to fractures — the deep conducting zones become available for MT soundings. It is clear that a formal (1-D) interpretation of such MT curves can lead to rough mistakes but using this interpretation the deep conducting zones can be at least qualitatively detected.

In all investigated models the conducting zones were excited by a normal magnetic field having only horizontal components. Now the effect related to the

exciting magnetic field modified by surficial inhomogeneities and having a significant vertical component will be estimated. A three layered model described above, which has a quasi 2-D inhomogeneity of horst and trench in its first layer, was used (Fig. 6). In the layer ρ_2 there was a thin horizontal well conducting disc, the diameter of which was 10 times larger than the depth of location. The model was excited by plane wave propagating downwards having electrical vectors polarized along the horst (and the graben). If the layer ρ_1 is homogeneous, the conducting disc has no effect on MTS curves (galvanic screening). In case of models of horst and graben a significant magnetic field component appears which excites the disc. The magnetotelluric effect of the disc means a small displacement of increasing and decreasing branches of curves ρ_T (Fig. 6).

Therefore when studying the resolution power of deep MT sounding, the excitation of conducting zones by anomalous field caused by superficial inhomogeneities can be ejected as it was shown.

Conclusions

The physical modeling proves that the inductive excitation mechanism of deep conducting zones can give a noticeable contribution to the anomalous electromagnetic field and can appear on MTS curves. It is to be mentioned that the inductive excitation of isolated conducting zones cannot be included into the Tikhonov–Cagniard model and the interpretation of MT curves must be made in the class of 3-D models.

It has been shown by physical modeling that the conductive current redistribution realized by fractures essentially increases the resolution power of deep MT soundings.

Inductive excitation of crustal and mantle conducting zones by the anomalous magnetic field of superficial origin does not give an essential contribution to the MT sounding curves.

References

Berdichevsky M N, Dmitriev V I, Mershikova N A 1978: Magnetotelluric sounding of the inhomogeneous asthenosphere (in Russian). Kiev, Naukova Dumka, 8–9.

Berdichevsky M N, Kobzova V M, Moroz I P 1980: Physical modeling of the magnetotelluric field over inhomogeneous asthenosphere (in Russian). *Izv. Akad. Nauk. SSSR, Fiz. Zemli*, No. 5, 121–124.

Berdichevsky M N, Lebedeva I A, Nechaeva G P 1981: Magnetotelluric sounding of conducting layers of finite dimensions (in Russian). *Izv. Akad. Nauk. SSSR, Fiz. Zemli*, No. 3, 72–78.

Berdichevsky M N, Dmitriev V I, Barashkov I S, Mershikova N V, Kobzova V M 1982: Magnetotelluric sounding of the conducting layers in the earth's crust and in the upper mantle (in Russian). *Izv. Akad. Nauk. SSSR, Fiz. Zemli*, No. 7, 69–77.

Dmitriev V I 1981: Computation methods of electromagnetic fields in three-dimensional inhomogeneous media (in Russian). In: *Investigation of the deep structure of the earth's crust and the upper mantle from sees and oceans using electromagnetic methods.* Moscow, Izmiran, 24–30.

Moroz I P, Kobzova V M, Timoshin B V 1975: Physical modeling of electromagnetic processes in inhomogeneous media (in Russian). Kiev, Naukova Dumka.

Svetov B S 1973: Theory and interpretation of low-frequency geoelectric exploration (in Russian). Moscow, Nedra.

Acta Geodaet., Geophys. et Montanist. Hung. Volume 19 (3–4), pp. 267–271 (1984)

TECHNICAL PRINCIPLES OF PHYSICAL MODELING IN GEOELECTRICS*

I P Moroz[1]

[Manuscript received March 25, 1983]

Physical modeling of electromagnetic fields has been widely applied in geophysics to solve 3-D geoelectric problems. A modeling equipment has been built in Lvov in the Institute of Applied Problems in Mechanics and Mathematics of the Ukrainian Academy of Sciences for modeling the magnetotelluric field and dipole-generated electromagnetic fields can be also modelled.

In this paper the modeling equipment is described. The construction method realized in Lvov assures a high measuring accuracy and many parameters of the EM field can be measured simultaneously both in E and H polarizations.

Keywords: analogue modeling; dipole method; geoelectric model; magnetotelluric modeling

Introduction

Physical modeling of electromagnetic fields has been widely applied to solve three-dimensional geoelectric problems as the mathematical modeling has certain limitations. Physical modeling has to be coupled to computers to process the measured data. Therefore it is necessary to assure a high reliability of the measured experimental amplitudes and phases of all field components.

A modeling equipment has been built in Lvov in the Institute of Applied Problems in Mechanics and Mathematics of the Ukrainian Academy of Sciences for modeling of the magnetotelluric field and dipole-generated harmonic electromagnetic fields can also be modelled.

Main parts of the equipment

Main parts of the equipment are as follows: an electrolytic tank containing NaCl-solution, two antennas perpendicular to each other, antenna amplifiers, a movable measuring probe by means of which the electromagnetic field is measured in the tank. Besides these parts, the equipment includes a frequency synthetizer, a block of

* Paper presented at the KAPG-Symposium on Electromagnetic Induction, Sopron, March 1983

[1] Institute of Applied Problems in Mechanics and Mathematics of the Ukrainian Academy of Sciences, Lvov

input filters for the intermediate frequencies ($f_i = 2.77$ kHz) with a phasemeter, a control oscillograph, AC–DC converters, millivoltmeters, analogue plotters with two coordinates, a frequency meter and a puncher.

Distortion effects to be eliminated

As it is known, a high accuracy can be reached in physical modeling if the antenna-effect is eliminated (first requirement) and a stable mutual orientation of the receiver dipoles in the primary generating magnetic field is assured (second requirement).

The first condition is fulfilled by carrying out the frequency transformation of the signal to be measured directly in the measuring block (MB) and by its transmission at first through an optical channel, then through a cable to the measuring and recording instruments. The measuring probe consists of two blocks: namely, the measuring block (MB) and the control block (CB). These units are stiffly connected to each other by an isolating tube. Inside of this tube there are luminours diodes to connect MB and CB. Figure 1 shows the functional scheme of MB. The frequency transformers have high-impedancy, symmetrical inputs for the receiver dipoles and also have a low output intermediate frequency, $f_i = f_h - f_s$. The intermediate frequency is amplified and by means of the luminous diodes transformed into a light signal which reaches through an optical fibre of 0.5 m length a photo-diode and a photoamplifier in CB. Signals coming from CB to the measuring and recording instruments are transmitted through an electric cable.

In magnetotelluric sounding (MTS) and profiling (MTP), the second condition mentioned above is fulfilled by generation of a circularly polarized primary magnetic field. In the frequency sounding method (FRS) there is usually an inflexible connection between the generating- and receiver dipoles and so the second condition can be fulfilled easily. As it is known, the directional characteristics of electromagnetic dipoles have sharp minima. The minima of dipoles measuring field components perpendicular to the primary field generally coincide with the primary magnetic field vector. If the mutually perpendicular orientation of the dipole and of the generating field vector is not ensured, the primary field is also sensed that in this case means a disturbance. In order to avoid such an effect, the primary field must be homogeneous at the surface of the tank and the receiver dipoles in the measuring probe must be in right orientation.

In case of a linearly polarized field and also in case of fields having a rotating polarization vector, there are at least two different disturbing effects: the presence of electric cables near to the tank, unsatisfactorily perpendicular orientation of the walls of the tank, etc. All of these effects increase the error of measurements and as a consequence the modeling of deep geoelectric structures becomes hopeless at frequencies higher than 3 MHz.

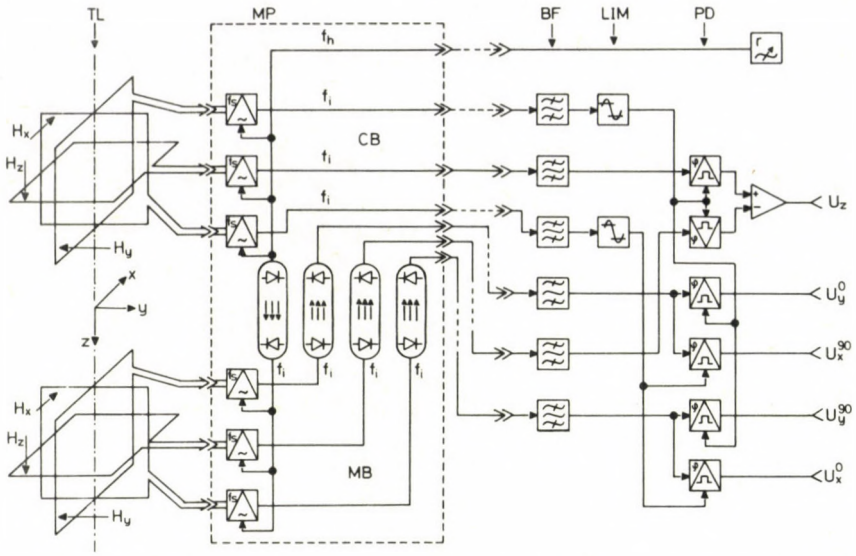

Fig. 1. Functional scheme of the modeling equipment. RD — receiver dipoles, MP — measuring probe, TL — transmitter lines, BP — processing block, FT — frequency transformer, BF — band filters, LIM — limiters, PD — phase demodulators, f_h — frequency of the heterodyn, f_s — frequency of the signal, CB — control block, MB — measuring block

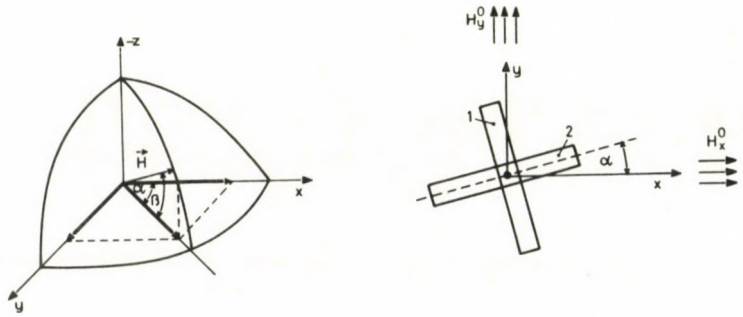

Fig. 2. Position of the magnetic dipoles in the horizontal plane of the tank, α — horizontal fault angle, β — vertical fault angle, $h = H_0 e^{-j(\omega t - kz + \varphi)}$ — vector of the generating field

Figure 2 shows the positions of the receiving magnetic dipoles in the horizontal plane of the tank for a plane-polarized magnetic field H_x^0 or H_y^0, using an xyz system of coordinates. In case of a generating field H_x^0 magnetic dipole 1 (at $\alpha = 0$) records its value, and dipole 2 records the quadrature component which appears in presence of geoelectric models. Similarly, in case of a field H_y^0, dipole 2 records H_y^0 and dipole 1 the quadrature component. This is valid in case of magnetic field generation with rotating

polarization vector too, namely with circular polarization being a superposition of two linearly polarized waves where the phase-shift in the plane is 90°. This field can be expressed by the following function: $\vec{H} = H_m e^{-j(\omega t - kz + \varphi)}$ where k is the wave number, z is the direction of propagation, φ is the phase oscillation of the current at $z = 0$ and $t = 0$.

Construction of the measuring unit

In the following the construction method of the measuring unit including MP will be surveyed. By the present method the error arising from an incorrect orientation of the measuring probe can be eliminated.

The field components H_x^0 and H_y^0 (Fig. 2) and the corresponding perpendicular secondary components H_y^{90} and H_x^{90} (which appear in presence of geoelectric models) are found by a multiplication (phase demodulation) of the e.m.f. produced in loops 1 and 2 by the potential differences of the basic oscillations with given phases. To obtain the primary fields H_x^0 and H_y^0 it is necessary that the zero values of the phase of the basic oscillation should coincide with the moment when the vector of the rotating magnetic field coincides with the axes y and x. In order to obtain the secondary horizontal fields H_x^{90} and H_y^{90} the zero values of the phase of the basic oscillations have to coincide with the moment when the vector of the rotating magnetic field coincides accordingly with the axes x and y.

Basic oscillations mentioned above can be directly obtained from the generating magnetic field $\vec{H}$ by means of perpendicular frame-like antenna-dipoles (Fig. 1), situated in the special control block (CB).

The frame-like receiver antennas of the control block (CB) are directly above the measuring block (MB). If these blocks are connected stably and the dipoles are co-orientated correctly, the necessary basic oscillation can be obtained. Using this method, the error caused by an incorrect orientation of the measuring probe and by the error of polarization is automatically eliminated. In this manner not only the measuring accuracy has been increased, but the following four components of the magnetic field can be also recorded in the circularly polarized field: the primary H_y^0 and the secondary H_x^{90} in case of an x-polarized field; the primary H_x^0 and the secondary H_y^{90} in case of an y-polarized field. This method can be also realized for electric fields using electric measuring dipoles.

An augmentation in the measuring accuracy of the horizontal electromagnetic field components increases the measuring accuracy of the vertical magnetic component H_z. The measurement is based on the mutual compensation of the errors which appear in MB and in CB when receiving the vertical magnetic field component. According to experiments the accidental deviation of the planes of the frame and of the primary rotating magnetic field can fluctuate from 0° (in case of a precise dipole unit) to $\pm 5°$ (in case of an inaccurate mechanism to move the MB along the profile). Besides, as it was

mentioned, the fault angle between the rotation plane of the primary magnetic field vector and the normal position ($\beta = 0°$, Fig. 2) may result in an inhomogeneity of the primary field. In order to avoid this effect, the following method has been applied (see Fig. 1): Inside the control block (CB) there is also a vertical dipole similarly as in MB. By means of the phase detector signals of both dipoles are detected and their difference is produced. One of the basic horizontal components (H_x^0 or H_y^0) is received to have a basic oscillation.

Multiplication of potential differences of the receiver dipoles with the basic voltage is carried out by a phase demodulator (PD) as it can be seen in Fig. 1. For reasons of comfort the phase demodulation is made at a fixed and low enough intermediate frequency. Therefore, before the signal coming from the electromagnetic dipoles would reach the phase demodulator, its frequency was transformed by a frequency transformer. Using this method, a good separation from the external generating magnetic field can be realized and a suppression of the signal by the strong primary field can be prevented. Besides, at low enough frequencies the error related to the transmission of the basic phase is a minimum and does not depend on the length of lines and on the displacement of the wires when moving the measuring probe along the investigated profile.

Axes x and y of the Cartesian system of coordinates are parallel with the bottom of the tank and the axis is parallel with the vertical walls.

Conclusions

If a magnetic field of circular polarization is generated and the basic oscillations are produced in a special control block (CB) of the measuring probe, not only the measuring accuracy can be increased, but also many parameters of the electromagnetic field can be measured simultaneously in E and H polarization. This is an important feature for a computerized data-processing. There is also a possibility to detect the direction of the extension of the investigated geostructure, and even to measure phase relations between optional field components.

Acta Geodaet., Geophys. et Montanist. Hung. Volume 19 (3–4), pp. 273–283 (1984)

HYDROMAGNETIC DIAGNOSTICS OF THE NONHOMOGENEOUS STRUCTURE OF THE SOLAR WIND

V A TROITSKAYA[1] and O V BOLSHAKOVA[1]

[Manuscript received April 10, 1983]

The determination of the parameters of the magnetosphere and of the solar wind by means of ground based observations of geomagnetic pulsations (GP) is defined as hydromagnetic diagnostics (HD). The connection of GP properties with different parameters which have to be determined involves complicated relationships. Therefore the development of the methods of HD is based at this stage mainly on empirical relations, describing the correlation of different parameters to be determined by GP properties and the analysis of the stability of the obtained correlation. Then empirical formulae are deduced, and criteria for HD elaborated. In this paper only the type of continuous GP as a tool for determination of solar wind (SW) properties is considered.

Keywords: geomagnetic pulsations; hydromagnetic diagnostics; nonhomogeneous structure; solar wind

The main parameters of Pc which are used in the diagnostics are periods, amplitudes, specific signatures and subdivision into groups (Pc 3, 4, 5). Special events, such as global Pc disappearances, sharp changes of their regimes, as well as the occurrence of one or other Pc groups are also important in the identification of inhomogeneities of the SW structure.

The goal of this investigation was to identify equatorial and polar coronal holes, solar flares, disappearance of filaments, and NCDE using specific combinations of Pc properties which reveal the type of the streams connected with the sources of the SW. In spite of the existence of direct observations of flares, coronal holes, filaments, NCDE, the development of indirect methods, the identification of these sources of different type solar streams is by itself valuable. Indeed, they can be used for a retrospective analysis for periods, when direct observations are absent. Moreover using ground based records of GP this identification can be tried at many observatories, without solar observations which are scarce, and the data of which are available only with significant delay. Finally, the proposed indirect method allows to conduct the diagnostics uninterruptedly by means of rather simple and inexpensive equipment.

[1] Institute Physics of the Earth, of the Acad. of Sci. of the USSR, B. Gruzinskaya 10, Moscow D-242

Strong equatorial coronal holes

A rather big number of coronal holes (CH) were observed in 1973–1974. Usually, the appearance of each CH near the solar equator was followed by a long lasting high speed stream (Krieger et al. 1973, Akasofu 1976, Shelly et al. 1976). Figure 1 shows the relative distribution of high speed streams from CH-s, and Pc3–4 regimes during several solar rotations. If we take into account the time (Δt) of propagation of the stream from the Sun to the Earth and shift the appearance of CH, the highest speeds of the streams are observed from the CH and in each case in addition to mixed Pc3–4 pulsations quasiregular "pure" Pc3 appears, too. The appearance of pure Pc3 is one of the most typical indicators of the connection of the high speed stream with a strong equatorial hole.

Using the results of previous investigations of Pc properties, we can define in a following way the requirements for high speed streams to generate "pure" Pc3:

1. Pc3 amplitudes due to SW streams from CH are usually high. As the Pc3 amplitudes depend on SW velocity, it can be estimated using e.g. the relation (Bolshakova et al. 1979)

$$V, \frac{\text{km}}{\text{sec}} = (380 \pm 60) + (150 \pm 50) \cdot Apc3\,(\text{nT}).$$

The estimates for streams from CH give usually high velocities.

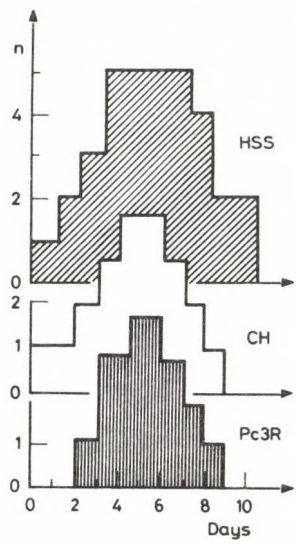

Fig. 1. Distribution of the frequency of occurrence of high speed streams (HSS), coronal holes (CH) and pure Pc3R regimes relative to the sector boundary for solar rotations N 1909–1913. Vertical axis: number of occurrence. Horizontal axis: days in the sector. Zero day in the sector boundary

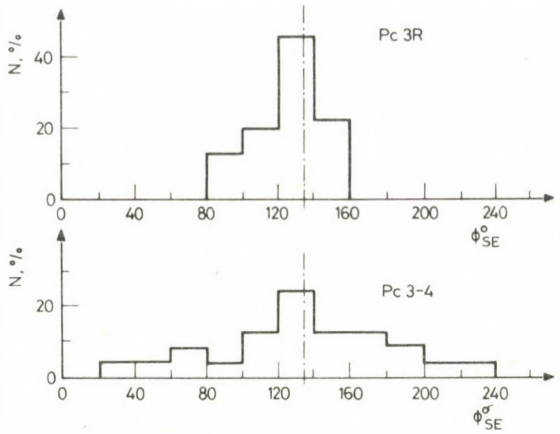

Fig. 2. Distribution of the IMF direction in the plane of ecliptic for pure Pc3R and Pc4R and for mixed Pc3–4 and Pc3–4–5 regimes. Vertical axis: frequency of occurrence of a given direction in percent from the total number of cases. Horizontal axis: the angle in the plane of ecliptic in degrees. The dotted line corresponds to the direction of the Parker spiral

2. Pc3 amplitudes are modulated according to the orientation of the interplanetary magnetic field (IMF) (Bolshakova and Troitskaya 1968). As the variability of intense pure Pc3-s is not significant, it can be assumed, that the orientation of IMF has only small deviations from its optimal position for Pc3 generation. This suggestion was confirmed by the character of the distribution of IMF directions for the periods of Pc3 occurrence (Fig. 2).
3. As the pure Pc3 is characterised by the quasiconstant period of pulsations, and its period is determined by the value of the IMF ($T\text{sec} \approx 160/B$, nT) (Vinogradov and Parchomov 1974, Troitskaya et al. 1971, Gul'elmi and Bolshakova 1973, Verő 1979) we expect that in case of pure Pc3 the fluctuations of the IMF magnitude should be small. The standard deviation (SD) of the IMF magnitudes Pc3 for mixed Pc-s are about 20% ($\text{SD} \approx (0.8 \div 1)$nT) and for pure Pc3 3–5% ($\text{SD} \approx (0.25 \div 0.3)$nT). For mixed irregular Pc-s the SD reaches values of several nT (Fig. 3).

The general conclusion from the analysis of the Pc signature is that high speed streams which generate pure Pc3 have more homogeneous structures than those which generate mixed Pc3–4.

Flares

Bolshakova et al. (1978) have investigated the connection between variations of the Pc regime before and after intense isolated proton solar flares. The modified index of the variability of Pc3 amplitudes was used for the diagnostics. This index represents the sum of time intervals in minutes for a whole day during which Pc3 is absent. Its

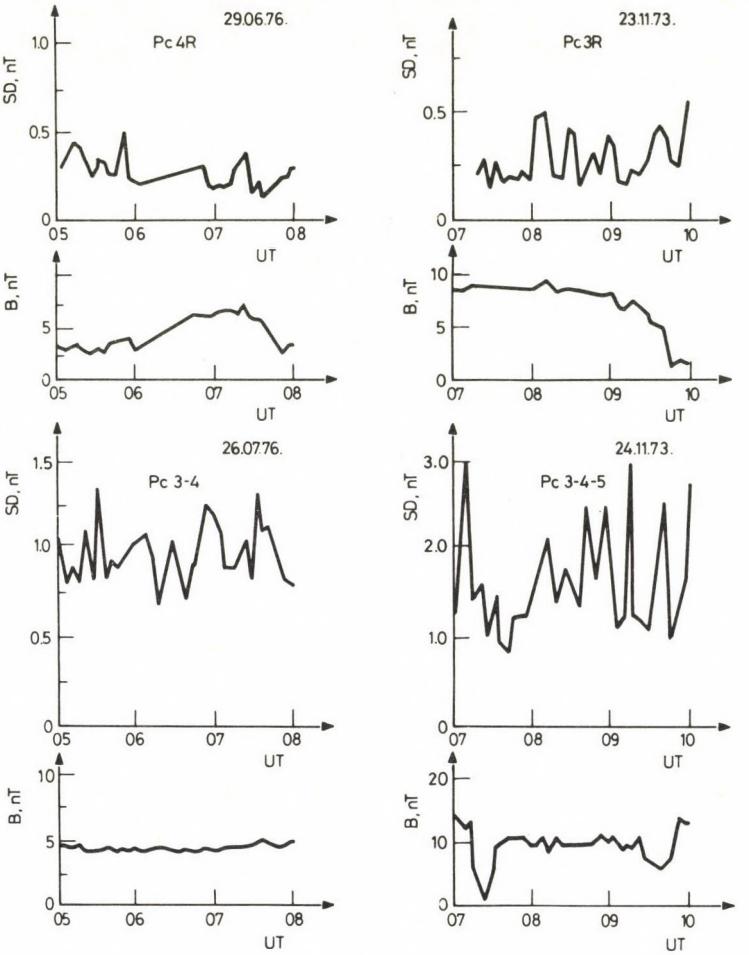

Fig. 3. Comparison of the standard deviations (SD) of the IMF magnitude for pure (above) and mixed (below) Pc-s

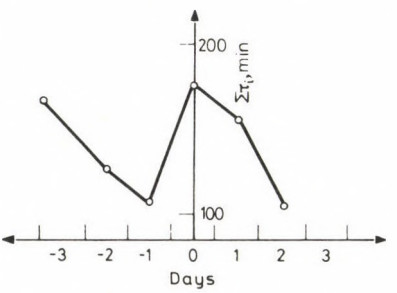

Fig. 4. The modified index of Pc3 variability $\Sigma\tau_i$ around a day with solar flare. Vertical axis: $\Sigma\tau_i$ in minutes. Horizontal axis: Days relative to the day of flare

changes in respect of the day of the flare were analysed. Investigations of its behaviour for a high number of flares showed that there exists a definite signature before the flares. Namely, $\Sigma\tau_i$ begins to rise 1–2 days before the flare, i.e. there is a greater number of time intervals during which Pc3 disappears. That means that the number and the dimensions of the inhomogeneities of the IMF in solar streams before the flares increase (Fig. 4). The increase of the disturbances of the magnetic fields on the Sun before the flare is confirmed by observations of the solar radioemissions, brightness and velocities in the photosphere. The estimation of inhomogeneities of the IMF based on information on the varability of Pc regimes is at this stage only qualitative. Further investigations aim to find quantitative criteria.

Weak polar coronal holes and solar filaments

Weak polar coronal holes and filaments were the main sources of high speed streams during the period of solar minimum (1976) and in the phase of solar activity increase. Practically no equatorial coronal holes were observed during these years. For some of the observed streams the sources can be identified with polar coronal holes (e.g. in September–October 1976 (Nolto et al. 1977, Fig. 5) and for others with the disappearance of filaments. E.g. the stream 03.10–03.11.1976 which originated most probably in the region of the disappearance of a filament (S 40°, E 40°), as at this time no other source could be found on the Sun (Joselyn and McIntosh 1981). The disappearance of a filament leads to the emission of a high speed stream which can reach the Earth and causes an increase of the geomagnetic activity only if some specific conditions are fulfilled (Joselyn and McIntosh 1981).

Direct solar observations, however, do not provide up to now quantitative criteria which enable to estimate the probability of occurrence and the intensity of the subsequent geomagnetic disturbance. The difficulties of these estimates are due to specific and changing conditions of the propagation of solar streams in the interplanetary space and their interaction with the magnetosphere. Geomagnetic pulsations give additional information on the details of such interactions and can be used as criteria for the estimates. The Pc regimes typical for streams emitted from polar coronal holes and from disappearing filaments belong to the classes of mixed Pc3–4 and Pc3–4–5. Pure Pc3 *R* are practically absent. The structure of these streams in respect of geomagnetic pulsations is presented in Fig. 6.

The figure shows that the occurrence of different Pc regimes in streams from different solar sources is quite different. The streams from equatorial coronal holes are dominantly characterized by pure Pc3 and Pc3–4. Streams from polar coronal holes and filaments excite mixed Pc3–4–5 and pure Pc4 regimes.

The last two types of streams are less stable judged from the corresponding type of Pc regimes as regards the IMF magnitude and direction, than streams from

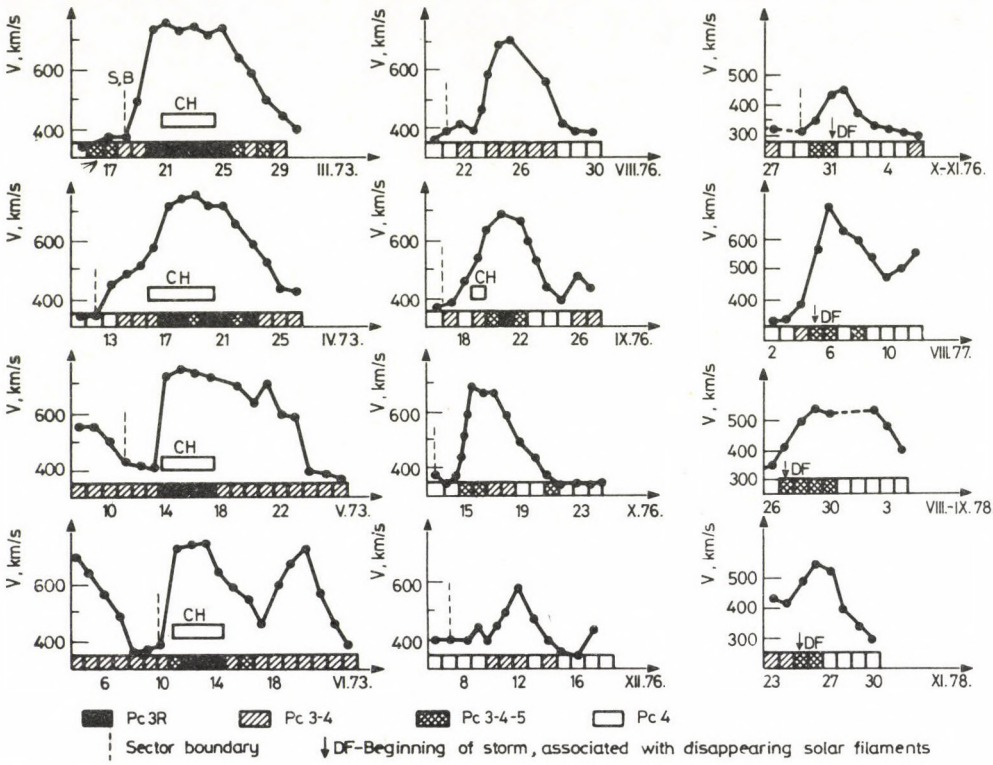

Fig. 5. Connection between HSS, CH and filament disappearences and geomagnetic pulsations in different phases of solar activity. (Explanation in the text.)

equatorial coronal holes. The degree of instabilities of these quantities in different streams can be seen comparing the corresponding plots presented in Figs 2, 3.

It should be mentioned that the streams from different sources differ not only by the magnitude and the direction of the IMF in the stream and its velocity, but also by the distribution of the density. For streams from strong equatorial holes, high values of the density are observed only in a narrow zone at the front of the stream. For streams from polar coronal holes and disappearing filaments high values of density are often observed not only at the front of the stream, but also inside it. This distribution of density explains the appearance of a great number of mixed Pc3–4–5 in these less intense streams, and the sharp changes from these regimes to pure Pc4 when the solar wind speed drops, but the density still remains relatively high.

Noncompressive density enhancements (NCDE) in the quiet solar wind

Using the same methods we have tried to identify the recently discovered NCDE near the orbit of the Earth. NCDE are large scale formations of cold plasma which move with the surrounding gas with an average speed 320 km/s (Gosling et al. 1977, King 1977). As NCDE have specific properties which distinguish them from other density enhancements in the solar wind it was expected, that they have also specific signatures in GP. The analysis of GP-s for 30 cases of NCDE lead to following conclusions as regards properties of geomagnetic pulsations corresponding to NCDE.

1. A sharp decrease of Pc3–4 intensity which is due to a decrease of SW velocity.
2. Occurrence of specific mixed irregular Pc3–4 which is the consequence of a large dispersion of the IMF magnitude.
3. A sharp increase of the index of the Pc variability which is for the same level of SW speed an indication of the dominantly azimuthal direction of the IMF.

The degree of irregularity in the IMF magnitude and direction for different cases of NCDE can be estimated by the dispersion of Pc periods and by the index of

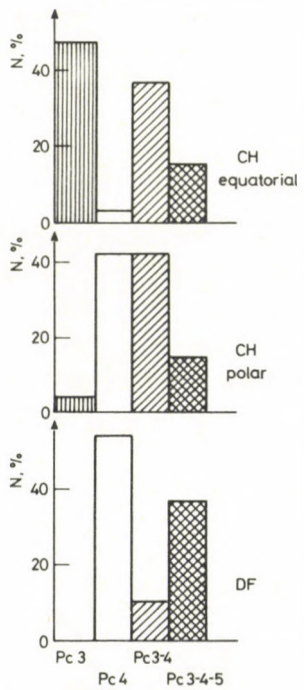

Fig. 6. Distribution of occurrence of different regimes of pulsations in solar streams from equatorial coronal holes (I) and from disappearing filaments (II)

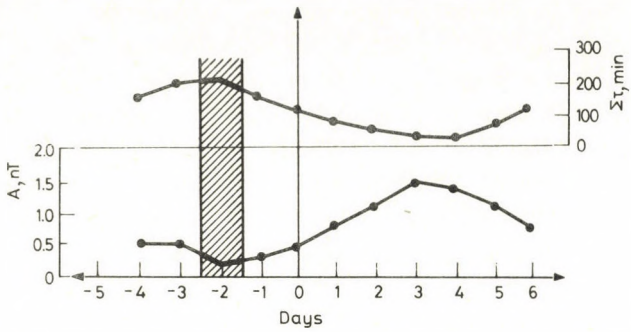

Fig. 7. Average distribution of Pc3–4 amplitudes and of the index of variability ($\Sigma\tau_i$) at sector boundaries

variability. The increase of these quantities indicates the increase of fluctuations in B and in its direction (Bolshakova and Troitskaya 1980b). Figure 7 shows the change of the average amplitude and of the index of variability in respect to several sector boundaries. The changes of these parameters can be used together as an indication of NCDE-s at the Earth's orbit. Moreover, the specific signature of these parameters can be considered as one of the precursors of the high speed streams which often occur after the crossing of sector boundaries.

Variations of the number of equatorial coronal holes and of NCDE in the solar cycle

Using the GP records and the previous criteria the number of CH-s and NCDE-s can be estimated in any phase of the solar cycle. These estimates can be especially important when direct observations of CH-s and NCDE-s are not available. Moreover, ground based observations encompass much longer time intervals than satellite and rocket observations on which direct observations were initiated only during the last decade. Figures 8 and 9 show the variation in the occurrence of CH-s and NCDE-s in the solar cycle obtained by GP records.

Data of direct observations of CH-s on board the satellites OSO–7 and Skylab for 1973–1974 on the same plots show a rather good coincidence of the values obtained by direct and indirect methods. The systematically higher number of CH-s obtained by direct observations can be understood from the following. Direct observations do not give the number of CH-s, but the number of days during which the CH crossed the central meridian. As pure Pc3 which is used to identify CH are observed only in the central part of the high speed stream from the CH—the number of days with pure Pc3 will be always less than the number of days of CH-observations. By introducing some coefficients, and taking into account the average longitudinal dimension of the CH,

better estimates can be obtained on the true CH-occurrence. One can argue that information on coronal holes can be obtained from the analysis of recurrent storms, and ask what additional contribution GP can give for improving the ground based methods for CH identification. The answer is that GP gives an insight into the fine structure of recurrent storms which is as important as general information on velocity and duration of high speed streams. Moreover, the signature of GP gives additional information on the number and dimensions of inhomogeneities of the IMF in the streams and in this way helps to distinguish the sources of these streams.

The occurrence of CH in the cycle of solar activity seems to depend on the phase of the complete (22 years) cycle. Indeed the main maximum of CH occurrence appears in the decreasing years of activity of the 20th cycle. The decreasing years of the previous (19th) cycle did not show significant enhancements of the magnetic activity (Ap) and correspondingly the increase in the number of identified CH is not very pronounced. It is interesting to note that a CH was first discovered by Waldmayer in the decreasing years of the 18th (even) cycle when their number was most probably great.

The variation of NCDE-s in the solar cycle was obtained also using their observed GP signature. Unfortunately we have no systematic direct data on NCDE during different years of solar activity. However, some data from different authors seem to confirm the shape of their variation presented in Figs 8, 9. By Newkirk et al. it was suggested that the maximum number of NCDE should be observed in the years of solar maximum. The cyclic variation of NCDE-s obtained as a result of diagnostics based on GP corresponds to this suggestion. The increase of the number of NCDE in the years of

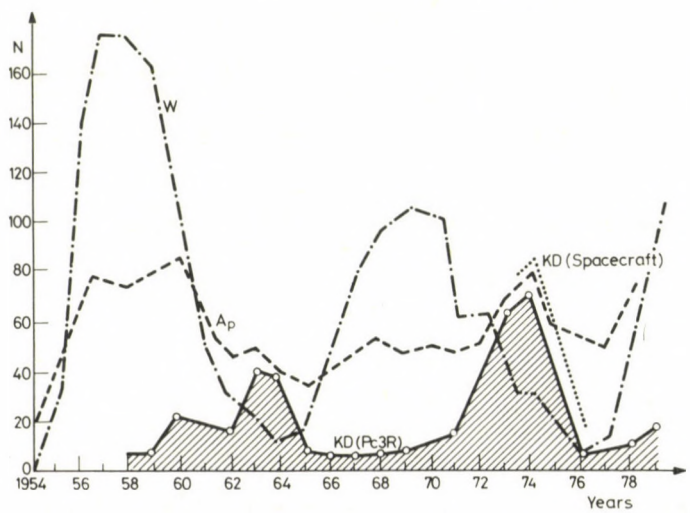

Fig. 8. Variation in the solar cycle of the: I. number of days when coronal holes were observed by satellites KD (Spacecraft), II. number of days when pure Pc3R regimes, identifying equatorial CH were observed KD (Pc3R), III. relative sunspot number

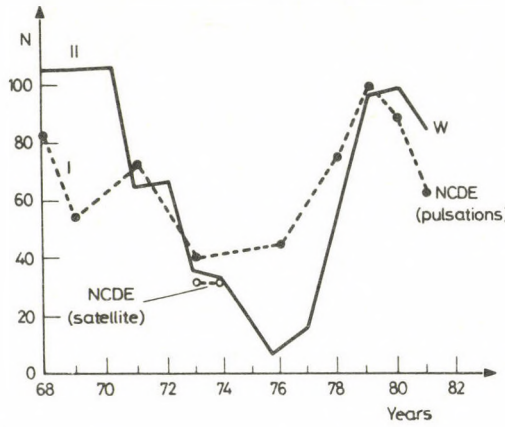

Fig. 9. Variation in the solar cycle of the: I. number of days when irregular mixed Pc3–4 regimes with small amplitudes (identifying NCDE) were observed, II. relative sunspot number — W, III. number of days with parameters of the solar wind corresponding to NCDE

the maximum of solar activity may be one of the factors influencing the solar cycle variations of cosmic ray intensity. Indeed NCDE-s present inhomogeneities on which cosmic rays can be scattered and cause their well known modulation of intensity in the solar cycle (Newkirk et al. 1976).

On the other hand Gosling et al. (1977) mentioned that in average 2.7 NCDE-s were observed in a month during 1973. If we take this number of NCDE per month as a representative one, we obtain for 1973—32 cases of NCDE. The analysis of GP records gives 39 cases of NCDE for 1973. These numbers are sufficiently close to each other.

The suggested hydromagnetic methods of diagnostics can be used for the clarification of differences in the fine structure and degree of inhomogeneity of solar streams from CH and in NCDE in different phases of the whole solar cycle.

The possibility to identify different sources of high speed streams using information on their fine structure using GP, presents a new direction of ground based studies of inhomogeneities in the SW. The development of the suggested method requires greater amount of direct observations and detailed comparisons with GP recorded on a number of stations ensuring uninterrupted monitoring on the sunlit side of the Earth.

References

Akasofu S I 1976: Solar cycle review. In: *Proceedings of the international symposium on Solar-Terrestrial Physics*, Boulder, Colorado, USA, vol. 1, 1–34.

Bolshakova O V, Troitskaya V A 1968: The connection of the direction of the IMP with Pc regime. *Reports of Ac. Sciences of USSR*, 180, 343.

Bolshakova O V, Troitskaya V A 1980a: Diagnostics of high speed streams and of the coronal holes by means of geomagnetic pulsations. *Geom. and Aeronomy*, 20, 102–106.

Bolshakova O V, Troitskaya V A 1980b: Diagnostics of big scale density enhancements in the quiet solar wind. *Geom. and Aeronomy*, 20, 163–165.

Bolshakova O V, Mirochaitchenko L, Troitskaya V A 1978: Continuous pulsations, conditions of propagation of solar cosmic rays and pre-flare situation on the sun. *Bul. Cosmic rays*, No. 19. 69–80.

Bolshakova O V, Lotova N A, Troitskaya V A, Chashey I V 1979: On the possibility of prediction of geomagnetic activity and pulsations using interplanetary scintillations. *Geom. and Aeronomy*, 19, 508–512.

Gosling J T, Hidner E, Asbridge J R, Bame S J, Feldman W C 1977: Noncompressive density enhancements in the solar wind. *Journ. of Geophys. Res.*, 82, 5005–5010.

Gul'elmi A V, Bolshakova O V 1973: Diagnostics of the IMF using data on the Pc2–4 periods. *Geom. and Aeronomy*, 18, 535.

Joselyn J A, McIntosh P S 1981: Disappearing solar filaments: a useful predictor of geomagnetic activity. *Journ. of Geophys. Res.*, 86, 4555–4564.

King G J 1977: Interplanetary Medium Data Book–Appendix. NSSDS/WDC–A–R ScS 77–04a, NASA/GSPC

Krieger A S, Timothy A F, Roelof E C 1973: A coronal hole and its identification as the source of a high velocity solar wind stream. *Solar Phys.*, 29, 505.

Newkirk G Jr, Hundhausen A J, Pizzo V 1976: Solar cycle modulation of galactic cosmic rays: the role of coronal transients. *Journ. of Geophys. Res.*, 81.

Newkirk G Jr, Hundhausen A J, Pizzo V 1981: Solar cycle modulation of galactic cosmic rays: speculation on the role of coronal transients. *Journ. of Geophys, Res.*, 86, 5387–5396.

Nolto J T, Davis J M, Gerassimenko M, Lazarus A J, Sullivan J D 1977: A comparison of solar wind streams and coronal structure near solar minimum. *Geophysical Research Letters*, 4, 291–294.

Shelly N R Jr, Harvey J W, Feldman W C 1976: Coronal holes, solar wind streams and recurrent geomagnetic disturbances: 1973–1976. *Solar Phys.*, 46, 201.

Troitskaya V A, Plyasova-Bakumina T A, Gul'elmi A V 1971: Connection between Pc2–4 pulsations and the IMF. *Reports of Ac. Sciences of USSR*, 197, 1312.

Verő J 1979: Geomagnetic pulsations and parameters of the interplanetary medium. Magnetospheric Study, 1979. Proceedings of the International Workshop on Selected Topics of Magnetospheric Physics, Tokyo

Vinogradov G A, Parchomov V A 1974: HM waves in the solar wind as a possible source of Pc3 pulsations. *Geom. and Aeronomy*, 15, 109.

Acta Geodaet., Geophys. et Montanist. Hung. Volume 19 (3–4), pp. 285–295 (1984)

SHORT-PERIOD VARIATIONS OF THE VERTICAL ELECTRIC CURRENT IN THE AIR

S V ANISIMOV[1], N N RUSAKOV[1], V A TROITSKAYA[1], J VERŐ[2]

[Manuscript received April 17, 1983]

Data are presented on the measurements of the variations of the electric current in the air at mid-latitudes in the ranges 2.5–0.1 Hz and 0.1–0.01 Hz. It is shown that there are essential differences in the character of the variations of the vertical electric current and of the magnetic field in the range 0.1–0.01 Hz, namely of their distribution in local time and dependence on Kp-index. Signals of unknown provenance with a *V*-shaped spectrum were recorded in the vertical electric current and in the magnetic field in the range 2.5–0.1 Hz. The model of an oscillation of the space charge in the near Earth layer due to infrasounds is suggested to explain some of the observed variations.

Keywords: atmospheric electricity; geomagnetic pulsations; infrasound; space charge in air; vertical current

The study of annual, seasonal, diurnal variations of the atmospheric potential gradient, electric conductivity and vertical electric current are traditional problems when dealing with atmospheric electricity. All these problems are closely connected with the verification of existing theories of atmospheric electricity, their development and the explanation of the unitary variation of the potential gradient. Measurements of the atmospheric electric parameters are of interest in connection with a number of other problems such as the nature of geomagnetic pulsations, magnetotelluric studies, analysis of solar-biological relations and investigation of electric phenomena before and during earthquakes.

Recently some experimental papers (Chetaiev et al. 1975, Olson 1971, Park 1976) have appeared with the results which cannot be explained by the static model of the atmospheric electricity and evidences were found for an interconnection of electric phenomena in the low atmosphere with geophysical processes in the magnetosphere. The observed disturbances of the potential gradient in fair weather conditions were connected in some cases with magnetospheric sources (Olson 1971). The correlation between potential gradient and the sector structure of the interplanetary magnetic field (Park 1976) indicates the interconnection of the atmospheric electric parameters with the processes in the cosmic space surrounding the Earth.

[1] Institute of the Physics of the Earth Academy of Science of the U.S.S.R. Moscow D-242, B. Grouzinskaya St. 10

[2] Geodetic and Geophysical Research Institute of the Hungarian Academy of Sciences H-9401 Sopron, Múzeum u. 6–8, Hungary

A new interpretation of ground based observations of the Earth's electromagnetic field in the range of short-period fluctuations (Chetaiev et al. 1975) suggests the existence of a vertical electric component of the geomagnetic field pulsations in the air. However, simultaneous measurements of short-period fluctuations of the electric field in the air and of the magnetic field at middle latitudes do not show any stable correlation. This can be connected with a high level of tropospheric electric noises as well as with the existence of different sources generating geomagnetic pulsations and variations of the potential gradient.

This paper presents an analysis of the short-period fluctuations of the vertical electric current density (VECD) in the air in order to estimate their amplitudes and to determine the regularities of these variations in two frequency ranges — namely 10–100 s and 0.4–10 s. Continuous measurements were made in calm atmospheric conditions in a region without industrial pollutions. The records were made on charts and on magnetic tape. VECD variations in the atmosphere were measured by the potential drop method on a resistance which connects the antenna area with the ground. The resistance value and the effective antenna area were calculated taking into account the amplifier noise level and its input impedance (Fig. 1).

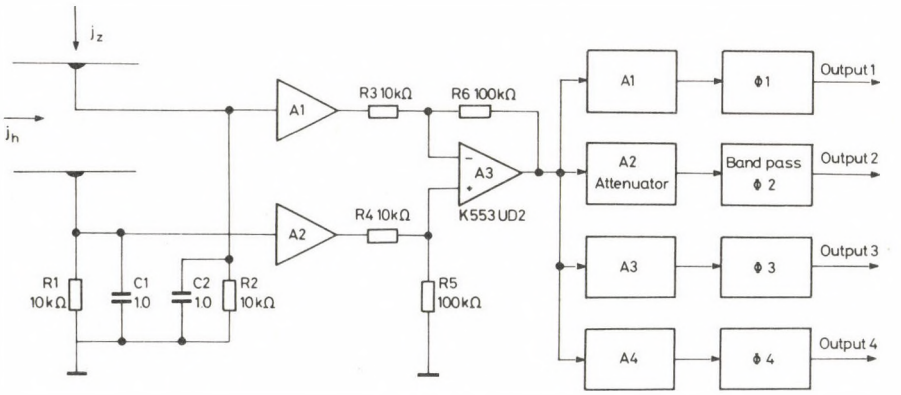

Fig. 1

Two wire grids situated parallel to the Earth surface one over the other at heights of 1.5 and 3 m were used as antennae. The area of each grid was 50 m^2.

The differential method of measurements was used in order to make no errors caused by the horizontal movements of local space charge. The third order active band filter was used to distinguish pulsations in the period ranges 10–100 s and 0.4–10 s. The threshold sensitivity of the device was 4×10^{-13} A/m^2. The study of fluctuations of the vertical atmospheric electric field and their correlation with pulsations of magnetospheric origin is hampered by frequent unfavourable atmospheric conditions such

as cloudiness, wind, precipitations, remote thunderstorms, fog, convective movements and atmospheric pollutions. The results of 20 round-the-clock continuous fair-weather observations at wind velocities less than 2 m/s were processed.

The fair-weather vertical current recorded at the Earth's surface is determined as a total current

$$j_z = j_{cd} + j_{cn} + j_{dp}$$

where j_{cd} — is the conductivity current
j_{cn} — the convective current
j_{dp} — the displacement current.

The method of measurements of the total VECD does not enable to distinguish these components, but it shows that the level of fluctuations is in the range of 10^{-11}–10^{-10} A/m^2 depending on the period of fluctuations. We evaluate each component and compare the results with observations.

An average level of the conductive current in atmospheric electricity is 10^{-12} A/m^2 (Chalmers 1974). The principle of quasi-stationary state being fulfilled, the amplitude of variations of the vertical current conductivity has the order of the average level. It is less than the value of the recorded fluctuations (Fig. 2).

The movement of the space charge driven by forces of non-electric origin determines the convective current. Turbulent diffusion is one of the mechanisms responsible for convective current. It is proportional to the wind velocity (Gul'elmi et al. 1979). The convective current generated by the movement of the space charge can be presented as

$$j_{cn} = \sigma \cdot V$$

where σ — is the space charge density
V — the charge movement velocity.

Data on the spectrum of the atmospheric turbulence are given by Fooks (1955). The average wind velocity being 2 m/s, the mean square velocity of the vertical movements is about 30 cm/s at a height of 70 cm from the surface. Taking the average value of the space charge equal to $500 \cdot 10^{-12}$ C/m^3 (Chalmers 1974) and assuming the velocity of the vertical movements of the wind in the above magnitude, the convective current is $j_{cn} \simeq 1.5 \cdot 10^{-10}$ A/m^2. It is close to the average value of the recorded variations of the current density (see Fig. 1).

The model of the horizontal propagation of inhomogeneous plane electromagnetic waves suggests the existence of a vertical component of the electric field intensity in the air as an integral part of the primary wave. In this case the variations of the potential gradient of the atmospheric electricity would be induced by the vertical component of the electromagnetic wave. According to the previous experimental data they can reach the value ~ 5 V/m (Chetaiev et al. 1975) for continuous Pc2, 3 pulsations at mid-latitudes.

The observed variation of the potential gradient with a period $T=10$ s yields for the displacement current:

$$j_{dp}=\varepsilon_0 \frac{\partial E_z}{\partial t} \sim 10^{-11} \text{ A/m}^2.$$

This value coincides with the amplitude of the observed fluctuations.

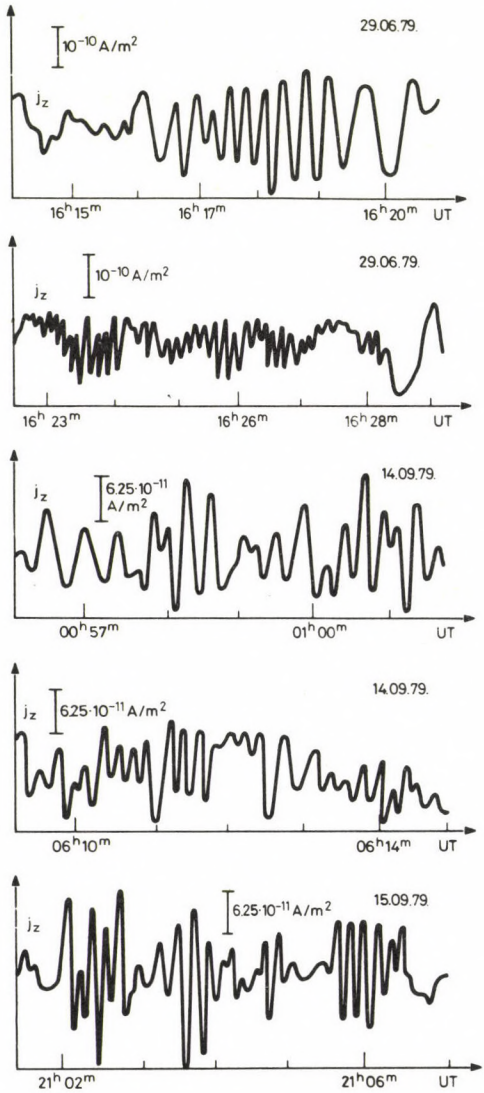

Fig. 2. Examples of short-period fluctuations of VECD in the air

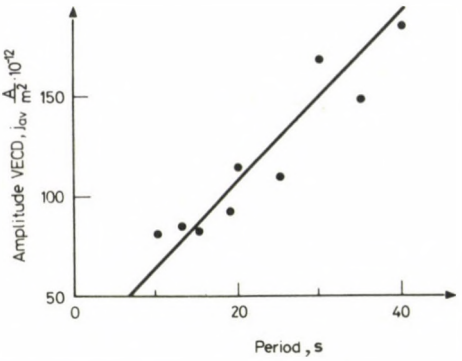

Fig. 3. Dependence of the average amplitudes of the VECD pulsations on their period

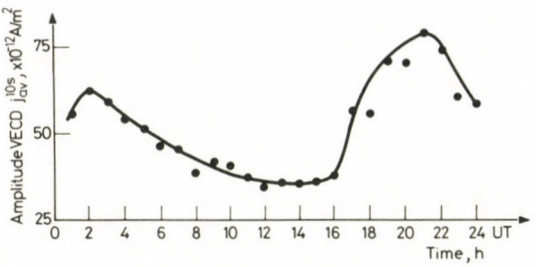

Fig. 4. Diurnal variation of the amplitude of the short-period VECD fluctuation. The average amplitude of the variations (j_{av} 10 s) is normalized to a period $T=10$ s, accounting for the dependence shown in Fig. 3

Figure 3 presents the dependence of the average amplitudes of the VECD pulsations on their period. The amplitude of pulsations increases by 6 db when periods increase by an octave. The function vertical current amplitudes *vs* period is similar to that of geomagnetic pulsations.

The diurnal variation of the vertical current during the observed period is given in Fig. 4. Taking into account the dependence in Fig. 3 the average amplitudes of the variations are normalized to a period of $T=10$s. The diurnal variation of the amplitudes have two maxima with values exceeding by 50% the average value. In contrast to the diurnal variation of the atmospheric potential gradient with maxima from 0700 to 1000 and from 1900 to 2200 UT, the maxima of short-period fluctuations of the VECD appear at 0100–0300 and at 2000–2300 UT. It is necessary to stress that mainly fluctuations with periods $T=10$–30s typical for these time intervals are responsible for these maxima. For the investigation of the correlation of these variations with magnetic activity the dependences of the variations of the amplitudes

(normalized to $T=10$ s) and of the relative number of VECD variations of different periods (10–30 s) were studied from Kp. In addition the number of observed cases was normalized for each Kp (Fig. 5). Fluctuations with $T=10$s have a maximum of occurrence at Kp = 2; 20 second fluctuations have a maximum at Kp = 4. Fluctuations with $T=30$ s were observed with approximately the same probability for all values of Kp.

It is important to note that the dependence of Pc2–3 occurrence on Kp in the vertical electric field does not coincide with that for geomagnetic pulsations. Indeed, it is known that for geomagnetic pulsations smaller periods are observed at higher values of Kp. Figure 5 shows that the dependence of the periods of fluctuations in the electric field on Kp is opposite.

Experimental results show that the variations with $T=20$–30 s are most typical in the range 10–100s, and their amplitudes reach the values $j_z = 10^{-11}$–10^{-10} A/m^2. They are usually observed near midnight. Regular geomagnetic pulsations Pc2, 3 with similar periods are observed, however, during morning and day-time hours. These facts indicate the different origin of the observed fluctuations in Pc2–3 range in the geomagnetic field and in the atmospheric electric field.

In the range of 0.4–10 s the spectrum of the variations of VECD has in most cases a noisy character. In the course of the experiment several clear cases of Pc1 geomagnetic pulsations were recorded. The comparison with simultaneous records of VECD did not show any signal of the Pc1 type at the level of sensitivity of our equipment. However, band limited emissions in the same range with the amplitude of the order of 10^{-12} A/m^2 were recorded during several hours (Fig. 6). The central

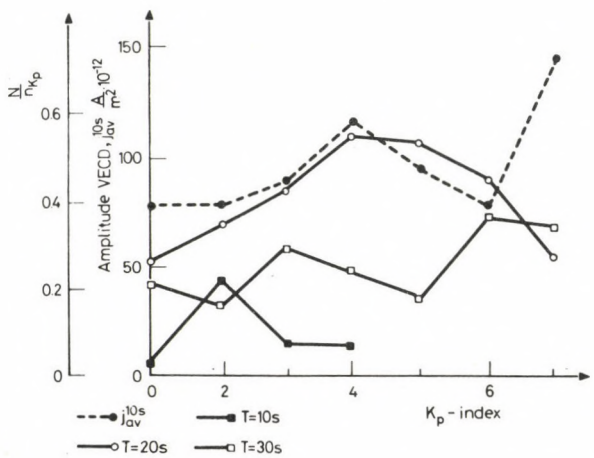

Fig. 5. Dependence of the amplitude of the VECD variations normalized to a period $T=10$ s (dashed line) and the relative number N/n_{kp} of the variations of the different periods in the range 10...30 s (solid line) on the Kp-index. The number of the observed cases was normalized to the number of the Kp-cases

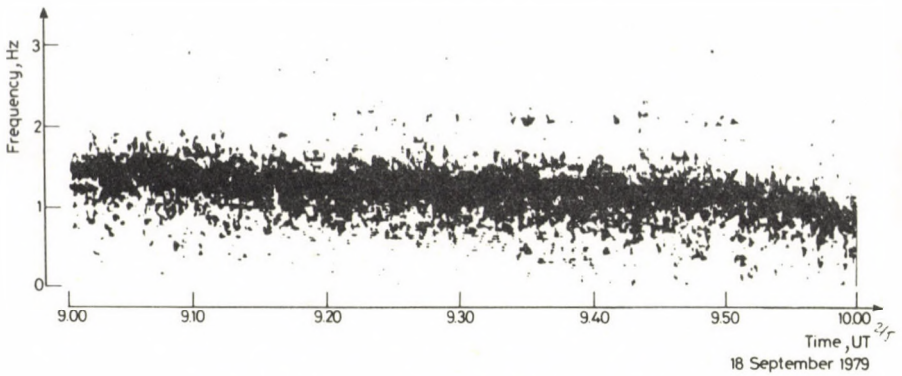

Fig. 6. Spectral display of the band-limited signal

frequency of such emissions is near 1 Hz with a relative width no more than 50%. In this case no pulsations with similar spectral structure were observed in the magnetic field.

A completely new and peculiar type (as regards its dynamic spectrum) of signal was observed in the considered and most probably higher frequency range (not covered by the frequency response of the equipment). During the experiment, 18 cases of such signals were registered. The example of their dynamic spectrum is given in Fig. 7. They have a clearly expressed *V*-type shape. Such signals occur mainly during morning and evening hours. Only in one of these cases the signals were observed simultaneously in the electric current density and in the magnetic field. Such cases were observed independently also in the magnetic field with high sensitivity equipment (private communication, Klain).

Fair-weather conditions mean generally the absence of the fluctuations in the velocity and space charge density in the near Earth layers of the air. However, one may assume that velocity fluctuations can arise in fair weather as a result of the infrasonic fluctuations on irregularly distributed space charges in the near Earth layer.

Let us consider the mechanism of generation of the convective current under the influence of such waves. The source of the infrasound should be located upwards and the infrasonic wave is incident at a right angle to the Earth's surface. The fluctuation of the ions in the surface layer under the influence of these waves will lead to fluctuations of the current. The relationship between the amplitudes of the fluctuations of ions to that of the medium is (Fooks 1955).

$$\frac{V}{U} = \frac{1}{\sqrt{1+\omega^2\tau^2}}; \qquad \tau = \frac{2r^2\gamma}{9\eta}$$

where r — is the radius of particle,
γ — ion density,
η — viscosity of the medium.

The magnitude of τ for the air does not exceed 10^{-5} s. Therefore $V \sim U$. It means that in the surface layer under the influence of infrasound the fluctuations of ions have the same amplitude and phase as those of the medium, i.e. they move as an integral part of the medium. In the medium the velocity of the particle oscillation under influence of infrasound is connected with the excessive pressure P as follows:

$$P = \gamma_g \cdot C_s \cdot V,$$

where γ_g — is the density of the medium
C_s — the velocity of the sound.

As the average magnitude of the pressure change due to infrasound is 10 μbar (Gossard and Hooke 1978), the amplitude of the velocity variations V is 0.2 cm/s. The corresponding local changes in vertical electric current density due to space charge velocity variations can be written as:

$$j = \sigma \cdot V \simeq 10^{-12} \text{ A/m}^2$$

(if the density of the volume charge is $\sigma = 500 \cdot 10^{-12}$ C/m^3). This value corresponds to the amplitudes of the observed fluctuations in the frequency range 0.4–10s.

Let's consider the possibility of occurrence of quasistationary, local fluctuations of the magnetic field connected with the space charge fluctuations generated by

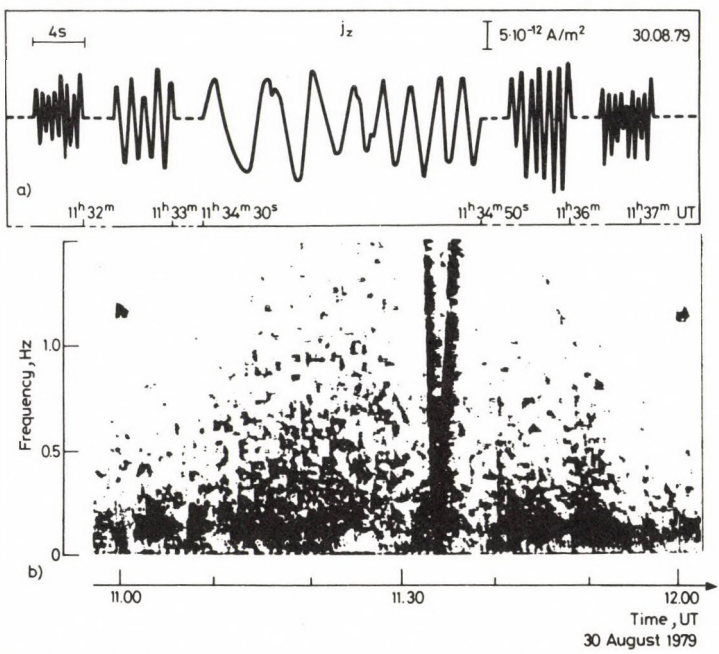

Fig. 7. Amplitude record of the *V*-shaped signal (a) and its spectral display (b)

infrasound. The linear dimensions of the space charges in the surface layer are around 100–400 m (Verg and Johnson 1974).

If the velocity of the volume charge fluctuations has the previous value $V=2\cdot 10^{-3}$ m/s, the amplitude of the magnetic field fluctuations is:

$$B=\frac{q}{4\pi\varepsilon\cdot C^2}\cdot\frac{V}{R}\simeq 0.1 \text{ pT}.$$

This corresponds to the threshold sensitivity of the induction magnetometers, used in the experiment. If the space charge and its linear dimension increase the fluctuation of the magnetic field reaches several pT and could be recorded by the present equipment (sensitivity ~ 0.2 pT).

The effect of infrasonic radiation of the space charges in the surface layer yields satisfactory estimations for the explanation of some types of the VECD variations. The natural sources of infrasound include, e.g. heavy thunderstorms, sea waves, aurora and earthquakes. Therefore the presented model can open new directions to elucidate the possible connection between the VECD variations and a variety of geophysical phenomena. Moreover, it paves the way for a physical understanding of these connections.

Comparison with records in the Nagycenk observatory

In the Nagycenk observatory in Hungary, a simple equipment, consisting of a 20 m^2 wire grid about 1 m above surface and amplifying-recording instrument was used for continuous recording during one month (September 1980). Some general conclusions of these records are summarized in the following, mostly coinciding with the result in the Soviet Union.

1. The amplitudes and spectral characteristics of the variations were generally similar to those in the Soviet Union.

2. The diurnal variation of the amplitudes was also similar to the Soviet results; the afternoon onset of the activity was mostly quite abrupt, whereas the decrease from the night maximum to the morning-a.m. minimum is continuous.

3. The records in fair weather are rather similar to those in wind, rain, storm etc., only the amplitudes are by one or more orders of magnitude less.

4. No correlation was found between the activity of VECD and any geomagnetic index, including Kp. An experiment to compute a transfer function between magnetic components and VECD failed due to very low coherences. There was only one case when coherences of about 0.8 were obtained for a short interval, else they were less than 0.5 (about random values).

5. There was a peculiar type of variations which appeared between 2200 and 0100 UT (23h–02h LT). They are continuous, regular variations with a frequency of

about 1Hz. In some cases durations up to 2–3 hours were found, while in other cases they lasted only for some minutes. The amplitudes did not show any regular modulation. No artificial source could be detected for these variations. Pc1 recording of the observatory, however, did not show any trace of similar activity in the geomagnetic field in either of the 6 cases found (i.e. about 20 percent of days), while in some cases of Pc1 activity, no traces of VECD variations with similar periods were found.

Conclusions

The obtained experimental results reveal the existence of specific oscillations of VECD in the air. Their frequencies are in the range 0.01–2.5 Hz, and their amplitudes are 10^{-12}–10^{-10} A/m^2. Investigation of the interconnection between VECD oscillations (20 days of continuous recording) and geomagnetic pulsations (about 50 cases of Pc2–3 and 6 cases of Pc1) showed significant differences between the oscillatory regimes in the magnetic and vertical electric fields. This conclusion was reached as a result of the comparison of their dynamic spectra, and amplitude time records. However, as it follows from some estimates (given in this paper), an identification of VECD connected with geomagnetic pulsations is hindered due to existence of convective currents in the lower troposphere.

It is necessary to stress that even in fair weather conditions the possibility of generation of VECD oscillation as a result of infrasonic action on space charges existing in the near Earth layer of the air is not excluded. Estimates show that changes in the pressure by 10μbar lead to local VECD changes of 10^{-12} A/m^2. This corresponds to the order of VECD amplitudes observed in the frequency range 0.1–2.5 Hz. Very small local oscillation can be simultaneously generated in the magnetic field with amplitudes of about 1pT.

Special interest presents the discovery of a new type of a signal, having a V-shape in the dynamic spectrum. These signals were observed mainly in the electric current, however, in one case this type of signals was recorded simultaneously in the magnetic and electric fields (Fig. 8).

The results of this investigation show:

— the presence of characteristic, short period VECD oscillation in the air, the sources of which need further studies;

— the morphological properties of VECD are different from those typical for geomagnetic pulsations,

— a possible relation of VECD oscillations with geophysical phenomena connected with the generation of infrasound (aurora, earthquakes, etc.). It is suggested that the measurements of the density of the vertical electric current can be used as a sensitive tool for the investigation of such processes.

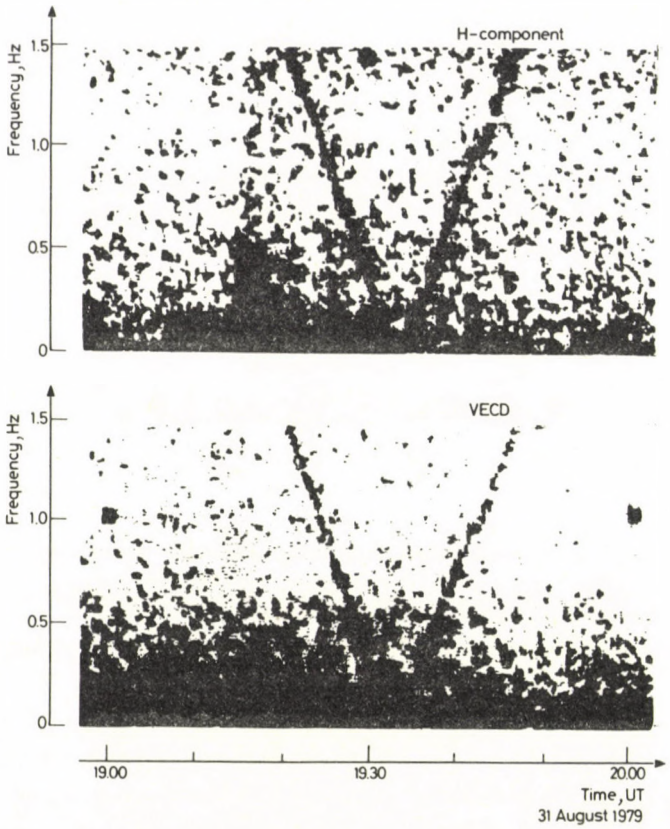

Fig. 8. Spectral display of a *V*-shaped signal observed simultaneously in VECD and in the magnetic field

References

Chalmers J A 1974: Atmospheric electricity (in Russian). Gidrometeoizdat, Leningrad

Chetaiev D N, Fedorov E N, Krylov S M 1975: On the vertical electric component of the geomagnetic pulsation field. *Planet. and Space Sci.*, 23, 311–314.

Fooks N A 1955: Mechanics of the Aerosols (in Russian). Academic Press, Moscow

Gossard E E, Hooke W H 1978: Waves in Atmosphere (in Russian). "Mir", Moscow

Gul'elmi A V, Klain B I, Rusakov N N 1979: Geoelectrical field in observations at the North Pole-22 drifting station (in Russian). *Geophys. Sbornik*, 88, 60–69.

Olson D E 1971: The evidence for auroral effects on atmospheric electricity. *Pageoph.*, 84, 118–138.

Park C G 1976: Solar magnetic sector effects on the vertical atmospheric electric field at Vostok, Antarctica. *Geophys. Res. Lett.*, 3, 475–478.

Verg D G, Johnson K R 1974: Short-period fluctuations in the fair-weather electric field. *J. Geophys. Res.*, 79, 2177–2184.

Acta Geodaet., Geophys. et Montanist. Hung. Volume 19 (3–4), pp. 297–304 (1984)

RELATIONSHIP BETWEEN THE PERIOD OF GROUND PULSATIONS AND THE PERIOD OF PULSATIONS IN THE SOLAR WIND

T J ODERA[1]

[Manuscript received May 3, 1983]

Data from ISEE-2 satellite and ground stations were used for comparison between the period of satellite pulsations and the period of pulsations on the ground. Very weak relationship was found between the periods of pulsations both in the satellite and on the ground.

Keywords: geomagnetic pulsations; pulsation periods; solar wind

Introduction

The periods of some Pc3, 4 pulsations which are controlled by the solar wind parameters have been found to depend on the magnitude (B) of the interplanetary magnetic field (IMF). Gul'elmi (1974) derived the relation $T=160/B$, between the period of the ground pulsations and the IMF magnitude. His idea was based on an early report by Troitskaya et al. (1971) that the period of pulsations observed on the surface of the Earth was proportional to the gyroperiod of protons in the interplanetary medium. Gul'elmi's idea was fundamental and formed a basis for a more rigorous theoretical treatment by Kovner et al. (1976) who showed that the period of ground pulsation was proportional to the gyroperiod of protons in the solar wind (interplanetary medium).

The waves discovered in the interplanetary medium have been found to have the same property as the pulsations on the ground, namely their period is proportional to the local proton gyroperiod. The consequence of this similarly is that the Pc3, 4 pulsations seen on the ground originate as low frequency waves generated locally in the solar wind and that spectra of the waves in the solar wind and on the ground may be similar.

Early experimental observation by Plyasova–Bakounina (1972) supported the idea that waves excited in the interplanetary medium may contribute to the spectrum of Pc3, 4 pulsations observed on the Earth's surface. A similar but more detailed study was made by Plyasova–Bakounina et al. (1978) who reported similarity in period

[1] Physics Department, Kenyatta University College, Nairobi

between the pulsations at Borok ground station and those seen on HEOS-1 satellite in the interplanetary medium.

More recently Russell and Hoppe (1981) found a linear relationship between the frequency of Pc3, 4 band 'upstream' waves and the strength of the IMF, which they expressed as $F = 5.81B$. The closeness of this result to the earlier ground results ($F = 6.25B$) led Russell and Hoppe to suggest that these upstream waves were a major source of magnetospheric Pc3, 4 pulsations, being convected through the magnetosheath to the magnetopause, and then transmitted to the ground.

A comprehensive investigation of the role of the solar wind parameters in pulsation generation and control on the ground and in the solar wind (Odera 1982) has brought out discrepancies and inconsistencies in the analysis of pulsations both on the ground and in the interplanetary space. This paper concentrates on one limited aspect of that analysis, namely comparison between the periods of ground pulsations at low latitude stations (Cambridge and Nagycenk) and those of low-frequency waves seen on the ISEE-2 satellite in the interplanetary medium.

Data

1. *Satellite data:* Data from the interplanetary medium were obtained from the ISEE-2 satellite, one of the three spacecraft forming the International Sun-Earth Explorer (ISEE) mission. The data were provided from the University College of Los Angeles (UCLA) fluxgate magnetometer aboard ISEE-2 spacecraft.

The instrumentation system is described in detail by Russell (1978). Details of the selection procedure for the wave-events in the interplanetary medium is found elsewhere by Odera (1982). Briefly the satellite data sampled at the rate of 4 seconds were plotted at a time scale of 3 mm/min, thus enabling the shortest possible period event (~ 10 sec) to be clearly identified. Plots of approximately 800 hours of data were produced. The absence or presence of upstream wave events were then determined (as low-frequency waves) by visual inspection. The period range of the selected wave events were estimated by handscaling the plots over about 10 cycles. The period was estimated only for events which were clearly identifiable. Where there was any doubt no measurement was done.

2. *Ground Data:* The ground data were provided from the Institute of Geological Sciences (IGS) magnetometers at Cambridge, UK ($L = 2.4$) and from Nagycenk Observatory ($L = 1.8$) in Hungary. Cambridge is about the same L value as Nagycenk. The IGS data were prepared using the standard method of data handling developed at IGS (Stuart and Green 1981).

The Nagycenk data are obtained from Earth current measurements which are characterized in 12-period bands. Details of the methods of characterization of the micropulsations measurements at Nagycenk are given by Holló et al. (1972). The data is in the form of handscaled hourly and daily mean amplitude, and a catalogue of the

period bands (lower and upper limits) of the pulsations occurring in each quarter hour and half hour intervals. For each interval the pulsation type and amplitude is given. Data used in this analysis were obtained from the catalogue containing indices for the micropulsation activity in 30 min intervals. The catalogue is based on the telluric records made at a chart speed of 6 mm/min.

From each 30 min interval a characteristic shorter interval is chosen which is considered typical for the whole interval. In this shorter interval the period and amplitude of pulsation is handscaled. The periods and amplitudes are distributed among 12-period bands which give a detailed description for the Pc3, 4 type pulsations at Nagycenk.

Before the analysis the following adjustments were made to the ground records.

a) The center of each period band was used to represent the ground period (T_{gr}) for each time interval corresponding to the satellite record.

b) Period bands within the range of Pc3, 4 only were used.

c) Only continuous types of pulsations were considered.

Direct comparison

The low-frequency waves recorded on board the ISEE-2 satellite were compared with simultaneous ground records of the Pc3, 4 events at Cambridge. Power spectra were used in the comparison.

Power spectral estimates were performed on both satellite and ground data set using maximum entropy method (MEM). MEM was developed by Burg (1967, 1968). The application of MEM spectral analysis to geophysics has been discussed by Ulrych and Bishop (1975). The MEM permits high frequency resolution in the spectral analysis, particularly for short data length. The resolving power of MEM depends on the percentage length for prediction error filter. Too short a length results in highly smoothed estimates, obviating the resolution advantage of MEM, whereas an excessive length introduces spurious details into the spectrum. Applying the MEM, successive five minutes intervals were spectrally analysed giving resolution of wave packets of 10 min duration.

Prediction error filters in the range of 10–40 percent (the percentage length for the prediction error filters) were used; this range gives the spectra which are clear and suitable for comparison. A sequence of spectra was presented as contour plot representing the dynamic spectrum. A low pass filter with a cut-off frequency of 100 mHz was used on the ground records before calculating the spectra to eliminate long period contamination and to make the overall spectra similar to those of the IMF waves. Although the estimation of the power spectral density was fairly course, the time resolution was sufficient to make reasonable comparison between the satellite data and the simultaneous ground records.

Figure 1 and Fig. 2 illustrate the procedure adopted in this analysis. The top panel is the dynamic spectrum for ISEE-2 and the bottom panel is the ground spectrum for day 325 covering the time interval 12.00–14.00 UT. Vertical lines in each panel represent hour marks. Start, finish and increment power spectral density contours (dB) along with the percentage of the prediction error filter are shown in the top right hand corner of each panel. Minimum and maximum frequencies on the ordinate are 10 mHz and 70 mHz respectively, the frequency resolution is 1 mHz. Although there is a good correspondence between the 'switch off' of activity in the interplanetary medium and on the ground (Fig. 3) the frequencies of the activity in the two media are different; the spacecraft has Pc activity of about 40 mHz ($T \sim 25$ s) while the ground has Pc3 activity with the frequency of about 25 mHz ($T \sim 40$ s).

The spacecraft position during the time interval 12.00–14.00 UT was at a radial distance of 22 RE; the local time of the spacecraft was about 8.30 morning. The IMF

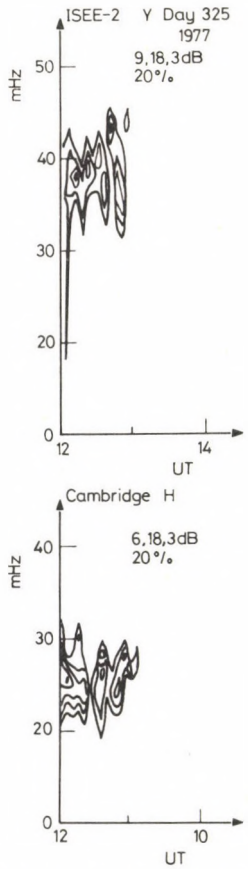

Fig. 1. Dynamic spectrum of waves in the solar wind (top panel) and the simultaneous Pc 3, 4 pulsations on the ground (bottom panel) for 12.00–14.00 UT on day 325 at Cambridge

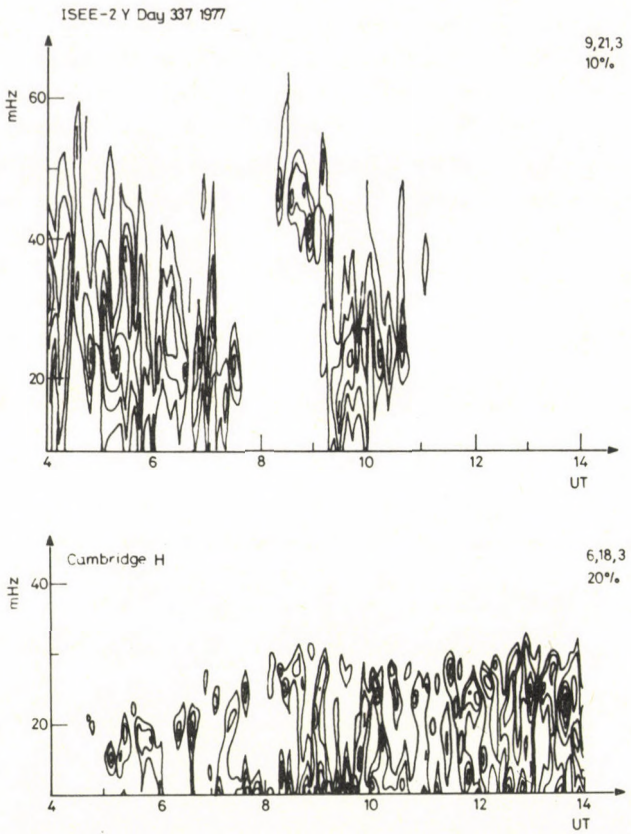

Fig. 2. Dynamic spectrum of waves in the solar wind (top panel) and the simultaneous Pc 3, 4 pulsations on the ground (bottom panel) for 04.00–14.00 UT on day 337 at Cambridge

magnitude at this time was, on the average 4.0 nT giving a frequency predicted by the empirical relation, $T=160/B$, of 25 mHz ($T=40$ s).

The predicted period is different from center band of the period of the satellite pulsation, but almost the same as the period of the ground pulsations.

In Fig. 2 the top panel is the dynamic spectrum for the ISEE-2 and the bottom panel is the ground spectrum for day 337 covering the time interval of 04.00–14.00 UT. Again the spectra of pulsations in space and on the ground are very different. The spacecraft has pulsations which are essentially Pc3 with the average frequency of 30 mHz ($T\sim 33$ s) while the ground has well developed Pc4 pulsations with the average frequency of about 20 mHz ($T\sim 50$ s).

About 200 hours of data were examined in this way (Odera 1982, and Odera and Stuart 1983) and no correspondence was found between the periods of satellite

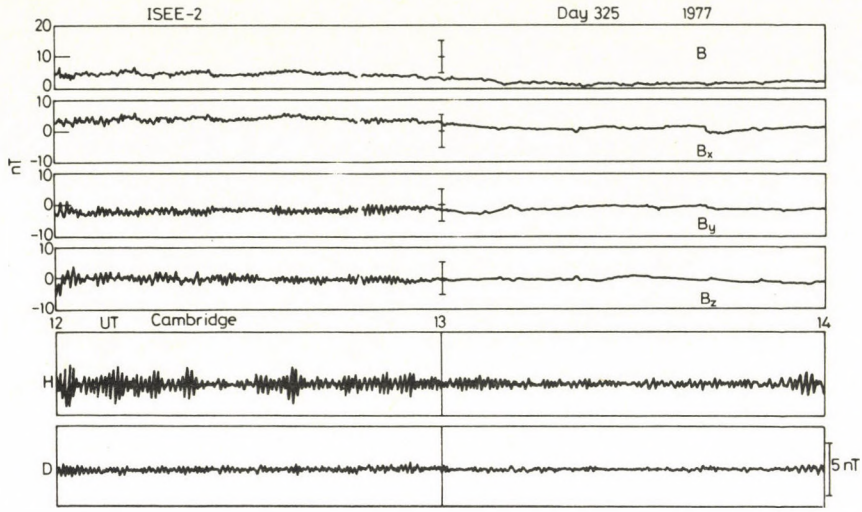

Fig. 3. Two-hour recordings of magnetic variations in space (ISEE-2) and on the ground (Cambridge) for 12.00–14.00 UT on day 325

pulsations and those of the ground pulsations. In fact for all cases it was found generally that the period (T_{sat}) of satellite pulsations was less than the period (T_{gr}) of ground pulsation, i.e. $T_{sat} < T_{gr}$.

Statistical comparison

Linear regression analysis was used to examine the relationship between the period (T_{sat}) measured on board ISEE-2 satellite and the period (T_{gr}) recorded on the ground at Nagycenk station. First the scatter plot shown in Fig. 4 was made. The high degree of scatter suggests that any relationship between the periods of pulsations in the solar wind and on the ground is weak or non existent. Nonetheless the least squares regression lines were derived and defined by

$$T_{sat} = (32.10 \pm 1.9) + (0.22 \pm 0.05) T_{gr}.$$

$$T_{gr} = (21.37 \pm 3.1) + (0.32 \pm 0.07) T_{sat}.$$

The lines are shown on the scatter diagram as full and dashed lines respectively. They intersect each other at a large angle (60°) implying that the correlation is poor. More to the point, the coefficient of linear correlation is small, $R = 0.26$, though it is significant at the 99.9 percent confidence level because of the large number of degrees of freedom (243). The upper and lower 95 percent confidence limits of the linear correlation coefficient is 0.31 and 0.21 respectively. The standard errors of the estimate

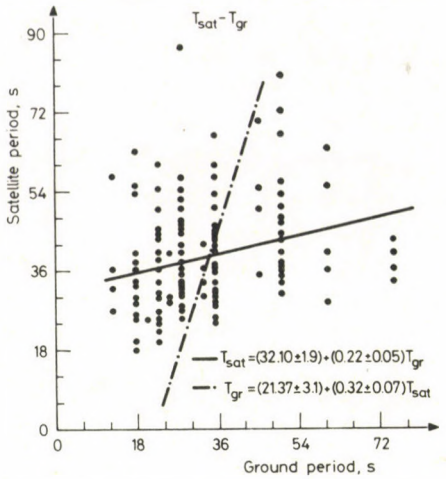

Fig. 4. Scatter diagram of measured periods (T_{sat}) of waves in the solar wind on board ISEE-2 satellite and measured periods (T_{gr}) on the ground at Nagycenk

of the regression lines (T_{sat} *Vs* T_{gr}) and (T_{gr} *Vs* T_{sat}) are 11.2 s and 13.5 s respectively, both indicating large scatter. The mean period ($\overline{T}_{sat}=39.54\pm0.74$ s) of the satellite pulsations is quite different from the mean period ($T_{gr}=34.01\pm0.89$ s) of the ground pulsations.

Discussion

That the mean period measured on the ground at Nagycenk is less the mean period on the ISEE-2 satellite is inconsistent with the results obtained by Odera (1982) using the Institute of Geological Science (IGS) magnetometer stations.

Odera (1982) results show that for the same set of B value $T_{gr} > T_{sat}$ all the time. The difference between the Nagycenk data and the IGS data is perhaps due to the different response characteristics of the instruments and different methods of selecting the Pc events. At Nagycenk the Earth current recording system has a frequency response that extends to higher frequencies than the IGS rubidium magnetometer, making it suitable for Pc3 and higher frequency events. The Pc3, 4 events at Nagycenk were (by practice) handscaled. The handscaling method is subjective and can be open to errors and bias in that the eye is always certainly drawn to the clearest most sinusoidal events. At the IGS, rubidium vapour magnetometer had a flat frequency from DC to 100 mHz which makes it ideal for identifying Pc4 and the larger Pc3 pulsation, but not suitable for the higher frequency pulsations which are typically an order of magnitude lower in amplitude. The Pc3, 4 events were clearly identified both by visual inspection and computation of power spectra, so errors were minimized in the IGS data.

The poor correlation obtained between the periods of satellite pulsations and those of ground pulsations is in agreement with Green et al. (in press) that the case for Pc3, 4 spectrum being the same in space and on the ground is very difficult. The idea that the period of pulsations in the two media (space and ground) would be similar originated from the theoretical assumptions (Gul'elmi 1974, Kovner et al. 1976, Hoppe and Russell 1982) based on rather generalized mathematical approximations. Green et al. (in press) indicated how it is hard to compare these theories with experiments. Perhaps the similarity between the periods of pulsations both in the interplanetary medium and on the ground is non-existent; if it does it may be a coincidence.

Acknowledgements

This work is part of the research carried out at the Geomagnetism Unit, Institute of Geological Sciences (IGS) U.K. The author wishes to thank the Director for permission to use IGS data and for facilities to carry out the work. I also thank Dr. J Verő for providing the ground pulsations data from Nagycenk Observatory, Hungary. Finally I am thankful to Dr. C T Russell for permission to use ISEE data.

References

Burg J P 1967: Maximum entropy spectral analysis. Paper presented at the 37th Annual International Meeting, Soc. of Expl. Geophys., Oklahoma City

Burg J P 1968: A new analysis technique for time series data. Paper presented at Advanced Study Institute on Signal Processing, NATO, Enschede, Netherlands

Green C A, Odera T J, Stuart W F (in press): The relationship between the strength of the IMF and the frequency of magnetic pulsations on the ground and in the solar wind. *Planet Space Sci.*

Gul'elmi A V 1974: Diagnostics of the magnetosphere and interplanetary medium by means of pulsations. *Space Sci., Rev.*, 16, 331.

Holló L, Tátrallyay M, Verő J 1972: Experimental results with the characterization of geomagnetic micropulsations, I. The method of characterization used in the investigations. *Acta Geod. Geoph. Mont. Hung.*, 7, 155.

Hoppe M M, Russell C T, 1982: Particle acceleration at planetary bow shock waves. *Nature* 295, 41.

Kovner M S, Lebedev V V, Plyasova, Bakounina T A, Troitskaya V A 1976: On the generation of low frequency waves in the solar wind in the front of the bow-shock. *Planet. Space Sci.*, 24, 261.

Odera T J 1982: The control and generation of magnetic pulsations on the ground and in interplanetary space by parameters of the solar wind. Ph. D. Thesis, University of Edinburgh

Odera T J, Stuart W F 1983 (in press): Morphology of low frequency waves in the solar wind and their relation to ground pulsations. *J. atmos. terr. phys.*

Plyasova, Bakounina T A 1972: Effect of interplanetary magnetic field on the characteristics of Pc2, 4 pulsations. *Geomagn. Aeron.*, 12, 772.

Plyasova, Bakounina T A, Golikov Y Y, Troitskaya V A 1978: Pulsations in the solar wind and on the ground. *Planet. Space Sci.*, 26, 547.

Russell C T 1978: The ISEE 1 and 2 fluxgate magnetometers. *ISEE, Trans. Geos. Electr.*, Ge 16, No. 3, 239.

Russell C T, Hoppe M M 1981: The dependence of upstream waves periods on the interplanetary magnetic field strength. *J. Geophys. Res., Lett.*, 8, 615.

Stuart W F, Green C A 1981: The array of magnetometers operated by IGS in N. W. Europe. Geomagnetism Unit Rep. No. 28, U.K., Institute of Geological Sciences

Troitskaya V A, Plyasova, Bakounina T A, Gul'elmi A V 1971: Relationship between Pc2–4 pulsations and the interplanetary magnetic field. *Dokl. Acad. Nauk. USSR.*, 197, 1312.

Ulrich T J, Bishop T N 1975: Maximum-entropy spectral analysis and auto-regressive decomposition. *Rev. Geophys. and Space Phys.*, 13, 183.

Acta Geodaet., Geophys. et Montanist. Hung. Volume 19 (3–4), pp. 305–338 (1984)

CONTROL OF THE SOLAR WIND PARAMETERS ON THE GROUND Pc3, 4 PULSATIONS*

T J ODERA[1]

[Manuscript received July, 20, 1983]

Data from five ground stations and the ISEE-2 Satellite have been used in the investigation of the problems of control by solar wind parameters of the generation of Pc3, 4 pulsations on the ground. The ground data have been correlated with the 1/2-hourly values of the solar wind velocity (V_{sw}), the IMF cone angle (θ_{xB}) and the IMF magnitude (B).

Results from statistical analysis of the ground data indicate that *a)* the energy level of Pc3, 4 pulsations on the ground increases with the increase in V_{sw} *b)* the energy level rises with the decrease in θ_{xB} *c)* the Pc3 pulsation is better related to the IMF cone angle than the Pc4 pulsation and *d)* the frequency of Pc3, 4 pulsations depends on the IMF magnitude. The quality of the frequency dependence on the IMF magnitude is found to be considerably improved when the same frequency of the Pc3, 4 activity is observed over a large area of the Earth's surface.

The results qualitatively suggest that the Pc3, 4 pulsations may originate from upstream waves of the subsolar bowshock region, the waves may be simply convected to the magnetopause where they couple to the magnetosphere through field line resonance.

Keywords: field line resonance; geomagnetic pulsations; interplanetary medium; Pc3; Pc4; solar wind

Introduction

The energy which drives many magnetospheric processes is provided by the solar wind. How this energy enters the magnetosphere and appears as hydromagnetic waves responsible for the appearance of the Pc3, 4 pulsations activity on the Earth's surface is not yet well understood.

Several approaches, notably Troitskaya et al. (1971), Gul'elmi and Bolshakova (1973), Greenstadt and Olson (1976), Webb and Orr (1976), Singer et al. (1977), Verő and Holló (1978), Wolfe et al. (1980) and Takahashi et al. (1981) have recently been used to attempt to establish experimentally what relationships exist between the dayside ground magnetic activities and the interplanetary medium. The relationships suggest that some Pc3, 4 pulsations are of external origin (i.e. outside the magnetosphere). Such relationship, if they exist, would be important for monitoring the state of the interplanetary space. Theoretical considerations have guided these studies to choose

* Paper presented at the KAPG-Symposium on Electromagnetic Induction, Sopron, March 1983

[1] Physics Department Kenyatta University College, Nairobi

the solar wind speed (V_{sw}) and the interplanetary magnetic field (IMF) as the two key interplanetary parameters controlling dayside Pc3, 4 activity on the ground. The generation of the surface waves at the magnetopause by the Kelvin–Helmholtz instability (Southwood 1968) and the convection and propagation of upstream waves to the magnetosphere (Greenstadt 1972, Kovner et al. 1976) have been shown theoretically to be controlled by the solar wind speed and IMF direction. Waves produced at the magnetopause by either increase of the solar wind or magnetic fluctuations arising from the upstream waves can excite field line resonance in the magnetosphere (Radoski 1966, Chen and Hasegawa 1974, Southwood 1974) thereby increasing the Pc3, 4 magnetic activity on the Earth's surface. The enhancement of the ground pulsation has been reported by Troitskaya (1967) and Webb et al. (1977) to be of global character.

A detailed study examining some of the relations which exist between the ground pulsations and three solar wind parameters has been recently carried out by Odera (1982). The three parameters considered were solar wind velocity (V_{sw}); the IMF cone angle (θ_{xB}) and the IMF magnitude (B). These parameters were obtained mainly from ONE spacecraft (ISEE-2) carrying the most recently developed equipment for field and solar wind plasma experiment. The purpose of this paper is to summarize Odera's (1982) study and bring out some outstanding features not discussed there.

Data

Satellite data

Data from the interplanetary medium were obtained mainly from the ISEE-2 satellite, one of the three spacecraft forming the International Sun-Earth Explorer (ISEE) mission. ISEE is a joint European Space Agency (ESA) and National Aeronautics and Space Administration (NASA) mission of three spacecraft designed to make the first comprehensive study of magnetospheric dynamics. The mission was timed to make a large contribution to the International Magnetospheric study (IMS). The main objectives of the ISEE mission and details of orbital parameters of the spacecraft was outlined by Durney (1977).

The nucleus of the ISEE mission is a pair of spacecraft, namely ISEE-1 and ISEE-2, which circulate the magnetospheric boundaries on the same orbit at a known and controllable distance apart. Since most of the events that occur inside the magnetosphere may be due to the varying conditions in the interplanetary medium, a third spacecraft ISEE-3 is stationed 235 RE at the libration point between the Sun and the Earth where it circulates in a 'halo' orbit monitoring the interplanetary medium.

The pair of spacecraft was launched as a stacked pair by a single Thor Delta 2914 from the Eastern Test Range on 22nd October, '77. The twin spacecraft travel in the

Table I
Orbital parameters of ISEE-2 satellite for different epoch

Launch date	22nd Oct., 1977		
Orbit Type	Geocentric		
Epoch (Month-Day-Year)	10–22–77	6–04–78	6–29–79
Period	3,453.1	3,441.8	3,444.2
Inclination	28.7°	39.5°	50.2°
Perigee (km)	280	1206	2940
Apogee (Km)	138,217	137,063	135,397

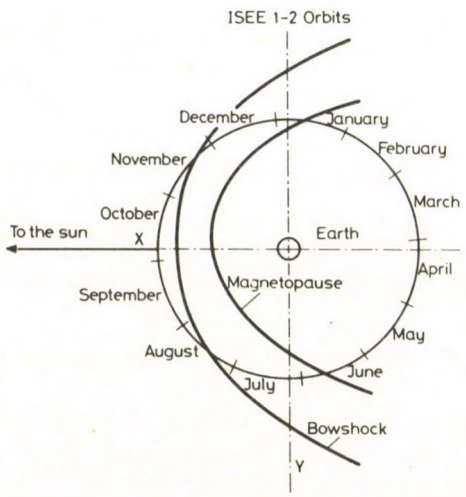

Fig. 1. The annual variation of apogee of ISEE-2 shown in relation to the magnetopause and bowshock in the ecliptic plane. The apogee moves completely round the date circle once each year

same orbit which had initial apogee and perigee of 22.6 RE and 280 km respectively. Table I shows some of the major orbital parameters of the spacecraft for different epoch. It was deliberately planned that the initial line of apsides should be such that the early apogee would be in the interplanetary space to ensure some measurements of the magnetopause, magnetosheath and the bow-shock in case of early failure. The orbit remains fixed in space and as the Earth revolves around the Sun the line of apsides rotates through the magnetosphere in a circular form as shown in Fig. 1. In the diagram the date circle indicates the position of the Earth's centre/apogee line at the time shown in calendar months. It should be noticed, for example, that apogees in October penetrated the interplanetary medium and will continue to do so in Autumn throughout the life of the mission, whereas apogees in the magnetotail occur during Spring.

The wide range of scientific experiments covered by the twin spacecraft, and which involved over a hundred investigators makes the ISEE a suitable source of the interplanetary data useful in this work. Generally the instruments carried aboard the spacecraft use the latest techniques and are more sensitive than the previous version. In particular a large effort went into reducing electric and magnetic interferences from the spacecraft itself, so the instruments have extraordinary low thresholds with high time resolution. UCLA-fluxgate magnetometers and solar wind plasma instrumentation aboard the ISEE-2 spacecraft provided the interplanetary medium data used in this work. There were two types of the interplanetary data, that is the interplanetary magnetic field (IMF) data and solar wind plasma data. Both types of data are described briefly below.

a) IMF Data. The IMF data were provided from the University College of Los Angeles (UCLA) fluxgate magnetometers experiment aboard the ISEE-2 spacecraft. The instrumentation system is described in detail by Russell (1978). The output rate of the magnetometers was either 4 or 16 vectors per second depending on the bit rate of the spacecraft telemetry system. Data for all the time periods used in this study were taken at a low bit rate corresponding to 4 vectors per second or the sampling interval of 0.25 sec. The raw data was sampled at four seconds interval.

Data from the instruments for the period from 22 October to 31st December, 1977 were used in this study. This period covers the first 30 orbits of the ISEE-2 spacecraft. The data tapes included three orthogonal components of the IMF records in geocentric solar ecliptic (GSE) coordinate system together with satellite position and time (UT). There were also 64- seconds average values of the IMF data.

The GSE system to which the original data refers is suitable for this study. The GSE coordinate system has its X-axis pointing from the Earth towards the sun; Z-axis is positively northwards normal to the ecliptic plane, and the Y-axis is chosen so that the rectangular Cartesian coordinate system is right handed. The position values of X, Y, Z are often given in terms of Earth radii (RE) Units. In the GSE system a magnetic vector **B** (X, Y, Z) can be speicified by magnitude (B) and two angles i.e., θ (ecliptic latitude) and φ (electiptic longitude). These quantities are related as follows.

$$B=(B_x^2+B_y^2+B_z^2)^{\frac{1}{2}}$$

$$\theta=\arctan B_z/(B_x^2+B_y^2)^{\frac{1}{2}}$$

$$\varphi=\arctan B_y/B_x\,.$$

Figure 2 shows the GSE coordinate system and the associated IMF parameters used in this work.

b) Solar wind data. The solar wind data were obtained from the positive ion electrostatic deflector on board the ISEE-2 spacecraft. A detailed description of the instrumentation system is found in Bonifazi et al. (1978). The instruments operate in

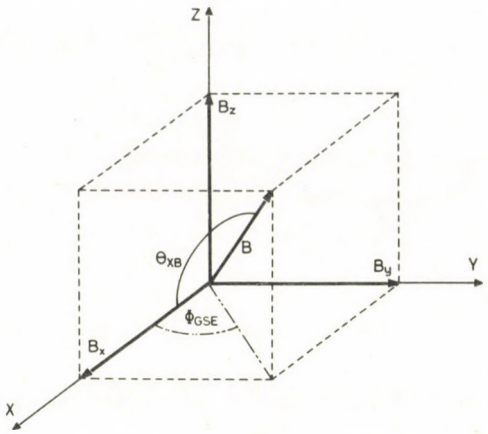

Fig. 2. The IMF parameters in the geocentric solar ecliptic (GSE) coordinate system

two different modes referred to as 'wide energy spectrum' (WES) and 'high time resolution' (HTR) modes which alternate automatically. In WES mode the instruments supply a full ion energy spectrum every ~96 seconds. In the HTR mode the instruments track the maximum of the ion energy spectrum obtaining significant observation of proton energy spectrum every two spacecraft revolutions (~6 seconds).

The values of the solar wind velocity used in the paper were obtained from the instruments operating in the WES mode. The data were received from the Consiglio Nazionale delle Recerche (CNR) Frascati, Rome. They were in the form of continuous 24 hr plots of the solar wind speed. The analogue records were digitized and scaled down every half-hour to obtain 30 min values of the solar wind speed. There were approximately 1402, 30 min data points.

Ground data

The ground data used in this work were obtained from five stations in the network of magnetometers in Europe operated during the International Magnetospheric Study (IMS) by the Geomagnetism Unit of the Institute of Geological Sciences (IGS). Figure 3 shows a map of North Western Europe and North Atlantic with most of the stations occupied by IGS magnetometers during the IMS. On the map are drawn *L*-values computed at 120 km altitude for epoch 1977.5 from the main field model of Barraclough et al. (1975). The geographic and geomagnetic coordinates and *L*-values along with the stations identifier of the five stations are listed in Table II. The stations are listed in order of decreasing geomagnetic latitude.

The instrument at each station was a three axis rubidium vapour magnetometer. The rubidium magnetometer is an atomic oscillator providing a frequency pro-

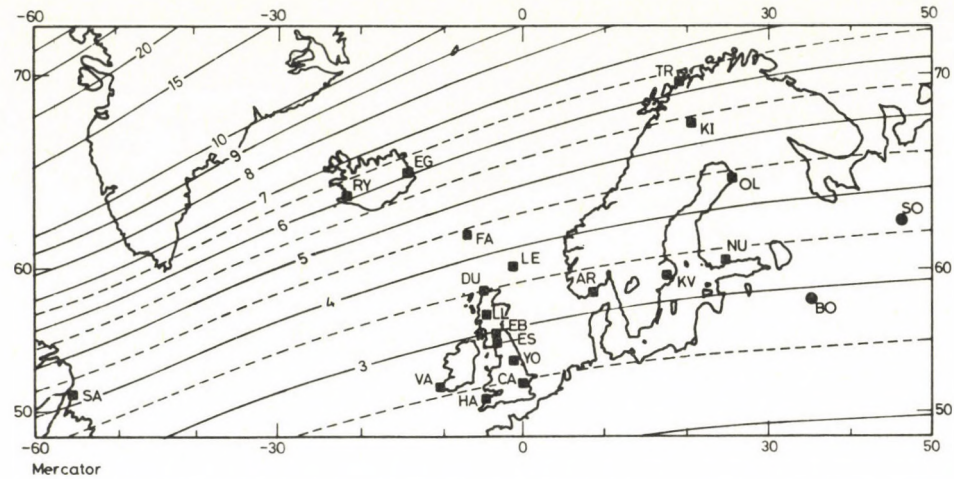

Fig. 3. Map showing the locations of the IGS magnetometers in the Northern hemisphere with superimposed *L*-shells for epoch 1977.5 calculated for 120 km altitude from Baraclough et al. 1975

Table II
Location of five ground stations in the IGS magnetometer array

		Geographic		Dipole		
Stations	Code	Latitude	Longitude	Latitude	Longitude	*L*-value*
Faroe	FA	62.03	− 6.78	65.03	86.02	4.30
St. Anthony	SA	51.35	−55.60	62.13	20.34	4.07
Oulu	OL	65.11	25.49	61.72	117.96	4.34
Eskdalemuir	ES	55.32	− 3.20	58.11	84.29	2.81
Cambridge	CA	52.23	+ 0.05	54.56	85.71	2.37

The coordinates are given in degrees, where (−) means West in Longitude and South in Latitude; unqualified numbers signify East in Longitude and North in Latitude.

* *L*-values computed at 120 km altitude for epoch 1977.5 from the main field model of Barraclough et al. (1975).

portional to the magnitude of the ambient magnetic field. The magnetometer had essentially flat frequency response and a noise level typically <0.05 nT. It recorded magnetic variations in three orthogonal directions—magnetic NE, NW and Z (Stuart 1971). H and D components can easily be recovered from the NE and NW components. The sensitivity of the magnetometer was usually in the range of $0.04-0.16$ nT. The magnetic variations were sampled at 2.5 sec intervals, timing accuracy being controlled by a crystal clock, and recorded digitally on cassette tapes as described by Riddick et al. (1975) who gave details of sensing and recording engineering. The recorded data were subsequently transcribed into computer compatible format (Mills et al. 1977) for

storage on master data bank tapes at the IGS. Analogue records were usually produced directly from the cassette tapes before transcription, but could also be obtained from the data bank tapes. The analogue records and the data bank tapes provided data used here. The data were prepared using the standard methods of data handling developed at the IGS (Stuart and Green 1981).

Selection of events

Selection of Pc3, 4 events on the ground was carried out in two stages, initial and final selection.

The initial selection of the Pc3, 4 events was made on the basis of 30 minute intervals. In each interval selected the amplitude of the Pc3, or Pc4 event must have been above the average background noise level most of the time; the period must have not changed by more than 10% of the apparent dominant period; the oscillations should be regular and fairly continuous for more than half the 30 min interval.

Analogue records were visually inspected and 30 minute interval beginning at the hour or half hour were selected during which there appeared to be good Pc3, or Pc4 pulsations. Good quality Pc activity usually occurred at times when the background field was relatively quiet and the Pc's could be selected quickly and easily.

In the final selection the technique of power spectral analysis was used. Power spectra were performed on the 30 minute segments of data. A low pass filter was first applied before the spectra were calculated by using Fast Fourier Transform (FFT) algorithm. During the spectral analysis data were converted from the recorded NE and NW to *H* and *D*- components which are physically more meaningful. Figures 4 and 5

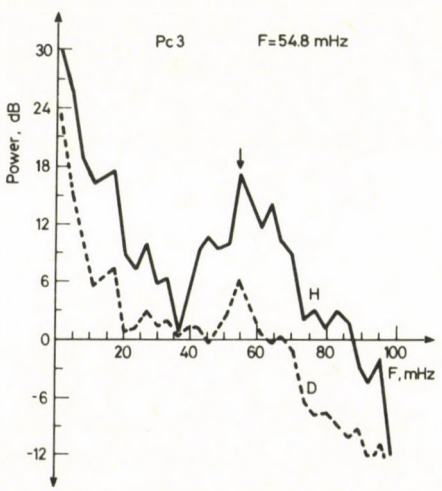

Fig. 4. An example of power spectral peak of Pc3 pulsation event on the ground, for *H* and *D* components

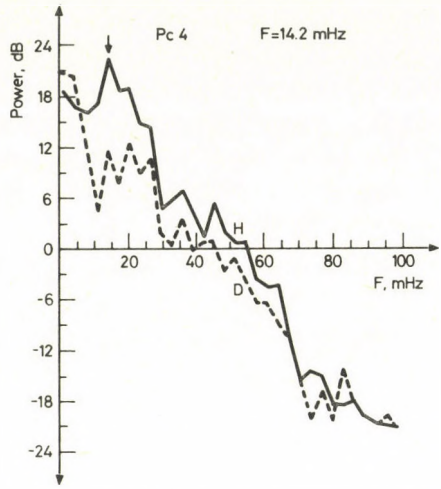

Fig. 5. An example of power spectral peak of Pc4 pulsation event on the ground, for *H* and *D* components

show typical power spectra for *H* and *D* components for events with energy mainly in the Pc3 and Pc4 frequency bands respectively. The power peak is shown by an arrow.

The procedure for the final selection of the pulsation events was as follows. Computer output for the spectral estimates was examined (1514, 30 minute spectra were treated in this way). It was determined whether a spectral peak appeared in the appropriate frequency band. If there was clearly identifiable power peak it was counted as an event and its power and corresponding period were noted. Whenever there was some ambiguity in identifying the peaks the event was rejected. Two components, *H* and *D* were considered equally in this exercise. If in one segment there were two outstanding peaks showing in both components at the same period band as shown in Fig. 4 only the component with the higher peak was chosen. If the peaks appeared in both components at different period bands in the same segment, then the peaks were treated as two separate events. Although the two components (*H* and *D*) were considered equally it turned out that *H*-components contained much more power than *D*-components. As a consequence the finally selected events were essentially *H*-components.

Analysis and results

Interrelation of V_{sw}, θ_{xB} and B

Before a correlation study was made the characteristics of the solar wind parameters themselves were studied first. The inter-relation of the solar wind velocity (V_{sw}) the cone angle (θ_{xB}) and the IMF magnitude (B) was examined by performing linear regression and correlation analysis using 713, 1/2-hourly data samples.

It should be noted that the cone angle (θ_{xB}) is used here instead of the ordinary polar angle θ (ecliptic latitude) and φ (ecliptic longitude) for two main reasons. First the use of one angular parameter simplifies the analysis. Second it had been earlier noted by authors, notably Greenstadt and Olson (1976), Arthur and McPherron (1977), Wolfe et al. (1980) and Takahashi et al. (1981) that the cone angle appreciably affect the Pc3–4 amplitude and occurrence.

The definition of 30 minute values for the cone angle adopted here is the average of 450 points taken from the 4 second IMF data, representing 30 minutes data length. By this definition and description of the cone angle according to Wolfe et al. (1980) the average value of the cone angle was calculated using the following expression.

$$\langle \theta_{xB} \rangle = \frac{1}{N} \sum_{i=1}^{N} \text{arc cos} \left(|B_{xi}| / B_i \right).$$

The 30 minute values for the IMF magnitude were computed using the following expression

$$\langle B \rangle = \frac{1}{N} \sum_{i=1}^{N} (B_{xi}^2 + B_{yi}^2 + B_{zi}^2)^{\frac{1}{2}}.$$

Scatter plots using 1/2-hourly average values of the solar wind parameters are shown in Fig. 6a, b, c. From these the least square best fit lines for the scatter plots and coefficient of linear correlation were computed. Generally there is a large scatter implying that any interrelation of V_{sw}, θ_{xB} and B is weak. More particularly there is a very small positive correlation coefficient of 0.02 between the IMF magnitude (B) and the solar wind velocity (V_{sw}); the correlation coefficient establishes the best fit line to be not significant at the 95% confidence level for the number of data points (713) used. The dependence of B on the cone angle (θ_{xB}) is also weak with a linear correlation coefficient of 0.18. This is however significant at the 95% confidence level. Similarly the dependence of θ_{xB} on the solar wind velocity (V_{sw}) is poor with a linear correlation coefficient of 0.19.

The results of the linear regression analysis are summarized in Table IH. In particular Table IV shows the linear correlation coefficient of pairs of the solar wind parameters. It is evident from the poor correlations shown in the table that B and θ_{xB} are not sufficiently related and that neither θ_{xB} nor B is correlated well to the solar wind velocity (V_{sw}). The evidence of poor correlations among the three parameters is brought out more clearly by the two regression lines drawn on each scatter diagram. The two regression lines, in each case intersect each other at an acute angle more than 65° (non correlation means that the angle of intersection is a right angle). In fact for the B and V_{sw} relation the angle of intersection (88°) is very nearly a right angle. Because of these results V_{sw}, θ_{xB} and B were regarded as independent parameters.

A network of five ground stations listed in Table II was used in the correlation study presented in this paper. The five stations were chosen from the IGS chain of magnetometers primarily to get sufficient ground coverage. Green (1981) has described

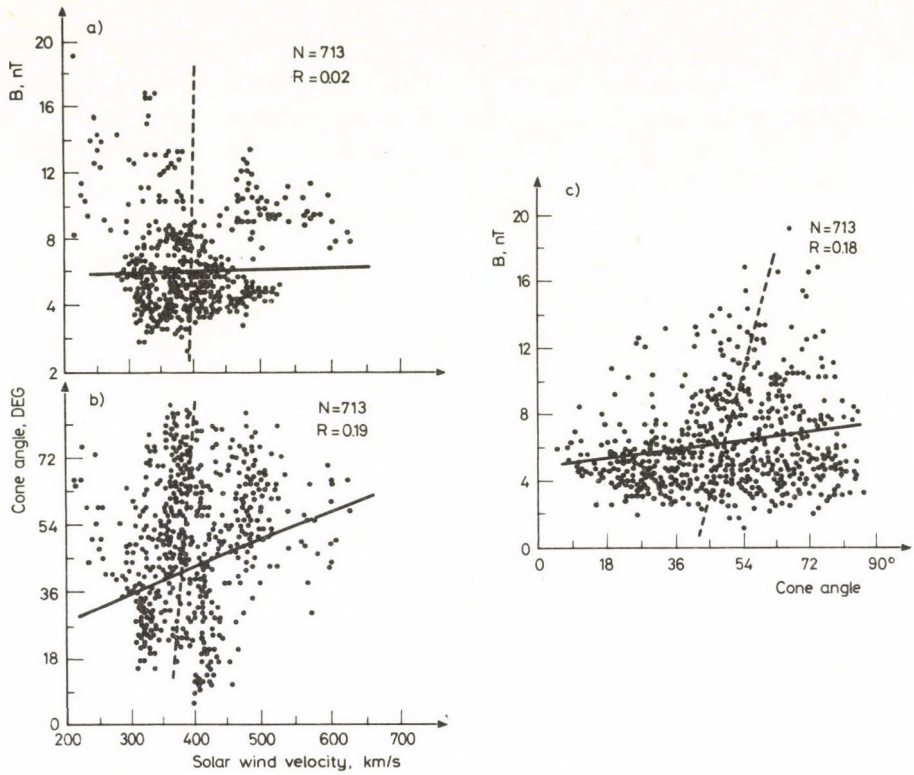

Fig. 6. Scatter plots of the 1/2-hour average solar wind parameters: *a)* dependence of magnetic field magnitude on solar wind velocity, *b)* dependence of cone angle on solar wind velocity, *c)* dependence of magnetic field on cone angle

the profile of the IGS magnetometer array during the period of this study. The basic configuration in Europe is of two lines approximately along the geomagnetic meridian about 2 hours apart. The eastern meridional line runs through Scandinavia and covers L-values of ~ 3.3–6.3, and the western line runs through the UK to Iceland, $L = 2.4$–6.5. In addition there is a station at St. Anthony in Newfoundland about 4 hours to the west of the UK line and 6 hours to the Scandinavia line—Oulu lies in the eastern meridional line; Faroe, Eskdalemuir and Cambridge lie in the UK line. In this configuration Cambridge and Faroe have the largest latitudinal separation of $\Delta\theta = 10.0°$ whereas St. Anthony and Oulu have the largest longitudinal separation of $\Delta\varphi = 81.09°$, giving 6 hours (to the nearest whole hour) local time difference between the two stations. These stations had relatively continuous good records for the geomagnetic field data during the most part of the period covered by this study. In addition the stations recorded good Pc3, 4 activity in terms of amplitude and continuity.

Table III
Results of linear regression analysis for the solar wind parameters

N	Mean values			Functional Relation	Slope (C_1)	Intercept (C_0)	R
	$\bar{B}$	$\bar{V}_{sw}$	$\bar{\theta}_{xB}$				
713				$B=C_1V_{sw}+C_0$	0.001 ± 0.002	5.86 ± 0.59	0.02
713	6.22 ± 0.1	393.02 ± 2.57		$V_{sw}=C_1B+C_0$	0.57 ± 0.94	389.46 ± 6.39	
713			49.24 ± 0.69	$B=C_1\theta_{xB}+C_0$	0.03 ± 0.006	4.90 ± 0.29	0.18
713				$\theta_{xB}=C_1B+C_0$	1.19 ± 0.25	41.85 ± 1.67	
713				$\theta_{xB}=C_1V_{sw}+C_0$	0.051 ± 0.01	29.12 ± 3.92	0.19
713				$V_{sw}=C_1\theta_{xB}+C_0$	0.72 ± 0.14	357.7 ± 7.24	

Table IV
Coefficients of linear correlation between the solar wind parameters

	B	V_{sw}	θ_{xB}
B		0.02	0.18
V_{sw}			0.19
θ_{xB}			

General distribution of V_{sw}, B, θ_{xB}

The general distribution of each of the solar wind parameters during the whole period of this study is shown by the histograms in Fig. 7a, b, c. The histograms were made from the same number of data points used in the scatter plots, Fig. 6a, b, c plus a few other points which could not be included in the scatter plots because they lacked correspondence in the records. The total number of 1/2-hour data points used in each diagram is shown in bracket. Each histogram represents the natural distribution of the parameter regardless of whether there was any pulsation activity observed or not.

Examination of the figures indicates that the distribution of the solar wind velocity has an outstanding maximum at 350–400 km/sec, Fig. 7a. There are few records for unusually high solar wind velocity, $V_{sw}>600$ km/sec and for unusually low velocity, $V_{sw}<250$ km/sec. Figure 7b shows an outstanding peak at 4–5 nT. There is a gradual decrease in the IMF distribution pattern for $B>^{6}$ nT. The cone angle distribution Fig. 7c peaks at 45°–60° with minima at $\theta_{xB}>75°$ and $\theta_{xB}<15°$.

The peaks of the three distribution diagrams are considered to be at the usual or normal values of the corresponding solar wind parameters during the period of this study, that is for V_{sw} the usual range is 350–400 km/sec, for B the usual range is 4–5 nT and for θ_{xB} the usual range is 45°–60°. It is to be noted that the usual values of the parameters may not necessarily be equal to their mean values.

The statistical analysis, to follow, involving the three solar wind parameters and the ground pulsation is divided in three main parts:

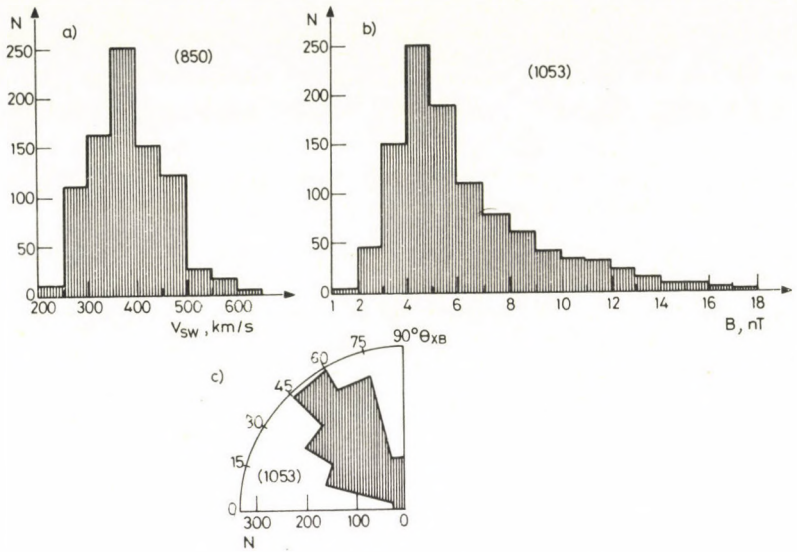

Fig. 7. General distribution of three major solar wind parameters: *a)* occurrence frequency of solar wind velocity (V_{sw}), *b)* occurrence frequency of IMF magnitude (B), *c)* occurrence frequency of cone angle (Θ_{xB})

Part 1: Effect of solar velocity

General occurrence pattern

The general occurrence patter of the Pc3, 4 pulsation events was presented in terms of the histograms shown in Fig. 8 for the five ground stations. Each event in the distribution diagrams represents the 30 min power spectral peak as described in the previous section. Few events at the end and beginning of each distribution diagram simply means that there were few records of the solar wind velocity $V_{sw} > 450$ km/sec and km $V_{sw} < 300$ km/sec and does not reflect any intrinsic property of frequency distribution of events against the velocity of solar-wind, see Fig. 7a.

In the range of velocity, $V_{sw} = 300$–450 km/sec there are more Pc3, 4 pulsation events for $V_{sw} > 400$ km/sec than for $V_{sw} < 400$ km/sec, in fact there is a clear maximum at $V_{sw} = 400$ km/sec for all the five stations. This result is shown below in a different way.

Diurnal occurrence pattern

The diurnal variation of the occurrence of Pc3, 4 activity at two ranges of solar wind velocity ($V_{sw} = 300$–400 km/sec and 400–500 km/sec) for the five stations is shown in Fig. 9. Each plot is a frequency polygon (a line graph) of occurrence frequency of Pc3, 4 events plotted against local time (LT).

The effect of the solar wind velocity on the diurnal occurrence pattern in positive. Before noon (LT) the occurrence of pulsations activity is generally higher for $400 < V_{sw} < 500$ km/sec than for $300 < V_{sw} < 400$ km/sec at all five stations, although Eskdalemuir does not show this trend very clearly. There is a pre-noon peak of the occurrence pattern.

One important feature visible in the plots is that high solar wind velocity drives the Pc3, 4 pulsations activity earlier, in the local morning sector, than low solar wind velocity does: the small triangles in the diagrams have their apex showing the median of the occurrence distribution of the Pc3, 4 activity at different local time; the median of each distribution moves towards the morning local time as the solar wind velocity increases, suggesting that high solar wind velocity affects the Pc3, 4 pulsations at earlier

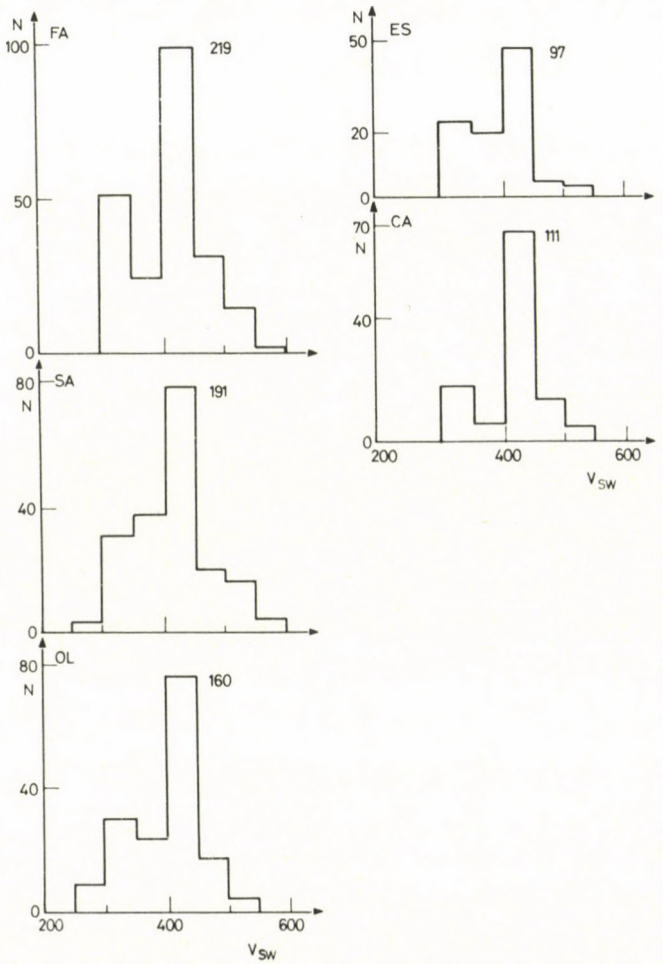

Fig. 8. Histogram showing the number of pulsation events against solar wind velocity at 5 ground stations

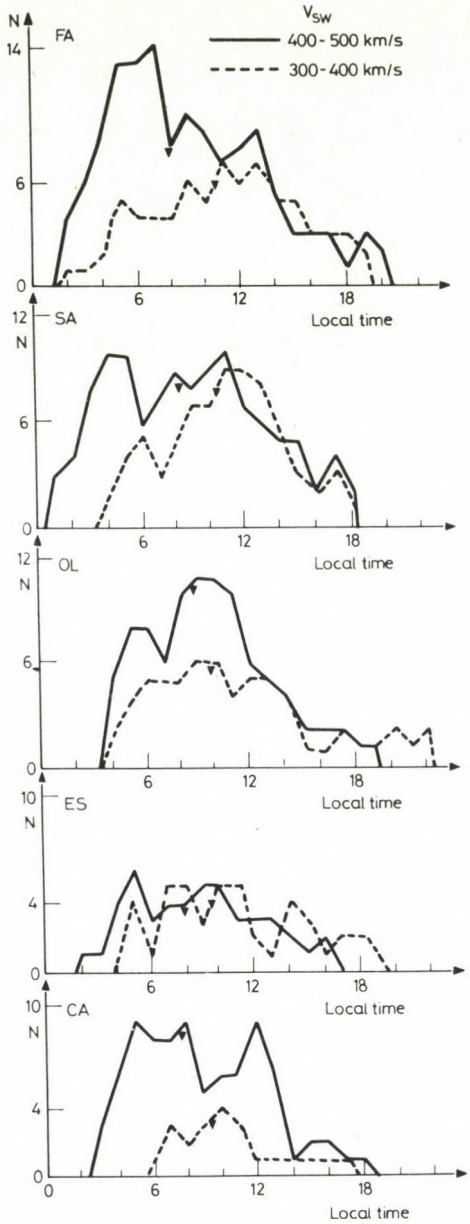

Fig. 9. Effect of solar wind velocity on the diurnal occurrence pattern of Pc3, 4 pulsation at 5 ground stations. The small triangles indicate the median local time for the occurrence of the pulsations

local morning hours than the time when low solar wind velocity is effective; for 400–500 km/sec the median is at around 08 LT, for 300–400 km/sec the median is at ~IOLT.

The precise relation of energy level of Pc3, 4 activity to the solar wind velocity cannot be judged from the results above. In the following section, the regression analysis performed to determine more precisely the relationship which exists between the solar wind velocity and the magnetic energy are presented.

Effect of V_{sw} on the Pc3, 4 pulsations energy

The power spectra provide measures of magnetic energy density in $(nT)^2/Hz$. The total energy of magnetic fluctuation is obtained by integrating the power spectral estimates over a given frequency range. Assuming that power is related to energy the magnetic energy density is referred to simply as magnetic energy.

Using the same number of events as was in Fig. 8 scatter plots were produced to illustrate the general trend of the relationship between the Pc3, 4 energy and the solar wind velocity as shown in Figs 10–14. The upper panel *a* of each figure shows the Pc3

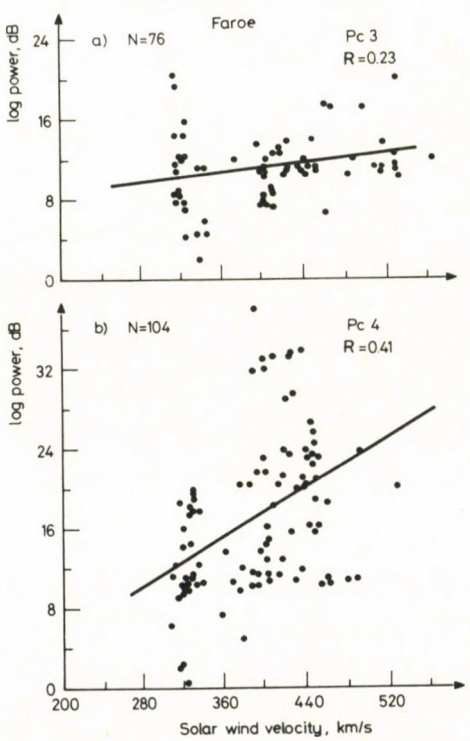

Fig. 10. Scatter plots of ground magnetic energy and solar wind velocity for Pc3 (a) and Pc4 (b) pulsations at Faroe

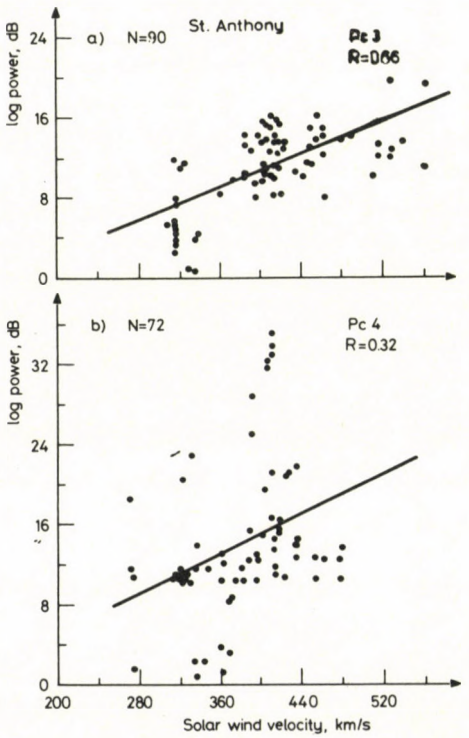

Fig. 11. Scatter plots of ground magnetic energy and solar wind velocity for Pc3 (a) and Pc4 (b) pulsations at St. Anthony

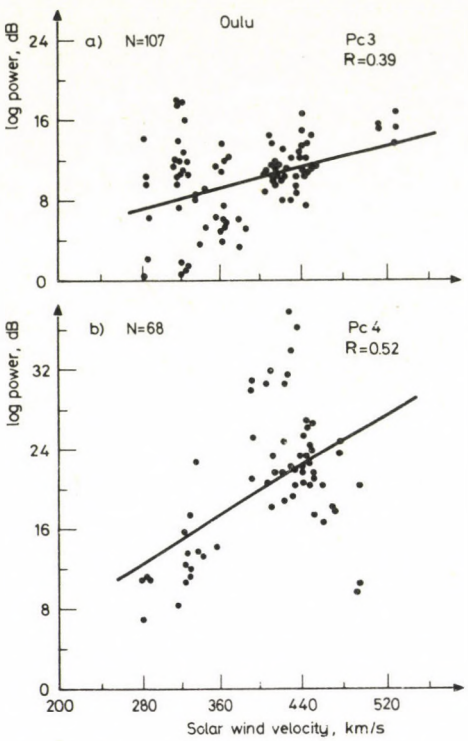

Fig. 12. Scatter plots of ground magnetic energy and solar wind velocity for Pc3 (a) and Pc4 (b) pulsations at Oulu

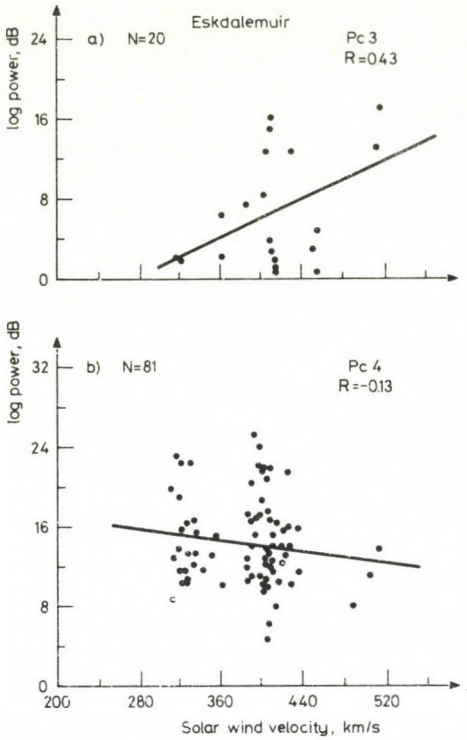

Fig. 13. Scatter plots of ground magnetic energy and solar wind velocity for Pc3 (a) and Pc4 (b) pulsations at Eskdalemuir

data and the lower panel *b* shows the Pc4 data, N is the number of data points used in each scatter diagram. The magnetic energy was measured in terms of log peak power density (dB). Each point in the scatter diagrams corresponds to the power peak of the power spectrum calculated at 30 mins segments and the corresponding 30 mins value of the solar wind velocity.

Linear regression analysis was performed to determine quantitatively the relationship between the energy of the ground pulsations and the solar wind velocity. The least square best fitting lines for the scatter plots were derived; the standard error of estimates (SEE) was determined to indicate the degree of scatter about the regression line; and the coefficient of the linear correlation (R) was calculated.

The results obtained are summarized in Table V. Taken in order of columns the table contains the following items: station (STN); number of events (N); average solar wind velocity ($\bar{V}_{sw}$); average energy level ($\bar{E}$), slope (C_1), intercept (C_0), coefficient of linear correlation (R) and type of pulsations. The table clearly indicates that there is no consistency in the influence of the solar wind velocity on the energy of pulsations

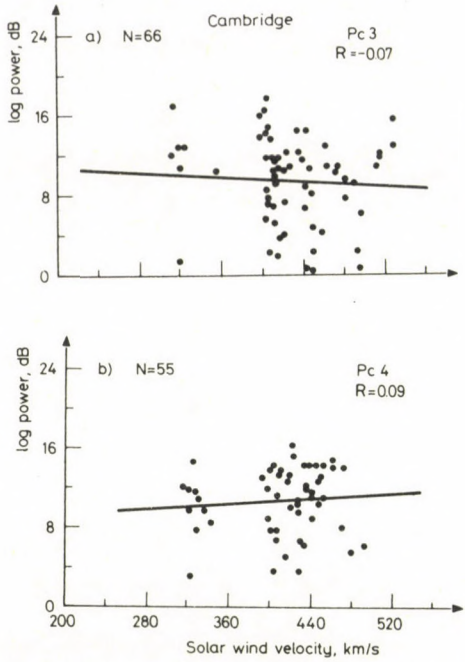

Fig. 14. Scatter plots of ground magnetic energy and solar wind velocity for Pc3 (a) and Pc4 (b) pulsations at Cambridge

Table V

Results of linear regression analysis of the dependence of magnetic energy on the solar wind veliocity ($E - V_{sw}$ relation) for five ground stations

Stn	N	$\bar{V}_{sw}$	$\bar{E}$	$E = C_1 V_{sw} + C_0$			Type
				C_1	C_0	R	
FA	76	411.85 ± 8.07	10.99 ± 0.38	0.01 ± 0.005	6.35 ± 2.25	0.23	
SA	90	406.78 ± 6.51	10.77 ± 0.40	0.40 ± 0.005	−5.76 ± 2.03	0.66	
OL	107	382.64 ± 5.86	9.94 ± 0.39	0.03 ± 0.006	0.19 ± 2.30	0.39	Pc3
ES	20	413.15 ± 11.29	6.61 ± 1.27	0.05 ± 0.02	−13.26 ± 9.94	0.43	
CA	66	424.76 ± 6.37	9.36 ± 0.55	−0.006 ± 0.011	11.98 ± 4.59	−0.07	
FA	104	391.00 ± 5.19	17.02 ± 0.77	0.06 ± 0.01	−6.98 ± 5.29	0.41	
SA	72	381.14 ± 5.97	14.24 ± 0.92	0.05 ± 0.02	−4.39 ± 6.71	0.32	
OL	68	406.46 ± 7.05	20.52 ± 0.84	0.06 ± 0.01	−4.96 ± 5.14	0.52	Pc4
ES	81	387.29 ± 4.84	14.27 ± 0.48	−0.01 ± 0.01	19.43 ± 4.34	0.13	
CA	55	411.75 ± 6.09	10.74 ± 0.44	0.007 ± 0.009	8.03 ± 4.09	0.09	
FA	180	399.45 ± 4.58	14.11 ± 0.52	0.03 ± 0.008	4.37 ± 3.38	0.22	
SA	162	395.98 ± 4.60	12.29 ± 0.48	0.03 ± 0.008	−1.02 ± 3.12	0.32	
OL	175	391.21 ± 4.61	14.01 ± 0.56	0.05 ± 0.008	−7.16 ± 3.26	0.45	Pc3, 4
ES	101	393.34 ± 4.62	12.75 ± 0.55	−0.01 ± 0.01	18.03 ± 4.65	0.11	
CA	121	419.18 ± 4.44	10.02 ± 0.36	−0.003 ± 0.007	11.06 ± 3.14	0.03	

among the five stations, at least in terms of the period of the magnetic activity; the variations in slope and coefficient of linear correlation do not follow any definite order with respect to the periods of pulsations. However, broadly there is a general tendency of rise in energy level of the pulsation with the increase of the solar wind velocity. The correlation coefficient, although consistently low and insignificant at Cambridge, is positive and significant at four other stations in the network. The average solar wind velocity for the pulsations activity at all stations and at the various period bands is approximately 400 km/sec.

Looking at the scatter plots more closely there is latitudinal effect on the dependence of magnetic energy (E) on the solar wind velocity (V_{sw}). [Later in this paper the dependence will be referred to simply as the $E - V_{sw}$ relation]. The two stations of lower latitudes, namely Cambridge and Eskdalemuir have weak magnetic energy and both stations show relatively poor $E - V_{sw}$ relation. Cambridge which is at the lowest geomagnetic latitude (52° N) in the array of five stations is the worst affected. It exhibits almost a flat $E - V_{sw}$ relation for all the period bands examined, the Pc3, Pc4 and Pc3, 4. The three stations at higher latitudes, Faroe, St. Anthony and Oulu have comparatively strong magnetic energy especially in the Pc4 band and have good $E - V_{sw}$ relation. In particular the Pc3 data at St. Anthony illustrates a convincing $E - V_{sw}$ relation, see Fig. 11.

Generally there is a large scatter in the $E - V_{sw}$ relation at all five stations. The large scatter is indicative of many factors that may be responsible for the generation of the Pc3, 4 activity at the ground stations.

Part 2: Effect of cone angle

a) General occurrence distribution pattern

The occurrence distribution pattern of the Pc3, 4 events at the five stations is shown in the form of the polar diagrams in Fig. 15. The radius of each shaded sector, which is 15° represents the number of the Pc events (N). It is noticeable that, at all ground stations, most events were observed when the cone angle was 15°–45° and hardly any events occurred when the cone angle was 60°–90°. In fact there was no events at a wider range of cone angle at Cambridge and Eskdalemuir than at Oulu, St. Anthony and Faroe; the three stations have larger L-values than Cambridge and Eskdalemuir.

The distribution pattern of the natural IMF cone angle is inserted in the bottom part of Fig. 15. The natural IMF orientation pattern was determined from 1053–1/2 hour data points regardless of whether or not there were pulsations activity observed at any of the five ground stations. The natural IMF orientation pattern is totally different from the general occurrence distribution pattern of the Pc3, 4 pulsations events. The

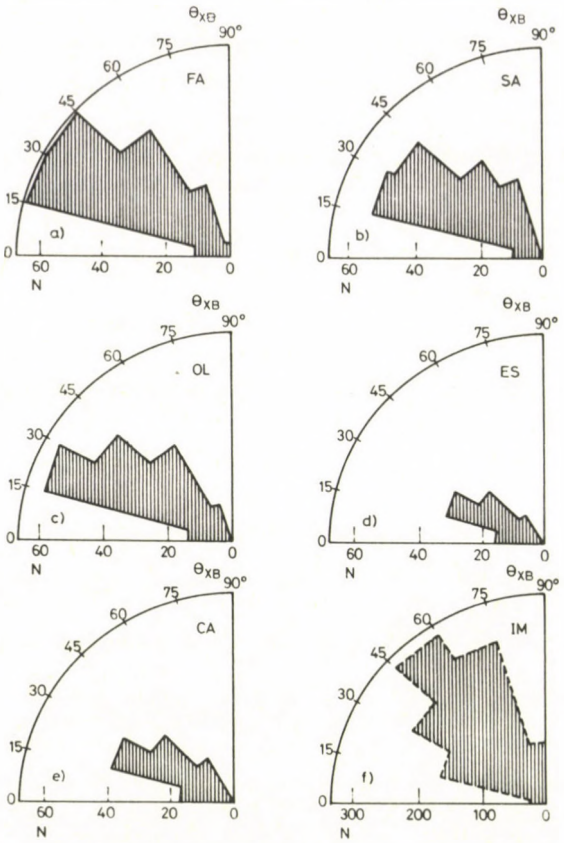

Fig. 15. Histograms showing the number of Pc3, 4 pulsation events against cone angle at five ground stations. The general distribution of cone angle is inserted in the bottom right hand side of the diagrams

distribution of the natural IMF orientation peaks at $\theta_{xB} \sim 50°$, whereas the general occurrence distribution for the Pc3, 4 events peaks at the angle $\theta_{xB} < 45°$.

It is evident that the occurrence of the ground pulsations takes place preferably at small cone angle of 15°–45°. The mostly preferred values of the cone angle for the occurrence of ground Pc3, 4 pulsations are shown in another way below, by means of cumulative distribution in Fig. 16.

The same number of Pc3, 4 events as used in Fig. 15 were used to produce the cumulative distribution curves. The distribution was made by determining for each station the number of Pc3, 4 events which fell below every 15° increment in the range of cone angle (θ_{xB}) from 0° to 90°; such cumulative distribution is known as 'less than' cumulative distribution. This format is convenient for showing the general occurrence distribution pattern of the Pc3, 4 events at once for all five stations. The median of the

occurrence distribution can easily be deduced straight from the cumulative distribution curves.

It is noticeable from Fig. 16 that the medians (the intersection of dotted line with the distribution curve) of the occurrence distribution at all the stations are at the cone angle range of 27°–37°. This means that for all the stations at least 50% of the Pc3, 4 pulsations occur when the cone angle is less than 27°–37°. It is also interesting to note that the stations with lower L-values (Cambridge and Eskadalemuir) have their medians at lower range of cone angle than the station with higher L-values (Faroe, Oulu and St. Anthony). This point will be discussed in later section.

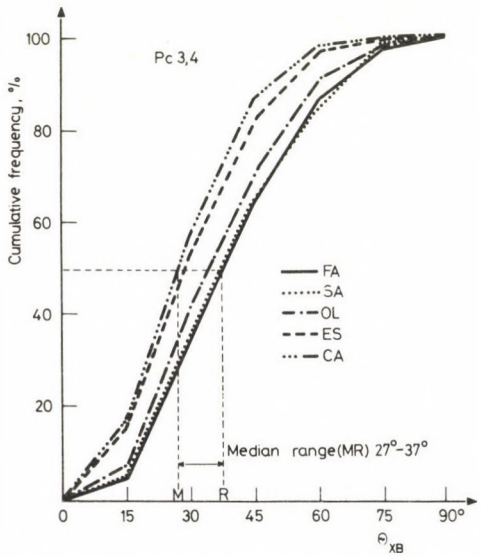

Fig. 16. Percentage cumulative frequencies of occurrence of cone angle from 5 ground stations for Pc3, 4 pulsations

b) The cone angle effect on Pc3 and Pc4 pulsations

The investigation of the dependence of the magnetic energy on the cone angle was carried out by the similar regression procedure as described previously for the solar wind velocity. The effect of the cone angle on the two period bands designated by Pc3 and Pc4 separately was investigated. The dependence of the ground magnetic energy in the two period bands on the cone angle is shown in Figs 17–21. The top panel (*a*) shows the Pc3 data, the bottom panel (*b*) shows the Pc4 data. The number in each scatter diagram is the number of the data points (N) in each of the scatter plots.

Table VI summarizes the results of the investigation of the dependence of the magnetic energy on the cone angle. There is a strong negative correlation between the

energy of the ground pulsations and the IMF cone angle— the magnetic energy decreases as the cone angle increases. The general negative correlation between the energy of the pulsations and the cone angle is clearly indicated by negative slopes (C_1) at the five stations and for all the three period bands Pc3, Pc4 and Pc3, 4. The Pc3 band is more strongly related to the cone angle than the Pc4 band. This is brought out clearly by generally higher linear correlation coefficient for the Pc3 band than for the Pc4 band. St. Anthony and Oulu (Figs 18 and 19) are good examples of showing the difference in effect of cone angle on the two frequency bands.

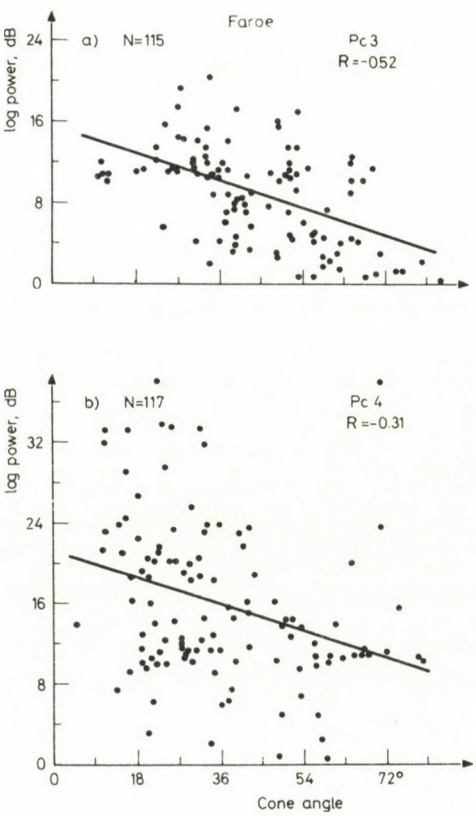

Fig. 17. Scatter plots of ground magnetic energy and cone angle for Pc3 (a) and Pc4 (b) at Faroe

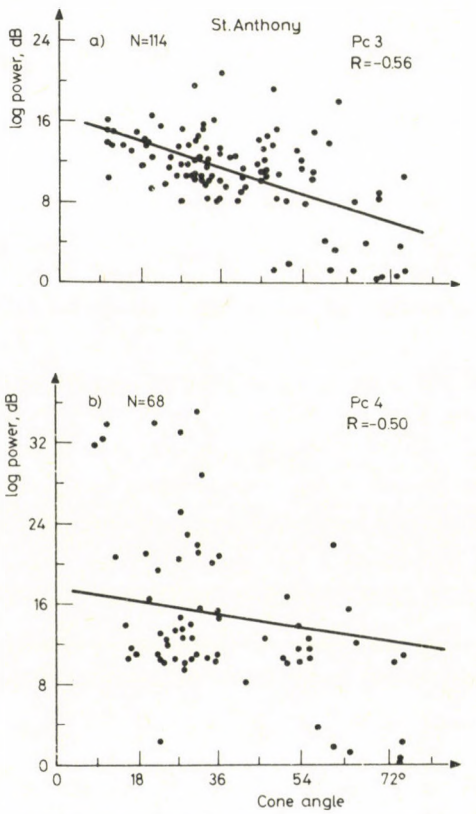

Fig. 18. Scatter plots of ground magnetic energy and cone angle for Pc3 (a) and Pc4 at St. Anthony

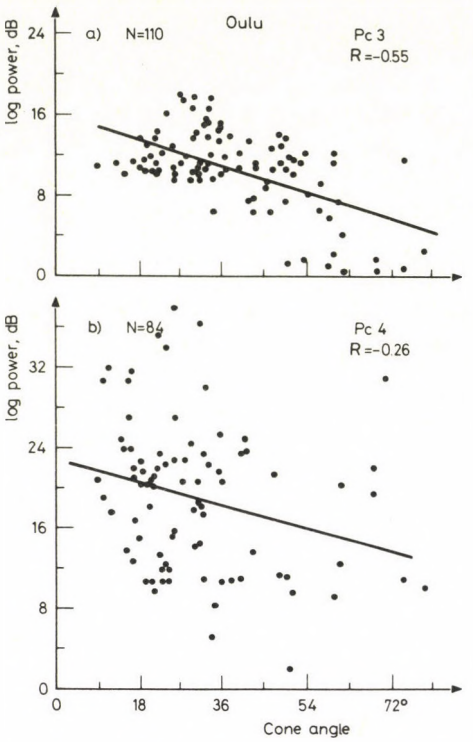

Fig. 19. Scatter plots of ground magnetic energy and cone angle for Pc3 (a) and Pc4 (b) at Oulu

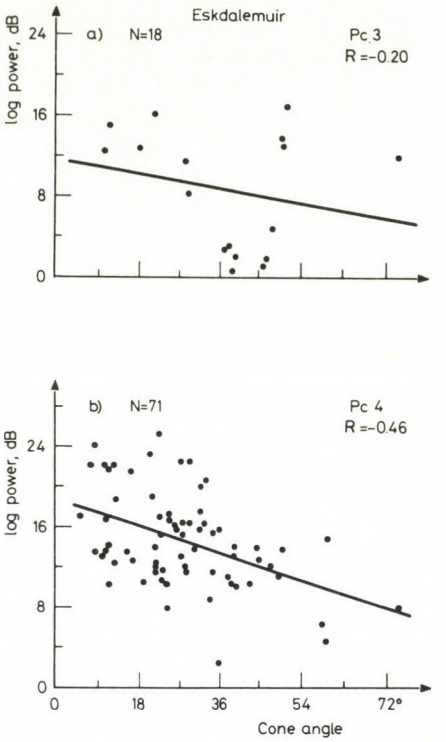

Fig. 20. Scatter plots of ground magnetic energy and cone angle for Pc3 (a) and Pc4 (b) at Eskdalemuir

Part 3: Effect of IMF magnitude (B) on the frequency of Pc3, 4 Pulsations

The relationship between the frequency of the ground pulsations and the IMF magnitude was tested. As before two separate bands of the ground magnetic activity that is the Pc3, and Pc4 were considered. The frequency of the ground pulsations was determined from the peak of the power spectrum calculated for the 30 min intervals. 30 min values of the IMF magnitude (nT) were plotted against the frequencies of the pulsation activity for the five stations. Then the same procedure of linear regression analysis already described in the previous sections was applied to these data.

The results generally indicate that the frequency of the ground pulsations increases with the rise in the IMF magnitude. The frequencies of the Pc3 band show strong dependence on the IMF magnitude whereas for the Pc4 band the dependence is considerably weak.

Detailed results are given in terms of regression lines in Fig. 22 and in tabular form, Table VII. Examination of the diagrams for the regression lines indicates that

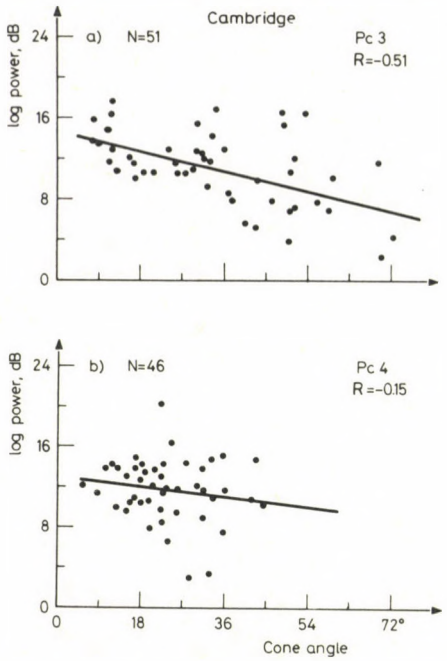

Fig. 21. Scatter plots of ground magnetic energy and cone angle for Pc3 (a) and Pc4 (b) pulsations at Cambridge

Table VI

Results of linear regression analysis of the dependence of magnetic energy on the cone angle ($E-\theta_{xB}$ relation) for five ground stations

Stn	N	$\bar{\theta}_{xB}$	$\bar{E}$	$E=C_1\theta_{xB}+C_0$		R	Type
				C_1	C_0		
FA	115	44.45±1.52	8.69±0.43	−0.15±0.02	15.31±1.08	0.52	
SA	114	39.03±1.53	10.79±0.40	−0.14±0.02	16.39±0.85	0.56	
OL	110	37.89±1.41	10.56±0.37	−0.14±0.02	15.96±0.86	0.55	Pc3
ES	18	37.46±4.0	8.65±1.43	−0.08±0.09	11.47±3.68	0.21	
CA	51	33.86±2.49	11.07±0.5	−0.10±0.02	14.57±0.95	0.51	
FA	117	35.62±1.61	15.77±0.75	−0.14±0.04	20.90±1.63	0.31	
SA	68	36.72±2.17	14.59±0.98	−0.23±0.05	22.91±1.97	0.31	
OL	84	30.43±1.72	19.03±0.81	−0.12±0.05	22.78±1.73	0.26	Pc4
ES	71	27.62±1.65	14.45±0.55	−0.15±0.04	18.65±1.10	0.46	
CA	46	23.58±1.33	11.76±0.46	−0.05±0.05	12.92±1.28	0.15	
FA	232	39.89±1.14	12.31±0.49	−0.19±0.03	19.87±1.11	0.44	
SA	182	38.30±1.25	12.19±0.48	−0.19±0.02	19.28±0.99	0.50	
OL	194	34.61±1.12	14.23±0.50	−0.19±0.03	20.75±1.13	0.41	Pc3, 4
ES	89	29.63±1.57	13.20±0.60	−0.17±0.04	18.24±1.17	0.46	
CA	97	29.25±1.55	11.35±0.34	−0.09±0.02	14.04±0.67	0.42	

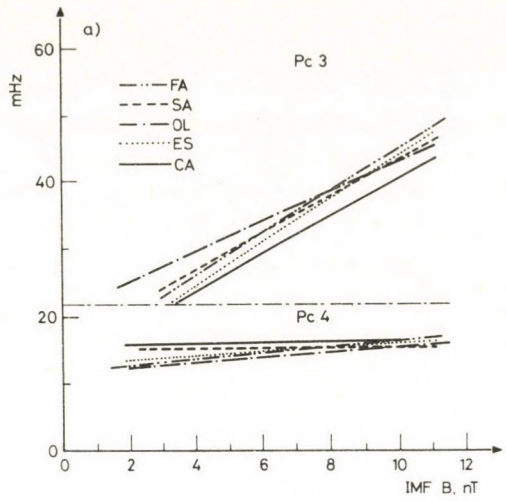

Fig. 22. Two groups of regression lines of the form $F = C_0 + C_1 B$ representing the F–B relation at 5 ground stations: *a)* 'inclined' regression lines for Pc3 pulsations, *b)* near 'horizontal' regression lines from the Pc4 pulsations

Table VII

Results of linear regression analysis of the dependence of frequency of pulsations on the IMF magnitude ($F - B$ relation) at five ground stations

Stn	N	$\bar{B}$	$\bar{F}$	$F = C_1 B + C_0$		
				C_1	C_0	
CA	67	5.22 ± 0.13	27.5 ± 0.7	2.75 ± 0.59	13.1 ± 3.2	
ES	18	5.65 ± 0.28	29.8 ± 2.7	3.31 ± 2.21	11.1 ± 12.8	
FA	126	5.83 ± 0.15	32.3 ± 0.8	3.19 ± 0.35	13.7 ± 2.1	Pc3
OL	149	5.43 ± 0.10	33.0 ± 0.6	2.18 ± 0.49	21.2 ± 2.7	
SA	137	5.92 ± 0.15	32.3 ± 0.6	2.61 ± 0.27	16.8 ± 1.7	
CA	52	4.27 ± 0.13	16.1 ± 0.4	0.14 ± 0.49	15.5 ± 2.1	
ES	76	4.36 ± 0.13	14.4 ± 0.4	0.33 ± 0.40	13.0 ± 1.8	
FA	124	4.91 ± 0.13	14.3 ± 0.4	0.43 ± 0.27	12.1 ± 1.4	Pc4
OL	85	4.96 ± 0.19	13.6 ± 0.5	0.40 ± 0.26	11.7 ± 1.3	
SA	68	5.19 ± 0.22	15.5 ± 0.6	0.10 ± 0.31	15.0 ± 1.7	
CA	119	4.80 ± 0.10	22.5 ± 0.7	3.60 ± 0.52	5.2 ± 2.6	
ES	94	4.60 ± 0.13	17.4 ± 0.9	2.82 ± 0.66	4.4 ± 3.1	
FA	250	5.38 ± 0.10	23.4 ± 0.7	3.46 ± 0.38	4.8 ± 2.1	Pc3, 4
OL	234	5.26 ± 0.10	26.0 ± 0.8	2.14 ± 0.49	14.7 ± 2.7	
SA	205	5.68 ± 0.13	26.7 ± 0.7	2.49 ± 0.35	12.6 ± 2.1	

there are two distinct groups of the regression lines, that is the 'inclined' regression lines representing the Pc3 band and the 'near horizontal' regression lines representing the Pc4 band.

The table indicates that the Pc3 magnetic activity has generally good correlation with the IMF magnitude at the five ground stations; the slope (C_1) of the linear regression line is fairly consistently about 3 mHz/nT among the stations. The Pc4 band has consistently flat but positive slope $C_1 < 1$ mHz/nT at all five stations considered here, implying that the Pc4 pulsations have poor correlation with the IMF magnitude. Combined Pc3 and Pc4 band (Pc3, 4) has different feature from either Pc3 band or Pc4 taken separately; the slope of the linear regression line for the Pc3, 4 band varies considerably from station to station. For instance Cambridge has the highest value for the slope ($C_1 = 3.6$ mHz/nT) whereas Oulu has the lowest ($C_1 = 2.14$ mHz/nT). Similarly the intercept (C_0) is not consistent among the stations as clearly indicated in the table.

Further investigation was made on the effect of the IMF magnitude on the Pc3 band only, by forcing the least square best fitted line through zero origin. The regression line passing through origin is defined by $F = CB$, the constant (C) gives the slope of the $F - B$ dependence. The Pc3 band was chosen for examination because the results described above indicate that the relationship between the IMF magnitude and the frequency of pulsations in the Pc3 band is promising. The following relations were derived for the five stations $F = 5.36 \pm 0.40B$ (Faroe); $F = 5.25 \pm 0.35B$ (St. Anthony); $F = 5.90 \pm 0.58B$ (Oulu); $F = 5.20 \pm 2.29B$ (Eskdalemuir); and $F = 5.16 \pm 0.67B$ (Cambridge). The least square best fitted lines representing above functional relation are shown in Fig. 23 along with the empirical relation $T = 160/B$ or $F = 6.25B$ of Gul'elmi et

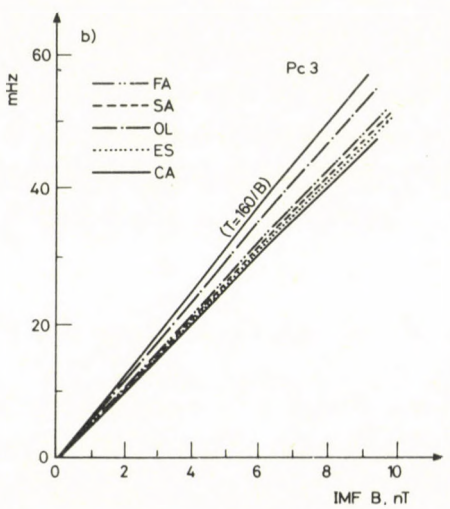

Fig. 23. Regression lines of the form $F = CB$ (forced through origin) from 5 ground stations together with the empirical relation $F = 6.25B$ (or $T = 160/B$)

Table VIII
Relation between the frequency of Pc3 pulsations and the magnitude of the IMF

Data	N	$\bar{B}$	$\bar{F}$	$F=CB$		$F=C_0+C_1B$		
				C	SEE	C_1	C_0	SEE
FA	126	5.83±0.15	32.3±0.8	5.36±0.40	7.74	3.19±0.35	13.7±2.1	6.69
S	137	5.92±0.15	32.3±0.6	5.25±0.35	7.16	2.61±0.27	16.8±1.7	5.44
OL	147	5.43±0.10	33.0±0.6	5.9±0.58	8.68	2.8±0.49	21.2±2.7	7.32
ES	18	5.65±0.28	29.8±2.7	5.2±2.29	11.25	3.31±2.21	11.1±12.8	11.32
CA	67	3.22±0.13	27.5±0.7	5.16±0.67	5.96	2.75±0.59	13.1±3.2	5.34

al. (1973). The lines for all the stations certainly indicate a clear frequency dependence on the IMF magnitude and fairly close to the empirically established relation, at least when the regression lines are forced through origin.

However Green et al. (1983) has shown that forcing the regression line through origin is not statistically good fit to the data. To illustrate this the results of the regression analysis for the Pc3 expressed in the form of $F=C_0+C_1B$ in Table VII were compared with the results obtained by forcing the regression lines through origin (i.e, $F=CB$) see Table VIII. A measure of statistically good fit to the data is chosen to be the standard error of estimate (SEE) of the regression lines, SEE is the degree of scatter about regression line.

A critical look at Table VIII reveals that the regression lines of the form $F=C_0+C_1B$ have less SEE than those of the lines $F=CB$. The ES data are rather unusual and may be considered unreliable in this respect probably because of small number of degrees of freedom. It is therefore implied that the form $F=C_0+C_1B$ is statistically better fit to the data than the form $F=CB$.

Simultaneous Pc3, and Pc3, 4

The exercise described in part 3 considers any Pc3, 4 pulsations activity regardless of whether the events are seen at only one station or simultaneously at, at least two stations in the network of five stations. Now the simultaneous events at station pairs in the E – W and N – S profile are analysed. The simultaneous events were selected on the basis of coincidence in their frequencies within ±10% error. The justification of this selection is that if the IMF does determine the frequency of magnetospheric pulsations it is expected, from geometry, that it is a wide source in longitude and therefore the stations with large longitudinal separation (>2 hrs) would see the same frequency of pulsations.

In the E – W profile the following pairs were considered; Oulu and St. Anthony separated by approximately 6 hrs, Faroe and St. Anthony separated by ~4 hrs; Oulu and Faroe separated by ~2 hrs; (the local time difference between the stations are

expressed to the nearest hour). In the N – S profile Faroe and Cambridge (separated by geographic latitude $\sim 10°$) were considered.

It is to be noted that the events which were simultaneously recorded among the stations were largely Pc3 pulsations; however, in the analysis, a few Pc4 that were also recorded simultaneously at the station pairs are included.

The results of the linear regression analysis show that there is a considerable improvement in the relationship between the frequency of the ground pulsations and

Table IX

Relation between the frequency and the IMF magnitude for the simultaneous Pc3, 4 events

Data	Separation	N	B	$\bar{F}$	$F=CB$		$F=C_0+C_1B$				Type
					C	SEE	C_1	C_0	SEE	R	
$T_{SA}=T_{OL}$	6 hrs	19	5.12±0.30	32.39±1.73	6.23	4.95	4.65±0.83	8.61±4.40	4.61	0.80	
$T_{SA}=T_{FA}$	4 hrs	24	5.82±0.42	31.61±2.9	5.28	6.85	3.97±0.65	8.51±4.02	6.39	0.79	
											Pc3
$T_{OL}=T_{FA}$	2 hrs	42	5.43±0.19	30.98±1.21	5.65	5.26	4.69±0.63	5.53±3.52	5.17	0.76	
$T_{CA}=T_{FA}$	10° lat	28	4.89±0.18	26.66±0.9	5.38	4.17	3.47±0.78	9.71±3.9	3.82	0.65	
$T_{SA}=T_{OL}$	6 hrs	20	4.99±0.31	31.66±1.30	6.24	4.83	4.88±0.75	7.28±3.89	4.54	0.83	
$T_{SA}=T_{FA}$	4 hrs	26	5.57±0.42	30.03±2.22	5.25	6.92	4.27±0.62	6.22±3.69	6.68	0.82	
											Pc3,4
$T_{FA}=T_{OL}$	2 hrs	57	5.22±0.16	26.11±1.43	5.03	8.15	5.71±0.87	−3.69±4.69	8.17	0.66	
$T_{CA}=T_{FA}$	10° lat	35	4.75±0.15	24.61±1.03	5.15	4.62	4.49±0.88	3.27±4.27	4.64	0.66	

the IMF magnitude when the same frequency is recorded simultaneously over a large distance separating the ground stations. The results for the Pc3 and Pc3, 4 bands are summarized in Table IX. The first column of the table contains pairs of the stations that saw the same period of pulsations activity simultaneously; for example $T_{SA}=T_{OL}$ means the same period measured at St. Anthony and Oulu simultaneously; the second column of the table contains the distance of separation between the stations (pairs) expressed in terms of local time in the case of E – W profile and degrees of latitudes in case of N – S profile, the rest of the columns contains the same statistical quantities that have already been described.

The least square best fitted lines for the simultaneous events are shown in the scatter diagrams in Figs 24–27. The top panel shows the Pc3 data and the bottom panel shows the Pc3, 4 data. The regression lines exhibit a convincing fit to the data suggesting that the $F-B$ relation for the station pairs is better than that for the single stations.

The correlation coefficient is very high ($R\sim 0.8$) particularly for the stations separated by more than two hours, local time. The improved relation is also indicated by the steep slope, on the average $C_1=4.2$ mHz/nT for the Pc3 and $C_1=4.8$ mHz/nT for the Pc3, 4 band.

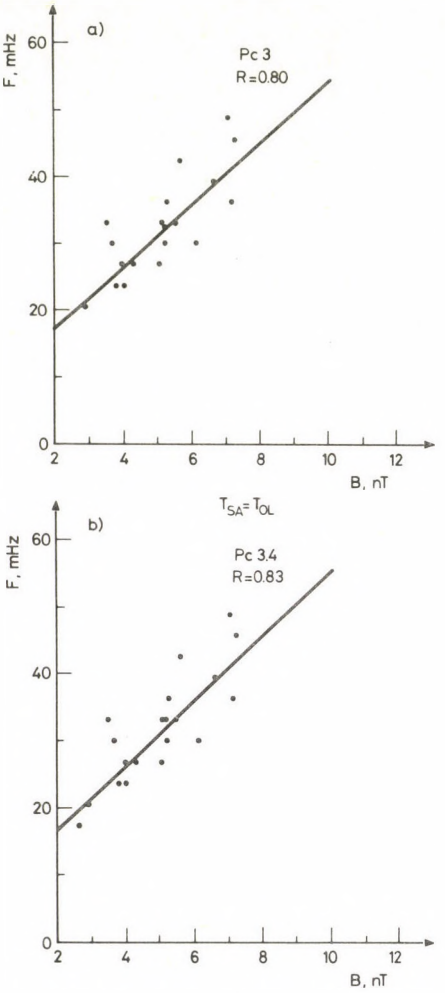

Fig. 24. Scatter plots of measured frequency (F) against the IMF magnitude (B) when the pulsation periods at St. Anthony and Oulu were the same within 10%, ($T_{SA}=T_{OL}$) for Pc3 (a) and Pc4 (b) pulsations

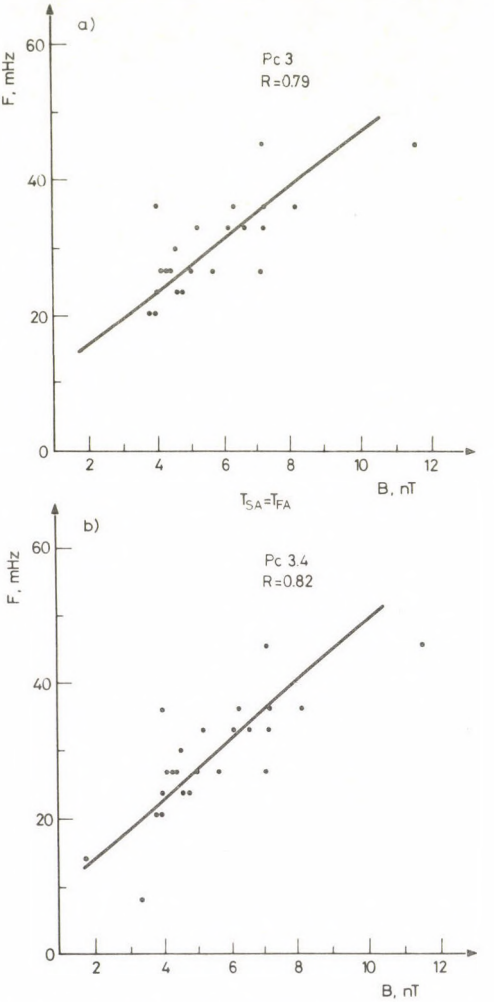

Fig. 25. Scatter plots of measured frequency (F) against the IMF magnitude (B) when the pulsation periods at St. Anthony and Faroe were the same within 10%, ($T_{SA}=T_{FA}$) for Pc3 (a) and Pc4 (b) pulsations

Generally there is not much difference in the improved relationships for the case of Pc3 and Pc3, 4 probably because the Pc3 events dominate in every case as noted above.

Looking at the Table IX more closely, once again the regression lines of the form $F \sim C_0 + C_1 B$ fit the data better than the form $F = CB$. This is judged from values of the standard error of estimates (SEE). Another point revealed by the table is that the SEE values for the simultaneous events are significantly lower than those for the single

station data shown in Table VIII. The results for the simultaneous events, particularly the $T_{SA} = T_{OL}$ data $F = (7.28 \pm 3.89) + (4.88 \pm 0.75)B$ compare quite well with the derived relationship by Gul'elmi and Bolshakova (1973), i.e. $F = 11.8 \pm 5.1B$, also using the simultaneous records with coincident frequencies from a pair of stations, Borok and Petropavlosk. This relationship was the original basis for the Borok B index. The relationship has been confirmed by Green et al. (1983) who used one year's data from a pair of stations Hartland and Borok to obtain $F = (10.1 \pm 1.5) + (5.16 \pm 0.21)B$. The

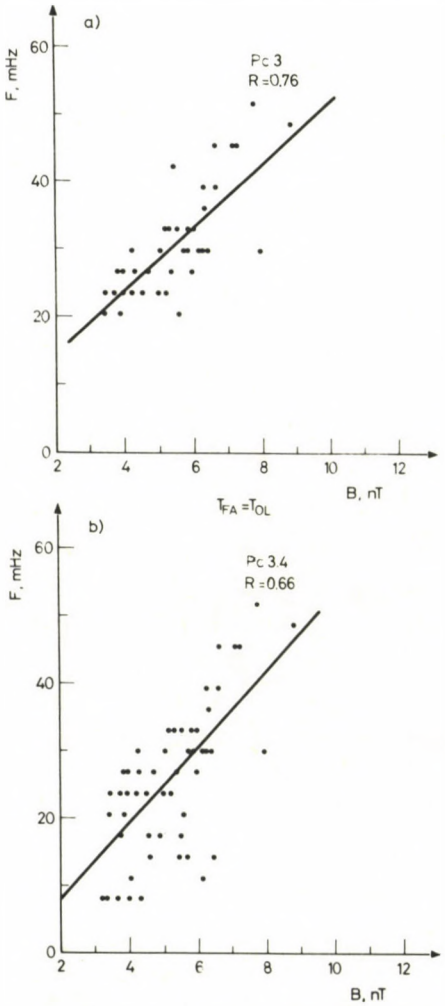

Fig. 26. Scatter plots of measured frequency (F) against the IMF magnitude (B) when the pulsation periods at Faroe and Oulu were the same within 10%, ($T_{FA} = T_{OL}$) for Pc3 (a) and Pc4 (b) pulsations

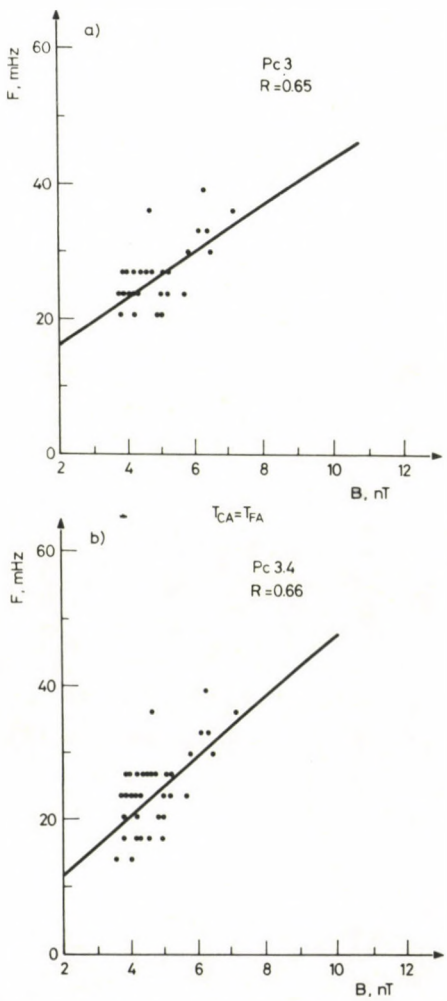

Fig. 27. Scatter plots of measured frequency (F) against the IMF magnitude (B) when the pulsation period at Cambridge and Faroe were the same within 10%, ($T_{CA} = T_{FA}$) for Pc3 (a) and Pc4 (b) pulsations

dependence of the frequency of pulsations on the IMF magnitude obtained from the use of coincidental frequencies at a pair of stations is perhaps the most reliable. The separation between the two stations, in longitude, should be preferably more than 4 hours local time.

Discussions

The results of the investigation made in this paper indicate that the pulsations observed at the five ground stations appear to be influenced strongly by three solar wind parameters, namely the IMF magnitude (B) and cone angle (θ_{xB}), and solar wind velocity (V_{sw}). The control by three solar wind parameters is suggesting external origin of some of the Pc3, 4 pulsations reported here. Such origin can be understood in a framework in which disturbances in the magnetosheath reach the magnetopause and amplified there by Kelvin-Helmholtz instability described by Southwood (1968).

The source of the magnetosheath disturbances that are amplified at the magnetopause may be the upstream waves such as the ones described by Barnes (1970). Barnes model for the generation of upstream waves was based on ion-cyclotron resonant instability associated with a stream of protons flowing upstream (along interplanetary magnetic field) from the bowshock: beam particles can interact strongly only with hydromagnetic waves whose frequency, as seen in the frame of the beam, has Doppler shifted up to ion gyrofrequency. According to the model, a proton streaming velocity of two or three times the solar wind velocity would locally generate hydromagnetic waves far upstream in the interplanetary medium. An attractive theory of the external origin of geomagnetic pulsations was given initially by Gul'elmi (1974). Gul'elmis idea was based on an early report by Troitskaya et al. (1971) that the period of pulsation observed on the surface of the Earth was directly proportional to the gyroperiod (T_p) of proton in the interplanetary medium, $T=(2.5\pm0.5)T_p$, and that waves discovered in the interplanetary medium had the same property, namely they are waves that are locally generated by a cyclotron resonant instability involving a beam of backstreaming energetic protons reflected from the bowshock; the waves have their frequency directly proportional to the protons' gyrofrequency. Gul'elmi estimated that the resonant frequency produced by the instability of the reflected proton is the same as the average frequency of the Pc3 pulsations ($F\sim30$ mHz).

Important consequence of Gul'elmis theoretical consideration is that if the ground spectrum was really formed in the interplanetary medium, the carrier frequency must be proportional to the magnitude of the IMF as follows,

$$F_{(\mathrm{mHz})}\simeq 6B_{(\mathrm{nT})} \quad \text{or} \quad T\simeq 160/B\,.$$

In fact Gul'elmi and Bolshakova (1973) derived the relation $F=11.8+5.1B$ between the frequency of ground Pc3, 4 pulsations and the IMF magnitude. This relation was used to define the Borok-B index; an hourly number designed to provide an indirect

measure of the IMF magnitude from pulsation data. The reliability of the Borok index was tested by Russell and Fleming (1976) who showed that the index was 54% successful when recalibrated. Recently Green et al. (1983) showed that the expression such as the one derived by Gul'elmi and Bolshakova is indeed a statistically better fit to the data.

Using similar expression this paper has shown the frequency dependence of Pc3, 4 pulsations, on the IMF magnitude particularly for the Pc3 pulsations. This dependence is improved considerably if the pulsations with the same frequency are observed simultaneously over a large area on the Earth's surface, (see Figs 24–27). The justification of this result is that if the upstream waves determine a source for the magnetospheric pulsations it is expected, from geometry, that it is a wide source in longitudinal extent and therefore stations with large longitudinal separation would see the same event simultaneously.

The waves in the interplanetary medium can reach the magnetopause in the way suggested by Greenstadt (1972). The cone angle is important in this respect. Greenstadt (1972) postulated that waves of large amplitude formed in the subsolar bowshock region when the cone angle is less than $50° - 70°$ are propagated and convected to the dayside magnetopause where they couple to the magnetosphere and reach the ground as geomagnetic micropulsations. Greenstadt et al. (1980) worked out a rough guide to indicate that waves reaching the magnetopause must originate at the shock region for a limited range of cone angle near Parker's spiral angle ($\sim 45°$). According to this picture the bulk of wave excitation is supposed to occur (on the average) as a result of large amplitude of shock induced oscillations, commonly known as quasi-parallel structure in the prenon sector, west of the sub-solar point itself. This is compatible with the experimental results presented in this paper. Recall that most of the Pc3, 4 pulsations, on the ground were observed when the cone angle was small and limited to $\theta_{xB} < < 50° - 60°$. The small cone angle is favourable for the quasi-parallel shock structure to prevail in the subsolar region.

It is difficult to visualize the coupling of the upstream disturbances to the magnetosphere because the transfer function is unknown. However the distribution patterns shown in Figs 15 and 16 are interesting in this respect, and may give some hints as to the way the upstream disturbance could reach the ground through the magnetosphere. Both figures show the variation of cone angle effect with L-values. Figure 15 shows that there are very little or no Pc3, 4 events for a wider range of cone angle at stations with low L-values (Cambridge and Eskdalemuir) than at stations with high L-values (Faroe, St. Anthony and Oulu). In fact there are no pulsations at Cambridge and Eskdalemuir for $\theta_{xB} > 60° - 90°$, whereas the absence of the events at Faroe, St. Anthony and Oulu occur at $\theta_{xB} > 75° - 90°$. Figure 16 shows that small cone angles (< 30) are more favorable for the appearance of Pc3, 4 pulsations at low L-values than at high L-value. These results qualitatively suggest that the Pc3, 4 pulsations may originate from the upstream waves of the subsolar bowshock region; the waves are

simply convected to the magnetopause by the magnetosheath plasma flows stream; from the magnetopause the waves may be coupled to the magnetosphere through field line resonance. In this context the waves convected along the surface of the magnetopause would be associated with small cone angles; from the magnetopause the coupled oscillations would reach the ground almost directly at low L-values. To reach high L-values the coupling would take place at the flanks of the magnetopause where stream line convection can transport waves from large cone angles.

A critical analysis has been carried out on the L-value dependence of the IMF cone angle effect using the same data by Russell et al. (1983). The analysis brings out the situation more clearly than what has been discussed above qualitatively. Russell et al. used normalized rate of occurrence of the dayside Pc3, 4 pulsations at the five stations and showed that there is a strong enhancement for low cone angle, and that the enhancement considerably decreases with the increase of L-values. The authors interpreted the results in terms of a source originating in the waves upstream of the subsolar bowshock, which are transported by convection to the magnetopause where they couple to oscillations of the magnetospheric field lines. Using a simplified magnetosheath flow pattern the authors attempted to justify the possibility of upstream waves reaching the Earth's surface as Pc3, 4 pulsations.

We now turn to the effects of solar wind velocity. It is observed in this work that the high solar wind velocity drive more pulsations than low; the energy of the pulsation increases with the increase in the solar wind velocity. Another important feature in the solar wind effect already noted earlier in this work (see Fig. 9) is that the high solar velocity drives the Pc3, 4 pulsations activity earlier, in the local morning sector, than low solar wind velocity does. There are three possible explanations for these results. First, high solar wind velocity would suggest that more energy in the quasi-parallel structure would be blown downstream into the magnetosheath adding its measure to energy already available for the excitation of the magnetopause. Second, the high solar wind velocity would cause the upstream waves to reach the magnetopause earlier in local time than low velocity. Third, the high solar wind speed would be associated with a disturbed magnetosphere in which a flux tube may readjust its position so as to bring enlarged amplitude of the waves of the shock origin to a limited latitude of ground stations where pulsations may be observed with enhanced energy.

In summary the discussion above implies both excitation and wave transfer. The instability at the magnetopause would simply act to amplify waves which have reached there from the upstream region.

Acknowledgements

This work is part of the research carried out at the Geomagnetism Unit, Institute of Geological Sciences (IGS). The author wishes to thank the Director for permission to use IGS data and for facilities to carry out the work. I also thank the Association of Commonwealth Universities which provided the fund for

carrying out the research. I am greatly indebted to W F Stuart and C A Green, both of IGS, for their constant encouragement and support to finish the work. Finally I am thankful to Prof. C T Russell for permission to use the ISEE data.

References

Arthur C W, McPherron R L 1977: Interplanetary magnetic field condition associated with synchronous orbit of Pc3 magnetic pulsations. *J. Geophys. Res.*, 5138.

Barnes A 1970: Theory of generation of bow-shock associated waves in the upstream interplanetary medium. *Cosmic Electrodynamics*, 1, 90.

Barraclough D R, Harwood J M, Leaton B R, Malin S R C 1975: A model of the geomagnetic field at epoch 1975. *Geophys. astr. Soc.*, 43, 645.

Bonifazi C, Cerulli-Irelli P, Egidi A, Formisano V, Moreno G 1978: The EGD positive ion experiment on the ISEE-B satellite. *IEEE Trans. Geosc. Electr.*, GE 16, 243.

Chen L, Hasegawa A 1974: A theory of long period magnetic pulsations; I. steady state of excitation of field line resonance. *J. Geophys. Res.*, 79, 1024.

Durney A C 1977: The International Sun-Earth-Explorer (formerly IME). *ESA Journal.* Vol. 1.

Green C A 1981: Continuous magnetic pulsations on the IGS array of magnetometers. *J. atmos. terr. Phys.*, 43, 883.

Green C A, Odera T J, Stuart W F 1983: The relationship between the strength of the IMF and the frequency of magnetic pulsations on the ground and in the solar wind. *Planet. Space Sci.*, 31, 559.

Greenstadt E W 1972: Field-determined oscillations in the magnetosheath as a possible source of medium period daytime micropulsations; paper prepared for Solar-Terrestrial Relation Symposium, Canada

Greenstadt E W, Olson J V 1976: Pc3, 4 activity and interplanetary field orientation. *J. Geophys. Res.*, 81, 5911.

Greenstadt E W, McPherron R L, Takahashi K 1980: Solar wind control of daytime, midperiod geomagnetic pulsations. *J. Geomag. Geoelect.*, 32, Suppl. II, SII 110.

Gul'elmi A V, Bolshakova O V 1973: Diagnostics of the interplanetary magnetic field from ground-based data on Pc2–4 micropulsations. *Geomagn. Aeron.*, 13, 331.

Gul'elmi A V, Plyasova-Bakounina T A, Shchepetnov R V 1973: Relationship between the period of geomagnetic pulsations Pc3, 4 and parameters of the interplanetary medium at the Earth's orbit. *Geomagn. Aeron*, 13, 535.

Kovner M S, Lebedev V V, Plyasova-Bakounina T A, Troitskaya V A 1976: On the generation of low frequency waves in the solar wind in the front of the bow-shock. *Planet. Space Sci.*, 24, 261.

Mills P M, Dyson K, Green CA, Stuart W F 1977: The data transcription and retrieval system used for cassette recording the IGS rubidium magnetometers. Geomagnetism Unit Rep. UK. Inst. of Geol. Sci. No. 20.

Odera T J 1982: The control and generation of magnetic pulsations on the ground and interplanetary space by parameters of the solar wind. Ph. D. Thesis, University of Edinburgh

Radoski H R 1966: Magnetic toroidal resonance and vibration field lines. *J. Geophys. Res.*, 71, 1891.

Riddick J C, Brown J, Forbes A J 1975: A low power movable observatory unit for magnetometer array application. Geomagnetism Unit Rep. UK. Inst. of Geol. Sci. No. 17.

Russell C T 1978: The ISEE 1 and 2 fluxgates magnetometers. *IEEE, Trans. Geos. Electr. GE.*, 16, No. 3, 239.

Russell C T, Fleming B K 1976: Magnetic pulsations as a probe of interplanetary magnetic field: A test of Borok-B-index, *J. Geophys. Res.*, 81, 5882.

Russell C T, Luhmann J G, Odera T J, Stuart W F 1983: The rate of occurrence of daytime Pc3, 4 pulsations: The L-value dependence of the IMF cone angle effect. IGPP publication No. 2409.

Singer H J, Russell C T, Kivelson M G, Greenstadt E W, Olson J V 1977: Evidence for the control of Pc3, 4 magnetic pulsations by the solar wind velocity. *Geophys. Res. Lett.*, 4, 377.

Southwood D J 1968: The hydromagnetic stability of the magnetospheric boundary. *Planet. Space Sci.*, 16, 587.

Southwood D J 1974: Some features of field line resonance in the magnetosphere. *Planet. Space Sci.*, 22, 483.

Stuart W F 1971: The high resolution magnetic stations operated in the Institute of Geological Sciences. Geomagnetism Unit Rep. UK, Inst. of Geol. Sci. No. 8.

Stuart W F, Green C A 1981: The array of magnetometers operated by IGS in NW Europe. Geomagnetism Unit Rep. UK. Inst. of Geol. Sci. No. 28.

Takahashi K, McPherron R L, Greenstadt E W, Neeley C A 1981: Factors controlling the occurrence of Pc3 magnetic pulsations at synchronous orbit. *J. Geophys. Res.*, 86, 5472.

Troitskaya V A 1967: Micropulsation and the state of the magnetosphere. Solar Terrestrial Physics, ed. King J W, Newman W S, Academic Press

Troitskaya V A, Plyasova-Bakounina T A, Gul'elmi A V 1971: Relationship between Pc2–4 pulsations and the interplanetary magnetic field. *Dokl. Akad. Nauk. U.S.S.R.*, 197, 1312.

Verő J, Holló L 1978: Connection between interplanetary magnetic field and geomagnetic pulsations. *J. atmos. terr. Phys.*, 40, 857.

Webb D, Orr D 1976: Geomagnetic pulsations (5–50 mHz) and the interplanetary magnetic field direction. *J. Geophy. Res.*, 81, 5941.

Webb D, Lanzerotti L J, Orr D 1977: Hydromagnetic wave observations at large longitudinal separations. *J. Geophys. Res.*, 82, 3329.

Wolfe A 1980: Dependence of mid-latitude hydromagnetic energy spectra on the solar wind speed and interplanetary magnetic field direction. *J. Geophys. Res.*, 85, 5977.

Wolfe A, Lanzerotti L J, MacLennan C G 1980: Dependence of hydromagnetic energy on the solar wind velocity and interplanetary magnetic field direction. *J. Geophys. Res.*, 85, 114.

Acta Geodaet., Geophys. et Montanist. Hung. Volume 19 (3–4), pp. 339–340 (1984)

SCIENTIFIC SESSION OF THE HUNGARIAN ACADEMY OF SCIENCES, FEBRUARY 15, 1983 AT THE 100TH AND 50TH ANNIVERSARIES OF THE FIRST AND SECOND POLAR YEARS AND AT THE 25TH ANNIVERSARY OF THE INTERNATIONAL GEOPHYSICAL YEAR

J VERŐ[1]

The Hungarian Academy of Sciences and the Hungarian National Committee of ICSU commemorated the two Polar Years and the International Geophysical Year (IGY) by a scientific session on February 15, 1983 according to the recommendations of the 19th ICSU General Assembly.

The session was opened by Professor J Tigyi, Chairman of the Hungarian ICSU Committee. Ten lectures were held, two by eminent foreign geophysicists, eight by Hungarian scientists. Professor Belousov from the Soviet Union who participated in the organization of the IGY, presented a review on the international cooperation in the study of the Earth. Professor Steinhauser from Austria lectured about the Austro–Hungarian Polar Expedition in 1872–74, closely connected with the idea of the First Polar Year. This paper is printed on the next pages.

Professor Gy Barta explained the realization of Weyprecht's idea from this expedition ten years later, and listed other predecessors of the Polar Years. Some highlights of this Year were the great magnetic storms on November 17 and 20, 1882 and the volcanic eruption of the Krakatoa in August, 1883 out of programme, but exactly within the fixed interval of observations.

Professor A Meskó outlined the role of international cooperation in Earth sciences. In order to obtain a comprehensive view of global phenomena, measurements have to be made at several observatories in different parts of the world. The first two intervals laid emphasis to less known polar regions, whereas in the IGY, the global components were of primary importance.

Dr. J Verő reviewed the history of geomagnetic research having developed during the IGY into magnetospheric physics. Hungary participated in these efforts

[1] Geodetic and Geophysical Research Institute of the Hungarian Academy of Sciences, H-9401 Sopron, P.O.B. 5, Hungary

quite early by magnetic observatories and analysis of certain variation types (L Steiner). Recently geomagnetic pulsations are of primary interest. This research was initiated during the IGY by the Hungarian Academy of Sciences in establishing the Nagycenk geomagnetic observatory. Dr. P Bencze reported on ionospheric research carried out since the IGY in Hungary, mainly also in the Nagycenk observatory. Ionospheric soundings are made at the Békéscsaba station of the Hungarian Meteorological Institute. Several Hungarian groups combined their efforts in the seventies to carry out the first ever Hungarian in situ ionospheric measurements (plasma parameters) onboard of rockets of the Vertical-series.

Professor A Somogyi described cosmic ray studies and planetological researches concentrated at the Central Institute of Physics of the Hungarian Academy of Sciences. Cosmic ray measurements have a long tradition in Hungary, and regular observations have been extended during and since the IGY, including cooperations with several foreign-based groups.

Meteorological aspects of the IGY were discussed by Professor B Bèll. He emphasized the importance of the First Polar Year as the first co-ordinated international observation. Aerological observations formed later a basis of the IGY-observation programmes. The first step toward cosmical meteorology was also made then by launching the first Soviet satellite during the IGY (Sputnik 1). Dr. G Götz dealt with the Global Atmospheric Research Programme (GARP) and the World Climate Programme, as continuations of the IGY. Past, present and future climates are in the focus of these programmes.

Solar physics was lastly reviewed by dr. B Kálmán, as a representant of the Heliophysical Observatory of the Hungarian Academy of Sciences in Debrecen. He mentioned the exceptionally high solar activity in 1957–58, and the International Quiet Sun Year in 1964–65. The latter was a success for the Debrecen group by the first observation of a complex sunspot group of the Proton Flare Project. Recently the 1979–81 Solar Maximum Years also contributed to our knowledge on solar-controlled terrestrial processes.

The scientific session was a welcome opportunity to survey past great personalities of Hungarian geophysics, important events and discoveries, as well as present problems of the researches in Earth sciences. In spite of economic problems, the basis of the observational, methodological and theoretical research develops further and offers good opportunities for future international cooperations. The material was mostly published in a mimeographed volume.

Acta Geodaet., Geophys. et Montanist. Hung. Volume 19 (3–4), pp. 341–346 (1984)

THE AUSTRO–HUNGARIAN POLAR EXPEDITIONS AS THE BASE OF INTERNATIONAL GEOPHYSICAL COOPERATION

P STEINHAUSER[1]

[Manuscript received June 17, 1983]

Keywords: Austro–Hungarian Polar Expedition; geophysical cooperation; Payer Julius von; polar expedition; polar year; Weyprecht Karl; Kepes Laszlo

The inspiration for the remarkable enterprise known as the First International Polar Year 1882–1883 has to be attributed to the foresight and determination of Karl Weyprecht, a navigation officer of the Austro–Hungarian Navy. Thus it is worthwhile to discuss how this idea was developed by Karl Weyprecht during his navy career and especially during the polar expeditions, he organized prior to the Polar Year.

Karl Weyprecht joined the Austro–Hungarian Navy being 18 years old in 1856. After 5 years of training he became an ensign at the frigate "Radetzky" under lieutenant commander Tegetthoff. This captain encouraged Weyprecht's interests in natural sciences and trained his skills within this field. The service on board of "Radetzky" and his scientific abilities resulted in his promotion to an instruction officer. During this time Karl Weyprecht was introduced to the wellknown German Geographer August Petermann, who rouse his interest in polar research. Petermann also interested another Austro–Hungarian Navy officer, the First Lieutenant Julius von Payer, in this subject. It was a lucky chance that both officers had interests and abilities supplementing each other. Weyprecht's main interests concentrated on scientific questions while Payer was an outstanding mountaineer, seafarer and organizer.

As a result, the first Austro–Hungarian Polar Expedition was organized in 1871 by Payer and Weyprecht with Petermanns assistance. Weyprecht defined three tasks for this expedition:

— First, to explore the King Charles Islands in the east of Spitsbergen.

— Second, to test a hypothesis which expected the southward drifting polar ice to be stopped by the Gulfstream in form of a huge ice barriere. As a consequence the warm water of the Gulfstream should open an icefree passage between Spitsbergen and Nowaja Semlja just south of the expected barriere.

— Third, to find the legendary "Gillis-Land", which was later identified as the "White Island", a small island NE of Spitsbergen.

[1] Institut für Meteorologie und Geophysik der Universität Wien, A-1190 Wien, Hohe Warte 38

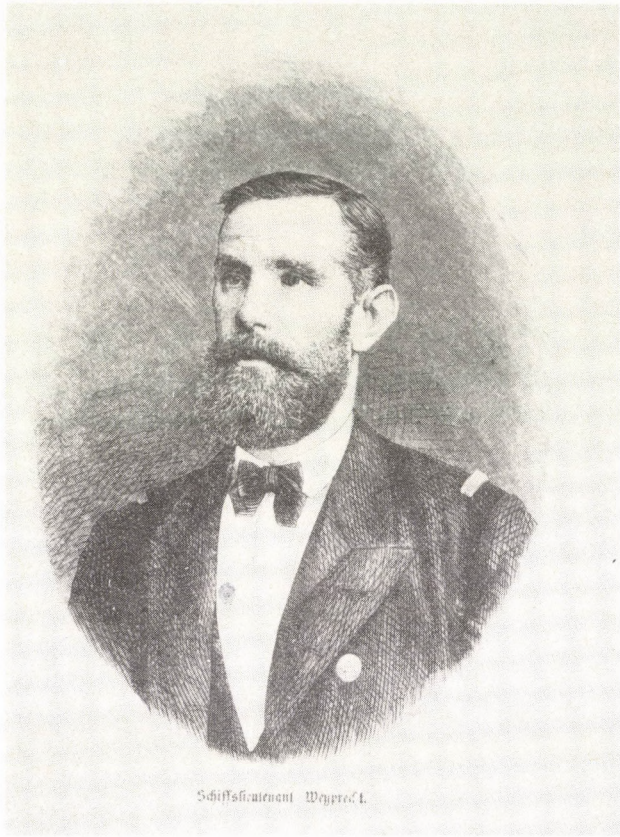

Fig. 1

Already this list of scientific subjects shows clearly that the scientific philosophy behind this expedition was completely different from that of other expeditions.

While other polar expeditions at this time simply aimed to the North Pole and — if at all — carried out only few scientific investigations the Austro–Hungarian expedition had dominant scientific tasks to fullfill.

For this expedition a ship named "Isbjörn" was chartered in Norway and therefore this expedition is often called the Isbjörn expedition. It started in June 1871 from Tromsö in Norway. It soon became evident that the "Isbjörn" was a too light weight vessel, which was not suitable for the requirements of the polar sea. Nevertheless it also became evident that there did not exist an ice barriere caused by the Gulfstream: the influence of the Gulfstream on the ice regime of the arctic sea was not as dramatic as expected, although the "Isbjörn" found ice free water with water temperatures around $+5\,^{\circ}C$ as far north as in 79° latitude, that is in the West and Nörthwest of Nowaja

Semlja. This was a very important discovery because everybody expected dense pack ice in this area. After carrying out oceanographic and meteorological investigations there as well as some geological work on Spitsbergen the Isbjörn returned back to Tromsö in October 1871.

Thus the Isbjörn-expeditions had gained very remarkable results within a short time. It demonstrated that planning an expedition on base of scientific considerations was an extremely powerful method. Further the discovery of an ice free sea, caused by the Gulfstream in the northwest of Nowaja Semlja, opened a breach for further investigations which had to be carried out evidently with better equipment especially with a ship which could better resist the rough arctic sea.

Already in December 1871 Weyprecht submitted the proposal for a new expedition to the Academy of Sciences in Vienna. Once again the definetely declared task was not to sail as far north as possible but to explore the open sea discovered by the Isbjörn expedition and to sail as far east as possible, ideally to the Bering strait.

A committee was created for fund raising which was headed by Count Wilczek who himself donated one fifth of the necessary budget. Besides contributions from various Austro–Hungarian Ministries, the Army and the Academy, a public campaign was started, which really made this expedition to a national project of Austro–Hungary.

In spring 1972 a research vessel was built according to the experiences of Isbjörn expedition. It was a 220 tons big screwsteamer which was designed to carry a crew of 23 persons together with equipment and supplies for three years. This ship was named "Admiral Tegetthoff".

The expedition started in 1872 on June 13th from Bremerhaven. It was headed by three persons: the Austrians First Lieutenant Julius von Payer as captain of the ship and Lieutenant Karl Weyprecht whose responsibility was the realization of the scientific program and the Hungarian Dr. László Kepes who served as the physician of the expedition.

First the "Tegetthoff" and the "Isbjörn" sailed together to Nowaja Semlja, were at the northwestend of the island an emergency deposit was established. Afterwards the "Isbjörn" returned to Norway while the "Tegetthoff" started the expedition in August 1872.

After a few weeks the "Tegetthoff" got stuck in packice and started a two years drift through the ice in a northeasterly direction.

On August 30th 1873 the "Tegetthoff" discovered land, which was named Franz Josefs Land — nowadays Semlja Frantsa Josifa. After exploring Franz Josefs Land till April 1874 the supplies of the expedition were fairly exhausted and at the instigation of Dr. Kepes the "Tegetthoff" was abandoned in the ice before Franz Josefs Land in May 1874 and the members of the expedition made an exhausting retreat over the packice by small boat and sledge to Nowaja Semlja, which took 3 months. Dr. Kepes' urgesledge for a retreat probably saved the lives of all expedition members.

After "Tegetthoff" became ice-bound in August 1872 Weyprecht, apart from continuing his research, seems also to have turned his thoughts to polar exploration and polar research in general; shortly after his return to Europe in September 1874 he presented a paper to the Austrian Geographical Society outlining his thoughts on polar exploration. In his talk to the Geographical Society he said:

"The key to many secrets of Nature, the search for which has now been carried on for centuries (I need only refer to magnetism and electricity and the greatest problems of meteorology) is certainly to be sought for near the Poles. But as long as Polar Expeditions are looked upon merely as a sort of international steeple-chase, which is primarily to confer honour upon this flag or the other, and their main object is to exceed by a few miles the latitude reached by a predecessor, these mysteries will remain unsolved...

Decisive scientific results can only be attained through a series of synchronous expeditions, whose task it would be to distribute themselves over the Arctic regions and to obtain one year's series of observations made according to the same method."

Weyprecht developed his idea for coordinated studies of the polar regions further in the months following his return from the Arctic, and put it to the 48th meeting of the Association of the German Naturalists and Physicians held in Graz on 18. September 1875. In his paper "Fundamental principles of Arctic exploration" Weyprecht outlined six principles:

1. Arctic exploration is of the greatest importance for a knowledge of the laws of nature.
2. Geographical discovery carried out in these regions has only a serious value inasmuch as it prepares the way for scientific exploration as such.
3. Detailed Arctic topography is of secondary importance.
4. For science the Geographical Pole does not have a greater value than any other point situated in high latitudes.
5. The greater the intensity of the phenomena to be studied the more favourable is the place for an observational station; the latitude as such is not an important parameter.
6. Isolated observations have only a relative value, research observatories are necessary.

He suggested the creation of a belt of five or six stations around the pole at Novaja Semlja (76 °N), Spitsbergen (80 °N), the east or west coast of Greenland (76°–78 °N), North America to the east of Bering Strait (70 °N), Siberia at the mouth of the Lena (70 °N), and the use of stations already existing near the polar circle. It was his opinion that the expenses necessary for one of the contemporary voyages of geographical exploration to reach the highest latitude achievable would be sufficient to defray the cost of upkeep of all the stations he had suggested.

Whenever possible during the course of a complete year the expedition should make simultaneous observations, using identical instruments and uniform in-

structions. First priority were observations of interest to various branches of physics and meteorology, then botany, zoology and geology, and finally detailed geography. If it would be possible to establish in the Antarctic regions one or more stations which would function simultaneously, Weyprecht expected that the importance of the results would be increased considerably. The idea was approved at Graz and Weyprecht began his efforts to have his plan adopted internationally.

The programme was developed still further, and reached its final form during May 1877 for presentation to the International Meteorological Congress which should have been held in Rome in September 1877 but which was postponed, because of the Balkan War, to April 1879. The 1879 Congress, noted in the report of the International Meteorological Commission for 1879, believed that the observations would be of the highest importance in developing meteorology and in extending knowledge of terrestrial magnetism. It adopted the following resolution:

Recognizing the great importance which should be attributed to synchronous meteorological and magnetical observations made in the polar regions, by means of simultaneous expeditions . . . recommends all governments to give the most effective support to such undertakings.

By the invitation of the International Meteorological Committee a series of polar conferences was held which decided on the following points of organizing the scientific program of the planned International Polar Year:

1. The number of observations and the most suitable localities for establishing them.
2. The exact period of the commencement of the observations, and their minimum duration.
3. Uniform instructions for the observations to determine in particular:
   a) the minimum of the elements to be observed at each station, both for meteorological and magnetical phenomena of the physics of the globe which are allied to them,
   b) the minimum number of observations to be made daily for the different elements,
   c) the first meridian to serve as a basis for simultaneous observations,
   d) the methods of observations and the methods of reduction for the different elements,
   e) the instruments of observation, and their erection, in so far as they may have an influence upon the comparability of the results.

Of course, the idea that decisive geoscientific results can only be attained through synchronous observations in different permanent observatories was not entirely novel. As a precursor especially the Göttinger Magnetic Union, launched by C F Gauß and M Weber, has to be named. In this Union, up to 44 observatories performed voluntary magnetic observations in 1836–1841 which were collected and evaluated in Göttingen.

However, full credit must be given to Weyprecht for recognizing that the following conditions are necessary for a successful international scientific cooperation:

— institutional contracts between partners instead of informal personal contacts,
— systematic organization of measurements and observations,
— continuing international cooperation for evaluating the data gained during the observation period in a post-observational period.

Thus the experiences of the Austro–Hungarian polar expeditions became the base of the international geophysical cooperation, because their scientific leader Karl Weyprecht did not launch only the idea of the International Polar Year but enforced also its realization in 1882–1883.

References

Baker F W G 1982: The First International Polar Year 1882–1883. *Polar Record*, 21, 275–285.
Corby G A 1982: The First International Polar Year. *WMO Bulletin*, 31, 197–214.
Tiggesbäumker G 1981: Carl Weyprecht 1838–1881. *Polarforschung*, 51, 213–218.
Weyprecht C 1874: Schlußfolgerungen aus dem Verlauf der zweiten Österr.-Ungar. Nordpolar-Expedition. *Petermanns Mitt.*, 20, 451–452.
Weyprecht C 1875: Grundprinzipien der arktischen Forschung. Vortrag bei der 48. Versammlung deutscher Naturforscher und Ärzte in Graz

Acta Geodaet., Geophys. et Montanist. Hung. Volume 19 (3–4), pp. 347–352 (1984)

THE MEASUREMENT OF THE AIR-EARTH CURRENT IN THE GEOPHYSICAL OBSERVATORY NEAR NAGYCENK (HUNGARY)

P BENCZE[1], I SZEMEREY[2], F MÄRCZ[1]

[Manuscript received June 22, 1983]

The equipment for the recording of the air-earth current set up in the Geophysical Observatory near Nagycenk is described. The problems connected with the placing of the collector plate are discussed and sample records are shown.

Keywords: air-earth current; atmospheric electricity; collector; Nagycenk Observatory

Introduction

The atmospheric electric field is one of the phenomena of the terrestrial environment, which is not yet sufficiently understood. This refers to the electric fields of both local and non local origin. The Middle Atmosphere Program (MAP) — and especially its studies of the electrodynamics of the middle atmosphere — sponsored by the Scientific Committee on Solar-Terrestrial Physics (SCOSTEP) shall contribute to the solution of the problems of the global electric field, too. Namely, the atmospheric electric field is connected with the middle atmosphere by the equalizing layer and the coupling of it with electric fields of ionospheric and magnetospheric origin is established also through the middle atmosphere.

For the detailed investigation of the global atmospheric electric field the recording of all three parameters (i.e. potential gradient, conductivity and air-earth current) of the atmospheric electric circuit is needed. The potential gradient is already recorded in the Geophysical Observatory near Nagycenk since 1961 (Bencze and Märcz 1967). (Actually it is the potential difference, which is measured, but we assume that the field is homogeneous.) However, the measurement of the air-earth current involves many difficulties. This is the reason, why it is recorded only at a few places of the world. The main problems are the measurement of small currents of a source of high inner resistance, the assurance of high insulation and the overcome of the effect of undesirable contact potentials at the collector plate. The experiences obtained during

[1] Geodetic and Geophysical Research Institute, Hungarian Academy of Sciences, Sopron, Hungary
[2] Central Institute for Physics, Hungarian Academy of Sciences, Budapest, Hungary

the recording of the potential gradient in the Geophysical Observatory near Nagycenk enabled us to solve the latter two problems, while the ideas gathered by the construction of small current amplifiers (femtoampermeters) in the Central Institute for Physics supported the implementation of the first task.

The measuring principle

The air-earth current is measured by substituting for a part of the Earth's surface with a plate insulated from the ground. The current (the flux of charges) collected by the plate is measured. The plate collects not only those charges, which reach the collector due to the potential difference between the equalizing layer and the Earth, respectively in consequence of the conductivity of the air (conduction current), but also charges transported by motions of the air (turbulence, exchange, wind) (convective current). In addition charges due to field changes appear also on the plate. Since the latter are undesirable, their effect have been eliminated by applying the method of Kasemir (1955). This method is based on the matching of the input circuit of the measuring amplifier an RC circuit formed — in the equivalent circuit diagram — by the resistivity and permittivity of the air above the collector plate. Taking the values $1.0 \cdot 10^{-14}$ Sm^{-1} and $8.86 \cdot 10^{-12}$ As/Vm for the resistivity, respectively permittivity of the air, one obtains $\sim$900 s for the time constant of the RC circuit of the air. To match these conditions an input resistance of 10^{11} Ω and an input capacitance of 9 nF have been chosen. Thus — assuming that neither the conductivity, nor the permittivity of the air above the plate change — the displacement current is excluded from the measurement (Dolezalek 1960a, 1960b).

The measuring equipment

The circular collector plate of 0.785 m^2 is made of wire grid and is located in a concrete trough on the flat area in front of the building, in which the recording instrument and the power supplies are situated (Figs 1, 2). The plate is held by three insulators used also at the radioactive collector in the measurement of the potential gradient (Dolezalek 1956). The high insulation resistance is assured under all weather conditions by the construction and heating of the insulators. For the reduction of the contact potential (Volta-potential) between the plate and its surroundings (Israël and Dolezalek 1957) the plate and the insulators are in a cylindrical cage without cover, made of wire grid, placed in the concrete trough and earthed. Since the measuring resistor (R) is only 10^{11} Ω, the potential of the collector plate can reach a maximum value of only 1 V. Therefore it is not necessary to hold the cage and the plate at the same potential.

The characteristics of the amplifier connected with the collector plate are determined by the measuring principle. Thus, the input circuit of it is an RC circuit consisting of a resistor of 10^{11} Ω and a condenser of 9 nF (Fig. 3). The Dual MOSFET transistor of the pre-amplifier is protected by a chain consisting of resistors, condensers, a glow tube and two reed relays, which prevents the damage of the transistor in case of harmful external influences — except a lightning stroke.

The signal is amplified by subsequent stages of operational amplifiers. The gain is 10. For the compensation of the temperature dependence of the resistor in the input circuit it is also provided. After the adjustment of the offset the output error is less than

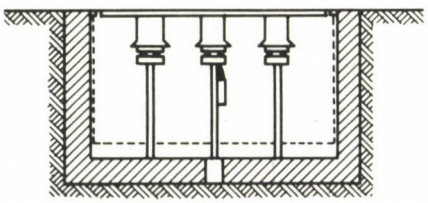

Fig. 1. Sketch of the sensing element of the air-earth current measuring equipment

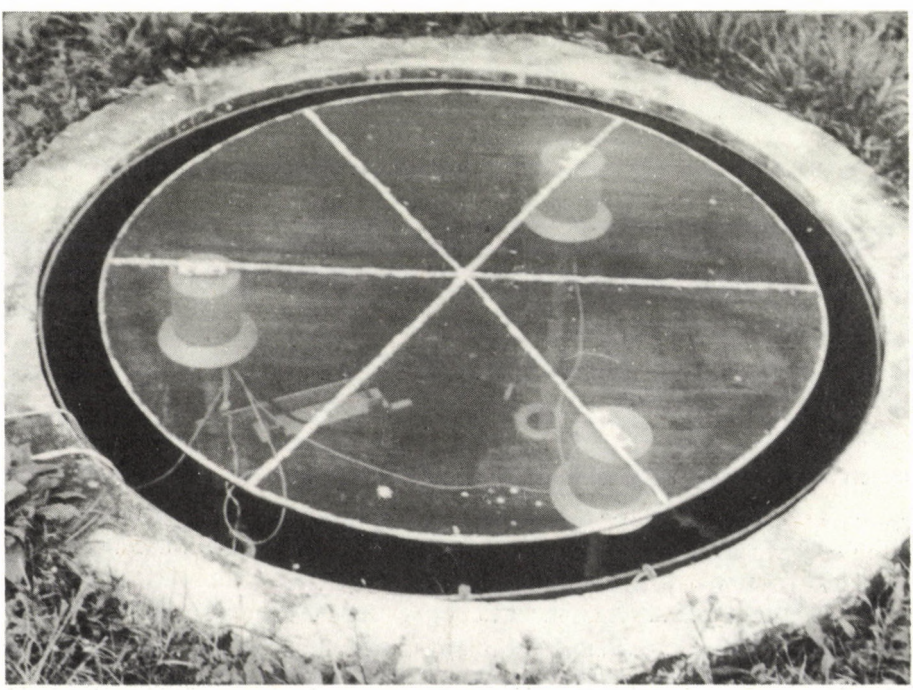

Fig. 2. Photograph of the collector plate unit

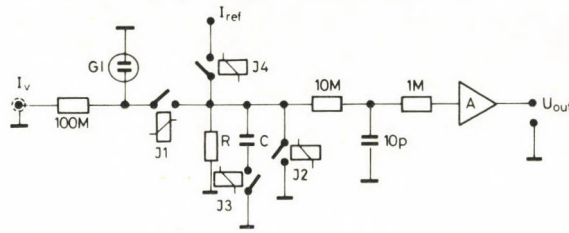

Fig. 3. Schematic circuit diagram of the electronic unit

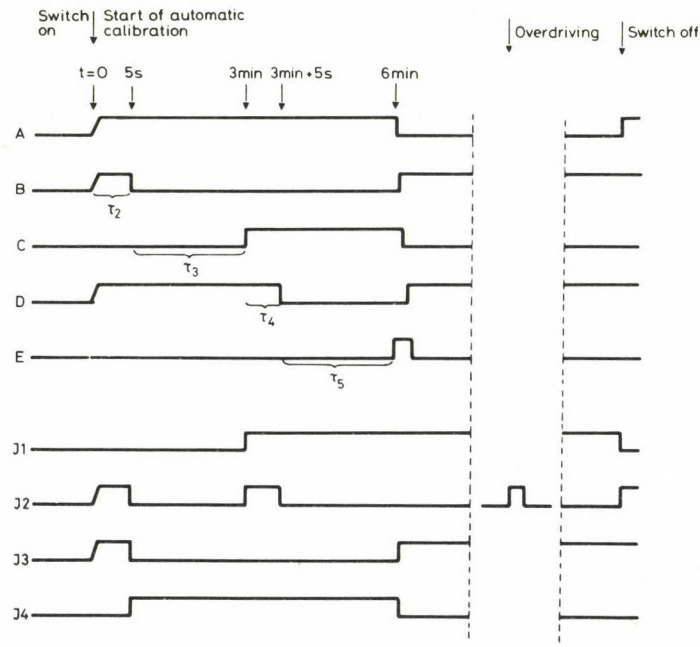

Fig. 4. Flow diagram of the automatic calibration, τ_2, τ_3, τ_4 and τ_5 are the time constants of the corresponding relays shown in Fig. 3

50 mV changing the environmental temperature from -20 to 60 °C. The output stage works as a current generator by inserting a series resistor. Thus, the recording galvanometer, located in a room at a distance of about 28 m from the collector plate and amplifier, can directly be connected with it.

The calibration of the equipment can be carried out by operating a relay, which initiates an internal timing chain. This timing chain performs in order the following operations: switching off the plate from the input it shorts the input, short circuit stopped and condenser in the input circuit switched off, calibrating current of $5 \cdot 10^{-12}$ A

is conducted to the input; collector plate is connected with the input; calibrating current is switched off and condenser in the input circuit entered. The flow diagram can be seen in Fig. 4 (see also Fig. 3).

The instrument is also protected against overdriving. If the output voltage exceeds +11 V, or −0.5 V, the input is short circuited. Since the time constant of the RC network in the input circuit is very large ($10^{11} \times 9 \cdot 10^{-9} = 15$ min), after an overdriving the output voltage reaches only after about 30 min the value corresponding to the input signal.

In case of cutoff or cessation of the supply voltage an automatic circuit operates the relay short-circuiting the input.

The amplifier is located below the collector plate. The supply voltage of 24 V is yielded by stabilized AC power supplies separately for the amplifier and for the heating of the insulators.

The output signal is first reduced by voltage division and then recorded on film by a galvanometer, the sensitivity of which can be changed with series resistors from $3 \cdot 10^{-7}$ to $3 \cdot 10^{-5}$ V/mm/m. Thus, the equipment enables the measurement of currents from 10^{-13} to 10^{-11}A. The recording speed is 20 mm/hour.

Results and conclusions

In Fig. 5 a sample record is shown, which was recorded with this equipment (upper curve) and where the potential gradient is also shown (lower curve). In this record a downward shift of the trace means an increase of the current, while in case of the potential gradient an upward displacement indicates increases (or decreases) of the positive (resp. negative) potential gradient. Time increases from left to the right. The vertical lines are hourly time signals. It can be seen that the variation of the air-earth current follows that of the potential gradient, which proves the correctness of the measurements. It should additionally be mentioned that conditions in and around the Geophysical Observatory near Nagycenk assure undisturbed atmospheric electric measurements. Since this preliminary record was made without the earthed cylindrical

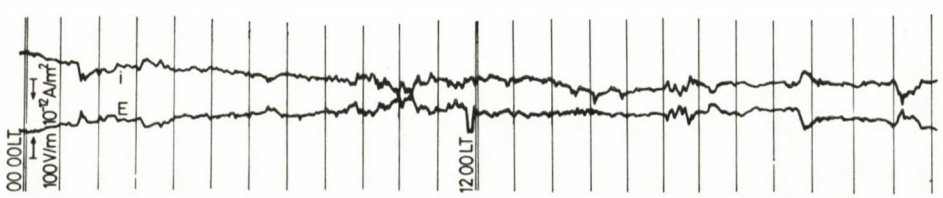

Fig. 5. A sample record of the air-earth current measuring equipment (i = air-earth current, E = potential gradient)

cage in the trough the disturbing effect of the contact potential may not be important. However, the contact potential is a parameter varying in time due to changes of environmental conditions. Therefore, the cage is placed into the trough and earthed to reduce the effect of occasionally occurring contact potentials.

References

Bencze P, Märcz F 1967: Atmosphärisch-elektrische und ionosphärische Messungen im Observatorium bei Nagycenk. In: *Observatoriumsberichte des Geophysikalischen Forschungslaboratoriums der Ungarischen Akademie der Wissenschaften vom Jahre 1966*, Sopron, 143–152.

Dolezalek H 1956: Freiluft-Isolator mit über 10^{14} Ohm Widerstand für alle Klimate (Ein Beitrag zur luftelektrischen Messtechnik). *Geofis. pura e appl.* 33, 223.

Dolezalek H 1960a: Zur Berechnung des luftelektrischen Stromkreises II. Über die Gültigkeit des Ohmschen Gesetzes in der Atmosphäre. *Geofis. pura e appl.* 45, 273–297.

Dolezalek H 1960b: Zur Berechnung des luftelektrischen Stromkreises III. Kontrolle des Ohmschen Gesetzes durch Messung. *Geofis. pura e appl.* 46, 125–144.

Israël H, Dolezalek H 1957: Zur Methodik luftelektrischer Messungen IV. Störspannungen in luftelektrischen Messfühlern und ihre Verhütung. *Geri. Beitr. Geophys.*, 66, 129–142.

Kasemir H W 1955: Measurement of the air-earth current density. Proc. Conf. Atm. Electr. AFCRC, Geophys. Res. Paper 42, 91–95.

Acta Geodaet., Geophys. et Montanist. Hung. Volume 19 (3–4), pp. 353–365 (1984)

COMPRESSION HEAT PUMPS FOR THE UTILIZATION OF GEOTHERMAL HEAT IN HUNGARY

B GÖLZ[1] and V MUČIĆ[2]

[Manuscript received June 22, 1983]

The paper points to new facilities for heating energy supply. In the following part modern economical types of heat pumps will be described. Enabled by them, we can now utilize a lot of environmental heat sources even when their temperature is low. Besides the waste heat of industry, in Hungary there are best preconditions for utilizing geothermal heat. In many places of the country tepid ground water can be considered as a good energy source. To avoid overstraining of the water balance, primary those wells come into question, whose water temperatures create a problem for using the water as planned. One needs only to mention the great number of tepid drinking-water wells. Elsewhere, tepid mine water and warm water of public baths are directed into brooks and rivers without any utilization of caloric. Further, the application of ground heat exchangers will be discussed.

Keywords: compression heat pump; geothermal heat; ground water; Hungary; utilization of geothermal heat

Introduction

The shortage of conventional energy sources and rising oilprices on a long-term basis have aroused interest in using new sources of energy. Especially for a country which is poor in fuel oil, the utilization of *all* available sources of energy has great importance. On this way foreign currency can be saved and coal stocks preserved. Alternative energies can only replace a part of conventional energies. However, in many cases, especially for heating, newly developed energy sources become more and more significant. Most of them can be used in a way which protects the environment.

The Council of Ministers of Hungary has therefore decided to promote the inclusion of new energy sources in the district heating supply. The guidelines for this are laid down in a "medium-term research and development program for the energy management (OKKFT A/1)" (Dudás and Varga 1982).

For *heating purposes* both natural heat sources and secondary energy sources are suitable. Amongst the first ones not only geothermal heat and the heat of ground water, but also the heat contained in rivers, lakes, ponds and in the air as well as the heat

[1] Scientific Adviser, D-6900 Mannheim, Merziger Str. 16, FRG
[2] TCH Thermo-Consulting Heidelberg Ltd., Heidelberg, FRG

produced by solar radiation comes into question. From all these energy sources, only geothermal heat and the heat gained from deep ground water (thermal water) are free from annual fluctuations. The fact that these energies are able to regenerate themselves without our help makes their utilization most attractive. Amongst the secondary energy sources, first of all the waste heat from industrial plants, heat generating and nuclear power stations play an important part. A lot of these energy sources have not been used for a long time, because often their temperature level is not sufficient for direct utilization.

Only since the *heat pump* has become economical, have cooler heat sources gained in significance. The investment costs of large-scale heat pumps are no longer an obstacle: in West Germany even medium-sized plants compensate for the higher investment within 10 years, compared with boiler-heating. Large-scale plants amortize quicker. When a plant is amortized, then the fuel savings take full effect. In a subprogram (4/b) of the before mentioned research and development project it is therefore planned to develop further the employment of heat pumps also in Hungary.

Technical features of compression heat pumps

Today heat pumps are available in numerous variations; they utilize different heat sources. The advantages of geothermal energy for the provision of heat in Hungary will be dealt with later on. Now we will shortly describe the energetic features of the most suitable heat pumps. We especially want to point out the energetic advantages of the resorption compression heat pump with solution circuit. This heat pump has already been proposed by Altenkirch (1950), but it was only realized by Mučić and Scheuermann quite recently.

In Fig. 1 the basic mode of operation of a *conventional* compression heat pump working with one medium can be seen. It is characteristic for a machine of this kind that the working medium shows *only one* evaporation or condensation temperature at a given pressure. To obtain the desired temperature of the heating water and of the heat source, the evaporated medium has to be compressed by the aid of mechanical energy from the pressure of the evaporator on the pressure of the condenser.

The COP ε_1 of the one medium heat pump (or refrigerating machine) corresponds in the *ideal case* to the COP of Carnot:

$$\varepsilon_1 = \frac{T_1}{T_1 - T_{01}} \tag{1}$$

T_1 = evaporation temperature of the working medium (K)
T_{01} = condensation temperature of the working medium (K).

The "outside irreversibilities" which are caused by the limited surface of the heat exchangers have already been taken into consideration.

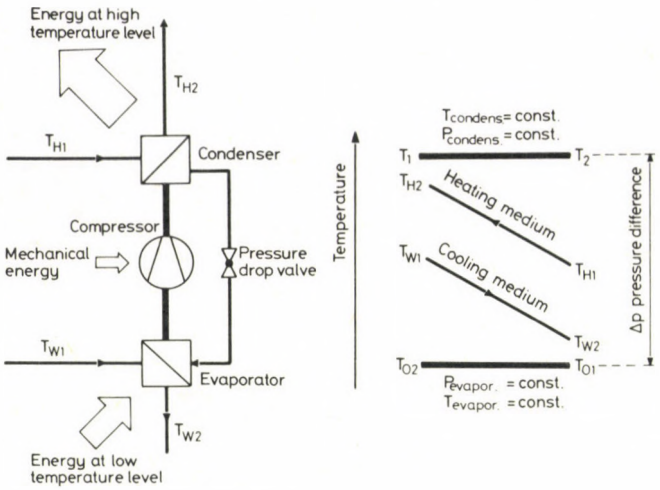

Fig. 1. Mode of operation of a conventional one medium compression heat pump.
$T_1 =$ $T_2 =$ temperature of the solution in the condenser,
$T_{01} =$ $T_{02} =$ temperature of the solution in the evaporator,
T_{H2}, $T_{H1} =$ maximum and minimum temperature of the heating medium,
T_{W1}, $T_{W2} =$ maximum and minimum temperature of the cooling medium

The basic mode of operation of the new compression heat pump can be seen in Fig. 2. This machine works with a two media mixture which has at a given pressure *an infinity* of degasification or resorption temperatures depending on the concentration of the component of solution which has a lower boiling point. In the desorber practically only the component of solution which has a lower boiling point is desorbed, whereby with decreasing concentration of the solution the degasification temperature increases.

The COP* ε_2 of the resorption compression heat pump (or refrigerating machine) corresponds in the *ideal case* to Joule's COP:

$$\varepsilon_2 = \frac{T_m}{T_m - T_{0m}}$$

T_m = medium resorption temperature of the solution (K)
T_{0m} = medium degasification temperature of the solution (K)

With the terms used in Fig. 2 follows

$$\varepsilon_2 = \frac{T_1 + T_2}{(T_1 + T_2) - (T_{01} + T_{02})}. \tag{2}$$

* COP = coefficient of performance

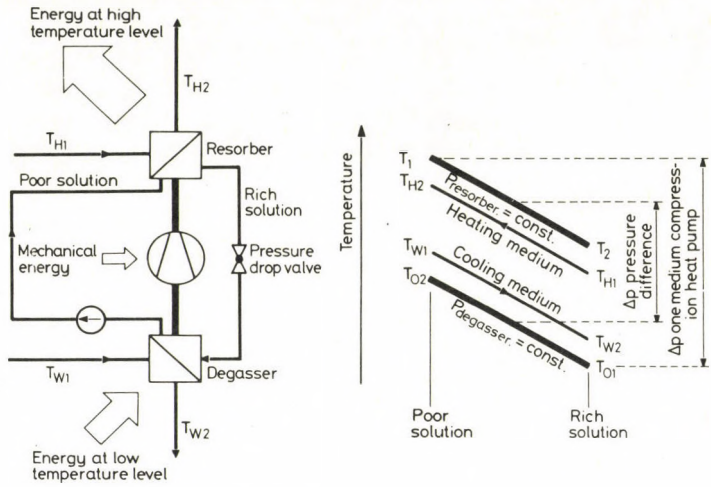

Fig. 2. Mode of operation of the new two media resorption compression heat pump with solution circuit.
T_1, T_2 = maximum and minimum temperature of the solution in the resorber,
T_{02}, T_{01} = maximum and minimum temperature of the solution in the degasser,
T_{H2}, T_{H1} = maximum and minimum temperature of the heating medium,
T_{W1}, T_{W2} = maximum and minimum temperature of the cooling medium

Hereby was calculated approximately with the arithmetic mean values

$$T_m = \frac{T_1 + T_2}{2}$$

and

$$T_{0m} = \frac{T_{01} + T_{02}}{2}$$

instead of the exact medium temperatures

$$T_m = \frac{\int_{s_1}^{s_2} T\mathrm{d}s}{s_2 - s_1}$$

and

$$T_{0m} = \frac{\int_{s_{01}}^{s_{02}} T\mathrm{d}s}{s_{02} - s_{01}}$$

(s signifies entropy).

Also in this case the "outside irreversibilities" are already considered.

The equation (2) can also be written as

$$\varepsilon_2 = \frac{T_1}{T_1 - T_{01}} \cdot \frac{1 + \dfrac{T_2}{T_1}}{1 + \dfrac{T_2 - T_{02}}{T_1 - T_{01}}}$$

and finally with (1)

$$\frac{\varepsilon_2}{\varepsilon_1} = \frac{1 + \dfrac{T_2}{T_1}}{1 + \dfrac{T_2 - T_{02}}{T_1 - T_{01}}}. \tag{3}$$

In Fig. 3 Eq. (3) is graphically shown for all T_2/T_1, $(T_2 - T_{02})$ and $(T_1 - T_{01})$. From this diagram follows that the ratio of COPs of both systems can reach considerable values, especially when the temperature drop by cooling and/or the temperature rise by heating is large. In this diagram the advantage of the compression heat pump working with a mixture is only demonstrated according to the theoretical calculations because there is no practical experience with this kind of heat pumps or cooling machines.

To obtain these experiences the Municipal Works of Mannheim, Federal Republic of Germany, decided to develop, build and test in operation a pilot plant of the resorption compression heat pump with the ammonia-water mixture driven by a gas Otto motor under the leadership of Mučić. This pilot plant with a capacity of about

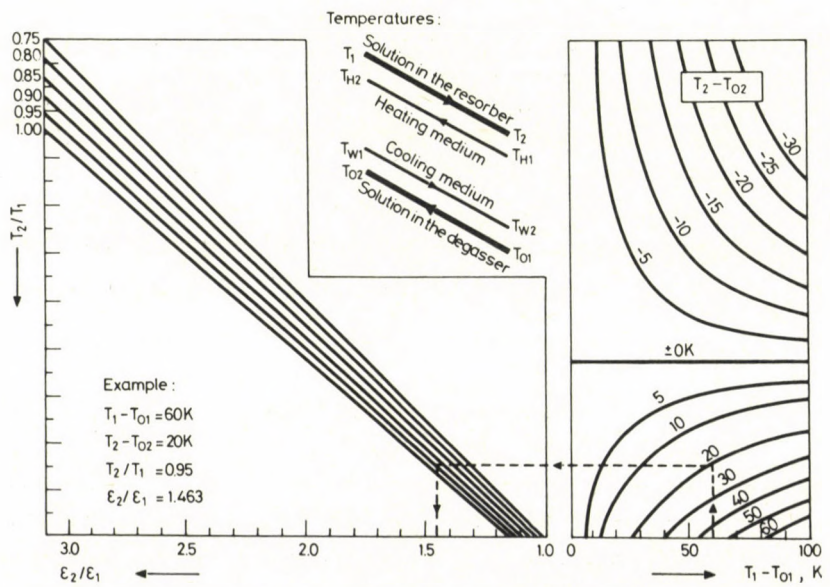

Fig. 3. Nomograph for the determination of the ratio of the theoretical COP at given process temperatures

500 kW was financially supported by the Federal Ministry of Research and Technology in Bonn with fifty percent of all costs.

The experimentation period on this pilot plant has been finished quite recently. The results corresponded to the values that had been calculated before, so that the theoretical advantages of the resorption compression heat pump compared with the one medium heat pump were also fully confirmed in the practical operation.

For example at the design point of the heat pump a COP of $\varepsilon_2 = 11.3$ was obtained. A well-known manufacturer of heat pumps offered under the same conditions (temperatures, capacity, kind of drive and so on) a heat pump with a COP of $\varepsilon_1 = 4.73$. The ratio is therefore $\frac{\varepsilon_2}{\varepsilon_1} = 2.39$. According to the attached diagram it follows a ratio of $\frac{\varepsilon_2}{\varepsilon_1} = 2.25$. This means, that the real ratio of COPs between a two media heat pump and a heat pump working with a single substance is even better than the ratio of COPs theoretically calculated.

The costs of the offered heat pump working with Frigen R12 amounts to 255,000 DM*. The heat pump of the pilot plant costed 256,000 DM*, this means that with the same investments great energy savings can be obtained with this new type of heat pump or refrigerating machine.

Geothermal energy as a source of heat

In Hungary *geothermal energy* can be especially well utilized with heat pumps. The geothermal gradient, in the continental average $3 \cdot 10^{-2}$ K/m, attains $5.6 \cdot 10^{-2}$ K/m in the country average. This is explained by a thinning out of the earth's crust i.e. high position of the MOHO-discontinuity and by an active tectonic structure. Whether in the highlands or in the lowlands, in the solid rock or in the loose rock — ground water and heat convection prefer everywhere fractures and dislocations. If the thermodynamics of the underground are known, then geothermal heat is one of the most reliable energy sources. It will mostly be exploited by thermal waters, in rarer cases by earth heat exchangers.

Thermal water as heat distributor

Already now heat pumps of a greater capacity (in the Scandinavian countries up to 10 MW) utilize ground water of 10 °C for district heating. With higher COP's it is possible to utilize *thermal water* which is often too cool for direct heating. Innumerable

* Both prices including mounting and putting into operation.

wells in Hungary provide such water. If a corresponding water supply is guaranteed, then this type of heat production will be chosen, because water is an excellent heat carrier. It transports heat not only by conduction, but mainly by convection, whereby the ground water movement plays an important part.

Wells in the *Great Hungarian Plain* produce a large amount of heat (Fig. 4). In the Danube–Tisza-interfluve and in the southern region around Szentes, Hódmezővásárhely, Szeged, Makó and Orosháza warm ground water rise up near to the surface. In a geothermal anomaly between Tiszakécske and Lakitelek the temperature gradients (0–50 m) reach over $2 \cdot 10^{-1}$ K/m. Even the wells of Hajdúszoboszló (26–78 °C), Kaba (44–47 °C) and Tótkomlós (31–80 °C) still have gradients from 6 to $6.5 \cdot 10^{-2}$ K/m. The ground water which stands under pressure is a reliable energy source on a long-term basis, too.

Also in *Transdanubia* (West Hungary) there exist various thermal wells. Their water springs from different geological formations. The geothermal reservoirs of the Little Hungarian Plain extend from Devonian to Tertiary sediments.

The crack waters of the *Trias blocks* occupy a special position in the hydrodynamical point of view (Fig. 5). In wide parts of the Hungarian mountain chain, in the Mecsek highlands and in the hills of Villány, limestone and dolomite rise up. Their karst surfaces take in many water. The Transdanubian mountain range alone has

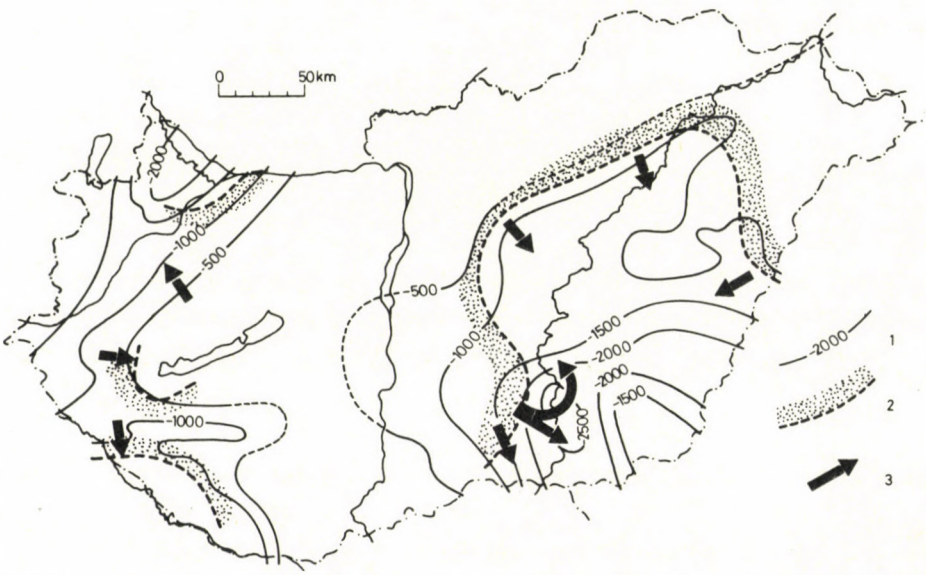

Fig. 4. Upper Pannonic thermal water reservoirs in Hungary. According to Erdélyi and Liebe (1977)
1 = Isohypse of the Upper Pannonic footwall in m under sea level,
2 = hypothetical recharge area
3 = probable movement of thermal water in virgin flow system

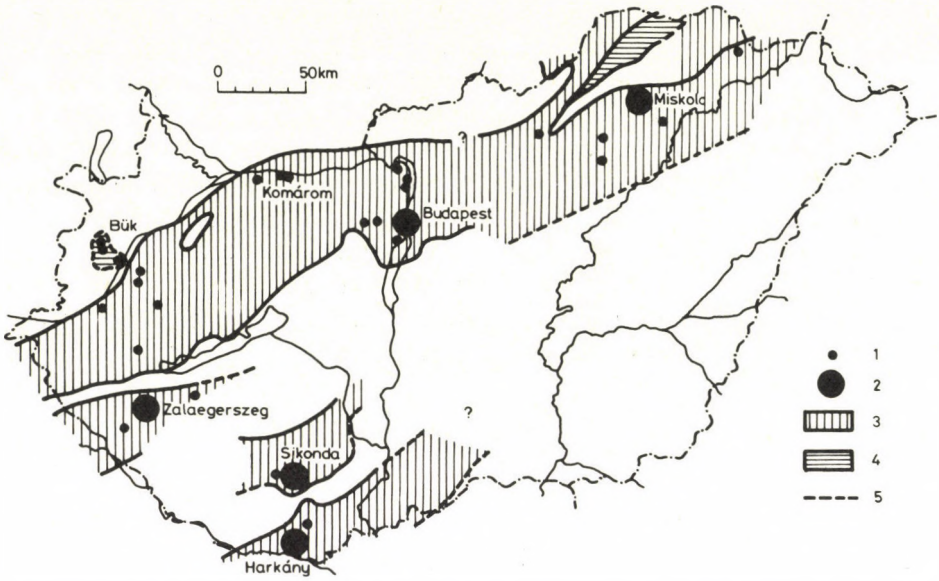

Fig. 5. Thermal water reservoirs in carbonatic rocks. According to Korim (1978), with modifications

1 = well > 35 °C
2 = well group > 35 °C,
3 = spreading of Triasic karst water reservoirs,
4 = spreading of Paleozoic karst water reservoirs

a dynamical heat stock of 319 MW (Gölz 1982). The water penetrates rock fissures as deep as 2000 m and more. In many places it reaches under intramontane sedimentary basins and lateral overlapping Tertiary mantles, where it warms up very much. The tense, widely communicating thermal water strives everywhere for a pressure balance. Especially in the fringe area of the highlands and in covered horsts the thermal water presses upwards. In this way Trias water with geothermal gradients $>10^{-1}$ K/m has been found by boring in many places at the *fringes* of the Hungarian mountain chain: near the Keszthely highlands in Nemesbük, Rezi and Hévíz, near the Buda highlands in Budapest and finally near the Bükk mountains in Eger, Egerszalók, Bogács and Miskolc-Tapolca. Also in many other places of this region exist warm drinking waters.

Even *covered horsts* which are far away from the highlands contain warm or hot waters. One needs only think of the geothermal anomaly of Táska, south of the lake Balaton. In South Transdanubia geothermal gradients of more than 10^{-1} K/m have been measured in the wells of Siklós, Harkány and Beremend. These waters are supplied from the highlands of Mecsek and Villány.

In Hungary up to 01. 01. 1977 545 wells had produced water of *more than* 35 °C. Only 9 of them were used for the heating of municipal buildings, 81 for the heating of

hothouses. For 53 wells above 35 °C there is at present no use. The wells producing a total of 637.833 l/s (2 296 200 m^3/h) are therefore closed. The number of wells dipped into groundwater of *more than 30°C* amounted 940 on January 1st of 1983. A great number of *tepid* wells produce particularly large quantities of water. Such wells supply a lot of kilowatts from shallow and permeable aquifers. The heat pump would enable the use of thermal water for heating on a larger scale than before. New borings would not be necessary; if water supply is guaranteed many wells already existing could be used completely or partially for heating.

Utilization of thermal water and cooling down of drinking water

From the 545 registered thermal wells (> 35 °C) 141, that is a good quarter, had been sunk for the drinking water supply. A number of cooler thermal wells should serve the same purpose. The high drinking water temperatures are a problem for many municipalities. They promote the increase in bacteria in the water and impair its pleasant taste.

To obtain favorable temperatures, warm drinking water is often mixed with cold. In this case the heat pump could make a virtue of necessity and use the warm wells entirely or partially for district heating. Already a single well could provide great quantities of energy.

To prevent toxical working substances getting into the drinking water by corrosion in the heat exchangers, *precautions* have to be taken. Use is partly made of regulating devices which need constant maintenance and which would immediately stop the plant in case the solvent overflows. Thus the overflow of ammonia can easily be registered by measuring conductivity or pH-index. Another security guarantor would be an intermediate circuit, which collects the overflowing working medium in case of leakage. In this case a loss of energy depending in the type and size of the heat exchangers must be taken into account.

As heat energy is only needed in winter, but water is needed all the year, the water supply has to include cold ground water too. Alternately the thermal well is to be used preferably in winter whereas the cold well would be used in summer. The well which is at a standstill can be serviced.

To the problem of the sintering process and corrosion

Thermal waters contain many dissolved substances. Some of them lead to depositions of sinter and ochre in the tubes. To prevent material depositions, the water has if necessary to be purified, or an easily cleanable heat exchanger has to be interposed. The latter solution is cheaper but only limitedly applicable.

As a result of acids and free carbon dioxide water has an aggressive effect on the pipe walls. Corrosion damage can also be prevented by water purification but better by corrosion-resistant material.

Every type of water considered as a heat supplier must be analysed for its sinter deposition and its corrosivity. The well-known methods of Papp (1942), Strohecker and Langelier (Hässelbarth 1963) serve as a basis for this. Many thermal waters, especially those which were tapped in the Great Hungarian Plain, have only a slight tendency to sintering and corrosion. In this case precautions are not necessary.

Winning of heat with ground heat exchangers

The thermal waters of Hungary possess a rich heat reservoir. Therefore, it is only seldom profitable to obtain geothermal energy directly out of the soil by heat exchangers. This comes into question only if the water supply is strained and if the ground is exceptionally warm. An example for this is the area of the Lukács- and Császárspas at Budapest. Here at 2 m depth the underground temperatures reach up to 29 °C (Fig. 6). The highest temperatures indicate the presence of aquiferous fissures.

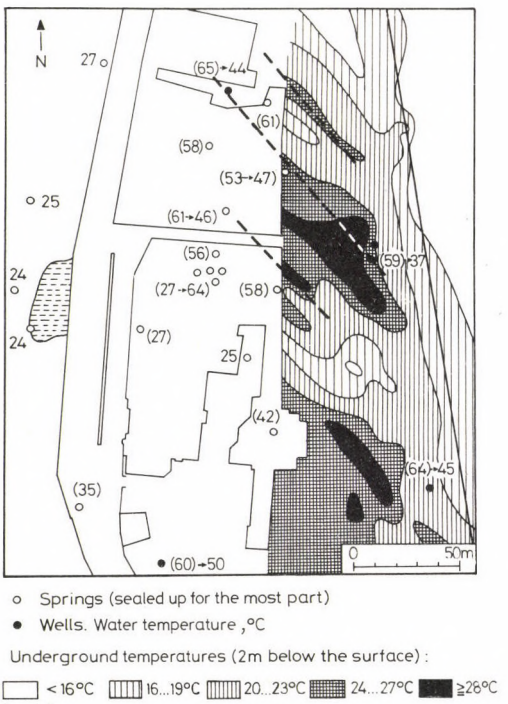

Fig. 6. Underground- and water temperatures in the Császár and Lukács spas at Budapest. Historical values are put in brackets

However, the additional withdrawals of water would strain much more the already disturbed water balance. Ground heat exchangers are laid in the ground as spiral pipes. They have already been used successfully under much more unfavorable circumstances than here.

Preconditions for the economical heating with heat pumps

It is not possible to make an economical forecast for a heat pump heating station which is valid overall. The economy must be investigated for each object. It is obvious that a complexly used heat pump heating station amortizes itself quicker than any small plant. As a complex method of use the combination of district heating and cooling down of drinking water among other things comes into question.

Let us take as an example the Eger waterworks' well situated on the Petőfi-Square. The well gives 50 litres of 28 °C warm water per second (= 180 m^3/h). A resorption compression heat pump, which cools the heat source down to 13 °C, could gain a refrigerating capacity of 3.14 MW. From the process temperatures shown in Fig. 7 the theoretical COP of the heat pump would lie at $\varepsilon_2 \simeq 8.0$.

Resorption compression heat pumps with turbo-compressor are expected to produce "inside irreversibilities" of about $\zeta_i \simeq 0.75$. Hence follows a real COP of

$$\varepsilon_{real} = \varepsilon_2 \cdot \zeta_i \simeq 8.0 \cdot 0.75 \simeq 6.$$

The compressor capacity needed for the working process amounts to

$$Q_C = \frac{Q_O}{\varepsilon_{real} - 1} = 0.63 \text{ MW}.$$

If the compressor is driven by a gas or oil motor, then part of the waste heat from the motor can also be used. As the compressor capacity Q_C amounts to about 38% and the utilizable waste heat of the motor Q_W amounts to 52% of the needed fuel, the farther utilizable heat is

$$Q_W = 0.63 \cdot \frac{0.52}{0.38} = 0.86 \text{ MW}.$$

The total *utilizable heat* from the heat pump is therefore

$$Q_H = Q_O + Q_C + Q_W = 3.14 + 0.63 + 0.86 = 4.63 \text{ MW}.$$

In order to operate a motor of 0.63 MW mechanical power and a mechanical efficiency of 0.38 a fuel capacity of

$$Q_F = \frac{0.63}{0.38} = 1.66 \text{ MW}$$

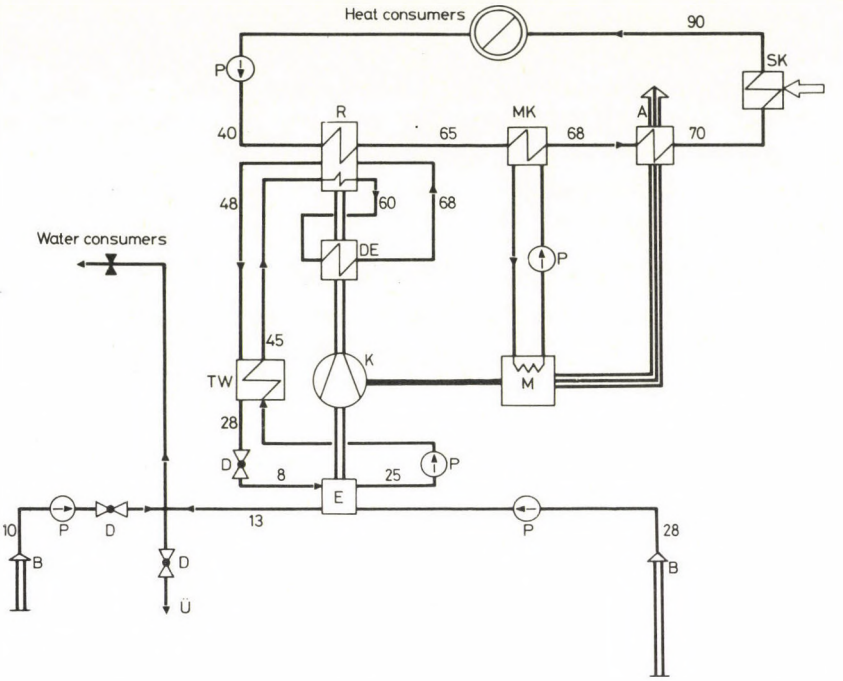

Fig. 7. Example for a residential heating by a 28 °C warm well with the help of a two media resorption compression heat pump and a peak boiler. The water which has been cooled down is directed into the drinking water system.
A = waste gas heat exchanger, B = well, D = pressure drop valve, DE = vapor cooling heat exchanger, E = desorber (degasser), K = compressor, M = motor, MK = motor cooling, P = pump, R = resorber, SK = peak boiler, TW = internal heat exchanger at the heat pump, $\dot{U}$ = overflow. The values mean the temperature in °C

is needed. From this follows a free efficiency of

$$\vartheta = \frac{Q_H}{Q_F} = \frac{4.63}{1.66} = 2.8.$$

This value speaks for an excellent energy exploitation.

Assuming that the maximal heat requirements of the residential area amounts to 10 MW, 46.3% of the peak load or 90% of the annual energy demand would be covered by the heat pump. The remaining 10% of the annual energy demand can be assured by a peak boiler.

Another example for a complex utilization method would be the combination of a residential heating and the heating as well as sprinkling of hothouses, which is not explained in detail.

The economy of a heat pump heating station increases with the following factors:

a) heating power of the plant,
b) number of consumers,
c) consumer density (favorable for blocks of flats),
d) rising prices for fossil fuel,
e) thermal and chemical quality of the heat source,
f) COP of the heat pump,
g) duration of life of the heat pump.

The duration of life of heat pumps is above all determined by the compressor. Compressors with about 1000 revolutions per minute work for 15 to 20 years. Slowly rotating compressors of technical veterans are usable for a longer period. Thus the town hall in Zürich has been heated by a heat pump since 1938.

References

Altenkirch E 1950: The resorption compression refrigeration machine with solution circuit (in German). *Kältetechnik*, 2, 251, 279 and 310.

Czipper Gy, Szőcs M 1981: Informations about the energy management program within the period of the 6. five year plan (in Hungarian). *Műszaki Élet*, 21–24.

Dudás Gy, Varga I 1982: An important research program (in Hungarian). *Műszaki Élet*, Supplement to No. 18.

Erdélyi M, Liebe P 1977: Hydrogeology of the clastic porous thermal water resources of Hungary (in Hungarian). In: *VITUKI, Magyarország hévizkútjai* III., Budapest, 29–43.

Gölz B 1982: Natural thermal power of springs in the Transdanubian Mountains (in Hungarian). *Földrajzi Értesítő*, 31, 427–447.

Hässelbarth U 1963: The equilibrium between Ca and HCO_3 in natural waters considering proper and extraneous electrolytic influences (in German). *Gas- und Wasserfach/Wasser*, 104, 89–93 and 157–160.

Korim K 1978: The hydrogeological fundamentals of the thermal water occurrences in Hungary (in Hungarian). *MTA X. Osztályának Közleményei*, 11, 255–275.

Mučić V 1982: The two media solution (in German). *Energie*, 34, 323–324.

Papp Sz 1942: The content of appropriate carbon dioxide in waters being in an equilibrium of Ca and HCO_3 and the calculation of lime corroding carbonatic acid (in German). *Gesundheits-Ingenieur*, 65, 322–327.

Acta Geodaet., Geophys. et Montanist. Hung. Volume 19 (3–4), pp. 367–381 (1984)

ENERGY RELEASE CURVE AND MAP OF HUNGARY

T Zsiros and L Tóth[1]

[Manuscript received September 15, 1983]

An energy release curve and map of Hungary were constructed based on the earthquakes occurring between 1859–1982. In this period the distribution of seismic energy has two peaks between 1904–1913 and between 1949–1958 while a significant minimum zone can be found between 1959–1968. The space distribution of earthquake energy is concentrated in the central part of the country but its form depends very much on the limit of the hypocentral distance used in the calculations.

Keywords: earthquake energy release; energy release map; Hungary; seismic energy

Introduction

In this paper the space and time distributions of the seismic energy released by earthquakes are estimated using the events occurred in the present territory of Hungary between 1859–1982. The calculations are based on macroseismic data being revaluated recently by Bisztricsány and Rónai (1984), Csomor and Kiss (1983) and Szeidovitz (1983). The Benioff-sums of Hungarian earthquakes were earlier published by Csomor and Kiss (1958) for the period 1880–1956. An energy release map of Hungary is presented here for the first time.

Focal depths in Hungary

The estimations of focal depths of earthquakes are based on the isoseismal maps using the Blake-method:

$$h = s_k(10^{\frac{I_0 - I_k}{3}} - 1)^{1/2}, \tag{1}$$

where I_0—epicentral intensity
I_k—intensity of the k-th isoseismal
s_k—mean epicentral distance of the k-th isoseismal (in km)
h—focal depth (in km).

The isoseismal maps used in the calculations are mainly compiled by Csomor and Kiss (1983). The results of depth estimations are summarized in Table I. This table

[1] Seismological Observatory, Budapest, Meredek u. 18. H-1112, Hungary

Table I

No.	Date	Location	I_0	h	σ_h	N^*
1.	Dec. 30. 1859.	Süttő	5			
2.	Jan. 20. 1860.	Zalaszántó	5			
3.	Apr. 13. 1860.	Győr	3			
4.	Apr. 18. 1862.	Komárom	4			
5.	Jan. 17. 1863.	Penc	5			
6.	June 14. 1863.	Kiskunmajsa	5			
7.	Sep. 30. 1863.	Komárom	4			
8.	Oct. 20. 1863.	Mór	5			
9.	Apr. 09. 1864.	Csatka	5			
10.	Apr. 09. 1864.	Magyaróvár	3			
11.	Dec. 19. 1864.	Nagykálló	4			
12.	Jan. 19. 1865.	Nagykőrös	4			
13.	Jan. 15. 1866.	Márianosztra	3			
14.	Feb. 27. 1866.	Komárom	4			
15.	Mar. 16. 1866.	Békéscsaba	3			
16.	Apr. 25. 1866.	Komárom	3			
17.	May 11. 1866.	Mór	3			
18.	1866.	Kazár	5			
19.	Sep. 22. 1867.	Pétervására	5			
20.	Feb. 04. 1868.	Tokaj	4			
21.	June 05. 1868.	Jászapáti	3			
22.	June 17. 1868.	Budapest (Pest)	3			
23.	June 21. 1868.	Jászberény	7.5			
24.	Aug. 24. 1868.	Eger	3			
25.	Sep. 01. 1868.	Jászfényszaru	4			
26.	Dec. 15. 1868.	Jásztelek	5			
27.	May 28. 1869.	Kétegyháza	5			
28.	Feb. 02. 1870.	Zsadány	3			
29.	June 30. 1870.	Alcsut	4			
30.	Sep. 10. 1870.	Abony	3			
31.	Dec. 01. 1871.	Hódmezővásárhely	3			
32.	Feb. 17. 1872	Magyaróvár	3			
33.	May 30. 1872.	Jászberény	4			
34.	Jan. 03. 1873.	Mosonmagyaróvár	3			
35.	Apr. 16. 1874.	Pécs	5			
36.	Dec. 27. 1874.	Kiskunhalas	5			
37.	Apr. 13. 1875.	Komárom	4			
38.	Oct. 17. 1875.	Pécs	4			
39.	July 06. 1876.	Nagyatád	6			
40.	Oct. 21. 1876.	Surd	6			
41.	Nov. 30. 1876.	Surd	6			
42.	Dec. 06. 1876.	Mohács	6			
43.	Mar. 03. 1878.	Makó	4			
44.	Dec. 31. 1878.	Gyöngyös	5			
45.	Apr. 30. 1879.	Pásztó	3			
46.	May 01. 1879.	Kazár	5			
47.	May 25. 1879.	Budapest (Buda)	4			
48.	Aug. 31. 1879.	Szőreg	5			
49.	Dec. 07. 1879.	Gyöngyös	5			
50.	Feb. 09. 1880.	Kaposvár	4			
51.	June 04. 1880.	Budapest (Buda)	4			

Table I (contd.)

No.	Date	Location	I_0	h	σ_h	N^*
52.	Nov. 28. 1880	Csengőd	3			
53.	June 22. 1881.	Sióagárd	4.5			
54.	Oct. 28. 1881.	Szarvas	4			
55.	Oct. 28. 1881.	Szentes	4			
56.	Nov. 08. 1881.	Kiskunmajsa	3			
57.	Jan. 18. 1882.	Nagyatád	4			
58.	Mar. 04. 1882.	Mosonszentjános	3			
59.	Oct. 29. 1882.	Tapolca	3			
60.	Nov. 24. 1882.	Bátaapáti	3			
61.	Dec. 12. 1882.	Mohács	3			
62.	Dec. 20. 1882.	Veszprém	3			
63.	Feb. 09. 1883.	Bonyhád	3			
64.	Mar. 28. 1883.	Miskolc	5	5.9	–	1
65.	Dec. 01. 1883.	Kisgyőr	3			
66.	Oct. 11. 1884.	Marcali	3			
67.	Dec. 05. 1884.	Eger	4			
68.	Jan. 12. 1886.	Pápa	4			
69.	Mar. 17. 1887.	Jászjákóhalma	3			
70.	Jan. 18. 1888.	Szend	4			
71.	Aug. 16. 1888.	Szend	5	12.5	0.1	3
72.	Aug. 17. 1888.	Bakonysárkány	4.5			
73.	Nov. 26. 1888.	Eger	3			
74.	Apr. 03. 1889.	Nemesvid	4	6.5	0.1	2
75.	June 18. 1889.	Esztergom	4			
76.	July 11. 1889.	Aka	4.5	9.1	–	1
77.	Aug. 19. 1889.	Somogyszil	3.5			
78.	Jan. 14. 1891.	Tápiószecső	3			
79.	Apr. 11. 1891.	Siklós	4.5			
80.	June 19. 1891.	Székesfehérvár	5	13.6	1.0	2
81.	July 07. 1891.	Elek	4.5	13.9	–	1
82.	June 21. 1892.	Székesfehérvár	3			
83.	June 22. 1892.	Pincehely	6.5	5.3	3.4	4
84.	Aug. 24. 1893.	Csesztreg	5.5	7.6	–	1
85.	June 11. 1895.	Cserháthaláp	5	9.2	0.0	2
86.	Apr. 26. 1896.	Somogyszob	3			
87.	Sep. 14. 1896.	Hidegkút	5	6.5	–	1
88.	Oct. 29. 1896.	Kecskemét	5	14.9	0.0	2
89.	Nov. 30. 1896.	Mezőkövesd	4	9.6	0.0	2
90.	Dec. 05. 1896.	Dédestapolcsány	4.5			
91.	Jan. 18. 1897.	Miskolc	5	7.9	–	1
92.	Mar. 18. 1898.	Isztimér	3			
93.	Nov. 30. 1898.	Miskolc	3.5			
94.	May 07. 1899.	Szentes	4	7.4	0.0	2
95.	June 14. 1899.	Csákány	4	4.9	0.0	2
96.	Aug. 06. 1899.	Kaposvár	3			
97.	Sep. 11. 1899.	Gyöngyös	3			
98.	Sep. 21. 1899.	Bükkszentlászló	4			
99.	Nov. 12. 1899.	Nagyecsed	5	5.5	–	1
100.	Mar. 23. 1900.	Szekszárd	3			
101.	Feb. 16. 1901.	Bakonytamási	5	11.1	0.8	2
102.	May 10. 1901.	Gic	4.5			

Table I (contd.)

No.	Date	Location	I_0	h	σ_h	N^*
103.	Nov. 15. 1901.	Bükkzsérc	4			
104.	Jan. 19. 1902.	Gyöngyöshalász	3			
105.	May 06. 1902.	Répáspuszta	4			
106.	May 31. 1902.	Kaposvár	3			
107.	Aug. 22. 1902.	Nyírkáta	4			
108.	Sep. 19. 1902.	Monor	5			
109.	Oct. 06. 1902.	Csány	3			
110.	Oct. 12. 1902.	Isztimér	4.5			
111.	Feb. 07. 1903.	Zalatárnok	4			
112.	June 09. 1903.	Zalakoppány	3			
113.	June 16. 1903.	Csány	3			
114.	June 26. 1903.	Eger	6.5	12.7	0.2	3
115.	July 07. 1903.	Tiszanána	3			
116.	Sep. 15. 1903.	Várpalota	5			
117.	Oct. 26. 1903.	Vésztő	3			
118.	Feb. 12. 1904.	Gölle	6			
119.	Feb. 24. 1904.	Tiszakécske	4			
120.	Mar. 04. 1904.	Nagylak	4			
121.	Aug. 03. 1904.	Komárom	4			
122.	Feb. 08. 1905.	Elek	4			
123.	May 30. 1905.	Dorogháza	3			
124.	Sep. 04. 1905.	Szentes	4			
125.	Nov. 12. 1905.	Komárom	3			
126.	June 05. 1906.	Zalaegerszeg	3			
127.	Aug. 12. 1906.	Szentmártonkáta	5.5	4.9	–	1
128.	Aug. 25. 1906.	Pétervására	4	2.6	0.0	2
129.	Dec. 30. 1906.	Abod	3			
130.	Jan. 21. 1907.	Veszprém	3			
131.	Mar. 25. 1907.	Bátaszék	4	8.5	–	1
132.	Mar. 26. 1907.	Mezőcsokonya	3			
133.	Oct. 16. 1907.	Nagyberény	4	1.9	0.0	2
134.	Nov. 02. 1907.	Szentiványfa	4	8.7	–	1
135.	Jan. 26. 1908.	Mátraszele	3			
136.	Feb. 28. 1908.	Zalaegerszeg	3			
137.	Mar. 07. 1908.	Kecskemét	3			
138.	Mar. 15. 1908.	Gomba	5.5	9.9	1.9	2
139.	Mar. 20. 1908.	Gödöllő	3			
140.	May 24. 1908.	Lajosmizse	5			
141.	May 28. 1908.	Kecskemét	7	20.2	0.4	5
142.	July 01. 1908.	Kecskemét	3			
143.	Aug. 26. 1908.	Kecskemét	5	15.4	0.0	2
144.	Sep. 08. 1908.	Kecskemét	5			
145.	Oct. 24. 1908.	Kiskunfélegyháza	3			
146.	Dec. 14. 1908.	Szigetszentmárton	3			
147.	Dec. 16. 1908.	Kecskemét	3			
148.	Jan. 06. 1909.	Kecskemét	3			
149.	Jan. 17. 1909.	Pilis–Gomba	4			
150.	Jan. 21. 1909.	Baja	5.5	9.6	0.2	2
151.	Jan. 23. 1909.	Nyáregyháza	3			
152.	Feb. 04. 1909.	Kakucs	3			
153.	Feb. 16. 1909.	Kecskemét	4.5	20.7	–	1

Table I (contd.)

No.	Date	Location	I_0	h	σ_h	N^*
154.	Mar. 12. 1909.	Veszprém	3			
155.	Mar. 14. 1909.	Kaposvár	4			
156.	Mar. 16. 1909.	Kecskemét	3			
157.	Mar. 19. 1909.	Gyöngyös	4			
158.	May 29. 1909.	Magyarsarlós	5	7.0	0.6	2
159.	Nov. 12. 1909.	Nadap	3			
160.	Dec. 13. 1909.	Isztimér	4			
161.	Dec. 19. 1909.	Cegléd	3			
162.	Jan. 12. 1910.	Zalaegerszeg	3			
163.	Apr. 07. 1910.	Szokolya	3			
164.	June 01. 1911.	Kecskemét	4	15.6	–	1
165.	June 19. 1911.	Kecskemét	6.5	22.7	–	1
166.	July 08. 1911.	Kecskemét	8	20.6	1.3	6
167.	July 26. 1911.	Pilis	3			
168.	Apr. 12. 1912.	Kecskemét	4			
169.	July 28. 1912.	Nagykőrös	3			
170.	July 29. 1912.	Dunakiliti	3			
171.	Aug. 17. 1912.	Gomba	4			
172.	July 27. 1913.	Győrszemere	4.5	5.2	–	1
173.	Nov. 11. 1913.	Monor	3			
174.	Nov. 23. 1913.	Lajosmizse	4			
175.	Feb. 04. 1914.	Győr	4.5			
176.	May 13. 1914.	Gomba	5.5	11.0	–	1
177.	Nov. 25. 1914.	Isztimér	5.5	13.9	0.4	2
178.	Jan. 06. 1916.	Bük	5			
179.	Jan. 19. 1916.	Eger	4			
180.	June 14. 1916.	Tápióbicske	3.5			
181.	Jan. 28. 1917.	Gyula	4.5			
182.	July 14. 1917.	Eger	3			
183.	Dec. 22. 1917.	Mátranovák	3.5			
184.	Feb. 22. 1919.	Gasztony	6			
185.	Mar. 29. 1921.	Szabadhídvég	3			
186.	Apr. 01. 1921.	Eger	3			
187.	May 21. 1921.	Isztimér	4			
188.	Dec. 14. 1921.	Komárom	4			
189.	Jan. 07. 1922.	Mór	4.5	12.5	0.7	2
190.	Jan. 21. 1922.	Kecskemét	4.5			
191.	Aug. 12. 1922.	Eger	3			
192.	Nov. 24. 1922.	Pécs	5.5			
193.	Dec. 22. 1922.	Sopronkövesd	5			
194.	Jan. 01. 1923.	Ivándárda	4			
195.	Feb. 09. 1923.	Noszvaj	3			
196.	Jan. 31. 1925.	Eger	7.5	6.9	0.2	3
197.	June 27. 1925.	Nagykanizsa	6.5			
198.	Mar. 04. 1927.	Várpalota	6.5	2.1	0.2	3
199.	Mar. 31. 1927.	Kecskemét	5			
200.	July 08. 1927.	Várpalota	6.5	2.1	0.0	2
201.	Oct. 11. 1927.	Kaposvár	4			
202.	June 20. 1928.	Eger	4	7.2	–	1
203.	Apr. 22. 1928.	Eger	4			
204.	Mar. 07. 1929.	Gödöllő	3			

Table I (contd.)

No.	Date	Location	I_0	h	σ_h	N^*
205.	Apr. 30. 1929.	Budapest (Pest)	4			
206.	July 25. 1929.	Abasár	4			
207.	Nov. 05. 1929.	Jakabszállás	5	19.8	1.1	3
208.	Nov. 15. 1929.	Komárom	4	6.1	–	1
209.	Mar. 20. 1930.	Kisbárkány	3			
210.	Apr. 11. 1935.	Pári	5	20.9	0.2	2
211.	May 11. 1930.	Pári	4	10.7	–	1
212.	July 20. 1930.	Eger	5	8.9	–	1
213.	Aug. 03. 1930.	Budapest (Buda)	4			
214.	Aug. 22. 1930.	Cserhátsurány	6	13.7	0.3	3
215.	Sep. 11. 1930.	Felpéc	5	4.8	–	1
216.	Sep. 27. 1930.	Mór	3			
217.	Oct. 25. 1930.	Berzence	4			
218.	Oct. 26. 1930.	Mosonszentjános	3			
219.	Apr. 06. 1931.	Vöröstó	3			
220.	Apr. 07. 1931.	Beregdaróc	6	9.9	0.5	3
221.	Apr. 18. 1931.	Várpalota	5	6.5	–	1
222.	Oct. 31. 1931.	Nagybörzsöny	5	10.0	–	1
223.	Mar. 04. 1932.	Hercegszántó	4			
224.	Mar. 05. 1932.	Várpalota	3			
225.	Dec. 29. 1932.	Gyöngyöspata	3.5			
226.	June 04. 1933.	Báta	3			
227.	June 26. 1933.	Kétegyháza	4			
228.	Aug. 27. 1933.	Lenti	4			
229.	Dec. 19. 1933.	Mór	3			
230.	Apr. 26. 1934.	Esztergom	5.5	4.7	–	1
231.	Sep. 01. 1934.	Búcsúszentlászló	6	9.4	0.3	2
232.	Dec. 14. 1934.	Eger	3			
233.	Aug. 04. 1935.	Babócsa	4			
234.	Aug. 06. 1935.	Békés	5	9.7	0.0	2
235.	Mar. 04. 1936.	Tiszaluc	5	10.6	0.9	2
236.	Apr. 14. 1936.	Nagygéc	4			
237.	Nov. 23. 1936.	Pécs	3			
238.	Apr. 26. 1937.	Kecskemét	4	13.0	–	1
239.	June 10. 1937.	Tarcal	6	12.4	0.8	3
240.	July 12. 1937.	Balatonvilágos	3			
241.	Nov. 08. 1937.	Nagykáta–Farmos	3.5			
242.	June 22. 1938.	Dunakiliti	3			
243.	July 13. 1938.	Eger	3			
244.	July 18. 1938.	Máriakéménd	5	15.5	–	1
245.	Sep. 13. 1938.	Nagylak–Apátfalva	3			
246.	Dec. 11. 1938.	Nagylak	3			
247.	Mar. 23. 1939.	Álmosd	6	29.4	1.4	3
248.	July 27. 1939.	Éger	4	5.9	–	1
249.	Nov. 01. 1939.	Elek	4	12.6	–	1
250.	Feb. 05. 1940.	Álmosd	4	16.3	–	1
251.	July 05. 1940.	Kimle	3.5			
252.	Dec. 08. 1940.	Újléta	5	12.2	–	1
253.	Feb. 17. 1941.	Harkapuszta	3			
254.	May 16. 1941.	Hajdúnánás	3			
255.	May 14. 1942.	Bakonybél	6	6.5	–	1

Table I (contd.)

No.	Date	Location	I_0	h	σ_h	N^*
256.	May 19. 1942.	Bácsa	4			
257.	May 28. 1942.	Tápiószele	3			
258.	Sep. 01. 1942.	Dáka	3			
259.	Sep. 30. 1942.	Tápiósüly	6	12.7	0.1	2
260.	Nov. 24. 1942.	Bezi	5	6.1	—	1
261.	June 07. 1945.	Szolnok	3			
262.	Apr. 26. 1946.	Eger–Felnémet	3			
263.	June 19. 1946.	Bodrogkeresztúr	4			
264.	Oct. 24. 1946.	Nagykőrös	3			
265.	Dec. 11. 1947.	Budapest (Buda)	4	13.2	—	1
266.	Mar. 08. 1948.	Budapest (Buda)	4	17.5	—	1
267.	Apr. 15. 1948.	Csobánka	5	6.3	—	1
268.	Aug. 07. 1948.	Bicske–Biatorbágy	4	26.1	—	1
269.	Nov. 21. 1949.	Dunaújváros	4			
270.	Aug. 21. 1950.	Izsák	4.5	13.9	—	1
271.	Nov. 29. 1950.	Becske	5	10.9	—	1
272.	Dec. 09. 1950.	Várpalota	4			
273.	Dec. 20. 1950.	Lábod	5	11.0	—	1
274.	Feb. 20. 1951.	Tereske	6.5	21.6	1.0	4
275.	Mar. 10. 1952.	Mór	5	10.9	0.8	2
276.	Apr. 04. 1952.	Nagybajcs	4.5	7.9	—	1
277.	May 14. 1952.	Esztergom	4	20.0	—	1
278.	Dec. 05. 1952.	Dad–Szák	4	7.1	—	1
279.	June 10. 1953.	Bajót	3.5			
280.	Sep. 13. 1953.	Ukk	6.5	7.4	0.6	4
281.	Jan. 12. 1956.	Dunaharaszti	8	19.0	0.3	6
282.	Mar. 04. 1956.	Dunaharaszti	5	10.5	—	1
283.	Mar. 31. 1956.	Pakod	6	12.7	0.7	3
284.	Apr. 28. 1956.	Csehimindszent	5	8.2	0.5	2
285.	May 02. 1956.	Csehi	5	9.4	0.4	3
286.	July 30. 1956.	Dunaharaszti	5	15.4	0.5	2
287.	Dec. 14. 1956.	Egerbakta	5.5	15.1	1.7	3
288.	Mar. 27. 1957.	Nagyléta	3	15.8	—	1
289.	Apr. 20. 1957.	Nagyigmánd	4			
290.	May 08. 1957.	Jánoshida	5	7.8	—	1
291.	May 30. 1957.	Miskolc	3			
292.	June 05. 1957.	Eger	4	5.6	—	1
293.	Dec. 03. 1957.	Vasvár	4	8.4	—	1
294.	Apr. 10. 1958.	Lőrinci	4	8.4	—	1
295.	Apr. 16.1958.	Pakod	3			
296.	Apr. 26. 1958.	Berkesz	5	11.6	0.8	2
297.	July 24. 1958.	Hetes	5	8.1	0.4	2
298.	July 28. 1958.	Dunaharaszti	4	10.8	—	1
299.	Oct. 15. 1958.	Csécse	4	8.2	—	1
300.	Dec. 17. 1960.	Ács–Bana	3			
301.	June 07. 1961.	Bérbaltavár	3			
302.	Aug. 23. 1963.	Jásztelek	3			
303.	July 23. 1965.	Dunaharaszti	3			
304.	Oct. 21. 1968.	Tapolca	4	10.1	—	1
305.	Feb. 10. 1969.	Bakonysárkány	5	27.4	0.2	2
306.	Jan. 30. 1974.	Törökbálint	5	14.0	—	1

Table I (contd.)

No.	Date	Location	I_0	h	σ_h	N^*
307.	Aug. 28. 1976.	Keszthely	3			
308.	Mar. 17. 1977.	Tamási–Regöly	5	17.1	0.4	2
309.	June 22. 1978.	Békés	6	17.5	2.8	2
310.	Sep. 26. 1978.	Délegyháza	5	15.4	0.9	2
311.	Oct. 30. 1979.	Békés	4.5	8.0	–	1
312.	Feb. 24. 1980.	Recsk	5	7.5	–	1
313.	Mar. 15. 1980.	Békés	4	8.0	–	1
314.	Mar. 25. 1980.	Portelek	5	8.5	0.1	2
315.	Mar. 31. 1980.	Farmos	4			
316.	Aug. 22. 1980.	Csemő	5	7.3	–	1
317.	Sep. 21. 1981.	Várpalota	4.5			
318.	Jan. 06. 1982.	Rácalmás	4.5	12.5	1.5	2

* I_0 — MSK intensity scale, h — focal depth (km), σ_h — standard deviation of h, N — number of isoseismals

includes also earthquakes which have no isoseismal maps but they were used for the construction of energy release maps.

Figure 1 shows the frequency distribution of the focal depths using a 3 km depth unit. The mean focal depth of the 107 earthquakes is 11 km. About 80 percent of the events occurred in the upper part of the earth crust ($h < 15$ km).

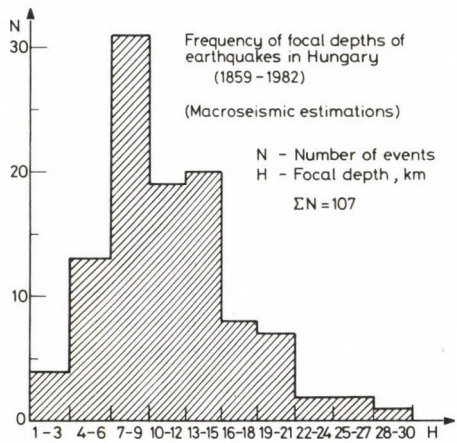

Fig. 1

Energy release curve

In order to examine the time distribution of energy released by earthquakes, the cumulative seismic energy is calculated for 5 year intervals using the Gutenberg–Richter equations (1942):

$$M = 0.6\, I_0 + 1.8 \log h - 1.0 \tag{2}$$

$$\log E = 1.5\, M + 4.8 \tag{3}$$

where

I_0 — epicentral intensity
h — focal depth of the earthquake (in km) (if it is unknown $h = 11$ km is used)
M — magnitude
E — seismic energy (in J).

Table I contains the input data and the results are shown in Table II and in Fig. 2.

It may be also interesting to examine the energy release in the aspect of the frequency of the events therefore the rates of energy releases per events are also

Table II

Period	N (number of events)	E (J)	E/N (J)
1859–1863	8	2.09×10^{11}	2.62×10^{10}
1864–1868	18	6.49×10^{12}	3.61×10^{11}
1869–1873	8	5.29×10^{10}	6.62×10^{9}
1874–1878	10	1.39×10^{12}	1.39×10^{11}
1879–1883	22	1.74×10^{11}	7.94×10^{9}
1884–1888	11	7.99×10^{10}	7.27×10^{9}
1889–1893	12	2.83×10^{11}	2.36×10^{10}
1894–1898	9	1.69×10^{11}	1.88×10^{10}
1899–1903	24	1.44×10^{12}	6.01×10^{10}
1904–1908	33	1.32×10^{13}	4.00×10^{11}
1909–1913	28	1.06×10^{14}	3.80×10^{12}
1914–1918	10	3.78×10^{11}	3.78×10^{10}
1919–1923	12	5.06×10^{11}	4.21×10^{10}
1924–1928	9	2.86×10^{12}	3.17×10^{11}
1929–1933	33	1.40×10^{12}	4.24×10^{10}
1934–1938	17	7.88×10^{11}	4.63×10^{10}
1939–1943	24	5.68×10^{12}	2.36×10^{11}
1944–1948	8	9.08×10^{10}	1.13×10^{10}
1949–1953	13	5.51×10^{12}	4.24×10^{11}
1954–1958	21	8.04×10^{13}	3.83×10^{12}
1959–1963	8	2.84×10^{9}	3.55×10^{8}
1964–1968	3	4.81×10^{9}	1.60×10^{9}
1969–1973	1	5.01×10^{11}	5.01×10^{11}
1974–1978	5	1.30×10^{12}	2.61×10^{11}

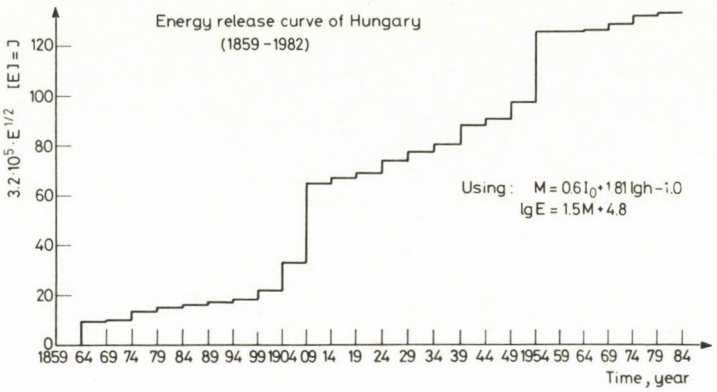

Fig. 2

summarized in Table II. In the investigated time period the distribution of seismic energy has two peaks between 1904 and 1913 and between 1949 and 1958, while a significant minimum zone can be found between 1959 and 1968.

Energy release maps

For the estimation of the space distribution of the seismic energy, based on the data of Table I Eqs (2), (3) were used and a model of the energy propagation:

$$E_i = E_k \exp(-\alpha_k R_i) R_i^{-\beta} \qquad \text{if} \quad i \neq k \tag{4}$$

$$E_i = E_k \qquad \text{if} \quad i = k \tag{5}$$

where

R_i — hypocentral distance (in km)
α_k — intensity attenuation coefficient of the earthquake (in 1/km) (if it is unknown, $\alpha = 0.024$/km is used)
β — numerical parameter (in this case $\beta = 2$)
E_k — energy radiated from the focus
E_i — energy at the distance R_i.

The intensity attenuation coefficients of the earthquakes were adopted from Zsiros and Mónus (1983). Three different maps are presented for this model of energy propagation with $R_i \leqq 25$, 50 and 100 km (Figs 3–5). The values of the square-root energies are summarized in every grid of 10×10 km.

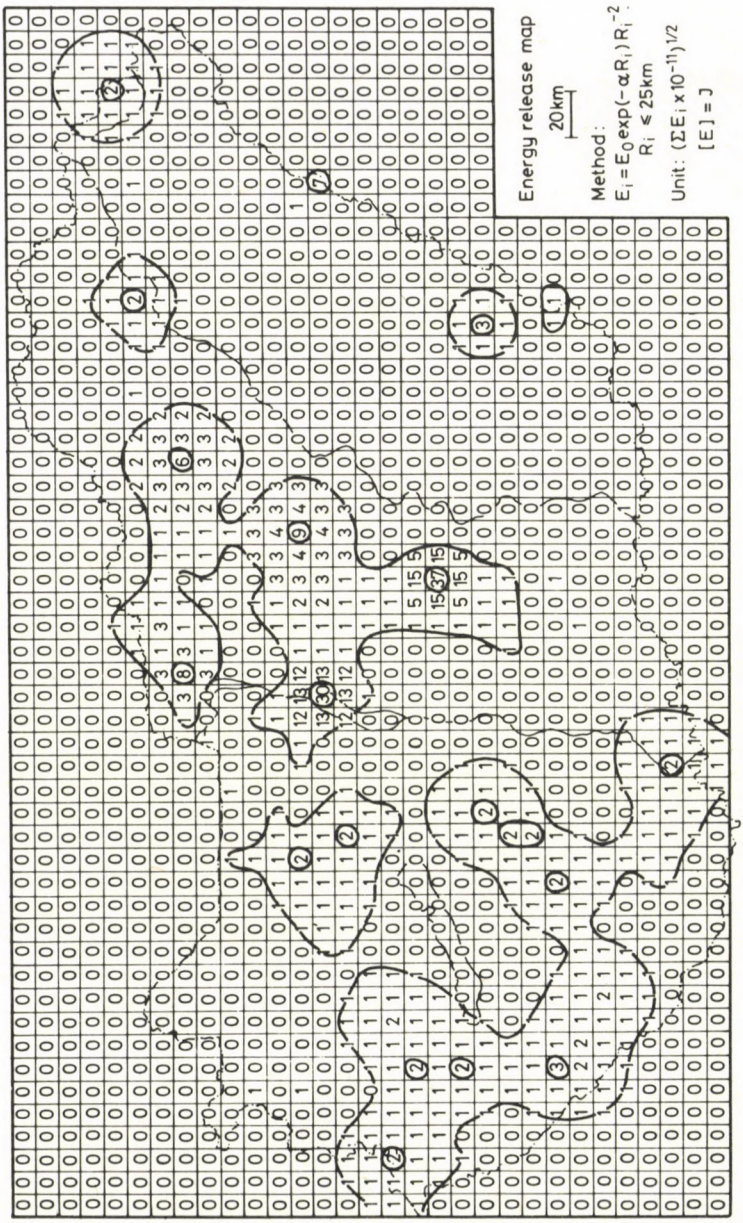
Energy release map
20km
Method:
$E_i = E_0 \exp(-\alpha R_i) R_i^{-2}$
$R_i \leq 25$km
Unit: $(\Sigma E_i \times 10^{-11})^{1/2}$
[E] = J

Fig. 3

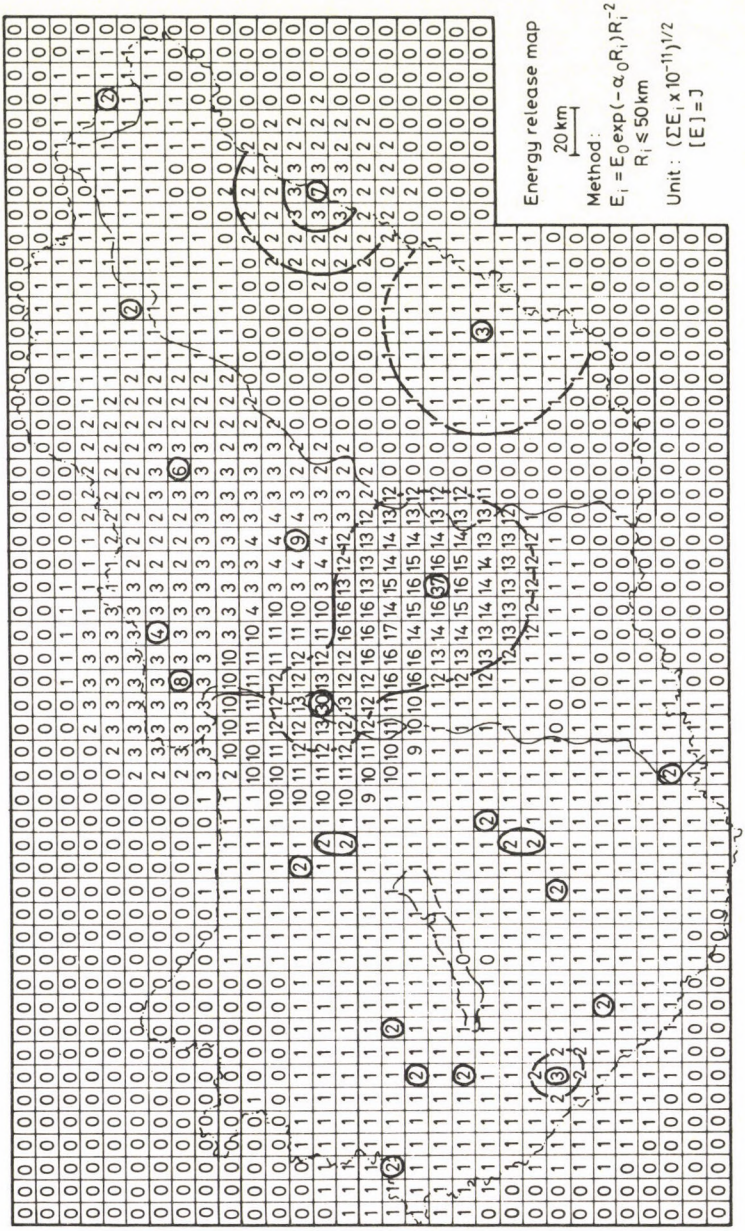
Energy release map
20 km
Method:
$E_i = E_0 \exp(-\alpha_0 R_i) R_i^{-2}$
$R_i \leq 50$ km
Unit: $(\Sigma E_i \times 10^{-11})^{1/2}$
[E] = J

Fig. 4

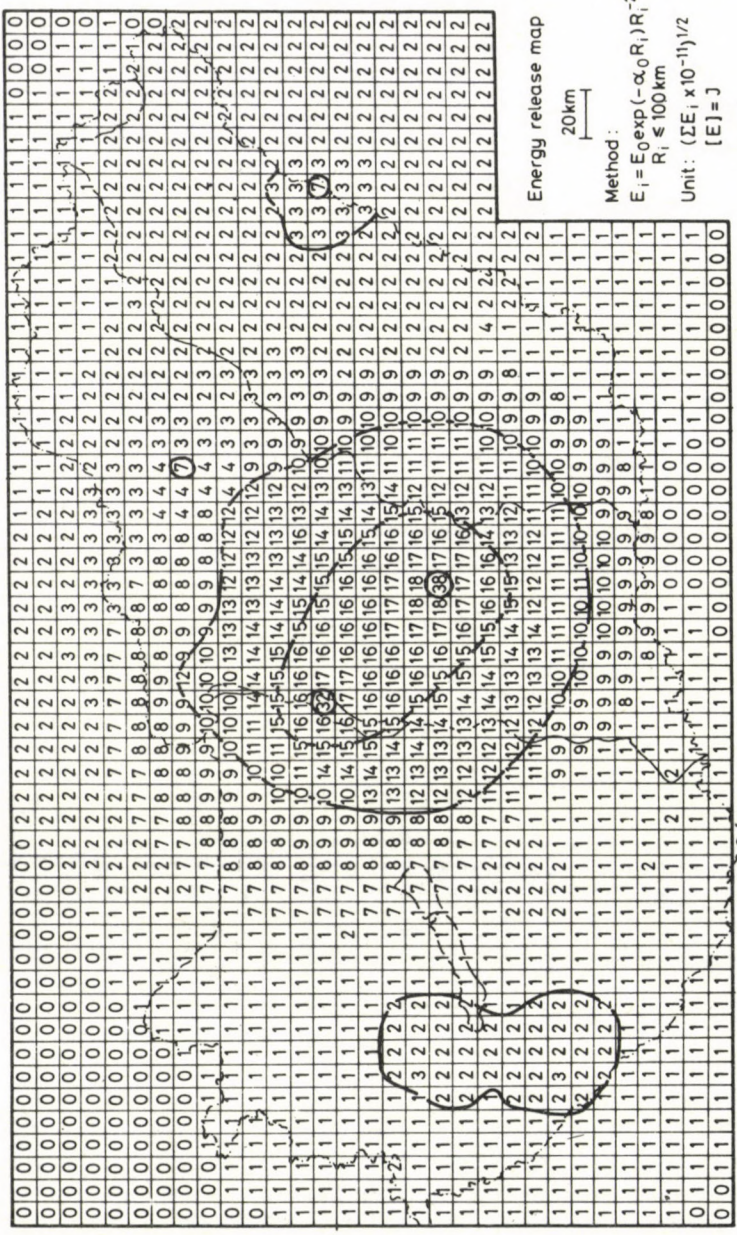
Energy release map
20km
Method :
$E_i = E_0 \exp(-\alpha_0 R_i) R_i^{-2}$
$R_i \leq 100$km
Unit : $(\Sigma E_i \times 10^{-11})^{1/2}$
[E] = J

Fig. 5

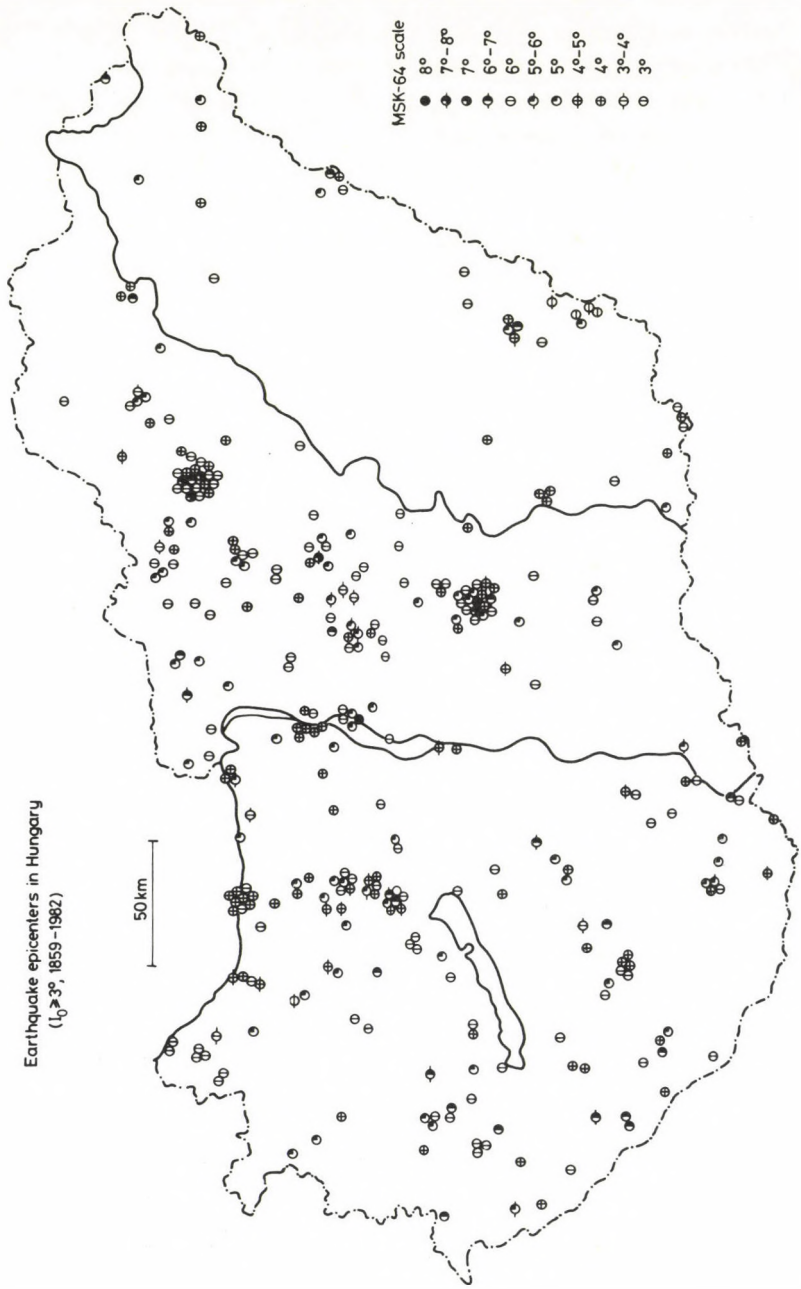
MSK-64 scale
8°
7°–8°
7°
6°–7°
6°
5°–6°
5°
4°–5°
4°
3°–4°
3°
50 km
Earthquake epicenters in Hungary
($I_0 \geq 3°$, 1859–1982)

Fig. 6

The results are determined mainly by the limit of the hypocentral distance (R_i) used in the calculations.* Comparing the energy maps with the epicentral map (Fig. 6) it can be seen that the high level of energy rate in the central part of Hungary is due to the largest earthquakes at Kecskemét and at Dunaharaszti.

As—according to the method of calculation—the energy of an earthquake depends not only on the epicentral intensity but on the focal depth too—so the energy release can be larger at epicenters with smaller intensities (e.g. Tereske, Álmosd) than it is at epicenters with greater intensities (e.g. Eger). Naturally the border zones—especially the western and south-western part—would certainly show higher energy levels if the earthquakes of the surrounding countries had been taken into account.

Acknowledgements

The authors thank D Csomor, Z Kiss and Gy Szeidovitz for letting use some unpublished macroseismic data.

References

Bisztricsány E, Rónai A 1984: Difficulties of the seismic risk determination in Hungary. *Acta Geod. Geoph. Mont. Hung.* (in press)

Csomor D, Kiss Z 1958: Seismicity of Hungary I. (in Hungarian) *Geofizikai Közlemények* 7, 3–4.

Csomor D, Kiss Z 1962: Seismicity of Hungary (in Hungarian) II. *Geofizikai Közlemények*, 11, 1–4.

Csomor D, Kiss Z 1983: Catalogue and isoseismal maps of Hungarian earthquakes (1880–1980). Manuscript

Gutenberg B, Richter C F 1942: Earthquake magnitude, intensity, energy and acceleration. *Bull. Seism. Soc. Am.*, 32.

Szeidovitz Gy 1983: Seismic risk in Budapest (in Hungarian). Manuscript

Zsiros T, Mónus P 1983: An estimation of maximum ground motions caused by earthquakes in Hungary. Manuscript

* The width of the zone along the Hungarian boundary, where the map is distorted due to the absence of earthquake data from foreign countries in the present study, is about 20, 30 and 50 km, respectively, for R_i-s of 25, 50 and 100 km.

Acta Geodaet., Geophys. et Montanist. Hung. Volume 19 (3–4), pp. 383–394 (1984)

ESTIMATION OF THE PARAMETERS TO BE USED IN THE REDUCTION TO THE MAGNETIC POLE

K Kis[1]

[Manuscript received October 6, 1983]

The transfer function of the reduction to the magnetic pole implies the originally unknown values of the angles fixing the direction of the magnetic polarization. The estimation of these parameters can be obtained by optimization, based on the Poisson's relation. The suggested procedure can be used if the specific density and the magnetic polarization of the geologic sources are homogeneous. The optimization is carried out by linearization of the objective function. The procedure is illustrated by an estimation of the parameters of a prismatic model.

Keywords: geomagnetic survey; parameter estimation; reduction to the magnetic pole; transfer function

Introduction

Field anomalies are often approximated by simple models in due course the interpretation of gravity and magnetic data. The estimation of the unknown parameters of the model constitutes an essential part of the interpretation.

An effective tool of the estimation is the optimization. In general the optimization aims at the determination of the extremum of a multivariable function. The optimization methods, used in gravity and magnetic interpretation were based on various techniques. Johnson (1969), Emilia and Massey (1974) used the Marquardt method; Whitehill (1973) applied the Simplex algorithm; Fisher and Howard (1980) worked out a version with the aid of quadratic programing. Al-Chalabi (1970) and Wilson (1970) summarized several other techniques.

In general an optimization procedure consists of the following elements: construction of a mathematical model and an objective function (which is the function to be minimized), determination of the extremum of the objective function, and the interpretation of results.

[1] Department of Geophysics, Eötvös Loránd University, Budapest, Kun Béla tér 2. 1083 Hungary

Mathematical model and objective function

In the case of a uniformly magnetized geologic source the transfer function of the reduction to the magnetic pole of the vertical magnetic anomaly is defined by

$$S(f_x, f_y) = \frac{(f_x^2 + f_y^2)^{1/2}}{N(f_x^2 + f_y^2)^{1/2} + j(Lf_x + Mf_y)} \tag{1}$$

where f_x and f_y are the spatial frequencies measured along the x and y axes, respectively. L, M, N represent the directional cosines of the constant unit vector **s** lying in the direction of the magnetic polarization. The development of Eq. (1) can be found e.g. in a paper by the present author (Kis 1981). The same equation was given by Syberg (1972). The directional cosines L, M, N can be expressed by the inclination α and the declination β of the magnetic polarization as follows

$$\begin{aligned} L &= \cos\alpha \cos\beta \\ M &= \cos\alpha \sin\beta \\ N &= \sin\alpha. \end{aligned} \tag{2}$$

If we know the angles α and β we can determine the coefficients of the reduction (Kis 1983a).

In many cases we have to estimate the value of the angles α and β. The suggested estimation can be carried out by optimization, based on the relation

$$W = \frac{J}{4\pi\mu_0 G\rho} \frac{\partial}{\partial \mathbf{s}} V \tag{3}$$

due to Poisson where W is the magnetic potential, V is the gravity potential, ρ is the specific density, J is the polarization, G is the universal gravitational constant, **s** is the direction of the polarization, μ_0 is the vacuum permeability. The Poisson's relation implies the following assumptions:

— the gravity and the corresponding magnetic anomalies are produced by the same geological source;
— the specific density and the magnetic polarization are homogeneous.

The derivative of the Eq. (3) with respect to the variable z gives the equation

$$Z = \frac{J}{4\pi G\rho}\left(\cos\alpha\cos\beta\frac{\partial}{\partial_x} g_z + \cos\alpha\sin\beta\frac{\partial}{\partial_y} g_z + \sin\alpha\frac{\partial}{\partial_z} g_z\right) \tag{4}$$

if the directional derivative with respect to **s** is expressed by the directional cosines (2). Z is the vertical component of the magnetic anomaly field and g_z is the vertical component of the gravity anomaly field.

Developing the objective function we start with Eq. (4). It is expected that the objective function contains the angles α and β and the polarization-to-density ratio J/ρ as its variables. According to Skeels and Watson (1949) these three variables can be determined unambiguously. Let us denote the components of the parameter vector to be determined, i.e. $\mathbf{p}=\mathbf{p}(p_1, p_2, p_3)$ by $p_1=\frac{J}{\rho}$, $p_2=\alpha$, $p_3=\beta$, respectively. Then the non-linear objective function $\varphi(\mathbf{p})$ can be expressed in the form

$$\varphi(\mathbf{p})=\sum_{i=1}^{n}\left(Z_i-\frac{1}{4\pi G}\left(p_1\cos p_2\cos p_3\frac{\partial}{\partial x}g_{zi}+\right.\right.$$
$$\left.\left.+p_1\cos p_2\sin p_3\frac{\partial}{\partial y}g_{zi}+p_1\sin p_2\frac{\partial}{\partial z}g_{zi}\right)\right)^2, \tag{5}$$

where n denotes the total number of the measured pairs of data while the subscript i indicates the i-th datum

Determination of the extremum of the objective function

The extremum of a non-linear objective function is often determined by linearization (Al-Chalabi 1970, Höpcke 1980). Let us expand the function defined by Eq. (4) into first order Taylor-series around the zeroth approximation of the parameter vector $\mathbf{p}_0$, i.e.

$$Z(\bar{p}_1, \bar{p}_2, \bar{p}_3)=Z(p_{10}, p_{20}, p_{30})+\left(\frac{\partial Z}{\partial p_1}\right)\Delta p_1+\left(\frac{\partial Z}{\partial p_2}\right)\Delta p_2+\left(\frac{\partial Z}{\partial p_3}\right)\Delta p_3. \tag{6}$$

Further calculations require the analytical expressions for the derivatives of the objective function with respect to each variable. These are as follows

$$a_{i1}=\frac{\partial Z_i}{\partial p_1}=\frac{1}{4\pi G}\left(\cos p_2\cos p_3\frac{\partial}{\partial x}g_{zi}+\cos p_2\sin p_3\frac{\partial}{\partial y}g_{zi}+\sin p_2\frac{\partial}{\partial z}g_{zi}\right)$$
$$a_{i2}=\frac{\partial Z_i}{\partial p_2}=\frac{p_1}{4\pi G}\left(-\sin p_2\cos p_3\frac{\partial}{\partial x}g_{zi}-\sin p_2\sin p_3\frac{\partial}{\partial y}g_{zi}+\cos p_2\frac{\partial}{\partial z}g_{zi}\right)$$
$$a_{i3}=\frac{\partial Z_i}{\partial p_3}=\frac{p_1}{4\pi G}\left(-\cos p_2\sin p_3\frac{\partial}{\partial x}g_{zi}+\cos p_2\cos p_3\frac{\partial}{\partial y}g_{zi}\right). \tag{7}$$

Let us define now the $n\times 3$ matrix $\mathbf{A}$ which includes the values of the derivatives for the parameters $p_1=p_{10}$, $p_2=p_{20}$, $p_3=p_{30}$, as follows

$$\mathbf{A}=\begin{bmatrix} a_{11} & a_{12} & a_{13} \\ a_{21} & a_{22} & a_{23} \\ \vdots & \vdots & \vdots \\ a_{n1} & a_{n2} & a_{n3} \end{bmatrix}. \tag{8}$$

The matrix **A** has as many rows as the total number of the data and three columns, i.e. as many columns as the number of the parameters. For the further calculations let us define the vectors **Z** and **v**

$$\mathbf{Z}=\begin{bmatrix} Z_1 \\ Z_2 \\ \vdots \\ Z_n \end{bmatrix}, \quad \mathbf{v}=\begin{bmatrix} v_1 \\ v_2 \\ \vdots \\ v_n \end{bmatrix}. \tag{9}$$

where Z_i is the i-th datum of the vertical component of the magnetic field and v_i is given by the equation

$$v_i=a_{i1}p_1+a_{i2}p_2+a_{i3}p_3-(Z_i-Z_i(p_{10}, p_{20}, p_{30})). \tag{10}$$

In the Eq. (10) $Z_i(p_{10}, p_{20}, p_{30})$ denotes a calculated value based on the Eq. (4) for $J/\rho=p_{10}$, $\alpha=p_{20}$, $\beta=p_{30}$, respectively.

Let us introduce the $n\times n$ weightmatrix **W**. The elements in its major diagonal denote the weight of the i-th data and the elements w_{ij} $(i\neq j)$ denote the correlation coefficients between i-th and j-th data. In due course of the calculation data are considered as having unit weights moreover they are regarded uncorrelated. In this case the matrix **W** is a unit matrix.

The next approximations of the parameters p_1, p_2 and p_3 are obtained as

$$\begin{aligned} \bar{p}_1&=p_{10}+\Delta p_1 \\ \bar{p}_2&=p_{20}+\Delta p_2 \\ \bar{p}_3&=p_{30}+\Delta p_3 \end{aligned} \tag{11}$$

where p_{10}, p_{20} and p_{30} are the previous approximations, and Δp_1, Δp_2, Δp_3 are the corrections derived from the solutions of the minimum problem:

$$\sum_{i=1}^{n} v_i^2=\min. \tag{12}$$

This problem formulated in matrix form reads as

$$\mathbf{A}^T\mathbf{W}\mathbf{A}\Delta\mathbf{p}-\mathbf{A}^T\mathbf{W}\mathbf{Z}=\mathbf{0}, \tag{13}$$

where the superscript T indicates the transposed matrix. The solution of the matrix equation (13) gives the correction vector $\Delta\mathbf{p}=\Delta\mathbf{p}(\Delta p_1\ \Delta p_2, \Delta p_3)$.

The components of the parameter vector $\mathbf{p}$ are calculated with an iterative procedure based on the previous equations. The trial values of the k-th iterative step are p_{10}, p_{20}, p_{30} and the corrections $\Delta p_1, \Delta p_2, \Delta p_3$ are determined by the solution of the Eq. (13). With the help of the Eq. (11) then we can calculate the values p_1, p_2, p_3 which are at the same time the next trial values of the iteration. Continuation or ending of the iteration can be decided by the decrease of the sum

$$F=\frac{1}{n}\sum_{i=1}^{n}(Z_i-Z_i(p_{10}, p_{20}, p_{30}))^2 \tag{14}$$

between the k-th and $(k+1)$-th steps.

Illustration of the method by a simple calculation

The procedure of the iteration is illustrated by a model calculation. We estimate the angles of the direction of the magnetic polarization and the ratio of the polarization and the specific density of a uniformly polarized prismatic body. The depth and the size of this rectangular prismatic body are shown in Fig. 1. The specific differential density $\Delta\rho$ is equal to 300 kgm^{-3} the magnetic polarization J is equal to 30 000 nT; consequently $J/\rho=100\ \mathrm{nTkg}^{-1}\ \mathrm{m}^3$. The values of the direction angle of the polarization are $\alpha=60°$ and $\beta=0°$.

The vertical component of the gravitational attraction of a rectangular prismatic body having a uniform specific density was given by Nagy (1966) in the form

$$g_z(x, y, z)=-G\Delta\rho\left|\left|\left| u\ln(v+r)+v\ln(u+r)-w\,\mathrm{tg}^{-1}\frac{uv}{wr}\right|\right|\right|_{u_1v_1w_1}^{u_2v_2w_2} \tag{15}$$

where

$$r=(u^2+v^2+w^2)^{1/2}$$

and

$$\begin{aligned} u_1&=x_1-x & u_2&=x_2-x\\ v_1&=y_1-y & y_2&=y_2-y\\ w_1&=z_1-z & w_2&=z_2-z. \end{aligned} \tag{16}$$

The vertical component of the magnetic field of a rectangular prismatic body having a uniform magnetic polarization was given by Whitehill (1973) as follows

$$Zx, y, z)=\frac{J}{4\pi}\left|\left|\left| \frac{M}{2}\ln\frac{r+u}{r-u}+\frac{L}{2}\ln\frac{r+v}{r-v}-N\,\mathrm{tg}^{-1}\frac{uv}{rw}\right|\right|\right|_{u_1v_1w_1}^{u_2v_2w_2}. \tag{17}$$

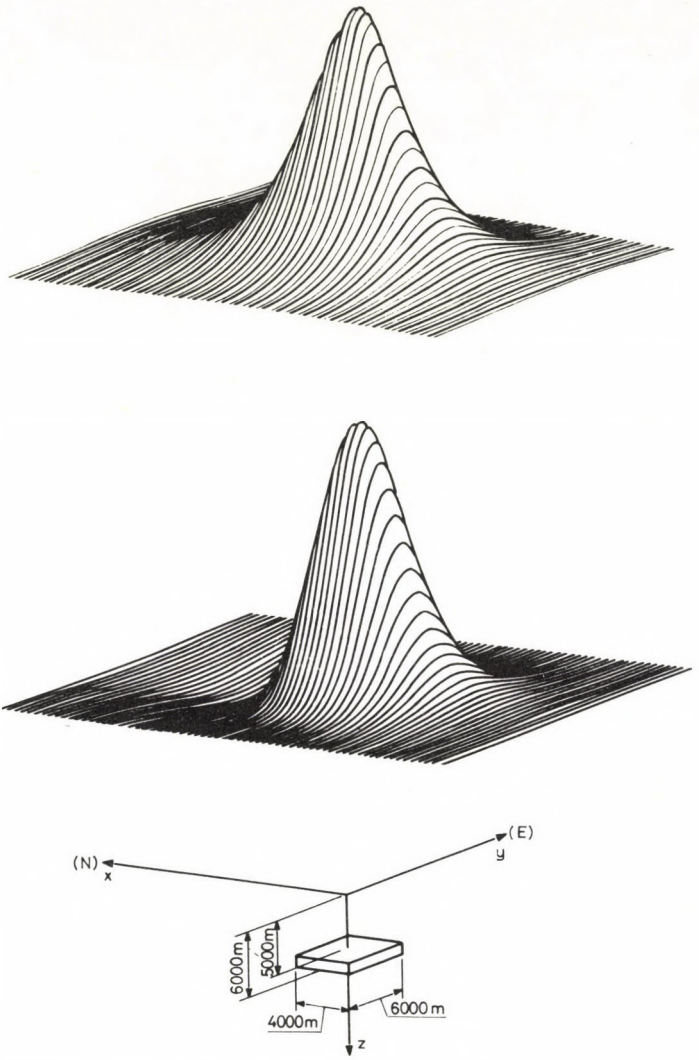

Fig. 1. The coordinate system and the rectangular prism with its dimensions indicated (lower); the perspective view of the vertical component of the magnetic field of the prism (middle); the perspective view of the vertical component of the gravitational attraction of the prism (upper)

The objective function (5) requires the determination of the derivatives of the function (15) with respect to the variables x, y and z. Although these derivatives can be determined analytically, allowing for a more general utilization of the method (which includes the case of discrete data), they are calculated numerically by convolution of coefficients.

The well-known property of the theoretical transfer functions

$$S_{dx}(f_x, f_y) = j2\pi f_x$$
$$S_{dy}(f_x, f_y) = j2\pi f_y \qquad (18)$$
$$S_{dz}(f_x, f_y) = 2\pi(f_x^2 + f_y^2)^{1/2}$$

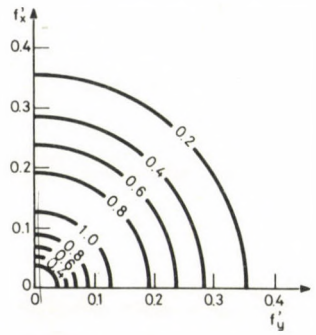

Fig. 2. The two-dimensional window ($m_1 = 9$, $m_2 = 3$), the independent variables are the dimensionless frequencies f'_x and f'_y, respectively

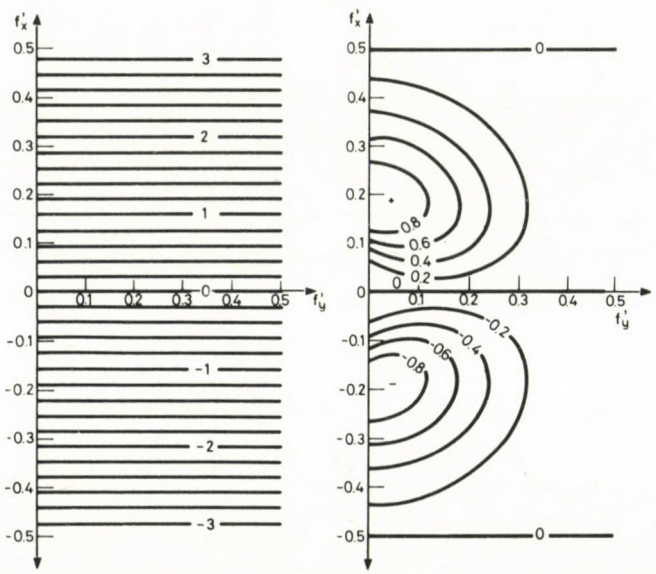

Fig. 3. The imaginary parts of the theoretical (left) and the actual (right) transfer functions of the computation of the derivative with respect to x. The independent variables are the dimensionless frequencies f'_x and f'_y, respectively

of the derivations is an undesirable amplification in the high frequency range. In order to remove this undesirable property of the theoretical transfer functions each of them is multiplied with a two-dimensional window. The window function

$$S_{BP}(f_x, f_y) = C\left(\exp\left(-\frac{36^2(f_x^2+f_y^2)}{m_1^2}\right) - \exp\left(-\frac{36^2(f_x^2+f_y^2)}{m_2^2}\right)\right) \tag{19}$$

suggested by Meskó (1969) is used in the present calculation. The windowing corresponds to band-pass filtering of the input. In Eq. (19) the normalization factor C equals to

$$C = \frac{1}{\exp\left(-\frac{36^2 f_{r\max}^2}{m_1^2}\right) - \exp\left(-\frac{36^2 f_{r\max}^2}{m_2^2}\right)} \tag{20}$$

where

$$f_{r\max} = \frac{m_1 m_2}{36}\left(\frac{2}{m_1^2 - m_2^2} \ln \frac{m_1}{m_2}\right)^{1/2} \tag{21}$$

and the relation $m_1 > m_2$ is valid for the parameters of the band-pass filter. The numerical calculations have been carried out for the parameters $m_1 = 9, m_2 = 3$. We may

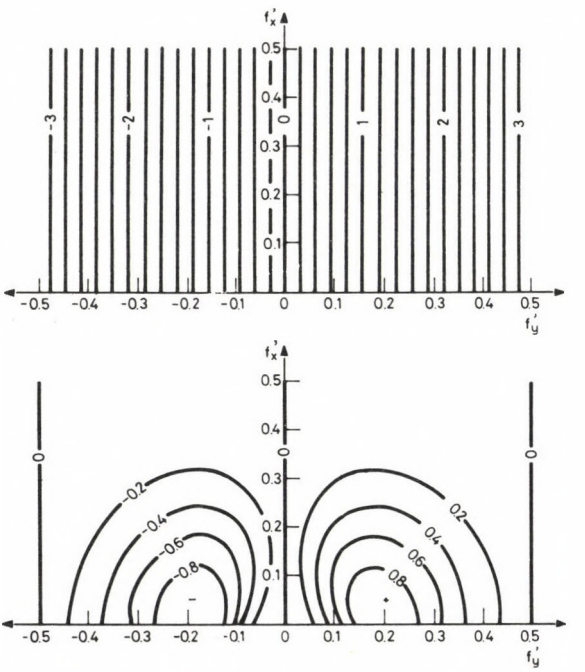

Fig. 4. The imaginary parts of the theoretical (top) and actual (bottom) transfer functions of the computation of the derivative with respect to y. The independent variables are the dimensionless frequencies f'_x and f'_y, respectively

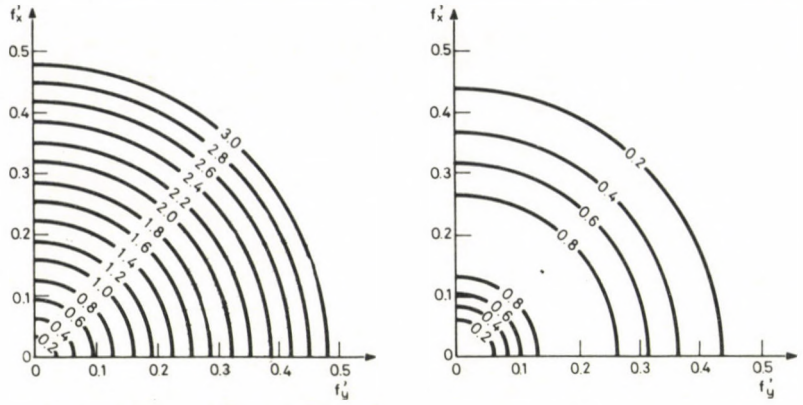

Fig. 5. The theoretical (left) and actual (right) transfer functions of the computation of the derivative with respect to z. The independent variables are the dimensionless frequencies f'_x and f'_y, respectively

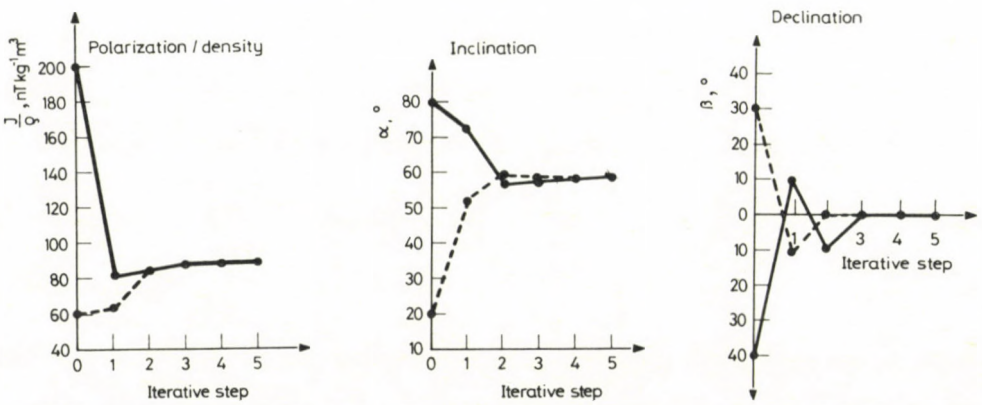

Fig. 6. Two series of the values of ratio J/ρ, inclination α and declination β determined by the iterative procedure, with two sets of starting values (shown by broken and continuous lines)

introduce dimensionless spatial frequencies by the definitions

$$f'_x = f_x \tau \qquad \text{and} \qquad f'_y = f_y \tau \tag{22}$$

where τ denotes the grid spacing. In Fig. 2 the transfer function (19) is shown as the function of the dimensionless frequency variables f'_x and f'_y, respectively. The coefficients (the digitized weight functions) for calculating the derivatives can be obtained by inverse Fourier transform of the appropriate functions, truncated by the above mentioned band-pass filter. The details has been given by the present author (Kis 1983b). Here as some illustration the theoretical transfer functions (18) are shown in Fig. 3, Fig. 4 and Fig. 5. The figures also show the actual transfer functions determined by

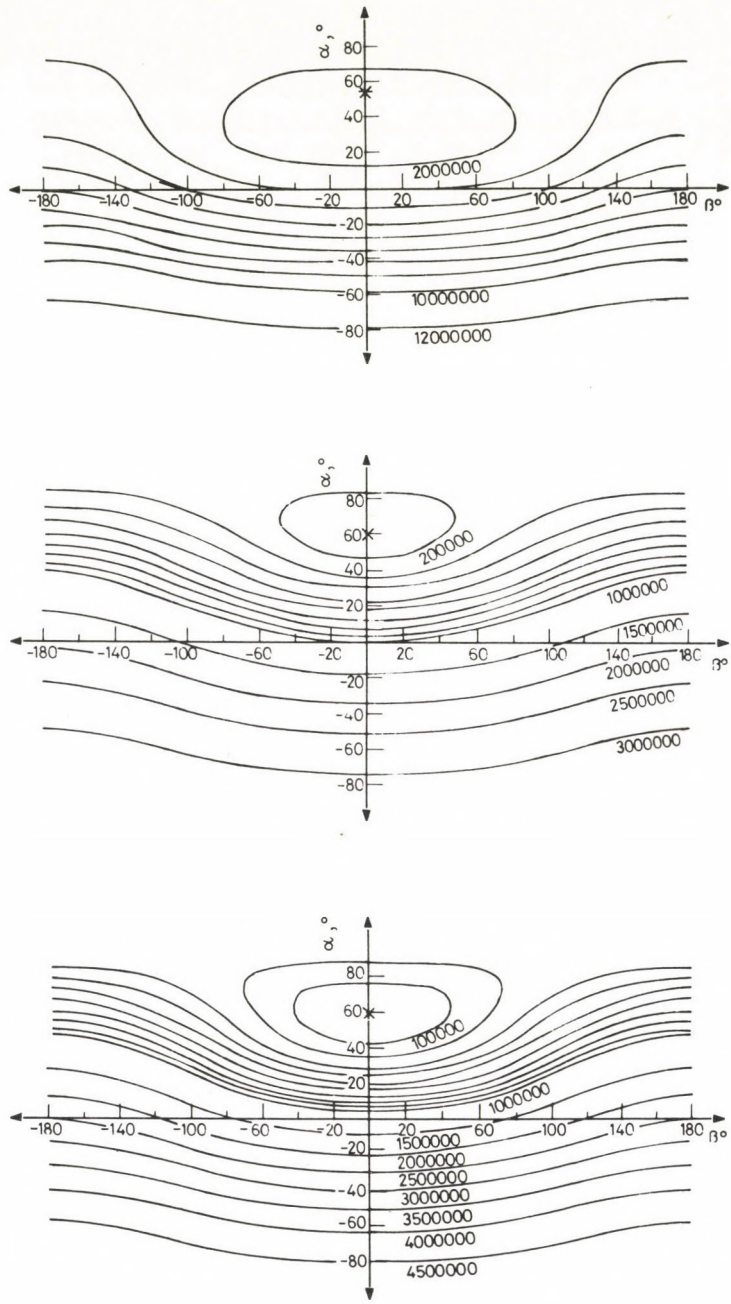

Fig. 7. Contours of three objective functions. The independent variables are the inclination α and the declination β, respectively, the fixed parameter is J/ρ. The upper part shows the contours for the value $J/\rho = 200\,\mathrm{nTkg^{-1}m^3}$, the middle part for $J/\rho = 60\,\mathrm{nTkg^{-1}m^3}$, the lower part for $J/\rho = 89.83\,\mathrm{nTkg^{-1}m^3}$

taking the digital Fourier transform of the computed sets of coefficients. The actual system functions are in a good concord with the theoretical ones in the chosen range.

In order to use the same frequency range for both sets of data the vertical component of the magnetic field of the prismatic body was also filtered by the same band-pass filter.

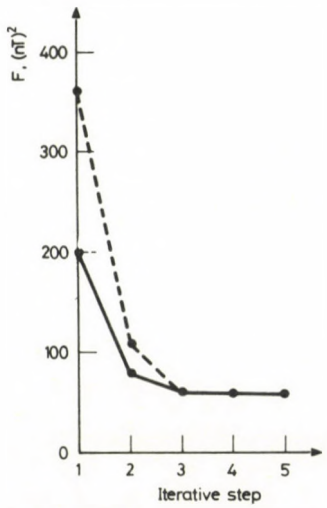

Fig. 8. Decrease of the value F (squared deviation) in the course of the two iterations, starting with two different sets of initial approximations

The input data of the iteration are the band-pass filtered magnetic field and the band-pass filtered vertical derivative of the gravity field, both due to the prismatic body. Two distinct series of the values determined by the iteration, starting with two distinct sets of the initial approximations can be seen in Fig. 6. From the results of the iterations it can be seen that after the third trial the values hardly change and both sets converge to the same values. Figure 7 depicts the contours of the objective function (5) as a function of the inclination α and declination β of the polarization for three different fixed values of J/ρ. The upper and middle parts of the Fig. 7 show the objective functions for the two different starting values of J/ρ. The lower part of Fig. 7 depicts the contours of the objective function the value determined by the iteration. The minimum of the objective function is denoted by an asterisk. Figure 8 shows the decrease of the sum of squares (14) in the course of the iteration. The notation in Fig. 8 is in accordance with the Fig. 6.

From the model calculation we can conclude that the estimation of the angles α and β is effective. The estimation of the ratio J/ρ derivates from the right value by 10 percent.

Acknowledgements

The author is indebted to Prof. A Meskó for the discussions and his help in the method of investigation.

Computations were done by the computer CDC-3300 of the Research Institute for Computing Methods and Automation of the Hungarian Academy of Sciences. The permission for using the computing facilities is being highly acknowledged.

References

Al-Chalabi M 1970: Interpretation of two-dimensional magnetic profiles by non-linear optimization. *Bolletino di Geophysica Teorica ed Applicata*, 12, No 45–46, 3–20.

Emilia D A, Massey R L 1974: Magnetization estimation for nonuniformly magnetized seamounts. *Geophysics*, 39, 223–231.

Fisher N J, Howard L E 1980: Gravity interpretation with the aid of quadratic programing. *Geophysics*, 45, 403–419.

Höpcke W 1980: Fehlerlehre und Ausgleichsrechnung. Walter de Gruyter, Berlin–New York.

Johnson W W 1969: A least-squares method of interpreting magnetic anomalies caused by two-dimensional structures. *Geophysics*, 34, 65–75.

Kis K 1981: Transfer properties of reduction of the magnetic anomalies to the magnetic pole and to the magnetic equator. *Annales Univ. Sci. Budapestiensis*, 23, 75–88.

Kis K 1983a: Derivation of coefficients reducing magnetic anomalies to the magnetic pole and to the magnetic equator. *Acta Geod. Geoph. Mont. Hung.*, 18, 173–186.

Kis K 1983b: Determination of coefficients for the computation of derivatives of potential fields with respect to x, y and z. *Acta Geod. Geoph. Mont. Hung.*, 18, 501–511.

Meskó A 1969: Gravity interpretation and filter theory: design and application of low-pass, high-pass and band-pass filter. *Annales Univ. Sci. Budapestiensis*, 13, 69–80.

Nagy D 1966: The gravitational attraction of a right rectangular prism. *Geophysics*, 31, 363–371.

Skeels D C, Watson R J 1949: Derivation of magnetic and gravitational quantities by surface integration. *Geophysics*, 14, 133–150.

Syberg F J R 1972: A Fourier method for the regional-residual problem of potential fields. *Geophysical Prospecting*, 20, 47–75.

Whitehill D E 1973: Automated interpretation of magnetic anomalies using the vertical prism model. *Geophysics*, 38, 1070–1087.

Wilson C D V 1970: The use of the Poisson relationship for separating the anomalies due to neighbouring bodies, and for recognizing inhomogeneities and structural deformation. *Bolletino di Geophysica Teorica ed Applicata*, 12, No. 45–46, 158–182.

Acta Geodaet., Geophys. et Montanist. Hung. Volume 19 (3–4), pp. 395–400 (1984)

TERRESTRIAL DIAGNOSTICS OF THE MAGNETOSPHERIC PLASMA AT FINITE VALUES OF β*

K DOBES[1], YU P KURCHASHOV[2], F Z FEYGIN[2]

[Manuscript received October 6, 1983]

Methods for the diagnosis of the magnetospheric plasma are studied in order to find the source region of the Pc1-type geomagnetic pulsations. Special attention is paid hereby to the finite pressure of the plasma. The observation material of Soviet stations served as data basis.

Keywords: geomagnetic pulsations; magnetospheric plasma; Pc1; plasma diagnostics

1. Introduction

The possibility of magnetospheric investigations using the transillumination by the MHD waves of natural origin, mainly those of the Pc1-type pulsations ("pearls") has been studied intensively in recent years (Gul'elmi and Troitskaya 1973). In these investigations, however, the effect of the plasma pressure on the dispersion of these pulsations has been neglected what is not always correct. It is known (Berko et al. 1975) that in a region at 4–6 Earth radii, where the "pearls" are excited and propagate, the pressure of the plasma may be equal to the pressure of the geomagnetic field. It was shown by Cornwall and Schulz (1971) that the finite pressure of the plasma significantly influences the dispersion of the Alfvén-waves in the magnetosphere. Since this parameter is one of the basic values for the diagnosis of the magnetospheric plasma, as proposed by Feygin et al. (1979), it is necessary to re-evaluate the method by taking the finite pressure into account.

2. Basic formulas

This paper is based on the same ideas about the generation of the pearls, as the previous one on the diagnostics (Feygin et al. 1979). The effect of a finite pressure will be considered at first in the generation of pulsations which — after a few reflections of the wave packet from the ionosphere — would be attenuated in plasmas with zero

* Paper presented at the KAPG-Symposium on Geomagnetic Pulsations, Sopron, March 1983

[1] Československá Akademie Věd Geofyzikálni Ústav 14131 Praha 4 — Spořilov, Bočni II, čp 1401

[2] Institute Physics of the Earth B. Gruzinskaya 10, Moscow D-242

pressure. In this aspect, the effect of the finite pressure has already been studied and described in the mentioned papers on the diagnosis. In case of finite plasma pressures the parameters which determine the propagation of the wave packets (group velocity, velocity of the frequency increase) strongly differ from the values in cold plasmas. Formally that means that corrections should be introduced into the dispersion relation due to the finite pressure not only in the imaginary, but also in the real part:

$$\kappa^2 \Phi = \frac{x^2}{1-x} - i\sqrt{\pi}\beta_\perp (B_{||})^{-\frac{3}{2}} \cdot \frac{(\tilde{A}-x)}{\kappa} \exp\left[-\frac{(1-x)^2}{B_{||}\kappa^2}\right]. \tag{1}$$

where $\kappa = ck/\omega_{pi}$ is the wave vector normalized by the relation of the Larmor-frequency of ions to the velocity of light; $x = \omega/\omega_{Hi}$ the frequency normed to the ionic gyrofrequency; $\beta_\perp = 8\pi n_g T_\perp / H_0^2$, n_g and T the concentration and the temperature of the hot plasma component; the symbols $\perp$ and $||$ denote components being perpendicular and parallel to the background magnetic field H_0; $B_{||} = 8\pi n_0 T_{||}/H_0^2$, n_0 is the concentration of the cold plasma, $\tilde{A} = 1 - T_{||}/T_\perp$. Further the values $\rho = n_g/n_0$ and $y = \gamma/\omega_{Hi}$ will also be used, the latter being the increment normed to the gyrofrequency of ions.

Equation (1) differs from the equation used by Feygin et al. (1979) in the multiplicator

$$\Phi = 1 + \frac{1}{2}\beta_\perp \frac{(\tilde{A}-x)}{(1-x)^3}. \tag{2}$$

In the following we shall omit all the computations which can be carried out in the same way as in the previous paper, and which, irrespective of their great extent, do not mean any basic difficulties.

Let us discuss the difference between the basic formulas due to the presence of the value $\beta_\perp \neq 0$. The equation for the real part of the frequency (with Im $\kappa = 0$) has here the additional multiplicator:

$$\kappa^2 \Phi = \frac{x^2}{1-x}. \tag{3}$$

If in the increment determined previously (Feygin et al. 1979), the finite pressure is taken into account, then we have instead of

$$y = \sqrt{\pi}\beta_\perp (B_{||})^{-\frac{3}{2}} \cdot \frac{(\tilde{A}-x)(1-x)^{\frac{5}{2}}}{x^2 \cdot (2-x)} \exp\left[-\frac{(1-x)^3}{B_{||} \cdot x^2}\right] \tag{4}$$

a form with the additional multiplicator:

$$\Phi^{\frac{1}{2}}\left[1 - \frac{x(1-x)}{(2-x)} \cdot \frac{\mathrm{d}}{\mathrm{d}x}(\ln \Phi)\right]^{-1} \cdot \exp\left[(1-\Phi)\frac{(1-x)^3}{B_{||} \cdot x^2}\right]. \tag{5}$$

It should be remarked that not all values appearing in the increment are independent, i.e. their values are determined by two parameters, the frequency and the distance of the zone of generation from the Earth. The increment in function of the frequency and distance has a rather sharp maximum (Feygin et al. 1979). If the instability has in consequence of a severe ionospheric attenuation a threshold character, then the generation takes place along this maximum. It is situated according to our results at the plasmapause where the concentration of the cold plasma changes quicker with the distance than all other parameters. Thus it is possible to use, instead of the extremum of the increment in function of frequency and distance, the extremum in function of the variables x and $B_{||}$. The condition for an extremum after $B_{||}$ is

$$B_{||} = \frac{2}{3} \frac{(1-x)^3}{x^2} \Phi . \tag{6}$$

The difference from the corresponding equation in the previous paper lies in the multiplicator Φ. The extremum in function of x is now considerably more complicated:

$$\beta_{\perp} = 2 \frac{(1-x)^2(2-x)}{x} \cdot \frac{1 - 2\dfrac{(1+x-x^2)}{(2-x)} \left[\dfrac{(\tilde{A}-x)}{x(1-x)}\right]}{2[(1-x)^2+x^2] \left[\dfrac{(\tilde{A}-x)}{x(1-x)}\right]^2 - 1} . \tag{7}$$

The diagnosis of the plasma parameters is based on the fact that some combinations of the derivatives of the increment y and of the frequency x with respect to the wave vector $\kappa_{|}$ namely

$$r_1 = - \frac{\partial^2 y / \partial \kappa^2}{\partial^2 x / \partial \kappa^2} \tag{8}$$

and

$$r_2 = \frac{x \cdot \partial^2 x / \partial \kappa^2}{(\partial x / \partial \kappa)^2} \tag{9}$$

can be obtained from ground observations of pulsations. Supposing that the derivatives in Eqs (8) and (9) are taken as constant $\tilde{A}$, $\beta_{\perp}$, $B_{||}$, and using Eqs (6) and (7) all the values appearing in these equations can be expressed by two variables, which are then used as independent ones, e.g. $\tilde{A}$ and x. By solving the system of two equations obtained so for the dependent variables, and by determining the others from the extremum condition, all parameters in the expression of the increment can be determined, i.e. x, $\tilde{A}$, $\beta_{\perp}$ and $B_{||}$.

In the previous paper we proposed a method for the determination of the left-hand side of Eqs (8) and (9) on the basis of the speed of the frequency increase and of the duration of the pulsation packets at the surface:

$$r_1 = \frac{4 \ln 2}{\pi} \left(\theta^2 \cdot \frac{\mathrm{d}f}{\mathrm{d}t} \right)^{-1} \tag{10}$$

$$r_2 = \frac{1}{1+r_1^2} \cdot \frac{f}{\tau} \frac{\mathrm{d}\tau}{\mathrm{d}f}. \tag{11}$$

Here θ denotes the duration of the packet till it decreases to the half of the maximum value, $\mathrm{d}f/\mathrm{d}t$ is the speed of the frequency increase within the packet ($f = \omega/2\pi$). The difference of the two reciprocal values of $\mathrm{d}f/\mathrm{d}t$ for two consecutive packets is accepted as the derivative of the repetition time at the given period ($\mathrm{d}\tau/\mathrm{d}f$); f and τ are the central frequency and the corresponding repetition time. It should be remarked that if in Eq. (11) the difference values for two packets are substituted, then in Eq. (10) the values for any of these packets can be substituted, i.e. $\theta^2 \cdot \mathrm{d}f/\mathrm{d}t = \text{const}$. Therefore the value of the deviation r_1 for the neighborous packets can be used for the preliminary estimation of the applicability of the proposed method for a given experimental sequence of Pc1-pulsations.

The proposed method enables the determination of mainly relative values, i.e.: the ratio of the concentration of hot and cold plasma $\rho = \frac{\beta_\perp}{B_{||}}(1-\tilde{A})$, the ratio of the perpendicular and field-aligned plasma pressures, $1/(1-\tilde{A})$ the ratio of the perpendicular pressure of the plasma to the pressure of the magnetic field $\beta_\perp$. From the absolute values, the ion gyrofrequency can be easily determined:

$$\omega_H = \frac{\omega}{x} \tag{12}$$

but, together with its distance from the generation zone (supposing the geomagnetic field as a dipole field) and the pressure of the magnetic field $H_0^2/8\pi$. From them using the values of $\beta_\perp$ and A, the perpendicular and field-aligned pressure of the plasma can also be found. For the determination of the absolute values n_0, n_r, $T_\perp$, $T_{||}$, it is necessary to determine one of these values by an independent method (any method can be used). Al'pert and Fligel (1977) proposed such a method: they computed the time needed for the wave packets to propagate along the field lines at different distances from the Earth, at different frequencies and at different plasma concentrations.

By solving the equation

$$\tau = \tau(\omega, \omega_H, n_0) \tag{13}$$

for n_0, the concentration of the cold plasma is obtained. As the ratio of the concentrations and the pressure tensor are already known, the values of n_r, $T_\perp$, $T_{||}$ can be easily obtained.

With the exception of the solution of the Eqs (8), (9) and (13) which can only be solved by computers or graphically in consequence of the complicated right-hand

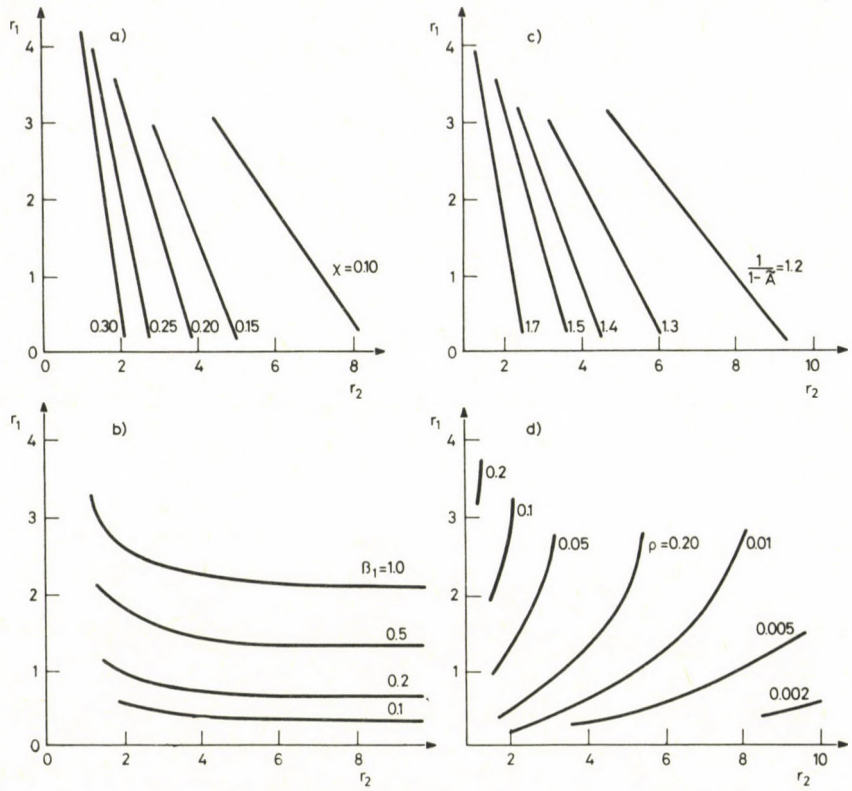

Fig. 1

Table I

Day	UT	f Hz	τ s	θ s	$\frac{df}{dt}\cdot 10^3$ Hz/s	$\frac{d\tau}{df}$ s/Hz	r_i	r_2	L	$\beta_\perp$	$\frac{T_\perp}{T_{\|\|}}$	$\rho\cdot 10^3$
17 October 1977	10.33	0.96	114	46	1.35	19	0.31	0.15	3.9	0.1	1.26	2.1
	11.10	1.065	122	51	0.29	105	1.2	0.38	4.7	0.29	1.57	30
	11.24	1.06	112	62	1.03	32	0.22	0.33	4.7	0.05	1.57	5.3
	11.31	1.04	114	48	1.58	34	0.25	0.29	4.6	0.06	1.5	5
	11.37	1.04	117	60	1.15	34	0.22	0.29	4.6	0.05	1.5	4.2
	11.49	1.055	122	67	0.89	27	0.23	0.22	4.3	0.06	1.4	3.1
16 October 1977	11.52	1.02	159	62	0.73	123	0.1	0.78	5.7	0.01	2.28	6.4

sides, all other computations are elementary ones. Figure 1 shows nomograms for the determination of x, $\tilde{A}$, $\beta_\perp$, ρ from the parameters r_1 and r_2.

The results of this method are presented on the basis of some events recorded at Soviet stations in Table I.

References

Al'pert Ja, Fligel D S 1977: *Planet. Space Sci.*, 25, 487.
Berko F W, Cahill L J, Jr Fritz T A 1975: *J. Geophys. Res.*, 80, 3549.
Cornwall J M, Schulz M 1971: *J. Geophys. Res.*, 76, 7791.
Feygin F Z, Kurchashov Yu P, Troitskaya V A, Fligel D S, Dobes K 1979: *Planet. Space Sci.*, 27, 151.
Gul'elmi A V, Troitskaya V A 1973: Geomagnetic pulsations and the diagnosis of the magnetosphere. Moscow, Nauka

Acta Geodaet., Geophys. et Montanist. Hung. Volume 19 (3–4), pp. 401–413 (1984)

SHORT-PERIOD PULSATIONS OBSERVED IN FINLAND DURING THE IMS AND CERTAIN ASSOCIATIONS WITH MAGNETIC AND IONOSPHERIC PARAMETERS*

F MÄRCZ[1], J VERŐ[1], P BENCZE[1]

[Manuscript received September 30, 1983]

Events of two types of short-period magnetic pulsations (Pc1 and IPDP) observed at five stations in Finland (between $L \simeq 6.0$ and $L \simeq 3.3$) are analysed. Sodankylä ($L \simeq 5.1$) at a higher latitude and Nurmijärvi ($L \simeq 3.3$) at a lower latitude seem to be rather favoured sites to short-period pulsations. The pulsation occurrences show certain seasonal variations with a quite stable minimum in June. The occurrence differences between individual stations have revealed some peculiarities, especially in dependence on geomagnetic activity and the *foF2* ionospheric parameter. *foF2* $\simeq 10$ MHz may represent a physical limit influencing the waveguide propagation of Pc1 pulsations.

Keywords: geomagnetic influence; geomagnetic pulsations; ionospheric influence; IPDP; latitude variation; Pc1

1. Introduction

The International Magnetospheric Study (IMS) yielded a lot of data on parameters characterizing the dynamical processes in the magnetosphere. Simultaneous measurements providing the data were carried out either in space or at the earth's surface. Some of the ground-based observations were organized in Scandinavia. Thus a north-south chain of five magnetic pulsation stations was established in Finland nearly at the same meridian between $L \simeq 6.0$ and $L \simeq 3.3$. Data of two types of short-period magnetic pulsations (Pc1 and IPDP) have been published for each station in the form of quick-look tables (Pikkarainen et al. 1982). The occurrences of the Pc1 and IPDP pulsation events are given for the period between October, 1976 and December, 1979.

As generally accepted, the generation of Pc1 type pulsations is connected with plasma instabilities in the plasmasphere. For the generation of IPDP pulsations the instability of the distribution of charged particles in the ring current may be responsible (Jacobs 1970). In addition to their magnetospheric origin, these pulsations observed at the ground may be influenced by propagation conditions (e.g. by ionospheric

* Paper presented at the KAPG-Symposium on Geomagnetic Pulsations Sopron, March 1983

[1] Geodetic and Geophysical Research Institute of the Hungarian Academy of Sciences, H-9401 Sopron, P.O.B. 5, Hungary

parameters). In the present paper data of both types of pulsations are analysed in order to show the latitude dependence and the seasonal variation in their occurrences. Some analyses are aimed at the study of pulsation occurrences in dependence on certain magnetic and ionospheric parameters.

2. Investigations and results

The five magnetic pulsation stations which have been operated in Finland during the IMS are listed by geographical latitude in Table I, where the geographical longitudes and the *L*-values of the stations are also given.

Table I

Station	Geographical		*L*-value
	latitude	longitude	
Kevo	69.8°N	27.0°E	6.0
Sodankylä	67.4°	26.6°	5.1
Oulu	65.1°	25.5°	4.3
Jyväskylä	62.4°	25.7°	3.7
Nurmijärvi	60.5°	24.7°	3.3

The quick-look tables published (by the Department of Physics, University of Oulu) contain the occurrences of Pc1 and IPDP pulsations for each station as a function of time (UT). The two types of pulsation events have not been separated from each other in the tables. Nevertheless, the Pc1 events mostly occur during the morning-day hours and the IPDP events in the afternoon-evening hours. On this basis we have summarized the individual occurrences separately for the two intervals from 00 00 to 12 00 UT (a.m.) and from 12 00 to 24 00 UT (p.m.). Thus total durations of both Pc1 and IPDP occurrences have been approximated for each day. (The accuracy limit for the individual sums might be half an hour or so). Though these daily values are approximations they should be suitable for analysing Pc1 and IPDP pulsations in dependence on different parameters.

2.1 Pc1 and IPDP pulsations at several stations during IMS years

To review the overall activity during the period from October 1976 to December 1979, the monthly sums of occurrences have been calculated for both types of pulsations. (Recordings were only a few times interrupted). Results presented in Fig. 1 top allow to study the Pc1 occurrences (a.m.) at three stations (Kevo, Sodankylä and Jyväskylä) located at different latitudes. At first, a comparison should be made between

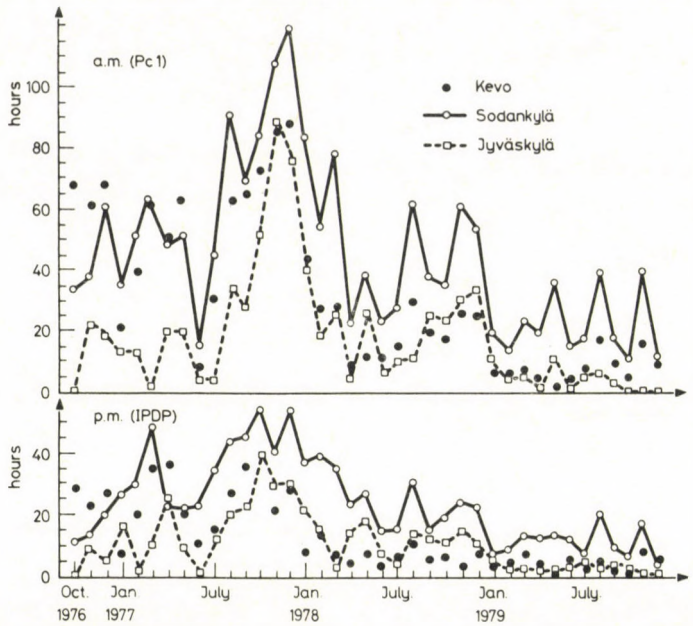

Fig. 1. Top: a.m. (Pc1) pulsation occurrences at three stations during the period from October 1976 to December 1979. Bottom: the same as above, but for p.m. (IPDP) occurrences

Sodankylä and Jyväskylä. There is a latitude difference of 5° between the two measuring sites. Pc1 activity at Jyväskylä (situated at a lower latitude) is much lower than at Sodankylä during the whole period investigated, however, the changes are rather similar at both stations. This is especially true in the time of highest activity from the second half of 1977 to the first months in 1978. As shown in Fig. 1 bottom for the IPDP pulsations (p.m.), the summarized monthly durations are also longer at Sodankylä than at Jyväskylä, excepting in April 1977. The trend of changes in IPDP activity is quite similar to that found for Pc1 activity. Nevertheless, it seems to be a general rule for both stations that a.m. (Pc1) pulsations have a longer duration than p.m. (IPDP) pulsations.

From the comparison between Sodankylä and Jyväskylä, it should be concluded that both Pc1 and IPDP activity is decreased towards the lower latitudes. This seems to be confirmed by a comparison between Kevo and Jyväskylä. In 31 months out of the investigated 39, Pc1 activity is higher at Kevo than at Jyväskylä. The IPDP activity is generally higher at Kevo during the first half of the total period but later the opposite is true.

Finally, a comparison between Kevo and Sodankylä reveals that in spite of the higher latitude of Kevo, the durations of both pulsation types are longer at the lower latitude Sodankylä. Consequently, the continuous decrease of the Pc1 and IPDP

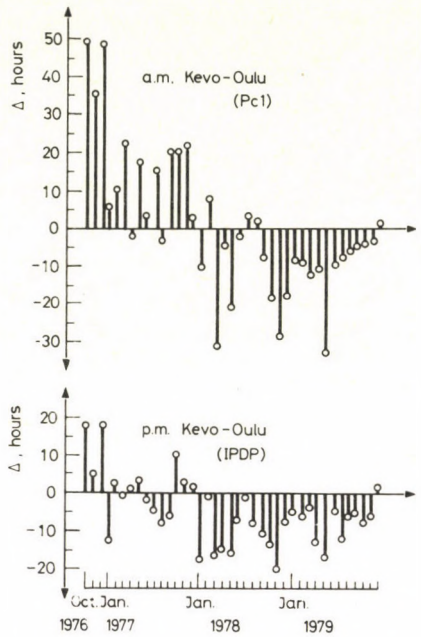

Fig. 2. Top: differences (Δ) between monthly duration sums of Kevo and Oulu during the period from October 1976 to December 1979 in case of a.m. pulsations. Bottom: the same as above, but for p.m. pulsations

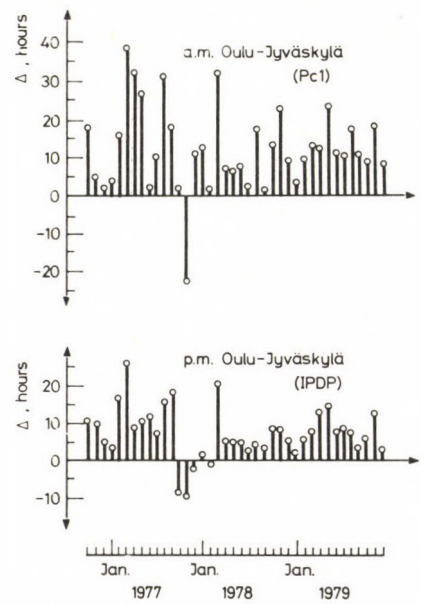

Fig. 3. Top: differences (Δ) between monthly duration sums of Oulu and Jyväskylä during the period from October 1976 to December 1979 in case of a.m. pulsations. Bottom: the same as above, but for p.m. pulsations

activity seems to be restricted to a distinct latitude range, or rather there may exist a belt around the latitude of Sodankylä where the magnetospheric conditions (configuration and processes) and/or the propagation conditions are excessively favourable to the appearance of Pc1 and IPDP.

The latter interpretation is in accordance with the results in Fig. 2 where the differences between monthly duration sums of Kevo and Oulu (situated between Sodankylä and Jyväskylä) are shown. The differences are positive when the durations of pulsations were longer at Kevo than at Oulu and negative in the opposite cases. Since for Pc1 pulsations (Fig. 2 top) these differences are mostly positive during the first half of the total period, the lower edge of the belt with favourable conditions to Pc1 occurrences was generally located somewhere between Oulu and Sodankylä till the beginning of 1978. After this time the negative differences dominate what indicates that then in addition to Sodankylä even Oulu was generally in an advantageous situation in comparison with Kevo. The mentioned belt extended towards lower latitudes between Oulu and Jyväskylä as shown by the differences between Oulu and Jyväskylä in Fig. 3 top, (see also Fig. 1 top). In case of IPDP's (Fig. 2 bottom) the situation is rather confused till 1978, however, from January 1978 to November 1979 each difference is negative. Consequently, during this interval the conditions were more favourable to IPDP occurrences at the Oulu station than at Kevo. This is also true for Oulu when comparing it with Jyväskylä (Fig. 3 bottom).

2.2 Seasonal variation in Pc1 and IPDP occurrences

Averaged duration sums for the individual months of the year and their changes are shown in Fig. 4 for the different stations. On the basis of the curves in Fig. 4, the months with the highest, respectively the lowest Pc1 and IPDP occurrences are listed in Table II.

Excepting one case, there is a fixed month for the absolute minimum in the occurrences of both pulsation types (namely June) independently of latitude. For Pc1 pulsations even the time of maximum occurrences is rather uniform along the investigated station chain. These pulsations are most frequent during early winter and only at Sodankylä in August. Fig. 4 shows, however, that a winter peak was also present at the latter station. In case of IPDP occurrences the maxima appeared in different months; in equinox at the higher latitudes and in winter at the two lower latitude stations.

Numbers in the last two columns of Table II indicate the ratios of the highest averaged monthly durations to the lowest ones, separately for the two pulsation types. Quite large ratios have been determined for the high latitude Kevo station and especially for Jyväskylä while the ratios are small in case of Sodankylä and Oulu. It is known from the previous section that Sodankylä and Oulu are favoured stations in comparison with Kevo or Jyväskylä. Consequently, the amplitude of the seasonal

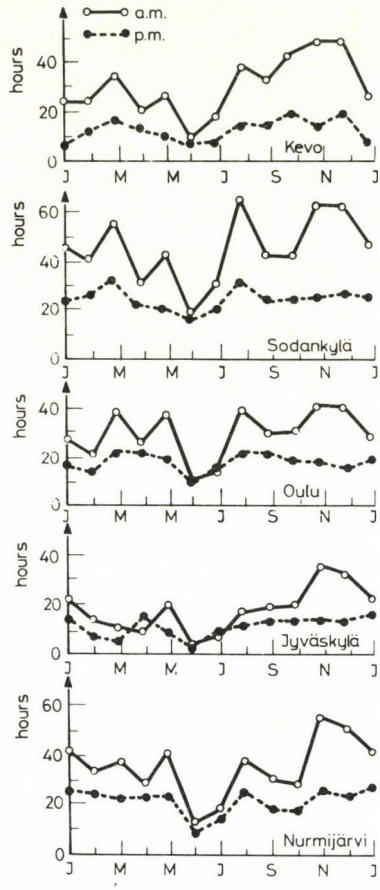

Fig. 4. Seasonal variation in a.m. and p.m. pulsation occurrences at five stations on the basis of averaged data of the period between October 1976 and December 1979

Table II

Station	Highest averaged monthly duration		Lowest averaged monthly duration		Ratio highest to lowest	
	a.m. (Pc1)	p.m. (IPDP)	a.m. (Pc1)	p.m. (IPDP)	a.m. (Pc1)	p.m. (IPDP)
Kevo	Dec.	Oct.	June	Jan.	6.0	3.0
Sodankylä	Aug.	March	June	June	3.6	1.9
Oulu	Nov.	April	June	June	3.9	2.2
Jyväskylä	Nov.	Jan.	June	June	9.3	4.6
Nurmijärvi	Nov.	Jan.	June	June	4.4	3.2

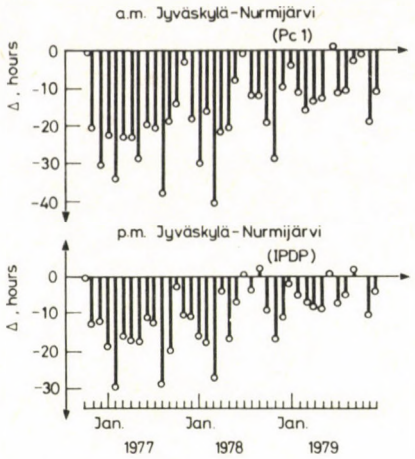

Fig. 5. Top: differences (Δ) between monthly duration sums of Jyväskylä and Nurmijärvi during the period from October 1976 to December 1979. Bottom: the same as above, but for p.m. pulsations

change (characterized by the ratio) is generally smaller at a favoured station than at some neighbouring sites.

On this basis it can be supposed that the Pc1 and IPDP occurrences of Jyväskylä should be surpassed by those of Nurmijärvi because of the smaller ratios determined for the latter. Fig. 5 shows the differences between the monthly duration sums of Jyväskylä and Nurmijärvi, situated at the lowest latitude (the presentation is the same as in Figs 2 and 3). Since these differences are almost all negative, the durations were really longer at Nurmijärvi than at Jyväskylä, as suggested on the basis of the ratios. At present, no clear explanation can be given for the relation experienced. It is to be mentioned, however, that the extremely low level of the minimum occurrences at Kevo and Jyväskylä (Fig. 4) contributed to the large ratios, and the generally lower level of pulsation activity to the disadvantageous situation of these stations in comparison with the others (Figs 2, 3, 5).

2.3 Associations with magnetic and ionospheric parameters

It was shown in earlier studies (Märcz and Verő 1977, Märcz 1980) that a distinct after-effect appears in Pc1 pulsations observed at mid-latitudes following geomagnetic storms. These pulsations may appear two times longer during the after-effect interval in comparison with the normal conditions. On the other hand, rather low Pc1 activity is generally found around severely disturbed days. In this section it will be studied whether geomagnetic activity might have played any part in some results presented previously.

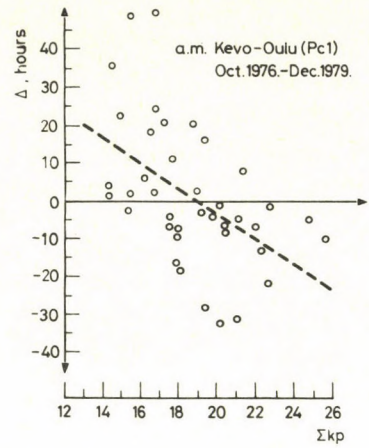

Fig. 6. Kevo-Oulu differences (Δ) of monthly duration sums of a.m. pulsation occurrences as a function of geomagnetic activity (Σ Kp)

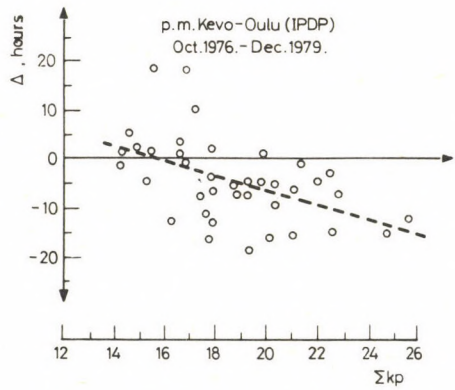

Fig. 7. The same as in Fig. 6, but for p.m. pulsations

For the investigated interval the yearly averages of the daily Kp-sums are the following: 17.9 (1976), 17.1 (1977), 20.1 (1978), 19.6 (1979). Thus, geomagnetic activity was higher in 1978 and 1979 than in the preceding years. In Fig. 2, the differences (Δ) between the monthly duration sums of Kevo and Oulu have also changed their sign, from mostly positive to negative around the beginning of 1978. A more detailed picture is presented in Fig. 6, where the Kevo-Oulu monthly differences (Δ) are shown for a.m. (Pc1) as a function of geomagnetic activity characterized by the monthly averages of daily Kp-sums (between October, 1976 and December, 1979). The influence of geomagnetic activity on the difference between Pc1 occurrences at the two stations is confirmed by the distribution of the 39 values in Fig. 6. The equation of the regression line can be given as $\Delta = -3.26\,\Sigma\mathrm{Kp} + 61.85$. For IPDP occurrences the connection is

shown in Fig. 7 and the equation of the corresponding regression line is the following: $\Delta = -1.5\,\Sigma Kp + 23.4$.

The Kevo-Oulu monthly differences for Pc1 pulsations (Δ) are presented in Fig. 8 as a function of the monthly averages of the daily *foF2* maxima, determined at a somewhat lower latitude ($\varphi_{geogr} \simeq 54.6°N$), in Juliusruh. Two distributions appear in Fig. 8, one is connected with *foF2* critical frequencies below about 10 MHz and another belongs to some values above 10 MHz. In the first case, the Kevo–Oulu differences are decreased with increasing frequency and become even negative, similarly to their distribution with increasing geomagnetic indices in Fig. 7. Above 10 MHz, the negative differences in Fig. 8 gradually decrease towards the higher *foF2* values, i.e. this smaller distribution may represent an opposite connection.

3. Discussion

As mentioned in the Introduction, the pulsation data of the IMS observations have been investigated on purpose to reveal certain latitudinal changes and to find associations with other parameters. The results presented in Section 2 hint at some peculiarities of the Pc1 and IPDP occurrences in dependence on latitude. The monthly sums of the occurrences do not show a proportional change in accordance with increasing or decreasing latitude of the individual stations. Sites favourable to the occurrences might be found both at higher and at lower latitudes as indicated by comparisons. Sodankylä station seems to be a rather favoured locus among the stations at higher latitudes and the situation at the lowest latitude Nurmijärvi is also advantageous.

In case of Pc1 pulsations it was considered (Jacobs 1970) that the source exciting the appropriate emissions has a diurnal variation in latitude. A strong day-time maximum at the higher latitudes could be contrasted with the night-time maximum at the lower latitudes. Troitskaya et al. (1975) have shown that in case of short-period ($T \leqq 2$ sec) Pc1 pulsations the meridional distribution of the pulsation amplitudes depends on local time. The maximum of the distribution (which indicates the L-parameter of the field line where Pc1's are generated) appears as a peak in day-time and is rather flat in the night and morning hours. Pc1 pulsations with longer periods mostly occur in day-time. Troitskaya et al. (1975) confirmed that Pc1's are generated at the day-side of the magnetosphere and get through waveguide propagation (from east to west) to the Earth's night-side. In addition, an increase of the waveguide attenuation with the decrease of Pc1 period was found.

These results indicate that the occurrence of Pc1 pulsations at the individual stations and their latitude variation is influenced both by the situation of the source and by the propagation conditions. The interaction of several parameters and processes (period, waveguide attenuation etc.) controls whether Pc1's do appear at one

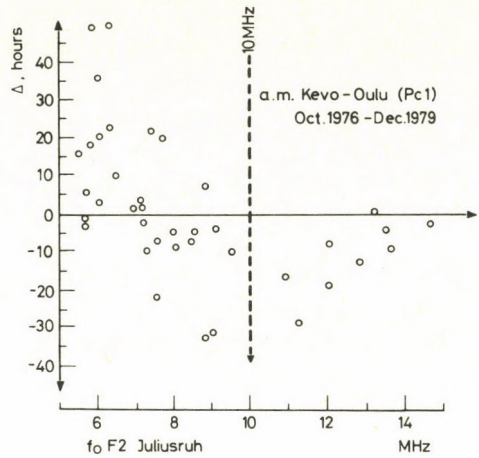

Fig. 8. Kevo-Oulu differences (Δ) of monthly duration sums of a.m. (Pc1) pulsation occurrences as a function of the $foF2$ parameter determined at Juliusruh (GDR)

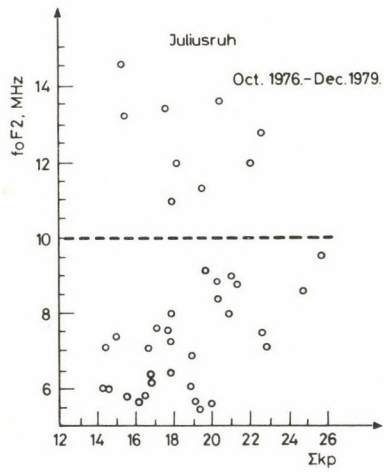

Fig. 9. The $foF2$ parameter as a function of geomagnetic activity (Σ Kp)

or another site. In the present paper short-period magnetic pulsations observed between 00 00 and 12 00 UT have been accepted as Pc1's, although within this interval, night-time and day-time occurrences may differently depend on latitude. Among others, this approximation and the unknown period spectrum prevent a detailed interpretation of the results given in the previous sections. Nevertheless, certain regularities and peculiarities, especially for the waveguide propagation, should be understood on the basis of some further facts.

Table III

parameter	cases	Σ Kp	*foF2*
Kevo-Oulu Pc1 diff.	all	−0.46	−0.49
	foF2 < 10 MHz	−0.41	−0.43
Σ Kp	all		+0.19
	foF2 < 10 MHz		+0.42

As shown earlier, the monthly differences between the pulsation occurrences at two stations depend on geomagnetic activity (Figs 6 and 7). Additionally, an association of the a.m. pulsations (Pc1) with the ionospheric parameter *foF2* can also not be excluded (Fig. 8). Now in Fig. 9, the *foF2* parameter is presented as a function of geomagnetic activity for the interval indicated. The *foF2* values regularly increase up to a limit of 10 MHz with increasing geomagnetic activity, but above the 10 MHz limit this connection is no more valid.

On this basis, it may be assumed that the change in the distributions of the Pc1 occurrence differences at 10 MHz (Fig. 8) could be associated with the different characteristics of two groups of *foF2* values in dependence on geomagnetic activity (Fig. 9). The supposition is refutable by partial correlation factors determined between the three parameters and shown in Table III both for all cases and for *foF2* < 10 MHz. The factors indicate that the Kevo–Oulu differences (in Pc1 occurrences) correlate with the geomagnetic and the ionospheric parameter in the same degree and even the separation according to the *foF2* limit does not change the situation. Such a separation, however, influences the correlation between ΣKp and *foF2* which is considerable only in case of *foF2* values below 10 MHz. (This connection has already been shown in Fig. 9).

Finally, a correlation analysis was carried out between the monthly duration sums of a.m. pulsations (Pc1) and the monthly averages of daily ΣKp respectively of daily maximum *foF2* values. The partial correlation factors are presented in dependence on the geographical latitude of the five measuring sites in Fig. 10. The latitudinal variation of the factors indicating the negative correlation between Pc1 pulsations and ΣKp (Fig. 10 top) is nearly the same whether all (monthly) data or only those with *foF2* < 10 MHz are taken into account. The largest correlation factor appears at Kevo ($\varphi \simeq 70°$) and the smallest at Oulu ($\varphi \simeq 65°$). Figure 10 bottom shows the change in correlations calculated between the Pc1 occurrences and the *foF2* parameter. When using all data, the closest correlation is again at Kevo, however, the lowest at Jyväskylä ($\varphi \simeq 62.5°$). If only the data with *foF2* < 10 MHz are regarded, practically no correlation exists, excepting at Kevo, i.e. in this case, for stations at lower latitudes than Kevo, the occurrence of Pc1 pulsations could not be influenced by the corresponding electron density of the *F2* layer.

This confirms that the *foF2* ≃ 10 MHz value may represent a real physical limit affecting the waveguide propagation of Pc1 oscillations. A similar value of about

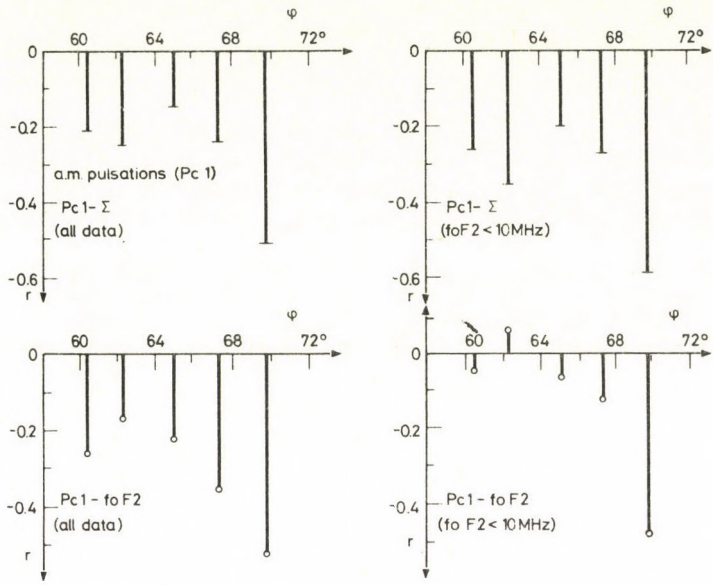

Fig. 10. Top: latitude variation in partial correlation factors determined between a.m. (Pc1) pulsation occurrences and geomagnetic activity (Σ Kp) considering also the *foF2* parameter. Bottom: latitude variation in partial correlation factors determined between a.m. (Pc1) pulsation occurrences and the *foF2* parameter considering also geomagnetic activity (Σ Kp)

(Correction: Top Pc1 – Σ should read Pc1 – Σ Kp)

10 MHz was else found as the lower limit of ionospheric-plasmaspheric damping of Pc3 pulsations (Verő 1981). Actually, at lower latitudes than Kevo, $foF2 > 10$ MHz values seem to be responsible for the negative correlation between this ionospheric parameter and the Pc1 occurrences. The degree of the correlation changing in dependence on latitude, together with the geomagnetic control (Fig. 10), indicates that complex causes may contribute to the situation revealed in Figs 1–5: that e.g. there are stations more favourable to the occurrences of short-period pulsations than other sites, which can be found both at the higher and the lower latitudes of the belt investigated. Thus, the ionospheric conditions that exist between source and site can differently affect the detection of pulsations at the individual stations. Nevertheless, the situation is even more complex as the influence of the ionosphere can be covered by changes in source intensity, too.

Acknowledgements

We are greatly indebted to the Department of Physics, University of Oulu for the quick-look tables of pulsation data made available for us.

References

Jacobs J A 1970: Geomagnetic micropulsations. Physics and Chemistry in Space 1. Springer-Verlag, Berlin, Heidelberg, New York

Märcz F, Verő J 1977: Ionospheric absorption and Pc1-type micropulsations following enhanced geomagnetic activity. *J. Atmos. Terr. Phys.*, 39, 295–302.

Märcz F 1980: Geomágneses utóhatás a rádióhullámok ionoszférikus abszorpciójában. Légköri és extraterresztrikus kapcsolatok. (Geomagnetic after-effect in ionospheric absorption of radio waves. Atmospheric and extraterrestrial relations). Cand. Dissertation, Sopron

Pikkarainen T, Lukkari L, Niskanen J, Kangas J 1982: Quick-look tables of Pc1 and IPDP magnetic pulsation events recorded in Finland during IMS-years 1976–1979. Data summary. Department of Physics University of Oulu. Report No. 92/1982.

Troitskaya V A, Baransky L N, Matveeva E T, Feigin F Z, Glangeaud F, Vinogradov P A, Koshelevsky V K 1975: O polozhenii istochnikov pulsatsii Pc1 v magnitosfere. (About location of Pc1 pulsation sources in the magnetosphere). *Geomagn. i Aeronomiya*, 15, 524–531.

Verő J 1981: Changes of pulsation activity during two solar cycles. *J. Atmos. Terr. Phys.*, 43, 919–926.

Acta Geodaet., Geophys. et Montanist. Hung. Volume 19 (3–4), pp. 415–420 (1984)

CONNECTIONS BETWEEN PARAMETERS OF THE INTERPLANETARY MEDIUM AND GEOMAGNETIC ACTIVITY

J STŘEŠTÍK*[1]

[Manuscript received October 6, 1983]

The paper deals with the determination of the correlation coefficients between some parameters of the interplanetary medium and the geomagnetic activity expressed by a number of indices (including pulsation indices). The connections and correlations are separately computed for different orientations of the interplanetary magnetic field (IMF) and also for high and low values of its scalar intensity, and of the velocity of the solar wind as well.

Keywords: geomagnetic activity; interplanetary medium; pulsation indices; solar wind velocity

It is generally accepted that the ultimate cause of the geomagnetic activity is in the sun. The propagation process of the disturbances from the sun to the earth is a chain: sun — interplanetary medium — magnetosphere — surface of the Earth. Since the launch of the first satellite we have *in situ* data from the cosmic space. Thus the possibility is also given to compare interplanetary data with data of the ground activity. The first discovery in this field was the connection between solar wind velocity and geomagnetic activity Σ Kp (Jacobs 1970). Many other interplanetary parameters influence significantly the geomagnetic activity, including the pulsation activity. In the present study connections between the two groups of parameters are looked for.

In the following only indices will be dealt with which describe the whole day with a single index. As measures of the geomagnetic activity the planetary indices Σ Kp and Ap, are used, further the local index Σ K of the observatory Niemegk (this will be here also denoted by ΣK_1, as in the Observatory Report 1966–1971). From pulsation indices, the K_2 index of the Niemegk observatory will be used. These indices characterize in intervals of three hours the microstructure of the activity of the geomagnetic field from four different aspects, from which in our case only the first one, i.e. that estimating the activity of the pulsations, is used. It is deduced from the amplitude of the pulsations. The values of this index lie between 0 and 3. In the following the sums for whole days will be denoted by ΣK_2. This method does not take into account the period of the pulsations.

* Paper presented at the KAPG-Symposium on geomagnetic pulsations, Sopron, October 1983

[1] Geophysical Institute of the Czechoslovak Academy of Sciences, 14131 Praha 4, Boční II

For a more detailed description of the pulsation activity, the pulsation indices of the observatory Fürstenfeldbruck are used. The amplitude level is determined there for four frequency ranges denoted by P1, P2, P3 and P4 and they coincide with the internationally adopted types Pc2, Pc3, Pc4, Pc5. Naturally these ranges include Pi1 and Pi2, too, and even all other disturbances with the appropriate period. These indices are directly connected with the average daily amplitudes of the corresponding frequency ranges. The numerical values are presented not in a form of the numbers 0, 1, 2,. . ., but similarly to the values of the index Ap. The indices are graphically published by Korschunow (1970 and following years). The indices are at disposal for the years 1966–1971.

The conditions in the interplanetary medium are described by several parameters. The most important ones are published by King (1977) on the basis of satellite measurements. A part of the days could not be used, as data from some hours are lacking. Only complete days have been taken into account, i.e. when data are available for all 24 hours, and from these hourly values, a daily average can be computed. King (1977) published the value B and its Cartesian components. In the present study, only the vertical component B_z is used. In addition, the velocity v and the number density, N of the solar wind will be used, too. These values are the basis for some further parameters: the Alfvén-velocity, $V_A = B(\mu_0 \rho)^{-1/2}$ (the plasma density, ρ, is determined from the value of N); further the tangential component of the interplanetary electric field, $E_y = vB_z$, then the function $vE_y = v^2 B_z$ (both parameters have already been used by Prigancová 1980, and Střeštík 1982).

For a detailed study the data sets are subdivided. At first, we use the two groups $B > 6$ nT and $B < 6$ nT, the second one as $v > 450$ km/s and $v < 450$ km/s (the values 6 nT and 450 km/s are considered as approximate averages of the corresponding parameters). On the basis of B_z, three groups shall be applied: northerly fields for $\vartheta > 10°$, southerly for $\vartheta < -10°$, and ecliptic for $-10° < \vartheta < 10°$, with $\vartheta = \arcsin(B_z/B)$. According to the orientation of the horizontal component of the IMF, in the quadrants I and II, the component B_{xy} points toward East, in the quadrants II and III, toward the Earth. In all groups one has a similar number of days, but in the quadrants II and IV the occurrence frequency is much higher than in the quadrants I and III.

In a first step, the averages of the parameters are determined for the different groups. In Table I the first column shows the averages of the indices Ap, Σ Kp, Σ K_1, Σ K_2 and P1, P2, P3 and P4. In the next columns the averages for the groups $B > 6$ nT, $B < 6$ nT, then for the days with $v > 450$ km/s and $v < 450$ km/s are given. All indices are higher if $B > 6$ nT and $v > 450$ km/s, but the differences are not the same. The greatest difference is found for Ap, for Σ K_2, it is rather small, and for the Fürstenfeldbruck pulsation indices, the difference increases with increasing period. In the following columns, the values for different orientations of the IMF are given. All parameters are greater for a southern orientation of B_z, the highest difference was found again for Ap and for the longest period pulsations. The difference between the values for ϑ_N and ϑ_s is

Table I
Means of the indices for different interplanetary situations

Index	All data	$B>6$	$B<6$	$v>450$	$v<450$	ϑ_N	ϑ_E	ϑ_S	I	II	III	IV
Ap	11.3	17.6	7.4	18.8	6.9	6.7	10.3	18.0	13.3	10.4	19.8	11.1
Σ Kp	15.8	20.8	12.6	21.4	12.1	11.2	15.7	19.7	15.1	15.9	19.4	15.5
ΣK_1	16.6	20.6	14.2	20.8	13.6	12.7	16.8	19.3	15.7	16.6	20.2	16.7
ΣK_2	12.7	13.7	12.0	14.5	11.5	11.9	12.7	13.2	12.7	12.5	14.8	12.6
P1	4.23	4.25	4.19	4.54	4.08	4.36	3.97	4.94	4.68	4.28	4.21	4.15
P2	15.5	16.9	14.7	18.2	13.6	13.8	15.7	16.1	14.4	16.0	14.5	15.3
P3	7.90	8.48	7.52	9.61	6.26	6.95	7.90	8.68	8.87	7.71	8.39	7.72
P4	4.42	5.68	2.82	5.60	2.92	3.83	4.40	4.98	5.77	4.10	7.66	4.24

Table II
Correlation coefficients between some interplanetary parameters and activity indices (all data)

Index	B	v	V_A	B_z	E_y	vE_y
Ap	0.56	0.68	0.40	−0.46	−0.58	−0.66
Σ Kp	0.53	0.64	0.51	−0.41	−0.49	−0.51
ΣK_1	0.53	0.65	0.43	−0.38	−0.43	−0.45
ΣK_2	0.42	0.60	0.25	−0.22	−0.22	−0.25
P1	−0.02	0.32	0.07	−0.01	−0.06	−0.12
P2	0.16	0.62	0.14	−0.17	−0.28	−0.32
P3	0.35	0.59	0.24	−0.21	−0.39	−0.48
P4	0.35	0.59	0.45	−0.19	−0.48	−0.54

about the same as for $B>6$ nT and $B<6$ nT. The last columns show the results for the quadrants. In the case of the first four indices, the values are the highest in the quadrant III, while for the pulsations the situation is very complicated.

Table II contains the correlation coefficients between geomagnetic indices and some parameters of the interplanetary medium for all days. The negative values for B_z, E_y and vE_y mean that the activity is higher for lower, i.e. the negative values of the parameters. The differences in the rows of Ap, Σ Kp and ΣK_1 are small, the best correlations can be found for Ap. Pulsation indices have generally lower correlations which increase, however, for increasing periods, as already mentioned by Střeštík (1982). The correlations with E_y and vE_y are closer than with the component B_z.

Table III contains the correlation coefficients between the interplanetary parameters and the indices Σ Kp and P2 separately for certain groups of days according to the second column of the Table. The orientation of the vector **B** significantly influences the correlations — the coefficients are much higher for days with southern B_z-components. The differences are the smallest for the solar wind velocity v, and greatest for E_y and vE_y, where else are the highest values found. The

Table III

Correlation coefficients between interplanetary parameters and the activity indices Σ Kp and P2 for different interplanetary conditions

Index	Condition	B	v	V_A	B_z	E_y	vE_y
Σ Kp	ϑ_N	0.61	0.69	0.43	0.37	0.42	0.44
	ϑ_E	0.44	0.60	0.31	−0.19	−0.19	−0.19
	ϑ_S	0.84	0.76	0.78	−0.78	−0.88	−0.89
P2	ϑ_N	−0.04	0.56	−0.02	0.19	0.22	0.37
	ϑ_E	0.13	0.58	0.13	−0.14	−0.17	−0.18
	ϑ_S	0.36	0.71	0.24	−0.30	−0.46	−0.54
Σ Kp	$B>6$	0.67	0.68	0.56	−0.51	−0.56	−0.56
	$B<6$	0.45	0.58	0.47	−0.32	−0.48	−0.49
P2	$B>6$	0.28	0.66	0.09	−0.21	−0.47	−0.58
	$B<6$	0.06	0.59	0.18	−0.13	−0.32	−0.41
Σ Kp	$v>450$	0.70	0.66	0.52	−0.59	−0.61	−0.62
	$v<450$	0.38	0.60	0.50	−0.30	−0.46	−0.44
P2	$v>450$	0.31	0.68	0.19	−0.19	−0.48	−0.57
	$v<450$	0.07	0.56	0.08	−0.15	−0.29	−0.39

correlations are generally very low for the ecliptic orientation of the vector **B**, the correlations for positive B_z-s are positive, i.e. the activity increases again if the positive value of B_z increases but not as strongly as for an increasing absolute value of the southern B_z. Some differences are also found for the groups $B>6$ nT, $B<6$ nT, $v>450$ km/s, $v<450$ km/s. In both cases the correlations are closer for higher values of the parameters (B and v). The differences are, however, much less than for different orientations of B. In Table III only correlations with Σ Kp and P2 are presented, but all other indices have similar correlations with the exception of P1, which has generally low correlation coefficients with the interplanetary parameters.

Some of the connections are presented also in a graphic form. Figure 1 shows the connection between the index P2 and the solar wind velocity v for the data of the year 1971. The step-like function shows the mean values for steps of 3 units in the index. The correlation coefficient is here 0.6. Figure 2 shows the connection for the activity index Ap and all interplanetary parameters. Here the single data are not represented, only the mean values are given by the step-like function. The step is here 2 Ap-units. In Fig. 2 some parameters are also represented which did not appear in the Tables. The lines refer to the following parameters from top to bottom: Intensity of the IMF, B, its components B_{xy} and $|B_x|$ (all have a common scale in nT), the velocities V_A and v (both in km/s) and the expression $v|E_y|$ (in V/s). All these parameters increase with an increasing index Ap. The single data have a rather great scatter similarly to that seen in Fig. 1.

The results presented here confirm the connections between different interplanetary parameters and the geomagnetic activity indices. It was found that the connection

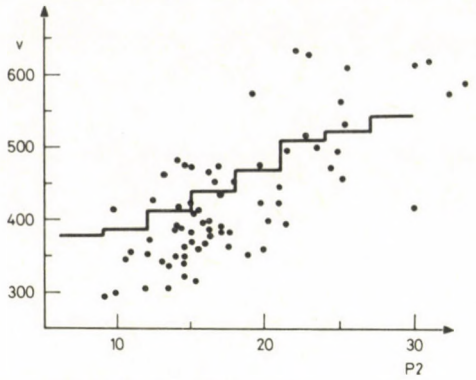

Fig. 1. Connection between the pulsation index *P2* and the velocity of the solar wind v (km/s) for days of the year 1971

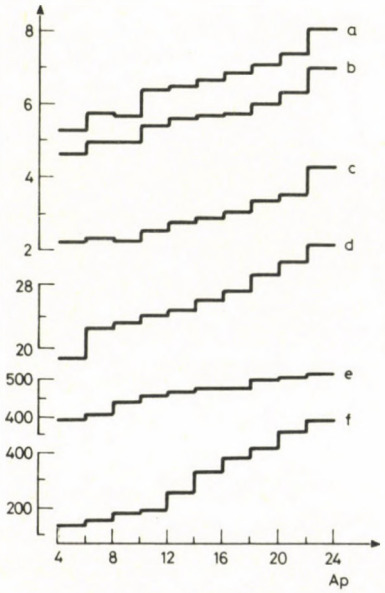

Fig. 2. Connection between the geomagnetic activity index Ap and interplanetary parameters for data of the years 1966–1971: *a)* intensity B of the IMF, *b)* its horizontal component B_{xy}, *c)* its radial component $|B_x|$, (all with a common scale in nT), *d)* Alfvén-velocity V_A, *e)* velocity of the solar wind v (both in km/s), *f)* the expression $v|E_y|$ (in V/s)

is in certain condition closer than in other cases. In knowledge of the connection it is possible to estimate the values of some interplanetary parameters, as e.g. B, v, E_y, etc. If some parameters are known from some other measurement, e.g. the orientation of the component B_z, then other parameters can be determined with higher accuracy.

References

Jacobs J A 1970: Geomagnetic Micropulsations. Physics and Chemistry in Space, 1. Springer Verlag Berlin, Heidelberg, New York.

Jahresbericht 1966 des Adolf-Schmidt-Observatoriums für Erdmagnetismus in Niemegk (und folgende Jahrgänge).

King J H 1977: Interplanetary Medium Data Book, Appendix. National Space Science Data, Center, VDC-A, Sept. 1977.

Korschunow A 1971: Erdmagnetische Pulsationen und Erdstrom an der Station FürsteFfeldbruck im Jahre 1970. Veröff. des Geophys. Observ. Fürstenfeldbruck, Serie A, Nr. 13, 9 (und folgende Jahrgänge).

Приганцова А 1980: Связь параметров солнечного ветра и геомагнитной возмущенности в 20-ом цикле солнечной активности. *Physica Solariterrestris*, Potsdam, No 12, 19.

Střeštík J 1982: Statistical Properties of Geomagnetic Pulsations at the Observatory of Fürstenfeldbruck Determined with the Aid of Pulsations Indices. Part III. Correlation with the Parameters of the Interplanetary Magnetic Field. Travaux Ints. Géophys. Acad. Tchécosl. Sci. No 574, Travaux géophysiques, Academia, Praha (in press).

Acta Geodaet., Geophys. et Montanist. Hung. Volume 19 (3–4), pp. 421–432 (1984)

LONG-PERIOD PULSATIONS AND PARAMETERS OF THE INTERPLANETARY MEDIUM

P K IVANOVA[1]*

[Manuscript received October 6, 1983]

The paper presents the results of a correlation analysis between parameters of the interplanetary medium and Pc5 pulsations occurring during geomagnetic storms (Pc5 Sc). The signatures of these events are presented for several events and as averages for the four seasons. It is suggested that the regression coefficients change in the moment of the storm onset. There are some possibilities for a short-term storm forecasting, too. A summary of phenomena is given which should be explained by a theory of these Pc5 Sc pulsations.

Keywords: geomagnetic activity; geomagnetic pulsations; interplanetary medium; Pc5; solar wind

1. Introduction

Short-period pulsations of the geomagnetic field have been studied by many authors. Among them, a number of theoretical (Gul'elmi and Troitskaya 1973) and experimental (Troitskaya et al. 1974) investigations were published in the last 10–15 years.

Verő (1980) investigated the connection of the excitation of geomagnetic pulsations with the Kp-indices, velocity and number density (D) of the solar wind (V_{SW}), and scalar magnitude of the interplanetary magnetic field (B). Ádám and Holló (1973) found that a 27 days recurrency exists in the pulsation activity. This fact can be well represented by autocorrelation functions. Miletits (1971) has shown on the basis of the material of 30 observatories that an increase of the geomagnetic activity is accompanied by a decrease of Pc-pulsation periods. Holló and Verő (1972) found an after-effect of the geomagnetic activity using cross-correlation functions between geomagnetic activity and pulsations. Verő (1975) analysed the effect of geomagnetic impulses on the pulsation periods that after the impulse, the motion outside of the plasmapause play a significant role in the excitation of the pulsations. On the basis of daily pulsation indices, Verő (1974) proved that the pulsation activity is a non-Markovian process.

[1] Geophysical Institute, ul. Akad. G. Bonchev, bl. 3, Sofia, 1113, Bulgaria

* Paper presented at the KAPG-Symposium on geomagnetic pulsations, Sopron, October 1983

Holló and Verő (1974) presented results on the comparison of the geomagnetic activity and pulsations. The method of daily pulsation indices was found to be effective in the detection of the interaction of the geomagnetic activity and pulsations. The velocity of the solar wind further the geomagnetic activity can be estimated from pulsation indices.

Kovalevsky (1981) studied an interplanetary energetic parameter:

$$\varepsilon = VB^2 \sin^4(\Theta/2) l^2 \qquad \text{(erg/s)}$$

$$\Theta = \operatorname{arctg}(|B_y/B_z|) \qquad \text{if} \quad B_z > 0 \quad \text{and}$$

$$\Theta = 180^\circ - \operatorname{arctg}(|B_y/B_z|) \text{if} \quad B_z < 0.$$

If $\varepsilon > 10^{19}$, geomagnetic storms are excited, consequently ε is an energetic function characterizing the connection between solar wind and magnetosphere and it is the most geoactive interplanetary index.

Pc5-type pulsations differ from other types of the continuous pulsations not only by their longer periods (150–600 s), but also by their greater amplitudes (Pudovkin et al. 1976, Oberts and Raspopov 1968). They are a phenomenon of the higher latitudes, their activity has a morning and an afternoon maximum at latitudes of 65–70°. Investigations have also shown that the diurnal variation of the Pc5-amplitudes is changing in different seasons: at equinoxes, both maxima, i.e. the morning and the evening ones, have about equal values, in summer the afternoon maximum is higher, in winter the morning one. Oberts and Raspopov have observed that the area of the maximum amplitudes of Pc5 coincides with the area where radiolocational reflections appear, hinting at a higher ionization in the ionosphere. The connection between the parameters of the Pc5 pulsations and the plasma inhomogeneities indicates a possible connection between Pc5 and substorms. The appearance of Pc5 is generally connected with a decrease of the geomagnetic activity of the stations where it is recorded (and also with a decrease of the planetary index AE).

It is known that long-period geomagnetic pulsations are observed mostly at higher latitudes (Gul'elmi and Troitskaya 1973). Their appearance at lower latitudes is considered as a rather exceptional phenomenon. Gogatishvili (1974, 1976) has shown that at middle latitudes ($\Phi = 36^\circ$, $L = 1.6$) not only Pc5 Sc pulsations are observed during the initial phase Sc of the geomagnetic storms, but in the main phase of the geomagnetic storm long-period pulsations are also observed with periods 5–8 min. It can be supposed that it is middle latitude Pc5. This problem deserves special attention. Gogatishvili (1974) has shown on the basis of middle latitude data for the years 1957–1975 that pulsations with periods 3–5 min are most frequent, and pulsations with even longer periods (5–8 min) appear only at high intensities of the geomagnetic field. In addition, at these latitudes pulsations of the beating type also appear (periods 8–15 min).

Gogatishvili found a difference between middle latitude and high latitude Pc5. He found three groups of middle latitude Pc5:

1. $Pc5_1$, with amplitudes of 0.5–1.0 nT. In case of high geomagnetic activity, the amplitude may increase to 15–20 nT. The correlation coefficient between the amplitude of the $Pc5_1$-type pulsations and the solar wind velocity is 0.7, and that with the scalar magnitude of the interplanetary magnetic field, 0.8. These Pc5-type pulsations have a linear relationship with the solar activity.

2. $Pc5_2$ appears only in the main phase of geomagnetic stroms at high IMF-intensities and southwards directed B_z components. The coefficient of correlation between $Pc5_2$ amplitudes and B is 0.7.

3. Special interest should be paid to Pc5 appearing in the initial phase of Sc-geomagnetic storms at middle latitudes. The amplitude and polarization of Pc5-pulsations also depend on the magnitude and orientation of the IMF.

It is known that the onset and the initial phase of Sc-geomagnetic storms are connected with the primary influences of the corpuscular streams on the magnetosphere. Pc5 Sc-type pulsations recorded simultaneously with the onset of the geomagnetic storms can be deduced from the same source. The difference of the high latitude and middle latitude Pc5 Sc-pulsations indicate that their generation is different in spite of the same source.

A further type of long-period pulsations is Pc6 (Pudovkin et al. 1976) observable day and night at high latitudes. The generation of the day-time Pc6-pulsations is connected with the position of the daytime cusp and their parameters are well correlated with the velocity of the solar wind. The night-time pulsations are correlated with changes in the structure of the tail. These pulsations have periods connected with the thickness of the plasma layer, and therefore this thickness can be diagnosticized by these pulsations.

2. Analysis of the data

As it has been mentioned in the previous section, long period pulsations are characteristic for higher latitudes. As they appear also at middle latitudes, their investigation at these latitudes is also possible. The stations used in the present study are Dusheti $\Phi = 36.8°$, $\Lambda = 122.5°$, Panagyurishte $\Phi = 40.5°$, $\Lambda = 103.2°$.

The primary aim of this investigation was to find the regularities of Pc5 at a middle-latitude station, at Panagyurishte. As in the case of normal magnetograms of the observatory Dusheti, Pc5 and Pc6 pulsations are mostly connected in Panagyurishte to Sc-events. The time interval of the investigation was 1966 to 1974. During this interval, about 50 geomagnetic storms with Sc were recorded being accompanied by Pc5 and Pc6 pulsations. According to these events, the maximum amplitude of Pc5 is 14 nT, the minimum detectable amplitudes were about 2–3 nT. The majority of the observed events have periods around 360 s. Nearly all Pc5 and Pc6 events were recorded simultaneously with the onset of Sc-storms.

On the basis of 36 Sc-storms, the distribution of the Kp-indices in 48 hours intervals were studied before the Sc-storms and the Pc5 pulsations. Two examples are shown in Fig. 1. Kp values more than 3 were found only in 5 cases, all other cases were characterized by low geomagnetic activities, $Kp \leq 3$. Figure 7 shows the number of cases with $Kp=0, 1 \ldots 8$ for the intervals $t=-12, -9 \ldots 0, +3$ hours. The geomagnetic storm began at $t=0$. It can be said, that the pre-storm Kp-indices do not correlate with the appearance of geomagnetic storms and Pc5-pulsations. In the intervals before the storm, the most common value is $Kp=1$, in the interval of the Sc and after it, $Kp=3$. Generally before the storm prevails $Kp \leq 3$, after it, $Kp > 3$.

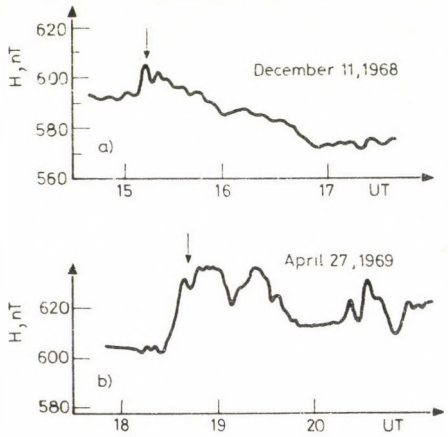

Fig. 1. Geomagnetic storms with sudden commencement and Pc5 on normal magnetogramms of the station Panagyurishte

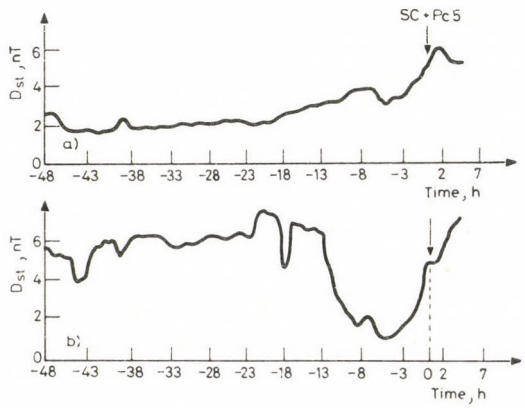

Fig. 2. Sums of the Dst indices for 48 hours before the geomagnetic storms and for 2 hours after it *a)* cases without significant minima on the Dst curve before the onset, *b)* cases with a deep minimum on the Dst curve Sc + Pc5 means geomagnetic storm and Pc5 pulsations

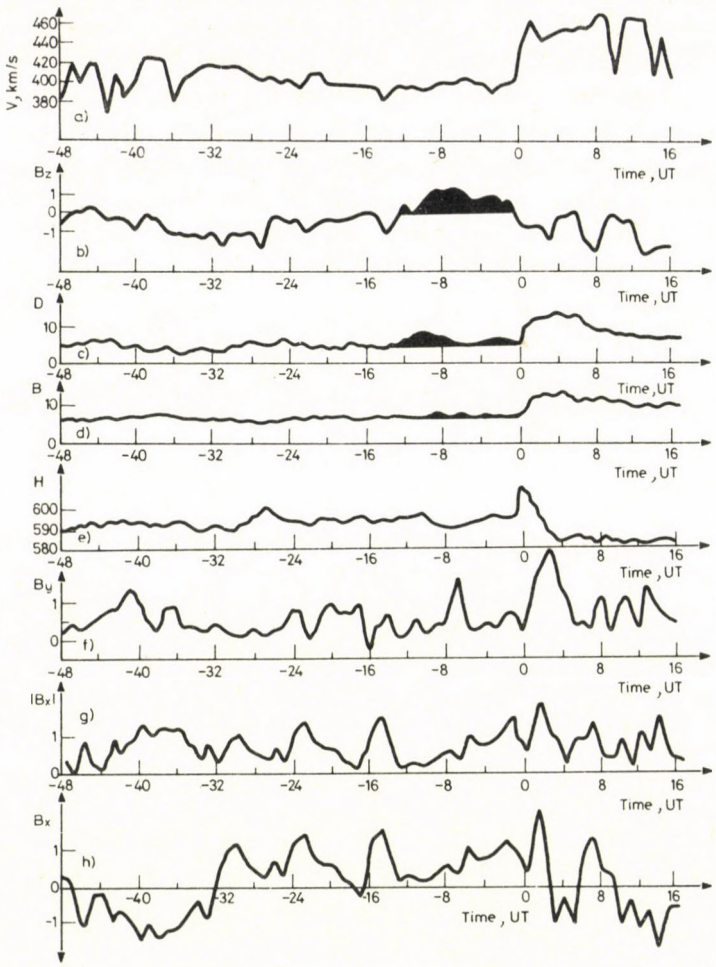

Fig. 3. Parameters of the interplanetary medium and the component H of the geomagnetic field for 48 hours before and 12 hours after Sc

The index Dst has also been analysed for 18 storms in the years 1966 and 1967 around the appearance of Pc5 pulsations. Figures 2a, b show the average value of this index for 48 hours before and 2 hours after the event. The events were distributed into two groups according to the form of the st-curves (if there is a minimum or not). The figure shows that Sc and Pc5 appears within a minimum of the Dst-index, which develops 5–6 hours previously to the appearance of the event at the observatory Panagyurishte. This fact can be used in the prognosis of ScPc5.

Figure 3 shows the changes of the parameters of the interplanetary medium for a 48 hours interval before and 12 hours after the event. The curves show average values

Table I

No.	a	b	c	d	x
1	−2.8	41.9	−35.7	10.2	$\frac{(DV^2)}{\min(DV^2)}$
	−59.9	60.1	−17.8	1.7	
2	3708.3	1853.6	−306.6	16.9	B
	929.6	−251.3	22.6	−0.7	
3	127.6	−55.6	8.8	−6.2	D
	−265.8	71.4	−0.4	0.2	
4	18.2	−17.2	19.4	−6.7	B_x
	−2.5	24.2	−22.6	5.6	
5	14.0	−0.8	2.0	−1.3	B_y
	6.3	−14.4	13.6	−3.3	
6	15.9	0.0	0.0	0.0	$V-380$
	402.3	−10.9	0.0	0.0	
7	14.5	0.0	0.0	0.0	$\frac{VB_z}{\min\lvert VB_z\rvert}$
	0.5	−0.7	0.0	0.0	
8	14.5	0.3	−0.3	0.6	B_z
	0.5	−6.5	0.8	1.5	

for 21 Sc-storms and Pc5 Sc. In the curve of $B_z(t)$, a maximum is found 8 hours before the appearance of Sc and Pc5 Sc. Similar maxima are also present in the $D(t)$ and $B(t)$ curves. In the curve $H(t)$ a significant, but not very deep minimum is found.

These results may form the basis for theoretical considerations on the connection between Sc-storms and Pc5 on the one side, and parameters of the interplanetary medium on the other. Table I shows the results of regression analyses of the events in the magnetic field and these parameters in the form:

$$H = a + bx + cx^2 + dx^3,$$

where x means the values of $(DV^2)/\min(DV^2)$; B, D, B_x, B_y, V-380, $(VB_z)/\min(|VB_z|)$ and B_z. It is clear that before Sc-storms and Pc5 there is a certain regression, after the events a different one. The polynomials obtained from this analysis approximate rather well the expected exponential function which can be also used for the diagnosis of the corresponding parameter of the interplanetary medium. Any deviation from the previous regression shows the appearance of an Sc-storm and Pc5-pulsations, or some other event. Table I shows that the H-component of the geomagnetic field is closely correlated with the scalar magnitude of the interplanetary magnetic field, B and with the density of the solar wind, D.

An analysis of the H-component at ground stations around Sc-s and Pc5 (Fig. 3) and the parameters of the interplanetary medium yielded the results presented in Table II. Here the following formulas were used: covariance:

$$S_{xy}=\frac{1}{n-1}\left(\Sigma x_i y_i-\frac{1}{n}\Sigma x_i \Sigma y_i\right),$$

coefficient of correlation:

$$\sigma_{xy}=\frac{S_{xy}}{S_x S_y}$$

where S_x and S_y are the standard deviations.

The variable means here the parameters denoted in the first column of the Table.

The correlation coefficients σ_{xy} between the H-component and the parameters of the Sc-storms differ significantly before and after the Sc-storms.

As the component H depends simultaneously on several variables, a three-component regression has also been computed in the form

$$H=a+bx+cy+dz$$

where a, b, c, d are the regression coefficients, and x, y, z the parameters of the interplanetary medium. The results of this analysis are presented in Table III. The first column of the table shows the choice of the variables x, y, z, the upper figures denote the regression coefficients for the pre-storm interval, the lower ones the coefficients after the storm. It is evident that these coefficients differ also here significantly. In addition, there are parameters which are closely correlated to the component H, such as $(DV^2)/\min(DV^2)$, B, B_z and $(VB_z)/\min(|VB_z|)$.

To decide if there is a seasonal variation in these connections between pulsations and the interplanetary medium, a monovariable regression analysis has been carried out for different seasons with the same data for which the earlier computations have also been made by distributing the earlier series according to seasons. It should be remarked that the closest connection were found in winter and spring. In the first column of the Table IV, the regression coefficients for the appearance of Sc and Pc5 are shown for each season before the event, in the second afterwards. The connections do change also here. Most regression have a linear form, while those with $H(B)$ and $H(B_z)$ are quadratic ones. These equations can be used for a prognosis of the dependent variable, i.e. the parameters of the interplanetary medium.

Table II

No.		B	D	B_x	V	B_y	VB_y	B_z	DV^2	
1	S_{xy}	−0.4	1.1	−0.2	−3.0	−0.2	−11.9	0.0	0.2	before Sc
		−1.7	−0.6	−0.1	−31.3	−0.5	−303.6	−0.7	−0.6	after Sc
2	σ_{xy}	−0.5	0.5	−0.2	−0.2	−0.2	0.0	0.0	0.3	before Sc
		0.3	0.0	0.0	−0.3	−0.1	−0.2	−0.2	−0.2	after Sc

Table III

	a	$\frac{(DV^2)}{\min(DV^2)}$	B	D	B_x	B_y	B_z	$V-380$	$\frac{VB_z}{\min\lvert VB_z\rvert}$
No.	1	2	3	4	5	6	7	8	9
1	14.88	3.47	−0.84		0.10				
	22.88	0.55	−2.08		1.39				
2	11.42	−0.35	−0.08	0.78					
	21.20	−0.04	−2.32	0.71					
3	13.27	3.13	−0.38			−1.67			
	24.63	0.49	−2.18			0.92			
4	20.88	−1.85	−0.68				1.42		
	22.62	0.56	−2.12				−2.13		
5	16.41	2.86	−1.03					0.06	
	41.59	−2.51	−0.59					−0.22	
6	15.73	2.86	−0.84						0.04
	22.17	0.55	−2.05						−0.19
7	14.29		−0.33	0.45	−0.72				
	16.82		−1.71	0.46	0.52				
8	12.98		−0.28	0.67		−1.69			
	26.55		−2.88	0.68		0.80			
9	15.75		−0.76	0.57			0.50		
	27.95		−3.26	0.81			−2.56		
10	16.22		−1.02	0.66				0.08	
	39.88		−1.05	−0.49				−0.20	
11	15.54		−0.69	0.54					0.07
	26.18		−3.22	0.93					−0.23
12	12.11			5.57	−0.33	−1.76			
	3.86			0.04	0.32	−0.97			
13	12.45			0.53	−0.48		−1.77		
	3.86			0.04	0.32		−0.97		
14	9.47			0.71	0.25			0.07	
	39.77			−0.87	−2.27			−0.25	
15	10.53			0.62	0.33				0.07
	6.72			−0.13	0.24				0.21
16	15.50			−0.50	−1.84	0.67			
	3.41			−0.25	−1.39	−2.05			
17	15.26			−0.83	−1.83		0.06		
	24.30			−2.03	−0.68		−0.18		
18	15.48			−0.49	−1.84			0.09	
	3.50			−0.15	−1.30			−0.18	
19	14.72				−1.81	0.64	0.04		
	19.74				−1.97	−1.93	−0.16		
20	15.01				−1.97	−18.29		2.38	
	3.44				−2.95	−92.76		8.92	
21	13.82					−10.33	0.05	1.35	
	10.45					−50.86	−0.08	4.91	

Table IV

No.		spring		winter		summer		autumn	
1	V	16.1	−126.8	85.0	232.0	−117.0	33.0	89.0	130.0
2		−0.2	5.9	1.3	2.5	43.5	−0.1	−0.2	−3.1
3		0.0	−0.1	−0.2	0.0	4.1	0.0	0.0	0.1
4		0.0	0.0	0.0	0.0	0.1	0.0	0.0	0.0
1	D	111.0	69.0	58.2	105.0	−128.0	88.0	643.0	453.0
2		−37.0	−12.0	18.4	−19.0	156.5	10.2	345.0	−85.0
3		4.4	0.7	−4.4	2.2	−47.3	−29.6	−54.0	6.4
4		0.0	0.2	0.3	0.0	4.6	3.0	2.7	−0.1
1	B	−217.0	489.0	−407.0	−967.0	78.1	51.6	959.0	279.0
2		100.0	−106.0	366.0	257.0	−52.1	205.0	−417.0	−38.4
3		−13.6	7.7	83.0	−21.0	13.3	−48.0	67.0	2.3
4		0.6	−0.2	6.0	0.6	−0.0	3.0	−3.6	0.0
1	B_x	13.0	17.0	80.0	72.2	23.0	44.0	53.0	94.0
2		−3.2	8.8	−20.0	0.9	−2.1	−22.6	53.0	−1.8
3		−1.3	1.4	−12.0	−1.5	4.6	10.1	−21.0	0.1
4		2.0	1.2	−1.4	0.2	0.2	−1.4	4.5	0.0
1	B_y	12.7	12.3	85.0	63.0	32.2	−161.0	85.9	95.1
2		0.1	−1.8	2.0	2.0	5.9	115.0	0.5	1.7
3		0.8	0.0	−0.9	3.7	−0.6	−22.0	−0.1	−0.3
4		0.1	0.0	−0.3	0.7	−0.2	1.35	0.0	−0.1
1	B_z	15.6	9.6	85.8	55.1	11.5	22.3	86.3	89.7
2		−1.6	−5.6	−0.5	−11.0	19.2	3.6	1.12	3.7
3		−1.6	0.6	−1.4	−2.0	−4.7	0.4	−0.7	2.1
4		0.1	0.3	0.0	−0.1	0.3	−0.1	−0.2	−0.8

Table V

	V		D		B		B_x		B_y		B_z	
					winter							
σ_{xy}	−0.3	−0.7	0.5	0.5	0.8	0.3	−0.0	−0.2	−0.2	−0.2	−0.3	−0.3
S_{xy}	−29.2	−136.3	1.5	22.8	0.1	23.5	−0.2	−5.8	0.6	−5.0	−0.9	−7.7
					summer							
σ_{xy}	0.4	0.7	0.2	0.6	0.4	−0.2	−0.2	38.1	0.4	−0.1	0.4	0.6
S_{xy}	9.7	59.1	1.5	2.1	8.5	−0.5	−3.3	−4.9	−2.9	−0.7	8.5	11.3
					spring							
σ_{xy}	−0.3	−0.6	0.4	0.6	−0.3	−0.2	0.3	0.1	0.8	−0.3	−0.1	−0.6
S_{xy}	−22.3	−617.9	4.0	33.4	−1.5	−2.8	0.9	1.5	5.2	−9.4	−0.6	−17.6
					autumn							
σ_{xy}	0.9	0.0	0.4	0.3	−0.8	−0.4	0.3	−0.6	0.2	0.4	0.3	0.7
S_{xy}	45.1	−1.6	1.3	4.7	−1.2	−1.5	0.5	0.8	5.2	1.2	1.0	4.0

From the data of different seasons, variances, covariances and correlation coefficients were computed. It is evident that the values change not only at the moment of an Sc or Pc5, but also in different seasons (Table V).

Many studies were devoted to the problem of latitudinal and longitudinal changes of the pulsations. Gogatishvili (1979) carried out an analysis of the phase changes, and a similar effort was made in the present study, too. Figure 4 shows the

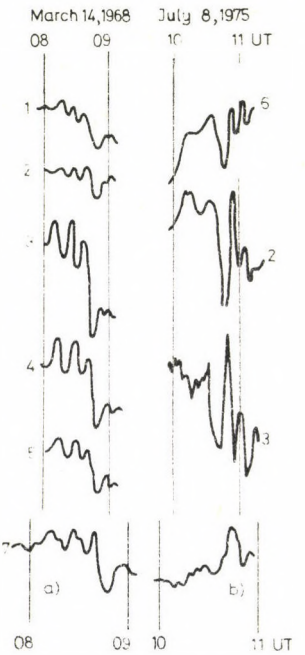

Fig. 4. A Pc5-event at eight geomagnetic observatories

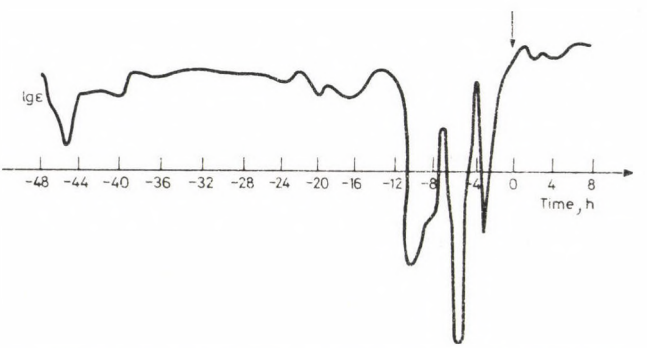

Fig. 5. The function log ε, for 48 hours before the onset of the geomagnetic storm and Pc5 and after the onset

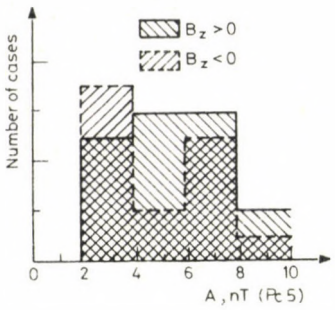

Fig. 6. The amplitude of Pc5-events in case of positive and negative B_z-components

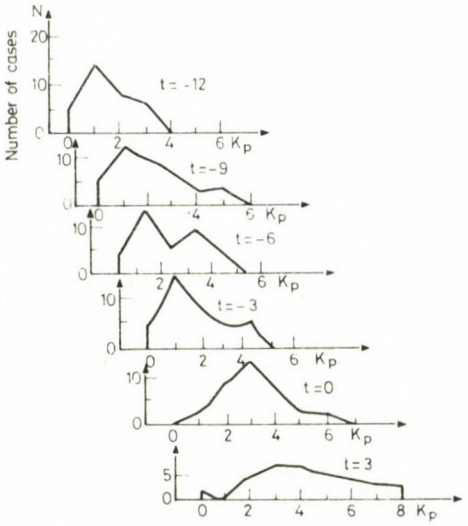

Fig. 7. Connection of the Kp values with the onset of the geomagnetic storm and Pc5. The plot at $t=0$ represents situation at the beginning of the storm, $t=3$, -6, -9, -12 in the previous 34-intervals

simultaneous records of the following stations: 1. Magadan ($\Phi=53.0°$, $\Lambda=214.2°$), 2. Borok ($\Phi=53.0°$, $\Lambda=123.0°$), 3. Dusheti ($\Phi=36.8°$, $\Lambda=122.5°$), 4. Alma Ata ($\Phi=38.6°$, $\Lambda=147.0°$), 5. Irkutsk ($\Phi=40.7°$, $\Lambda=174.0°$), 6. Lovozero ($\Phi=62.9°$, $\Lambda=127.0°$) and 7. Panagyurishte ($\Phi=40.5°$, $\Lambda=103.2°$). The figure proves that there is a phase shift at different latitudes, but no phase shift appears at different longitudes. It is a very characteristic feature of the middle latitude Pc5 Sc that it appears earlier than high latitude Pc5. This fact should be included in any theory of Pc5 (Gul'elmi and Troitskaya 1973).

The function ε proposed by Kovalevsky (1981) could be used as an indication of the appearance of Sc-storms. This function has also been determined for 48 hours prior

to Sc-s and Pc5, and for some hours afterwards. The results are presented in Fig. 5. The sudden changes of the function $\varepsilon(t)$ can be clearly seen before the onset of the geomagnetic storm, and after the first precursor, there two more maxima of not very high values. This function allows to conclude to the mechanism which causes the Sc-storm and the Pc5-pulsations.

Figure 6 shows the amplitudes of the Pc5-pulsations at different values of the sign of B_z. In the range 2–4 nT, there are more cases with positive B_z, but in the interval 4–6 nT, the negative B_z-values prevail. These results need further confirmation, as if it is true then it should take an important role in the theory of these pulsations.

The presented results were obtained by using King's data (1975) and the records of the observatory Panagyurishte concerning Sc-storms and Pc5 pulsations. The results show that the long-period pulsations Pc5 appear also at middle latitudes and they differ from the high-latitude phenomena not only by their amplitudes. Their study is necessary not only for the investigation of the ionosphere and magnetosphere, but also in studies of the Earth's interior by electromagnetic methods.

References

Ádám A, Holló L 1973: On the prognosis of micropulsations activity. *Acta Geod. Geoph. Mont. Hung.*, 8, 207–216.

Gogatishvili J M 1974: On the appearance of long-period pulsations at middle latitudes (in Russian). *Geomagn. i Aeronom.* 14, 767–769.

Gogatishvili J M 1976: The interplanetary geomagnetic field and the long-period pulsations at middle latitudes (in Russian). *Geomagn. i Aeronom.* 16, 382–384.

Gogatishvili J M 1979: Regularities of the appearance of long-period pulsations at middle latitudes (in Russian). *Geomagn. i Aeronom.* 19, 382–384.

Gul'elmi A V, Troitskaya B A 1973: Geomagnetic pulsations and the diagnosis of the magnetosphere (in Russian). Nauka, Moscow

Holló L, Verő J 1972: Experimental results with the characterization of geomagnetic micropulsations. *Acta Geod. Geoph. Mont. Hung.*, 7, 167–175.

Holló L, Verő J 1974: Investigation of the connection between geomagnetic activity and pulsations with the maximum probability method. *Acta Geod. Geoph. Mont. Hung.*, 9, 121–127.

Isaev S I, Pudovkin M I 1972: Aurora and processes in the magnetosphere (in Russian). Nauka, Leningrade

King, 1975: Interplanetary Medium Data Book — WDC — A

Kovalevsky I V 1981: Response of the AE and *D*st indices on the energetic function of connection in 1972. Physica Solaris-terrestris No 15.

Miletits J Cz 1971: On the latitude dependence of Pc-type pulsations. *Acta Geod. Geoph. Mont. Hung.*, 6, 141–153.

Oberts P, Raspopov O M 1968: Study of the propagation characteristics of the Pc5-type pulsations of the geomagnetic field (in Russian). *Geomagn. i Aeronom.*, 8, 534–539.

Pudovkin M I, Raspopov O M, Kleimenova N G 1976: Disturbances of the electromagnetic field of the Earth (in Russian), Part 2. Leningrade

Troitskaya V A, Kleimenova N G, Gokhberg N B, Gul'elmi A V, Chetaev D N, Barsukov O M 1974: Study of the variations of the electromagnetic field of the Earth. (in Russian) *Fiziki Zemli*, No 10, 46–57.

Verő J 1974: Pulsation activity as a non-Markovian process. *Acta Geod. Geoph. Mont. Hung.*, 9, 291–296.

Verő J 1975: Geomagnetic pulsations around impulses. *Acta Geod. Geoph. Mont. Hung.*, 10, 247–253.

Verő J 1980: Geomagnetic pulsations and parameters of the interplanetary medium. *J. of Atmospheric and Terrestrial Physics*, 42, 371–380.

Acta Geodaet., Geophys. et Montanist. Hung. Volume 19 (3–4), pp. 433–449 (1984)

AN ESTIMATION OF MAXIMUM GROUND MOTIONS CAUSED BY EARTHQUAKES IN HUNGARY

T ZSIROS[1] and P MÓNUS[1]

[Manuscript received October 8, 1983]

A theoretical maximum intensity map of Hungary was constructed based on the earthquakes occurred between 1859 and 1982. These intensity values were transformed into acceleration, velocity and displacement data.

Keywords: earthquake effects; Hungary; isoseismal maps; maximum ground motion; maximum intensity map

Introduction

Macroseismic data of Hungarian earthquakes were revaluated in the years past. As a result a complete set of isoseismal maps of earthquakes occurred in the present territory of Hungary between 1880 and 1980 is going to be published by Csomor and Kiss (1983). This paper is based mainly on this unpublished material which made it possible to calculate attenuation coefficients of intensities.

Attenuation coefficients of intensities

The calculations are based on the assumption of an exponential attenuation of intensities with epicentral distance

$$I_k = I_0 \exp(-\alpha R_k) \tag{1}$$

where

I_0 — epicentral intensity
I_k — intensity of the isoseismal k
R_k — mean radius of the isoseismal k (in km)
α — attenuation coefficient of intensity (in km^{-1}).

Mean radii (R_k) were usually determined from the radii in the available directions and occasionally by calculating the radius of an equivalent circle having the same area

[1] Seismological Observatory, Budapest, Meredek u. 18. H-1112, Hungary

as the area enclosed by the isoseismal k. The attenuation coefficients were estimated for all isoseismals of an earthquake and their arithmetical mean was chosen as the representative value. The results are summarized in Table I. This table includes also the earthquakes which have no isoseismal maps but were used for the construction of the theoretical maximum intensity map.

Table I

No	Date	Location	I_0	α	σ_α	N
1.	Dec. 30. 1859.	Süttő	5			
2.	Jan. 20. 1860.	Zalaszántó	5			
3.	Apr. 13. 1860.	Győr	3			
4.	Apr. 18. 1862.	Komárom	4			
5.	Jan. 17. 1863.	Penc	5			
6.	June 14. 1863.	Kiskunmajsa	5			
7.	Sep. 30. 1863.	Komárom	4			
8.	Oct. 20. 1863.	Mór	5			
9.	Apr. 09. 1864.	Csatka	5			
10.	Apr. 09. 1864.	Magyaróvár	3			
11.	Dec. 19. 1864.	Nagykálló	4			
12.	Jan. 19. 1865.	Nagykőrös	4			
13.	Jan. 15. 1866.	Márianosztra	3			
14.	Feb. 27. 1866.	Komárom	4			
15.	Mar. 16. 1866.	Békéscsaba	3			
16.	Apr. 25. 1866.	Komárom	3			
17.	May 11. 1866.	Mór	3			
18.	1866.	Kazár	5			
19.	Sep. 22. 1867.	Pétervására	5			
20.	Feb. 04. 1868.	Tokaj	4			
21.	June 05. 1868.	Jászapáti	3			
22.	June 17. 1868.	Budapest (Pest)	3			
23.	June 21. 1868.	Jászberény	7.5			
24.	Aug. 24. 1868.	Eger	3			
25.	Sep. 01. 1868.	Jászfényszaru	4			
26.	Dec. 15. 1868.	Jásztelek	5			
27.	May 28. 1869.	Kétegyháza	5			
28.	Feb. 02. 1870.	Zsadány	3			
29.	June 30. 1870.	Alcsut	4			
30.	Sep. 10. 1870.	Abony	3			
31.	Dec. 01. 1871.	Hódmezővásárhely	3			
32.	Feb. 17. 1872	Magyaróvár	3			
33.	May 30. 1872.	Jászberény	4			
34.	Jan. 03. 1873.	Mosonmagyaróvár	3			
35.	Apr. 16. 1874.	Pécs	5			
36.	Dec. 27. 1874.	Kiskunhalas	5			
37.	Apr. 13. 1875.	Komárom	4			
38.	Oct. 17. 1875.	Pécs	4			
39.	July 06. 1876.	Nagyatád	6			
40.	Oct. 21. 1876.	Surd	6			

Table I (contd.)

No	Date	Location	I_0	α	σ_α	N
41.	Nov. 30. 1876.	Surd	6			
42.	Dec. 06. 1876.	Mohács	6			
43.	Mar. 03. 1878.	Makó	4			
44.	Dec. 31. 1878.	Gyöngyös	5			
45.	Apr. 30. 1879.	Pásztó	3			
46.	May 01. 1879.	Kazár	5			
47.	May 25. 1879.	Budapest (Buda)	4			
48.	Aug. 31. 1879.	Szőreg	5			
49.	Dec. 07. 1879.	Gyöngyös	5			
50.	Feb. 09. 1880.	Kaposvár	4			
51.	June 04. 1880.	Budapest (Buda)	4			
52.	Nov. 28. 1880	Csengőd	3			
53.	June 22. 1881.	Sióagárd	4.5			
54.	Oct. 28. 1881.	Szarvas	4			
55.	Oct. 28. 1881.	Szentes	4			
56.	Nov. 08. 1881.	Kiskunmajsa	3			
57.	Jan. 18. 1882.	Nagyatád	4			
58.	Mar. 04. 1882.	Mosonszentjános	3			
59.	Oct. 29. 1882.	Tapolca	3			
60.	Nov. 24. 1882.	Bátaapáti	3			
61.	Dec. 12. 1882.	Mohács	3			
62.	Dec. 20. 1882.	Veszprém	3			
63.	Feb. 09. 1883.	Bonyhád	3			
64.	Mar. 28. 1883.	Miskolc	5	0.034	—	1
65.	Dec. 01. 1883.	Kisgyőr	3			
66.	Oct. 11. 1884.	Marcali	3			
67.	Dec. 05. 1884.	Eger	4			
68.	Jan. 12. 1886.	Pápa	4			
69.	Mar. 17. 1887.	Jászjákóhalma	3			
70.	Jan. 18. 1888.	Szend	4			
71.	Aug. 16. 1888.	Szend	5	0.021	0.004	3
72.	Aug. 17. 1888.	Bakonysárkány	4.5			
73.	Nov. 26. 1888.	Eger	3			
74.	Apr. 03. 1889.	Nemesvid	4	0.049	0.011	2
75.	June 18. 1889.	Esztergom	4			
76.	July 11. 1889.	Aka	4.5	0.019	—	1
77.	Aug. 19. 1889.	Somogyszil	3.5			
78.	Jan. 14. 1891.	Tápiószecső	3			
79.	Apr. 11. 1891.	Siklós	4.5			
80.	June 19. 1891.	Székesfehérvár	5	0.016	0.000	2
81.	July 07. 1891.	Elek	4.5	0.019	—	1
82.	June 21. 1892.	Székesfehérvár	3			
83.	June 22. 1892.	Pincehely	6.5	0.019	0.004	4
84.	Aug. 24. 1893.	Csesztreg	5.5	0.033	—	1
85.	June 11. 1895.	Cserháthaláp	5	0.029	0.003	2
86.	Apr. 26. 1896.	Somogyszob	3			
87.	Sep. 14. 1896.	Hidegkút	5	0.041	—	1
88.	Oct. 29. 1896.	Kecskemét	5	0.017	0.004	2
89.	Nov. 30. 1896.	Mezőkövesd	4	0.033	0.007	2
90	Dec. 05. 1896.	Dédestapolcsány	4.5			

Table I (contd.)

No	Date	Location	I_0	α	σ_α	N
91.	Jan. 18. 1897.	Miskolc	5	0.026	—	1
92	Mar. 18. 1898.	Isztimér	3			
93.	Nov. 30. 1898.	Miskolc	3.5			
94.	May 07. 1899.	Szentes	4	0.042	0.009	2
95.	June 14. 1899.	Csákány	4	0.065	0.013	2
96.	Aug. 06. 1899.	Kaposvár	3			
97.	Sep. 11. 1899.	Gyöngyös	3			
98.	Sep. 21. 1899.	Bükkszentlászló	4			
99.	Nov. 12. 1899.	Nagyecsed	5	0.048	—	1
100.	Mar. 23. 1900.	Szekszárd	3			
101.	Feb. 16. 1901.	Bakonytamási	5	0.018	0.007	2
102	May 10. 1901.	Gic	4.5			
103.	Nov. 15. 1901.	Bükkzsérc	4			
104.	Jan. 19. 1902.	Gyöngyöshalász	3			
105.	May 06. 1902.	Répáspuszta	4			
106.	May 31. 1902.	Kaposvár	3			
107.	Aug. 22. 1902.	Nyírkáta	4			
108.	Sep. 19. 1902.	Monor	5			
109.	Oct. 06. 1902.	Csány	3			
110.	Oct. 12. 1902.	Isztimér	4.5			
111.	Feb. 07. 1903.	Zalatárnok	4			
112.	June 09. 1903.	Zalakoppány	3			
113.	June 16. 1903.	Csány	3			
114.	June 26. 1903.	Eger	6.5	0.014	0.004	3
115.	July 07. 1903.	Tiszanána	3			
116.	Sep. 15. 1903.	Várpalota	5			
117.	Oct. 26. 1903.	Vésztő	3			
118.	Feb. 12. 1904.	Gölle	6			
119.	Feb. 24. 1904.	Tiszakécske	4			
120.	Mar. 04. 1904.	Nagylak	4			
121.	Aug. 03. 1904.	Komárom	4			
122.	Feb. 08. 1905.	Elek	4			
123.	May 30. 1905.	Dorogháza	3			
124.	Sep. 04. 1905.	Szentes	4			
125.	Nov. 12. 1905.	Komárom	3			
126.	June 05. 1906.	Zalaegerszeg	3			
127.	Aug. 12. 1906.	Szentmártonkáta	5.5	0.051	—	1
128.	Aug. 25. 1906.	Pétervására	4	0.122	0.027	2
129.	Dec. 30. 1906.	Abod	3			
130.	Jan. 21. 1907.	Veszprém	3			
131.	Mar. 25. 1907.	Bátaszék	4	0.032	—	1
132.	Mar. 26. 1907.	Mezőcsokonya	3			
133.	Oct. 16. 1907.	Nagyberény	4	0.168	0.034	2
134.	Nov. 02. 1907.	Szentiványfa	4	0.031	—	1
135.	Jan. 26. 1908.	Mátraszele	3			
136.	Feb. 28. 1908.	Zalaegerszeg	3			
137.	Mar. 07. 1908.	Kecskemét	3			
138.	Mar. 15. 1908.	Gomba	5.5	0.022	0.004	2
139.	Mar. 20. 1908.	Gödöllő	3			
140.	May 24. 1908.	Lajosmizse	5			

Table I (contd.)

No	Date	Location	I_0	α	σ_α	N
141.	May 28. 1908.	Kecskemét	7	0.009	0.000	5
142.	July 01. 1908.	Kecskemét	3			
143.	Aug. 26. 1908.	Kecskemét	5	0.017	0.004	2
144.	Sep. 08. 1908.	Kecskemét	5			
145.	Oct. 24. 1908.	Kiskunfélegyháza	3			
146.	Dec. 14. 1908.	Szigetszentmárton	3			
147.	Dec. 16. 1908.	Kecskemét	3			
148.	Jan. 06. 1909.	Kecskemét	3			
149.	Jan. 17. 1909.	Pilis-Gomba	4			
150.	Jan. 21. 1909.	Baja	5.5	0.027	0.001	2
151.	Jan. 23. 1909.	Nyáregyháza	3			
152.	Feb. 04. 1909.	Kakucs	3			
153.	Feb. 16. 1909.	Kecskemét	4.5	0.013	—	1
154.	Mar. 12. 1909.	Veszprém	3			
155.	Mar. 14. 1909.	Kaposvár	4			
156.	Mar. 16. 1909.	Kecskemét	3			
157.	Mar. 19. 1909.	Gyöngyös	4			
158.	May 29. 1909.	Magyarsarlós	5	0.015	0.003	2
159.	Nov. 12. 1909.	Nadap	3			
160.	Dec. 13. 1909.	Isztimér	4			
161.	Dec. 19. 1909.	Cegléd	3			
162.	Jan. 12. 1910.	Zalaegerszeg	3			
163.	Apr. 07. 1910.	Szokolya	3			
164.	June 01. 1911.	Kecskemét	4	0.017	—	1
165.	June 19. 1911.	Kecskemét	6.5	0.009	—	1
166.	July 08. 1911.	Kecskemét	8	0.007	0.000	6
167.	July 26. 1911.	Pilis	3			
168.	Apr. 12. 1912.	Kecskemét	4			
169.	July 28. 1912.	Nagykőrös	3			
170.	July 29. 1912.	Dunakiliti	3			
171.	Aug. 17. 1912.	Gomba	4			
172.	July 27. 1913.	Győrszemere	4.5	0.052	—	1
173.	Nov. 11. 1913.	Monor.	3			
174.	Nov. 23. 1913.	Lajosmizse	4			
175.	Feb. 04. 1914.	Győr	4.5			
176.	May 13. 1914.	Gomba	5.5	0.024	—	1
177.	Nov. 25. 1914.	Isztimér	5.5	0.017	0.002	2
178.	Jan. 06. 1916.	Bük	5			
179.	Jan. 19. 1916.	Eger	4			
180.	June 14. 1916.	Tápióbicske	3.5			
181.	Jan. 28. 1917.	Gyula	4.5			
182.	July 14. 1917.	Eger	3			
183.	Dec. 22. 1917.	Mátranovák	3.5			
184.	Feb. 22. 1919.	Gasztony	6			
184.	Mar. 29. 1921.	Szabadhídvég	3			
186.	Apr. 01. 1921.	Eger	3			
187.	May 21. 1921.	Isztimér	4			
188.	Dec. 14. 1921.	Komárom	4			
189.	Jan. 07. 1922.	Mór	4.5	0.022	0.005	2
190.	Jan. 21. 1922.	Kecskemét	4.5			

Table I (contd.)

No	Date	Location	I_0	α	σ_α	N
191.	Aug. 12. 1922.	Eger	3			
192.	Nov. 24. 1922.	Pécs	5.5			
193.	Dec. 22. 1922.	Sopronkövesd	5			
194.	Jan. 01. 1923.	Ivándárda	4			
195.	Feb. 09. 1923.	Noszvaj	3			
196.	Jan. 31. 1925.	Eger	7.5	0.020	0.006	3
179.	June 27. 1925.	Nagykanizsa	6.5			
198.	Mar. 04. 1927.	Várpalota	6.5	0.100	0.013	3
199.	Mar. 31. 1927.	Kecskemét	5			
200.	July 08. 1927.	Várpalota	6.5	0.099	0.005	2
201.	Oct. 11. 1927.	Kaposvár	4			
202.	June 20. 1928.	Eger	4	0.037	—	1
203.	Apr. 22. 1928.	Eger	4			
204.	Mar. 07. 1929.	Gödöllő	3			
205.	Apr. 30. 1929.	Budapest (Pest)	4			
206.	July 25. 1929.	Abasár	4			
207.	Nov. 05. 1929.	Jakabszállás	5	0.010	0.003	3
208.	Nov. 15. 1929.	Komárom	4	0.032	—	1
209.	Mar. 20. 1930.	Kisbárkány	3			
210.	Apr. 11. 1930.	Pári	5	0.011	0.002	2
211.	May 11. 1930.	Pári	4	0.025	—	1
212.	July 20. 1930.	Eger	5	0.023	—	1
213.	Aug. 03. 1930.	Budapest (Buda)	4			
214.	Aug. 22. 1930.	Cserhátsurány	6	0.015	0.003	3
215.	Sep. 11. 1930.	Felpéc	5	0.056	—	1
216.	Sep. 27. 1930.	Mór	3			
217.	Oct. 25. 1930.	Berzence	4			
218.	Oct. 26. 1930.	Mosonszentjános	3			
219.	Apr. 06. 1931.	Vöröstó	3			
220.	Apr. 07. 1931.	Beregdaróc	6	0.021	0.002	3
221.	Apr. 18. 1931.	Várpalota	5	0.041	—	1
222.	Oct. 31. 1931.	Nagybörzsöny	5	0.027	—	1
223.	Mar. 04. 1932.	Hercegszántó	4			
224.	Mar. 05. 1932.	Várpalota	3			
225.	Dec. 29. 1932.	Gyöngyöspata	3.5			
226.	June 04. 1933.	Báta	3			
227.	June 26. 1933.	Kétegyháza	4			
228.	Aug. 27. 1933.	Lenti	4			
229.	Dec. 19. 1933.	Mór	3			
230.	Apr. 26. 1934.	Esztergom	5.5	0.053	—	1
231.	Sep. 01. 1934.	Búcsúszentlászló	6	0.021	0.005	2
232.	Dec. 14. 1934.	Eger	3			
233.	Aug. 04. 1935.	Babócsa	4			
234.	Aug. 06. 1935.	Békés	5	0.024	0.004	2
235.	Mar. 04. 1936.	Tiszaluc	5	0.023	0.006	2
236.	Apr. 14. 1936.	Nagygéc	4			
237.	Nov. 23. 1936.	Pécs	3			
238.	Apr. 26. 1937.	Kecskemét	4	0.021	—	1
239.	June 10. 1937.	Tarcal	6	0.016	0.002	3
240.	July 12. 1937.	Balatonvilágos	3			

Table I (contd.)

No	Date	Location	I_0	α	σ_α	N
241.	Nov. 08. 1937.	Nagykáta–Farmos	3.5			
242.	June 22. 1938.	Dunakiliti	3			
243.	July 13. 1938.	Eger	3			
244.	July 18. 1938.	Máriakéménd	5	0.013	—	1
245.	Sep. 13. 1938.	Nagylak–Apátfalva	3			
246.	Dec. 11. 1938.	Nagylak	3			
247.	Mar. 23. 1939.	Álmosd	6	0.006	0.002	3
248.	July 27. 1939.	Eger	4	0.046	—	1
249.	Nov. 01. 1939.	Elek	4	0.021	—	1
250.	Feb. 05. 1940.	Álmosd	4	0.016	—	1
251.	July 05. 1940.	Kimle	3.5			
252.	Dec. 08. 1940.	Újléta	5	0.017	—	1
253.	Feb. 17. 1941.	Harkapuszta	3			
254.	May 16. 1941.	Hajdúnánás	3			
225.	May 14. 1942.	Bakonybél	6	0.033	—	1
256.	May 19. 1942.	Bácsa	4			
257.	May 28. 1942.	Tápiószele	3			
258.	Sep. 01. 1942.	Dáka	3			
259.	Sep. 30. 1942.	Tápiósüly	6	0.017	0.001	2
260.	Nov. 24. 1942.	Bezi	5	0.044	—	1
261.	June 07. 1945.	Szolnok	3			
262.	Apr. 26. 1946.	Eger–Felnémet	3			
263.	June 19. 1946.	Bodrogkeresztúr	4			
264.	Oct. 24. 1946.	Nagykőrös	3			
265.	Dec. 11. 1947.	Budapest (Buda)	4	0.020	—	1
266.	Mar. 08. 1948.	Budapest (Buda)	4	0.015	—	1
267.	Apr. 15. 1948.	Csobánka	5	0.033	—	1
268.	Aug. 07. 1948.	Bicske–Biatorbágy	4	0.010	—	1
269.	Nov. 21. 1949.	Dunaújváros	4			
270.	Aug. 21. 1950.	Izsák	4.5	0.012	—	1
271.	Nov. 29. 1950.	Becske	5	0.019	—	1
272.	Dec. 09. 1950.	Várpalota	4			
273.	Dec. 20. 1950.	Lábod	5	0.019	—	1
274.	Feb. 20. 1951.	Tereske	6.5	0.008	0.002	4
275.	Mar. 10. 1952.	Mór	5	0.022	0.005	2
276.	Apr. 04.1952.	Nagybajcs	4.5	0.035	—	1
277.	May 14. 1952.	Esztergom	4	0.013	—	1
278.	Dec. 05. 1952.	Dad–Szák	4	0.038	—	1
279.	June 10. 1953.	Bajót	3.5			
280.	Sep. 13. 1953.	Ukk	6.5	0.024	0.007	4
281.	Jan. 12. 1956.	Dunaharaszti	8	0.008	0.000	6
282.	Mar. 04. 1956.	Dunaharaszri	5	0.020	—	1
283.	Mar. 31. 1956.	Pakod	6	0.016	0.003	3
284.	Apr. 28. 1956.	Csehimindszent	5	0.026	0.011	2
285.	May 02. 1956.	Csehi	5	0.028	0.006	3
286.	July 30. 1956.	Dunaharaszti	5	0.014	0.002	2
287.	Dec. 14. 1956.	Egerbakta	5.5	0.014	0.005	3
288.	Mar. 27. 1957.	Nagyléta	3	0.024	—	1
289.	Apr. 20. 1957.	Nagyigmánd	4			
290.	May 08. 1957.	Jánoshida	5	0.034	—	1

Table I (contd.)

No	Date	Location	I_0	α	σ_α	N
291.	May 30. 1957.	Miskolc	3			
292.	June 05. 1957.	Eger	4	0.048	—	1
293.	Dec. 03. 1957.	Vasvár	4	0.032	—	1
294.	Apr. 10. 1958.	Lőrinci	4	0.032	—	1
295.	Apr. 16. 1958.	Pakod	3			
296.	Apr. 26. 1958.	Berkesz	5	0.021	0.005	2
297.	July 24. 1958.	Hetes	5	0.029	0.004	2
298.	July 28. 1958.	Dunaharaszti	4	0.025	—	1
299.	Oct. 15. 1958.	Csécse	4	0.033	—	1
300.	Dec. 17. 1960.	Ács–Bana	3			
301.	June 07. 1961.	Bérbaltavár	3			
302.	Aug. 23. 1963.	Jásztelek	3			
303.	July 23. 1965.	Dunaharaszti	3			
304.	Oct. 21. 1968.	Tapolca	4	0.026	—	1
305.	Feb. 10. 1969.	Bakonysárkány	5	0.009	0.001	2
306.	Jan. 30. 1974.	Törökbálint	5	0.015	—	1
307.	Aug. 28. 1976.	Keszthely	3			
308.	Mar. 17. 1977.	Tamási–Regöly	5	0.014	0.002	2
309.	June 22. 1978.	Békés	6	0.011	0.000	2
310.	Sep. 26. 1978.	Délegyháza	5	0.015	0.003	2
311.	Oct. 30. 1979.	Békés	4.5	0.034	—	1
312.	Feb. 24. 1980.	Recsk	5	0.027	—	1
313.	Mar. 15. 1980.	Békés	4	0.031	—	1
314.	Mar. 25. 1980.	Portelek	5	0.026	0.003	2
315.	Mar. 31. 1980.	Farmos	4			
316.	Aug. 22. 1980.	Csemő	5	0.028	—	1
317.	Sep. 21. 1981.	Várpalota	4.5			
318.	Jan. 06. 1982.	Rácalmás	4.5	0.018	0.008	2

I_0 — MSK intensity scale
α — attenuation coefficient
σ_α — standard deviation of α
N — number of isoseismals

Theoretical maximum intensity map of Hungary

Based on the intensities and their attenuation coefficients (Table I) the maximum intensities are calculated for all points on a 10 × 10 km grid of Hungary using the model

$$I_i = I_0 \exp(-\alpha R_i), \tag{2}$$

where

I_0 — epicentral intensity
R_i — epicentral distance (in km)
α — attenuation coefficient of intensity (in km^{-1}); if it was unknown $\alpha = 0.024\ km^{-1}$ was used
I_i — intensity at a distance R_i.

Each division of the grid was characterized by the maximum intensity value and the results are contoured in Fig. 1.

The calculated map has the lowest intensities—irregardless of some border zones—in the north-western part of Hungary and in the central part of Transdanubia, followed by the territory east of the river Tisza which is generally regarded as the lowest seismicity region of Hungary. This result is certainly due to the effect of the Kecskemét, Eger and Jászberény earthquakes with intensities 8°, 7.5° and 7.5° respectively. As only Hungarian earthquakes were considered the border regions—especially at Austria and Yugoslavia—have considerably smaller intensity values than expected. After the compilation of the new observed intensity map of Hungary it might be useful to compare the theoretical intensity map with the observed one in order to trace the effects of local conditions on intensities.

Estimation of maximum ground accelerations, velocities and displacements

Based on the theoretical intensity map (Fig. 1) the intensity values can be transformed into acceleration, velocity and displacement parameters of the ground motion using the equations proposed by Trifunac and Brady (1975)

$$\log A_h = -0.014 + 0.30\, I \tag{3}$$

$$\log A_v = -0.18 + 0.30\, I \tag{4}$$

$$\log V_h = -0.63 + 0.25\, I \tag{5}$$

$$\log V_v = -1.10 + 0.28\, I \tag{6}$$

$$\log D_h = -0.53 + 0.19\, I \tag{7}$$

$$\log D_v = -1.13 + 0.24\, I \tag{8}$$

(h—horizontal component; v—vertical component).

The units of acceleration (A), velocity (V) and displacement (D) are cm/sec^2, cm/sec and cm respectively. The relationships are based on data from Western United States and the intensity scale used by the authors was the Modified Mercally one. The range of intensity data was from 3° to 10°.

In the theoretical maximum intensity map (Fig. 1) the values are in MSK intensity scale ranging from 2.5° to 8°. Concerning the two different intensity scales we accepted Medvedev, Sponheuer and Karnik's opinion that there is no significant difference between the two intensity scales. (See Manual of Seismological Observatory Practice, 1979, MAC 1.1.4.)

The results are shown in Figs 2–7. The main features of these maps, naturally, are the same as we obtained in the theoretical maximum intensity map. The peak values of

Theoretical maximum intensity map of Hungary (1859–1982)
20km
Method: $I_K = I_0 \exp(-\alpha R_K)$
α – attenuation coefficient of intensity
I_0 – epicentral intensity
R_K – epicentral distance (≤200 km)

Fig. 1

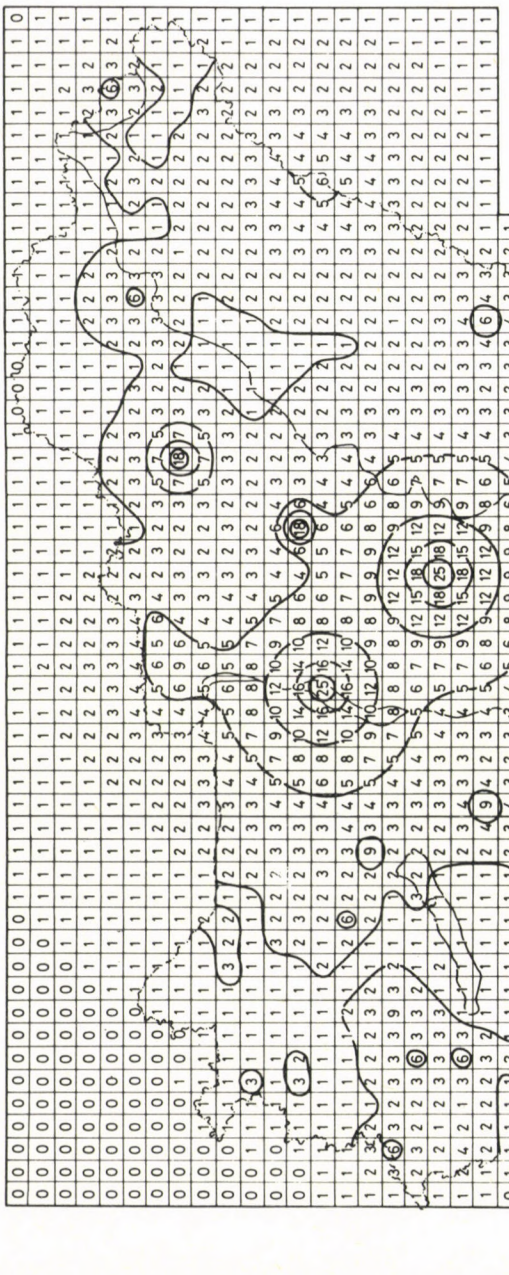
Theoretical values of the maximum horizontal ground accelerations caused by earthquakes in Hungary (1859–1982)
20km
Unit: 10^{-2} g (g=981cm/s^2)

Fig. 2

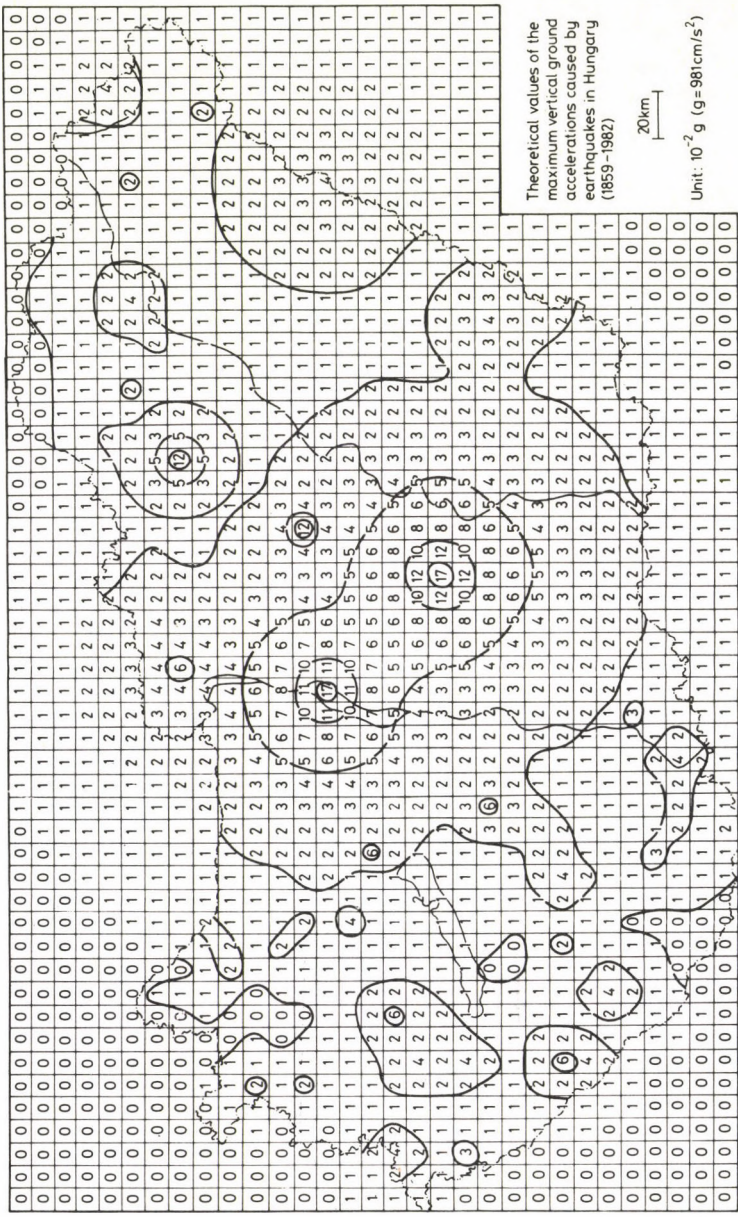
Theoretical values of the maximum vertical ground accelerations caused by earthquakes in Hungary (1859–1982)
20km
Unit: 10^{-2} g (g=981cm/s^2)

Fig. 3

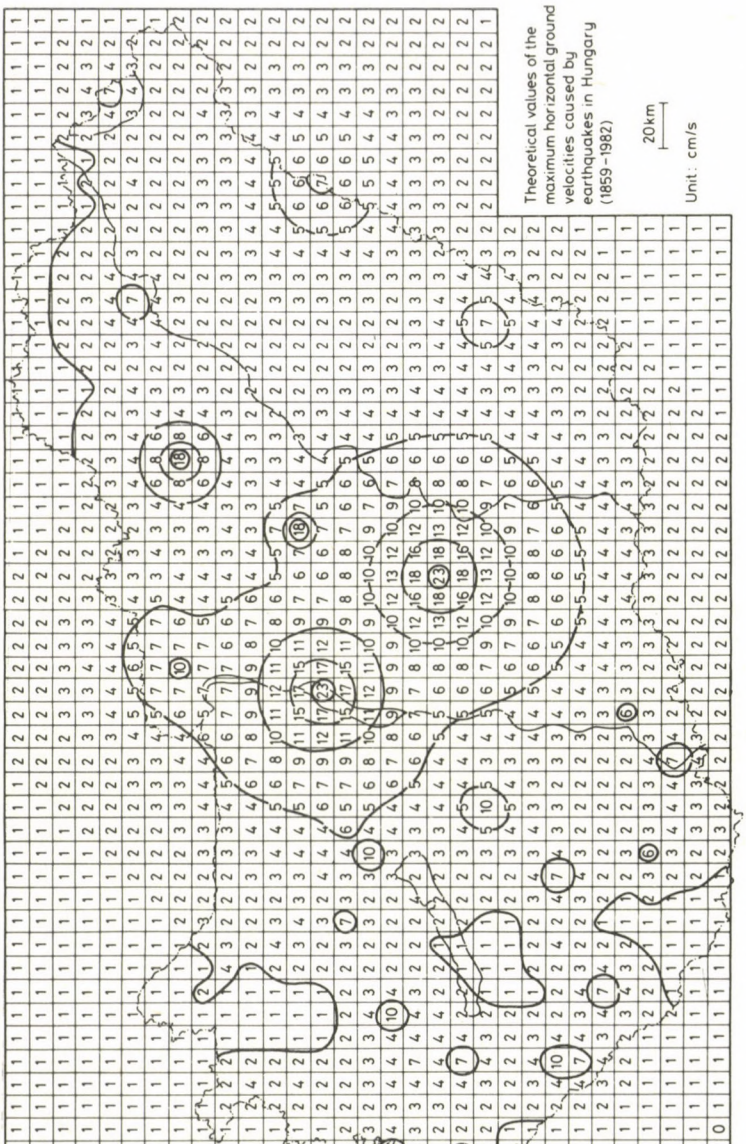
Theoretical values of the maximum horizontal ground velocities caused by earthquakes in Hungary (1859–1982)
20km
Unit: cm/s

Fig. 4

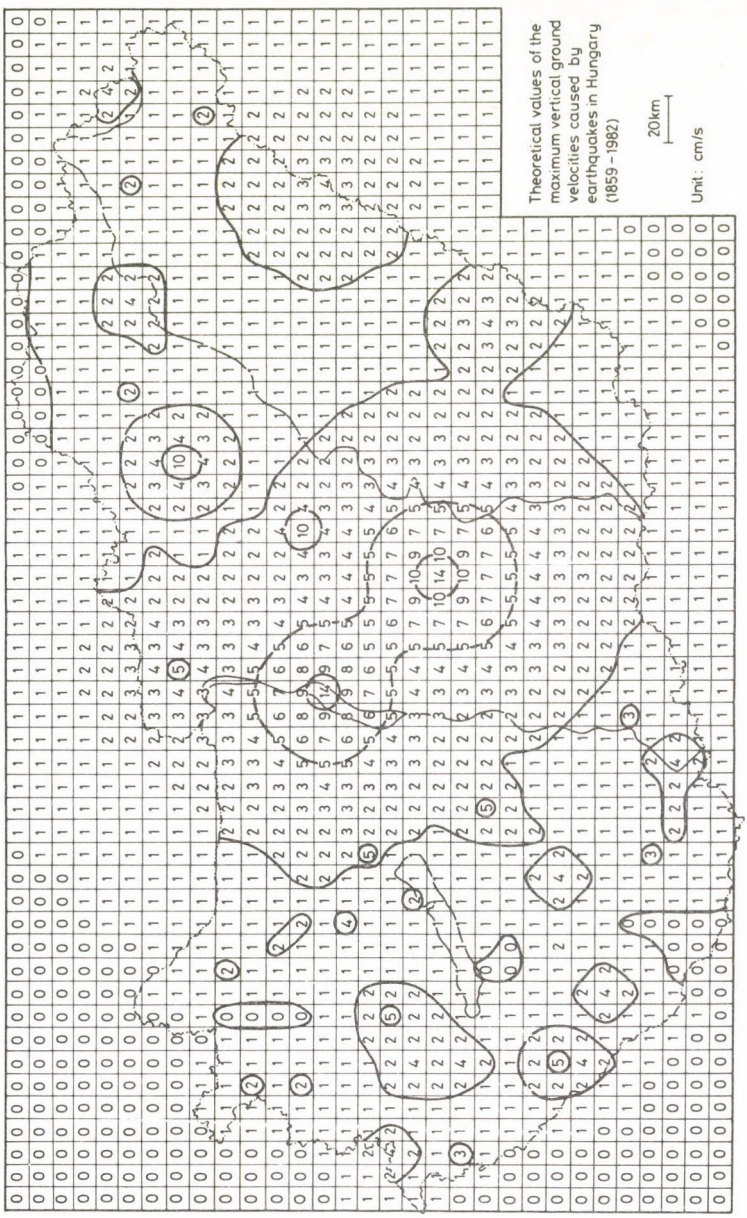
Theoretical values of the maximum vertical ground velocities caused by earthquakes in Hungary (1859 – 1982)
20km
Unit: cm/s

Fig. 5

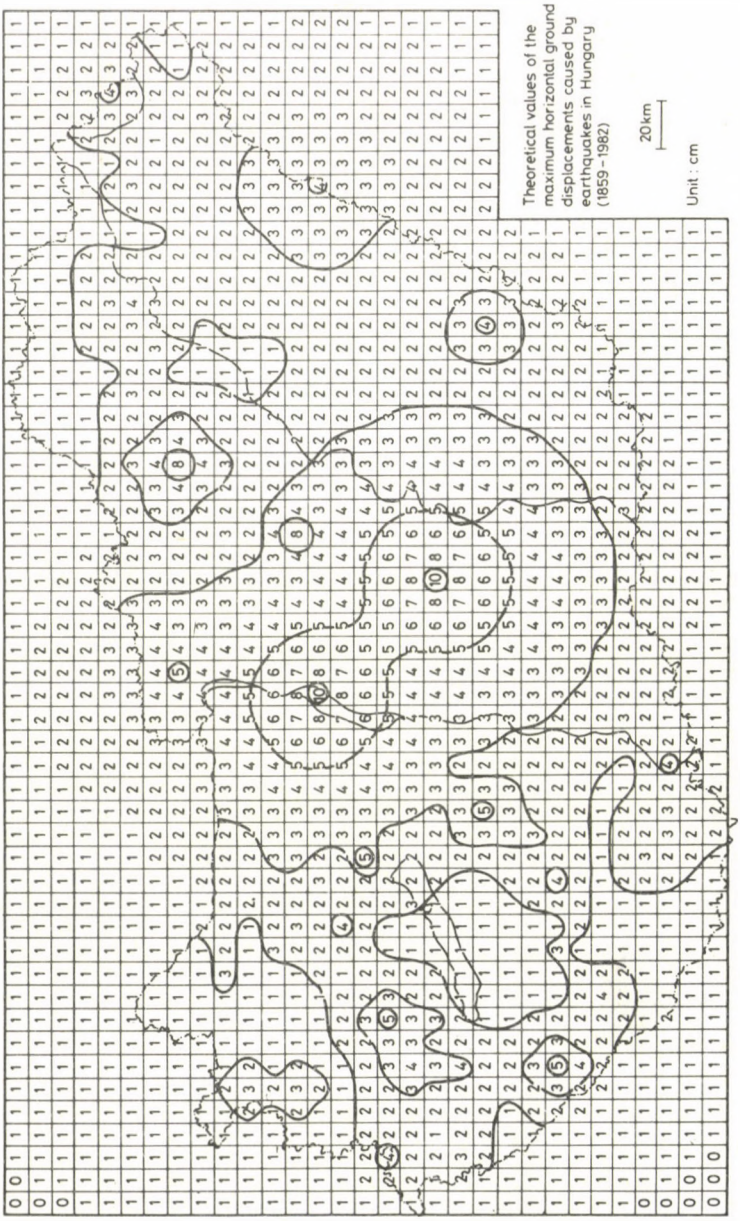
Theoretical values of the maximum horizontal ground displacements caused by earthquakes in Hungary (1859–1982)
20km
Unit : cm

Fig. 6

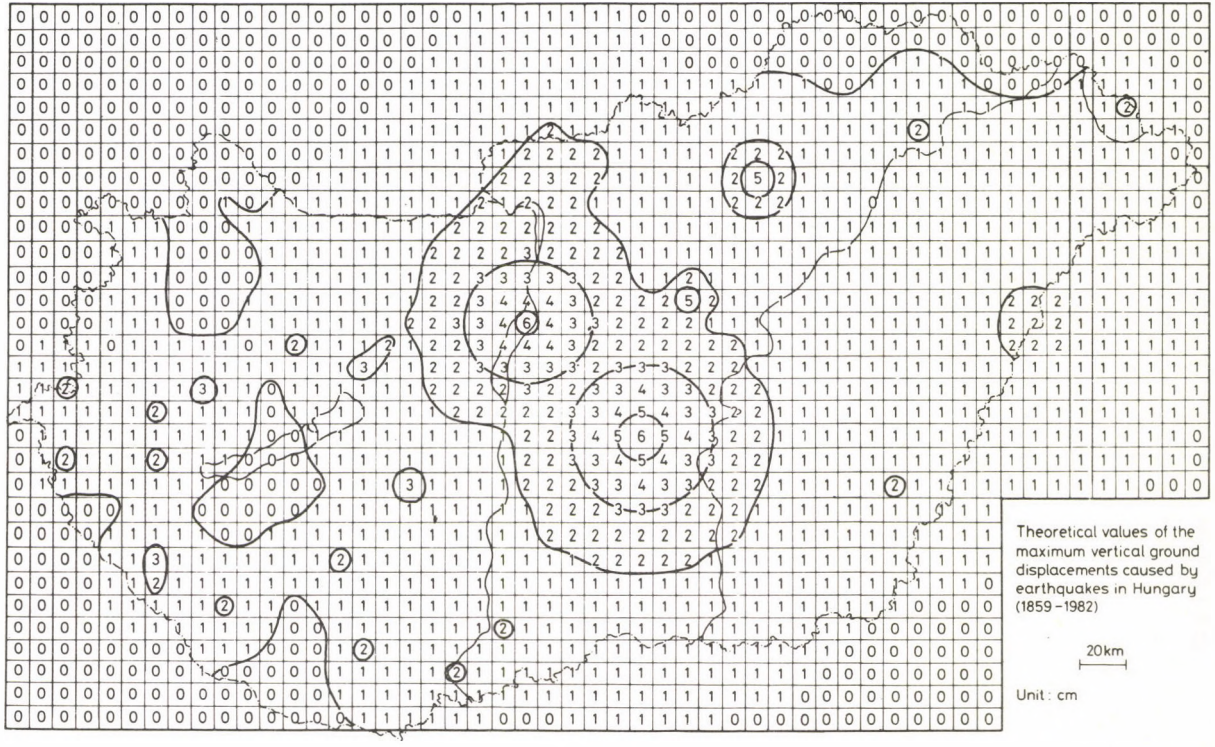
Theoretical values of the maximum vertical ground displacements caused by earthquakes in Hungary (1859–1982)
20km
Unit : cm

Fig. 7

acceleration, velocity and displacement are 2.4 m/sec^2, 23 cm/sec and 10 cm, respectively.

In spite of the fact that the results can only be regarded as simple and rough estimations of the ground motions it is hoped that this qualitative estimation of shaking effects provides a step forward in the field of earthquake engineering in Hungary.

Acknowledgements

The authors thank D Csomor, Z Kiss and Gy Szeidovitz for letting use some unpublished macroseismic data.

References

Bisztricsány E, Rónai A 1983: Difficulties of the seismic risk determination in Hungary. *Acta Geod. Geoph. Mont. Hung.* (in press)

Csomor D, Kiss Z 1983: Catalogue and isoseismal maps of Hungarian earthquakes (1880–1980). Manuscript

Szeidovitz Gy 1983: Budapest szeizmikus kockázata. Manuscript

Trifunac M D, Brady A G 1975: On the correlation of seismic intensity scales with the peaks of recorded ground motion. *Bull. Seism. Soc. Am.*, 65, 139–162.

Acta Geodaet., Geophys. et Montanist. Hung. Volume 19 (3–4), pp. 451–465 (1984)

ANALOGUE MODELING OF DC MAPPING METHODS OVER HIGH RESISTIVITY BASEMENT STRUCTURES

L SZARKA[1]

[Manuscript received October 14, 1983]

The characteristics and the resolution power of several geophysical DC mapping methods in investigation of high resistivity basement inhomogeneities have been studied by means of analogue modeling.

Mainly anomalies over 2-D and 3-D ramp-, ridge- and valley-like structures have been investigated using the potential mapping method (PM) and the hole-to-surface resistivity method (HSR).

According to analogue model measurements, the responses of high resistivity basement structures in the hole-to-surface method are more difficult to interpret and are smaller than the responses in the potential mapping method.

A close connection between the normal magnetic field H_y of the magnetometric resistivity method (MMR) and the normal electric field E_x of the potential mapping method has been shown. On this basis the horizontal electrical conductance of the top layer can be determined from the impedance E_x/H_y and a combined PM-MMR method is proposed to investigate such high resistivity basement inhomogeneities.

Keywords: analogue modeling; DC mapping; geoelectric model; high resistivity basement; hole-to-surface method; magnetometric resistivity

Introduction

In the electromagnetic modeling laboratory of the Geodetic and Geophysical Research Institute of the Hungarian Academy of Sciences various DC methods can also be modeled.

There are numerous geological environments (e.g. the two layered half-space having high resistivity basement inhomogeneities) where a significant part of the geophysical prospecting problems can be solved using cheap DC mapping methods. A detailed investigation of the mentioned type geological formations is very important in Hungary, especially in bauxite exploration.

The potential mapping method (PM) and the hole-to-surface resistivity method (HSR) have been employed by the Hungarian Geophysical Institute Loránd Eötvös (ELGI) for several years. A study of the characteristics of these methods by means of

[1] Geodetic and Geophysical Research Institute of the Hungarian Academy of Sciences, Sopron, Pf. 5, H-9401

analogue modeling over 2-D and 3-D high resistivity basement inhomogeneities was supported by the ELGI.

When the model measurements were made an idea came to apply the magnetometric resistivity method (MMR) also in investigation of the high resistivity basement.

Description of the modeled methods

The potential mapping means the measurement of the quasi-static electric field between two distant electrodes A and B. Figure 1 shows a typical measuring arrangement of the PM method as used in practice.

Usually the horizontal electric field component E_x is measured at stations in a grid over an area shown in Fig. 1. For high resistivity basement structures the two layered half-space with a ρ_∞-bottom is the basic model. The basic model of the measuring area supposes a quasi-homogeneous current density forming the so-called S interval. This S interval exists in points at a distance from the current electrode at least twice the depth of the basement.

The measured field anomalies in the surface are caused by the horizontal inhomogeneities of the basement surface. The measured electric fields are normalized to the theoretical values as follows:

$$S_m = -\frac{E_{\text{basic model}}}{E_{\text{measured}}}. \tag{1}$$

The negative sign transforms the S_m profile (or map) to show the geologic cross section upside up. Far of basement inhomogeneities $S_m \approx -1$, over trenches $|S_m| > 1$, and over ridge-like structures $|S_m| < 1$. This S_m distribution is called a PM anomaly.

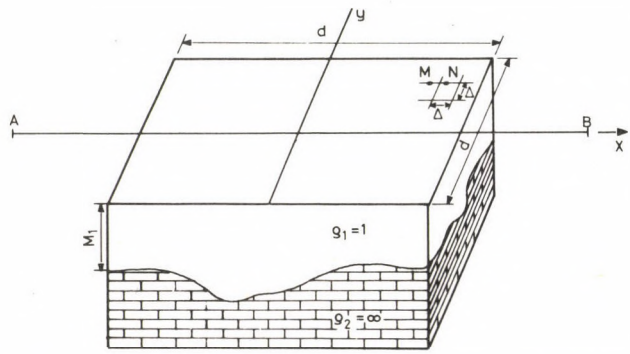

Fig. 1. A typical measuring arrangement of the potential mapping (PM) method. M_1—average depth of basement; A and B—current electrodes; usually $\overline{AB} \approx 8$–$10\,M_1$; M and N—measuring electrodes; Δ—distance between measuring points on the grid; d—length of side of the survey area, usually $d \approx 0.5\,\overline{AB}$

A more detailed description of this method for the investigation of high resistivity basement structures is given by Simon (1974).

The hole-to-surface resistivity method is similar to the PM, but one of the current electrodes is placed in a borehole and two orthogonal electrical components are measured at stations over an area enclosing the borehole. An overview of this method and results of field measurements are given in a recent paper by Daniels (1983). The so called underground potential mapping which is essentially the same as HSR method was applied in Hungary already in the seventies first of all to investigate sinks of the high resistivity basement filled with conducting sediment (bauxite) and covered by a layer of higher resistivity. Its first description is given in the Annual Report of the ELGI for the year 1973.

This paper deals only with two-layered cases with uncovered sinks, faults and horsts (that is valley-like, ramp-like and ridge-like inhomogeneities) of the high resistivity basement.

The magnetometric resistivity method means the measuring of the magnetic field due to galvanic currents flowing in the earth. The measuring arrangement is similar to that of the PM method, only sensitive component magnetometers are used instead of potential electrodes. Usually the horizontal magnetic component perpendicular to the *AB* line is measured (Edwards 1974).

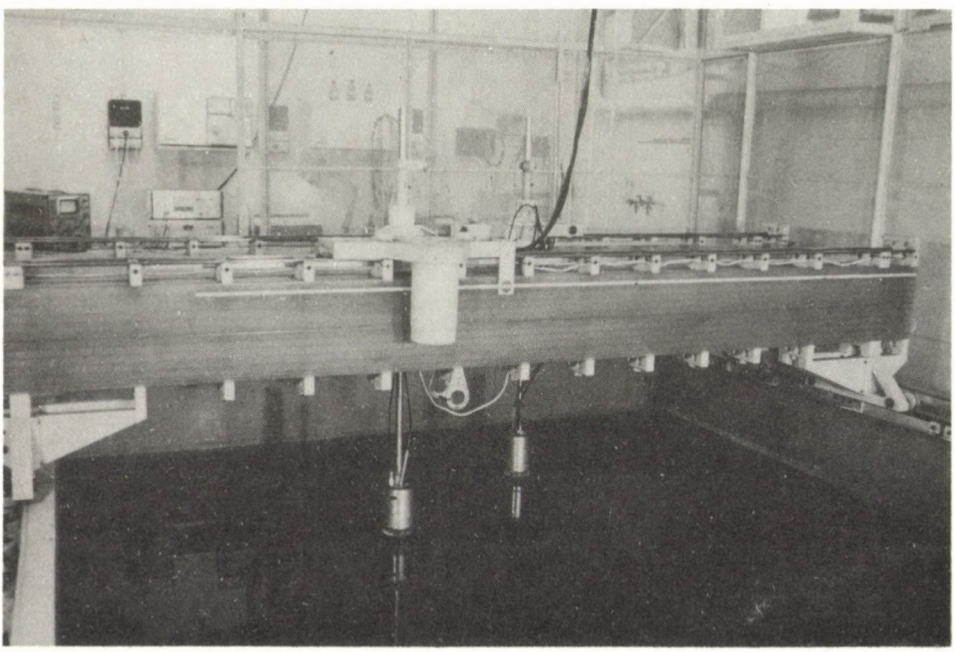

Fig. 2. Electromagnetic analogue modeling laboratory at the Geodetic and Geophysical Research Institute of the Hungarian Academy of Sciences

DC analogue modeling

The analogue modeling of the DC exploration methods mentioned above has been developed in the modeling laboratory of the Geodetic and Geophysical Research Institute of the Hungarian Academy of Sciences (Fig. 2).

The models of basement inhomogeneities are built at the bottom of a plastic tank with dimensions of 3 m × 4 m, containing sodium chloride solution. The measurements are carried out on the surface of the electrolyte. The modeling frequency of 500 Hz is low enough to produce a quasi-static field in the medium with a resistivity of about 0.1 ohmm. The potential differences on the measuring (electrical or magnetic) dipoles moved by a rolling bridge are punched automatically on tape.

More details on the laboratory are published in a paper by Ádám et al. (1981).

Results of PM modeling

PM anomalies of 2-D basement inhomogeneities have been determined not only by analogue modeling, but also by a mathematical modeling method, namely by conform transformation (Szigeti 1980).

Results of mathematical and physical modelings over 2-D basement inhomogeneities are summarized in a paper by Szarka and Szigeti (1982). Here only a short overview of PM anomalies over prism-like 2-D structures is given. 3-D anomalies are described in more details by Szarka (1982).

Figure 3 shows the PM anomaly extremes over prism-like 2-D high resistivity structures as a function of the relative width b/M_1. The curve parameter is M_2/M_1. For horsts $M_2/M_1 < 1$, and for trenches $M_2/M_1 > 1$.

On the basis of Fig. 8, it can be seen that

1. In case of wider horsts ($b/M_1 > 1$) the extreme values of the S_m anomalies are linear functions of M_2/M_1. The limit of the applicability of the linear depth calculation is denoted roughly by dashed line.

2. Narrow trenches ($b/M_1 < 0.5$) cannot be detected at all, and only in the range $b/M_1 > 1$ some difference appears between the PM anomalies of trenches having finite and infinite depth. A linear depth calculation can be applied only for very wide ($b/M_1 > 5$, the exact value depending on M_2/M_1) trenches.

Summarizing the conclusions of Fig. 3, the PM anomalies of 2-D horsts and trenches significantly differ from each other. Contrary to trenches, narrow horsts have already significant anomalies as it has been quantitatively shown in Fig. 3.

Figures 4, 5 and 6 show PM anomaly maps (plotted by Závoti's method 1981) over 3-D structures. Their main features are as follows (Fig. 7):

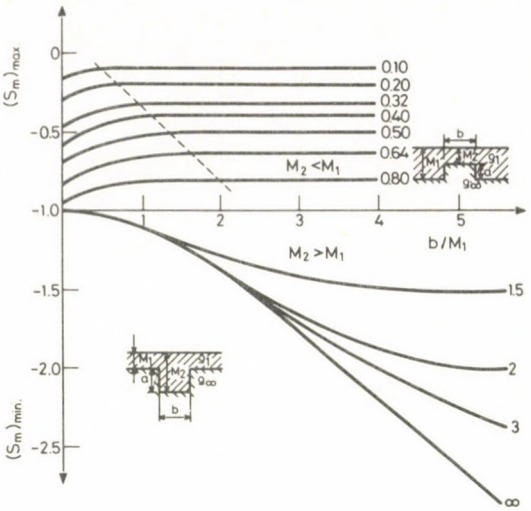

Fig. 3. Extreme values of PM anomalies for 2-D horsts and trenches *vs.* width of the structure. The curve parameter is M_2/M_1

1. The anomaly over 3-D structures is smaller than over 2-D structures of the same height and thickness.

2. The anomaly is much wider than the structure itself.

3. Fictitious anomalies appear at the front ends of the structure (in case of horsts, a deepening, in case of trenches, an uprise).

These phenomena have simple reasons. A part of the current flows round the horsts. The trenches collect the currents due to their larger cross-sections. Meanwhile in the region (2) there is an opposite effect in form of the current distortion, so the summarized effect of both phenomena causes a spreading of the superficial current density distortion. Fictitious anomalies at the front sides (3) are formed due to current branching.

On the basis of the measured distortion, master curves were made, but due to the complicated shape of 3-D anomalies, they did not come in use. It proved to be more useful in practice to make a transformation of the measured maps which results in anomalies following the forms of the investigated structures.

According to the method applied by ELGI, two PM maps are measured using two orthogonal layouts and the geometric mean of the values obtained in a measuring point is calculated. This treatment is called a $\bar{S}$-transformation.

The results of analogue modeling have supported the validity of this procedure as it can be seen for horsts in Fig. 8 and for trenches in Fig. 9.

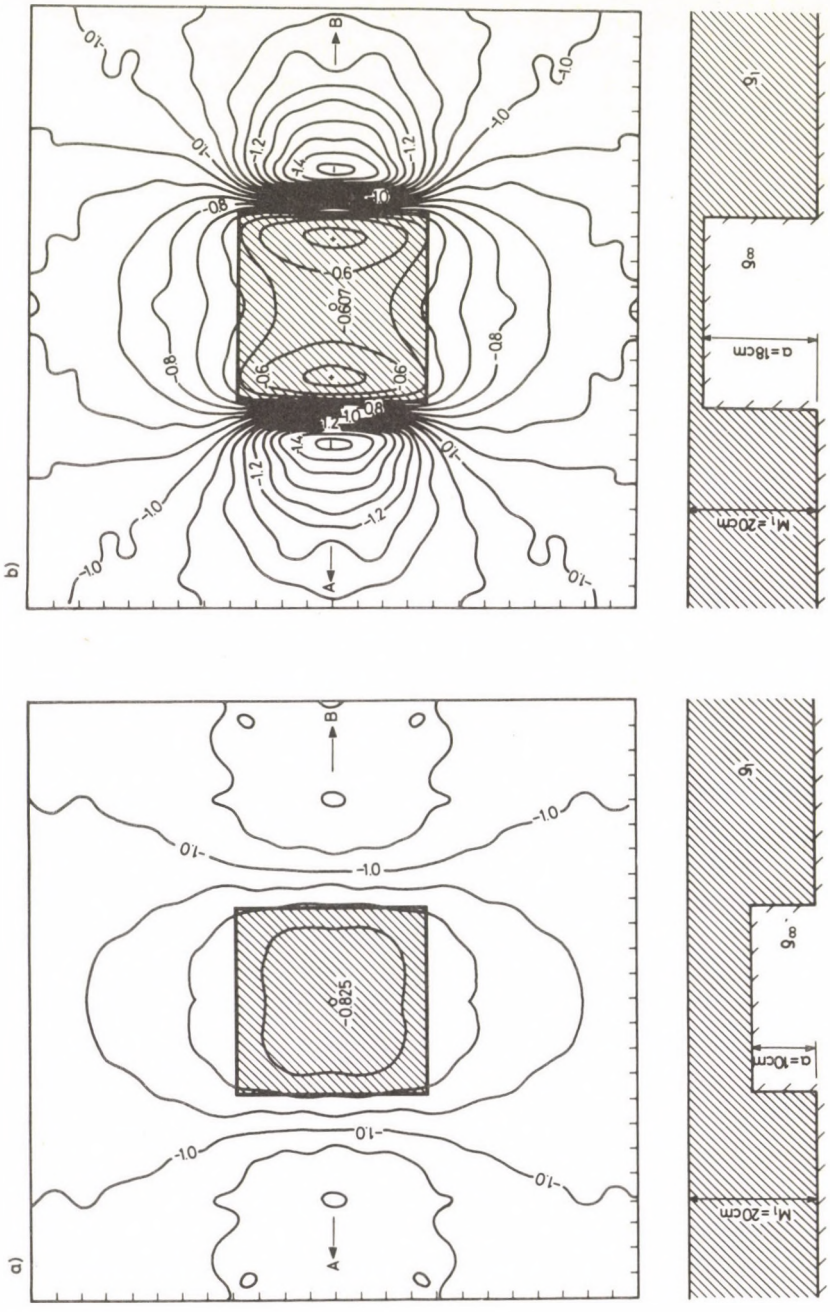

Fig. 4. PM anomaly maps over high resistivity basement horsts

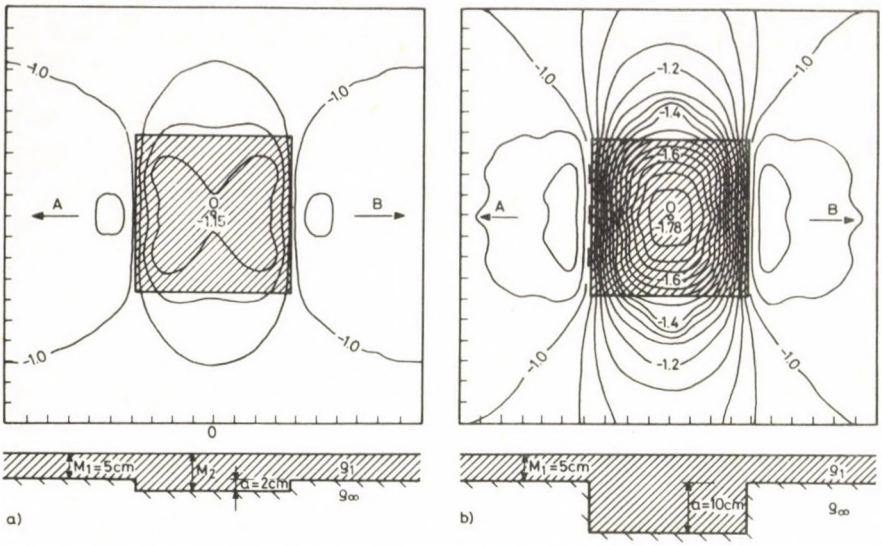

Fig. 5. PM anomaly maps over isometric sinks of the high resistivity basement

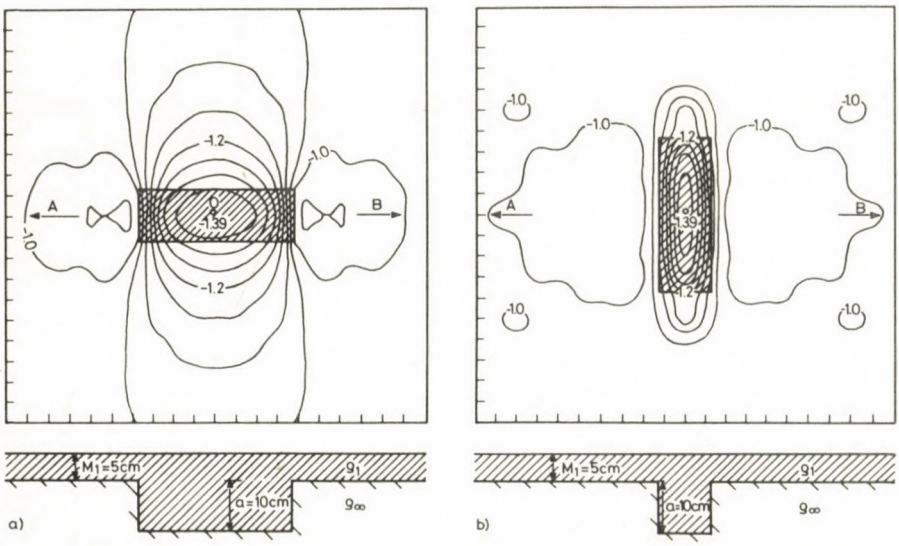

Fig. 6. PM anomaly maps over non-isometric prism-like sinks of the high resistivity basement

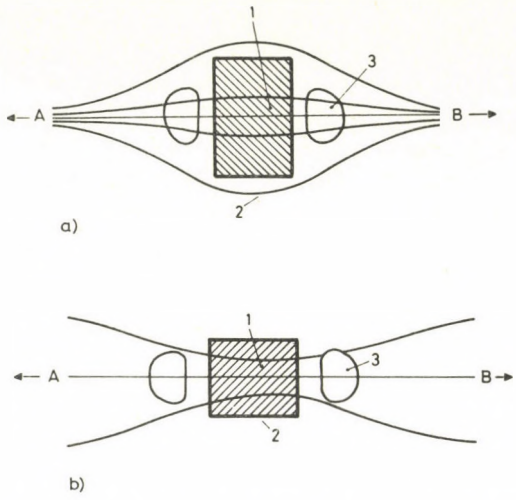

Fig. 7. Explanation of PM anomalies over 3-D structures

a) horsts
1 — Anomaly decreases due to by-pass currents
2 — Spreading of anomaly due to by-pass currents
3 — Fictitious anomalies due to current branching

b) sinks
1 — Anomaly decreases due to cumulative currents
2 — Spreading of anomaly due to cumulative currents
3 — Fictitious anomalies due to current branching

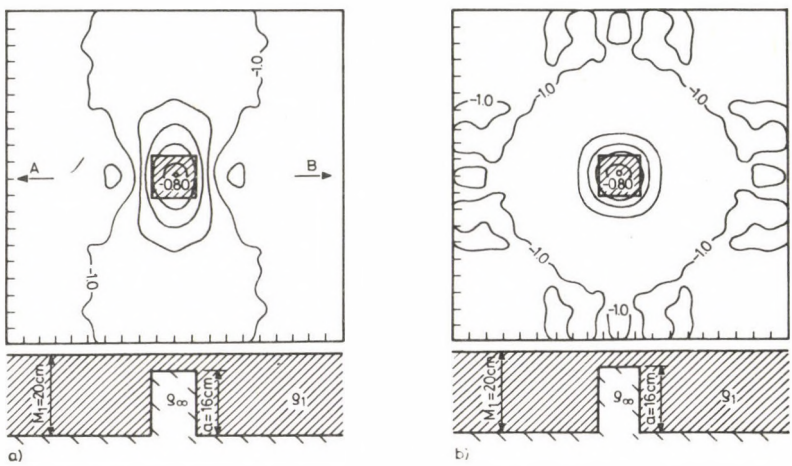

Fig. 8. Effect of the $\bar{S}$-transformation on the PM anomaly map over 3-D horsts. *a)* PM anomaly map of one layout *AB b)* Relative $\bar{S}$ map obtained from two orthogonal layouts

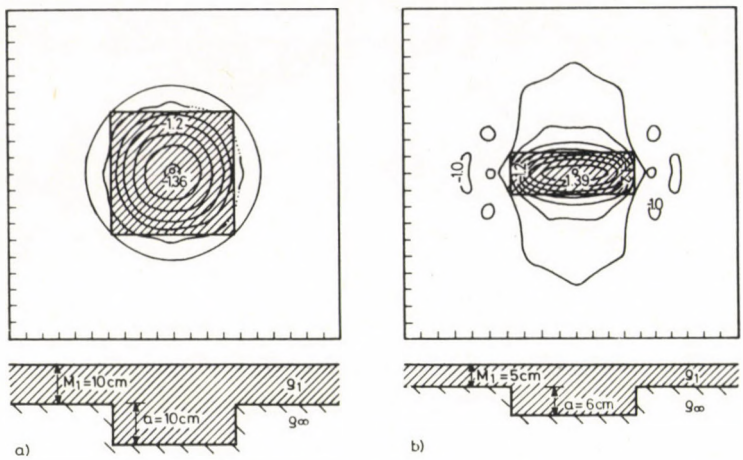

Fig. 9. Relative $\bar{S}$ maps over 3-D sinks

Results of the hole-to-surface resistivity modeling

According to several authors (e.g. Snyder and Merkel 1973) the buried electrode can significantly increase the response of a buried structure. These calculations were made for models placed in a homogeneous medium. Scale model experiences made by the HSR method over high resistivity basement inhomogeneities have not verified the previous expectations concerning the resolution power of the method in such geological environments.

The hole-to-surface resistivity method over 2-D inhomogeneities of the resistive basement did not give unambiguous results as the form of the anomaly strongly depends on the direction of the distant (placed in "infinity") electrode B, as it can be seen in Fig. 10. (In case of Fig. 10b, too, the field vectors starting from the electrode A point towards the electrode B. Moving away from the line AB, their directions become more and more parallel to the strike i.e. an equalization appears in the superficial current density, and the anomaly disappears.)

Figure 11 shows a fault where the sunk electrode A comes closer to the fault on its thrown side while the electrode B is fixed on the elevated side, far of the horizontal inhomogeneity. According to the HSR/PM anomaly profile the HSR anomaly is much less if the electrode A is placed near to the fault. When the distance between the electrode A and the fault is large (more than $3M_1$) the PM and HSR anomalies agree as the development of the S-interval does not depend on the vertical coordinate of the electrode A.

Figure 12a shows that only one sidewall of the 2-D trench can be detected depending on the position of the distant electrode B. This feature exists also in case of 3-D structures (Fig. 12b).

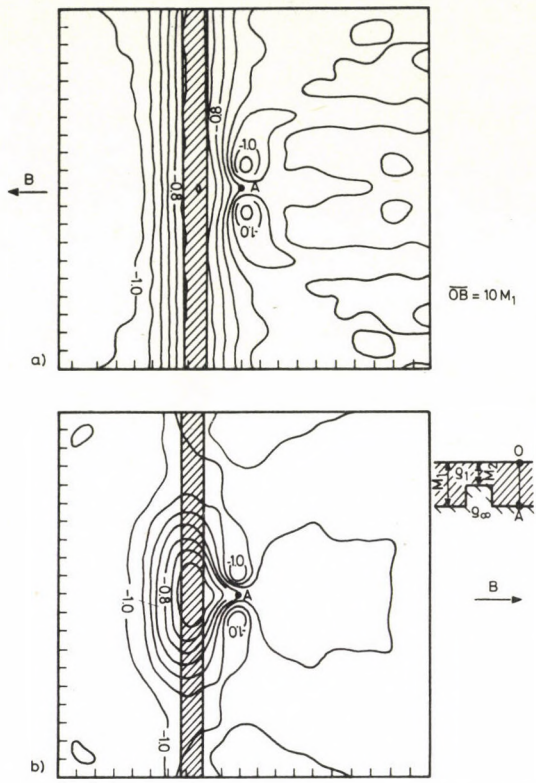

Fig. 10. Hole-to-surface resistivity anomaly over a 2-D horst. *a)* The horst is between the two electrodes *b)* The horst is out of the section *AB*

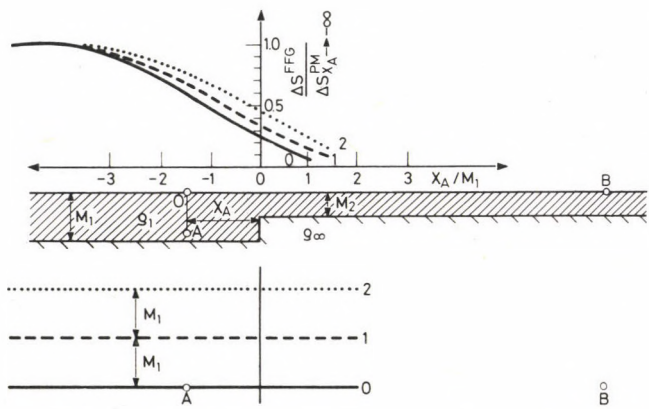

Fig. 11. HSR/PM anomaly profiles over a 2-D fault in the high resistivity basement. 0, 1 and 2 identify the measuring profiles which are shown at the bottom of the figure

Figure 13 shows a comparison of the PM and HSR methods over six 3-D sinks in the basement. The PM method gave the expected results: wide anomalies with fictitious maxima between them. With the HSR method similar anomaly values were obtained except for the trench containing the sunk electrode. The HSR anomaly forms are prolating the isolines of the HSR normal field.

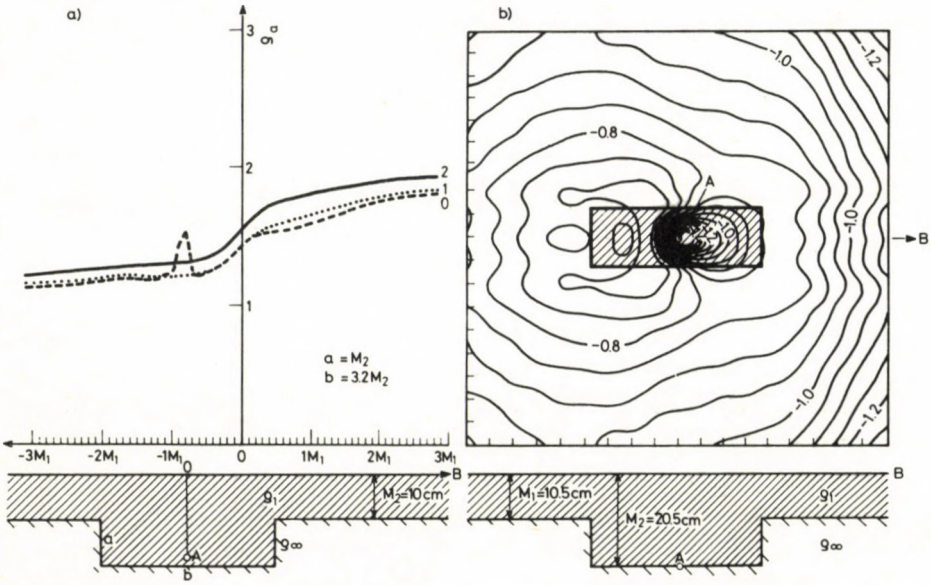

Fig. 12. HSR modeling over sinks of the high resistivity basement *a)* HSR profiles over a 2-D trench *b)* HSR profiles over a 3-D sink

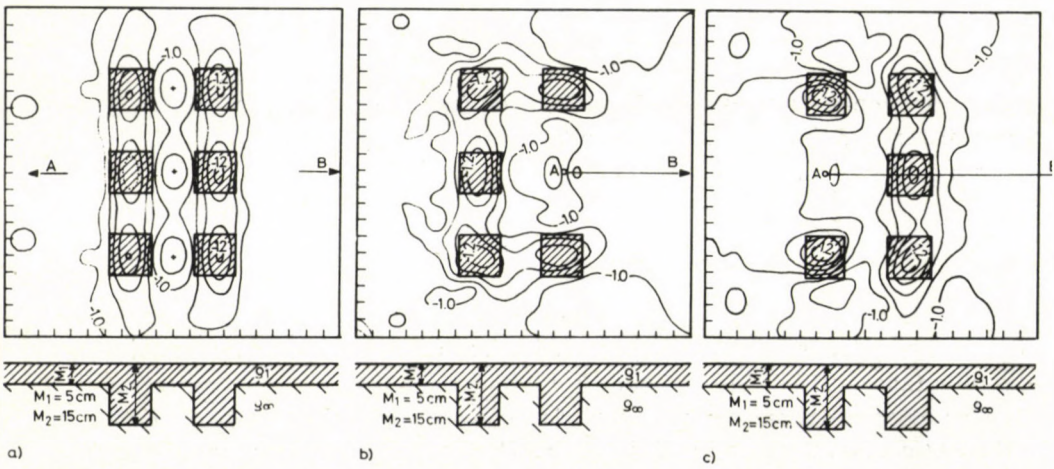

Fig. 13. Comparison of PM and HSR anomaly maps over six small sinks *a)* PM map *b)* and *c)* HSR maps

On the basis of the scale modeling it can be summarized that the HSR anomalies over uncovered high resistivity basement inhomogeneities also depend on the development of the *S*-interval. The HSR anomalies of horizontal inhomogeneities near to the sunk electrode are strongly distorted.

Perspectivity of the MMR method in the investigation of the high resistivity basement

According to Edwards (1974) in case of any axial symmetry around the point electrode (including the horizontally layered half-spaces) the magnetic field distribution on the surface agrees with the field distribution over a homogeneous half space.

This field distribution has an axial symmetry, where $H_z=0$, $H_r=0$ and

$$H_\varphi = \frac{I}{4\pi R} \tag{2}$$

where I is the current flowing in the earth, R is the distance between the measuring point and the current electrode.

In the *S*-interval (when $R>2H$) over isolator basement there is a homogeneous current density in the conducting layer. In the right-side of the relation $\vec{E}=\rho\vec{j}$, the current density can be replaced by the whole current divided by the surface of the cylindre around the electrode.

In this case over a conducting layer of resistivity ρ_1

$$E_r = \frac{\rho_1 I}{2\pi R H}. \tag{3}$$

A comparison of relations 2 and 3 shows that the ratio E_r/H_φ does not depend on the distance R but this ratio is an absolute function of the horizontal electric conductance of the conducting layer S_1:

$$Z = \frac{E_r}{H_\varphi} = 2\frac{\rho_1}{H} = \frac{2}{S_1}. \tag{4}$$

This relation is valid for superposed point sources too, so the horizontal electric conductance can be determined from horizontal electric and magnetic field distributions using any current electrode arrangements. In field measurements using the PM method shown in Fig. 2 the E_x and H_y distributions also give the conductance S_1.

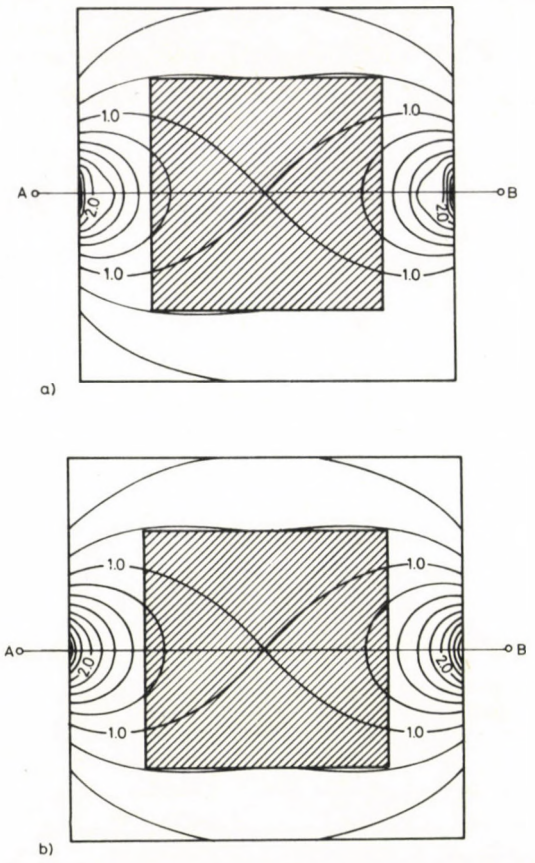

Fig. 14. Normal fields of the PM and MMR methods *a)* Normal field E_x of the PM method *b)* Normal field H_y of the MMR method

Figures 14a and 14b show that the normal fields of the PM and the MMR methods over a high resistivity basement are the same disregarding the close vicinities of the current electrodes.

Over a high resistivity basement, the MMR method can be applied together with the PM method and this combination yields several further advantages.

Possibilities of the combined PM-MMR method

Figure 15 shows results over a fault in the high resistivity basement. (The angle between the direction of the current electrodes and the strike direction was 45°) Figure 15a shows the well-known phenomenon, i.e. the electrical field distribution depends

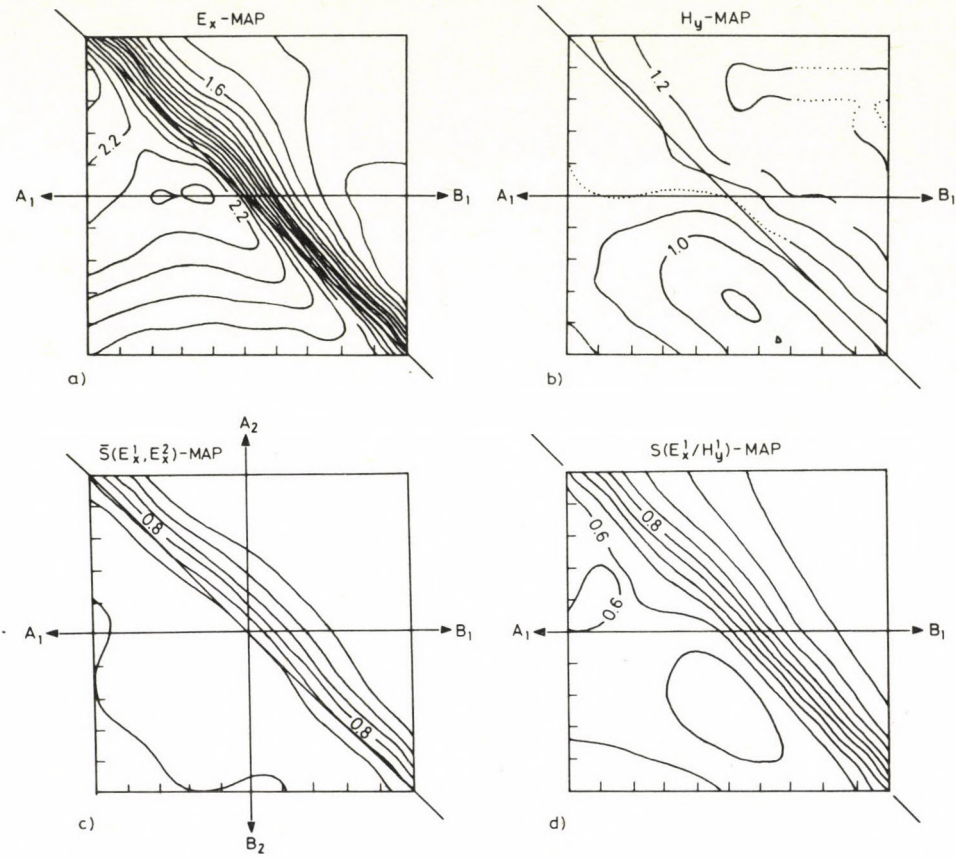

Fig. 15. $S(E_x)$ and $S(E_x/H_y)$ maps over a fault in the resistive basement. Angle between the AB line and the strike is 45°. *a)* Relative S map of the PM method using only one layout *b)* Relative H_y map of the MMR method *c)* $\bar{S}$ map of PM method using two orthogonal layouts *d)* S map of the combined PM-MMR method

not only on the geological structure but on the direction of the current electrodes as well. In the PM method this distortion effect can be eliminated using the $\bar{S}$-transformation, as it can be seen in Fig. 15c.

Figure 15b shows the distribution of H_y over the fault. According to Fig. 15d the S-map determined from the E_x and H_y field distributions of only one single layout also reflects the geological structures.

An advantage of the PM-MMR method is that here is no need for geometric coefficients and normal field calculations. Quasi-static signals coming from sources of unknown position and intensity also can be interpreted (Szarka 1983).

In field measurements the $\bar{S}$ anomaly map of the PM method reflects real structural effects but naturally a part of these effects may be of near-surface origin. As

the magnetic field gives a more averaged picture of the currents flowing in the earth, some limited possibilities appear in distinguishing deep and localized near-surface effects.

Summary

Analogue modeling experiments have given an addition to clear the real possibilities of the PM and HSR methods over 2-D and 3-D high resistivity basement inhomogeneities. The modelings have supported the effectivity of the potential mapping method and have pointed out some distortion effects of the HSR method.

In the interpretation of difficult anomalies of 3-D structures it is advantageous to use a transformation to make disappear the fictitious anomalies. The $\bar{S}$-transformation gives satisfactory results, but it requires two orthogonal AB-lines. If measuring the horizontal magnetic field perpendicularly to the measured electrical component, a realistic picture for the high resistivity basement could be obtained in case of only one single layout. To develop this "combined PM-MMR method", further investigations are to be made.

Acknowledgements

The author thanks the support of the Hungarian Geophysical Institute Loránd Eötvös and wishes to express his gratitude to Prof. E Takács for valuable comments.

References

Ádám A, Pongrácz J, Szarka L, Nagy Z, Zimányi I, Kardeván P, Szabadváry L, Kormos I, Régeni P 1981: Analogue model to study geoelectric methods at the Geodetic and Geophysical Research Institute of the Hungarian Academy of Sciences. *Acta Geod. Geoph. Mont. Hung.*, 16, 359–380.

Annual Report of the Geophysical Institute Loránd Eötvös for the year 1973. 1974, 59–60.

Daniels J J 1983: Hole-to-surface resistivity measurements. *Geophysics*, 48, 87–97.

Edwards R N 1974: The magnetometric resistivity method and its application to the mapping of a fault. *Can. J. Earth Sci.*, 11, 1136–1156.

Simon A 1974: Theory of potential mapping and its several processing methods. ELGI-report, Budapest

Snyder D D, Merkel R M 1973: Analytic models for the interpretation of electrical surveys using buried current electrodes. *Geophysics*, 83, 513–529.

Szarka L 1982: Analogue modeling of geophysical DC mapping methods. Doctoral Thesis (in Hungarian). Technical University, Miskolc

Szarka L 1983: Exploration of the high resistivity basement using electric and magnetic fields of quasi-static point sources. *Geophysical Prospecting*, 31, 829–839.

Szarka L, Szigeti G 1982: Combined application of mathematical and physical modeling for potential mapping. *Geophysical Transactions*, 28/2, 33–46.

Szigeti G 1980: Application of the conform transformation to determine the electric field distribution over high resistivity semicylinders using line source field generation (in Hungarian). *Magyar Geofizika*, 21, 121–133.

Závoti J 1981: Digital map construction using bicubic spline interpolation. *Acta Geod. Geoph. Mont. Hung.*, 16, 237–244.

Acta Geodaet., Geophys. et Montanist. Hung. Volume 19 (3–4), pp. 467–474 (1984)

METHODOLOGY OF EVALUATION OF THE DATA MEASURED BY RETARDING POTENTIAL ANALYZERS

P BENCZE[1], K KOVÁCS[1], I SZEMEREY[2],
V V AFONIN[3], V V BEZRUKIH[3]

[Manuscript received November 25, 1983]

The methodology of the evaluation of the characteristic curves measured by plane-gridded retarding potential analyzers (planar ion trap) is described. In course of the evaluation first a primary processing of the data is necessary for the conversion of the telemetric data into characteristic curves suitable for the curve fitting procedure. Then the determination of the plasma parameters follows by comparing the experimental characteristic curves with theoretical curves, while the values of the plasma parameters are changed. Finally, the validity of the planar ion trap approximation is discussed.

Keywords: retarding potential analyzer; curve fitting procedure; planar trap approximation

Introduction

Within the scope of the Intercosmos programme retarding potential analyzers have also been used on rockets for the determination of the plasma parameters (Apáthy et al. 1981, Bencze et al. 1985). Thus, the elaboration of a procedure was necessary by means of which plasma parameters can be determined from the telemetric data received at the ground. The procedure consists of two steps. The first step called primary processing includes the conversion of the telemetric data forming a characteristic curve into currents and voltages cutting out those parts of the characteristic curve, where the sensitivity was changed and smoothing the curve by using sliding averages instead of single values. The second step includes the actual determination of the plasma parameters by means of curve fitting (Whipple 1959, Knudsen 1966, Moss and Hyman 1968, Hanson et al. 1970). Since the planar ion traps were used to a height of 1500 km, the consideration of the validity of the planar approximation was also necessary.

[1] Geodetic and Geophysical Research Institute, Hungarian Academy of Sciences, Sopron, Hungary
[2] Central Institute for Physics, Hungarian Academy of Sciences, Budapest, Hungary
[3] Institute for Space Research, Academy of Sciences of the USSR, Moscow, USSR

Primary processing of the data

As it is known, in case of a retarding potential analyzer the result of the measurements is a characteristic curve, which represents the current due to positive ions as a function of the retarding potential, i.e. as a function of the energy and mass of the particles. This positive ion current can be expressed as a function of the retarding potential in analytical form. The unknowns in this equation are determined by means of the fitting of the computed characteristic curve to the measured one changing the values of the unknowns. The unknown parameters which determine the dependence of the current on the retarding potential are the plasma parameters, i.e. the concentrations of the different ions, the ion temperature and the rocket (container) potential. The accurate determination of these parameters is possible only in that case, when the scatter of the measured data is small. The analysis of the noise has shown that the noise is produced outside the instrument. Namely, the noise level is independent of the amplification. For the determination of the source of the noise that part of the characteristic curve belonging to large retarding potentials has been analysed, where the signal to noise ratio is small (Fig. 1). First the deviations of the current values from a parabola approximating the data have been computed. The harmonic analysis of these deviations has shown that in the spectrum there are two peaks with periods of 0.012 and 0.007 s, respectively (Fig. 2). The first peak corresponds to the rotation period of the commutator, while the second peak to that of its first harmonic. Thus, according to this analysis the noise originates from the commutator. In the course of the data processing no filtering was used. Practice has shown that the manipulation of the data may lead to incorrect results. Since there are enough experimental characteristic curves, the best curves have been selected on the basis of the scatter of the data.

The retarding potential corresponding to the measured current (during one revolution of the commutator the current is measured four times, but the retarding

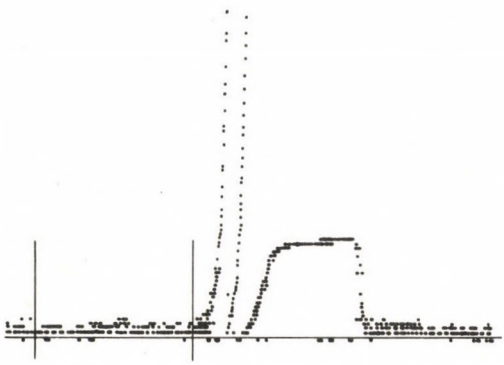

Fig. 1. Part of characteristic (current-voltage) curve which has been used for the determination of the noise spectrum

potential only once) is determined as follows: The retarding potential corresponding to the measured current consists of two parts — one part is connected with the change of the retarding potential during one complete revolution of the commutator, the other part corresponds to its variation between two measurements within one period of revolution of the commutator. The difference between the voltages corresponding to

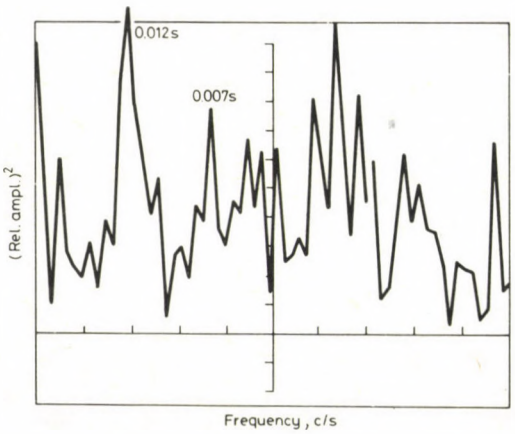

Fig. 2. The noise spectrum of the characteristic curve shown in Fig. 1

the beginning and end of the characteristic curve is divided by the number of rotations of the commutator (the period of the saw-tooth voltage divided by the period of the commutator). Thus, the change of the retarding potential during one revolution of the commutator is obtained. Then dividing the change of the retarding potential during one revolution of the commutator by the number of channels of the commutator the change of the potential between measurements carried out in adjoining channels is found. Since the current was measured in every eighth channel, the retarding potential was calculated by means of the following formula:

$$V = 16 - (I-1)C_k - 8JK_k,$$

where C_k is the change of the retarding potential during one revolution of the commutator, K_k being the variation of the potential between measurements carried out in two adjoining channels (in case of the measurement of the current every eighth channel is used), $I = 1, \ldots N$ and $J = 0, 3$.

Preparing the current data for the computation of the parameters those parts of the experimental characteristic curves have been omitted, where the amplification respectively the sensitivity of the equipment was changed. In order to reduce the scatter

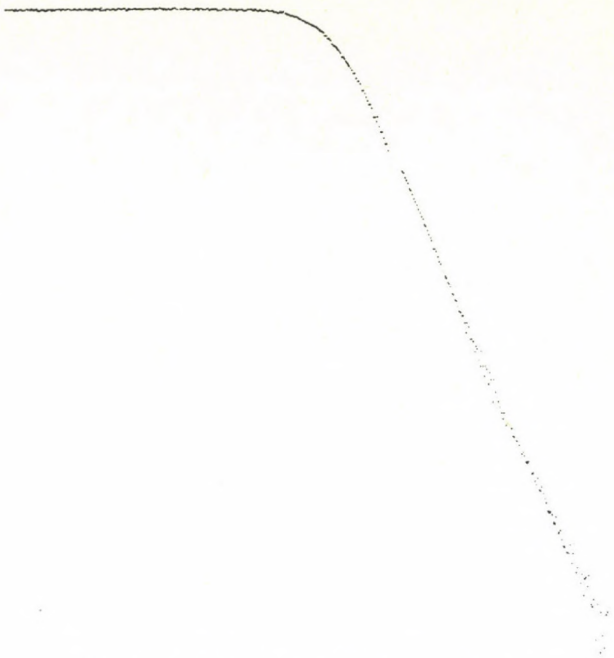

Fig. 3a. Characteristic curve before smoothing

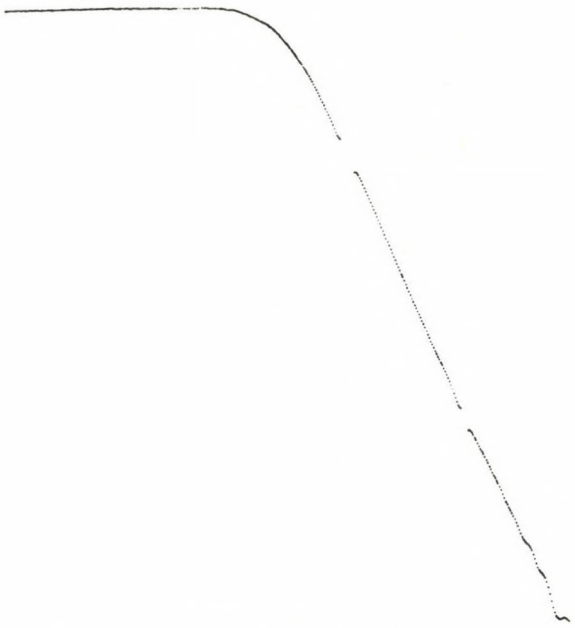

Fig. 3b. The same curve after smoothing

of the data in different parts of the curve recorded with the same sensitivity the data were smoothed using the formula

$$y_n = \frac{S_1 y_{n-1} + S_2 y_n + S_3 y_{n+1}}{S_1 + S_2 + S_3}$$

where $S_1 = S_3 = 1$ and $S_2 = 2$ are weighting coefficients. This procedure is repeated ten times. The efficiency of the smoothing is illustrated by Figs 3a and b, where the same experimental characteristic curve is shown respectively before and after smoothing. Before starting the data processing the telemetric data are converted into current intensities. This conversion is performed by means of the data obtained by checking the amplifier in different ranges of amplification. The current intensity is calculated from the formula

$$i = (TD - 0\%) \frac{6300}{100\% - 0\%} \cdot G$$

where TD is the current in telemetric units, 0% and 100% are respectively the beginning and end of the measuring range in telemetric units, 6300 is the calibrating voltage in millivolts, G being the sensitivity of the amplifier corresponding to the given range.

Determination of the plasma parameters

The parameters of the plasma are determined by fitting the computed curve (on the basis of the equation of the characteristic curve) to the measured characteristic curve, while the values of the unknowns, i.e. the magnitude of the plasma parameters are changed. The curve fitting is started with approximate values of the unknown plasma parameters. As it is known, the relation of the ion current i to the retarding potential V is given by the equation (Whipple 1959, Knudsen 1966):

$$i = \alpha A e \sum_j n_{ij} \left\{ v_r \cos \Theta \left[\frac{1}{2} - \frac{\operatorname{erf}(X_j)}{2} \right] + \frac{C_{ij} \exp(-X_j^2)}{2\sqrt{\pi}} \right\};$$

$$X_j = \frac{1}{C_{ij}} \left[\sqrt{\frac{2e(v+\varphi)}{m_{ij}}} - v_r \cos \Theta \right]$$

where α is the transparency of the grids, A is the area of the aperture of the trap, v_r is the velocity of the container, n_{ij} and m_{ij} are respectively the concentration and the mass of the positive ions of type j, $C_{ij} = \sqrt{\frac{2kT_i}{m_{ij}}}$ being the most probable velocity of the j-th ion, T_i is the common ion temperature, Θ is the angle between the direction of the relative velocity vector and the normal to the trap aparture (angle of attack), φ is the potential of the container relative to the undisturbed plasma.

The values of the plasma parameters are obtained, when the sum of the deviations of the computed current intensities (forming the theoretical characteristic curve) from the measured current intensities becomes minimum. Since the number of measurements (the number of related voltages and current intensities), determining a characteristic curve is greater than the number of unknowns, the problem is overdetermined and can be solved by means of the mathematical statistics. Expanding in series the equation above the following expressions are obtained:

$$v_1 = a_1\delta x_1 + b_1\delta x_2 + c_1\delta x_3 + d_1\delta x_4 + e_1\delta x_5 - l_1$$

$$v_2 = a_2\delta x_1 + b_2\delta x_2 + c_2\delta x_3 + d_2\delta x_4 + e_2\delta x_5 - l_2$$

$$\vdots$$

$$v_n = a_n\delta x_1 + b_n\delta x_2 + c_n\delta x_3 + d_n\delta x_4 + e_n\delta x_5 - l_n$$

where

$$a = \alpha Ae\left\{v_r\cos\Theta\left[\frac{1}{2} - \frac{\operatorname{erf}(X_{O^+})}{2}\right] + \frac{C_{O^+}\exp(-X_{O^+}^2)}{2\sqrt{\pi}}\right\} \qquad \delta x_1 = \delta n_{O^+}$$

$$b = \alpha Ae\left\{v_r\cos\Theta\left[\frac{1}{2} - \frac{\operatorname{erf}(X_{He^+})}{2}\right] + \frac{C_{He^+}\exp(-X_{He^+}^2)}{2\sqrt{\pi}}\right\} \qquad \delta x_2 = \delta n_{He^+}$$

$$c = \alpha Ae\left\{v_r\cos\Theta\left[\frac{1}{2} - \frac{\operatorname{erf}(X_{H^+})}{2}\right] + \frac{C_{H^+}\exp(-X_{H^+}^2)}{2\sqrt{\pi}}\right\} \qquad \delta x_3 = \delta n_{H^+}$$

$$d = \alpha Ae\sum_j n_{ij}\left\{v_r\cos\Theta\,\frac{1}{2}\,\frac{x_j\exp(-X_j^2)}{\sqrt{\pi}\,T} + \frac{\exp(-X_j^2)}{2\sqrt{\pi}}\left(\frac{k}{mc} + \frac{c_{ij}X_j^2}{T}\right)\right\} \qquad \delta x_4 = \delta T_i$$

$$e = \alpha Ae\sum_j n_{ij}\left\{-v_r\cos\Theta\,\frac{1}{\sqrt{\pi}}\,\frac{\exp(-X_j^2)e}{C_{ij}\sqrt{\dfrac{2e(v+\varphi)}{m_{ij}}\,m_{ij}}} - \frac{\exp(-X_j^2)}{\sqrt{\pi}}\,X_j\,\frac{e}{\sqrt{\dfrac{2e(v+\varphi)}{m_{ij}}\,m_{ij}}}\right\}$$

$$\delta x_5 = \delta\varphi$$

$$l = \alpha Ae\sum_j n_{ij}\left\{v_r\cos\Theta\left[\frac{1}{2} - \frac{\operatorname{erf}(X_j)}{2}\right] + \frac{C_{ij}\exp(-X_j^2)}{2\sqrt{\pi}}\right\} - i$$

and the coefficients of the observation equations are computed by means of the approximate values of the unknowns. The same equations in matrix form are

$$v = \mathbf{A}x - y\,.$$

Since the condition

$$\sum_{i=1}^{n} v_i^2 = \text{Min}$$

is equivalent to the condition

$$\sum_{i=1}^{n} v_i \frac{\partial v_i}{\partial x_j} = 0 \qquad (j = 1, 2, \ldots k)$$

from equation

$$\frac{\partial v'}{\partial x_j} \cdot v = e'_j \mathbf{A}'(\mathbf{A}x - y) = e'_j(\mathbf{A}'\mathbf{A}x - \mathbf{A}'y) = 0$$

the formula for the computation of the unknowns is obtained as

$$x = \frac{\mathbf{A}'y}{\mathbf{A}'\mathbf{A}} = \mathbf{A}'y\,(\mathbf{A}'\mathbf{A})^{-1},$$

where $\mathbf{A}'$ is the matrix transpose.

This procedure is repeated till the supplementary quantity δx_5 (supplementary quantity for the common ion temperature) will be less than about 1% of the approximate value. The characteristic curves included in the further analysis are selected on the basis of the mean square error. This quantity is determined by the deviation of the measured from the computed curves on the basis of the parameters of the characteristic curves.

On the validity of the planar ion trap approximation

As it is known, the rockets type Vertical reach an altitude of 1500 km. Since the density of the plasma decreases with increasing height, the mean free path of the ions increases and becomes commensurable with the dimensions of the trap. However, the planar ion trap approximation used here presumes that the flux density of the positive ions is constant over the surface of the aperture and the plasma sheath, as well as the electric field of the grids affect only the velocity component of the ions perpendicular to the aperture. These conditions are fulfilled only in case of small Debye length, that is in the dense layers of the ionosphere. Computations show that in case of Debye lengths less than 10 cm, the retarded positive ion current can be determined on the basis of the planar approximation with an accuracy better than 10%, if the angle of attack is $<45°$, the potential of the aperture grid is equal to the potential of the body (container) (no drawing-in potential) and the negative potential of the body is less than 3 V (Parker and Whipple 1970). The planar approximation does not give accurate results in case of large Debye lengths, if the retarding potential is small. Since the Debye-length does not reach 10 cm in 1500 km altitude, the planar trap approximation gives reliable results to these heights. However, the deviation of the circumstances from the above mentioned conditions may result in scatter of the data.

References

Apáthy I, Szemerey I, Bencze P, Kovács K, Afonin V, Bezrukih V, Gringauz K, Shutte N 1981: Comprehensive investigation of the basic parameters of the upper atmosphere at the time of the flight of the geophysical rocket "Vertical-6". *Adv. Space Res.*, 1, 101–105.

Bencze P, Kovács K, Szemerey I, Afonin V V, Bezrukih V V 1985: Measurement of the plasma parameters in the ionosphere by night with retarding potential analyzers on board of the geophysical rocket Vertical-10. *Acta Geod., Geoph. Mont. Hung.* 20 (in press)

Hanson W B, Sanatani S, Zuccaro D, Flowerday T W 1970: Plasma measurements with the retarding potential analyzer on Ogo 6. *J. Geophys. Res.*, 75, 5483–5501.

Knudsen W C 1966: Evaluation and demonstration of the use of retarding potential analyzers for measuring several ionospheric quantities. *J. Geophys. Res.*, 71, 4669–4678.

Moss S J, Hyman E 1968: Minimum variance technique for the analysis of ionospheric data acquired in satellite retarding potential analyzer experiments. *J. Geophys. Res.*, 73, 4315–4323.

Parker L W, Whipple E C Jr 1970: Theory of spacecraft sheath structure, potential and velocity effects on ion measurements by traps and mass spectrometers. *J. Geophys. Res.*, 75, 4720–4733.

Whipple E C 1959: The ion trap results in exploration of the upper atmosphere with the help of the third Soviet Sputnik. *Proc. IRE*, 47, 2023–2024.

BOOK REVIEWS

S AKIMOTO and M H MANGHNANI eds: *High-Pressure Research in Geophysics (Advances in Earth and Planetary Sciences 12)*. Center for Academic Publications Japan/Tokyo D Reidel Publishing Company/Dordrecht–Boston–London, ISBN 90-277-1439-8, XIII + 632 pages, Cloth Dfl 260.—/ US $ 113.— 1982

The Center for Academic Publications Japan and the Japan Scientific Societies Press undertake the publication of a series "*Advances in Earth and Planetary Sciences*" for which Professor Rikitake works as General Editor. The proceedings of the second U.S.–Japan Seminar on "*High-Pressure Research: Applications in Geophysics*" held in Hahone, Japan, 12–15 January, 1981 was published in this series. Of forty-seven papers presented during the seven scientific sessions covering a wide spectrum of recent advancements in the field forty-five appear as contributed papers in this volume.

The themes of the sessions are as follows:

I. Instrumentation and Pressure Calibration
II. Elasticity, Attenuation and Rheology of the Crust and Upper Mantle
III. Mechanical Properties and Melting of the Crust and Upper Mantle
IV. Geophysics and Geochemistry of the Mantle
V. High-Pressure Phase Transformations and Crystal Chemistry
VI. Thermochemistry and Crystal Growth
VII. Shock Wave Experiments.

As it is emphasized in the Preface "Since holding of the first U.S.–Japan Seminar on "High-Pressure Research Applications in Geophysics", in Honolulu, 1976, interest and activity have been increasing with notable acceleration in experimental techniques and interpretation of the experimental data both in the U.S.A. and Japan. The new diamond-anvil techniques have not only extended the working pressure range up to the earth's core conditions, but have incorporated, in addition to X-ray measurements, Brillouin, Raman, infrared, viscosity, and melting studies." Investigations of the kinetics of phase transformation and shock wave experiments with high velocity and light gas guns should be mentioned.

Only a few papers are devoted to the "Geophysics and Geochemistry of the Mantle". Such a very important parameter of the mantle rocks as the electrical properties are not mentioned in this volume in spite of the large amount of the field data got by electromagnetic induction soundings all over the world.

The content of this volume is at high scientific level. The proceedings are warmly recommended not only to the experts on the high pressures techniques but to those also who want to get an overview on the present state of the laboratory research techniques aimed at the better understanding the physics and chemistry of earth's interior.

A Ádám

I I ROKITYANSKY: *Geoelectromagnetic Investigation of the Earth's Crust and Mantle*. Translated from the Russian by Chobotova N L, Pestryakov G M, Pristay M N, Shilman B G. 1982. 129 figs. XIII, 381 pages. 820 g. Cloth DM 148.—; approx. US $ 65.80. Berlin–Heidelberg–New York: Springer-Verlag ISBN 3-540-10630-8

The author of this monograph Prof. Rokityansky (Kiev, USSR) is a well-known Soviet scientist whose name can be found among the pioneers of the electromagnetic induction methods already in the early sixties. He has written in Russian a few books dealing with the development of these methods, the first field results and the interpretation of the conductivity anomalies, such as the Carpathian Anomaly, Kirovograd Anomaly, etc., some of them discovered by him and his co-workers. In his

last papers he also looked for general relations in the distribution of the conductivity anomalies. His main research field is the Magnetic Variation Profiling (MVP) and he is strongly interested in Geomagnetic Deep Soundings (GDS), too. His interest is well reflected by the content of this monograph. (The first part of this book is the English translation of his book published in Russian in 1981.)

We should cite the intention of the author in writing this monograph from the introduction of the book: "This monograph is intended to present mainly the physical basis of the deep electromagnetic methods and to describe the problems arising in interpretation of experimental data. Discussion of complicated mathematical problems is kept to a minimum, data processing of measurements is given very briefly, instrumentation is not described at all".

"The present monograph attempts to "fill the gap", i.e. to summarize principal results obtained in the last 15 years".

The book consists of the following chapters:

Chapter 1 Geoelectromagnetic Field (pp 1–27)
2 Elements of the Theory of Electromagnetic Field (pp 27–60)
3 The Inverse Problems (pp 60–106)
4 Global and Regional Geomagnetic Deep Sounding (pp 106–186)
5 Magnetotelluric Sounding (pp 186–247)
6 Magnetic Variation Profiling (MVP) (pp 247–308)
7 Electrical Conductivity Anomalies (pp 308–345)
8 Conclusions (pp 345–349).

The first three chapters are of introductory character, or "auxiliary to the further chapters" as it has been formulated by the author. The chapter on inversion gives a good insight to the difficult problems to be solved in case of the induction methods. The Geomagnetic Deep Sounding (GDS) is separated from the so-called "Magnetic Variation Profiling", nevertheless their boundary is generally becomes indistinct in the practice mainly in the western countries. The magnetotelluric soundings are treated from the most actual point of view taking into account the effect of the lateral inhomogeneities. The description of the induction methods seems to me well balanced.

Each chapter has its conclusions emphasizing the most important results and problems.

The book presents some of the newest field results measured on well-known conductivity anomalies in different parts of the world. The author seeks for general but in the given form yet a little rough relations in the distribution of conductivity anomalies depending on their tectonic settings. In this large book we should make allowances for such a mistake as the ranging Transdanubia among platforms (in Table 28) with its extremely high heat flow and thin crust. (Other important discriminations should not be mentioned here.)

In the Conclusions the main physical and petrological causes of the conductivity anomalies are summarized.

In an Appendix the Geomagnetic Observatories of World-wide Network are listed as a valuable contribution to the methodical part of the book. (It is a pity that even the two Hungarian observatories — Nagycenk and Tihany — are confused and united to only one.)

The references contain the most important papers from east and west.

The quality of the figures does not always correspond to the high level of this monograph.

The book is warmly recommended not only to the experts on electromagnetic induction methods but all the geoscientists who are interested in the structure and dynamics of the Earth.

A Ádám

Ch C BATES, T F GASKELL, R B RICE *Geophysics in the Affairs of Man.* (A Personalized History of Exploration Geophysics and Its Allied Sciences of Seismology and Oceanography.) Pergamon Press, Oxford–New York. 492 pages + many illustrations, $ 25.00

The subtitle of the book states quite exactly what it is, a really personalized history of some branches of geophysics. It is personal in the sense, too, that developments in three countries, United States, United Kingdom and Canada, are treated most intensively while other countries are only occasionally mentioned, e.g. Hungary appears in connection with the Eötvös (torsion) balance a few times.

After a short introductory chapter dealing with the beginnings of geophysics, a little more is said on the development between the two wars when foundations for most modern geophysical methods were laid and even presently existing companies founded. Then the greatest part of the book is devoted to geophysics in World War II and later developments. Both technical and economic problems are treated in details, sometimes the "official" text being somewhat difficult due to the acronyms of

government institutions, international organizations etc. The authors, however, do not forget to make their book interesting: they raccont stories about persons and methods, often in footnotes which are sometimes more interesting and informative then the main text itself. It is not intended to write a comprehensive history of all geophysics, the authors speak mostly of topics they were interested in and participating in. This personal style and viewpoint is what makes the book a most interesting reading for all geophysicists.

The surprising fact is when one sees the many connections between geophysics and everyday life, politics, human environment, economy. Some of these were discussed at international forums for a long time, e.g. the seismological detection of nuclear tests. Other major issues recently met by public interest and also covered in the book are continent spreading (plate tectonics) and modification of the earth atmosphere by human activity.

The most positive aspect of geophysical cooperation was the International Geophysical Year a quarter of a century ago. The history of this Year is also told as the first great international, even worldwide effort in science.

Special interest is due to the rich illustrations in the book, portraits of eminent geophysicists, events etc. Some of them add personal recollections about their achievements at the end of the book, together with the history of major geophysical contractors.

Especially when reading these last parts of the book, the necessity to have a complete history of geophysics is strongly felt — as long as the key figures of its beginning can tell their story.

J Verő

A R RITSEMA and A GÜRPINAR eds: *Seismicity and Seismic Risk in the Offshore North Sea Area.* Proceedings of the NATO Advanced Research Workshop, held at Utrecht, the Netherlands, June 1–4, 1982. D Reidel Publishing Company, Dordrecht, Boston, London, 1983. 420 pp.

The assessment of the Earth's seismicity became an exceedingly significant theme in the second half of the twentieth century.

The reason of the grown interest is double, namely, the increase in number and value of the structures and political views. The main theme of the proceedings of this workshop held at Utrecht was the study of the actual and potential seismic risk at such an area where the historical seismic hazard was not so great, but this zone shows some unique and complicated characteristics, which increases the uncertainty at planning of different structures.

In accordance with the long list of participants, the authors came from different institutes, observatories, universities, oil companies and insurance firms. Except a few countries, numerous nationalities along the North Sea shore were present on this workshop, in addition to some experts from outside the region.

This volume consists of six sections namely: Geology and Tectonics on 46 pages, Seismicity on 68 pages, Tides Ocean Waves and Sea Level Changes on 24 pages, Instrumentation on 44 pages, Oilmechanics, Liquefaction, Geotechnology on 108 pages and Risk Analysis on 80 pages. The six sections contain altogether the papers of thirty-four lectures with nearly 150 figures and discussions for the different themes, furthermore the conclusions and recommendations for the future tasks.

It can be found, that this fruitful meeting similarly to other wide range geophysical discussions shows certain information gaps among different professions, therefore stronger coordination is needed between national and international seismological services and other different branches of professions of the themes mentioned above.

As a final note my firm opinion is that the participants of this workshop achieved a good job, their purpose and discussions were clear and the text was well compiled.

E Bisztricsány

T RIKITAKE: *Earthquake forecasting and warning.* Developments in Earth and Planetary Sciences 03 Center for Academic Publications Japan. D Reidel Publishing Company, 1983

If somebody thinks that there are books in a sufficient number about earthquake prediction, and nothing new could be written, this volume could convince him that this is not the case. Professor Rikitake presents here the process of earthquake warning, as made in the four greatest powers of this field, in Japan, in China, in the United States and in the Soviet Union. This order is the order of decreasing information used in the book, mostly due to the quantity of information obtainable for the author.

The process of prediction is described from the very first steps, i.e. from the collection of material to be used as basis for future prediction, ample examples are given for precursors of all kinds, including many less well known Chinese results,

then the use of the collected knowledge is outlined in form of special observation networks in areas where earthquakes are expected, and the administrative and legislative measures to be taken are summarized with special emphasis on the reaction of citizens to earthquake warnings and also to false rumours. This social impact is one of the most interesting aspects for countries too, where up to now no similar earthquake warning system has been developed, be it due to the less frequent occurrence of earthquakes, be it due to administrative problems, e.g. observations from neighborous countries would be also necessary due to the small area of the country. Hungary is a country of both categories, nevertheless, earthquake prediction would also be important here, as even during the last century, some destructive earthquakes happened. In this respect, the Japanese and American legislature is of great interest, being at present the unique examples for such measures.

It is a very interesting fact that from the few successfully predicted earthquakes, there were one in Japan and all others in China. That means that Chinese geophysicists were most successful in this area (there could be also one more Soviet success). In spite of quite simple instrumentation, they succeeded in predicting three consecutive quakes in one province. This success makes it very important to know more about Chinese methods, and Professor Rikitake tries to tell as much about Chinese methods as he can. He supposes that the rural environment, the low noise level and the close connection of men with nature in these areas may contribute significantly to the success.

An interesting aspect of the prediction is the animal behaviour. In this respect, many new facts were discovered in recent years, so the author considers as a proven fact that at least some animals are able to "predict" earthquake. The mechanism behind this predictory capability is unknown, nevertheless, the effect itself seems to be of increasing importance.

Professor Rikitake's book is a very interesting lecture, and at the same time, a valuable contribution to a rapidly developing field, not only for geophysicists, but also for everybody who has to do with earthquakes, including administrative bodies, too.

J Verő

P BÍRÓ: *Time Variation of Height and Gravity.* Akadémiai Kiadó, Budapest, 1983. 160 pages, 15 figs.

Height determination has always had an important role in the field of geodesy. Without it the numerical and graphical representation of the earth's surfaces would be unimaginable. In our age the instruments of height measurements and the different mathematical methods permit the precise determination of heights. It is possible to detect the elevation changes for a relatively short time period. In this way it is no problem to monitor the vertical displacements of certain areas on the earth. In the classical geodesy the basic assumption of height determinations has been so far that the spatial position of the equipotential surface as a vertical datum level for the height measurements remained unchanged with time. In the dynamical aspect of our time we know that in the universe everything is in continuous progress and change. In fact, the movements of the earth's surface are continuously changing too. Under such conditions it is necessary to revise the classical principle of height determination. The book deals with these problems. The author gives a summary about his research work which was done at the Department of Geodesy of the Technical University in Budapest.

Chapter 1 gives a brief summary of basic definitions.

Chapter 2 deals with the effect of time variations of the gravity field. The subchapters are as follows: The effect of time variations of the gravity field of a model earth with rigid crust. The effect of time variations of the gravity field at the surface of a model earth covered by an ideal fluid. The effect of time variations of the gravity field at the surface of a model earth with elastic crust. The effect of time variation of the real earth's gravity field.

Chapter 3 summarizes the geodynamic conclusions.

The book is well illustrated with numerous figures, and is very clearly written.

J Somogyi

W D PARKINSON: *Introduction to Geomagnetism.* Scottish Academic Press, Edinburgh. 1983, 434 pp, 121 figs, £ 27.50

One has seldom the feeling of completeness, not to say perfectness when reading a book. Professor Parkinson succeeded to reach this success. It is really admirable, how many aspects of geomagnetism he could collect in this rather slim volume (especially when compared to its predecessor, the thick two volumes by Bartels-Chapman). He is always very precise and concrete in his data, be it about the first reports of Southern aurora by Captain Cook, Legendre polynomials or biomagnetism. Just this that everything can be found in a book, properly ordered and balanced is the most difficult thing which makes this book a necessary tool for everybody interested in geomagnetism.

In the introductory part a short description is given on the geomagnetic field, its constituents and sources. Ample space is devoted to the principles of magnetism, discussing problems of fundamental interest which cause sometimes much confusion. Geomagnetic instruments, measurements and observatories are dealt with in the remaining sections of this chapter.

The second Chapter deals with the main field, its morphology and origin, with respect to the secular variation. The theoretical background, magnetohydrodynamics and hydromagnetic dynamos are very clearly reviewed in spite of being one of the most complicated problems of geophysics.

Local fields are due to crustal (or deeper) anomalies. Many aspects of this topic are rapidly developing, thus e.g. rock magnetism (paleomagnetism) and ocean floor spreading, or the use of magnetic records in earthquake prediction (tectonomagnetism). Naturally, "normal" geomagnetic surveys are also mentioned.

The external field, the magnetosphere and its processes are reviewed in Chapter 4. Following a short introduction on plasma physics, at first the two most characteristic regions i.e. ionosphere and magnetosphere, are reviewed, then some characteristic variations of the geomagnetic field, diurnal variations, magnetic storms and substorms, and pulsations. The chapter is well-balanced, in the short place at disposal the most important facts and events are summarized.

From the point of view of exploration geophysics, the most important aspect of geomagnetism is the induction. Both the theory of induction (eddy currents) and the distribution of the electric conductivity are dealt with in sufficient details, followed by a description of different conductivity anomaly-types. The implications of conductivity determinations are finally surveyed.

Among miscellaneous topics, the history of geomagnetism is summarized, and then biomagnetism, being a quite new, but recently more and more current topic, for the first time appearing just in this year in a US IAGA Report for the Hamburg General Assembly — IAGA is also represented among Miscellaneous Topics.

The appendices include some useful mathematical methods, such as e.g. spherical trigonometry, spherical harmonics and filter theorem.

I think that if a student has to get acquainted with geomagnetism, the best advice is for him for the next decade to take this book. Even those dealing for many years with geomagnetism, will find it interesting to read it. It can be only congratulated to the author and to the publisher for this excellent book.

J Verő

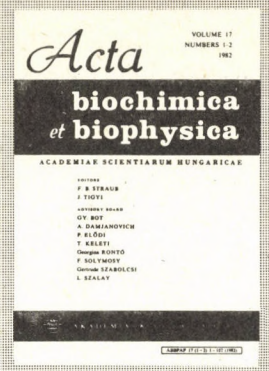

ACADEMIAE SCIENTIARUM HUNGARICAE

EDITORS
F. B. STRAUB and J. TIGYI

Acta Biochimica et Biophysica publishes original papers on biochemistry and biophysics in English. Papers on proteins (structure and synthesis), enzymes, nucleic acids, regulatory and transport processes, bioenergetics, excitation, muscular contraction, functional structure and ultrastructure will be accepted.

Published in one volume (4 issues) annually
Subscription rate per volume $ 40.00

AKADÉMIAI KIADÓ
Publishing House of the Hungarian Academy of Sciences
Budapest

Distributed by KULTURA
Hungarian Foreign Trading Co.
PO Box 149, H-1389 Budapest

CONTENTS
VOLUME 17, NUMBERS 3–4

ACTA AGRONOMICA

ACADEMIAE SCIENTIARUM HUNGARICAE

CHAIRMAN OF THE EDITORIAL BOARD

S. RAJKI

EDITED BY

GY. PÁL

TOMUS XXXI FASCICULI 3–4

CONTENTS

PRINTED IN HUNGARY
Akadémiai Kiadó és Nyomda, Budapest

— treble underlining: bold-face italics
— red underlining: Greek letters
— green underlining: script letters.

Rules for mathematical-physical notations:

— trigonometric, logarithmic, analytic symbols, symbols for units and functions are in roman type (not underlined)
— letter symbols in mathematical and physical formulas, scalars, and subscripts of algebraic and physical quantities are in italics (underlined)
— vectors, matrices, operators in probability theory are in bold-face roman type (double underlining)
— tensors, operators and some special functions are in script letters (green underlining). These cannot be bold.
— Greek letters (red underlining) cannot be bold or extra bold type (thus they cannot be used for vectors or tensors)
— void upper lines e.g. for vectors
— avoid possible confusion between o (letter) and 0 (zero), l (letter) and 1 (one), ν (Greek nu) and v, u (letters) etc.
— explain ambiguous or uncommon symbols by making marginal notes in pencil
— be careful about superscripts and subscripts
— formulae must be numbered consecutively with the number in parentheses to the right of the formula. References in text to the equations may then usually be made by the number in parenthesis. When the word equation is used with a number, it is to be abbreviated, Eq. or Eqs in the plural
— the International System of Units (SI) should be used.

Authors are liable for the cost of alteration in the *proofs*. It is, therefore, the responsibility of the author to check the text for errors of facts before submitting the paper for publication.

3. *References* are accepted only in the Harvard system. Citations in the text should be as:

...(Bomford 1971)...or Bomford (1971)

...(Brosche and Sündermann 1976)...

...(Gibbs et al. 1976b)...

The list of references should contain names and initials of all authors (the abbreviation et al. is not accepted here); for *journal articles* year of publication, the title of the paper, title of the journal abbreviated, volume number, first and last page.

For *books* or *chapters in books*, the title is followed by the publisher and place of publication.

All items must appear both in the text and references.

Examples:

Bomford G 1971: Geodesy. Clarendon Press, Oxford

Brosche P, Sündermann J 1976: Effects of oceanic tides on the rotation of the earth. Manuscript. Univ. of Bonn

Buntebarth G 1976: Temperature calculations on the Hungarian seismic profile-section NP-2. In: *Geoelectric and Geothermal Studies (East-Central Europe, Soviet Asia), KAPG Geophysical Monograph.* Akadémiai Kiadó, Budapest, 561–566.

Gibbs N E, Poole W G, Stockmeyer P K 1976a: An algorithm for reducing the bandwidth and profile of a sparse matrix. *SIAM J. Number. Anal.*, 13, 236–250.

Gibbs N E, Poole W G, Stockmeyer P K 1976b: A comparison of several bandwidth and profile reduction algorithms. *ACM Trans. on Math. Software,* 2, 322–330.

Szarka L 1980: Potenciáltérképezés analóg modellezéssel (Analogue modeling of potential mapping). *Magyar Geofizika,* 21, 193–200.

4. *Footnotes* should be typed on separate sheets.

5. *Legends* should be short and clear. The place of the tables and figures should be indicated in the text, on the margin.

6. *Tables* should be numbered serially with Roman numerals. Vertical lines are not used.

All the illustrations should contain the figure number and author's name in pencil on the reverse.

Figures will be redrawn. Therefore the most important point is clearness of the figures, even pencil-drawings are accepted (with a duplicate).

Photographs and *half-tone* illustrations should be sharp and well contrasted.

If a specific reduction or enlargement is required, please indicate this in blue pencil on the figure.

The editors will send information to the first author about the *arrival* and acceptance of the papers. A galley proof is also sent to the first author for *correction*. Hundred *offprints* are supplied free of charge.

Periodicals of the Hungarian Academy of Sciences are obtainable at the following addresses:

AUSTRALIA
C.B.D. LIBRARY AND SUBSCRIPTION SERVICE
Box 4886, G.P.O., *Sydney N.S.W. 2001*
COSMOS BOOKSHOP, 145 Ackland Street
St. Kilda (Melbourne), Victoria 3182

AUSTRIA
GLOBUS, Höchstädtplatz 3, *1206 Wien XX*

BELGIUM
OFFICE INTERNATIONAL DE LIBRAIRIE
30 Avenue Marnix, *1050 Bruxelles*
LIBRAIRIE DU MONDE ENTIER
162 rue du Midi, *1000 Bruxelles*

BULGARIA
HEMUS, Bulvar Ruszki 6, *Sofia*

CANADA
PANNONIA BOOKS, P.O. Box 1017
Postal Station "**B**", *Toronto, Ontario M5T 2T8*

CHINA
CNPICOR, Periodical Department, P.O. Box 50
Peking

CZECHOSLOVAKIA
MAD'ARSKÁ KULTURA, Národní třida 22
115 66 Praha
PNS DOVOZ TISKU, Vinohradská 46, *Praha 2*
PNS DOVOZ TLAČE, *Bratislava 2*

DENMARK
EJNAR MUNKSGAARD, Norregade 6
1165 Copenhagen K

FEDERAL REPUBLIC OF GERMANY
KUNST UND WISSEN ERICH BIEBER
Postfach 46, *7000 Stuttgart 1*

FINLAND
AKATEEMINEN KIRJAKAUPPA, P.O. Box 128 *SF- 00101 Helsinki 10*

FRANCE
DAWSON-FRANCE S. A., B. P. 40, *91121 Palaiseau*
EUROPÉRIODIQUES S. A., 31 Avenue de Versailles, *78170 La Celle St. Cloud*
OFFICE INTERNATIONAL DE DOCUMENTATION ET LIBRAIRIE, 48 rue Gay-Lussac
75240 Paris Cedex 05

GERMAN DEMOCRATIC REPUBLIC
HAUS DER UNGARISCHEN KULTUR
Karl Liebknecht-Straße 9, *DDR-102 Berlin*
DEUTSCHE POST ZEITUNGSVERTRIEBSAMT Straße der Pariser Kommüne 3–4, *DDR-104 Berlin*

GREAT BRITAIN
BLACKWELL'S PERIODICALS DIVISION
Hythe Bridge Street, *Oxford OX1 2ET*
BUMPUS, HALDANE AND MAXWELL LTD.
Cowper Works, *Olney, Bucks MK46 4BN*
COLLET'S HOLDINGS LTD., Denington Estate *Wellingborough, Northants NN8 2QT*
WM. DAWSON AND SONS LTD., Cannon House *Folkstone, Kent CT19 5EE*
H. K. LEWIS AND CO., 136 Gower Street
London WC1E 6BS

GREECE
KOSTARAKIS BROTHERS INTERNATIONAL BOOKSELLERS, 2 Hippokratous Street, *Athens-143*

HOLLAND
MEULENHOFF-BRUNA B. V., Beulingstraat 2,
Amsterdam
MARTINUS NIJHOFF B.V.
Lange Voorhout 9–11, *Den Haag*
SWETS SUBSCRIPTION SERVICE
347b Heereweg, *Lisse*

INDIA
ALLIED PUBLISHING PRIVATE LTD., 13/14
Asaf Ali Road, *New Delhi 110001*
150 B-6 Mount Road, *Madras 600002*
INTERNATIONAL BOOK HOUSE PVT. LTD.
Madame Cama Road, *Bombay 400039*
THE STATE TRADING CORPORATION OF INDIA LTD., Books Import Division, Chandralok 36 Janpath, *New Delhi 110001*

ITALY
INTERSCIENTIA, Via Mazzé 28, *10149 Torino*
LIBRERIA COMMISSIONARIA SANSONI, Via Lamarmora 45, *50121 Firenze*
SANTO VANASIA, Via M. Macchi 58
20124 Milano
D. E. A., Via Lima 28, *00198 Roma*

JAPAN
KINOKUNIYA BOOK-STORE CO. LTD.
17-7 Shinjuku 3 chome, Shinjuku-ku, *Tokyo 160-91*
MARUZEN COMPANY LTD., Book Department, P.O. Box 5050 Tokyo International, *Tokyo 100-31*
NAUKA LTD. IMPORT DEPARTMENT
2-30-19 Minami Ikebukuro, Toshima-ku, *Tokyo 171*

KOREA
CHULPANMUL, *Phenjan*

NORWAY
TANUM-TIDSKRIFT-SENTRALEN A.S., Karl Johansgatan 41–43, *1000 Oslo*

POLAND
WĘGIERSKI INSTYTUT KULTURY, Marszalkowska 80, *00-517 Warszawa*
CKP-I W, ul. Towarowa 28, *00-958 Warszawa*

ROUMANIA
D. E. P., *Bucuresti*
ILEXIM, Calea Grivitei 64–66, *Bucuresti*

SOVIET UNION
SOJUZPECHAT — IMPORT, *Moscow*
and the post offices in each town
MEZHDUNARODNAYA KNIGA, *Moscow G-200*

SPAIN
DIAZ DE SANTOS, Lagasca 95, *Madrid 6*

SWEDEN
GUMPERTS UNIVERSITETSBOKHANDEL AB
Box 346, *401 25 Göteborg 1*

SWITZERLAND
KARGER LIBRI AG, Petersgraben 31, *4011 Basel*

USA
EBSCO SUBSCRIPTION SERVICES
P.O. Box 1943, *Birmingham, Alabama 35201*
F. W. FAXON COMPANY, INC.
15 Southwest Park, *Westwood Mass. 02090*
READ-MORE PUBLICATIONS, INC.
140 Cedar Street, *New York, N.Y. 10006*

YUGOSLAVIA
JUGOSLOVENSKA KNJIGA, Terazije 27, *Beograd*
FORUM, Vojvode Mišića 1, *21000 Novi Sad*

Index: 26.031